JAERI-Conf
96-010

PROCEEDINGS OF
THE 3rd JAERI SYMPOSIUM ON HTGR TECHNOLOGIES
February 15~16, 1996, Oarai, Japan

July 1996

(Ed.) Executive Committee of
The 3rd JAERI Symposium on HTGR Technologies

日本原子力研究所
Japan Atomic Energy Research Institute

本レポートは，日本原子力研究所が不定期に公刊している研究報告書です。
入手の問合わせは，日本原子力研究所研究情報部研究情報課（〒319-11 茨城県那珂郡東海村）あて，お申し越しください。なお，このほかに財団法人原子力弘済会資料センター（〒319-11 茨城県那珂郡東海村日本原子力研究所内）で複写による実費頒布をおこなっております。

This report is issued irregularly.
Inquiries about availability of the reports should be addressed to Research Information Division, Department of Intellectual Resources, Japan Atomic Energy Research Institute, Tokai-mura, Naka-gun, Ibaraki-ken 319-11, Japan.

© Japan Atomic Energy Research Institute, 1996

編集兼発行　日本原子力研究所
印　　刷　㈱原子力資料サービス

JAERI−Conf 96−010

Proceedings of
The 3rd JAERI Symposium on HTGR Technologies
February 15～16, 1996, Oarai, Japan

(Ed.) Executive Committee of
The 3rd JAERI Symposium on HTGR Technologies

Japan Atomic Energy Research Institute
Oarai-machi, Higashiibaraki-gun, Ibaraki-ken

(Received June 3, 1996)

Japan Atomic Energy Research Institute (JAERI) held the 3rd JAERI Symposium on HTGR Technologies from February 15 to 16, 1996 at Oarai, Ibaraki-ken, Japan.

In the Symposium, the worldwide present status of HTGR Projects and the future perspective of HTGR development, safety, operation experience, fuel and heat utilization technology were reviewed and discussed with 17 papers including 2 invited lectures.

The Symposium was attended by 115 participants from official circles, universities, national institutes and manufacturing industries, and 24 overseas participants from China, Germany, the United States of America, Indonesia, Russia, The Netherlands, Israel, Myanmar and the International Atomic Energy Agency (IAEA).

This paper was edited as the proceedings of the 3rd JAERI Symposium on HTGR Technlogies, collecting the 17 papers presented in the oral and the 22 papers presents in the poster.

Keywords: HTR, HTGR, Gas-cooled Reactor, HTGR Technology, Environmental Problem, Future Perspective, HTGR Project, Nuclear Safety, Coated Particle Fuel, Operation Experience, Heat Utilization

JAERI－Conf 96－010

第３回高温ガス炉技術国際シンポジウム論文集

1996年２月15日～16日，大洗町

日本原子力研究所

（編）第３回高温ガス炉技術国際シンポジウム実行委員会

（1996年６月３日受理）

日本原子力研究所（原研）は，平成８年２月15日，16日の両日，茨城県大洗町にて第３回高温ガス炉技術国際シンポジウムを開催した。

本シンポジウムでは，各国における高温ガス炉計画の現状と高温ガス炉開発の将来展望，安全性，燃料，運転経験，熱利用等を中心に招待講演２件含む17件の論文発表があった。

今回のシンポジウムでは，官界，大学，国立研究機関及び産業界から 115名と海外から中国，ドイツ，アメリカ，インドネシア，ロシア，オランダ，イスラエル及びＩＡＥＡより24名の参加者があった。

本報は，本シンポジウムで発表された17件の論文と22件のポスター発表を収録しプロシーディングとしてまとめたものである。

日本原子力研究所：〒311-13　茨城県東茨城郡大洗町成田町新堀3607

JAERI－Conf 96－010

Proceedings of

The 3rd JAERI Symposium on HTGR Technologies

Japan Atomic Energy Research Institute

Members of Executive Committee

Chairman Toshiyuki TANAKA: Director, Department of HTTR Project, JAERI

Vice Chairman Osamu BABA: Deputy Director, Department of HTTR Project, JAERI

Vice Chairman Yuichiro KAMBAYASHI: Head, HTTR Project Management Division, Department of HTTR Project, JAERI

Maturou OGAWA: Senior Staff, Office of Planning, JAERI

Takashi OKABE: Administrative Manager, Department of Reactor Engineering, JAERI

Takehiko MUKAIYAMA: Deputy Director/Head, Thermal Reactor Physics Laboratory, Department of Reactor Engineering, JAERI

Takamitsu MORI: Administrative Manager, Department of Materials Science and Engineering, JAERI

Masami SHINDO: Head, Material Performance and Testing Laboratory, Department of Materials Science and Engineering, JAERI

Yasunori HIROHARA: Administrative Manager, Department of Chemistry and Fuel Research,JAERI

Kousaku FUKUDA: Deputy/Head, Fuel Irradiation And Analysis Laboratory, Department of Chemistry and Fuel Research, JAERI

Koichi SAKAMOTO: Administrative Manager, Department of High Temperature Engineering, JAERI

Motokuni ETO: Head, Energy Materials Development Laboratory, Department of High Temperature Engineering, JAERI

Hideo OSONO: General Manager, Administrative Services Division, Department of Administrative Services, Oarai Research Establishment, JAERI

Shinichi SUGA: Administrative Manager, Department of HTTR Project,JAERI

Shusasku SHIOZAWA: Deputy Director/Head, HTTR Reactor Development Division, Department of HTTR Project, JAERI

Secretariate: HTTR Project Management Division, Department of HTTR Project JAERI

Contents

Participant List 1
Program of the Symposium 5
Foreword 10
Opening Address 11
M.Yoshikawa (JAERI, Japan)
1. Session Ⅰ-Invited Lecture 13
1.1 Global Environmental Problems and Perspective of Nuclear Energy 15
H.Komiyama (University of Tokyo, Japan)
1.2 Nuclear Safety and the Expectation to HTGR's Deployment 21
K.Kugeler (KFA, Germany)
2. Session Ⅱ-Present Status of HTGR Projects and Perspectives of HTGR Deployment 37
2.1 Present Status of the HTR-10 Project 39
Y.Sun (INET, China)
2.2 Present Status of HTGR Projects and Their Heat Applications in Russia 50
V.N.Grebennik (Kurchatov, Russia)
2.3 High-temperature Reactor Developments in the Netherlands 76
R.Schram (ECN, The Netherlands)
2.4 Status of the GT-MHR 89
W.A.Simon (GA, USA)
2.5 Construction of the HTTR and Its Testing Program 97
T.Tanaka (JAERI, Japan)
3. Session Ⅲ-Safety of HTGR, Development of Fuel and Component, and Operation Experience of HTGR 105
3.1 Safety Studies on Heat Transport and Afterheat Removal for GCR Accident Conditions 107
M.Hishida (JAERI, Japan)
3.2 Safety Experiments for the Demonstration of Fission Product Retention in Fully Irradiated Fuel Elements 119
H.Nabielek (KFA, Germany)
3.3 Research and Development on C/C Composite Control Rod for HTGR 138
M.Eto (JAERI, Japan)

3.4 General Design of the 10MW HTR ····· 149
Z.Qin (INET, China)
3.5 Construction of the HTTR In-core Components ····· 161
T.Miki (Fuji Electric Co., Ltd.)
3.6 Experimental Reactivity Assessment During AVR Defuelling ····· 177
P.Pohl (KFA, Germany)
4. Session Ⅳ-Heat Utilization of HTGR ····· 191
4.1 Design and Evaluation of Heat Utilization Systems for the HTTR through International Cooperation ····· 193
I.Lewkowicz (IAEA)
4.2 Design Procedures of Small Pebble Bed HTGR for Electric Generation in Isolated Islands ····· 213
L.P.Hong (BATAN, Indonesia)
4.3 Recent Test Results of CO_2 Reforming of Methane in a Closed Loop ···· 228
M.Epstein (Weizmann Institute of Science, Israel)
4.4 Design of a steam Reforming System to be Connected to the HTTR ····· 229
K.Hada (JAERI, Japan)
5. Session Ⅴ-Panel Discussion "Future Perspectives of Nuclear Energy Utilization and Expected Role of HTGR" ····· 241
5.1 Future Perspective of Nuclear Energy Utilization and Expected Role of HTGR-JAERI's Energy Systems Analysis Research ····· 243
O.Sato (JAERI, Japan)
6. Poster Session ····· 259
6.1 Preliminary Study on the Use of the Heat Pipe to the Passive Decay Heat Removal System of the Modular HTR ····· 261
K.Ohashi (Fuji Electric Co., Ltd., Japan)
6.2 Safety Considerations and Countermeasures against Fire and Explosion at an HTGR-hydrogen Production System ····· 264
T.Nishihara (JAERI, Japan)
6.3 Analysis of Air Ingress Process during the Primary-pipe Rupture Accident of the HTGR ····· 272
T.Takeda (JAERI, Japan)
6.4 Availability of Steam Generator against Thermal Disturbance of Hydrogen Production System Coupled to HTGR ····· 289
T.Shibata (JAERI, Japan)
6.5 On the Improvement of HTGR Fuel Elements Corrosion Resistance ····· 294
A.Chernikov (Lutch, Russia)

6.6 Design and Fabrication of He-he Intermediate Heat Exchanger for HTTR ····· 305
H.Koikegami (Ishikawajima-Harima Heavy Ind., Japan)

6.7 Design and Fabrication of the Reactor Vessel Cooling System (VCS) in HTTR ····· 322
H.Kodama (Babcock-Hitachi K.K., Japan)

6.8 Evaluation of Long-term Creep Properties of Hastelloy XR in Simulated High-temperature Gas-cooled Reactor Helium ····· 338
Y.Kurata (JAERI, Japan)

6.9 Development of a Ni-Cr-W Superalloy for Application to High-temperature Gas-cooled Reactor Systems ····· 353
- Creep Properties and Weldability -
Y.Kurata (JAERI, Japan)

6.10 Evaluation on Materials Performance of Hastelloy Alloy XR for the High Temperature Engineering Test Reactor Components ····· 368
-Weldability and High Temperature Strength Properties-
K.Watanabe (JAERI, Japan)

6.11 Comparison of Creep Behavior under Varying Load/Temperature Conditions between Hastelloy XR Alloys with Different Boron Content Levels ····· 383
H.Tsuji (JAERI, Japan)

6.12 Operation Experience with In-pile Gas Loop OGL-1 for HTTR Fuels and Materials Irradiation ····· 400
T.Ishii (JAERI, Japan)

6.13 Applicability of Carbonation/Decarbonation Reactions for Storing Thermal Energy from Nuclear Reactors ····· 408
K.Kyaw (University of Nagoya, Myanmar)

6.14 Fundamental Study of Fission Product Behavior in HTGR; Effect of Graphite Environment on Vaporization of $SrUO_3$ and $BaUO_3$ ····· 421
J.Huang (University of Tokyo, China)

6.15 Plant Concept of Heat Utilization of High Temperature Gas-cooled Reactors ····· 429
M.Tonogouchi (Ube Ind., Japan)

6.16 Performance of High Temperature Chemical Heat Pump with Metal Hydride Reaction ····· 435
S.Ishiyama (JAERI, Japan)

6.17 Disposition of Plutonium with HTGRs Using Pu Burner Balls and Th Breeder Balls ····· 450
K.Yamashita (JAERI, Japan)

6.18 Studies on Water Splitting Hydrogen Production 462
K.Onuki (JAERI, Japan)
6.19 Transmutation of Minor Actinides(MA) with Pebble Bed Type HTGRs 475
N.Fujimoto (JAERI, Japan)
6.20 Start-up Physics Test Plan of the HTTR 484
M.Takeuchi (JAERI, Japan)
6.21 Highlights from the IAEA Coordinated Research Programme on Fuel Performance and Fission Product Data 501
H.Nabielek (KFA, Germany)
6.22 Some Topics on Improvement in Production Technology and Fission Product Behavior of HTTR Coated Particle Fuel 516
K.Hayashi (JAERI, Japan)
Closing Address 531
T.Tanaka (JAERI, Japan)

目　　次

参 加 者 …… 1
プログラム …… 5
まえがき …… 10
開会の辞 …… 11
吉川　允二（原研）
1. セッションⅠ：招待講演 …… 13
1.1 地球環境問題と原子力エネルギーの展望 …… 15
小宮山　宏（東京大学教授）
1.2 原子力の安全性と高温ガス炉への期待 …… 21
Kugeler, K.（ドイツユーリッヒ研究所）
2. セッションⅡ：高温ガス炉計画の現状と将来展望 …… 37
2.1 ＨＴＲ－10計画の現状 …… 39
Sun, Y.（中国清華大学核能技術研究所）
2.2 ロシアにおける高温ガス炉計画と熱利用の現状 …… 50
Grebennik, V.N.（ロシアクルチャトフ研究所）
2.3 オランダにおける高温ガス炉開発 …… 76
Schram, R.（オランダＥＣＮ）
2.4 ＧＴ－ＭＨＲの現状 …… 89
Simon, W.A.（米国ゼネラルアトミック社）
2.5 ＨＴＴＲの建設とその試験計画 …… 97
田中　利幸（原研）
3. セッションⅢ：ガス冷却炉の安全性，燃料・機器開発及び運転経験 …… 105
3.1 ガス炉の異常時における熱移送と崩壊熱除去の安全性研究 …… 107
菱田　　誠（原研）
3.2 照射済燃料要素の核分裂生成物閉じ込め実証のための安全性実験 …… 119
Nabielek, H.（ドイツユーリッヒ研究所）
3.3 高温ガス炉用Ｃ／Ｃコンポジット制御棒の研究開発 …… 138
衛藤　基邦（原研）
3.4 ＨＴＲ－10の設計概要 …… 149
Qin, Z.（中国清華大学核能技術研究所）
3.5 ＨＴＴＲ炉心機器の製作 …… 161
三木　俊也（富士電機）
3.6 ＡＶＲ燃料取り出し中の実験的反応度評価 …… 177
Pohl, P.（ドイツユーリッヒ研究所）

4. セッションⅣ：高温ガス炉における熱利用 …… 191
4.1 国際協力を通じたＨＴＴＲ熱利用システムの設計及び評価 …… 193
Lewkowicz, I. （ＩＡＥＡ）
4.2 離島における発電用小型ペブルベット型高温ガス炉の計画 …… 228
Hong, L.P.（インドネシア　バタン）
4.3 閉ループでのメタンのCO_2改質のテスト結果 …… 229
Epstein, M. （イスラエルワイズマン研究所）
4.4 ＨＴＴＲ接続用水蒸気改質システムの設計 …… 241
羽田　一彦（原研）
5. セッションⅤ：パネルディスカッション「各国における原子力利用の将来見通しと高温ガス炉の役割」 …… 243
座長：飛岡　利明（原研）
5.1 基調講演
－原研におけるエネルギーシステムの評価研究－ …… 259
佐藤　　治（原研）
6. ポスターセッション
6.1 ヒートパイプを用いたモジュラ型ＨＴＲの静的な崩壊熱除去の基礎的研究 …… 261
大橋　一孝（富士電機）
6.2 ＨＴＧＲにおける水素製造システムの火災と爆発に対する安全考察と対策 …… 264
西原　哲夫（原研）
6.3 ＨＴＧＲの主配管破断事故時の空気侵入過程の解析 …… 272
武田　哲明（原研）
6.4 ＨＴＧＲに接続した水素製造システムの熱的障害に備えた蒸気発電機の可能性 …… 289
柴田　大受（原研）
6.5 ＨＴＧＲ燃料要素腐食抵抗の改善について …… 294
A. Chernikov. （Lutch, ロシア）
6.6. ＨＴＴＲのＨｅ－Ｈｅ中間熱交換器の設計と製作 …… 305
小池上　一（石川島播磨重工）
6.7 ＨＴＴＲの炉容器冷却設備の設計と製作 …… 322
児玉　　裕（バブコック日立）
6.8 高温ガス炉ヘリウムを模擬したハステロイＸＲの長期クリープ特性の評価 …… 338
倉田　有司（原研）
6.9 高温ガス炉システムに適用するＮｉ－Ｃｒ－Ｗ合金の開発 …… 353
－クリープ特性及び溶接性－
倉田　有司（原研）
6.10 ＨＴＴＲ機器のハステロイＸＲの材料性能の評価 …… 368
－溶接性及び高温強度特性－
渡辺　勝利（原研）

6.11 異ホウ素含有量のハステロイＸＲの荷重／温度状況の変化に伴うクリープ挙動の比較 …… 383
辻　宏和（原研）
6.12 ＨＴＴＲ燃料及び照射材料のためのインパイルガスループ１号（ＯＧＬ－１）の運転経験 …… 400
石井　忠彦（原研）
6.13 原子炉からの熱エネルギー蓄積のための酸化還元反応の適用性 …… 408
Kyaw, K （名古屋大学）
6.14 高温ガス炉における核分裂生成物挙動の基礎的研究；$SrUO_3$と$BaUO_3$の気化における黒鉛環境の影響 …… 421
Huang, J. （東京大学）
6.15 高温ガス炉の熱利用の施設概念 …… 429
殿河内　誠（宇部興産）
6.16 金属水素反応を用いた高温ケミカルヒートポンプの性能 …… 435
石山　新太郎（原研）
6.17 Ｐｕ燃焼球及びＴｈ増殖球を用いた高温ガス炉でのプルトニウム処分 …… 450
山下　清信（原研）
6.18 水分離による水素製造の研究 …… 463
小貫　薫（原研）
6.19 ペブルベットタイプ高温ガス炉でのマイナーアクチノイドの変換 …… 475
藤本　望（原研）
6.20 ＨＴＴＲの出力上昇試験計画 …… 484
竹内　光男（原研）
6.21 燃料性能及び核分裂生成物データにおけるＩＡＥＡ協力研究計画からのハイライト …… 501
Nabielek, H.（ユーリッヒ研究所）
6.22 ＨＴＴＲ被覆燃料粒子の製造技術の改善と核分裂生成物の挙動に関する概要 …… 516
林　君夫（原研）
閉会の辞 …… 531
田中　利幸（原研）

Participant List

Family Name	Given Name	Institute	Country
A			
Akino	Fujiyoshi	JAERI	Japan
Akino	Norio	JAERI	Japan
Amano	Noboru	JAERI	Japan
Amir	Rusli	BATAN	Indonesia
Aoki	T.	Fuji Electric Co., Ltd.	Japan
Arai	T.	JAERI	Japan
B			
Baba	O.	JAERI	Japan
Brey	H.L.	International Atomic Energy Agency	U.S.A
C			
Chen	Shulin	Nuclear Power Institute of China	China
E			
Epstein	Michael	Weizmann Institute of Science	Israel
Eto	M.	JAERI	Japan
F			
Fujimoto	N.	JAERI	Japan
Fujisaki	S.	JAERI	Japan
Fuketa	T.	RIST	Japan
Fukuda	K.	JAERI	Japan
Fukuda	Shigeru	MHI	Japan
Fumizawa	Motoo	JAERI	Japan
Futakawa	Masatoshi	JAERI	Japan
G			
Grebennik	V.N.	Russian Research Center, Kurchatov Institute	Russia
H			
Hada	K.	JAERI	Japan
Haga	Katsuhiro	JAERI	Japan
Hassel	Horst W.	JECTA Consulting Gmbh	Germany
Hayakawa	H.	Fuji Electric Co., Ltd.	Japan
Hayashi	Kimio	JAERI	Japan
Hayashi	Shigeo	Kawasaki Heavy Industries, Ltd.	Japan
Hayashi	T.	JAERI	Japan
Hayashi	Takao	Tokai University	Japan
Hino	Ryutaro	JAERI	Japan
Hirao	S.	Hitachi Ltd.	Japan
Hirata	Mitsuho	Mitsui Engineering & Shipbuilding Co., Ltd.	Japan
Hishida	M.	JAERI	Japan
Hontani	kouji	Babcock-Hitachi K.K.	Japan
Huang	J.	University of Tokyo	China

I			
Ichikawa	M.	JAERI	Japan
Ide	A.	Fuji Electric Co., Ltd.	Japan
Inaba	Y.	JAERI	Japan
Inagaki	Yoshiyuki	JAERI	Japan
Inoue	Toyokazu	Toshiba Co., Ltd.	Japan
Ishihara	Masahiro	JAERI	Japan
Ishii	H.	Fuji Electric Co., Ltd.	Japan
Ishii	Tadahiko	JAERI	Japan
Ishikawa	H.	JAERI	Japan
Ishiyama	S.	JAERI	Japan
Itoh	J.	Fuji Electric Co., Ltd.	Japan
K			
Kambayashi	Y.	JAERI	Japan
Kashimura	S.	JAERI	Japan
Katagiri	Masaki	JAERI	Japan
Kawae	Hidetoshi	Kawasaki Heavy Industries, Ltd.	Japan
Kita	Satoshi	JAERI	Japan
Kitano	Masanori	Mitsubishi Electric Co.	Japan
Kodama	Hiroshi	Babcock-Hitachi K.K.	Japan
Koikegami	Hajime	Ishikawajima-Harima Heavy Industries Co., Ltd.	Japan
Komiyama	H.	University of Tokyo	Japan
Korei	Yoshiaki	Nippon Nuclear Fuel Development Co., Ltd.	Japan
Kotani	T.	Deputy Mayor of Oarai-machi	Japan
Kubota	Hideo	Atoms in Japan	Japan
Kugeler	Kurt	Research Center Jülich GmbH	Germany
Kurata	Y.	JAERI	Japan
Kyaw	Kyaw	Nagoya University	Myanmar
L			
Lewkowicz	Irene	International Atomic Energy Agency	Israel
Li	Jing-he	Beijing Association for Science and Technology Exchanges with Foreign	China
Li	Zhinong	The State Science and Technology Commission of P.R.C	China
Liem	Peng Hong	National Atomic Energy Agency	Indonesia
M			
Matsuda	Hitoki	Nagoya University	Japan
Matsumiya	Masayuki	Mitsubishi Co.	Japan
Matsuura	S.	JAERI	Japan
McEligot	Donald M.	JAERI	U.S.A
Miki	T.	Fuji Electric Co., Ltd.	Japan
Minato	K.	JAERI	Japan
Miyamoto	Yoshiaki	JAERI	Japan
Mogi	H.	JAERI	Japan
Muto	Yasushi	JAERI	Japan

N			
Nabielek	Heinz	Research Center Jülich GmbH	Germany
Nakagawa	Shigeaki	JAERI	Japan
Nakata	Hirokatsu	Ibaraki-ken	Japan
Nishihara	T.	JAERI	Japan
Nomura	Sinichi	Mitsubishi Co.	Japan
O			
Ogawa	M.	JAERI	Japan
Ogawa	Yutaka	Tohoku University	Japan
Ohashi	K.	Fuji Electric Co., Ltd.	Japan
Ohtsuki	Takaichi	Mitsubishi Electric Co.	Japan
Okamoto	Futoshi	Fuji Electric Co., Ltd.	Japan
Onuki	K.	JAERI	Japan
P			
Pohl	P.	Arbeitsgemeinschaft Versuchsreaktor AVR GmbH	Germany
Q			
Qin	Zhenya	Tsinghua University	China
S			
Saigo	Masao	Fuji Electric Co., Ltd.	Japan
Saito	S.	JAERI	Japan
Sakano	Kosuke	Kawasaki Heavy Industries, Ltd.	Japan
Sakama	Iwao	Toshiba Co., Ltd.	Japan
Sakashita	Toshio	Toyo Tanso Co., Ltd.	Japan
Sanokawa	K.	JAERI	Japan
Sasaki	Yasuichi	Yazaki Co., Ltd.	Japan
Sato	Osamu	JAERI	Japan
Sato	S.	JAERI	Japan
Sato	Tadao	National Institute for Research in Inorganic Materials	Japan
Satoh	Keisuke	Kawasaki Heavy Industries, Ltd.	Japan
Sawa	K.	JAERI	Japan
Schram	R.P.C	Netherlands Energy Research Foundation ECN	The Netherlands
Serizawa	H.	JAERI	Japan
Shi	Guobao	Shanghai Nuclear Engineering Research and Design Institute, China	P.R.China
Shibata	Taiju	JAERI	Japan
Shiina	Y.	JAERI	Japan
Shimizu	Saburo	JAERI	Japan
Shimomura	Hiroaki	JAERI	Japan
Shiozawa	S.	JAERI	Japan
Shiratori	Tetsuo	JAERI	Japan
Simon	W.A.	General Atomics	U.S.A
Singh	Jasbir	KFA	Germany
Sudo	Yukio	JAERI	Japan
Sun	Yuliang	Tsinghua University	China
Suzuki	Y.	JAERI	Japan

T			
Takeda	A.	Japan Atomic Power Co., Ltd.	Japan
Takeda	Takeshi	JAERI	Japan
Takeda	Tetsuaki	JAERI	Japan
Takenaka	Yutaka	Kawasaki Heavy Industries, Ltd.	Japan
Takenoshita	Masataka	Babcock-Hitachi K.K.	Japan
Taketani	Kiyoaki	Nuclear System Research Association	Japan
Takeuti	M.	JAERI	Japan
Takitani	Koichi	Kawasaki Heavy Industries, Ltd.	Japan
Tanaka	Toshiyuki	JAERI	Japan
Tchernikov	Albert	Scientific Industrial Association "Lutch	Russia
Tobioka	T.	JAERI	Japan
Tokushita	Yoshitaka	Electric Power Development Co., Ltd.	Japan
Tonogouchi	Makoto	Ube Industries, Ltd.	Japan
Tsuchie	Y.	Japan Atomic Power Co., Ltd.	Japan
Tsuji	Hirokazu	JAERI	Japan
W			
Wada	T.	STA	Japan
Wakayama	Naoaki	Nippon Advanced Technology Co., Ltd.	Japan
Watanabe	K.	JAERI	Japan
Watanabe	T.	Fuji Electric Co., Ltd.	Japan
Y			
Yamada	M.	Fuji Electric Co., Ltd.	Japan
Yamagishi	Hideshi	JAERI	Japan
Yamashita	K.	JAERI	Japan
Yamawaki	K.	NASDA	Japan
Yamawaki	M.	University of Tokyo	Japan
Yasuno	T.	Fuji Electric Co., Ltd.	Japan
Yoshikawa	M.	JAERI	Japan
Yoshimuta	Shigeharu	Nuclear Fuel Industries,	Japan
Z			
Zhao	B.	PNC	China

Program of the Symposium

Thursday, February 15

9:30- 9:40 **Opening Address** Room Shakko — M. Yoshikawa (President, JAERI, Japan)

9:40-11:30 **Session Ⅰ−Invited Lectures** Room Shakko

Chairpersons: T. Tanaka (JAERI, Japan) & H. Nabielek (KFA, Germany)

9:40-10:25	Ⅰ-1	Global Environmental Problems and Perspective of Nuclear Energy	H. Komiyama (Univ. of Tokyo, Japan)
10:25-11:10	Ⅰ-2	Nuclear Safety and the Expectation to HTGR's Deployment	K. Kugeler (KFA, Germany)

11:10-16:45 **Poster Session** Room Kohrin

11:30-13:00 Lunch

13:00-15:05 **Session Ⅱ−Present Status of HTGR Projects and Perspectives of HTGR Deployment** Room Shakko

Chairpersons: L. Brey (IAEA) & Y. Miyamoto (JAERI, Japan)

13:00-13:25	Ⅱ-1	Present Status of the HTR-10 Project	Y. Sun (INET, China)
13:25-13:50	Ⅱ-2	Present Status of HTGR Projects and their Heat Applications in Russia	V. N. Grebennik (Kurchatov, Russia)
13:50-14:15	Ⅱ-3	High-Temperature Reactor Developments in the Netherlands	R. Schram (ECN, Netherlands)
14:15-14:40	Ⅱ-4	Status of the GT-MHR	W. A. Simon (GA, USA)

14:40-15:05 Ⅱ-5 Construction of the HTTR and its Testing Program — T. Tanaka (JAERI, Japan)

15:05-15:20 Coffee break

15:20-18:20 **Session Ⅲ −Safety of HTGR, Development of Fuel and Component, and Operation Experience of HTGR** Room Shakko

Chairpersons: V.N.Grebennik (Kurchatov, Russia) & O. Baba (JAERI, Japan)

15:20-15:50 Ⅲ-1 Safety Studies on Heat Transport and Afterheat Removal for GCR Accident Conditions — M. Hishida (JAERI, Japan)

15:50-16:20 Ⅲ-2 Safety Experiments for the Demonstration of Fission Product Retention in Fully Irradiated Fuel Elements — H. Nabielek (KFA, Germany)

16:20-16:50 Ⅲ-3 Research and Development on C/C Composite Control Rod for HTGR — M. Eto (JAERI, Japan)

16:50-17:20 Ⅲ-4 General Design of the 10MW HTR — Z. Qin (INET, China)

17:20-17:50 Ⅲ-5 Construction of the HTTR In-Core Components — T. Miki (Fuji Electric Co.,Ltd., Japan)

17:50-18:20 Ⅲ-6 Experimental Reactivity Assessment During AVR Defuelling — P. Pohl (KFA, Germany)

18:45-20:15 **Reception** Room Kohrin

Friday, February 16

9:30-11:30 **HTTR Site Tour** JAERI-Oarai

11:30-13:00 Lunch

13:00-15:00 **Session Ⅳ−Heat Utilization of HTGR** Room Shakko

Chairpersons: Y. Sudo (JAERI, Japan) & Y. Sun (INET, China)

13:00-13:30	Ⅳ-1	Design and Evaluation of Heat Utilization Systems for the HTTR through International Cooperation	I. Lewkowicz (IAEA)
13:30-14:00	Ⅳ-2	Design Procedures of Small Pebble Bed HTGR for Electric Generation in Isolated Islands	L. P. Hong (BATAN, Indonesia)
14:00-14:45	Ⅳ-3	Recent Test Results of CO_2 Reforming of Methane in a Closed Loop	M. Epstein (Weizmann Institute of Science, Israel)
14:45-15:15	Ⅳ-4	Design of a Steam Reforming System to be Connected to the HTTR	K. Hada (JAERI, Japan)

15:15-15:25 Coffee Break

15:25-17:20 **Session Ⅴ−Panel Discussion "Future Perspectives of Nuclear Energy Utilization and Expected Role of HTGR"** Room Shakko

Chairpersons: K. Kugeler (KFA, Germany) & T. Tobioka (JAERI, Japan)

15:25-15:55 **Keynote speech on**

"Future Perspective of Nuclear Energy Utilization and Expected Role of HTGR - JAERI's Energy Systems Analysis Research - " O. Sato (JAERI, Japan)

15:55-16:55 **Contribution of Participants**

Y. Sun	(INET, China)
R. Schram	(ECN, Netherlands)
V. N. Grebennik	(Kurchatov, Russia)
K. Kugeler	(KFA, Germany)
A. Rusli	(BATAN, Indonesia)
S. Shiozawa	(JAERI, Japan)

16:55-17:20 **Discussion**

17:20-17:30 **Closing Address** Room Shakko K. Sanokawa (JAERI, Japan)

Poster Session Room Kohrin

P-01 Preliminary Study on the Use of the Heat Pipe to the Passive Decay Heat Removal System of the Modular HTR — K.Ohashi (Fuji Electric Co.,Ltd., Japan)

P-02 Safety Considerations and Countermeasures against Fire and Explosion at an HTGR-Hydrogen Production System — T.Nishihara (JAERI, Japan)

P-03 Analysis of Air Ingress Process during the Primary-Pipe Rupture Accident of the HTGR — T.Takeda (JAERI, Japan)

P-04 Availability of Steam Generator against Thermal Disturbance of Hydrogen Production System Coupled to HTGR — T.Shibata (JAERI, Japan)

P-05 On the Improvement of HTGR Fuel Elements Corrosion Resistance — A.Chernikov (Lutch, Russia)

P-06 Design and Fabrication of He-He Intermediate Heat Exchanger for HTTR — H.Koikegami (Ishikawajima-Harima Heavy Ind., Japan)

P-07 Design and Fabrication of the Reactor Vessel Cooling System(VCS) in HTTR — H.Kodama (Babcock-Hitachi K.K., Japan)

P-08 Evaluation of Long-Term Creep Properties of Hastelloy XR in Simulated High-Temperature Gas-Cooled Reactor Helium — Y.Kurata (JAERI, Japan)

P-09 Development of a Ni-Cr-W Superalloy for Application to High-Temperature Gas-Cooled Reactor Systems
- Creep Properties and Weldability - — Y.Kurata (JAERI, Japan)

P-10 Evaluation on Materials Performance of Hastelloy Alloy XR for the High Temperature Engineering Test Reactor Components
- Weldability and High Temperature Strength Properties - — K.Watanabe (JAERI, Japan)

P-11 Comparison of Creep Behavior under Varying Load/Temperature Conditions between Hastelloy XR Alloys with Different Boron Content Levels — H.Tsuji (JAERI, Japan)

P-12 Operation Experience with In-pile Gas Loop OGL-1 for HTTR Fuels and Materials Irradiation — T.Ishii (JAERI, Japan)

P-13 Applicability of Carbonation/Decarbonation Reactions for Storing Thermal Energy from Nuclear Reactors — K.Kyaw (University of Nagoya, Myanmar)

P-14 Fundamental Study of Fission Product Behavior in HTGR; Effect of Graphite Environment on Vaporization of $SrUO_3$ and $BaUO_3$ — J.Huang (University of Tokyo, China)

P-15 Plant Concept of Heat Utilization of High Temperature Gas-Cooled Reactors — M.Tonogouchi (Ube Ind., Japan)

P-16 Performance of High Temperature Chemical Heat Pump with Metal Hydride Reaction — S.Ishiyama (JAERI,Japan)

P-17 Disposition of Plutonium with HTGRs using Pu Burner Balls and Th Breeder Balls — K.Yamashita (JAERI, Japan)

P-18 Studies on Water Splitting Hydrogen Production — K.Onuki (JAERI, Japan)

P-19 Transmutation of Minor Actinides(MA) with Pebble Bed Type HTGRs — N.Fujimoto (JAERI, Japan)

P-20 Start-up Physics Test Plan of the HTTR — M.Takeuchi (JAERI, Japan)

P-21 Highlights from the IAEA Coordinated Research Programme on Fuel Performance and Fission Product Data — H.Nabielek (KFA, Germany)

P-22 Some Topics on Improvement in Production Technology and Fission Product Behavior of HTTR Coated Particle Fuel — K.Hayashi (JAERI, Japan)

Foreword

The 3rd JAERI Symposium on HTGR Technologies was held by Japan Atomic Energy Research Institute (JAERI) from February 15 to 16, 1996 at Oarai, Ibaraki-ken, Japan.

In the Symposium, the worldwide present status of HTGR Projects and the future perspective of HTGR development, safety, operation experience, fuel and heat utilization technology were reviewed and discussed with 17 papers including 2 invited lectures by Prof. H. KOMIYAMA, Tokyo university and Prof. K. Kugeler, Director of KFA in Germany.

The Symposium was attended by 115 participants from official circles, universities, national institutes and manufacturing industries, and 24 overseas participants from China, Germany, the United States of America, Indonesia, Russia, The Netherlands, Israel, Myanmar and the International Atomic Energy Agency (IAEA).

In the first day, the Symposium was opened by Dr. H. Yoshikawa, President, JAERI. Session Ⅰ, Invited lecture, was provided with 2 papers and Session Ⅱ, entitled "Present Status of HTGR Projects and Perspective of HTGR Deployment" was provided with 5 papers from China, Russia, the Netherlands, the United States of America and Japan, and Session Ⅲ, entitled "Safety of HTGR, Development of Fuel and Component, and Operation Experience of HTGR", was provided with 6 papers from Japan, Germany and China. Poster Session was provided with 22 papers.

In the second day, the technical tour organized by 18 overseas participants and 12 inland participants to the High Temperature engineering Test Reactor (HTTR) site at Oarai Research Establishment, JAERI, were conducted in the morning. In the afternoon, Session Ⅳ, entitled "Heat Utilization of HTGR" was provided with 4 papers from IAEA, Indonesia, Israel and Japan and Session Ⅴ, Panel Discussion entitled "Future Perspectives of Nuclear Energy Utilization and Expected Role of HTGR" was provided by keynote speech, and panelists from Germany, China, The Netherlands, Russia, Indonesia and Japan remarked on its idea.

It is regretful that we could not express our profound acknowledgments individually to all persons who contributed so much to the Symposium, we highly appreciate kind suggestions, cooperations and assistances given by the participants and the persons concerned directly and indirectly forwarded to the great success in the Symposium which was never expected at the preparation stage of the Symposium.

We look forward to seeing successful development of HTGR nationally and internationally after next three years when we are planning to hold subsequent symposium Japan.

Toshiyuki TANAKA
Chairman, Executive Committee

The 3rd JAERI Symposium on HTGR Technologies

OPENING ADDRESS

Masaji YOSHIKAWA
President, JAERI

Good morning, Distinguished guests, ladies and gentlemen.

I am Masaji YOSHIKAWA, the President of the Japan Atomic Energy Research Institute, JAERI.

I sincerely appreciate your participation to the Symposium.

This Symposium is organized, following the 2nd Symposium held in Oarai in October 1992and is held, at the same place, here at Oarai, where the JAERI is proceeding with the construction of a high temperature gas-cooled reactor.

Now, the JAERI has, of course, been enthusiastically conducting researches and developments of nuclear energy. To speak concretely, there are safety research aiming at upgrading the safety and confidence of nuclear facilities and their environment, and high temperaturegas-cooled reactors as well as nuclear fusion research aiming at the realization of new energy sources. Moreover, the JAERI is proceeding with leading projects on the radiation utilization, construction of Spring-8 facilities and the computer science. At the same time, basic researches and fundamental technology development are also being carried out in various areas. Neutron science and advanced photon researches have newly been introduced.

Particularly, as you will be well aware, the high temperature gas-cooled reactor will be expected to make significant contributions to the diversity of energy sources, stable energy supply together with the preservation of global environmental problems.

Since 1969, the JAERI has carried out research and development works on high temperature gas-cooled reactors. In 1989, the High Temperature engineering Test Reactor, HTTR, was determined to be constructed in the Oarai Research Establishment, integrating the results accumulated so far. At present, fabrication work is going on satisfactorily aiming at the first criticality scheduled in 1997.

Talking about the study on high-temperature nuclear heat application, I am glad to announce that the HTTR Hydrogen Production System Project and feasibility study of the Gas Turbine System by HTGR will be initiated this year.

It is my great honour to be able to hold this Symposium so prosperously with such a lot of specialists and concerned persons from all over the world and I would like to express my greatest appreciation to your ceaseless and warm support to us.

In this Symposium, we have two invited lectures by special guests, Prof. Hiroshi

KOMIYAMA, Tokyo University, who has contributed how to solve Global Warming and Dr. Kurt KUGELER, Director of KFA in Germany, who has proposed a catastrophe−free reactor concept of the HTGR.

In general and poster sessions, 13 papers from foreign countries and 22 papers from Japan are planned to be presented, focusing on the present status of HTGR Projects in each country and safety, fuel, operating experiences, nuclear heat utilization and so on. A panel discussion chaired by Dr. Kurt KUGELER and Dr. Toshiaki TOBIOKA, Director General of Oarai Research Establishment, with 6 distinguished specialists from home and abroad is also planned on "Future Perspectives of Nuclear Energy Utilization and Expected Role of HTGR", which is now a worldwide subject.

I heartily would like to ask all of you vigorous discussions among you to make the Symposium fruitful.

In concluding my address, I sincerely hope that, with your kind cooperation, the Symposium becomes significant to the development of HTGRs not only for Japan but also for each country, through a fruitful information exchange in these two days. I believe that the Symposium shall be doing a lot for the international cooperation through this information exchange, and, consequently, a contribution to the world welfare would be expedited.

Thank you very much for your kind attention.

1. Session I

-Invited Lecture-

1.1 Global environmental problems and perspective of nuclear energy

University of Tokyo
Hiroshi KOMIYAMA

1 What is the global environmental problems?

1-1 Categorization of global environmental problems

global warming, acid rain, ozone layer depletion, desertification, decrease of species diversity, decrease of tropical rain forest, oceanic contamination

1-2 Why now?

Essential reasons of the occurrence of the global environmental problems include,
5.6 gigapersons and 6 gigatons of fossil fuel combustion
finite capacity of environment, finite resources of energy
% order increase of the atmospheric CO2 a year
Fig.1 shows abrupt increase of world population and atmospheric CO2

1-3 Is the global warming caused by the increase of atmospheric CO2 an illusion?

π R2J=4 π R2 σ T4 yields T=278K.(Fig.2)
Green house effect is 33K for the time being.
It is a matter of energy and materials balance, not a matter of taste.
Global warming will certainly proceed, as far as the atmospheric CO2 will continue to increase.

2 How can human beings respond to the CO2 problem?

energy saving
CO2 fixation
non-fossil energy source(solar,nuclear or geothermal)

2-1 Is the effect of energy saving trivial?

Fig.3 shows that 4.2% of the annual economic growth really occurred in Japan at a constant rate of energy consumption during the decade starting from 1973.

2-2 What is the real fixation of CO2 in the CO2 issue and what can we do ?

Fixation of atmospheric nitorgen means chemical reactions of N2 to yield chemical substances which are soluble in water, since plants can absorb them. The meaning of fixation depends on the purpose of the fixation. The purpose of fixation of CO2 is to mitigate the increase of the atmospheric CO2 concentration. The neccessary conditions of a measure for satisfying this porpose include:

1) it increases the carbon content in the ocean or on the land (Fig.4 tells that do not drink!)
2) the quantity of the carbon increase is compatible with the total emission of anthropogenic CO2 which amounts to 6 gigatons per year
3) duration of the carbon sequestered is long enough
4) carbon emission to do the process is much less than the carbon emission avoided

Bioprocesses for the fixation of CO2 as biomass is not the fixation in the present definition, if the biomass is assumed to be burned as energy source. Production of an antibiotic from CO2 is not the fixation in the definition, since the quntity is too small. Production of CocaCola is not, since the deration period is too short. Greening of a desert seems to be a good measure to fix CO2 in the present definition. But, the greening of a desert which is being conducted in the Gulf countries fails to satisfy the fourth condition. A study was carried out to calculate the carbon budget of the greening by assuming the most energy-efficient desalination of sea water and the most energy-efficint watering by trickling at the plant roots. The conclusion was that CO2 emitted from the desalination process is larger than the CO2 captured by the plant which grows by the water.

Fig.5 shows the Gulf nations forrestation.

Another important feature as a countermeasure to mitigate atmospheric CO2 increase is non-regret. Even if the capture and sequestering of CO2 from stuck gases is technologically feasible, it consumes energy source by the reduced net power generation. It is,therefore, categorized as a regret measure. Iron-fertilization of some part of the ocean, though it seems atractive, has not been proved to be effective.

We have to admit that there are no means of CO2 fixation which satisfy the four neccessary conditions as well as the non-regret policy. In the light of the consideration of the present state of the art, a study is now being conducted to investigate the possibility of the climate modification of a desert by a large scale of forestation. Forestataion of a desert needs watering. If the water fed to the forest precipitates around the forestation region, the forest is self-sustainable or requires less watering.

Yes, we can modify the climate by a large scale forestation!

The simulation of the climate north Perce in the western Australia was carried out by constructing a computer model. It was assumed that the forestation changes the boundary conditions on the surface including humidity, roughness, and albedo. Size of the area afforested, location, arrangement of the forest area and the uncovered area were changed. Calculation was carried out at least for a day. Precipitation increased by the change of the surface coverage. The ratio of the precipitation to the evaporation from the forest was used as a indicatior of the efficiency. It amounted to 50 to 70 %, if the forested area is greater than 200kmx200km. With decreasing size of the forested area, the ratio decreased.

Figs.6 and 7 show that precipitation increases around the forrested region.

2-3 Non-fossil energy resources

Renewables include wind, biomass, hydrauric, photovoltaic, all solar in their origin, and geothermal.

Solar energy

Abundant. Ten thousand times the present energy consumption by human beings!

High quantum mechanical quality. Even water can be splitted!

Low density. Maximum instantaneous power of a solar photovoltaic car is only 2 hp!!!

Energy payback time of the photovoltaic system

3 years for pannel and another 3 years for a large-scale power station.

Solar will not wait. It has started from a roof-mounted system, then will go to desert solar stations and [moon factory (Fig.8)]

2000yen per watt (1995), 1500yen per watt (1996)----------250yen per watt (2005)

3 Conclusion

Can we rely on the CO2 fixation and/or the photovoltaic systems? No, for the moment.

SOLAR or NUCLEAR, what is the energy source in the future? It has to run at least from the latter half of the 21st century.

SOLAR should be more efficient. NUCLEAR should be more open and safe.

RECOMMENDATION!

Read now a book entitled Answer to Global Warming Problem, published by the Tokyo University Press(Tel 03-3812-2111),「地球温暖化問題に答える、東京大学出版会, 1995」in Japanese. Even foreigners can imagine from cartoons and figures.

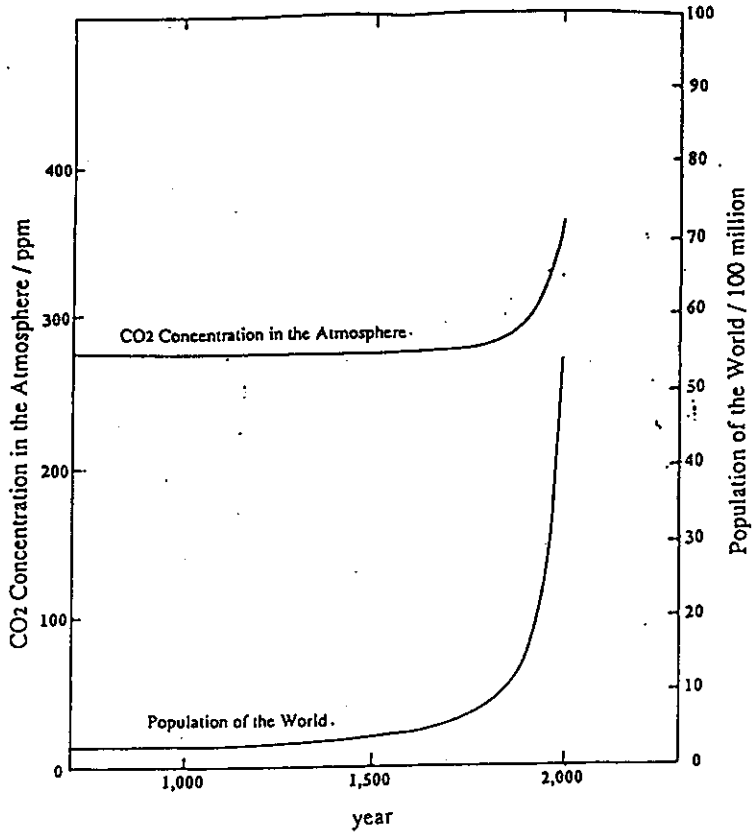


Fig. 1 Population and CO2 has increased abruptly

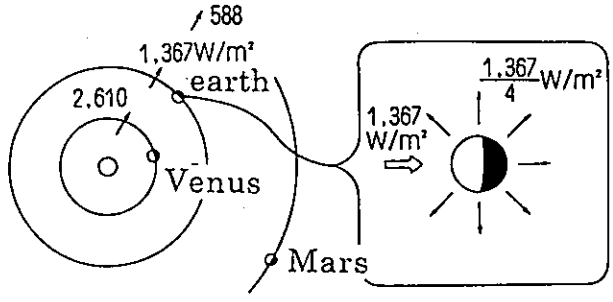


Fig. 2 How is the temperature governed?

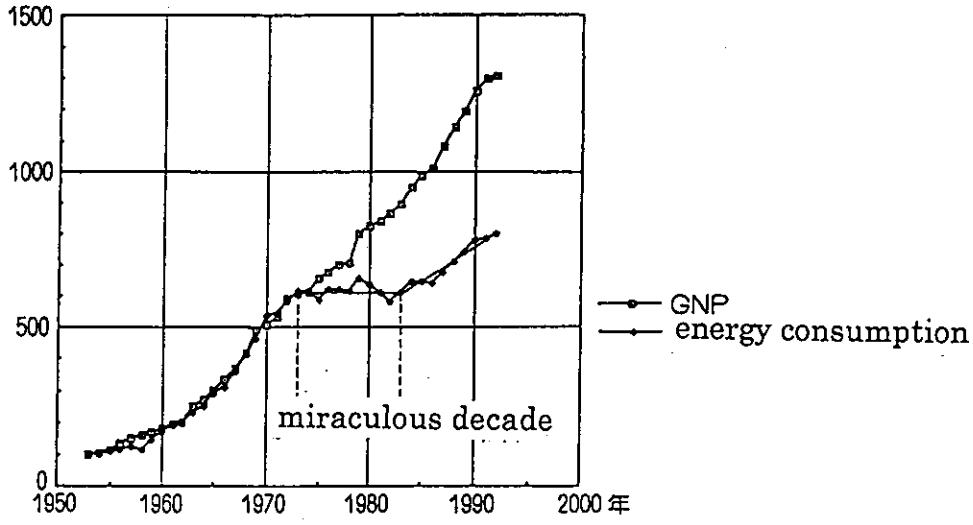


Fig. 3 miraculous decade

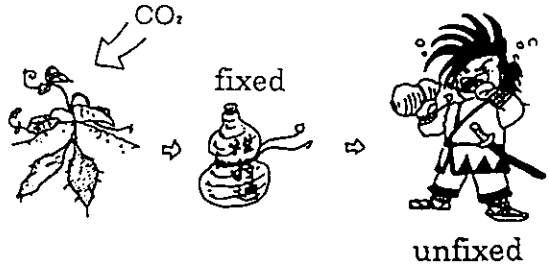


Fig. 4 Don't drink it

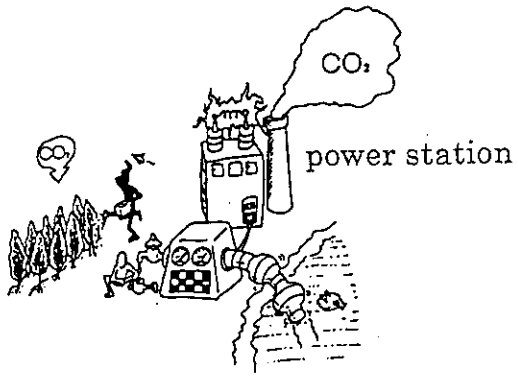


Fig. 5 Afforestation on gulf nations makes CO_2 balance minus

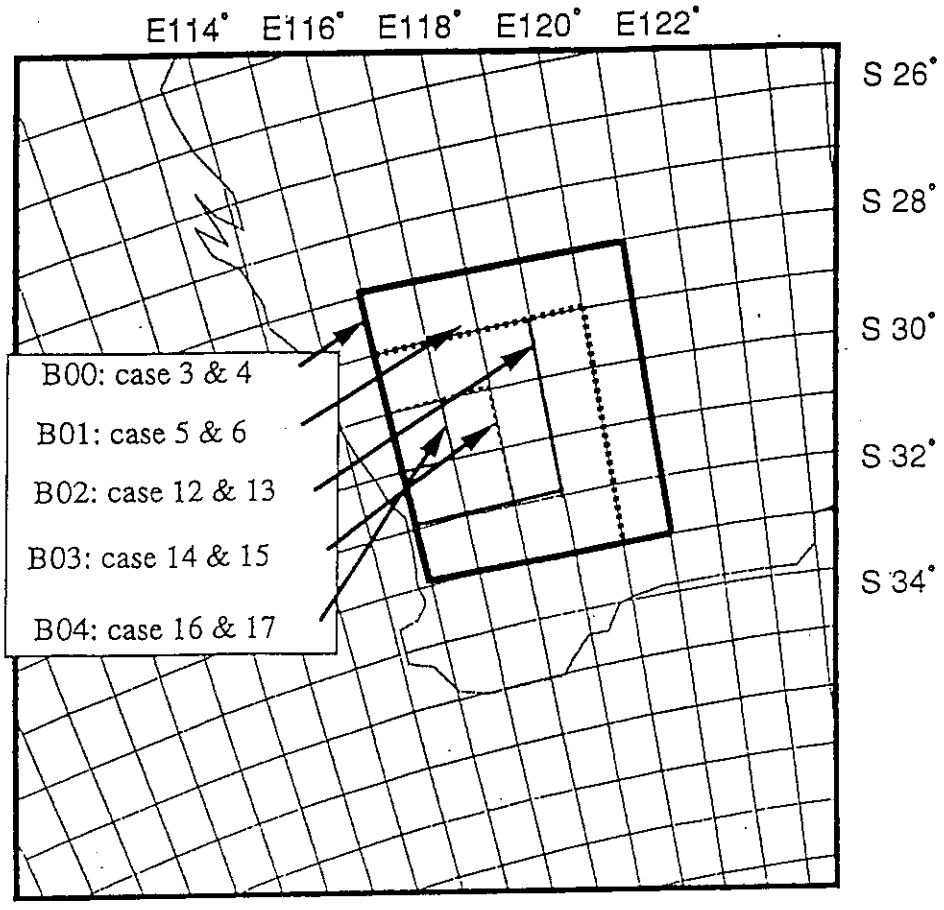


Fig. 6 large scale forestation in Australia

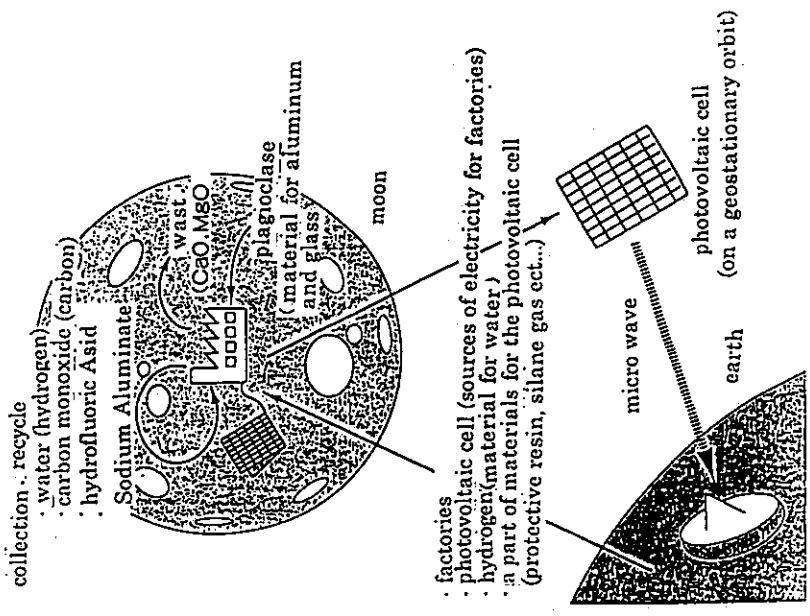


Fig. 8 moon factory

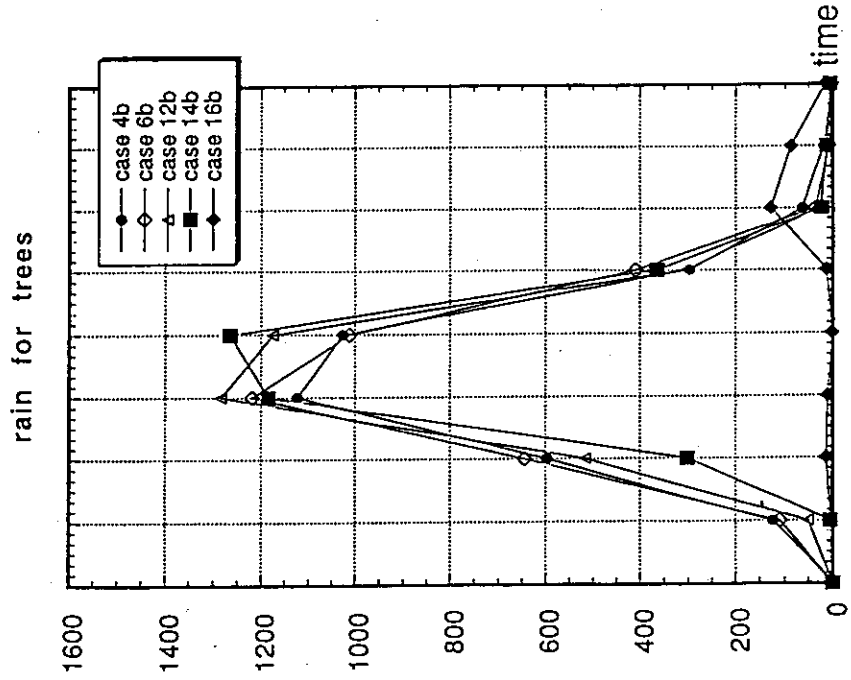


Fig. 7 Precipitation will increase

Prof. Dr.-Ing. Kurt Kugeler
Institute for Safety Research and Reactor Technology
Reseach Center Jülich

1.2 Nuclear Safety and the Expectation to HTGR's Deployment"

Because of world-wide rise in energy consumption use of nuclear energy will be very important in the future in the market of electricity and heat.

Nuclear energy needs a very high standard of safety for future application. In the modified new German atomic act, future nuclear technology without radiological consequences outside the nuclear plant in case of accidents is required. This must be valid for all accidents caused by internal or by foreseeable external reasons.

The high temperature reactor has the capability to fulfil this requirement and it is possible to show this behaviour in a 1/1-scale experiment and in the nuclear reactor itself.

The preconditions for this safety behaviour is that the reactor core never can melt, that the fuel elements can never be destroyed by nuclear transients, by corrosion or by mechanical impacts.

The fuel elements and the core must fulfil the fundamental principles of nuclear, thermal, chemical and mechanical stability.

Especially coated particle fuel, suited core design, corrosion resistant fuel elements and prestressed burst protected reactor vessels are preconditions to this safety behaviour even in extreme accident situations.

The totally ceramic fuel elements and specific technologies for the fuel element containers allow a similar safety standard for the final storage. Fuel cycles with a minimal production of actinides can be used in the HTGR, too.

Finally there is the opportunity to realize an HTGR-system, which fulfills the requirement to be a catastrophe-free system in the total chain of nuclear technology, i.e. in the reactor, in the intermediate and in the final storage.

Nuclear Safety and the Expectation to HTGR's Deployment

KUGELER, Kurt
Research Centre Jülich GmbH , Institute for Safety and Reactor Technology, Postfach 1913, D-52425 Jülich, Germany

1. Future Significance of Nuclear Energy

Global energy requirements will greatly increase within the next few decades, in particular due to the additional demand in developing and threshold countries. According to present estimates, an energy amount of about 20 billion tce/a (tons coal equivalent per year) will have to be made available after 2020. If the climatologists' demands are not met, roughly 80 % of this energy will then still be covered by fossil resources.

According to the today predictions, the capacity of nuclear energy utilization would have to be doubled worldwide by the year 2020 in comparison to the present situation. If, on the other hand, the climatologists' warnings are taken seriously, a reduction of global anthropogenic CO_2 emissions to roughly 10 billion t CO_2/year must be achieved by the year 2020. This means that only about 4 billion tce/year may then be covered by fossil resources so that 80 % of the world energy supply would have to come from non-fossil energy sources. Intensive efforts at saving energy in the developed countries are required and will be feasible to a certain extent, but they do not fundamentally change the picture outlined here.

If it is necessary in the next century to restrict the fossil energy supply to the mentioned 10 billion tCO_2/year, a greatly increased use of nuclear energy will be indispensable worldwide in addition to expanding the supply of renewable energies. From the supply aspect, it is conceivable that the present nuclear capacity will then be expanded to several 1000 GW_{el} worldwide.

2. Safety Requirements for Future Nuclear Power Plants

A worldwide expansion of nuclear energy, requires a continuous and remarkable enhancement of safety standards. This has been the case in the past already, when considerable progress has indeed been made in reactor safety. However, there is a number of older plants worldwide which do not correspond to present conceptions concerning engineered nuclear safety. Decisions on upgrading these plants or even shutting them down are urgently required whereas new plants must fulfil higher safety requirements.

The German Government has come to this obvious conclusion. Recently, it has amended the German Atomic Energy Act [1] according to which no undue amounts of radioactive substances may be released into the environment from future nuclear plants after extreme accidents, including core meltdown (Fig.1). In a simplified but distinct formulation, this implies the demand for "catastrophe-free nuclear technology" [2]. Catastrophe-free nuclear technology is achieved if the radioactive substances remain practically completely contained inside the reactor plant in all possible cases of accidents. Consequently, no appreciable radiological consequences will result for the environment, i.e. no immediate fatalities, no late fatalities, no evacuation and relocation.. This very far-reaching demand must be fulfilled for all cases of accidents resulting from inner causes and for all events caused by predictable outer impacts. Extreme cases of accidents due to

unpredictable outer causes, which even go beyond the above two scenarios (e.g. sabotage, war, extreme earthquakes) will require specific additional measures (Fig. 2).

The principle of catastrophe-free nuclear technology, as defined above, is already applied today e.g. for the dry interim storage of spent fuel elements and the dry interim storage of vitrified final disposal packages in cast iron containers. The relocation problem, which again and again burdens the discussion on nuclear energy especially from the acceptance perspective, is illustrated referring to the fraction of released ^{137}Cs, Fig. 3.

Whereas the current probabilistic principle still involves the possibility of a large-area contamination, although with low probability, catastrophe-free nuclear energy permits only very small amounts of radioactivity to be released from the plant (for example a fraction of 10^{-5} of the ^{137}Cs inventory). This requirement must be fulfilled with no need to specify any probability as usual.

Modified German Atomic Act

Amendent of the Atomic Energy Act as a further precaution against risks to the general public (7th Amendment to the Atomic Energy Act of 27.07.1994): The amended German Atomic Energy Act (1) (Art. 7, para. 2a) for future plants stipulates "that even such events whose occurence is practically excluded by the precautions to be taken against damage would not necessitate decisive measures for protection against the damaging effects of ionizing radiation outside the plant fencing,...". In the substantiation of the bill for parliamentary discussion, terms from the text of paragraph (2a) are defined in more detail. It is thus postulated that "accidents with core melt" are controlled and "evacuations" are not necessary.

Consequences:

- no evacuations necessary
- no relocations necessary

Requirements:

- Future nuclear energy uses (including waste disposal) must avoid serious radiological impacts outside the plant.
- Evidence (as integral as possible) must be provided for the safety behaviour of reactors.

Fig. 1: Modified German atomic act and consequences

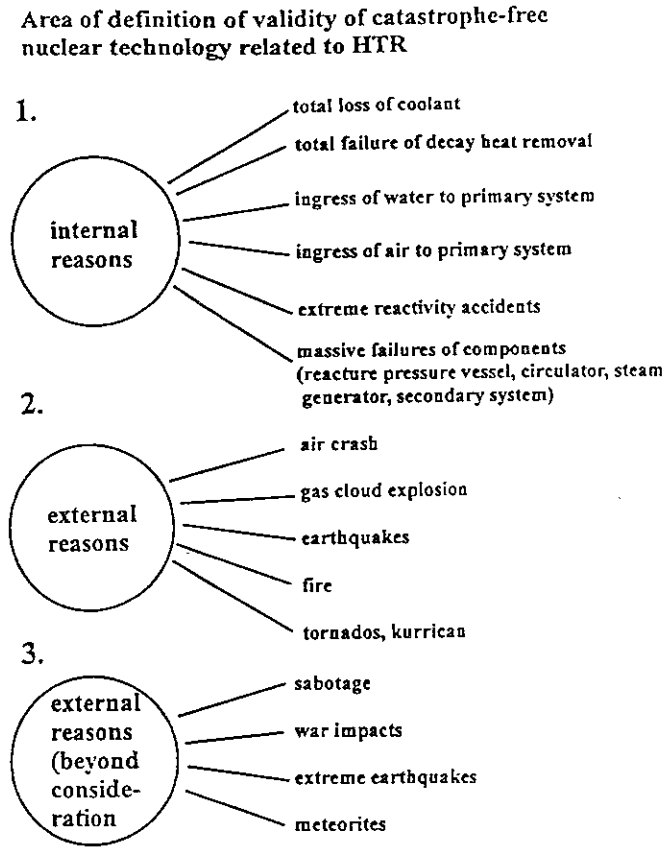


Fig. 2: Requirements of the safety of future reactors (e.g. HTR)

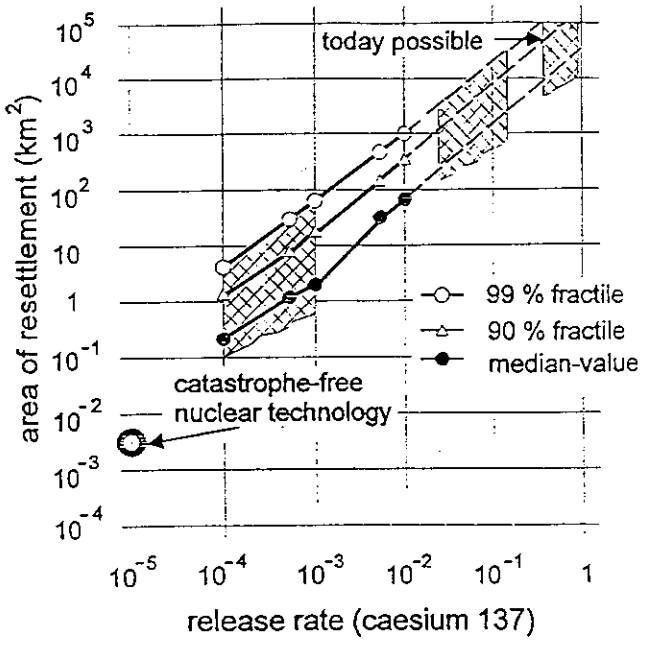


Fig. 3: **Genesis of the term "catastrophe-free nuclear energy".**
Resettlement area dependent on the release of radionuclids from a pressurized-water-reactor (Cesium- contamination as the determining parameter) and aims to be achieved by the "catastrophe-free nuclear energy (curve after [3]).

3. Innovative Reactors

Various efforts are under way worldwide aiming to develop reactors with a new quality of safety standards. The following objectives can be differentiated, Fig. 4:

a) Improvements on the basis of the light-water reactors currently established worldwide, in which core melting is still possible. The probability of a core melt is further reduced by introducing additional active or passive cooling devices. In the sense of catastrophe-free nuclear technology, this improvement is not yet sufficient.

b) Further developments of the light-water reactor concept comprise systems with which a core melt is to be controlled, once it has occurred. Core catchers are to accommodate the melt and enable long-time core cooling [4, 5]. The reactor containment must be designed to cope with all conceivable consequences of a core melt accident. Fission product retention in the reactor containment must be adequately ensured for long periods of time. The release of fission products to the environment must be very small.

c) A retention of the core melt with the aid of a core catcher is also conceivable inside the reactor pressure vessel. Radioactive substances are then partially retained and cooled in the reactor pressure vessel and ultimately in the reactor containment.

d) An appropriate design and dimensioning of the fuel elements, of the reactor core and the entire primary system physically excludes reactor core melting after loss of coolant and failure of all active cooling systems. Radioactive substances are then retained in the fuel elements. It must be ensured that fuel element integrity is not impaired by neutron physical, thermal, chemical or mechanical impacts [6].

The capability of future reactors to retain radioactive fission products and fuel inside the reactor plant even after extreme accidents can be most convincingly demonstrated by means of integral large-scale experiments.

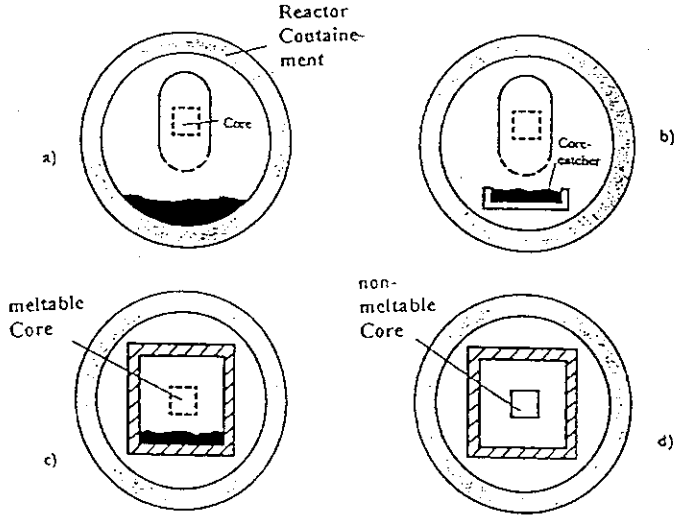


Fig.4: Objectives pursued in a worldwide development of innovative reactors
a) Improvements to current light-water reactors
b) Further development of light-water reactors (external core catcher)
c) Further development of light water cooled reactors (internal core catcher)
d) Reactors without core melting and without fuel element destruction

4. High Temperature Reactors and their Safety Behaviour

The high-temperature reactor represents a nuclear engineering solution which excludes melting of the reactor core and thus inadmissible fission product releases from the fuel elements . Fig. 5 shows the concept of this type of plant with the following specific features: coated fuel particles embedded in spherical graphite fuel elements will retain practically completely the fission products during accidents up to a fuel temperature of 1600°C These characteristics have been confirmed by detailed experiments with this type of fuel element [9] . The fuel elements are corrosion-resistant to air and water vapour due to silicon carbide coatings (100 to 200 μm thickness) which are under development. The core is built into a burstproof prestressed reactor pressure vessel.

In recent years, a modular high-temperature reactor of 200 MWth capacity was developed by Siemens [7, 8, 10], largely in agreement with the above mentioned safety principles. This concept aims at excluding catastrophic vessel failure by the use of a basically safe reactor pressure vessel. For future worldwide application, however, burstproof prestressed reactor pressure vessels should be more suitable also from the aspect of manufacturing and transport. In Fig. 5 such a reactor pressure vessel is shown, prestressing is achieved by a lot of axial and radial tendons. The material of the vessel is cast steel. Tight-weldings are outside between the blocks and rings, which are used to build up the vessel.

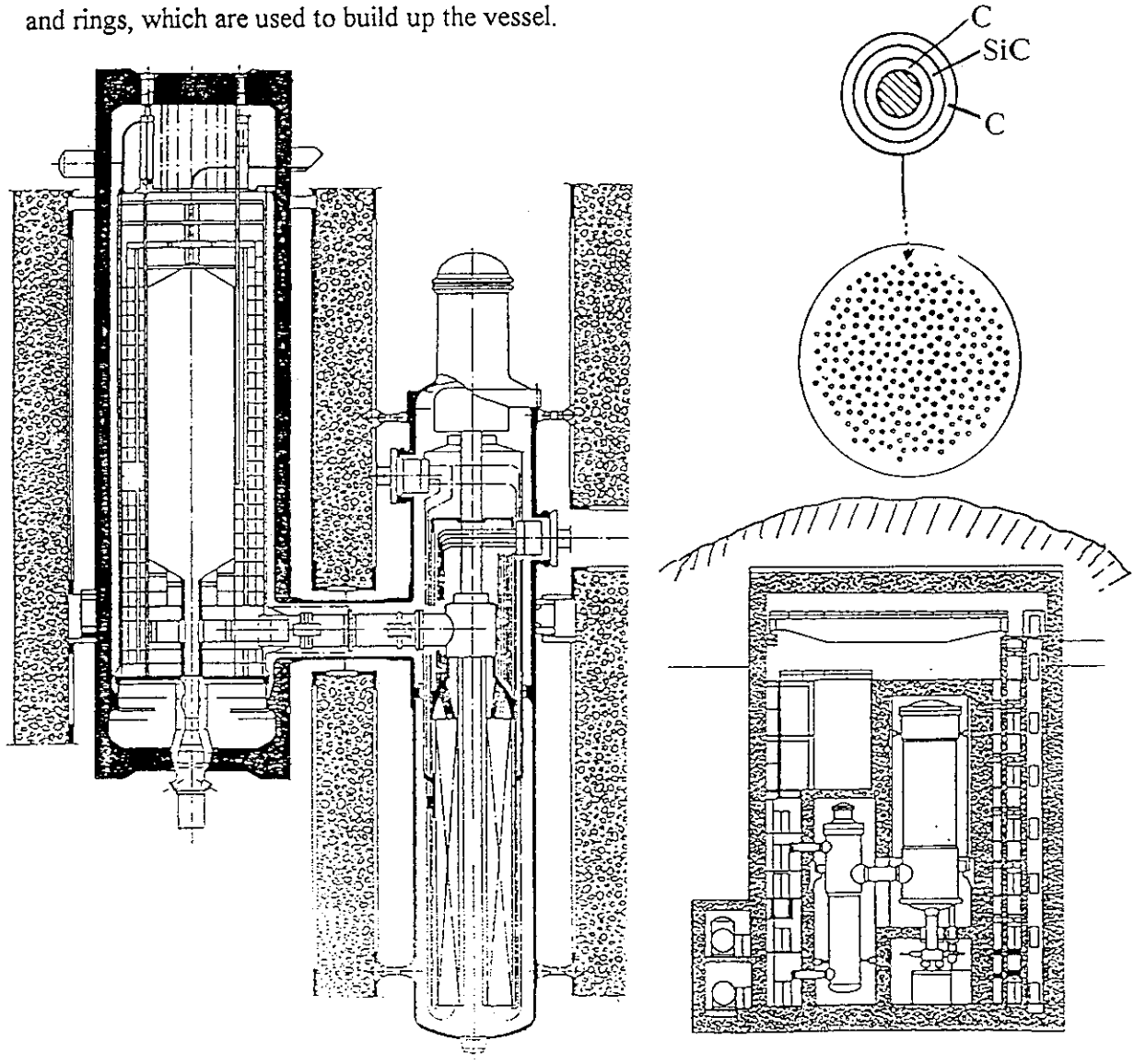


Fig. 5: High Temperature Reactor (pebble bed, 200 MWth) as an example of a non-melting System

Decay heat removal from the reactor system after loss of coolant accident and failure of all active decay heat removal systems takes place in a self-acting way solely by heat conduction, thermal radiation and natural convection. The decay heat is finally removed to the environment in a self-acting manner through the reactor, containment internals and containment wall. Fig. 6 shows the time dependent temperatures for an accident in such a system for a thermal power of 200 MWth of the reactor system. In this case the fuel temperatures stays below 1600°C. Only very few fuel elements get this temperature for a short time (Fig. 6).

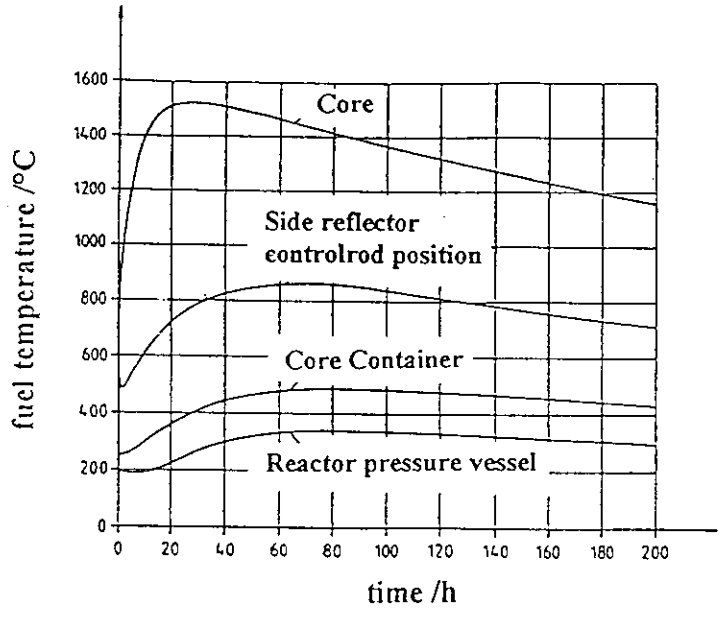


Fig. 6: Temperature variations in the core of a high-temperature pebble-bed reactor after loss of coolant and failure of all active cooling systems [10]

The experience from the HTR development programme is that the integral release fractions of radioactive fission products are below 10^{-5} of the core inventory if the fuel temperature is kept below 1600°C [9].

The predictions that the above mentioned limitation of maximal fuel temperature and the concept of the self-acting decay heat removal are fulfilled are as follows:

- Effective heat transport in the core and reactor system by heat conduction, thermal radiation and natural convection.
- Large permanent external heat sink outside the reactor pressure vessel.
- Temperature-resistant core due to the use of ceramic materials.
- Retention of radioactive substances in the fuel elements up to high temperatures.
- Maintaining admissible fuel temperatures for all conceivable accidents and accident combinations.
- Protection of the fuel elements against inadmissible power transients.
- Protection of the fuel elements against inadmissible corrosion.

Naturally a sufficient low power density in the core, short transport path of heat in the core and high effective heat conductivity in the pebble bed are necessary conditions of the system behaviour.

If all these conditions are fulfilled, the system is named "thermal stable". Today it is well-known that this principle of self-acting decay heat removal can be used in pebble bed HTR upto 500 MWth using an annular core geometry. The principe already has been tested in the AVR reactor (50 MWth) in a real nuclear system.

Analyses have so far not revealed any reactivity transients which could lead to inadmissible temperature increases in the fuel elements. This behaviour is basically attributable to constantly negative feedback coefficients (e.g. temperature coefficients) and to the lack of appreciable excess reactivities in the core. This is a consequence of the continuous loading scheme of the pebble bed reactor. Fig. 7 shows calculations in which a sudden withdrawal of the first shutdown system from the module reactor core was assumed to occur whithin a short time (reactivity change $\Delta k/k = 1.2$ % in 10 s, 1 s, 0.1 s). No inadmissibly high fuel temperatures result even under these extreme conditions [12]. The reason is again the high heat capacity in the core. Furthermore it is very important, that the fuel particles are embedded in graphite. This causes, that the temperature of the particles rises up fast enough to enable the negative temperature coefficient to stabilize the nucelar reactor and that the heat produced in the transient can be transfered and stored inside the graphite matrix.

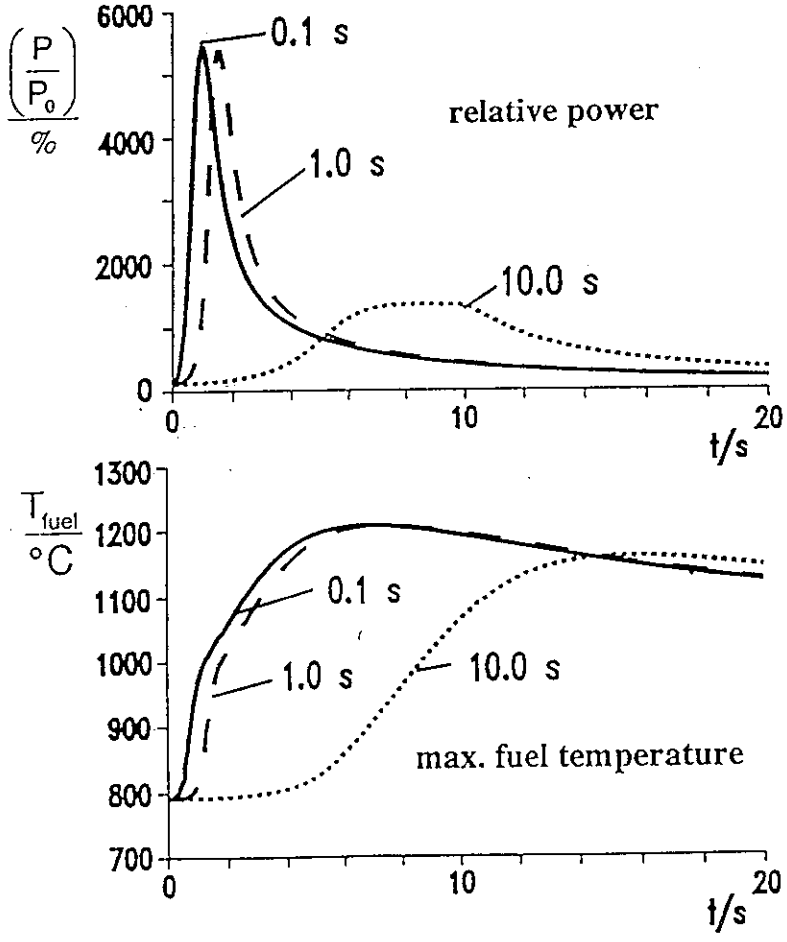


Fig. 7: Withdrawal of the first shutdown system in the 200 MWth modular reactor (Δ k/k = 1.2 % in 10 s, 1s, 0.1 s)

The main conditions of a system, which behaves "nuclear stable, as, shown above, are as follows:

- There must always be a negative feedback coefficient of reactivity (e.g. temperature coefficient, void coefficient).
- Reactivity perturbations must be so small that they can be compensated through the negative feedback coefficients maintaining admissible values.
- There must not be any inadmissible power transients caused by changes in the core structures due to an infringement of the principle of mechanical stability.
- There must not be any inadmissible power transients caused by changes in the core structures due to an infringement of the principle of chemical stability.
- Sufficiently high and rapid heat storage in the fuel and in the fuel element must be ensured.
- High temperature stability must be ensured for the fuel and structural material in the core.

Corrosion resistant graphite fuel elements, which are coated with a thin (100...200 μm) SiC-layer, have been tested in air upto 1400 °C for more than 200 hours without loss of mass by corrosion. This enables a design which is "chemical stable".
The following topics are important:

- Use of fuel elements protected against corrosion, which are e.g. corrosion-resistant to water vapour and air even in the case of extreme corrosive media ingress.
- Fuel elements remain at a high temperature level for a short time only, a few fuel elements only reach high temperature ranges at all.
- Fuel particles are additionally protected by silicon carbide coatings applied to each individual particle.
- Fuel particles do not become hotter than 1600°C.
- Use of a burstproof primary circuit containment (excluding rupture) prevents a rapid ingress of very large amounts of foreign media into the core.

The arrangement of the reactor core in a burst-protected vessel guarantees that the dimensions and composition of thecore never can be changed. This feature of "mechanical stability" includes the following:

- Use of a burstproof reactor pressure vessel (excluding rupture) prestressed by a large number of axial and radial cables. There are only compressive stresses in the vessel wall so that cracks cannot grow. At overpressure, the vessel blows the primary circuit medium off through joints; bursting never occurs, even after a failure of pressure limiting devices.
- No fuel element destruction in the case of a depressurization accident.
- No ejection of shutdown elements from the core is possible.
- No core deformations and thus no reactivity increases are possible.

In an overview, Fig. 8 shows all the explained principles of stability.

A reactor system which is nuclear, thermal, mechanical and chemical stable never will release catastrophic amounts of fission products, if the coated particle fuel fulfills the condition of retention to the above mentioned temperature (1600 °C).

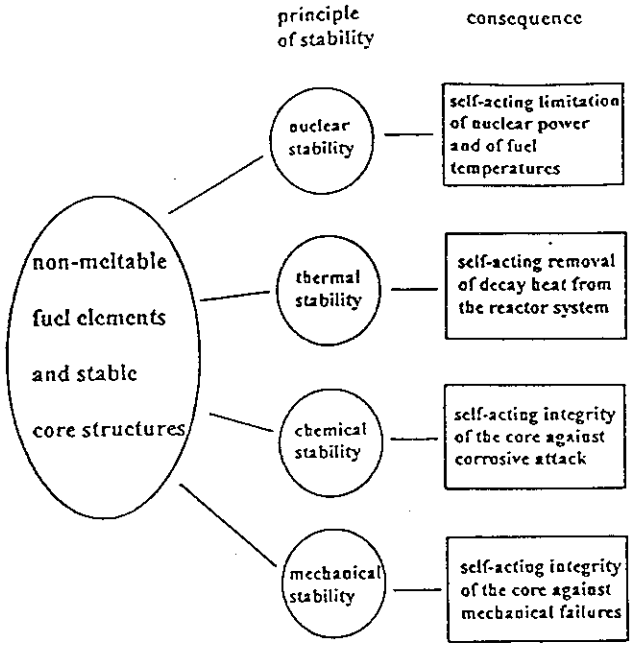


Fig. 8: Correlations between requirements and consequences for indestructible core-melt-proof fuel elements and core structures

As a consequence of these features the high temperature reactor will be able to fulfil the requirements of the German Atomic Act for future nuclear power plants. Fig. 9 shows in a compilation the results of the analysis for the main accidents:

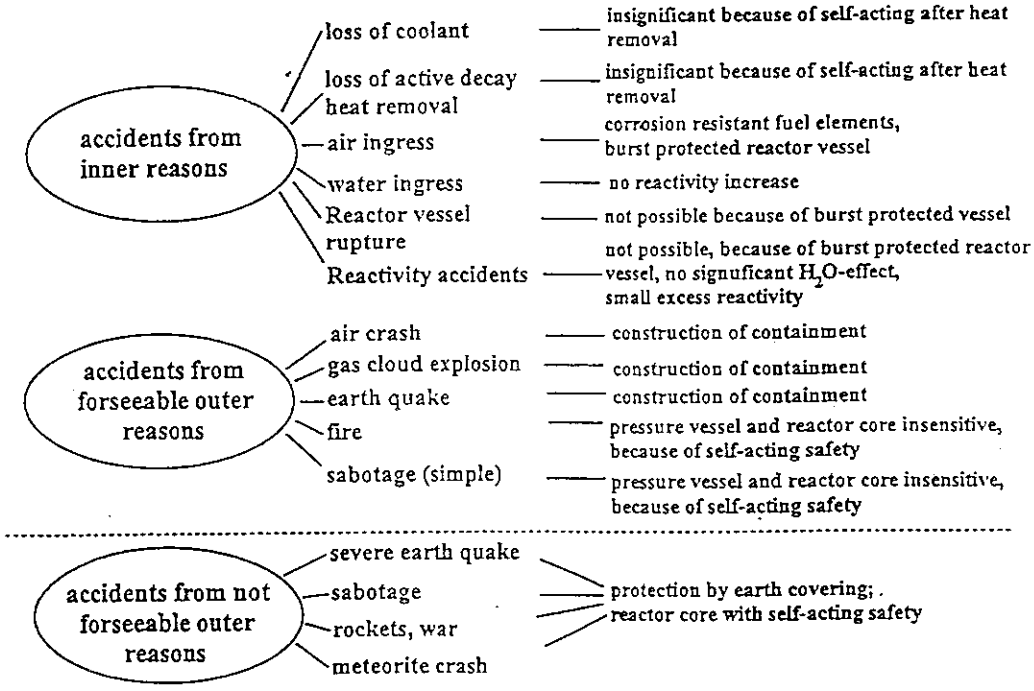


Fig. 9: Compilation of accidents due to inner and predictable outer causes, and evaluation for an HTR design according to the criteria of nuclear, thermal, chemical, and mechanical Stability

Accidents due to inner reasons are normally analysed with respect to a total loss of coolant, failure of all active afterheat removal systems, extreme air ingress, extreme water ingress, catastrophic failure of vessel and extreme reactivity events. As shown on the right in Fig. 9, these effects are insignificant if the principle of self-acting afterheat removal is applied and corrosion-resistant fuel elements and burstproof reactor pressure vessels are used. Accidents due to predictable outer impacts (aircraft crash, gas cloud explosion, earthquake, fire and simple cases of sabotage) are also controlled by an adequately designed reactor core and the before mentioned principles and by an appropriately designed reactor containment. The reactor pressure vessel and core are insensitive since the self-acting safety principles are applied. Finally, coverage with large volumes of earth or underground construction of the plant would help in most cases. This is facilitated by the fact that the core safety functions are generally independent of any active systems whose functioning is necessary.

On the whole, there are reasonable prospects that catastrophe-free nuclear technology can be demonstrated for the HTR. Since core melting and thus a release of appreciable amounts of fission products can never occur, it may be expected that all safety features can be verified in integral large-scale experiments at reasonable expenditure and within predictable periods of time.

5. Application of High Temperature Reactors

Three main applications are characteristic for the HTR: electricity production, cogeneration, production of high temperature process heat.

In case of electricity production efficiencies of 40...43 % are possible using steam turbines; gas turbines processes allow efficiencies of 45 to 48 %; a very attractive solution for the future will be combined gas turbine steam turbine processes (see Fig. 10) which can be operated with 48 to 50% efficiency. The reactor inlet temperature is 250 °C which corresponds to today's technology. The direct coupling of reactor and gas turbine depends on the quality of the fuel elements.

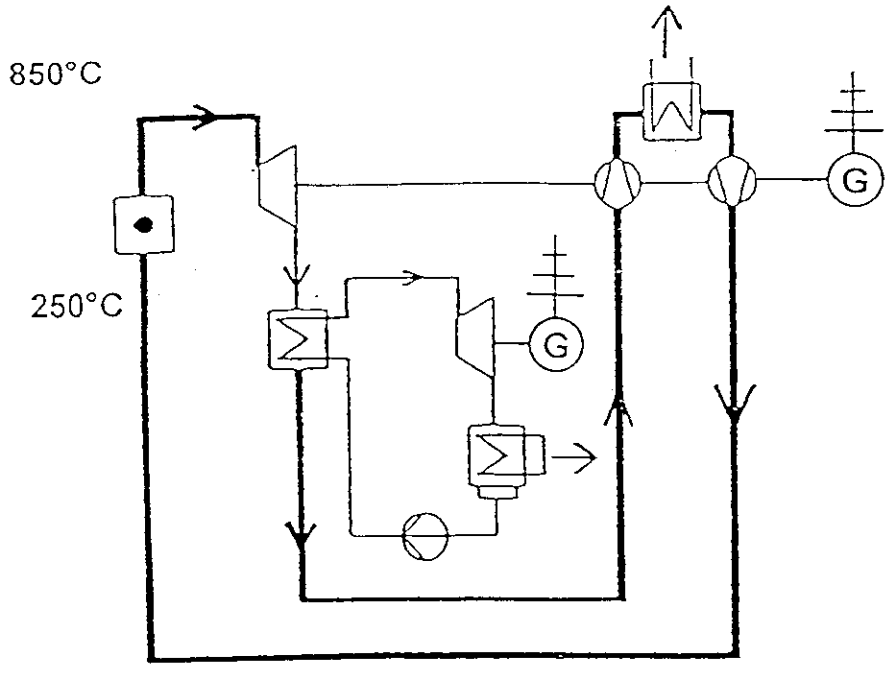


Fig. 10: HTR combined to gas turbine - steam -turbine cycle

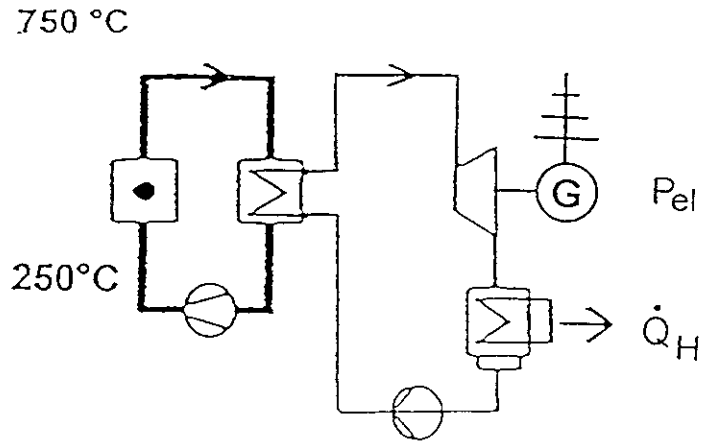


Fig. 11: HTR application in cogeneration plants

Especially plants with small power are very well suited for the cogeneration processes. Fig. 11 shows a back pressure turbine process, which results in a total efficiency of energy use of 80 to 90 %. Naturally gas turbine or combined processes can deliver process heat, too. Cogeneration is very important in sea water desalination, district heat, process heat production for refineries, enhanced oil recovery and the chemical industry. In these applications oil and natural gas can be substituted.

As it is well known and already tested in non-nuclear plants, process heat from helium cycles at temperatures of 950 °C can be used for the chemical processes of steam reforming of methane or hydrocarbons, of coal gasification and all the different processes connected to these fundamental procceses. By all these processes the process energy, in most cases nearly 40 % of the fossile energy, can be substituted by nuclear process heat. The application of nuclear process heat from the HTR in the energy economy can help very much to reduce the CO_2-emission worldwide in the future.

6. Final disposal of spent fuel elements of HTR

The final disposal of spent fuel elements of the HTR must also comply with the high demands of catastrophe-free nuclear technology. The problem of direct final disposal presents itself as follows for the HTR, Fig. 12. The spent fuel elements are stored in a cast steel container. This container is emplaced in a salt dome or possibly also in granite formations covered by cap rock. Consequently, five barriers are available for fission product retention: the coated fuel particles with their three protective layers (C/SiC/C), the fuel element provided with an outer SiC coating, the thickwalled steel container, the salt dome or granite formation, and the cap rock.

Of advantage is longterm intermediate storage above ground (e.g. 100 years) during which the activity and decay heat of the fuel elements already decreases to very low levels. The spent HTR fuel elements can then be classified as intermediate-level waste [13, 14, 15].

An extreme accident in a salt dome repository is usually considered to involve the permanent unimpeded ingress of water into the emplacement zone of repository packages. It has been found that particles and SiC-coated fuel elements are leachresistant in brine. This is a known property of ceramics. The surrounding steel container would even be resistant to brine for a period of approximately 1000 years and thus withstand the mechanical outer loads and the

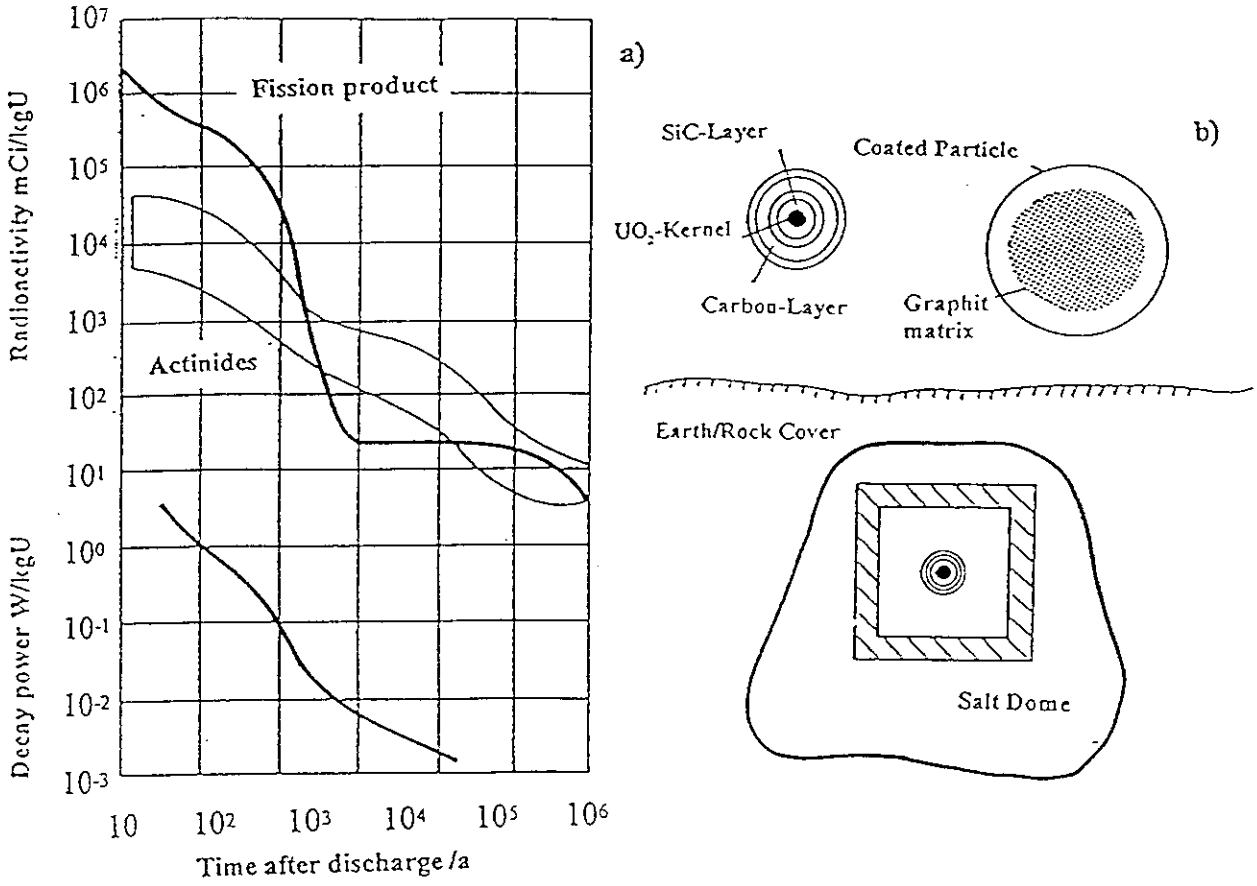


Fig12: Final disposal of spent high-temperature reactor fuel elements;
a) radioactivity and decay heat of spent fuel elements
b) barrier concept in HTR fuel element disposal

corrosive attack of brine. If fuel element leaching in brine after massive water ingress then had to be considered in the following actinide phase, the advantageous properties of ceramics would come into play. Actinides are practically not leached from the fuel elements. Calculations have shown that the additional radiological load due to actinides could increase the natural radioactivity by a few percent at the most unfavourable point of impact after about 10^4 years. These values are within the normal variation width of natural radiation exposure. This type of release from a repository certainly does not have to be regarded as a catastrophe.

The amount of building up plutonium inside the burnt fuel elements can be minimized by using thorium as a resonance absorber in the fuel . Expecially plutonium from weapon technology can be burnt very efficient togheter wiht thorium in HTR fuel cycles.

Finally, it should be noted that long-lived radioactive substances could also be destroyed by transmutation processes, spallation, in the future. This could make the problem of radioactive waste storage a comparatively shortterm task. A subcritical accelerator-driven transmutation facility can be used for the conversion of transuranic wastes and long-lived fission products. Since the annihilation of transuranic wastes always proceeds through nuclear fission, a considerable amount of electrical energy can be produced in addition.

7. Investment Costs of HTR Plants

There are three main aspects to be considered in connection with investment costs of future nuclear power plants:

- A proven safety concept (catastrophe-free nuclear technology) allows the fabrication of cheap components, especially in the conventional parts of the plant (steam cycle) the rules of conventional engineering can be valid.
- Modular design of larger power allows reduction of costs of auxiliary systems, buildings and infrastructure. Engineering expenses are reduced, too.
- Series production of primary components allows reduction of specific cost numbers.

Related to German conditions (1990 number) a 2 x 200 MWth modular plant was estimated to cost twice time compared to a pressurized water reactor with 3800 MWth power (convoi-type). It was estimated by the responsible company that for a plant consisting of 8 modular reactors (200 MWth) the investment cost are in the same order as large LWR-plants if series production becomes valid. The real problem is to get a reference plant and to reach the status of series production. In any case for future applications it can be stated, that high temperature reactors will have similar or even better cost structure compared to today nuclear technology.
Therefore in a first step in applications in cogeneration plants or in processes substituting oil and gas, these reactors will have good chances in the future.

8. Conclusions

In view of the energy resources, for environmental reasons and due to climatological problems, nuclear energy must and can in future furnish a much higher contribution to the long-term world energy supply than at present. Research and development efforts in the field of nuclear technology will have to provide convincing evidence of the safety features of innovative reactors in the next few years and to develop the required new components. Once this evidence has been provided, nuclear engineering solutions will be available featuring the new quality of safety standards required for catastrophe-free operation, the HTR is a convincing candidate to reach this goal. It will be possible to meet practically all requirements of the electricity and heat market. The acceptance problem can and must be redefined. In the long run, nuclear energy is not only necessary for the world energy supply, but also justifiable from a safety-engineering point of view.

9. Literature

[1] Deutscher Bundestag, 12. Wahlperiode, Sachgebiet 750, Gesetzentwurf der Bundesregierung, C. Kernnenergie, Einzelbegründung zu Artikel 5 (Siebentes Gesetz zur Änderung des Atomgesetzes) Zu Nummer 1 (§ 7 Abs. 2a) Drucksache 12/6908, 25.02.1994

[2] K. Kugeler: Hat Kernenergie Zukunft? - Neue Sicherheitsanforderungen und neue Lösungen, Monographien des Forschungszentrums Jülich, Band 8/1993

[3] G. Keßler, F. Daude, J. Ehrhard: Sicherheitskonzept gegenwärtiger Druckwasserreaktoren, KfK Nachrichten 25 (1993) Heft 1, S. 20-28

[4] H. Hennies, G. Keßler J. Eibl: Sicherheitskonzept zukünftiger Druckwasserreaktoren, KfK Nachrichten 25 (1993) Heft 1, S. 29-41

[5] B. Kuczera: Innovative Trends in der Leichtwasserreaktor-Technik, KfK-Nachrichten 25 (1993) Heft 4, S. 219-249
[6] K. Kugeler, R. Schulten: Überlegungen zu den sicherheitstechnischen Prinzipien der Kerntechnik, Forschungszentrum Jülich, Jül-2720, Januar 1993
[7] G.H. Lohnert: Technical Design Features and Essential Safety Related Properties of the HTR-Module, Nuclear Engineering and Design 121 (1990) p. 259-275
[8] N.N.: The HTR-Module, Interatom GmbH, Bensberg, 1986
[9] W. Schenk, D. Pitzer, H. Nabielek: Fission Product Release Profiles from Spherical HTR-Fuel Elements at Accident Temperatures, Kernforschungsanlage Jülich, Jül-2234, September 1988
[10] Hochtemperaturreaktors-Modul-Kraftwerksanlage, Sicherheitsbericht, Bd. 1-3, Siemens/Interatom, Bensberg, November 1988
[11] Hochtemperaturreaktor-Modul-Kraftwerksanlage, Kurzbeschreibung, Siemens/Interatom, Bensberg, November 1988
[12] W. Scherer et al: Zur selbsttätig sicheren Begrenzung von nuklearer Leistung und Brennstofftemperatur in innovativen Kernreaktoren, Forschungszentrum Jülich, Jül-2960, August 1994
[13] H. Brücher, H.U. Brinkmann: Direkte Endlagerung von HTR-Brennelementen, atomwirtschaft, 36 (1991) S. 88-93
[14] B.-G. Brodda, E. Merz: Leachability of actinides and fission products from spent HTR fuel, Radiochemica acta 44/45, (1988) pp. 3-6
[15] H. Brücher et al: Auf dem Weg zur direkten Endlagerung von HTR-Brennelementen

2. Session Ⅱ

－Present Status of HTGR Projects and Perspectives of HTGR Deployment－

To be presented at the 3rd JAERI Symposium on HTGR Technologies, Feb. 15-16, 1996, JAERI, Japan

2.1 Present Status of the HTR-10 Project

Yuliang Sun Yuanhui Xu

Institute of Nuclear Energy Technology
Tsinghua University, Beijing, China

Abstract:

China has selected high temperature gas-cooled reactor (HTGR) to be developed as an advanced reactor type to prepare for more intensified utilization of nuclear power in the next century. As the first important step, a 10MW pebble bed HTGR test reactor (termed HTR-10) will be erected within this century.

The project of the construction of HTR-10 was approved in 1992. After that, a number of important proportion work items have been carried out. Design criteria have been established. Siting and Seismic Report, Environmental Impact Report were reviewed and approved. Basic design was reviewed and approved in November 1994. Preliminary Safety Analysis Report was reviewed by the national nuclear safety authority and the construction permit for HTR-10 was issued at the end of 1994. Since then detailed design has been intensively performed. Contracts for the fabrication of large time-consuming components like pressure vessels have been signed.

The construction of the HTR-10 reactor was formally started in 1995 with the first concrete of the reactor building fundament being poured on June 14. of that year. The construction work has been since then continuously underway.

Present Status of the HTR-10 Project

Yuliang SUN Daxin ZHONG Yuanhui XU Zongxin WU

Institute of Nuclear Energy Technology

Tsinghua University, Beijing, China

Abstract

China is experiencing a period of rapid economic development. Energy supply is one of the key issues of the national economic development. Great importance has been attached to nuclear energy implementation within the overall primary energy mix. Construction of a number of water cooled reactors has been planned for electricity generation. As part of the national nuclear policy, China is developing advanced reactor types to prepare for the more intensified utilization of nuclear energy in the future. High temperature gas-cooled reactor (HTGR) is one of them to be developed.

Within the HTGR development programme, a high temperature gas-cooled test reactor with a thermal power rating of 10MW (termed HTR-10) is now being designed and constructed. The design of the HTR-10 represents the advanced features of the modular HTGR. The conceptual design of the HTR-10 was completed under cooperation between China and Germany. Basic design and its safety review by the national nuclear safety authority were completed so that the construction permit of the HTR-10 was issued at the end of 1994. Construction of the HTR-10 formally started in June 1995. Detailed design, building construction, component procurement, research and development are now intensively underway in parallel. The majority of the key components will be manufactured domestically in China. The HTR-10 test reactor is scheduled to be erected before the year 2000.

1. The HTR-10 Project

1.1 Project background

The rapid economic development in China at present and in the future demands correspondingly rapid increases in energy supply. Coal plays the dominant role in China's energy

supply systems, which causes great problems in terms of transport burden and environmental pollution. To ease the overall problem of energy supply shortage and the problems caused by coal burning, China has decided to make much use of nuclear energy. Besides the erection of nuclear power plants with water cooled reactors, the national nuclear policy also includes the development of advanced nuclear reactor types to prepare for more intensified utilization of nuclear energy in the next century.

The high temperature gas-cooled reactor (HTGR) is the only reactor type which can offer a coolant temperature over 700°C. This feature has two benefits: it makes power generation very efficient; and it can supply process heat for a variety of industrial applications. In the last decades, the development of HTGR technology has focused on modular reactor designs. These designs are characterized by favourable safety features, particularly in the area of inherent safety. China recognizes the advantages of the modular HTGR and has decided to develop this technology. In the energy supply systems of the next century, the HTGR will have two roles, namely to supplement water-cooled reactors for electricity generation and to provide an environmentally friendly heat source, providing process heat at different temperatures for various industrial applications.

As the first important step of the modular HTGR development, a 10 MW helium cooled test reactor (termed as HTR-10) shall be built. It is projected within the framework of China's High Technology Programme. The test reactor will be erected on the site of the Institute of Nuclear Energy Technology (INET) in a northwest suburb of Beijing.

In China, research and development work on HTGR technology started in the 1970s. Before the HTR-10 project was finally approved in 1992, R&D activities had focused on fuel fabrication, helium technology, design methodology, concept design and application potential studies.

1.2 Project objectives

The HTR-10 project is to be carried out in two phases. In the first phase, the reactor will be operated with a coolant outlet temperature of 700°C. It will be coupled with a steam generator providing steam for a steam turbine cycle which works on an electricity / heat co-generation basis. The process flow diagram of the first phase is given in Fig. 1. In the second phase, it is planned to raise the reactor coolant outlet temperature to 900°C. A gas turbine cycle, with an intermediate heat

exchanger (IHX) in between, will be coupled to the reactor in addition to the steam turbine cycle. The process flow diagram of the second phase is given in Fig. 2. Experimental studies on high temperature process heat application, e.g., coal gasification, are also planned to be performed using the nuclear heat of HTR-10. Construction of HTR-10 is scheduled to be completed before the end of the century. When the HTR-10 has been erected, it will enable the following aims to be met:

- Acquiring know-how in the design, construction and operation of HTGRs.
- Establishing an irradiation and experimental facility.
- Demonstrating the inherent safety features of modular HTGR.
- Testing electricity / heat co-generation and closed gas turbine technology.
- Carrying out R&D work on high temperature process heat application.

1.3 Technical design of the HTR-10 test reactor

Technical design of the HTR-10 test reactor represents the features of modular HTGR design. Reactor core and steam generator are housed in two steel pressure vessels which are arranged in a "side-by-side" way. The two vessels are connected to each other by a connecting vessel in which the hot gas duct is designed. All these steel pressure vessels are in touch with the cold helium of about 250°C coming out from the circulator which sits over the steam generator tubes in the same vessel.

Spherical fuel elements (6 cm in diameter) with coated particles are used. The reactor core contains about 27,000 fuel elements forming a pebble bed which is 180 cm in diameter and 197 cm in average height. Graphite serves as the main material of core structures which mainly consist of the top, bottom and side reflectors. The ceramic core structures are housed in a metallic core vessel which is supported on the steel pressure vessel. Side reflector is 100 cm thick. In the side reflector, cold helium channels are designed in which helium flows upward after entering the reactor from between the connecting vessel and the hot gas duct. Helium flow reverses at the top of reactor core into the pebble bed, so that a downward flow pattern takes place in it. After being heated in the pebble bed, helium enters into a hot gas chamber in the bottom reflector, and from there it flows with reactor outlet temperature through hot gas duct to the heat exchanging components.

The steam generator is composed of a number of modular helical tubes which are arranged in a circle between two insulation barrels inside the steam generator pressure vessel. The place inside the inner barrel is envisaged for the IHX which is to be installed in the second phase of the project. The IHX will be a large helical tube type with the primary helium flowing outside the tubes.

Decay heat removal is accomplished on a completely passive basis. At a loss of pressure accident, against which no core cooling is envisaged at all, decay power will dissipate through the core structures by means of heat conduction and radiation to the outside of the reactor pressure vessel, where, on the wall of the concrete housing, a surface cooling system is designed. This system works on the principle of natural circulation of water and it takes the decay heat via air coolers to the atmosphere. In fact, this surface cooling system is designed to protect the vessel and concrete structures more than the ceramic reactor core from being overheated by decay power.

There are two reactor shutdown systems, one control rod system and one small absorber ball system. They are all designed in the side reflector. Both systems are able to bring the reactor to cold shutdown conditions. Since the reactor has strong negative temperature coefficients and decay heat removal does not require any circulation of the helium coolant, turning off the helium circulator can also shut down the reactor from power operating conditions.

Spherical fuel elements go through the reactor core in a "multi-pass" pattern. Fuel pebbles are continuously discharged via a pneumatic pulse single-exit gate (or better called "serializer") which is placed inside the reactor pressure vessel. The burn-up of the discharged fuel elements is measured individually and those fuel elements which have not reached the limit value will be sent back pneumatically to the reactor core.

No pressure-containing and leak-tight containment is designed. The concrete compartments, which house the reactor and the steam generator as well as other parts of the primary pressure boundary and which are preferably called as confinement, together with the accident ventilation system, serve as the last barrier to the radioactivity release into the environment.

Fore more information on the design of HTR-10, Ref. [1] is referred.

2. Status of the HTR-10 Project

2.1 Safety review and licensing

For the design and licensing requirement, INET has prepared two technical documents, namely the Design Criteria for HTR-10 and the Format and Content of the Safety Analysis Report of HTR-10. These two documents were reviewed and approved by NNSA in August 1992 and March 1993 respectively.

The Environmental Impact Report (EIR) of HTR-10 was compiled and submitted it to the National Environmental Protection Administration (NEPA) in the mid of 1992. The report was reviewed by an expert committee, then NEPA approved the EIR of HTR-10 in November 1992.

The Siting and Seismic Report (SSR) of HTR-10 was submitted to the National Nuclear Safety Administration (NNSA) and the reactor site was approved in December 1992.

The Preliminary Safety Analysis Report (PSAR) and the Quality Assurance Programme were completed and submitted to NNSA for the application of the construction permit (CP) in December 1993. The activities of the CP licensing procedure lasted for one year. NNSA formally issued the construction permit for HTR-10 in December 1994.

2.2 Design of HTR-10

The conceptual design of the HTR-10 was jointly completed by INET, Siemens/Interatom and KFA in 1988. Modifications of the conceptual design have been made by INET in 1990 based on Chinese conditions.

The basic design and budget estimate of HTR-10 was carried out in the mid of 1994 and then examined and approved by both the State Education Commission (SEC) and the State Science and Technology Commission (SSTC) before the end of 1994.

The detailed design of the components, systems and buildings is being carried out by INET under cooperation with sub-contractors who are respectively responsible for the reactor building and ventilation buildings, the helium purification system with other helium auxiliary systems and the

turbine generator system and its building. For the detailed design of the main components, e.g., the reactor pressure vessel, the steam generator and the helium circulator, design engineers of INET have closely contacted and discussed with the manufacturing engineers to modify and improve the designs. The detailed design of HTR-10 is scheduled to be completed in 1996.

2.3 Engineering experiments

A programme of engineering experiments for the HTR-10 key technologies is being conducted in INET. The main aims of these engineering experiments are to verify the designed characteristics and performance of the components and systems, to give feedback on design and to obtain operational experiences.

A number of experimental facilities have been set up or are being established. Some experiments are being made. The key engineering experiments are as following:

- high temperature helium test loop and the relevant helium technology
- hot gas duct test facility
- fuel handling system test
- control rod driving mechanism test
- small absorber ball simulating system
- stability test of the steam generator
- helium flow temperature mixing
- pebble bed flow pattern

The test components of the fuel handling system and the small absorber ball releasing mechanism, the prototype of the control rod driving mechanism and the test section of the hot gas duct are designed in 1:1 scale. The tests are to be performed at operation temperatures and under helium atmosphere condition. The tests of the fuel handling system and the small absorber ball system under air condition at room temperature have been carried out.

2.4 Manufacturing of the key components

The key HTR-10 components, such as the reactor pressure vessel and its metallic internals, the steam generator vessel and its internals and the helium circulator are fabricated by domestic factories which have the ability and experience of manufacturing PWR's components. Graphite blocks for core internals and part of the safety grade helium valves will be imported from foreign suppliers. Spherical fuel elements will also be made indigenously.

The reactor pressure vessel is a safety grade I component. It has an overall height of 11.4 m, and a diameter of 4.2 m. The total weight is 142 t. It is fabricated by Shanghai Boiler Works. The metallic core internals, which consist of the metallic core vessel, top thermal shielding structure and the bottom support structures, will be manufactured by Shanghai Machine Works No.1. The reflector graphite blocks will be supplied by Toyo Tanco Co. Ltd. of Japan. The final machining of the graphite blocks is to be done in the workshop of INET. The carbon bricks of the reflector will be domestically fabricated.

The steam generator pressure vessel as part of the primary pressure boundary is also a safety grade I component. It has a height of 11.2 m, a diameter of 2.5 m and the total weight is 70 t. The once-through type steam generator consists of 30 small helical heating tubes. This component (vessel and internals) is fabricated by Shanghai Power Station Auxiliary Equipment Works.

The helium circulator is a vertical single-stage centrifugal one with the impeller at the end of the shaft. The circulator has the same axle with its driving motor and is fixed in the circulator pressure vessel which is the top part of the steam generator vessel. The helium circulator is fabricated by the Shanghai Blower Works.

The original German NUKEM manufacturing apparatus for fuel elements fabrication were transferred to INET in the first half of 1995. Most of them have been moved in and installed in the fuel fabrication building. It is scheduled to have all the necessary facilities and conditions ready in the mid of 1996, and experimental work will be started right afterwards. Process capability of the production line is set at 500 g uranium, i.e., 100 fuel elements a day.

The components of the fuel handling system, the helium purification system and other auxiliary systems will also be domestically made.

2.5 Building construction

The HTR-10 test plant includes a reactor building, a turbine generator building with two cooling towers and a ventilation centre with a stack. The buildings are to be arranged and constructed on an area of 100x130m^2.

Civil engineering work of the buildings are contracted to engineering companies of China National Nuclear Corporation (CNNC). The ground excavation was completed at the end of 1994. The first concrete of the reactor building fundament was poured on 14. June 1995. The fundament of the reactor building was finished in September 1995 (Fig. 3). Civil work of building construction is now underway.

2.6 Time schedule

The time schedule for the HTR-10 project is shown in Table 1. The reactor building construction will last for two and a half years and is scheduled to be completed at the end of 1997. In parallel, the manufacturing and installation of components, and systems will closely follow the progress of building construction and will be completed at the end of 1998. The first criticality of the reactor is planned to be reached at the beginning of 1999.

3. Summary

China is now projecting a 10MW high temeprature gas-cooled test reactor (HTR-10). The construction of the HTR-10 started in June 1995. Currently, detailed design, building construction, component procurement, research and development are now intensively underway in parallel. First criticality of the reactor is scheduled for 1999.

References

[1] Qin Zhenya, "The General Design of the 10MW HTR", the 3rd JAERI Symposium on HTGR Technologies, February 15-16, 1996, Oarai, Ibaraki, Japan

Table 1 Time Schedule of the HTR-10 Test Reactor Project

	1994	1995	1996	1997	1998	1999
Milestone	Construction Licence	First Concrete			FSAR Critical	Operatinon Power Operation
Basic Design						
Detailed Design						
Construction						
• Site Preparation						
• Building						
• Manufacture of Components						
• Installation						
Commissioning						
• Critical						
• Test						
• Power Operation						

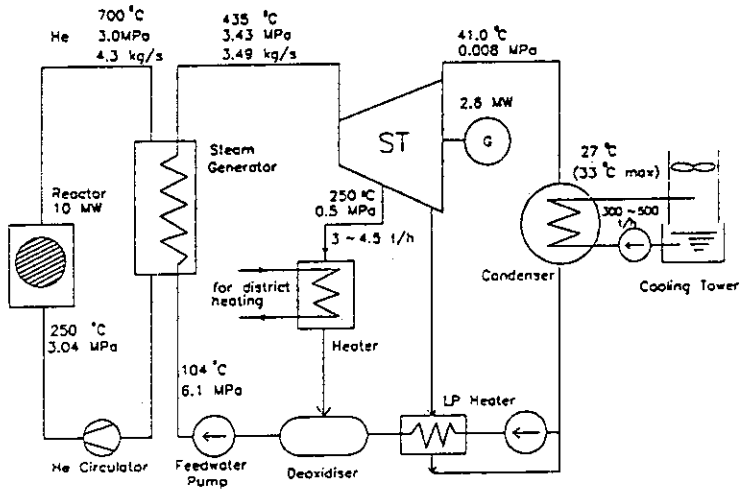


Fig. 1 Flow Scheme of the HTR－10 Steam－Turbine Cycle

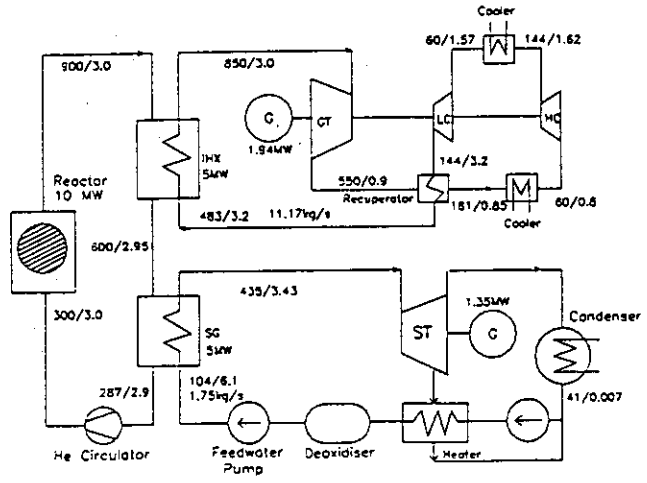


Fig. 2 The HTR－10 Gas－turbine/Steam－turbine Combined Cycle



Fig. 3 Concrete Pouring of the HTR-10 Reactor Building Fundament Was Completed in September 1995

2.2 PRESENT STATUS OF HTGR PROJECTS AND THEIR HEAT APPLICATIONS IN RUSSIA.

Grebennik V.N., Glushkov E.S., Kukharkin N.E.,
Ponomarev-Stepnoi N.N.

Russian Research Center "Kurchatov Institute",
Moscow.

Abstract

The constantly increasing needs in supplying the mankind with power require the search of the most economic and safe, as well as the most environmentally clean way of generation heat and electric power. Use of mostly organic energy resources in industry and at homes results on the one hand in the exhaust of their supplies and thus in the increase of cost, and one the other hand in the intensification of the CO2 impact and environmental pollution. Due to all this, despite all the negative phenomena, that took place, nuclear power engineering is a real source of power supply for many dozens of years.

Taking into consideration the increased requirements to safety, nuclear power engineering is to be developed due to modification of the traditional reactor technologies and due to development of new reactor concepts, possessing good safety and economic efficiency. High temperature gas cooled modular reactors, using the closed gas turbine cycle (MVGR-GT) could be reviewed as the concept of advanced reactor of new generation. Nuclear system with the helium turbine allows to general electricity with high thermal efficiency (45-50%), than the reactors with steam turbine cycle.

This results in less specific nuclear fuel rate per electricity generation, decrease of the amount of radioactive waster per unit of the generated power, and sufficient decrease of the heat release into the environment. The systems with gas turbine cycle require less cooling media, as they can operate with the air cooling. High temperature gas cooled modular reactor (MVGR), meeting all the modern requirements in regard to safety and protection of the people and environment from the radioactive influence, serves as the source of thermal power for the GTC.

Main characteristics and advantage of MVGR are determined by using of fuel elements on the basis of coated fuel particles of uranium dioxide with the multilayer protecting coating, graphite as the core structural material, and helium coolant.

These factors provide unique inherent safety of this reactor type, that means that in case of the accident with the temperature excursion, nuclear reaction will

be stopped by itself, and residual heat will be released by passive means without actuation of the active protection systems.

MVGR-GT is a nuclear power plant consisting of the high temperature gas cooled reactor and closed cycle gas turbine unit.

Significant scientific and technical experience on HTGR is accumulated in Russia in the area of their design and R&D during more than 30 years. A number of detailed designs of reactors have been made for a wide range power (VGR-50 MW el., VGM-200 MW th., VG-400 MW el.), and many investigations have been performed on fuel elements development, testing of equipment and facilities, safety assuring, heat application in industry, etc.

In the area of development and manufacturing of gas-turbine systems in Russia there is also accumulated a significant experience of using them in power production, aircraft and space industry. Power production GTC used as peak power production systems and drive gas-turbine engines at natural gas lines have been fabricated and are in service. Experimental investigations on gas-turbine model using helium have also been started.

Considering advantages of GTC HTGR development, investigation in this area recently resumed. Different concept of gas-turbine systems use with HTGR are considered:

- a direct helium cycle;
- an indirect helium cycle with high temperature intermediate heat exchanger;
- a combined gas-steam cycle.

This paper describes the main technical decision and parameters of the HTGR of different power and considers a few schemes of HTGR plants with a gas turbine cycle. Also, the future prospects on heat utilization of HTGR in Russia is presented.

RECENT STATUS AND PROSPECTS OF APPLICATION OF HIGH-TEMPERATURE GAS-COOLED REACTORS (HTGR) IN RUSSIA

V.N.Grebennik, E.S.Glushkov,
N.N.Ponomarev-Stepnoi, N.E.Kukharkin,
A.A.Khrulev

Russian Research Center "Kurchatov Institute"
Moscow

Prepared for: The 3rd JAERI
Symposium on HTGR Technology
February 15-16, 1996
Oarai, Ibaraki, JAPAN

1. INTRODUCTION

At the present time it has become clear, taking into account severe accidents at nuclear power plants and growing negative public attitude towards nuclear option, that further development is possible if nuclear and radiation safety and reliability of nuclear plants (NP) are significantly improved and humanity and environment are guaranteed to be protected against radiation effects.

This requires that major improvements be made in recently operating nuclear reactors all over the world and in the reliability of equipment, fundamentally new engineering concepts and reactor technologies be created to provide development of ecologically safe nuclear power sources.

This problem becomes most pressing because of extended application area of nuclear energy (NE) for domestic and industrial heating, as well as for production of high-potential heat for different industrial processes.

The experience in developing nuclear plants in Russia based on light-water reactors demonstrates advantages of NE application for these purposes because of lower consumption of organic fuel and improved ecological situation in densely populated regions.

The next step to expand potentialities of NE should be application of nuclear reactors to produce high-potential heat for different branches of industry.

Examination of different reactor concepts for generation both electricity and high-potential heat has demonstrated that high-temperature gas-cooled reactors are the most applicable for this purpose. The main features and advantages of

HTGR are based on helium coolant, graphite used as structural material for the core, as well as fuel elements made of coated particles of uranium or plutonium with multi-layer protective coatings. These factors allow to reach the temperature of up to 1000°C at the HTGR reactor outlet, as well as provide improved safety characteristics.

In this report a brief review of modern situation in works on HTGR in Russia, as well as key problems of their application for industrial purposes, are considered.

2. HTGR CONCEPTS IN RUSSIA.

Significant scientific and technical experience was accumulated in Russia during more than 30 years in the area of design and R&D of HTGR. Several detailed designs of reactors have been made for a wide range of powers (VGR - 50 MW el., VGM - 200 MW th., VG - 400 MW el.), and many investigations have been performed on development of fuel elements, testing of equipment and facilities, safety assuring, etc.

Taking into account unique HTGR properties in generation of high-potential heat the designs developed in Russia have provided for production both of electricity and heat. The usual industrial steam-turbine cycle has been used for electricity production, providing in NP with HTGR the higher efficiency (~38%) compared to light-water reactors, but not completely utilizing high potential of a helium coolant at the reactor outlet.

The HTGR advantages should become more evident when using gas-turbine cycle providing the higher efficiency of NP (48%), as well as ensure the further improvement in safety and decreasing of capital investments comparing to steam-turbine cycle.

In Russia the great experience in development and construction of gas-turbine systems, as well as in their application to power production, aircraft and space engineering, has been accumulated.

Considering advantages of GTC HTGR development, investigations in this area have recently been resumed. Different concepts of application of gas-turbine systems with HTGR are under consideration:

- direct helium cycle;
- indirect helium cycle with high temperature intermediate heat exchanger;
- combined gas-steam cycle.

A direct cycle provides more efficiency and economical benefits but requires to solve problems related to complexity of turbines, compressors, generator and heat exchangers arrangement in a single vessel. Furthermore, there are restrictions on temperature level of helium at reactor inlet related to reactor vessel material resistance.

For indirect cycle, these factors are less significant because there are more opportunities of GTC equipment arrangement, their maintenance and repairing. However, this option requires development of a high temperature intermediate heat exchanger with adequate lifetime. The system efficiency is also partially decreased because of temperature level reduction at a turbine inlet.

Combined cycle provides more efficiency of heat conversion into electricity but has more complicated thermal scheme and more units of power equipment.

Gas-turbine cycle in combination with HTGR having different power has recently been considered:

MVGR-GT - 200 MW (th)

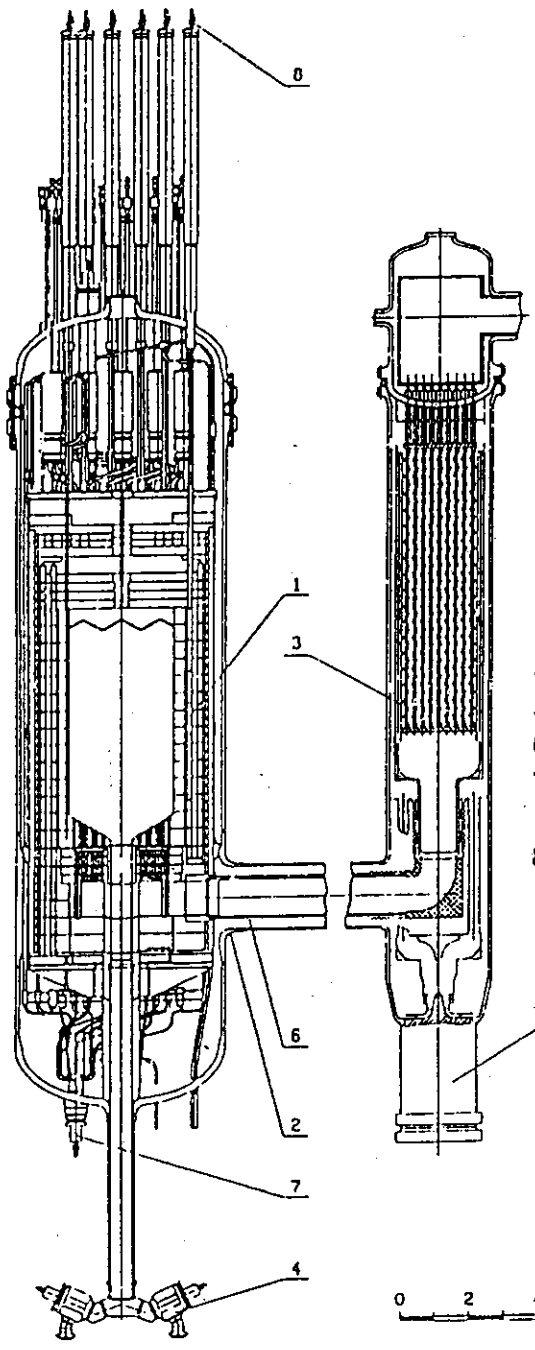
The MVGR-GT is a nuclear power plant consisting of a high temperature gas-cooled reactor and a closed-cycle gas-turbine system. All main units of a reactor are located in the steel high-pressure vessel. The reactor has a cylindrical core consisting of spherical fuel elements.

Engineering concepts and reactor materials used for this reactor enable to reach, in operation mode, helium temperature in the range 850-950°C at the reactor outlet. General view of the reactor is shown at Fig. 2.1.

Two options of arrangement of the reactor with gas-turbine system have been considered:

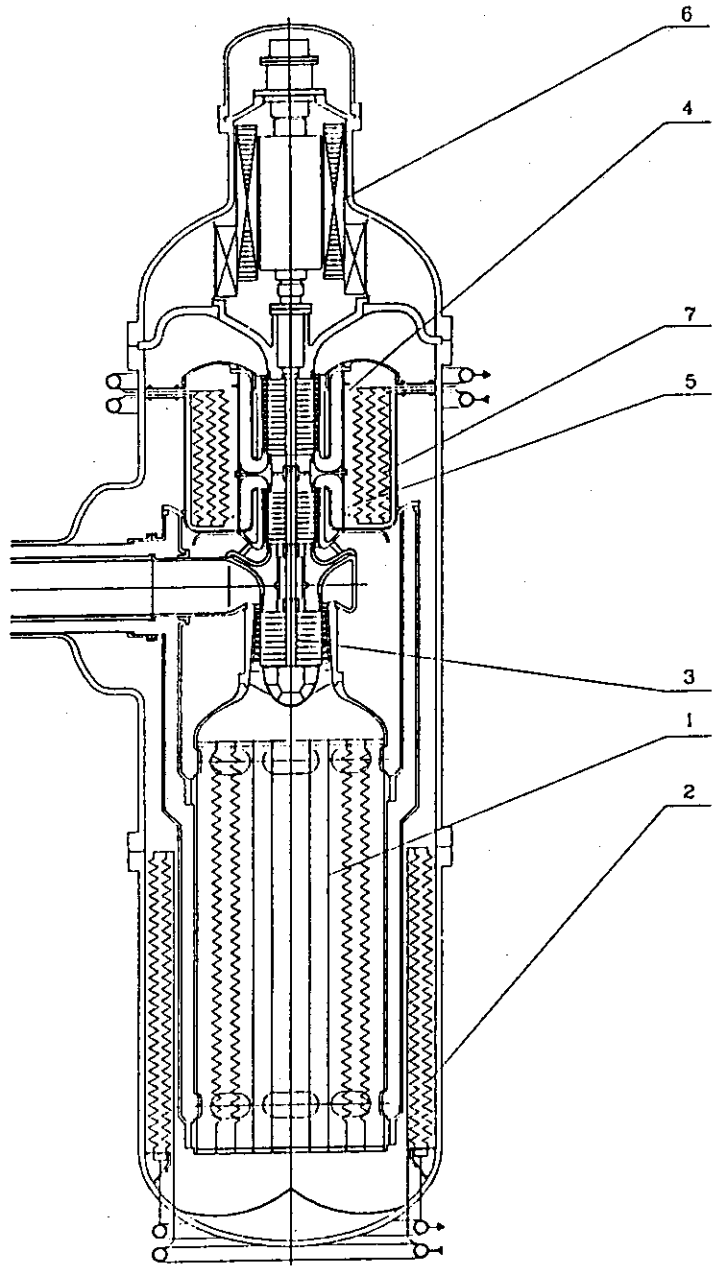
- With direct cycle and turbines, compressors and heat exchanging equipment arranged in a single pressure vessel (Fig. 2.2);
- With indirect cycle, power and heat exchanging equipment arranged in separate vessels (Fig. 2.3).

The first option is preferable by its leak-tightness and compactness, while the other has more simple and reliable design and accessibility for servicing and repair.



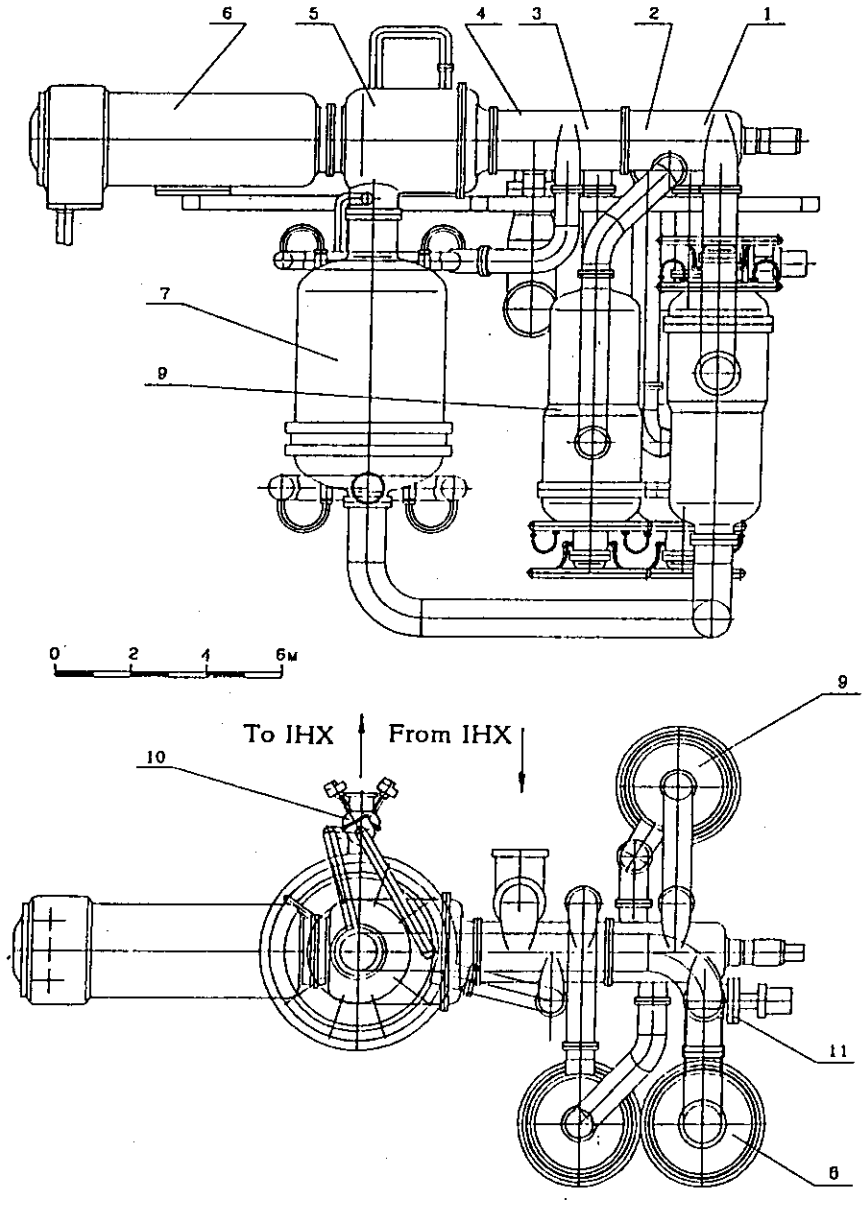
1. Reactor
2. Vessel section
3. High-teemperature intermediate heat exchanger
4. Refueling system
5. Gas blower
6. Hot gas duct
7. Ball-type reactivity compensation system
8. CPS rod drive

Fig.1. Reactor Unit



1. Recuperator
2. End cooler
3. Turbine
4. Low pressure compressor
5. High pressure compressor
6. Generator
7. Intermediate cooler

Fig.2.2 Direct-Cycle GTC with Intermediate Cooling



1. Low pressure compressor
2. Medium pressure compressor
3. High pressure compressor
4. High pressure turbine
5. Low pressure turbine
6. Generator
7. Recuperator
8. End cooler
9. Intermediate cooler
10. Control accessories
11. Throttle valve

Fig23. GTC with Indirect Cycle

An option with indirect cycle and temperature 850°C at the reactor outlet has been accepted as basis one for the stage of building the pilot system.

Main parameters of a power plant with MVGR-GT reactor are given in Table 2.1.

The more efficient cycle with double-stage intermediate cooling of compressors is used in this system.

GTC is designed according to double-shafted scheme where a driving turbine, low, medium and high pressure compressors, as well as a start-up motor, are located at the high-speed shaft (15000 rpm), while the high-pressure power turbine and generator are located at the low-speed one (3000 rpm).

HTGR - 10 MW (t)

HTGR-10 is a high temperature gas-cooled low-powered reactor designed to develop an independent nuclear power plant for power supply of far regions of Russia.

The distinct feature of these regions is their low population density and wide dispersion of small settlements (5000 persons). Population of settlements is usually 600-2000 persons. Centralized power supply is impossible in these regions. Total power produced by available power sources in far north regions of Russia is recently 1200 MW. Utilization of diesel oil to produce this power seems unprofitable.

According to that, proposals on providing power supply for these regions with nuclear power sources has been considered in RF. Power sources based on different reactors (water/water, gas-cooled, thermionic) have been compared. The main requirement to nuclear power sources for far north of RF is high safety that ensures reliable protection of environment from radioactive contamination under conditions of lack of well-experienced personnel.

Investigations have demonstrated that a concept of HTGR with a core of uranium-graphite fuel elements made of coated particles with multilayer coatings of pyrocarbon and silicon carbide provides the best compliance with this requirements.

HTGR-10 reactor design includes intermediate loop and combined gas and steam cycles. NPP schematic is shown at Fig. 2.4.

Table 2.1.

Parameters of Power Plant with MVGR-GT.

Parameter	Cycle	
	Indirect	Direct
Reactor thermal power, MW	215	215
Temperature:		
- at reactor outlet,°C	850	950
- at reactor inlet, °C	400	490
Helium pressure in reactor, MPa	7.5	7.5
Core dimension, height/diameter	9.0/3.0	9.0/3.0
Average power density, MW/m^3	3.0	3.0
Fuel type, size, mm	sphere ∅60	sphere ∅60
Fuel	UO2	UO2
^{235}U enrichment, %	8.5	8.5
Reactor vessel diameter, m	6.0	6.0
Turbine generator	double-shafted	single-shafted
Shaft revolutions, rpm	15000/ 6000 (3000)	6000
Turbine steps	4/7	8
Intermediate coolers	2	1
Helium temperature ahead of turbine, °C	810	950
Helium pressure in GTC, max, MPa	7.7	7.5
Generator power, MW (el)	99	105
Internal-purpose power MW (el)	5.5	2.0
Net power, MW el.	93.5	103
Power plant efficiency	0.435	0.479

A core of spherical fuel elements is located in a pressure steel vessel 3250 mm in diameter and 7650 mm in height. In the bottom there is a special facility to discharge fuel elements after lifetime. Two gas blowers located at side ducts of a vessel provide helium circulation. The reactor structure is shown at Fig. 2.5.

Main parameters of the power plant are given in Table 2.2.

Power plants of this type can provide power supply for more than 50% of the largest settlements in the far north of Russia.

MHR-GT - 600 MW (th)

Work on development of the conceptual design of the modular gas-cooled MHR-GT reactor with direct cycle and 600 MW (th) power are recently in progress in the context of joint Russian-American project.

The reactor and gas-turbine system units are located in steel vessel connected with a coaxial gas pipe.

The annular core consists of prismatic fuel elements made of coated particles with ceramic protective coatings. Schematic diagram of MHR-GT is shown at Fig. 2.6.

This reactor makes it possible, besides of producing electricity in traditional uranium cycle, to burn weapon-grade plutonium up to condition that puts it out of military use.

Main parameters of reactor are shown in Table 2.3.

The main participating institutions of this project are: Russian institutions - RRC "Kurchatov Institute" and OKBM, American institution-General Atomic Company.

3. PERSPECTIVES OF HTGR HEAT APPLICATION.

In the present time nuclear power engineering (NE) attempts to solve the problem to substitute organic fuel in electricity production; some countries have achieved good results in this field.

However, it is well known that the leading industrial countries spend only one fourth of the consumed primary power sources for generating electricity.

Table 2.2.

Main Parameters of Independent Power Plant with HTGR-10.

Plant power, MW th.	20
Reactor units	2
Reactor power, MW th.	10
Helium coolant temperature, °C	
- at the core outlet	850
- at the core inlet	300
Pressure in reactor, MPa	1.0
Fuel elements type, size, mm	Sphere ∅60
^{235}U fuel enrichment, %	21
Fuel burnup, MW.day/t	95,000
Average power density in core, MW/m^3	1.98
One fueling lifetime, eff.years	11.3
Secondary loop coolant	air
Air temperature in a heat exchanger, inlet/outlet, °C	175/800
Working pressure of air, MPa	1.0
Power system	gas-steam turbine
Gas turbine power, MW el.	3.4
Steam turbine power, MW el.	3.9
Net efficiency, %	35
Plant operation time, years	40
Electricity output per year, KW.h	64.10^6
Annual displacement of diesel oil, t	15,000

Table 2.3.

Main Parameters of MHR-GT.

Reactor power, MW th.	600
Helium temperature in reactor: inlet/outlet, °C	490/850
Helium pressure in primary loop, MPa	7.0
Fuel blocks in a core:	
- in plan	102
- in height	10
Average power density, KW/l	6.5
Fuel elements type	prismatic
Fuel	UO2 (PuOx)
Reactor vessel diameter, m	8.5
Turbine generator	vertical single-shafted
Shaft speed, rpm	5160
Bearings	magnetic
Turbine steps	9
Compressors steps	11/15
Intermediate cooler	1
Generator	asynchronous 50/60
Diameter of turbine generator vessel, m	8.0
Generator power, MW el.	298
Net power, MW el.	286
Net efficiency, %	48

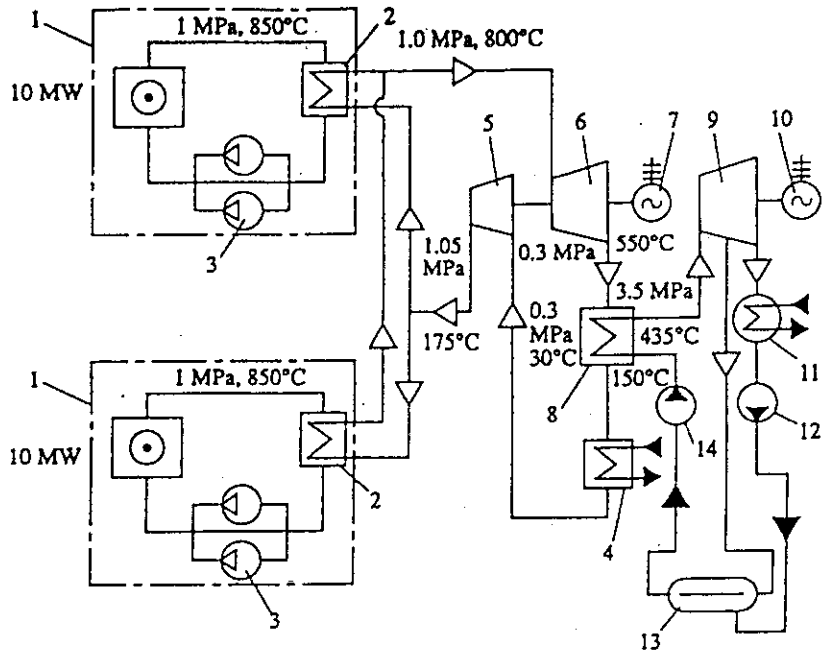


Fig. 2.4. Cycle Arrangement for NPP with HTGR-10 Reactor and Gas-Steam Turbine Installation.

1. HTGR-10 reactor
2. Helium-air heat exchanger
3. Blower
4. Heat exchanger
5. Compressor
6. Gas turbine
7,10. Electric generator
8. Steam generator
9. Steam turbine
11. Turbine condenser
12. Condensate pump
13. Deaerator
14. Feed pump

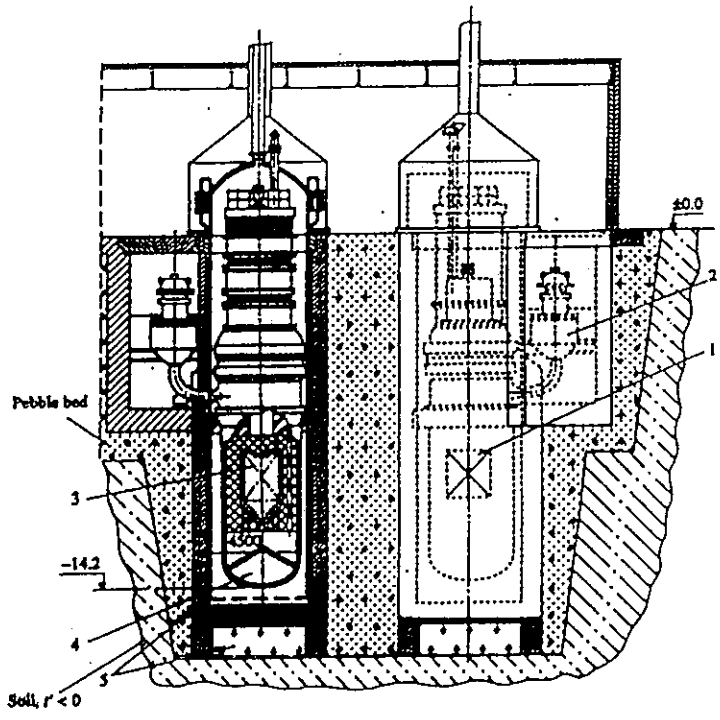


Fig. 2.5. Small Reactor HTGR-10.

1. Reactor
2. Blower
3. Reactor core and its fuel assemblies of uranium-graphite spheres
4. Burned-up fuel storage place
5. Biological shielding

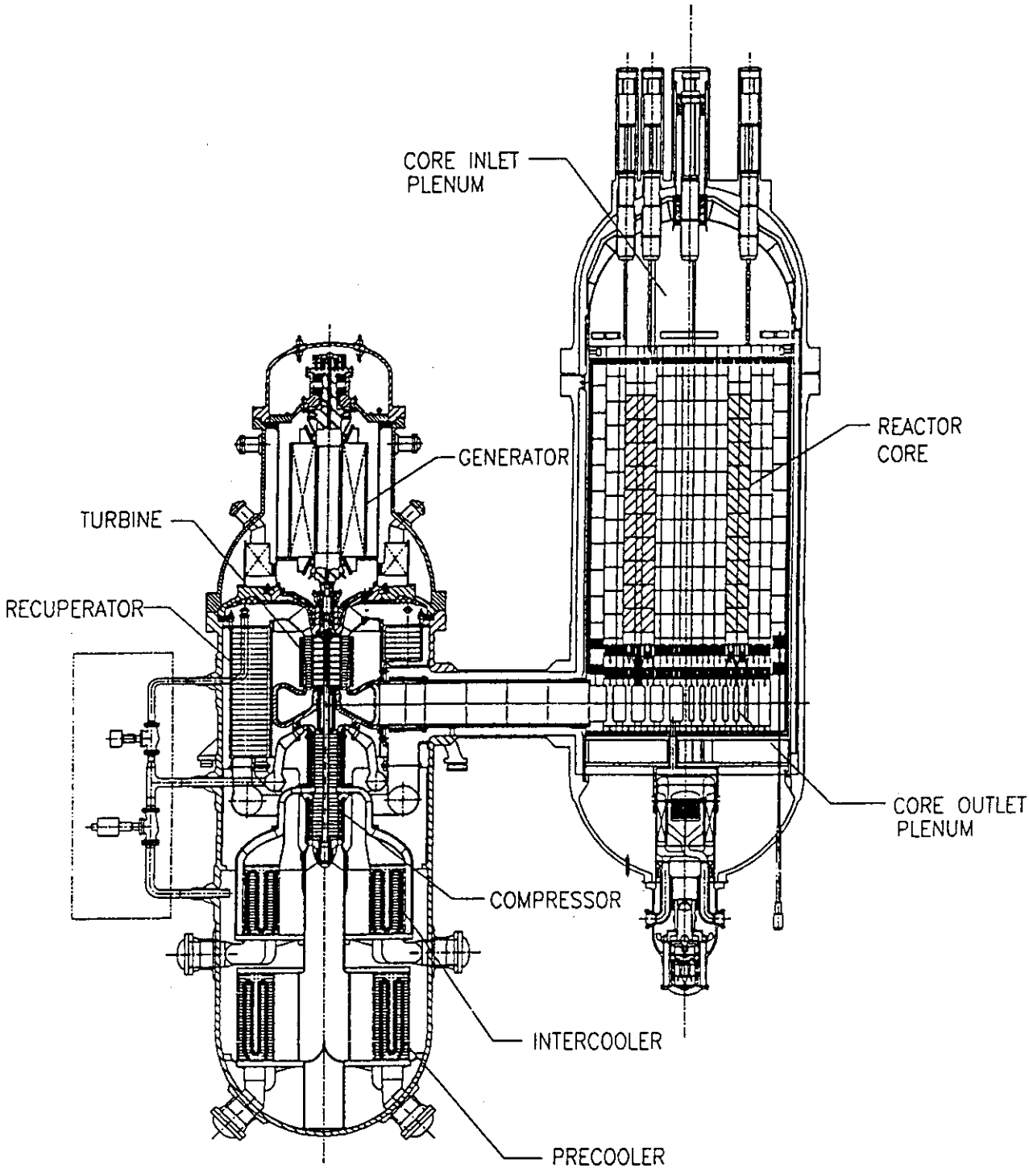


Figure 2.6 GT-MHR Single Module Reactor Arrangement

That is why the problem of nuclear reactor application to different industrial technologies consuming thermal power has become vital. Solution of this problem will allow not only to reduce consumption of the organic fuel, but also to improve the environment in the industrial regions with a high density of population.

Nuclear power engineering is to make important contribution into the reduction of gases release into the environment intensifying warming up (mainly CO_2 and CH_4), as well as the hazardous products due to the burning of organic fuel (such as SO_2, NO_2 and others.)

Unique possibility to have the coolant of a very high temperature in HTGR give us wide perspectives in application of this reactors to power engineering. HTGRs allow to perform complete power supply of technological industries with high-parameter heat and steam and also with electricity.

During the passed years, the research on possible application of HTGR in different branches of industry has been carried out in RF. About 20 different technologies where HTGRs are conceptually possible to be used were reviewed. Nuclear power technological plants based on HTGRs can be used for thermal and power supply of different industrial processes of methanol, hydrogen, ammonia production, coal conversion, district heating, etc. Steam catalytic methane conversion carried out on the basis of HTGR at the temperature of 850-900°C is the key item for many of these processes. Taking into consideration the real situation of HTGR development in our country, we evaluated all the possibilities of the use of HTGR in near and remote future.

One of the possible fields of the power technological use of HTGRs in the near future would be oil-reprocessing and oil-chemical industries. This branch of industry consumes lots of energy and occupies, among all the branches of heavy industry, the first place in the consumption of steam, the second place, after the ferrous metal industry, in the fuel consumption, the third place, after ferrous and non-ferrous metal industries, in the consumption of electricity. Oil-reprocessing and oil-chemical industry uses for its own need the amount of energy, equivalent to 6-10% of the total amount of reprocessed oil.

The processes of oil industry can be divided, according to the heating level of oil products, into three types: low-, medium- and high-temperature. For the low-temperature processes the maximum heating temperature is 400°C, for the medium temperature ones - 550°C, for the high-temperature ones - 900°C. The thermal energy consumption fractions for these temperature ranges are 0.65, 0.23 and 0.12, respectively.

The basic process of primary oil reprocessing aims at to crack petroleum at the temperature of 400°C into the fractions which serve as raw material for the majority of processes of oil-chemistry. Catalytic reforming is carried out at the temperature of 530°C to improve quality of gasoline fractions and produce high-

.octane gasoline. These most energy-consuming processes could be quite easily supplied with energy by HTGR.

The most important oil industry high-temperature processes are those of pyrolysis and conversion which take place at temperatures of 800-900°C.

Fig. 3.1 represents possible scheme of HTGR heat application for the purpose of pyrolysis of hydrocarbon raw, heating and reprocessing of oil products, and steam generation.

Preliminary research carried out in Russia has demonstrated that HTGRs can be widely used in oil recovery industry. Development of far heating nuclear plants based on HTGR can intensify recovery of viscous petroleum and bitumen, by means of heat transfer to petroleum wells in a chemically bound form.

An important item is production of synthetic liquid and gaseous fuel on the basis of coal conversion. It is of major interest to the countries possessing great resources of coal. For Russia this problem becomes more burning because of the expensive transportation of coal to the European part of the country, where 3/4 of the fuel energy resources are consumed.

The carried out research shows that the processes of coal reforming into liquid and gaseous fuel could be realized by the means of thermal power of HTGR. Temperature level of about 850-900°C is satisfactory for efficient gasification processes with external power supply. Two processes of coal gasification are reviewed due to utilization of HTGR thermal power:

- hydrogasification $CH_4+H_2O=3H_2+CO$ - 60 kcal/mol;
  $C+2H_2=CH_4$ - 20.9 kcal/mol;
-steam gasification $C+H_2O=H_2+CO$ - 23.8 kcal/mol.

The schematic diagram of the combined process of steam gasification of coal, hydrogen production, and hydrogenization of coal to produce liquid fuel, is presented at Fig. 3.2.

Coal reforming by utilization of thermal power of nuclear reactor is the more efficient and ecologically clean process. This method allows to reduce two times, comparing to existing methods, the coal consumption to produce the same amount of synthetic fuel, thus reducing expenses for its mining and transportation. This will result in sufficiently less cost of the final product.

The process of obtaining synthetic fuels out of coal due to nuclear energy can become economically competitive in the beginning of the next century, especially as prices for the organic fuel are constantly growing.

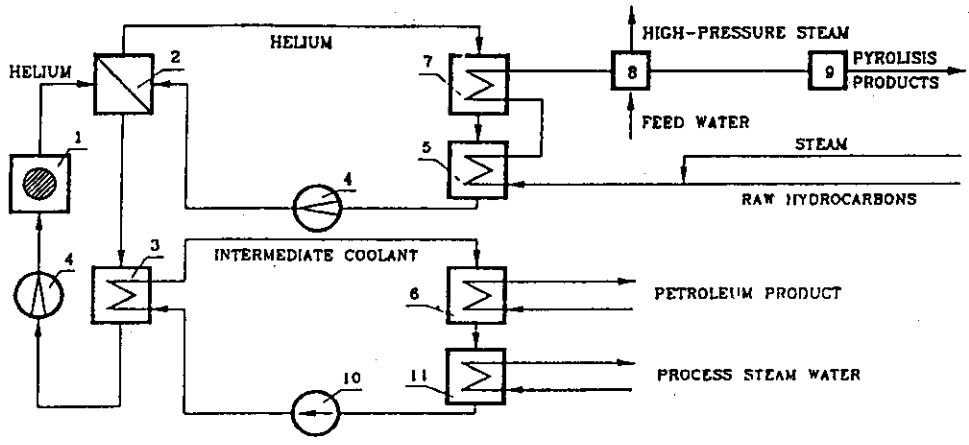


Fig. 3.1. Schematic Diagram of HTGR Application for Pyrolysis, Steam Generation and Heating of Petroleum Products

1. HTGR
2. Helium-helium heat exchanger
3. helium-intermediate coolant heat exchanger
4. Gas blower
5. Preheater for raw hydrocarbons
6. Intermediate coolant-petroleum product heat exchanger
7. Pyrolysis unit
8. High-pressure steam generating system
9. Separator for pyrolysis products
10. Pump
11. Steam generator

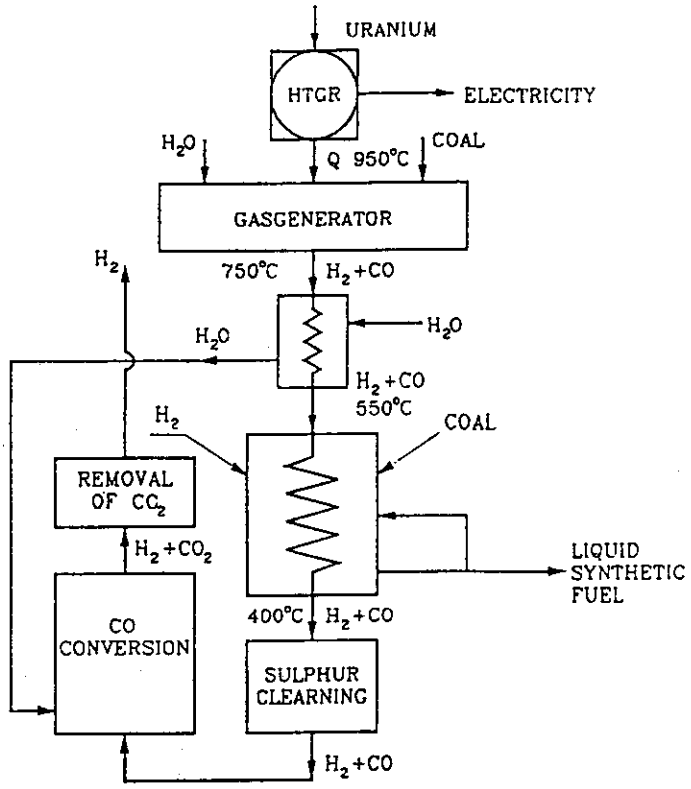


Fig. 3.2.. Combined Process of Steam Coal Gasification, Hydrogen Production and Coal Hydrogenation for Liquid Synthetic Fuel Production

If HTGR is used as a source of thermal power for the industrial processes, it is to meet certain requirements on the level of power and temperature, unified equipment, power redundancy, etc.

The advantages of modular HTGR systems are easily seen when being produced on the large scale. Construction of multi-unit NPP of high power will allow to reduce specific capital investments, and these NPPs will be competitive at the power market.

4. HTGR SAFETY

Further improvement in nuclear and radiation safety and reactor reliability is the major criterion to dictate development of nuclear industry in the modern situation.

Main requirements to a new generation of reactors are eventually summarized in a major reducing of the accident risk at operation, as well as in the ensuring of a reliable protection of people and environment against radiation. The probability of severe accidents causing sufficient radiation release must be, in the large-scale development of nuclear industry, extremely reduced (10^{-5} - 10^{-6} 1/reactor.year), that will require radical improvement in existing nuclear power sources and introduction of fundamentally new reactor technologies. A problem of development of ecologically clean reactor must be therewith considered due to development of such a protection that ensures sufficient improvement in reactor safety including external effects such as earthquake, airplane fall, nearby explosion, diversion and so on.

Investigations showed that the most efficient protective means are so-called inherent reactor safety properties that are based on physical laws and are related to thermal-hydraulic, nuclear-physical, chemical parameters and construction of the reactor. Passive protective means, i.e. engineering means that do not require outer power supply and are always ready to operate, are also efficient.

The combination of inherent properties and passive means for reactor shutdown and release of residual heat provide high protection of nuclear power source, this means that, if accident happens, the environmental impact would be low even without use of active protective means and actions of operating staff.

Such a protective system is to be provided not only for reactor operation but also for spent fuel storage and reactor decommissioning.

These criteria are substantially met by HTGR reactors that ensure high safety by the means of their inherent safety and the following features:

- Graphite used as a structural material for the core and reflector, withstanding high temperature (up to 3500°C) without being melted.

- Single-phased, non-activated, chemically inert helium coolant precluding increase in reactivity caused by coolant leakage.
- High thermal capacity and low power stress in a core providing slow increase of temperature at accidents with cooling cease or depressurization, thus giving time to make appropriate decisions.
- Improved resistance of ceramic fuel elements, made of coated particles with multi-layer coatings, to temperature excursions in a core.
- Sufficient temperature margin from operating (1200°C) to maximum permissible (1600°C) level.
- Negative temperature coefficient of reactivity in all operating range of temperature, ensuring inherent protection of a reactor.
- High burn-up of fuel (10% Fima) giving the chance, according to economic reasons, do not reprocess fuel, making it easier to localize activity.

In the last years in Russia and other countries (USA, Germany, Japan, China) there has been developed a concept of a modular HTGR having the following main features:

-high safety ensured by inherent characteristics of a reactor.
- a possibility to develop the universal power source for generation both of thermal and electrical power.
- high level of unification, at serial-scale building of NP, of main and auxiliary equipment.
- competitive ability against high-power NP using organic fuel, etc.

The interest in modular reactors has been increased not only in industrially developed countries but, in the IAEA view, this path development of power engineering may be acceptable for small and developing countries.

The prototype of modular reactors in Russia is MVGR reactor of 200 MW(th) power intended to produce electrical and thermal power for industrial and domestic needs. This kind of application is a reason to locate NPs near the large populated areas and industrial units and to meet safety standards for nuclear heating plants.

According to this, main design concepts of safety for MVGR reactors have been stated, assumed to be used for commercial NPs in future.

To ensure radiation safety (RS), a system of independent barriers against expanding radioactive substances is provided for MVGR operation. The composition and performance of these barriers are given in Table 4.1.

A fuel element made of coated particles (CP) is a main barrier against radioactive substances in HTGR. The criteria of radiation safety for different states of MVGR reactor accepted in the design are given in Tables 4.2. and 4.3.

To ensure radiation releases from MVGR, that determines staff and population radiation exposure, to be within boundaries established by regulations, the permissible leakage limits of main radionuclides from damaged fuel elements are defined (Table 4.4.)

Parameters of primary circuit activity that characterize these requirements to fuel elements have the following values:

1. Balanced state activity of the primary circuit due to volatile FP (Xe, Kr, I, Tl) is to be no more than 100-200 Ku.
2. Activity due to Cs and Sr is to be no more than 10-20 Ku by the end of lifetime.

Assuming impossibility of MVGR core melting, the following criteria of safety are stated:

- Maximum temperature of 1600°C for a fuel element (FE), allowing to meet requirements on the FE damage, is not exceeded during a long time. This temperature is not exceeded for all designed accidents including depressurization, as well as for the prearranged accident with a failure of all designed cooling systems, maximum designed boundary of FE damage is not therewith exceeded. Residual heat is removed by natural physical processes, without staff actions and power consumption.
- The possibility of prompt criticality is eliminated for all accidents including emergency protection failure accident.
- Possible positive reactivity is compensated by negative temperature feedback for all accidents.

These criteria are ensured by physical and structural characteristics of the core and fuel elements, low specific power, high thermal capacity, low reactivity margin on burnup, etc. Values of reactivity coefficients due to MVGR reactor fuel temperature and power are therewith negative within all range of parameters at normal operation and in design-basis accidents.

Along with properties of coated particles, reactor vessels are also of great importance for activity confining because of their disruption probability to exceed designed level being no more than 10^{-7} 1/reactor.year.

When designing MVGR the full list of possible accidents has been studied and engineering measures on equipment reliability have been provided for, to ensure, in combination with MVGR inherent safety properties, reliability of protective and confining systems of NP.

One of the most severe accidents of MVGR is air and/or water ingress into a core.

Table 4.1.

MAIN BARRIERS TO CONFINE RADIOACTIVITY

Barrier	Type of Barrier	Confining Factor
Fuel element and CP with protective coatings (FP crushing and localization)	Passive	Number of FE in reactor ~$4 \cdot 10^5$ CP ~10^9 - 10^{10}
Helium purification system	Active	0.1 - 1.0 h^{-1}
Self-purification of helium of the primary circuit from radionuclides J, Cs, Sr	Passive	10^3 - 10^4 h^{-1}
Pressurized equipment of the primary circuit	Passive	Helium release rate <0.3% vol/day
Special ventilation of pressurized premises	Active	Purification ratio K≥10
Protective leaktight containment	Passive	Medium release rate ~1% vol/day
Sanitary protective zone	Active	Defined in design

Table 4.2

HTGR RADIATION SAFETY CRITERIA ON NORMAL OPERATION AND IN DESIGN-BASIS ACCIDENTS

Name	Value	Comment
NORMAL OPERATION:		Gas-aerosol radiation releases are at normal operation and in design-basis accidents an order less than those set by regulations for NPP
Whole body external dose for critical group of population, mrem/year	<2	
Thyroid gland dose for critical group of population, mrem/year	<10	
DESIGN-BASIS ACCIDENTS (at a boundary of 2.5 km sanitary-protective zone):		
External exposure, rem	<1	
Child thyroid gland exposure, rem	<3	

Table 4.3

HTGR RADIATION SAFETY CRITERIA
FOR BEYOND DESIGN-BASIS ACCIDENTS

Name	Value	Comment
External exposure within the year after accident, rem	<3	Without regard for filter cleaning
Child thyroid gland dose, rem	<5	
Probability of ultimate accidental release beyond NP boundaries per year	$<10^{-8}$	
Accidental release to atmosphere:		
- ^{137}Cs, Ku	<20	
- ^{131}J, Ku	<1000	
Effective equivalent dose (during 50 years), rem	<5	Evacuation of population excluded
Thyroid gland dose, rem	<50	

Table 4.4

DAMAGE LIMITS FOR HTGR FE

Limit Name	Radionuclide	Value
Operational limit	^{133}Xe, balanced relative release (R/B)	$<10^{-5}$
	^{131}J, balanced relative release (R/B)	$<10^{-5}$
	^{137}Cs, ^{90}Sr, Ku/year	<2
Safe operation limit	^{133}Xe, relative release	$<5{\cdot}10^{-5}$
	^{131}J, relative release	$<5{\cdot}10^{-5}$
	^{137}Cs, relative release	$<10^{-5}$
Maximum designed limit	^{133}Xe, relative release	$<10^{-4}$
	^{131}J, relative release	$<10^{-4}$
	^{137}Cs, relative release	$<5{\cdot}10^{-5}$

This can cause, on the one hand, graphite oxidization (burning) followed by FE disruption and significant radiation release, and, on the other hand, impermissible reactivity growth.

Performed design-scale investigations on MVGR reactor have shown that such accidents proceed predictably and will not cause catastrophic consequences.

The simultaneous prompt rupture of gas tubes located in the top and bottom parts of the reactor vessel, that may cause so-called "hood effect", i.e. the process of oxidizing of spherical fuel element claddings and graphite bricks when streamed with air penetrating a reactor through derived holes, is assumed in the design to be the most severe (hypothetical) accident. Even having the most conservative estimation of such an accident with depressurization in the primary circuit, it was shown that graphite in a core is oxidizing (burning) slowly and one has many dozen hours to locate and put out the accident.

The effective measure to sufficiently decrease or to prevent completely graphite oxidization in a core in the depressurization accident can be the protection system based on accidental inert gas supply into reactor vault.

A safety containment considered in the design operates as protection against external impact, prevents activity release to environment, as well as reduces intensive oxidization of a core.

The further step to preclude such accidents will be development of protective barriers on FE and on reflector blocks to ensure resistance of FE against air at high temperatures in the case of severe and hypothetical accidents.

A protective barrier is not only protecting FE against oxidization and disruption under interaction with air and water, but preventing water absorption by the FE graphite as well, precluding the possibility of reactivity growth. A protective barrier on fuel elements also allows to make requirements to the spent FE storage less strict, ensuring their safety on fire or flooding of a storage facility.

A problem to intensify works on development of non-combustible fuel elements for HTGR has occurred after analysis of Chernobyl accident and its consequences because it has become obvious that all significant releases of radioactivity in accidents, including graphite oxidization, are to be ruled out.

It has been shown by preliminary analysis that one of the practical methods is to construct the protective barrier from silicon carbide. Technological works along this line in Russia have begun in 1988-1990. In first experiments it has been found that silicon additives in a cladding of a fuel element will sufficiently (2 orders) increase FE oxidization resistance in air. To compensate neutron absorption by silicon it is enough to slightly increase, for example, enrichment (for MVGR reactor from 8% to 9-10%), that will be insignificant for technical and

economic properties of a facility. To prevent rather high wear of FEs, graphite stack and channels, it is expedient to arrange protective barrier from SiC to be an abrasive located slightly under surface of a FE or a reflector retaining tribological and wear characteristics of graphite.

Such FEs ensure very low release levels in any severe accidents - preliminary assessed value is less than 20 Ku due to cesium-137 and less than 200 Ku due to iodine.

Our opinion is that proposed concept of fuel element and reflector protection against oxidization is additional measure to improve HTGR safety in severe accidents.

5. CONCLUSIONS

In our opinion, the HTGR reactors are, in spite of unsuccessful attempt of their commercial application in several countries, the most advanced type of reactors for NP. The accumulated positive experience in safe and reliable operation enables to anticipate that ecologically pure reactor, meeting the advanced modern requirements on population and environment protection against radioactivity, will be constructed.

Construction of pilot HTGR reactors in Japan and China, joint design development of high-powered HTGR with GTC in USA and Russia, activities of these and other countries, under the aegis of IAEA, demonstrate a trend of developed countries to introduce this advanced generation of reactors.

There is also a potential market for modular HTGR in small and developing countries.

On the other hand, in order to succeed in HTGR introduction a number of key problems on developing mature technology of new reactor generation is needed to be solved. According to that, it is important to join efforts and experience of countries involved in activities on HTGR. Despite of differences in concepts and actual engineering implementation of HTGR in different countries, there is a wide field of common problems to be effectively solved in active international cooperation.

The real step may be in development, with participation of several countries involved in this technology, of international modular HTGR project.

REFERENCES

1. N.N.Ponomarev-Stepnoi, V.N.Grebennik, E.S.Glushkov et al., "The Workshop on the Modular High-Temperature Gas-Cooled Reactors as Option for Future Nuclear Power Generation", July 13-14, 1995, GTDC, Vienna.

2. V.N.Grebennik, "Status of Works on HTGR in the World", Nuclear Hydrogen and Technology, Issue 7, Energoatomizdat, 1986, 232 p, Moscow.

3. N.N.Ponomarev-Stepnoi, V.N.Grebennik, E.S.Glushkov, "Development Prospects of High-Temperature Gas-Cooled Reactors and their Role in Nuclear Power", June 19-20, 1989, Dimitrovgrad, USSR.

2.3 High-Temperature Reactor developments in The Netherlands

R.P.C. Schram, E.H.P. Cordfunke and A.I. van Heek
Netherlands Energy Research Foundation ECN,
P.O. Box 1, 1755 ZG Petten, The Netherlands

Abstract

The high-temperature reactor development in the Netherlands is embedded in the WHITE reactor program, in which several Dutch research institutes and engineering companies participate. The activities within the WHITE program are focused on the development of a small scale HTR for combined heat and power generation. In 1995, design choices for a pebble bed reactor were made at ECN. The first concept HTR will have a closed cycle helium turbine and a power level of 40 MWth. It is intended to make the market introduction of a commercially competitive HTR feasible. The design will be an optimization of the Peu-à-Peu (PAP) concept of KFA Jülich. Computer codes necessary for the evaluation of reactor physics aspects of this reactor are developed in cooperation with international partners. An evaluation of a 20 MWth PAP concept showed that the maximum fuel temperature after depressurization does not exceed 1300 $^{\circ}C$.

As a part of the HTR program at ECN, chemical aspects of HTR fuel and coated particles are studied. Experimental work on the oxidation resistance of coating materials and fission product attack on coating materials as well as thermochemical calculations of the fuel particles are done at ECN. The concept-HTR of ECN is fuelled with UO_2, but the use of thorium is considered. The composition of the fuel determines the oxygen potential, which plays a key role in chemical safety of the fuel. Thermochemical calculations of the chemical form of cesium inside the HTR fuel particles were performed for a wide oxygen potential range. The chemical form of cesium determines the cesium pressure inside the fuel particle, which in turn determines the release behavior of Cs from defective particles. At normal operating temperatures and low oxygen potentials, the chemical form of cesium is $C_{60}Cs$. It is known that cesium carbon compounds decompose above 650 $^{\circ}C$ in vacuum. The stability of these compounds in the fuel particles at high temperatures (1000-1600 $^{\circ}C$) is questioned. Decomposition of these compounds may result in high cesium pressures even at normal operating conditions. Experimental work on the thermodynamic properties of cesium compounds at high temperatures is currently performed.

1 Introduction

In 1993, ECN started the WHITE (Widely applicable High Temperature Reactor) program, for the development of a safe and enviromental-friendly high-temperature reactor HTR. This modular-type HTR is considered as an interesting option for small scale combined heat and power generation in the Netherlands. In 1995 some design choices were made and at present the WHITE program focuses on an optimized concept based on the Peu-à-Peu design of KfA Jülich [1]. A small pebble bed reactor with a closed cycle gas turbine is chosen, the power level of the current concept is 40 MWth. The design is very simple; no emergency cooling system, backup shutdown systems or containments should be needed. The reactor will shut down after a core heat accident due to the negative temperature coefficient. Even in the worst case, the fuel temperature does not exceed 1300 °C. The TRISO-coated fuel particles contain uranium oxide fuel kernels. The use of thorium will also be considered.

The activities of ECN within the WHITE program include studies of the reactor physics of the HTR, as well as chemical aspects of the fuel. Physics aspects of the HTR being studied include safety analyses, optimization of the design and the thorium fuel cycle. The chemical studies concern the oxidation and Pd-attack of coating materials, the stability of carbide fuel, and the thermochemical processes inside the fuel particles during normal and off-normal conditions.

Thermochemical properties of reactor materials are vital for fuel fabrication, reprocessing and behaviour of the fuel during reactor operation. The understanding of the processes in the fuel particle, such as thermal migration and corrosion of the SiC coating, requires thorough knowledge of chemical reactions inside the particles. The release of fission products from defect particles, the interaction of fission products with the coating layers are important issues of HTR safety. The long term stability of stored HTR-waste (i.e. the integrity of the fuel particle and elements, the corrosion resistance of the coating layers) may be estimated by means of thermochemical assessments based on accurate experimental data.

In order to study the above mentioned processes, the nuclear chemistry group at ECN performs thermodynamic measurements of compounds that appear in nuclear systems. Data of various compounds are collected and continuously updated in a Thermodynamic Database (TBASE), part of which is published [2]. As an example of this thermochemical research, the chemical form of one of the hazardous fission products, Cs, in the HTR fuel particle will be discussed in this paper.

In the interior of the TRISO-coated fuel particle, a porous carbon layer is used for the retention of fission products. Fission products such as cesium are absorbed on carbon [3] but can also form lamellar cesium carbon (CsC_n) compounds. Kwasny, Hilpert and Nickel [4] have

performed an extensive series of measurements of the sorption of cesium on various types of graphite at 950-1820 K. The formation and decomposition of intercalation compounds with the formula CsC_n (n=8,10,24,36,48,60) was studied by Aronson and Salzano [5]. The same authors also measured the cesium vapour pressure of these compounds in the temperature range 670-1070 K [6, 7].

Thermochemical calculations of Minato *et al.* [8], show that the predominant chemical form of cesium inside the carbon buffer layer is Cs_2MoO_4 for temperatures up to 1600-1800 K. For temperatures higher than 1800 K cesium carbon compounds, CsC_n, are formed. Aronson and Salzano [5] have studied the decomposition of lamellar cesium graphite compounds and found that all compounds (CsC_n) have decomposed at 923 K *in vacuo*. Tromp and Cordfunke [9] state that the stability of KC_n compounds in a purified helium-flow is limited to a temperature of 875 K. The question that rises is: Are the CsC_n compounds stable at temperatures up to 1600 K? It may be that the cesium carbon compounds are stabilized by their own Cs pressure inside the HTR fuel particle, even at elevated temperatures. Decomposition of the cesium carbon compounds may result in a sudden increase of the cesium pressure inside the fuel particle. However, no thermodynamic measurements of CsC_n above 1080 K are available in literature.

Obviously, the chemical form of the relatively large amount of cesium inside the HTR fuel particle is of great importance for estimates of the release of cesium under normal/off-normal conditions.

2 Formation of cesium carbon compounds

Salzano and Aronson studied the stability and the equilibrium Cs vapour pressures of CsC_n compounds in the temperature range 400-800 Celsius using Knudsen effusion in conjunction with a tracer technique [5, 6, 7, 10]. From the vapour pressure measurements, they derived the Gibbs energy of formation of CsC_n [7], described by:

$$nC(s) + Cs(g) \rightleftharpoons CsC_n(s) \tag{1}$$

The thermodynamic parameters of the formation of cesium intercalates are given in Reference [7]. We have used these data and the thermodynamic data of C(s) [11] and Cs(g) [2] to calculate the Gibbs energy function of CsC_n. These thermodynamic data were used for further thermodynamic calculations.

The vapour pressure of cesium in a carbon enviroment is plotted in Figure 1. In the figure the threshold Cs-pressure for the formation of Cs intercalates is shown. From their vapour pressure measurements Aronson and Salzano [10] derived the equation:

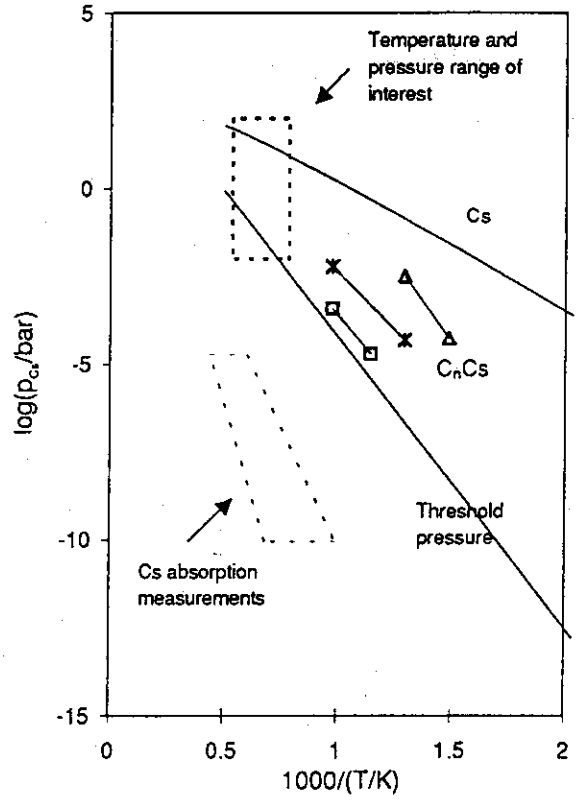


Figure 1: Cesium vapour pressures [7]: (□): $C_{60}Cs/C_{48}Cs$; (*) $C_{24}Cs/C_{10}Cs$; (Δ): $C_{10}Cs/C_8Cs$. Dashed area refers to the sorption measurements [3]. Upper solid line is the vapour pressure of pure Cs, the lower solid line is the threshold pressure for the formation of intercalation compounds 2. The dashed box refers to the temperature range of 1273-1873 K for which no thermodynamic data of CsC_n are available.

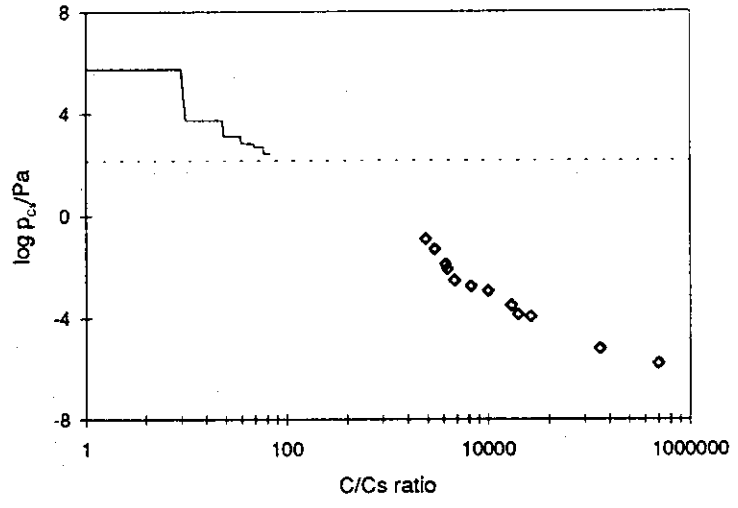


Figure 2: Cesium pressure versus C/Cs ratio, T=1200 K. Solid line: Intercalates [7] ; Dashed curve: threshold pressure (Eq. 2). ◇ Sorption measurements [4]

$$\ln p_{Cs}/\mathrm{bar} = -\frac{158992}{RT} + \frac{78.34}{R} \tag{2}$$

For cesium pressures below the threshold pressure cesium absorbs on carbon and above the threshold pressure cesium intercalates are formed. The predicted threshold pressure was experimentally verified by Merz and Scharf [12] for pyrographite and reactor graphite. As the threshold pressure is exceeded, $C_{60}Cs$ is formed. Further increase of the pressure leads to formation of $C_{48}Cs$, $C_{36}Cs$ etc. and finally a C_8Cs/Cs mixture remains. Note that the measurements of Aronson and Salzano are performed in a limited temperature range. Extrapolation of the $C_8Cs/C_{10}Cs$ vapour pressure curve shows that C_8Cs cannot be stable above 1000 K, even if the cesium pressure is increased. The question is whether the other intercalates are stable at temperatures up to the maximum fuel temperature of the HTR (1873 K). Below the threshold pressure sorption of Cs on graphite takes place, as was extensively studied by Kwasny, Hilpert and Nickel [4]. Vapour pressures of cesium were measured using Knudsen effusion and mass spectrometry for different cesium concentrations. In Figure 2 the cesium vapour pressures for the intercalates [7] and of chemisorbed cesium Kwasny [4] extrapolated to 1200 K are shown. The data are plotted versus the carbon/cesium ratio in the condensed phase. For large cesium concentrations (small C/Cs ratio) the cesium pressure changes stepwise at C/Cs = 8,10,24 etc. Below the threshold pressure sorption of cesium on carbon is expected. In the HTR fuel particle, the overall C/Cs ratio can be as large as 160 (see Table 1), so that formation of intercalates may be expected.

3 Chemical form of cesium

Both the cesium pressure and the oxygen potential play an important role for the chemical form of cesium in the condensed phase. As was pointed out by Lindemer [13] cesium molybdate is the stable form of Cs if a certain oxygen potential is exceeded. Since MoC is the stable form of Mo in a carbon enviroment, the formation of cesium molybdate from MoC has to be considered:

$$C_nCs(s) + MoC(s) + 2O_2(g) + Cs(g) \rightleftharpoons Cs_2MoO_4(s) + (n+1)C(s) \tag{3}$$

The formation of Cs_2MoO_4 and MoO_2 are given by the following reactions:

$$\begin{aligned} MoC(s) + 2Cs(g) + 2O_2(g) &\rightleftharpoons Cs_2MoO_4(s) + C(s) \\ MoC(s) + O_2(g) &\rightleftharpoons MoO_2(s) + C(s) \end{aligned} \tag{4}$$

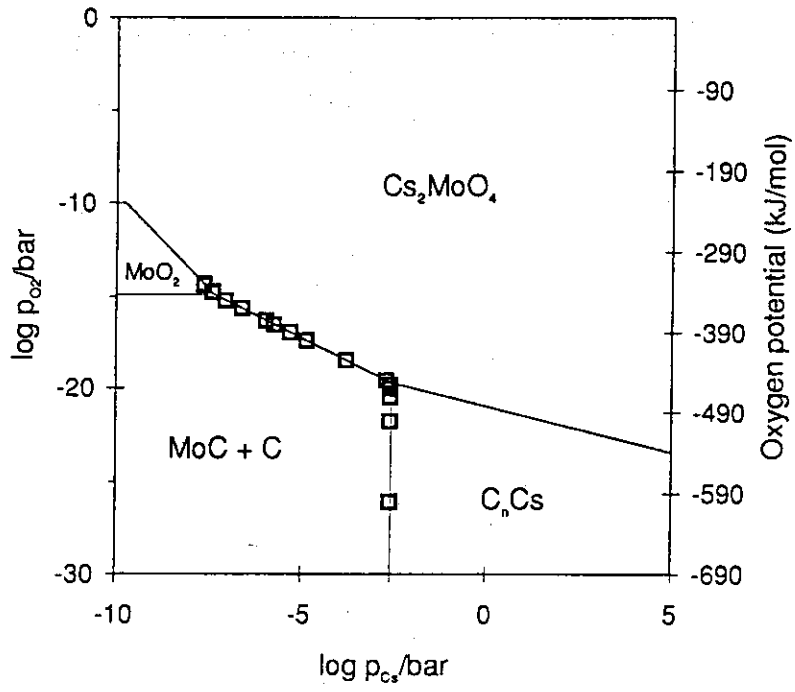


Figure 3: Predominance area diagram of the C-Cs-Mo-O system at 1200 K. The boxes refer to the calculations of the HTR fuel at 5.5 % FIMA and 1200 K.

As was shown by Cordfunke and Konings [14] Cs_2ZrO_3 can be formed at low oxygen potentials from ZrO_2. At T=1200 K Cs_2ZrO_3 is formed below an oxygen potential of -508 $kJ \cdot mol^{-1}$ at a minimum cesium pressure of 0.16 bar.

At the normal fuel temperature of the HTR (1200 K) the threshold oxygen potential for the formation of Cs_2MoO_4 out of $C_{60}Cs$ is -460 $kJ \cdot mol^{-1}$. C_nCs is more stable than Cs_2ZrO_3 according to the present calculations, but it should be stressed that these calculations are based on extrapolations of the thermodynamic measurements of $C_{60}Cs$ [6, 7] that were performed in the range 670-1070 K. The thermodynamic parameters Cs_2ZrO_3 at room temperature were taken from [2], and were recently updated with enthalpy increment measurements up to 640 K. The thermodynamic properties of both cesium compounds at HTR fuel conditions are presently experimentally determined at ECN.

4 Thermodynamic calculations of the HTR particle

During the lifetime of a fuel particle both the burnup and the fuel temperature will change. The burnup and the temperature are the most important parameters for the thermochemical description of the fuel, for they determine the inventory of the particle, the oxygen potential,

Table 1: Inventory of the HTR fuel particle at 5.5 % FIMA [8]

	Amount (10^{-8} mol)	mol %
C	755.00	62.44
UO_2	411.08	34.00
Total F.P.	43.01	3.56
Kr	0.74	0.06
Rb	0.70	0.06
Sr	1.78	0.15
Zr	6.49	0.54
Mo	5.74	0.47
Tc	1.47	0.12
Ru	3.63	0.30
Rh	1.03	0.08
Te	0.57	0.05
I	0.29	0.02
Xe	5.32	0.44
Cs	4.79	0.40
Ba	1.57	0.13
La	1.46	0.12
Ce	2.75	0.23
Nd	4.62	0.38
Eu	0.07	0.01

the chemical form of the fission products and the pressure inside the fuel particle. For the present calculations TRISO-coated UO_2 fuel particles will be considered. The fuel kernel is coated with a porous carbon layer, an inner PyC layer, a SiC coating and an outer PyC layer, but in the present case only the fuel kernel and the porous carbon layer are taken into account. It will be assumed that the PyC layers and the SiC coating remain intact, and no gas transport through these layers will take place. Normal conditions are assumed; the fuel temperature is 1200 K, and the burnup is 5.5 % FIMA. Both the particle dimensions and the inventory at 5.5 % FIMA are taken from the study of Minato *et al.* (Reference [8]) and are summarized in Table 1. The buffer volume of the porous carbon layer is 3.14×10^{-11} m^3 [8], and the total amount of carbon is 7.55×10^{-6} mole and the initial amount of uranium oxide is 4.35×10^{-6} mole. At 5.5 % FIMA 4.11×10^{-6} mole of UO_2 remains and 0.48×10^{-6} mole of fission product is formed, which are specified in Table 1. It is commonly assumed that the oxygen potential increases with increasing burnup [15], although this could not be confirmed experimentally by Matzke [16]. Since the burnup dependence of the oxygen potential remains a point of discussion in literature, the calculations are performed as a function of the oxygen potential. The thermochemical calculations are performed using the ChemSage code [17]. The

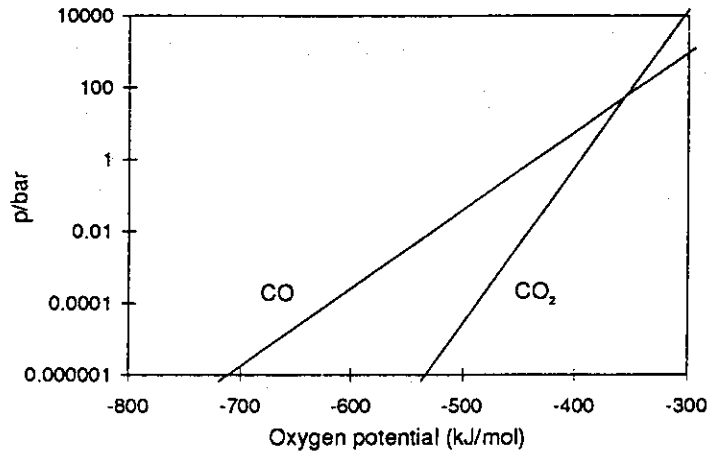


Figure 4: Pressure of CO and CO_2 as a function of the oxygen potential assuming an excess of carbon. T=1200 K

thermochemical data were taken from the ECN thermodynamic database [2]. The condensed compounds that were used in the present calculations are listed in Table 2.

Because of the excess amount of carbon inside the fuel particle, the CO and CO_2 pressures can be become quite large. This is demonstrated in Figure 4, where both pressures are plotted as function of the oxygen potential at 1200 K. The CO/CO_2 equilibrium plays an important

Table 2: List of compounds used in thermochemical calculations [2]

Solids				Gases			
Ba	CeO_2	La	$SrUO_4(\beta)$	Ba	Cs_2I_2	La_2O_2	SrO
$BaMoO_4$	Cs	La_2O_3	$SrZrO_3$	Ba_2	Cs_2MoO_4	LaO	Tc
BaO	$Cs_2Mo_2O_7$	$La_2Zr_2O_7$	Tc	$BaMoO_4$	Cs_2O	Mo	Te
BaU_2O_7	Cs_2MoO_4	Mo	Te	BaO	Cs_2O_2	Mo_2	Te_2
$BaUO_3$	Cs_2O	MoC	TeO_2	C	CsI	Nd	TeO
$BaUO_4$	Cs_2Te	MoO_2	U	C_2	CsO	NdO	TeO_2
$BaZrO_3$	$Cs_2U_2O_7$	Nd	UO_2	C_3	CsTe	NdO_2	UO
C	$Cs_2U_4O_{12}$	Nd_2O_3	$UO_3(\beta)$	C_4	Eu	O	UO_2
C_8Cs	Cs_2UO_4	Rb	$UO_3(\gamma)$	C_5	Eu_2O	O_2	UO_3
$C_{10}Cs$	Cs_2ZrO_3	Rh	Zr	Ce	Eu_2O_2	O_3	Xe
$C_{24}Cs$	CsI	Ru	ZrO_2	CeO	EuO	Rb	Zr
$C_{36}Cs$	Eu	Sr		CeO_2	I	Rb_2	ZrO
$C_{48}Cs$	$Eu_2O_3(\beta)$	Sr_2ZrO_4		CO	I_2	Rh	ZrO_2
$C_{60}Cs$	$Eu_2O_3(\gamma)$	$Sr_3Zr_2O_7$		CO_2	Kr	Ru	
Ce	EuO	$Sr_4Zr_3O_{10}$		Cs	La	Sr	
Ce_2O_3	I_2	SrO		Cs_2	La_2O	Sr_2	

role in the thermal migration (or amoeba effect) of the fuel kernel up the temperature gradient. When the PyC layer becomes defective due to the amoeba effect, CO gas can oxidize the SiC layer.

The thermodynamic calculations of the HTR fuel particle based on the inventory of Table 1 showed that the total pressure inside the buffer volume (at T=1200 K and 5.5 % FIMA) is 200 bar, which is essentially the sum of the Xe (170 bar) and the Kr (24 bar). The actual noble gas pressure may be lower since part of the noble gases remains dissolved in the fuel kernel. Only at high oxygen potentials (larger than ≈ -390 $kJ \cdot mol^{-1}$) the contribution of the CO and CO_2 pressure to the total pressure is significant which is shown in Figure 5. In the same plot the partial pressure of some cesium compounds are shown. The predominant chemical form of Cs in the gas phase is a saturated CsI vapour with a partial pressure of 0.033 bar. Cesium iodine (CsI) is the dominant chemical form of Iodine in both the condensed and the gas phase. Only 6 % of the total amount of cesium is present as CsI. (Figure 6). The CsI pressure is independent of the oxygen potential which shows that condensed CsI is a very stable compound. $C_{60}Cs$ is the most stable compound up to -460 $kJ \cdot mol^{-1}$, and Cs_2MoO_4 is found at higher oxygen potentials. At -390 $kJ \cdot mol^{-1}$ Cs_2Te disappears and more Cs_2MoO_4 is formed.

Post-irradation studies on uranium oxide revealed that molybdenum is found in metallic precipitates ("white inclusions") in the fuel [15]. The present study indicates that the thermodynamic stable form of Mo in the carbon-rich enviroment of the HTR particle is molybdenum carbide. The chemical form of Mo in the condensed phase is shown in Figure 7. Oxidation of Mo occurs at oxygen potentials larger than -342 $kJ \cdot mol^{-1}$. At lower oxygen potentials Cs_2MoO_4 (-452 $kJ \cdot mol^{-1}$) and $BaMoO_4$ (-370 $kJ \cdot mol^{-1}$) are formed.

In Figure 8 it is shown that a large portion (about 27 %) of the porous carbon layer used for the formation of $C_{60}Cs$. For oxygen potentials larger than -452 $kJ \cdot mol^{-1}$cesium forms cesium molybdate and $C_{60}Cs$ disappears.

It is interesting to compare the thermodynamic calculations with the predominance diagram Figure 3. The cesium pressures were calculated in the oxygen potential range from -800 to -330 $kJ \cdot mol^{-1}$, and the results are plotted in Figure 3. For the lowest oxygen potentials the cesium pressure is controlled by the $C/C_{60}Cs$ equilibrium. For larger oxygen potentials (>-452 $kJ \cdot mol^{-1}$) the cesium pressure decreases moves along the MoC/Cs_2MoO_4 phase line. For the highest oxygen potentials (> -342 $kJ \cdot mol^{-1}$) MoO_2 is formed. This plot shows that as the oxygen potentials increases the partial cesium pressure decreases. The total amount of Cs in the vapour phase, however, is governed by the CsI pressure which was constant for all oxygen potentials. When both $C_{60}Cs$ and Cs_2ZrO_3 are not stable at 1200 K, however, the cesium pressure can reach high values. When no cesium compounds exist at this temperature the cesium pressure can increase to a maximum of 152 bar at 5.5 % FIMA.

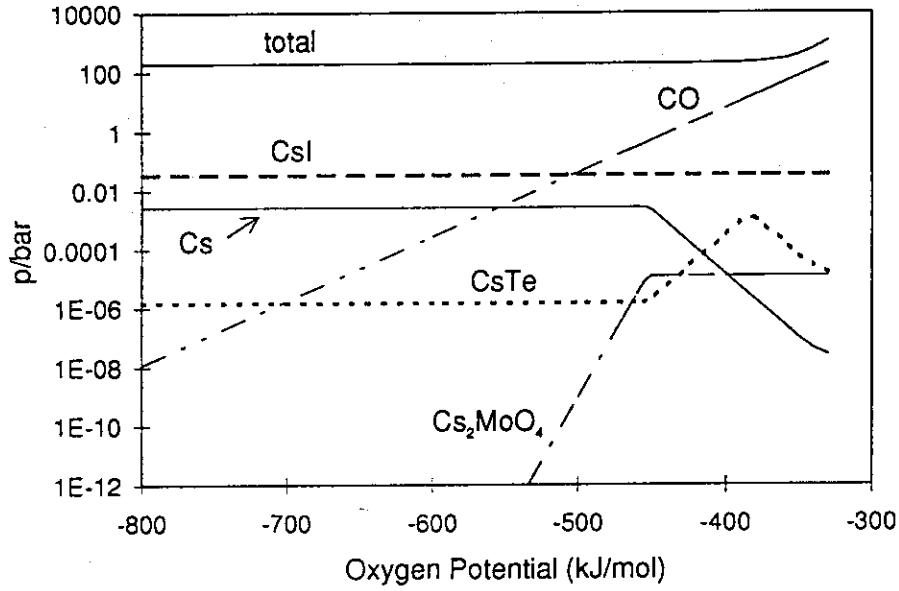


Figure 5: Pressure of different compounds in the HTR-particle buffer volume at T = 1200 K, and 5.5 % FIMA

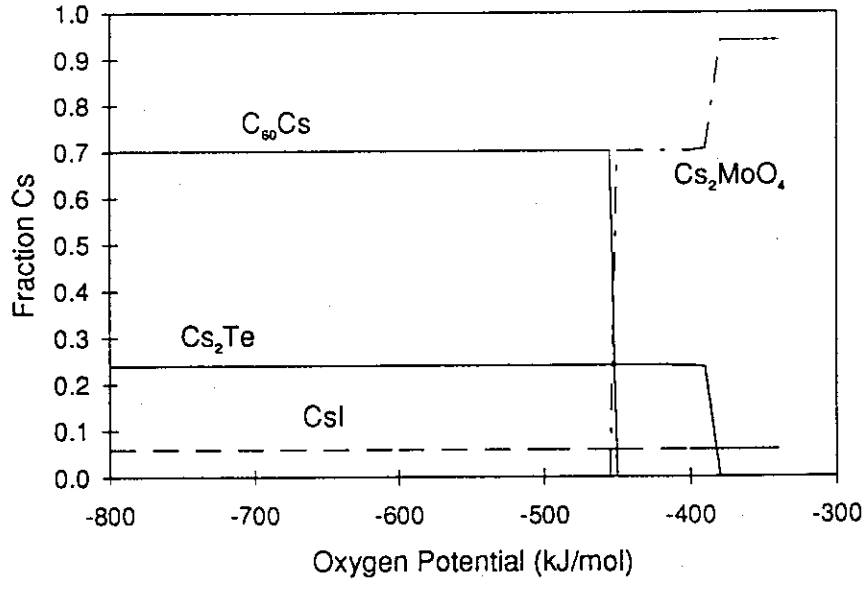


Figure 6: Fraction of Cs in the condensed phase

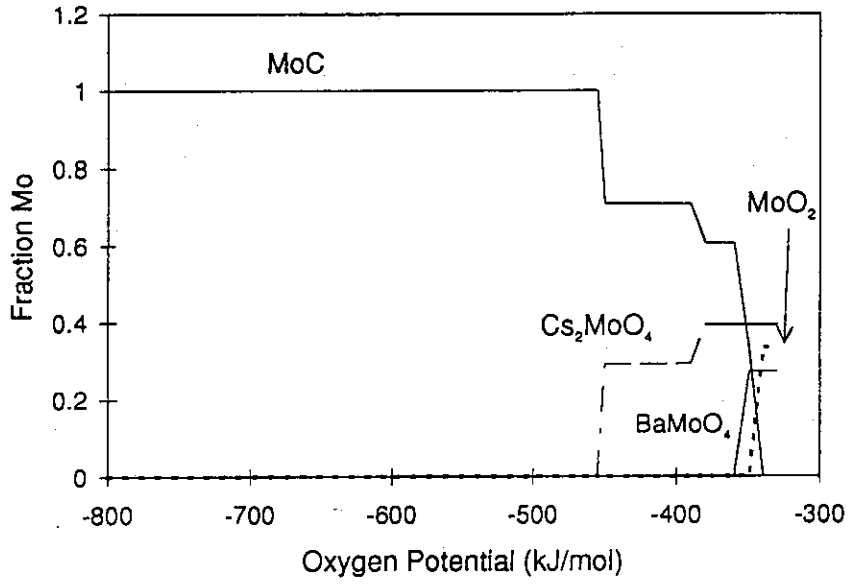


Figure 7: Fraction of Mo in the condensed phase

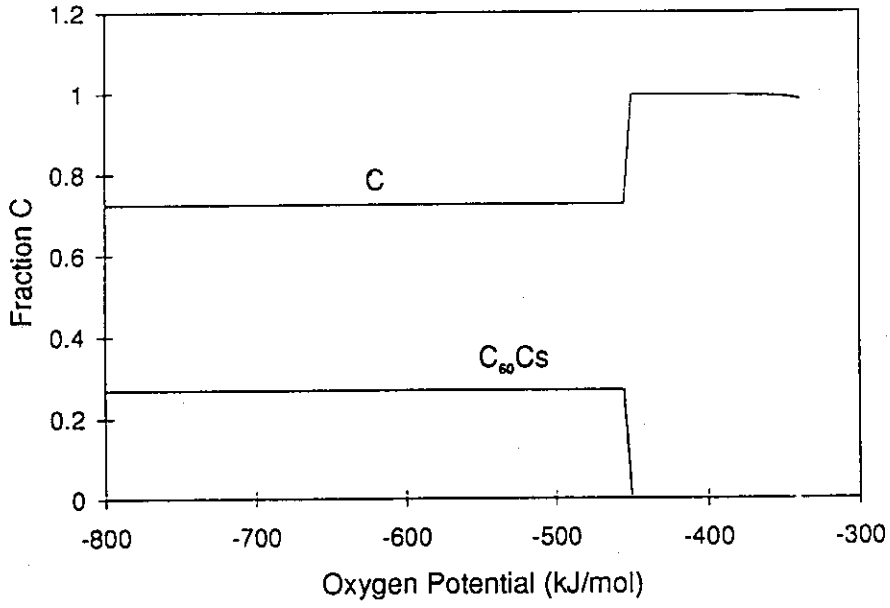


Figure 8: Fraction of C in the condensed phase

5 Conclusion

After a familiarization phase the Dutch HTR program is well underway. The HTR developments have resulted in design choices for a small Peu-à-Peu HTR. The reactor will be fuelled with spherical fuel elements, filled with UO_2 fuel particles. Part of the HTR research at ECN deals with the chemistry of the TRISO-coated fuel particles. Thermochemical calculations show that the predominant chemical form of Cs in the condensed phase inside the HTR fuel particle is, depending on the oxygen potential, either $C_{60}Cs$ or Cs_2MoO_4. In the vapour phase inside the buffer volume of the fuel particle, CsI is the predominant form of Cs. For these calculations, extrapolated thermochemical data of the cesium intercalates and Cs_2ZrO_3 had to be used. Stability measurements of both compounds in the temperature range 1200-1800 K are required. Decomposition of these compounds in this temperature range can give a considerable increase in the cesium pressure.

References

[1] H. Gerwin E. Teuchert and K.A. Haas. Simplification of the pebble bed high-temperature reactor. In *International Specialists' Meeting on Potential of Small Nuclear Reactors for Future Clean and Safe Energy Sources, Tokyo, October 23-25*, 1991.

[2] E.H.P. Cordfunke and R.J.M. Konings. *Thermochemical data for reactor materials and fission products.* Elsevier Science Publishers, 1990.

[3] R. Moormann and K. Hilpert. Chemical behavior of fission products in core heatup accidents in high-temperature gas-cooled reactors. *Nucl.Technol.*, 94:56–67, 1991.

[4] J. Kwasny, K. Hilpert, and H. Nickel. Investigation of the sorption of cesium by graphitic reactor materials. Juel-2353, Forschungszentrum Jülich Gmbh, 1990.

[5] F.J. Salzano and S. Aronson. Kinetic study of the decompostion of cesium-graphite lamellar compounds. *J.Chem.Phys.*, 42(3):1323–1330, 1965.

[6] F.J. Salzano and S. Aronson. Thermodynamic properties of the cesium-graphite lamellar compounds. *J.Chem.Phys.*, 43(1):149–154, 1965.

[7] F.J. Salzano and S. Aronson. Stability of phases in the cesium-graphite system. *J.Chem.Phys.*, 45(6):2221–2227, 1966.

[8] K. Minato, T. Ogawa, K. Fukuda, M. Shimizu, Y. Tayama, and I. Takahashi. Fission product behavior in Triso-coated UO_2 fuel particles. *J.Nucl.Mater.*, 208:266–281, 1994.

[9] P.J.J. Tromp and E.H.P. Cordfunke. A thermochemical study of the reactive intermediate in the alkali-catalyzed carbon gasification. I. x-ray diffraction results on the alkali-carbon interaction. *Thermochim.Acta*, 77:49–58, 1984.

[10] F.J. Salzano and S. Aronson. The compatibility of Graphite with Cesium. *Nucl.Sci.Eng.*, 28:51–54, 1967.

[11] L.V. Gurvich, I.V. Veyts, and C.B. Alcock. *Thermodynamic properties of individual substances.* Hemisphere Publishing Corporation, 4th edition, 1991.

[12] E. Merz and H. Scharf. Zum Verhalten von Spalt-Caesium in graphithaltigen Brennelementen. *Atomkernenergie*, 17(4):287–292, 1971.

[13] T.B. Lindemer. Chemical thermodynamics of iodine species in the HTGR fuel particle. *Calphad*, 7(2):87–102, 1983.

[14] E.H.P. Cordfunke and R.J.M. Konings. The release of fission products from degraded UO_2 fuel: Thermochemical aspects. *J.Nucl.Mater.*, 201:57–69, 1993.

[15] H. Kleykamp. The chemical state of the fission products in oxide fuels. *J.Nucl.Mater.*, 131:221–246, 1985.

[16] A. Nakamura and T. Fujino. Thermodynamic analysis on point defects of UO_{2+x} at relatively small deviation from stoichiometry between 600 and 1400 $^{\circ}C$. *J.Nucl.Mater.*, 140:113–130, 1986.

[17] G. Eriksson and K. Hack. ChemSage - A computer program for the calculation of complex chemical equilibria. *Metall.Trans.*, 21B:1013–1023, 1989.

2.4 STATUS OF THE GT-MHR

A. J. Neylan and W. A. Simon (General Atomics)

Abstract

The Gas Turbine-Modular Helium Reactor (GT-MHR) program in the U.S. sustained a major setback with the recent Congressional decision to fund only an orderly closeout in fiscal year 1996. The program fell victim to the current Administration's strong anti advanced reactor sentiment and the U.S. Congress' effort toward balancing the budget. Despite this reality, and driven by its conviction that the GT-MHR simply is too good to let go, General Atomics (GA) remains committed to a continuing program.

Clearly, within the spectrum of nuclear options, gas reactors have unique high-temperature capabilities. With state-of-the-art technology, they can be applied to modern steam power conversion equipment and a wide range of industrial process heat and cogeneration applications. In particular, because of its helium coolant, the reactor is unique in that it can be coupled to closed-cycle gas turbine power conversion equipment. The direct cycle GT-MHR has been evaluated to have:

- the highest safety margins of any current or proposed nuclear power plant (it is "meltdown proof"!);
- about 50% higher efficiency than current or proposed nuclear-generating systems;
- highly competitive power generation costs;
- the least environmental impact of any nuclear alternative (significantly less thermal discharge and spent fuel per unit of electricity generated);
- utilizing ceramically coated fuel, the capability to use alternative fuel cycles, e.g., low/highly enriched uranium and/or plutonium; and
- superior radionuclide retention for long-term spent fuel disposal.

This paper discusses the background and status of the GT-MHR design and the opportunity to move forward in an international cooperative program.

INTRODUCTION

The GT-MHR is a second generation meltdown-proof nuclear power plant that is under development and planned to be operational early in the next century. The plant design evolved from the more than 50 gas cooled nuclear reactors which have operated worldwide, and the more recent advances in industrial gas turbine, plate-fin recuperator, and magnetic bearing technology. Five helium cooled reactors, which operated into the 1970's, demonstrated the inherent characteristics of a helium cooled reactor design: inert, single phase coolant: refractory coated particle nuclear fuel which prevents significant release of fission products at temperatures of up to about 2000°C; and high heat capacity structural graphite providing long thermal response times and high temperature stability. In the 1980s, under the sponsorship of the U.S. Department of Energy, the modular gas cooled reactor design emerged with inherent passive characteristics that provided the capability of meeting stringent safety goals without relying on active safety systems or operator action.

By 1992, advances in industrial gas turbine technology and related equipment suggested that the unique high temperature capability of the reactor could be economically coupled to a closed cycle helium turbine using the Brayton cycle. The small passively safe modular helium reactor size matched available gas turbine sizes. Magnetic bearings had become commercially proven. Highly efficient, compact plate-fin recuperator designs had become available. And because forced cooling is not relied on for safety, turbine failures posed no nuclear consequence. With this technology available, the GT-MHR evolved from the steam cycle design and promises significant (~30%) reductions in power generating costs. A standard plant comprised of 4x600 MWt modules was selected based on utilizing existing technology and the ability to meet similar safety requirements as imposed on the former steam cycle plant (Ref. 1).

OVERALL GT-MHR PLANT CONFIGURATION

Since the power plant concept has been described previously (Refs. 1-4) only a summary will be given here. Each module is installed in a below grade reinforced concrete containment structure (Fig. 1). The module components are contained within three steel pressure vessels: a reactor vessel, a power conversion vessel and a connecting cross vessel. The reactor vessel is made from 9 Cr-1 Mo-V alloy steel, and is approximately 8.3 m in diameter. It contains the reactor system which includes the annular reactor core, reactor internals, and neutron control assemblies.

The power conversion vessel, also ~8.3 m in diameter and made from 9 Cr-1 Mo-V material, contains the entire power conversion system, which consists of the helium turbomachine, recuperator, precooler and intercooler, and internal ducts and shroud supports. The turbomachine includes the turbine, compressors, generator, magnetic bearings, and supports and ducts. The recuperator is a compact plate-fin design. The precooler and intercooler are low temperature finned tube, helical bundle, helium to water heat exchangers that remove reject heat from the thermodynamic cycle.

The process flow diagram is shown on Fig. 2.

DESIGN STATUS

Significant progress has been made on the GT-MHR conceptual design since the power level evaluation and selection study in February 1994 (Ref. 1).

Although the focus and priority has concentrated on the power conversion module, considerable progress has also been made on the design of the 600 MWt core and related components. The reactor core system uses the same components and technology as that successfully demonstrated on Fort St. Vrain and further adopted for the annular core design in the prior steam cycle concepts. Reactor physics analyses confirm the acceptability of core design parameters, neutron control requirements, fuel loadings, operational stability and thermohydraulic behavior under normal, transient and accident conditions.

In addition, significant effort has been applied to assessing reactor performance under alternatives to the reference LEU fuel cycle. Specific emphasis has been put on the capability to destroy surplus weapons grade plutonium while concurrently generating electricity (Ref. 4). Erbium is used as a burnable poison to control excess reactivity and ensure a negative temperature coefficient at all times over life. No fertile material is used in this fuel cycle, and hence no additional fissile material, particularly plutonium, is produced. The loading of weapons-grade plutonium and the erbium poison loading are adjusted to provide the maximum fuel burnup and maintain the negative temperature coefficient over each cycle. Both the fuel and the poison are zoned to meet power peaking requirements and fuel temperature limits. The erbium poison is used in the form of coated erbium oxide particles formed into rods identical to the fuel rods and distributed in a uniform pattern in each fuel block. Design studies have shown that a three-year fuel cycle, in which one-third of the core is refueled each year, destroys 90% of the weapons-grade Pu-239 resulting in discharged fuel having high diversion resistance, due to the limited Pu per fuel block, and minimal attractiveness for subsequent weapons use. No recycling of the plutonium is required to achieve these high destruction levels, and the discharged fuel elements are suitable for disposal as is in a geologic waste repository.

The GT-MHR operating in the plutonium destruction mode described above also could take the plutonium discharged from an LWR and achieve the same high level of consumption as for weapons-grade plutonium.

The significant progress on the development of the power conversion module was reported at the IAEA Technical Committee Meeting on October 30-November 2, 1995 in Beijing, China (Ref. 6).

An experienced capable team needs to be credited for the status of the design and development of the power conversion system. AlliedSignal Aerospace (Tempe, Arizona, USA) had the overall responsibility as the turbomachine vendor, GEC-Alsthom (Belfort, France) worked on the generator and Mechanical Technology Inc. (Latham, New York, USA) worked on the magnetic and auxiliary catcher bearings. General Atomics, the overall system designer, has integrated this turbomachine team with the AlliedSignal (Torrance, California, USA) efforts on the helium recuperator and the ABB-CE (Windsor, Connecticut and Chattanooga, Tennessee, US) work on the precooler, intercooler and

pressure vessel. This team has addressed and identified solutions to many key design issues. Evaluation of an external versus internal (submerged) generator and modifications as a result of an internal seal task force were completed. Significant progress was made on the design of the generator utilizing existing technology. Conceptual design of the turbocompressor was confirmed, including extensive evaluation of the entire turbomachine (turbocompressor and generator) rotor dynamics. Results concluded in a somewhat revised configuration for the location and access to magnetic bearings supporting the entire machine. Integration of the turbomachine with the recuperator, precooler, intercooler and internal ducts and seals progressed to improve maintenance and operation.

The results of this progress continue to support earlier conclusions that there are no feasibility issues and that continued design and development can indeed lead to a breakthrough technology.

A key event in the U.S. GT-MHR program was the review by utility/Electric Power Research Institute representatives held June 20 and 21, 1995 at General Atomics in San Diego. The review was prompted by an Advanced Reactor Corporation report that characterized the GT-MHR as potentially a "breakthrough technology" due to its combination of built-in safety and high plant efficiency. The ARC report proposed that a broader, intensive review be conducted by utility representatives assembled by EPRI.

Two paragraphs are reproduced here from the subsequent EPRI report (Ref. 7).

> "The review team concludes that the GT-MHR makes bold and innovative use of emerging technologies that have the potential for much improved efficiency, simplification, and reduction of cost and waste. However, the current GT-MHR conceptual design needs substantial development, detailed design, experimental verification, and licensing effort before it can be viewed with confidence as a breakthrough technology that provides a technically and economically viable future option for potential utility customers."

> "The review team found no obvious show stoppers that would prevent the GT-MHR from eventually meeting regulatory safety goals and achieving the many technical and economic goals set by DOE and the design team. Meeting these goals is viewed as both a major challenge and a prerequisite to the GT-MHR joining the ALWR in future U.S. nuclear power plant deployment."

The EPRI review team concluded that development and testing could be completed within 7 years and a first plant could be deployed within 11 years. This compares to 10 years estimated by GA.

ECONOMICS

Preliminary economic assessments, using U.S. DOE prescribed guidelines, indicate that proposed operating costs for the four-module equilibrium GT-MHR plant rated at 600 MW(t) per module is in the range of 34 mills/kWh. This is about a 33% decrease in busbar power costs compared to the early 1980's design of the steam cycle MHTGR (Ref. 8). As shown in Table 1, these costs are

now competitive with even the combined cycle combustion gas turbine plants coming into service at the same time even if only modest real escalation in natural gas prices are assumed.

Table 1
Comparison of GT-MHR Equilibrium* Generation Costs with Power Generation Alternatives

	GT-MHR	Passive ALWR	Evolutionary ALWR	Integrated Gasified (Coal) Combined Cycle	Combined Cycle Gas Turbine
Performance Parameters					
Plant thermal rating, MW(t)	4x600	3659	3582	2625	2203
Net thermal efficiency, %	47.7	32.8	33.5	38.1	45.4
Plant electrical rating, MW(e)	4x286	2x600	1200	4x250	4x250
Plant capacity factor, %	84.0	80.0	80.0	84.0	84.0
Plant Economic Evaluation Results, 1992 Dollars					
Total capital cost, M$	1740	2034	1860	1611	531
Unit capital cost, $/kW(e)	1520	1695	1550	1611	531
Annual O&M, M$/yr	31.2	54.5	45.5	48.4	11.2
Fuel cost, $/MBTU	1.27	0.77	0.77	1.45	2.33
Fuel real escalation, $/yr	0.0	0.0	0.0	1.0	2.2
Levelized busbar generation costs, mills/kWh					
- Capital	19.6	23.2	21.2	21.5	7.1
- O&M	4.2	7.8	6.5	6.6	1.5
- Fuel	9.1	8.0	7.9	18.5	38.4
- Decommissioning	0.6	0.9	0.9	0.1	0.0
Total busbar costs	33.5	39.9	36.5	46.7	47.0

*For a standard plant coming on line in year 2015

POTENTIAL INTERNATIONAL PROJECT

The gas reactor has enjoyed international following for quite some time. Up to now, however, the development has largely been supported and conducted on a national basis. But "going it alone" carries considerable business risk and a large financial commitment. International collaboration would allow a pooling of resources and expertise to help meet the cost of bringing an advanced reactor technology, which the GT-MHR represents, to the market place.

The first significant step to broaden the GT-MHR program occurred as a result of discussions between officials of the Russian Ministry for Atomic Energy (MINATOM) and GA in early 1993.

Subsequently MINATOM and GA signed a Memorandum of Understanding for development and deployment of a GT-MHR in Russia that can be fueled with either uranium or weapons-grade plutonium. In 1994 a specific proposal was made by Russia to the U.S. government to cooperate in the design and construction of a GT-MHR at Tomsk to destroy excess weapons-grade plutonium and provide electric power to the surrounding community. An additional benefit would be progress in the conversion of the Russian weapons complex to the peaceful use of nuclear power and the employment of existing staff and facilities having plutonium handling and fabrication expertise. Pending the U.S. government response, continued development of the GT-MHR conceptual design is ongoing funded by MINATOM and GA.

The proposed joint program to be performed under an agreement between the participant countries would be implemented in two phases: (1) a design and development phase, and (2) a single power unit prototype plant construction, startup, and initial operation phase. The product of the first program phase would be the design, development of a prototype GT-MHR power unit, including testing of major components, and licensing. In the second phase, a prototype power unit would be built in Russia and used for Pu destruction. Successful operation of the prototype would provide data to support design certification of the GT-MHR in the U.S..

This cooperation makes the most effective use of combined resources and is an essential part of the strategy to continue GT-MHR development. It is estimated that this design and development program can be carried out at approximately one-third the cost of a U.S.-only development program. Further, it is anticipated that construction and operation of a demonstration plant in Russia also can be completed at approximately one-third the cost of a demonstration project carried out exclusively in the U.S..

GA's commitment to the GT-MHR is evident with the anticipation that renewed U.S. government support in the future is not out of the question. In the meantime, GA is fortifying the support base by looking to expand the roster of international participants and sponsors with the long-term goal to advance the design and eventually see GT-MHRs deployed on a worldwide basis.

At the same time GA is trimming its GT-MHR work force, but will retain a core group of gas reactor experts with know-how in all key areas of the GT-MHR. The principal ingredient in its strategy to advance the technology is to attract international support through cooperation in a reactor demonstration project.

CONCLUSIONS

Considerable progress has been made on the GT-MHR design since the concept was accepted as the U.S. reference design in February 1994. An experienced capable team has been assembled to address the design and development of the power conversion system. Alternative plutonium destruction concepts have been developed. Many key design issues have been addressed and solutions identified. The results of this progress and independent reviews continue to support earlier conclusions that there are no feasibility issues and that continued design and development can indeed lead to a breakthrough technology. The high efficiency and resulting power generation costs are competitive with alternative

power generation concepts. The design simplicity, modularization, passive safety and reduced environmental impact make the GT-MHR a strong contender for international deployment.

Despite recent setbacks in the U.S. government funded program, an opportunity exists to economically deploy a prototype plant in Russia which would also contribute to the destruction of weapons-grade plutonium and the conversion of weapons complex to peaceful purpose. GA continues to support the GT-MHR program and believes international cooperation on the Russian project is the key to success.

References:

1. U.S. DOE "Evaluation of the GT-MHR," DOE-GT-MHR-10002, issued by Gas Cooled Reactor Associates, February 1994.

2. Simon, W. A., A. J. Neylan, and F. A. Silady, "Design Features of the Gas Turbine Modular Helium reactor (GT-MHR)," Paper Presented at the 4th Annual Scientific & Technical Conference of the Nuclear Society "Nuclear Energy and Human Safety" (NE-93), June 28-July 2, 1993, Nizhny Novgorod, Russian Federation.

3. "GT-MHR Design, Performance, and Safety," (GA-A21924), "A. J. Neylan, A. Shenoy, F. A. Silady, and T. D. Dunn presented at the IAEA Technical Committee Meeting on "Development Status of Modular High Temperature Reactors and Their Future Role," November 28-30, 1994, ECN, Petten, The Netherlands.

4. "Gas Turbine Modular Helium Reactor (GT-MHR), A Multipurpose Passively Safe Next Generation Reactor," (GA-A21920, Rev. 1), A. J. Neylan, F. A. Silady, and A. M. Baxter presented at the 3rd International Conference on Nuclear Engineering, April 23-27, 1995, Kyoto, Japan.

5. "The GT-MHR for Destruction of Weapons Plutonium", A. M. Baxter, A. J. Neylan presented at the American Nuclear Society, June 25-29, 1995, Philadelphia, Pensylvania.

6. "Status of GT-MHR with Emphasis on The Power Conversion System," A. J. Neylan, F. A. Silady, B. Kohler, D. Lomba, and R. Rose, October 30-November 2, 1995, Beijing, China.

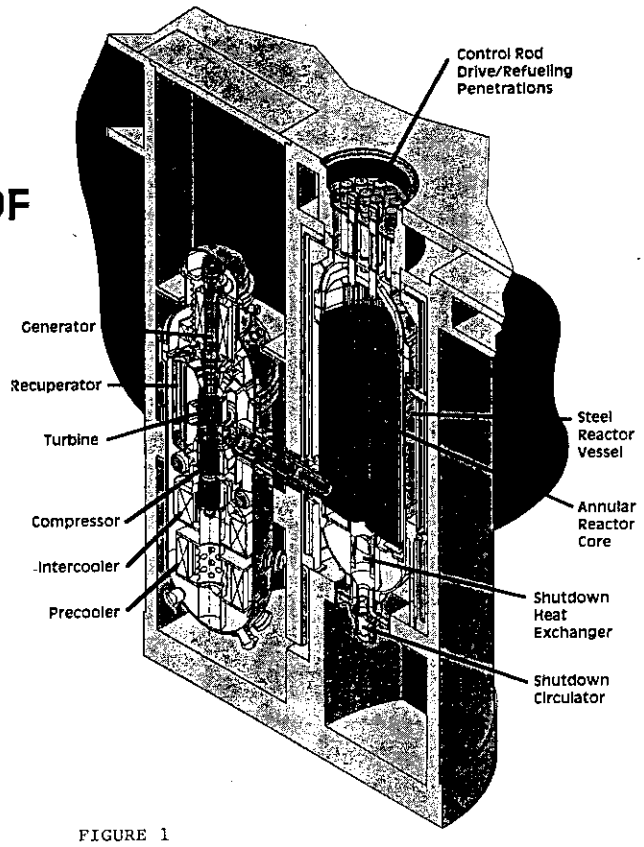
7. "Utility Industry Review of Design Progress on the Gas Turbine-Modular Helium Reactor," EPRI Report, September 1995.

8. LaBar, M. P., and W. A. Simon, "Comparative Economics of the GT-MHR and Power Generation Alternatives," GA-A21772, Paper Presented at the International Joint Power Generation Conference, October 3-5, 1994, Phoenix, AZ, USA.

GT-MHR COMBINES MELTDOWN-PROOF ADVANCED REACTOR AND GAS TURBINE

POWER LEVEL 600 MWt

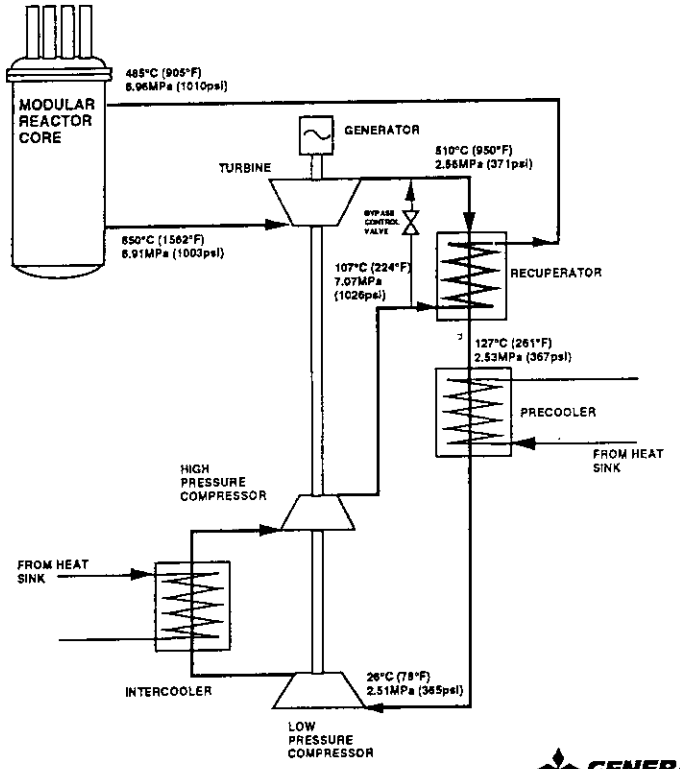
GENERAL ATOMICS



L-170(4)
8-1-94

FIGURE 1

FLOW SCHEMATIC



L-339(14)
11-15-94

GENERAL ATOMICS

FIGURE 2

3rd JAERI Symposium
on HTGR Technologies,
Oarai, Japan 15-16 Feb. 1996

2.5 Construction of the HTTR and its Testing Program

T. Tanaka, O. Baba, S. Shiozawa, M. Okubo and Y. Kambayashi
Department of HTTR Project
Japan Atomic Energy Research Institute
Narita-Cho, Oarai-Machi, Higashiibaraki-Gun, Ibaraki-Ken, Japan

Abstract

Concerning about global warming due to emission of greenhouse effect gas like CO_2, it is essentially important to make efforts to obtain more reliable and stable energy supply by extended use of nuclear energy including high temperature heat from nuclear reactors, because it can supply a large amount of energy and its plants emit only little amount of CO_2 during their lifetime. Hence, efforts are to be continuously devoted to establish and upgrade technologies of High Temperature Gas-cooled Reactor (HTGR) which can supply high-temperature heat with high thermal efficiency as well as high heat-utilizing efficiency. It is also expected that making basic researches at high temperature using HTGR will contribute to innovative basic research in future. Then, the construction of High Temperature engineering Test Reactor (HTTR), which is an HTGR with a maximum helium coolant temperature of 950 ℃ at the reactor outlet, was decided by the Japanese Atomic Energy Commission (JAEC) in 1987 and is now under way by the Japan Atomic Energy Research Institute (JAERI).

The construction of the HTTR started in March 1991, with first criticality in 1997 to be followed after commissioning testing. At present the HTTR reactor building and its containment vessel have been constructed and its main components, such as a reactor pressure vessel, an intermediate heat exchanger, hot gas pipings and core support structures, have been installed in the containment vessel. Final construction works have been proceeded to start the functional test of the reactor cooling system in May 1996. Fuel fabrication has been started for the fuel loading in September 1997.

The project is intended to establish and upgrade the technology basis necessary for advanced HTGR developments. Some heat utilization system is planned to be connected to the HTTR and demonstrated at the former stage of the second core.

After attaining rated power, the JAERI plans to carry out safety demonstration tests to confirm the salient inherent safety features of the HTGR. In addition material and fuel irradiation tests as upgrading HTGR technologies will be conducted.

Preliminary tests on selected research subjects such as composite material and ZrC coated fuel developments, have been carried out at high temperature and under irradiation.

At the same time use will be made of the HTTR to carry out innovative basic research. Special irradiation facility has been considered to have a large irradiation space and flat thermal neutron irradiation atmosphere.

1. Introduction

A High Temperature Gas-cooled Reactor (HTGR) can supply high temperature heat as high as 1000℃, which has a potential of obtaining high thermal efficiency as well as high heat-utilizing efficiency. It also has excellent features such as high inherent safety, easy operation and high fuel burnup. From the view point of the global environmental protection and diversification of energy usage, non-electrical application of nuclear energy, hydrogen production for example, is very important. Therefore, in order to establish and upgrade the technological basis for HTGRs and also to use as a tool of basic researches for high temperature and neutron irradiation, the Japan Atomic Energy Research Institute (JAERI) has been constructing a 30MWt High Temperature engineering Test Reactor (HTTR) at the Oarai Research Establishment. Since the 2nd JAERI symposium on HTGR technologies which was held in Oarai in October 1992[1], construction works of the HTTR have progressed well and have been near the final stage of the functional test in 1996. The first criticality is scheduled in 1997. Testing program using the HTTR has been developed to start preliminary tests on innovative basic researches at high temperature and under irradiation in 1994 and also to identify the candidate system and key components for the nuclear heat utilization system connected to the secondary helium cooling circuit of the HTTR for the demonstration test. Also the testing program for advanced HTGR development have been assessed[2]. This report describes present status of the HTTR construction and its testing program.

2. Present status of HTTR construction

The HTTR plant is composed of a reactor building, a spent fuel storage building, a machinery building and so on. The reactor building is 48m x 50m in size with two floors on the ground and three under ground. Major components such as the reactor pressure vessel (RPV), primary cooling system components etc. have been installed in the containment vessel in 1994. Air cooling towers for the cooling system are located on the roof of the reactor building. The construction of reactor building started in March 1991 and has been almost completed. The external view of the reactor building is shown in Photo 1. The major specification of the HTTR are shown in Table 1.

The block type fuel is adopted in the HTTR considering the advantages of fuel zoning, control of coolant flow rate in each column, easy insertion of CRs, irradiation flexibility in the core. Core components and reactor internals have been

installed in the RPV from May to August 1995. Gaps between core components and reactor internals are carefully controlled to be maintained to be the required minimum during the assembling. The installed core arrangement of a top replaceable reflector region is shown in Photo 2. In order to verify the seal performance between permanent reflector blocks, the air leakage test had been carried out to measure leakage flow rate. The measured value was found to be less than the assumed limit in the core thermal hydraulic design. The core is cooled by helium gas of 4MPa flowing downward. The core has 30 fuel columns and 7 CR guide columns, which is surrounded by replaceable reflector blocks. The reactivity is controlled by the control rods system which consists of 32 control rods (16 pairs) and 16 control rods drive mechanisms. The installation of the system in the RPV started in December 1995 after placing the upper biological shielding structure.

The reactor cooling system is composed of the MCS, ACS and VCS as schematically shown in Fig. 1. The MCS is operated in normal operation condition to remove heat from the core and send it into the environment. The ACS and VCS have incorporated safety features. The ACS is initiated to operate in case of a reactor scram. Besides one out of two components of VCS has sufficient capacity to remove residual heat, the ACS is provided to cool down the core and core support structure. A helically coiled intermediate heat exchanger (IHX) whose heat-resistant material is Hastelloy-XR developed by the JAERI has been installed in September 1994. Primary helium gas is transported from the reactor core to the IHX and primary pressurized water cooler (PPWC) through a concentric hot gas duct. It consists of a pressure tube, an inner tube and an internal insulation reinforced with the liner. The helium gas at temperature of 400℃ flows in annular path and of 950℃ inside the inner tube. The pressure tube (outer diameter 860mm, thickness 42mm) can contain high pressure helium gas at 4.0MPa. The inner tube, which separates the high and low temperature helium gas paths, supports the pressure difference between the high and low temperature helium gas. The internal insulation is placed between the liner and inner tube. Assembling of T shaped concentric hot gas duct have been carefully conducted with welding taking into account that the RPV is supported with the skirt while the IHX and PPWC are with floating support structures. In March 1996 the pressure-proof and leakage test of the reactor cooling system will be carried out with the nitrogen gas at 6.0MPa. No leakage for the nitrogen gas will be confirmed because the amount of helium gas leaking into the atmosphere shall be less than 0.2 percent of the inventory per a day.

A functional test operation of the reactor cooling system will be performed from May 1996 to September 1997. At first the whole reactor cooling system shall be evacuated by several vacuum pumps and filled with the helium gas. Because of the large volume of the system and the outgases from both the graphite and the ceramic insulation with the temperature increase, a large quantity of chemical impurities in the helium gas are expected, which shall be removed by the helium purification system (HPS) to the concentration sufficient to reduce oxidation of the graphite. The helium gas flow rate in the HPS for the primary cooling system (670kg) is 200kg/h. In the copper oxide fixed bed, hydrogen and carbon monoxide are converted to water vapor and carbon dioxide, which are absorbed by a molecular sieve trap. Noble gases, methane, oxygen and nitrogen are absorbed by a cold charcoal trap. At the stage of a

functional test without nuclear heating, the helium gas will be heated by gas circulators up to about 200 ℃ at 2MPa. Functional tests of the cooling system will be performed at this operation condition to accumulate operational experiences. Plant control system will be fully checked. The fuel fabrication started in June 1995 and will complete in 1997. Fuel will be loaded into the core around in September 1997 and the first criticality is expected in December 1997. Fuel will be column-vise loaded from the outer fuel column to the inner one and 20 of the total 30 fuel columns will make the reactor critical. The first criticality will be attained in a shape of annular core. The excess reactivity and control rod worth will be measured by the Inverse Kinetic method. Preliminary tests to validate the measuring method have been conducted in the Very High Temperature Reactor Critical assembly (VHTRC).

3. HTTR Testing Program

The HTTR project is intended to establish and upgrade the technology basis necessary for advanced HTGR developments. The design studies and R&D works on the future promising HTGRs have been started in order to make the best of testing program using the HTTR. Around in 1998 the results of these studies will be reviewed by the Japanese Atomic Energy Commission (JAEC) at the revision of long-term program for research, development and utilization of nuclear energy.

Some heat utilization system is planned to be connected to the HTTR and demonstrated at the former stage of the second core. At present, steam-reforming of methane is the first candidate.

Besides the demonstration of the heat utilization system, the JAERI plans to carry out safety demonstration tests to confirm the salient inherent safety features of the HTGR. In addition material and fuel irradiation tests as upgrading HTGR technologies will be conducted after attaining rated power. Preliminary tests on selected research subjects such as composite material and ZrC coated fuel developments, have been carried out at high temperature and under irradiation.

In order to conduct innovative basic research in the HTTR, special irradiation facility has been considered to have a large irradiation space and flat thermal neutron atmosphere with low gamma heating. Preliminary tests on research items have been initiated since 1994.

3.1 Nuclear heat utilization tests

The HTTR is designed to transfer the thermal energy of 10MW to secondary helium at temperature of 905℃ and pressure of 4.1MPa through an intermediate heat exchanger (IHX).

Design works of the HTTR steam reforming system have been started since 1990 aiming at demonstration test of the HTTR at the beginning of the 21st century.

Design of main system arrangement, of key components such as a steam reformer and a steam generator and of control method, especially start-up procedure and development of computer code for transient thermal-hydraulics analysis have been conducted. The steam generator is designed to have a safety function as an interface.

The heat utilization efficiency of 78% using steam reformer is possible to be achieved, competitive to non-nuclear process (80%-85%).

3.2 Safety demonstration tests

The following safety demonstration tests are planned in the HTTR to verity inherent safety features of HTGRs.

1) Abnormal control rod withdrawal tests and
2) Coolant flow reduction tests

For these tests the code as a simulator has been developed for performing analyses of HTTR core transients and accidents.

3.3 Material and fuel irradiation tests as upgrading HTGR technologies

To develop advanced HTGRs (reactor outlet coolant temperature about 1100℃, power density 3-6w/cm³ and fuel burnup about 100GWd/t are targeted respectively), overall R&D program on upgrading HTGR technologies has been drafted in March 1995. Design studies and R&D works on advanced HTGRs have been started in order to incorporate the results in the long-term program revised by the JAEC around in 1998.

At present the first priority is dedicated to the medium-sized modular and severe accident free HTGR with high temperature heat. In order to upgrade core performance achieving higher power density, higher burnup of the core and higher allowable temperature design limit of the fuel, ZrC coated fuel and c/c composite material for control rod sleeves have been pre-tested.

3.4 High temperature irradiation tests as innovative basic researches

The HTTR can accommodate the large space for tests at high temperature and under irradiation. There established the Evaluation Committee on HTTR Utilization for Innovative Basic Researches in 1993. From researchers at universities, industries and JAERI's laboratories, more than 60 research subjects have been proposed and evaluated in the Committee. Four items such as development of high-temperature semi-conductors, upgrading of super-conductors characteristics, decomposition mechanism of high molecular compounds and trial fabrication of optical fibre for a high temperature use have been selected and their preliminary tests have been carried out since 1994. Design of special irradiation facility, which controls the irradiation condition with axial reversible movement of the specimen, started in 1995.

4. Concluding remarks

The HTTR is a high temperature gas cooled test reactor which has various aims and operational modes. The construction of the HTTR has progressed smoothly and its first criticality is foreseen in December 1997.

The various tests by the HTTR will make a great contribution to confirm salient characteristics of HTGRs including reliable supply of high temperature heat as high as 950℃ and high inherent safety and the application of high temperature heat from HTGRs to various fields will also contribute to relax global environmental problems. Furthermore, the HTTR has a unique and superior capability for carrying out high temperature irradiation tests not only for development of advanced HTGRs but also for basic researches such as new semi-conductors, super-conductors, composite material developments and tritium production and continuous recovery testing of fusion reactor blanket materials. The HTTR is highly expected to contribute so much to promoting the international cooperation in these fields.

5. References

1) Saitoh, S. 1993. Present Status of HTTR Project and Associated International Cooperation. JAERI-M 92-215, pp106-120. January

2) Tanaka, T. Baba, O. Shiozawa, S. Okubo, M. and Kunitomi, K. 1995. Construction of the HTTR and its Testing Program for Advanced HTGR Development. Proceedings (In Preparation) : TCM and Workshop on Design and Development of Gas-Cooled Reactors with Closed-Cycle Gas Turbines, Beijing, China. IAEA, Vienna, Austria. November

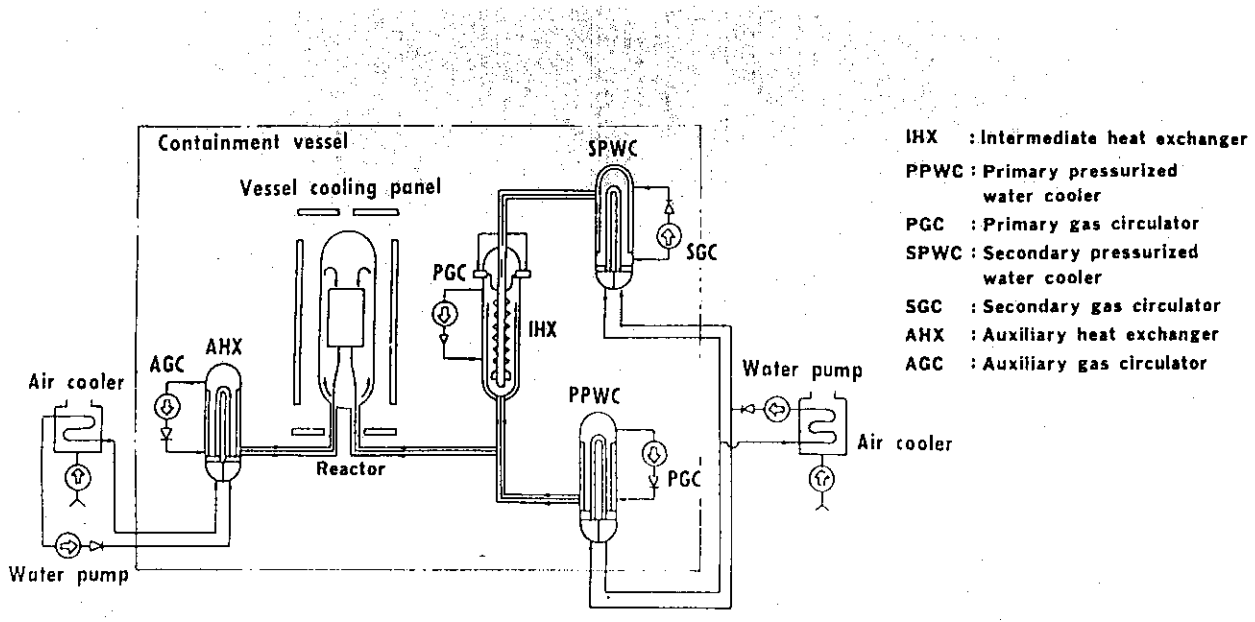


Fig. 1 Flow diagram of cooling system of HTTR

Table 1. Major specifications of HTTR

Thermal power	30MW
Outlet coolant temperature	850°C/950°C
Inlet coolant temperature	395°C
Fuel	Low enriched UO_2
Fuel element type	Prismatic block
Direction of coolant flow	Downward
Pressure vessel	Steel
Number of cooling loop	1
Heat removal	IHX and PWC (parallel loaded)
Primary coolant pressure	4MPa
Containment type	Steel containment
Plant lifetime	20 years

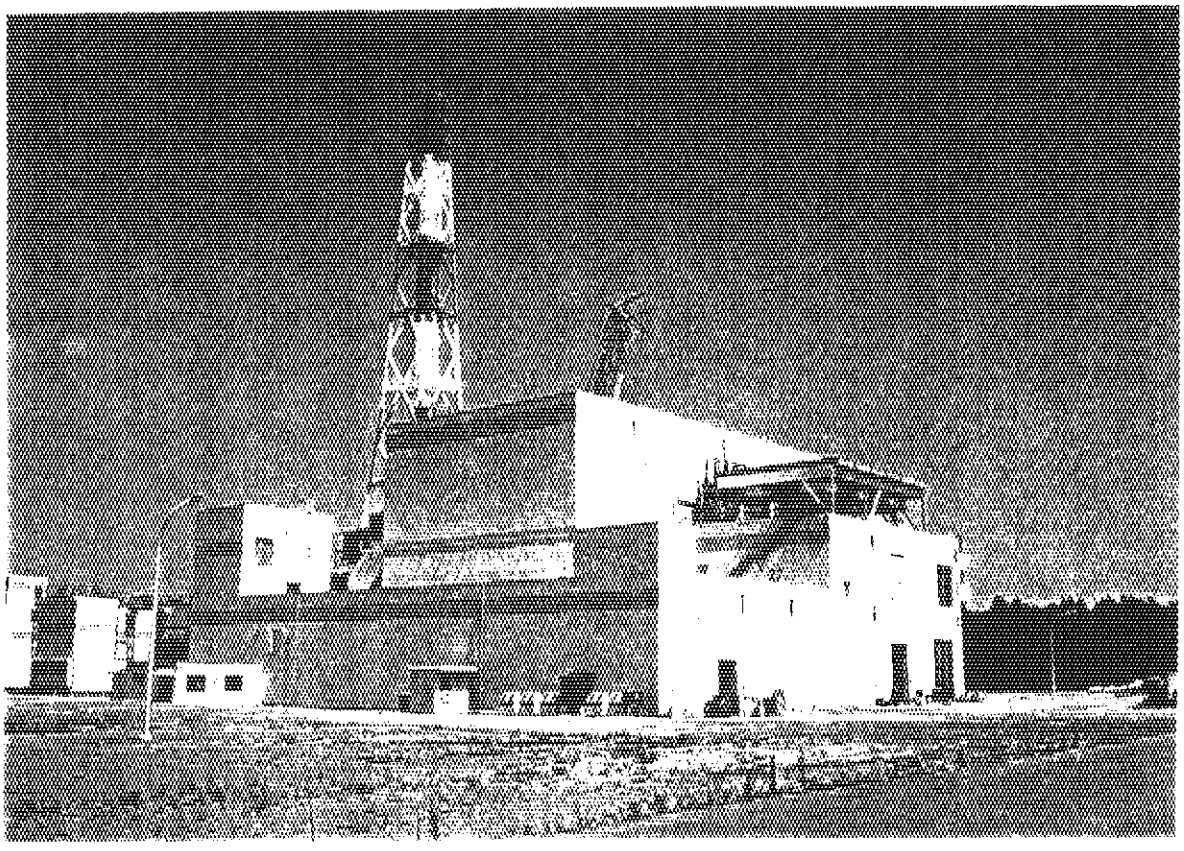


Photo 1. External view of the reactor building

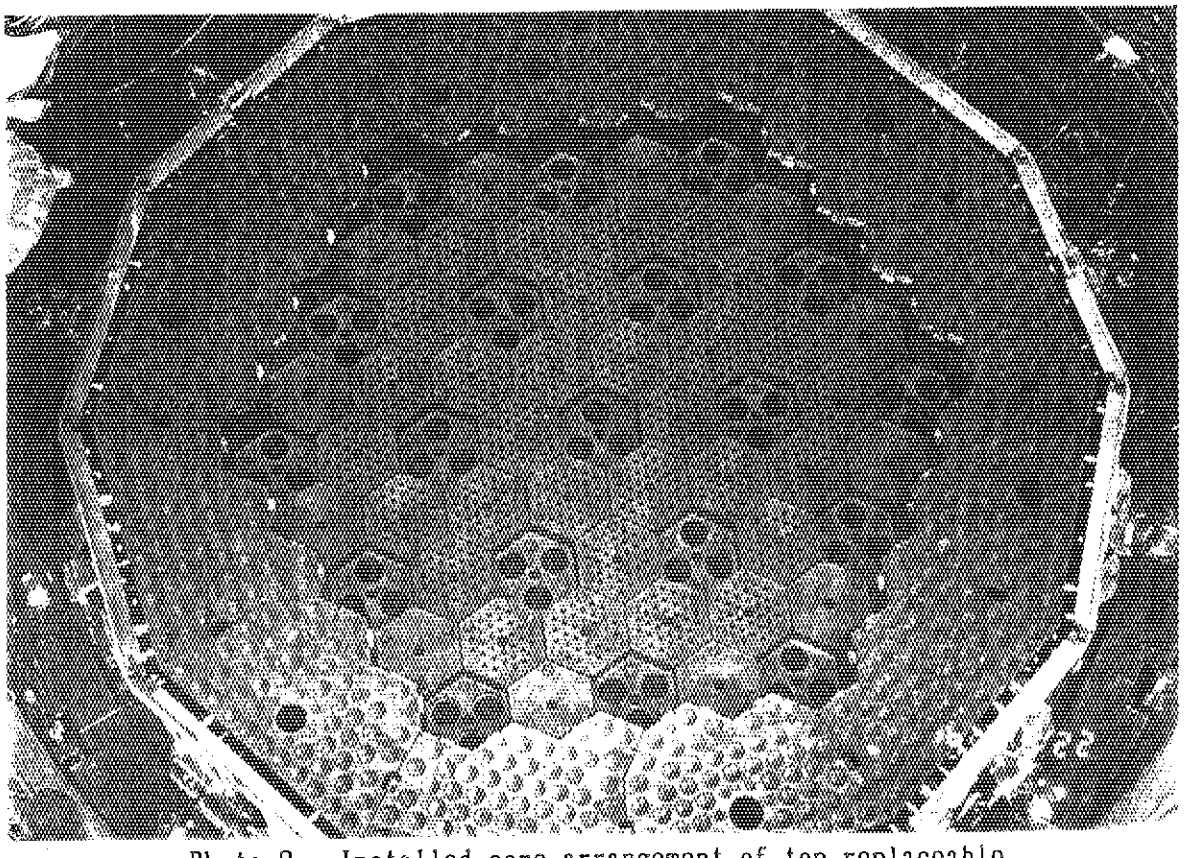


Photo 2. Installed core arrangement of top replaceable reflector region

3. Session Ⅲ

－Safety of HTGR, Development of Fuel and Component, and Operation Experience of HTGR－

3.1 Safety Studies on Heat Transport and Afterheat Removal for GCR Accident Conditions

Makoto Hishida
Nuclear Heat Application Laboratory
Department of High Temperature Engineering , JAERI

1. Introduction

The IAEA coordinated an international research program on "Heat Transport and Afterheat Removal for GCRs under Accident Conditions (CRP-3)". America, China, France, Germany, Japan, Netherlands and Russia participate the program.

Final goal of the program is to show clearly to the world one of the most important salient features of the HTGR, that is the HTGR reactor can be cooled down by passive measures without causing any damage to the nuclear reactor system even in accidental conditions, and to make clear the boundaries (or restrictions) for the passive cooling regime.

The first 5 year term of the coordinate program started in 1993 and established a goal to improve common knowledge for decay heat removal and to improve our tools, like computer codes and analytical models for the prediction of the performance of decay heat removal system. We are now performing benchmark problems for these purposes. The present efforts are concentrated on the benchmark for the passive heat removal performance outside the reactor vessel, partly because we have two different type of the HTGR in the world, the pebble bed type and the block type reactor. They have quite different heat dissipation behavior inside the reactor vessel. However, they have quite similar residual heat removal process outside the reactor vessel. For the first step of the international cooperation, we selected the common problem. After finishing the present benchmark we are planning to proceed to tackle the inside heat removal problem.

2. Benchmark Problems

We are now pursuing following benchmark problems.

(1) Benchmark problems of the HTTR VCS out-of pile test rig

(code-to-experiment benchmark problem provided by Japan)

The Japan Atomic Energy Research Institute had been performing extensive tests with the HTTR VCS (Vessel Cooling System) test model to investigate and demonstrate the passive cooling performance of the HTTR. The test model consists of a partial-scale model of the HTTR reactor

vessel and water cooling panel, with 6 individually-controlled heaters corresponding to the HTTR's core barrel and top and bottom reflectors. Four sets of test data were supplied for the benchmark problems to analyze thermal performance of the VCS system.

(2) Benchmark problem of the SANA out-of-pile test rig

(code-to-experiment benchmark problem provided by Germany)

The KFA (Research Center Jülich GmbH) has been making experiments to investigate passive heat removal of the residual heat in the pebble bed reactor with a primary concern with heat transport inside the pebble bed. The test rig called SANA is a test model of pebble bed reactor. Four benchmark experimental data were supplied.

(3) Benchmark problems of the HTR-10 reactor

(code-to-code benchmark problem provided by China)

The Institute of Nuclear Energy Technology of Tsinghua University is now constructing the HTR-10 pebble type high temperature reactor with 10MW thermal output and 700℃ reactor outlet temperature. It is equipped with two independent reactor cavity cooling systems (RCCS) to dissipate residual heat out of the reactor. Primary working fluid of the RCCS is water. Two benchmark problems were defined to predict temperature fields and thermal performance of the reactor vessel, RCCS system and associated components during a heatup experiment which is planned to perform with the HTR-10 and during of a design-base depressurization accident.

(4) Benchmark problems of the VGM reactor

(code-to-code benchmark problem provided by Russia)

OKBM in Russia is now developing the VGM pebble type high temperature reactor with 200 MW thermal output and 750℃ outlet temperature. It has three independent RCCSs with water as working fluid. The benchmark problem for the VGM reactor was given to predict temperature fields and thermal performance of the RCCS systems and the reactor vessel during a design base accident of loss of forced cooling with and without pressurized Helium in the reactor vessel.

(5) Benchmark problem of the HTTR reactor

(code-to-code benchmark problem provided by Japan)

JAERI has proposed a benchmark problem to predict reactor transient for the ATWS (anticipated transient without scram) accident of the HTTR.

The participants have calculated the benchmark problems which they are interested in and compared with the experimental data or with each other's computed results. The calculated temperature fields on the reactor vessel and thermal performance of the VCS and RCCS of the participants have shown good agreement with the experimental data or each other's calculated results.

We found that our computer programs and analytical models are satisfactory for the prediction of the performance of the passive cooling system and analyzing the temperature fields of the reactor vessel. However, we also found the importance natural convection which can give a large influence on the maximum temperature of the reactor vessel.

3. Future prospective of the CRP-3

It is desirable that the present first phase of CRP-3 (will end in 1997) develops into the second one, in which our effort should placed on the benchmark problems based on the safety experiments with the Japanese HTTR. The HTTR will be put into operation in 1998 and several tests relevant to the safety features of the HTGRs will be carried out.

Safety Studies on Heat Transport and Afterheat Removal for GCR Accident Conditions

Makoto Hishida
Nuclear Heat Application Laboratory
Department of High Temperature Engineering
JAERI

1. Introduction

The IAEA coordinated an international research program on "Heat Transport and Afterheat Removal for GCRs under Accident Conditions (CRP-3)". America, China, France, Germany, Japan, Netherlands and Russia participate the program. This paper reviews international cooperation researches going on in the framework of the CRP-3.

Final goal of the program is to show clearly to the world one of the most important salient features of the HTGR, that is the HTGR reactor can be cooled down by passive measures without causing any damage to the nuclear reactor system even in accidental conditions, and to make clear the boundaries (or restrictions) for the passive cooling regime.

Up to now a lot of work have been carried out in the world to investigate the passive decay heat removal of the HTGRs. Figure 1 is an pioneering work made by W.Rehm[1], which shows the plot of the maximum fuel temperatures of the various designs of HTGR against reactor output. The maximum fuel temperature was calculated with an assumption that active cooling of the reactor failed. It is not surprising that the maximum fuel temperatures of old design (or the early stage) of the HTGRs like Vort St. Vrain, THTR-300 and so force exceed 1600℃ (limiting temperature for the fuel), because those reactor relied on active cooling measures for the decay heat removal, in other words, they were not designed to remove the decay heat by passive cooling measures. In addition they had large reactor output because of economical reason. On the other hand, modern design adopts the passive cooling system and modular concept with less reactor output.

The figure shows that smaller reactors with the thermal output less than about 300 to 500 MW can achieve the passive decay heat removal of the residual heat without exceeding the maximum fuel temperature of 1600℃. The figure also indicates that the maximum fuel temperature can be reduced by improving the designs of the reactor and passive decay heat removal system.

It is quite timely for the IAEA to organize the international cooperation researches to improve

common knowledge for decay heat removal and to improve our tools, like computer codes and analytical models for the prediction of the performance of decay heat removal system. The first 5 year term of the coordinate program was started in 1993.

We are now performing benchmark problems for these purposes. The present efforts are concentrated on the benchmark problems for the heat removal performance outside the reactor vessel, partly because we have two different types of the HTGR in the world, the pebble bed type and the block type reactor. Although the two types of reactor have quite different heat dissipation behavior inside the reactor vessel, they have quite similar residual heat removal process outside the reactor vessel. For the first step of the international cooperation, we selected the common problem. After finishing the present benchmark we are planning to proceed to tackle the inside heat removal problem.

2. Benchmark Problems

We are now pursuing following benchmark problems.

2.1 Benchmark problems of the HTTR VCS out-of pile test model [2]

(code-to-experiment benchmark problem provided by Japan)

The Japan Atomic Energy Research Institute had been performing extensive tests with the HTTR VCS (Vessel Cooling System) out-of-pile test model to investigate and demonstrate the performance of the residual heat removal system of the HTTR.

Figure 2 shows the test model consisting of a partial-scale model of the HTTR reactor vessel and water cooling panel, with 6 individually-controlled heaters corresponding to the HTTR's core barrel and top and bottom reflectors. The vessel is 3000mm in height and 1000mm in diameter. Helium or Nitrogen is filled inside the vessel to simulate pressurized loss of forced cooling accident. The water cooling panel is composed of two sets of upper, side and lower sub-water-cooling-panels, each set of which have 12, 44 and 6 tubes, respectively. Figure 3 shows temperature measuring points. About 200 K-type thermocouples are attached to measure detailed temperature distributions on the pressure vessel, water cooling panel and thermal insulation, and gas temperature. The detailed temperature measurement is essential for the present test because one of the key issues of the CRP-3 is to establish reliable data base.

Five sets of test data listed in Table 1 have been supplied so far for the benchmark problems to

analyze the thermal performance of the VCS system and to investigate the detailed process of the decay heat removal. The test rig was originally designed to test water cooling panels. However, in the discussion of the CRP-3 technical meeting, the member countries requested JAERI to carry out experiments with an air cooling panel. The JAERI's research group involved in the test generously accommodated the request and supplied experimental data of an air cooling panel for an additional benchmark problem.

All the participant countries have been making calculation with their computer programs and comparing the calculated results with the experimental data. Figure 4 shows an example of the comparison made by JAERI[3]. Calculated temperature fields on the reactor vessel and thermal performance of the VCS of the participants have shown good agreement with the experimental data.

We found that our computer programs and analytical models are satisfactory for the prediction of the performance of the residual heat removal systems and analyzing the temperature fields of the reactor vessel. However, we also found the importance of natural convection which can give a large influence on the maximum temperature of the reactor vessel.

2.2 Benchmark problem of the SANA out-of-pile test rig[4]

(code-to-experiment benchmark problem provided by Germany)

The KFA (Research Center Jülich GmbH) has been making experiments to investigate passive heat removal of the residual heat in the pebble bed reactor with a primary concern with heat transport inside the pebble bed. The test rig called SANA involves a test model of pebble bed reactor with 1.5m diameter and 1m height and a central electric heater in the bed. Approximately 9500 graphite pebbles with a diameter of 6cm are filled in the reactor vessel. Four benchmark experimental data were supplied. The experiments were performed with Nitrogen and Helium inside the vessel and with 10kW and 30kW heater output, and temperature distributions in the pebble bed were measured with about 50 N- and W- type thermocouples.

The benchmark problems require us to predict the temperature distributions in the pebble bed. Participants are now making the calculations.

2.3 Benchmark problems of the HTR-10 reactor[5]

(code-to-code benchmark problem provided by China)

The Institute of Nuclear Energy Technology (INET) of Tsinghua University is now constructing

the HTR-10 pebble bed type high temperature reactor with 10MW thermal output and 700℃ reactor outlet temperature. It is equipped with two independent reactor cavity cooling systems (RCCS) to dissipate residual heat out of the reactor by completely passive manners. Each of the RCCS system consists of a water cooling panel surrounding the reactor vessel and a natural circulation loop of water to transport residual heat from the water cooling panel to a air cooler which eventually dissipate heat to air draft driven by natural convection in a chimney.

Two benchmark problems were defined to predict temperature fields and thermal performance of the reactor vessel, RCCS system and associated components during a heatup experiment (benchmark problem 1) which is planned to perform with the HTR-10 and during a design-base depressurization accident (benchmark problem 2).

The INET is planning to make safety demonstration test with the HTR-10. The test will be performed under following conditions: the reactor is in operation with 200kW power and 0.1MPa helium pressure, two water coolers are working, helium blower in the reactor primary cooling system is turned off. Giving the surface temperature field of the core barrel which was predicted by the INET, the benchmark problem 1 requests us to predict the temperature fields of the reactor vessel, water cooler, air cooler, thermal shield and reactor cavity, and to predict the mass flow rate or the water coolers.

The benchmark problem 2 requires us to predict the same items as the problem 1 for the design base depressurization accident of the HTR-10. The variation of temperature field of the core barrel was given as the function of time.

Participants have been calculating and comparing their results with each other. So far good agreements have been obtained.

2.4 Benchmark problems of the VGM reactor[6]

(code-to-code benchmark problem provided by Russia)

OKBM in Russia is now developing the VGM pebble type high temperature reactor with 200 MW thermal output and 750℃ outlet temperature. It has three independent RCCSs with water as working fluid. The benchmark problem for the VGM reactor was given to predict temperature fields and thermal performance of the RCCS systems and reactor vessel during a design base accident of loss of forced cooling with and without pressurized Helium in the reactor vessel.

Participants have been calculating and comparing the results.

2.5 Benchmark problem of the HTTR reactor[7]

(code-to-code benchmark problem provided by Japan)

JAERI has proposed a benchmark problem to predict reactor transient for the ATWS (anticipated transient without scram) accident of the HTTR.

Participants have been calculating and comparing the results.

3. Future prospective of the CRP-3

It is desirable that the present first phase of CRP-3 (will end in 1997) develops into the second one, in which our effort should placed on the benchmark problems based on the safety experiments with the Japanese HTTR. The HTTR will be put into operation in 1998 and several tests relevant to the safety features of the HTGRs will be carried out.

4. Conclusion

The international research program on "Heat Transport and Afterheat Removal for GCRs under Accident Conditions (CRP-3)" coordinated by the IAEA has turned out to be very effective for the participant countries to have common knowledge about the passive cooling of the residual heat of HTGRs, to validate the computer programs and analytical models developed for the prediction of the thermal performance of passive cooling systems, encourage researchers to proceed with further advanced studies.

In order to prove the salient features of the HTGRs achieved by the passive cooling system, with firm ground, it is desirable that the present first phase of CRP-3 develops into the second one, in which primary effort should be placed on the benchmark problems based on the safety experiments with the Japanese HTTR.

References

(1) Rehm W., "Compilation and Presentation of the Thermodynamic Safety Analyses for HTR-Concepts with Pebble-Bed Core", KFA-ISR-4/91 Re(1991)

(2) Takada S. et. al., "Benchmark Problem of the HTR VCS test for IAEA Coordinated Research Program (CRP-3)" to be published in IAEA-TECDOC (1998)

(3) Takada S. et. al., "Study of the Cooling Characteristics of the Water Cooling Panel System - Pressure Vessel without Stand Pipes -", JAERI-Research 95-049 (1995)

(4) Nießen H. F. et. al., "Benchmark Problem of the SANA test for IAEA Coordinated Research Program (CRP-3)" to be published in IAEA-TECDOC (1998)

(5) Gao Z. et. al., "Benchmark Problem of the HTR-10 for IAEA Coordinated Research Program (CRP-3)" to be published in IAEA-TECDOC (1998)

(6) Kuzavkov N. et. al., "Benchmark Problem of the VGM for IAEA Coordinated Research Program (CRP-3)" to be published in IAEA-TECDOC (1998)

(7) Saikusa A. et. al., "Benchmark Problem of the HTTR Safety Test for IAEA Coordinated Research Program (CRP-3)" to be published in IAEA-TECDOC (1998)

Table 1 Benchmark Problems of HTTR VCS Out-of-pile Test

Case	Maximum Temperature of Vessel (℃)	Decay Heat (kW)	Gas in Vessel	Pressure in vessel (Pa)	Remarks
Vacuum	150 ℃	13 kW	Vacuum	1.3 Pa	Water Cooling Panel
Low Temperature	200 ℃	29 kW	Helium	0.73 MPa	Water Cooling Panel
High Temperature	420 ℃	94 kW	Nitrogen	1.1MPa	Water Cooling Panel
With Stand Pipe	420 ℃	77 kW	Helium	0.47 MPa	Water Cooling Panel with Stand Pipes
Air Cooling Panel	500 ℃	30 kW	Helium	0.64 MPa	Air Cooling Panel with Stand Pipes

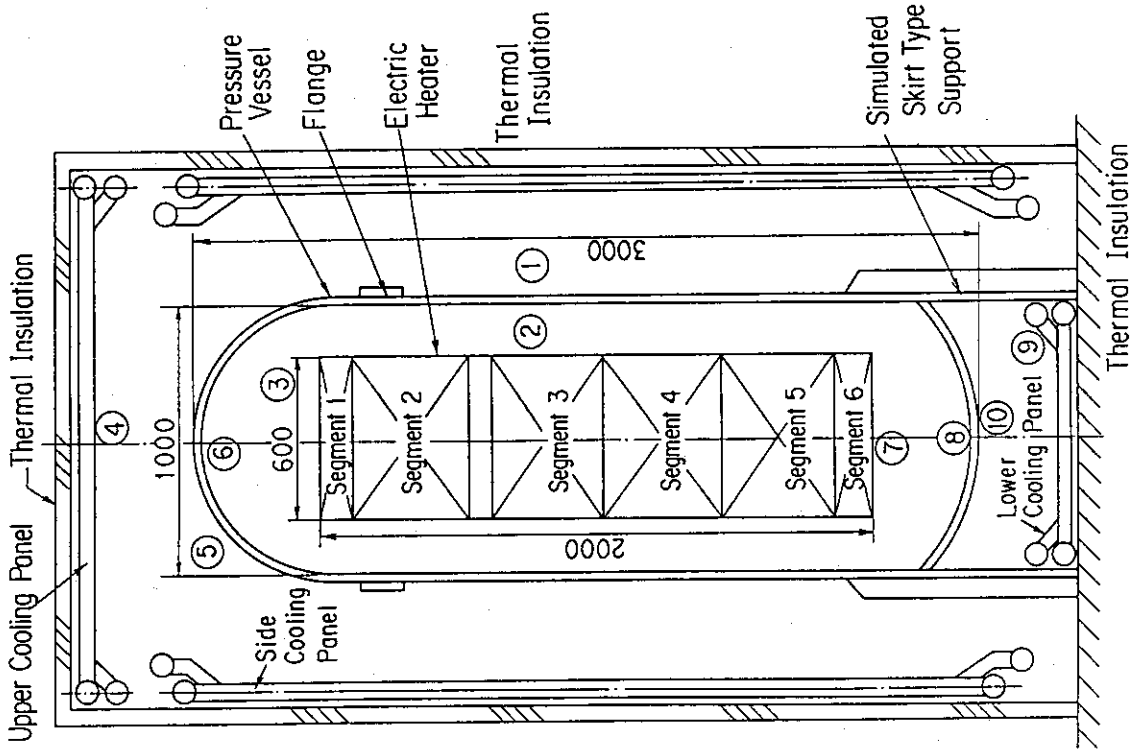


Figure 2 Out-of-pile test model of the HTTR VCS

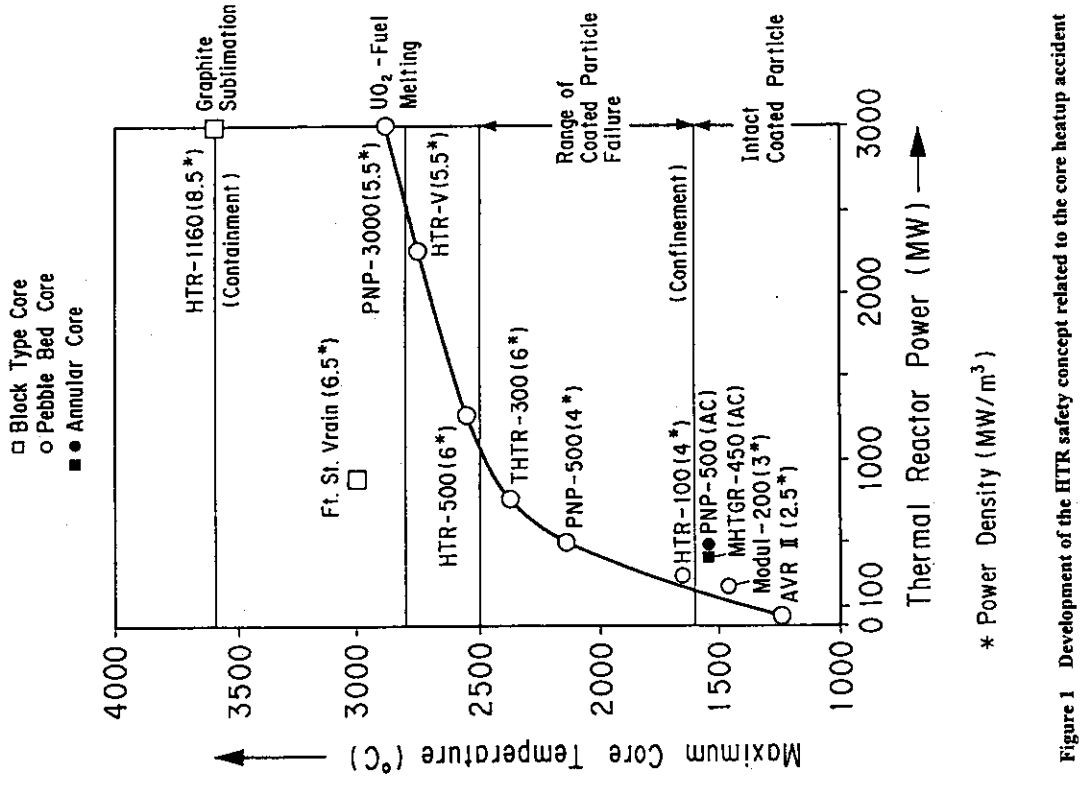


Figure 1 Development of the HTR safety concept related to the core heatup accident with depressurization

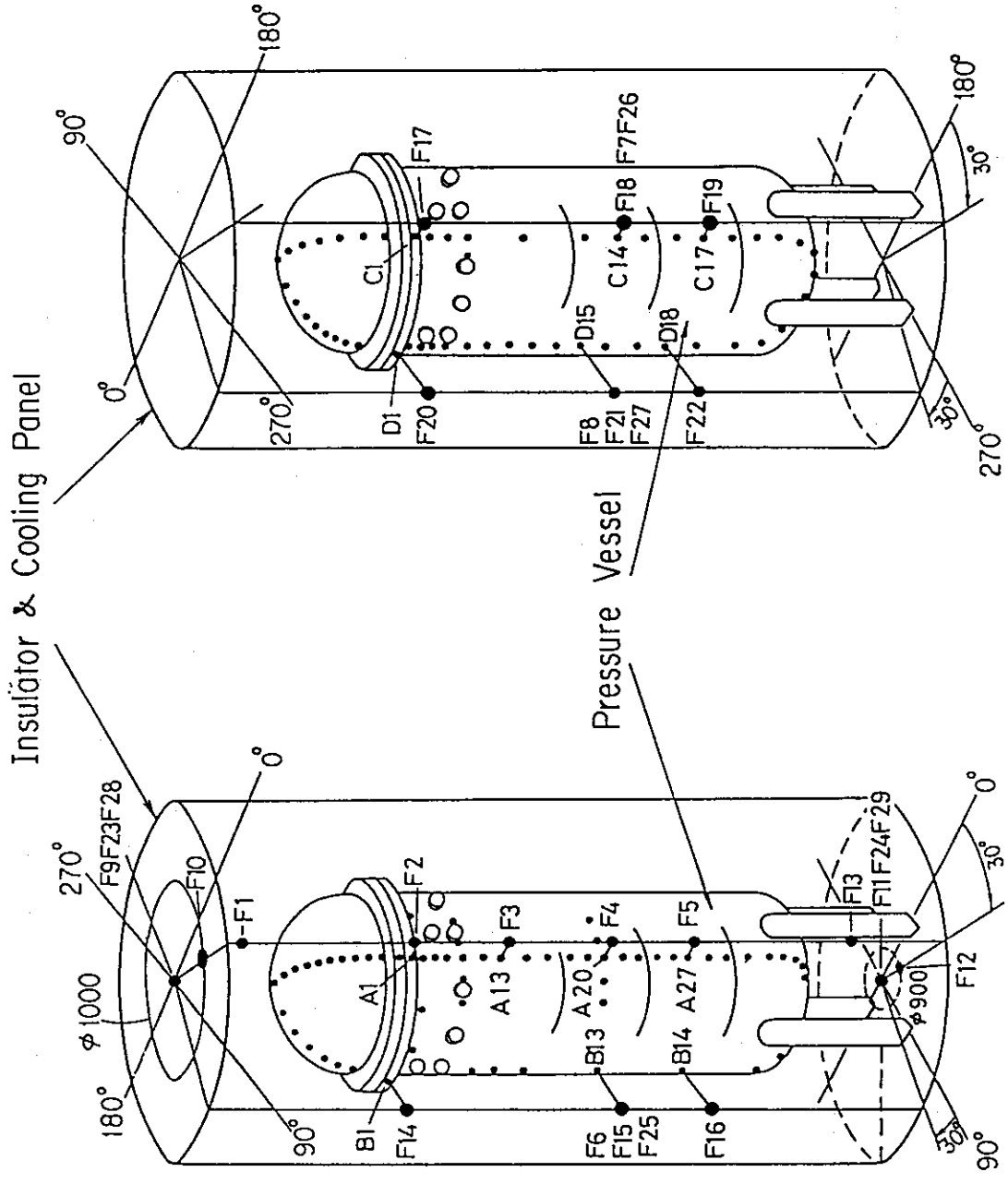
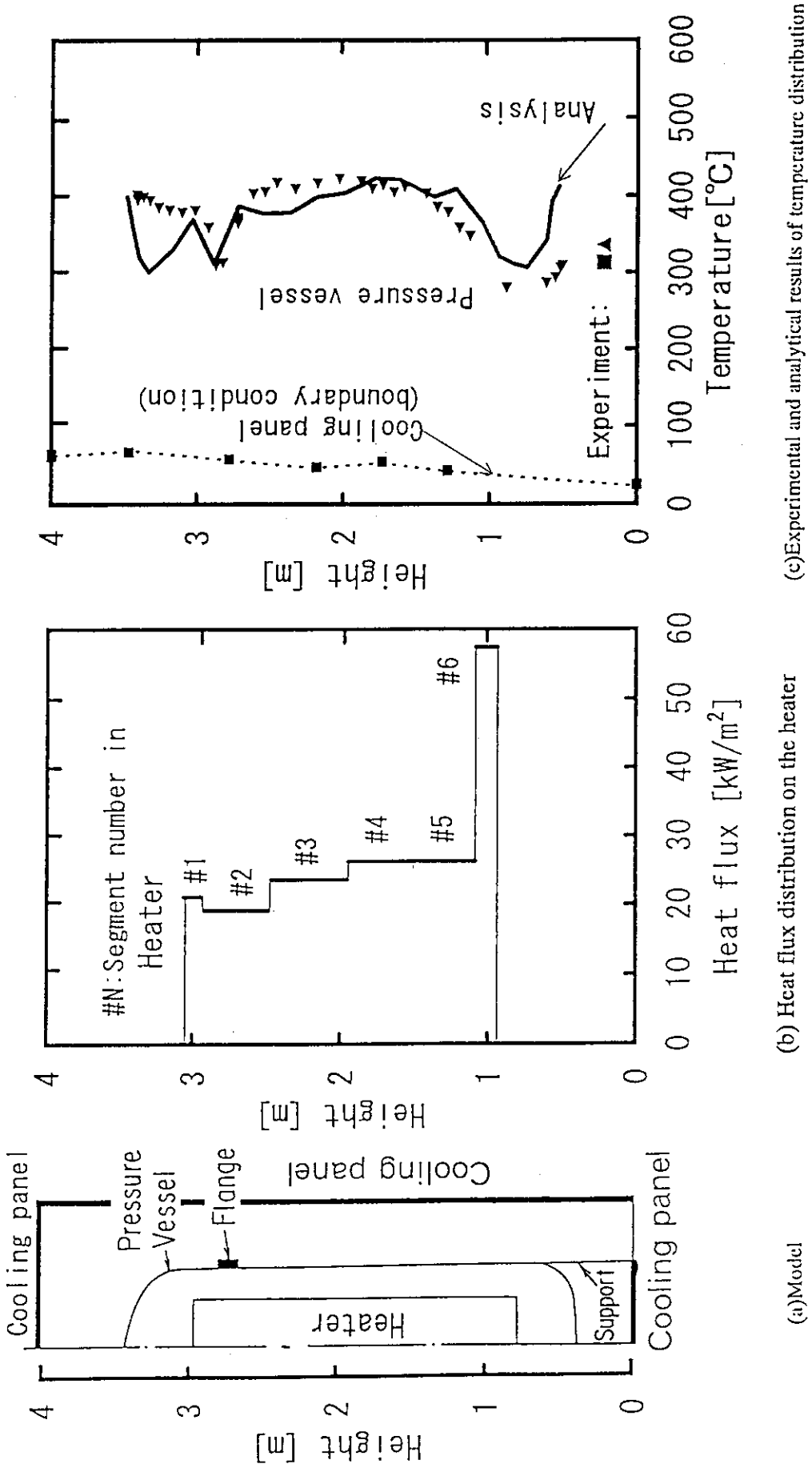


Figure 3 Temperature measuring points.



(a)Model

(b) Heat flux distribution on the heater (Boundary condition)

(c)Experimental and analytical results of temperature distribution on the surfaces of components

Figure 4 An example of the comparison between calculation and experiment for the HTTR VCS test made by JAERI[3]

FORSCHUNGSZENTRUM JÜLICH GmbH KFA

Third JAERI Symposium on HTGR Technology, Section IV:
Safety of HTGR, Development of Fuel and Components, Operation Experience

3.2 Safety Experiments for the Demonstration of Fission Product Retention in Fully Irradiated Fuel Elements

by
Werner Schenk and Heinz Nabielek
Research Centre Jülich (KFA), Germany

Abstract:
Since 1977, fuel elements from AVR operation and MTR irradiation tests have been investigated in accident simulation tests. In the first phase, the temperature margins were explored up to 2500 °C where fission product release is massive.

While suitable safety measures can minimise the probability of accidents involving temperatures beyond 2000°C, the novel design of a small modular reactor limits the maximum temperature to 1600°C by inherently passive mechanisms. In consequence, the second phase of the investigations concentrated on a new set of equipment enabling the measurement of minute fractions of fission product release in the temperature range from 1600°—1800°C (KÜFA furnace).

We were able to demonstrate that modern, TRISO coated, UO_2 particles will retain all safety-relevant fission products up to 1600°C at a level not exceeding release under normal operating conditions which in itself is very low. If the maximum burnup is strictly kept within the limits of the SIEMENS-designed 200 MW_{th} MODUL reactor (in the range 9-11% FIMA), the allowable temperature limit may be between 1700°—1800°C; while very high burnup fuels (14-15% FIMA) will have to be limited to 1600°C.

The third phase of the investigation - still ongoing - is dedicated to the study of fission product release under oxidising conditions. Again, special equipment designed for the purpose (the KORA furnace) enables the simulation of

- steam ingress, typically at 800 °C
- air ingress exploring coated particle limitations in the range from 1300 to 1600°C.

Steam ingress can lead to large releases of fission gases and iodine from defective and failed particles. Detailed results are presented and will be compared to in-pile experiments.

The work on air ingress has only recently started, but first results are encouraging. While the original assumptions - lacking representative experimental work - assumed complete particle failure at 1100°C during unimpeded air ingress, we can show that it takes several days at 1100°C to disintegrate the graphitic spherical fuel element still leaving the particles intact. Only prolonged air ingress at 1300° C or higher initiates the failure of particles.

The first phase (2500°C) and the third phase (air ingress) were performed for hypothetical accident scenarios to enable the reliable prediction of accident consequences.

The second phase (1600°—1800°C) concerns the design basis accident of small, modular HTRs. The results are useful not only for safety calculations and licensing purposes, but provide a direct demonstration of the potential for a catastrophe-free form of nuclear energy.

Safety Experiments for the Demonstration of Fission Product Retention in Fully Irradiated Fuel Elements

Werner Schenk and Heinz Nabielek
Research Centre Jülich (KFA)
Germany

1. Introduction

Since 1977 accident simulation tests on irradiated fuel specimens - mostly spherical fuel elements - have been carried out at the KFA Hot Cells at temperatures up to 2500 °C with the aim of obtaining data for analyses of hypothetical accidents in medium-sized HTRs (e.g. THTR 300) /1/. Considerable fission product release above 2000 °C has led to the development of smaller reactors, such as the HTR MODUL, in which the fission products are retained in the fuel element even in the extreme case of a depressurization accident /2/.

In order to demonstrate fission product retention in the temperature range of interest between 1600 and 1800 °C, experiments were carried out with the cold finger apparatus (KÜFA) with which even minute activity releases of important fission products of I, Cs, Sr and the noble gases can be measured /3/.

In recent years, safety experiments with the specifically developed corrosion apparatus (KORA) have been focused on tests with fuel specimens under oxidising conditions.

Water vapour in the sweep gas may lead to considerable release increases from defective fuel particles depending on burnup. Knowledge about the release behaviour of fission products, especially of iodine, as a function of temperature, water vapour partial pressure and UO_2 burnup is therefore necessary /4/.

For experiments with fuel specimens in air it is important to know at which temperature/time load the SiC coating fails as a function of specimen burnup.

There are still a number of essential outstanding questions especially in the field of UO_2 fuel particles in oxidising atmosphere.

2. Apparatus

Important features of the apparatus installed in the Hot Cells of KFA Jülich are compiled in Tab. 1.

2.1. Cold finger apparatus (KÜFA)

The KÜFA can be used to examine fuel specimens at temperatures up to 1800 °C in inert gas up to 130 kPa. The experimental aim is to measure the fission product retention of specimens with coated fuel particles at 1600 to 1800 °C and to obtain information about defect behaviour at high temperatures.

Table 1: Accident simulation tests (KFA Jülich)

Apparatus	**KÜFA**	**KORA**	
Max. temperature	1800°C	1000°C	1600°C
Gas	Helium	Helium and H20	O2, N2, CO2
Accident simulation	High temperature	Oxidizing conditions	Air ingress
Meas. of fission gases	Continuous release during whole test (Kr-85, Xe-133)		
Measurement of solid fission products	Cs-, Sr-, I-, Ag-release profiles	Overall release of Cs	
Examination of heated samples	Distribution of fission products, defect mechanism		

The fuel specimens (particles, compacts, spherical fuel elements) are heated in a laboratory resistance furnace accommodated in the gastight box of a Hot Cell. The furnace is integrated in a sweep gas circuit for measuring the fission gases (Fig. 1). The fission gases released from a fuel specimen, normally ^{85}Kr, are entrained in the sweep gas, collected in liquid-nitrogen-cooled activated charcoal traps outside the Hot Cell and measured with NaI detectors.

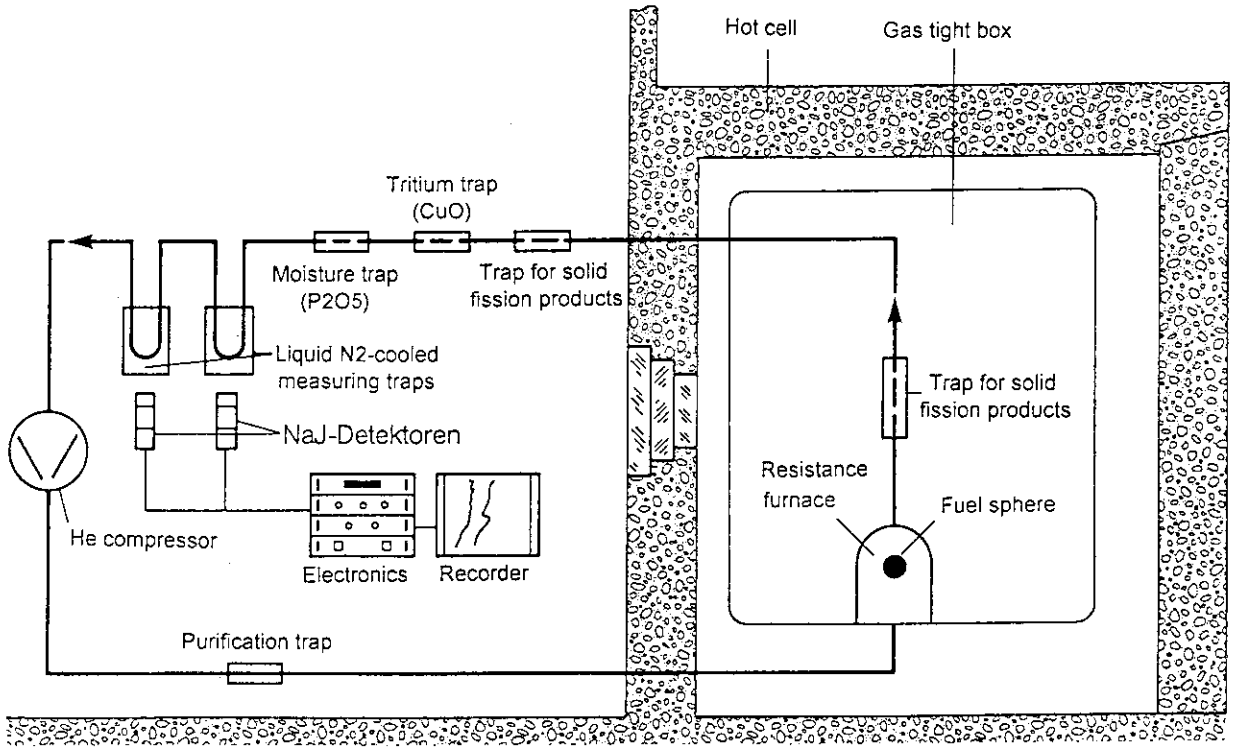


Fig. 1: Diagram of the cold finger apparatus (KÜFA) with sweep gas circuit

The measurement of all solid fission products released, such as Cs, Sr, Ag and I (unless ^{131}I has already decayed), is possible by the cold finger method (Fig. 2). A water-cooled tube, the cold finger, with an exchangeable "condensation plate" at the bottom extends into the furnace. A high portion of the solid fission products released, i.e. 60 to 70 % Cs and iodine depending on the specimen type, deposit on this condensation plate. The cold finger can be removed from the furnace through an airlock during the heating experiment to exchange the condensation plate. The plates are then measured by gamma and beta spectrometry outside the Hot Cell so as to obtain the release profile for solid fission products.

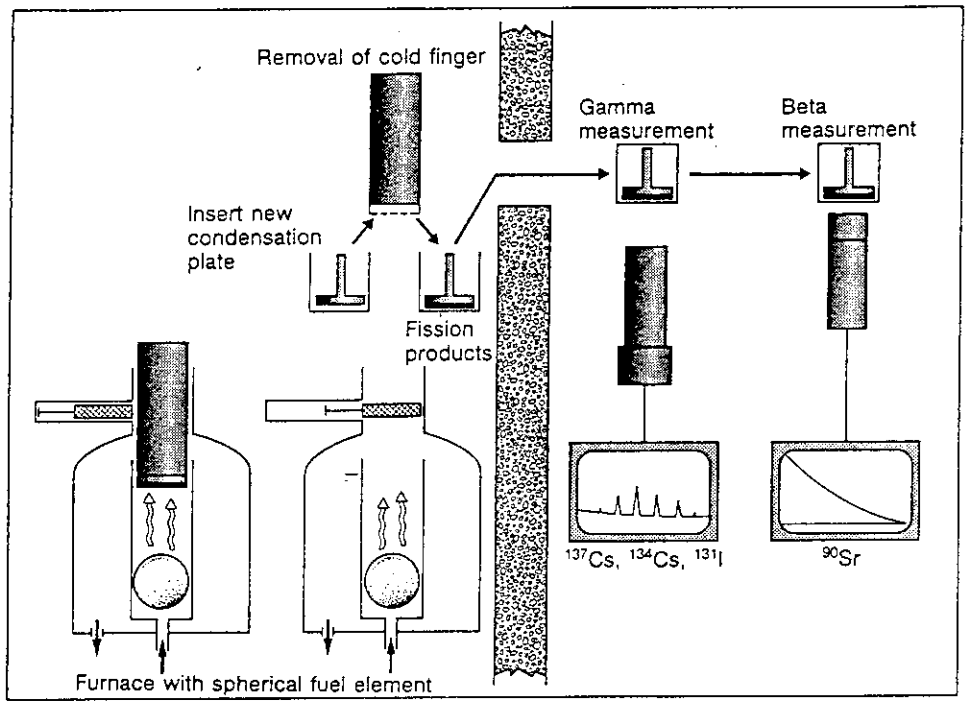


Fig. 2: Method for determining the release of solid fission products with KÜFA

2.2. Corrosion apparatus (KORA)

The KORA can be used to examine fuel specimens in oxidising atmosphere, i.e. both in helium with defined moisture content and in gas mixtures such as air. The aim of the experiments with intermittent water vapour additions is to measure the influence of moisture on the fission gas and thus iodine release from defective fuel particles in the temperature range from 600 to 1200 °C. The most important aim of the experiments in air is to examine the stability of SiC coatings at temperatures up to 1600 °C in addition to graphite corrosion.

The corrosion furnace KORA, in which fuel specimens up to spherical fuel element size can be heated, is also installed in the gastight box of a Hot Cell (Fig. 3). The resistance-heated furnace contains two concentric tubes placed into each other, which may consist of fused silica, alumina or SiC depending on the test temperature. The gas or gas mixture first flows into the annular gap between inner and outer tube at max. 1400 mbar and normally 30 l/h, where it is heated before reaching the specimen through an opening at the end of the inner tube.

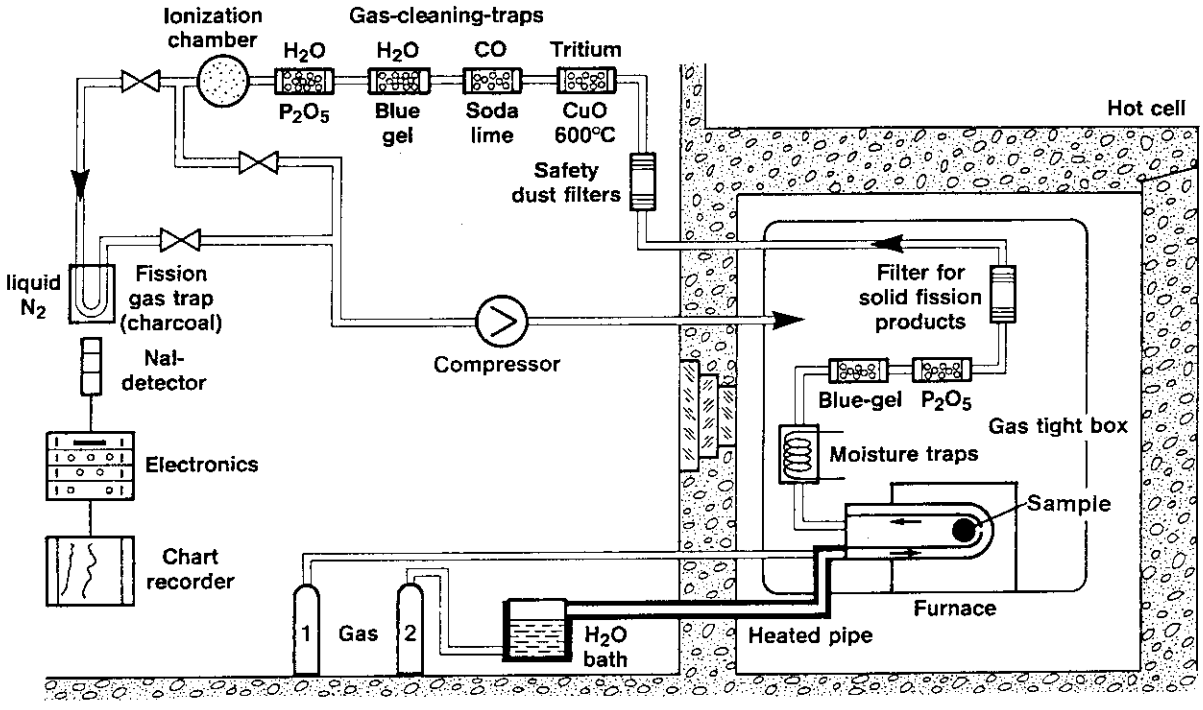


Fig. 3: Sweep gas circuit with moisturing equipment of the corrosion apparatus (KORA)

The water vapour partial pressure can be regulated through the bath temperature or by admixing dry gas. The gas coming from the furnace is cleaned of residual moisture and aerosols before measuring the entrained ^{85}Kr activity in an ionisation chamber outside the Hot Cell and, if possible, additionally with a cooled activated charcoal trap and a NaI detector.

3. Results

The most extensive results are available from tests with KÜFA (since 1984) and post-examinations of heated specimens /3/. KORA experiments with water vapour were started in 1991, with air in 1994. This paper reports on results with irradiated, state-of-the-art UO_2 fuel specimens.

3.1. Fuel specimens at high temperatures

3.1.1. Release from high burnup fuel elements

Spherical fuel elements and other fuel specimens with UO_2-TRISO particles were experimentally heated to temperatures from 1600° to 1800 °C, which were then maintained for 30 to 500 hours. Results are summarised in Tab. 2.

Table 2: Results from accident simulation tests with fuels pheres containing UO_2 TRISO particles

Fuel element UO2 TRISO	*Burnup (%FIMA)*	*Fast fluence (1E+25*1/m2) E>0,1MeV*	*Heating test*		*No. of failed particles ***		*Fractional release*				
			Temp. (°C)	*Time (h)*	*manuf.*	*heating*	*Kr-85*	*Sr-90*	*Ag-110m*	*Cs-134*	*Cs-137*
AVR 71/22	3.5	0.9	1600	500	no	no	4E-07	5E-06	9E-04	7E-05	2E-05
HFR-K3/1	7.7	3.9	1600	500	no	no	2E-06	2E-07	3E-02	1E-04	1E-04
FRJ2-K13/2	8.0	0.1	1600	138	no	no	6E-07	3E-07	3E-03	1E-04	4E-05
AVR 82/20	8.6	2.4	1600	100	no	no	2E-07	4E-06	4E-03	1E-04	6E-05
AVR 82/9	8.9	2.5	1600	500	no	no	5E-07	8E-05	2E-02	6E-04	8E-04
AVR 89/13	9.1	2.6	1620 *	~10	no	no	2E-07	***	8E-04	1E-05	1E-05
			1620 *	~10		no	1E-09	***	1E-02	2E-06	1E-06
AVR 85/18	9.2	2.6	1620 *	~10	no	no	1E-07	***	7E-03	1E-05	1E-05
AVR 90/5	9.2	2.7	1620 *	~10	no	no	2E-07	***	1E-03	8E-06	9E-06
			1620 *	~10		no	7E-09	***	9E-04	3E-06	3E-06
AVR 90/2	9.3	2.7	1620 *	~10	1	2	1E-04	***	4E-02	5E-05	5E-05
AVR 90/20	9.8	2.9	1620 *	~10	2	3	2E-04	***	8E-02	6E-06	7E-06
AVR 91/31	9.0	2.6	1700 *	~10	2	18	1E-03	***	6E-01	4E-03	2E-03
AVR 74/11	6.2	1.6	1700	184.5	1	no	3E-05	7E-06	5E-02	8E-05	8E-05
FRJ2-K13/4	7.6	0.1	1600	138	no	no	3E-07	2E-08	5E-04	6E-06	3E-06
			1800	100		2	7E-05	1E-03	5E-01	1E-02	1E-02
AVR 88/33	8.5	2.3	1600	50	no	no	1E-07	8E-06	1E-03	1E-04	1E-04
			1800	20		~4	2E-04	2E-04	2E-01	4E-04	5E-04
AVR 88/15	8.7	2.4	1600	50		no	6E-08	***	9E-03	9E-06	1E-05
			1800	50	1	~6	3E-04	1E-02	8E-01	1E-02	1E-02
AVR 76/18	7.1	1.9	1800	200	no	~3	1E-04	7E-02	6E-01	5E-02	5E-02
AVR 88/41	7.6	2.0	1800	24	no	no	2E-07	1E-04	8E-02	1E-04	2E-04
HFR-K3/3	10.2	6.0	1800	100	no	~12	7E-04	2E-03	7E-01	6E-02	6E-02

* simulating calculated core heatup curve　　** out of 16400 particles　　*** not measured

The ^{85}Kr release fractions of the isothermal accident phase of the tests in Fig. 4 show that no particle failure occurs at 1600 °C. ^{85}Kr and thus also the iodine nuclides behaving similarly only show a fractional release of $< 10^{-6}$. If a single particle becomes defective, about 50 % of the particle inventory is released within a few hours, which increases the release by two orders of magnitude. At 1800 °C, isolated pressure vessel defects and transport through coatings that are still intact lead to a further increase in krypton release. At 2100 °C, these effects are enhanced and, in addition, chemical decomposition begins to destroy the SiC coating. Ceramographic sections of particles from heated fuel elements (Fig. 5) show that the pores in the fuel kernels enlarge with increasing temperature. The most important fission product barrier in the HTR fuel element during irradiation and at accident temperatures up to about 2000 °C is the SiC interlayer, which only exhibited decomposition phenomena after the 2100 °C heating test, whereas no damage was apparent at 2000 °C /5/.

Tests on four fuel elements from the AVR reactor with more than 9 % FIMA after a calculated MODULE depressurization accident curve led to three particle defects in a single fuel element at about 1600°C. Investigations have shown that individual fuel elements in the AVR reactor may have been exposed to comparatively high irradiation temperatures, which may have contributed to particle failure /6/. Heating experiments are therefore particularly important to determine the particle load limits on fuel elements irradiated under real MODULE conditions in the proof tests (HFR-K5, -K6). Fig. 6 shows individual particle defects at 1600 °C in compacts with about 1650 UO_2-TRISO particles each, which had been irradiated before to significantly higher (compared to MODULE) burnup and fluence values /7/.
A large portion of the heated spherical fuel elements and compacts were electrolytically de-consolidated after the 1600 °C, 1700 °C and 1800 °C heating experiments, and the fission product distribution was then measured in the matrix and particles and, in part, in their components. The ^{137}Cs distribution in high burnup compacts after about 300 hours of heat testing is shown in Fig. 7 /7/.
The most important findings on the transport of solid fission products, which are also of significance for release calculations, are as follows:

Caesium is internally released most rapidly from the fuel kernels, mainly in the near-kernel buffer layer. However, a significant release from the particles was only measured at 1800 °C, retention in the matrix graphite preventing rapid release from the fuel element. Different caesium releases from single particles of a fuel element show the different degree of damage to the SiC layers.

Strontium in comparison to caesium is very well retained in the oxide fuel kernels and in the matrix graphite, which almost completely prevents release from the spherical fuel element at 1600°C. Strontium release approaches caesium release at 1800°C. The storage effect of the coating is relatively small for strontium in contrast to caesium.

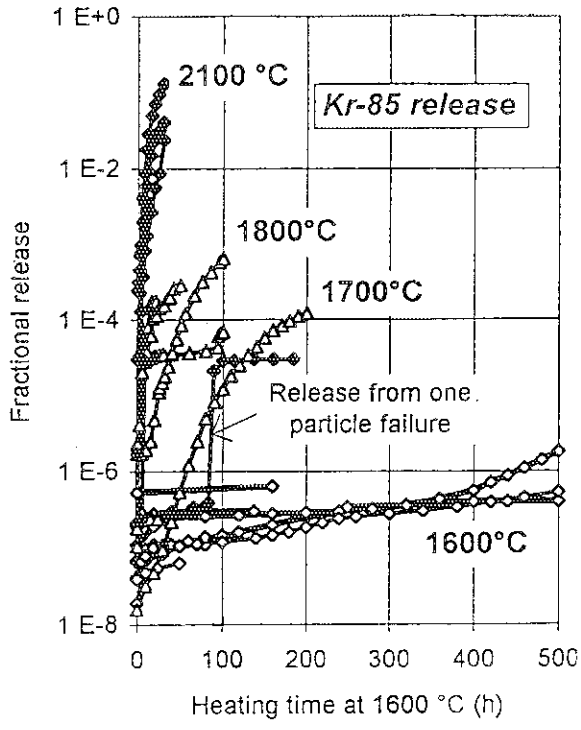


Fig. 4: ^{85}Kr release during heating tests with spherical fuel elements (9% FIMA)

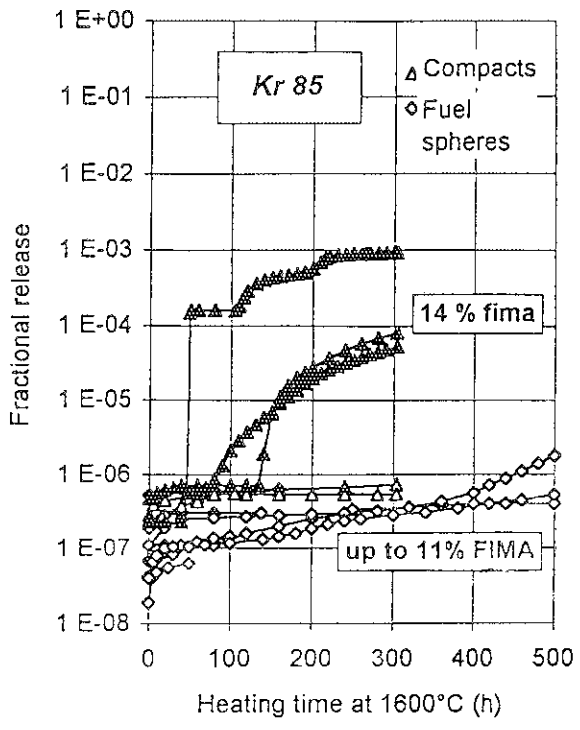


Fig. 6: ^{85}Kr release from compacts and spherical fuel elements during 1600 °C heating tests

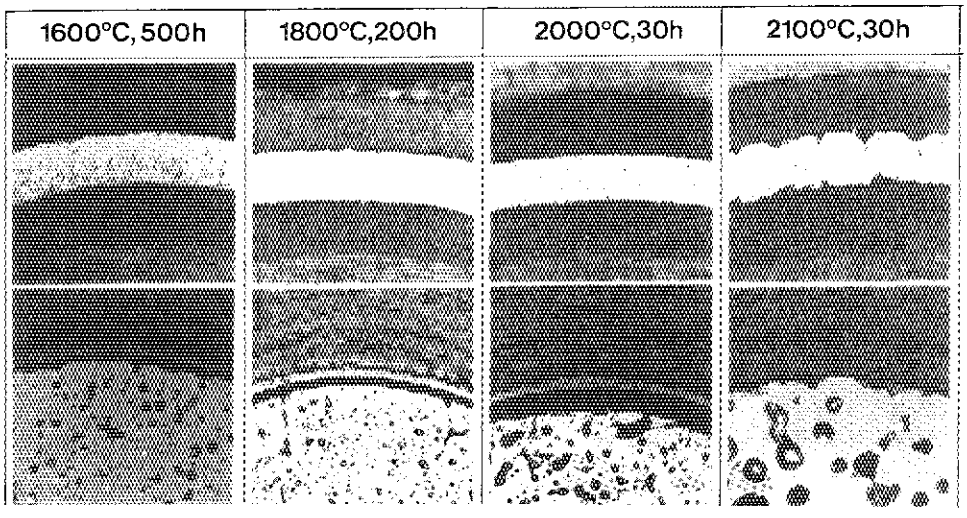


Fig. 5: Ceramographic sections from particles of heated fuel elements (7-8% FIMA)

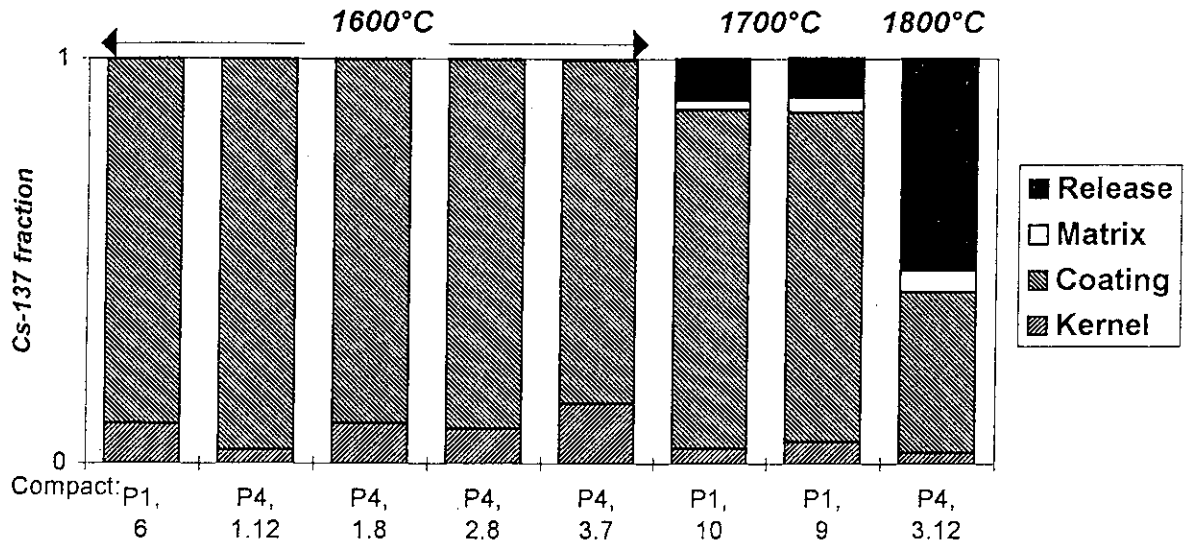


Fig. 7: Caesium distribution in particles and matrix graphite and release from high burnup compacts (10-14% FIMA) after about 300 hours at 1600/ 1700/ 1800°C

Silver was released with the highest fraction from the fuel elements, which is attributed to the good diffusion capability of the small atoms. Silver penetrates particularly rapidly through the matrix graphite, whereas the retention in the kernel is even higher than that of caesium and better than that of strontium in the coating.

Thus, we were able to demonstrate that modern, TRISO coated, UO_2 particles will retain all safety-relevant fission products up to 1600°C at a level not exceeding release under normal operating conditions. If the maximum burnup is kept to 11% FIMA, the "allowable" temperature may be 1700-1800°C, while high burnup fuels have to be limited to 1600

3.1.2 Release from low burnup fuel elements

In the DIDO reactor at Jülich, two experiments with three spherical fuel elements each, FRJ2-KA1 and FRJ2-KA2, were irradiated up to 0.6 and 2 % FIMA at temperatures below 500 °C, in order to determine the level of heavy metal contamination and iodine/fission gas release. One fuel element each from the two experiments was first heated for 50 hours at 1000 °C, 1200 °C and 1400 °C and then every 50 hours at 1600 °C. In one case, heating to 1800 °C and in another even to 2000 °C was carried out additionally. Particle defects did not occur. As shown by the fuel element results from experiment FRJ2-KA2 (Fig. 7), the expected similarity between iodine and fission gas release was observed at an extremely low activity level. Even if it is conservatively assumed that the entire ^{131}I release amounts to 10^{-7} after further heating at 1800 °C and originates solely from the free heavy

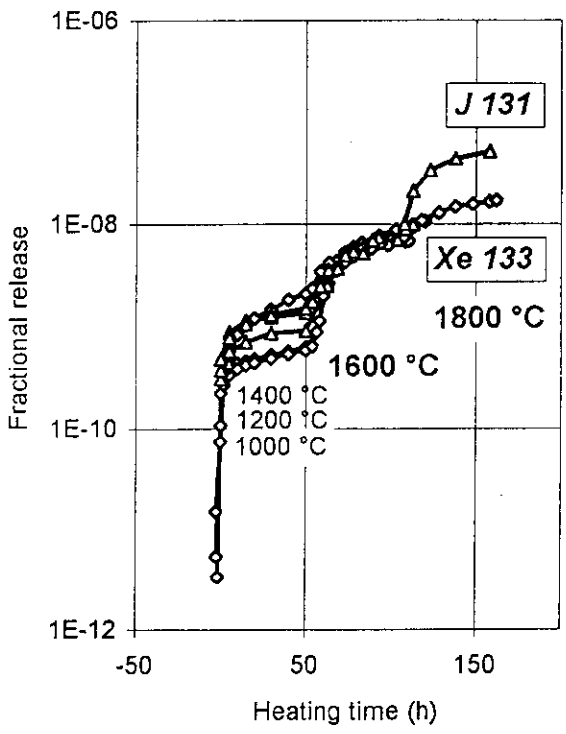


Fig. 8: ^{131}I and ^{133}Xe release during heating experiments on spherical fuel elements (max. 2 % FIMA)

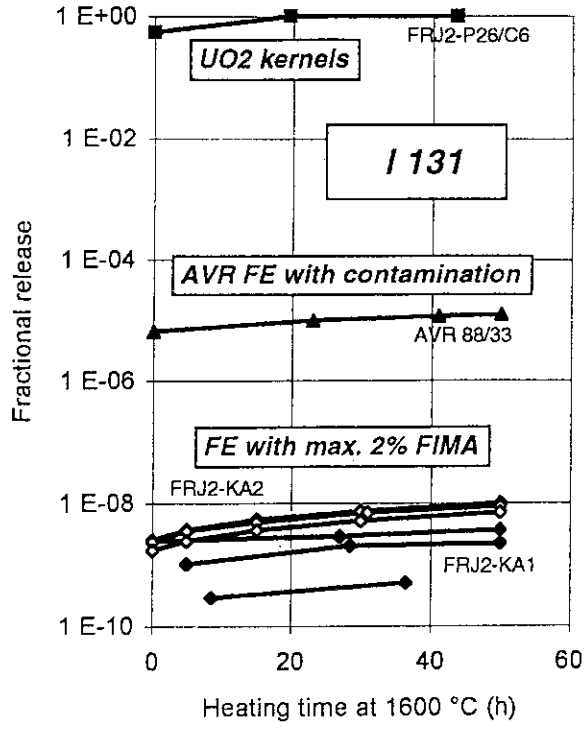


Fig. 9: ^{131}I release from UO_2 kernels and spherical fuel elements during 1600 °C heating experiments

Fig. 9 shows comparative measurements at 1600 °C on UO_2 kernels where iodine release is almost complete after 20 hours. One AVR fuel element shows the influence of cross contamination of old fuel element varieties still present in the AVR core together with the modern UO_2-TRISO fuel elements.

3.2. Fuel specimens under water vapour partial pressure

The influence of water vapour on fission product release from defective fuel particles was examined in-pile in two US irradiation experiments /8/ and, in addition, with the experiment HFR-K6 in Petten with state-of-the-art UO_2-TRISO spherical fuel elements /9/.

In the out-of-pile KORA tests, three UO_2-TRISO fuel element spheres and specimens with five UO_2 and UCO kernels each were tested /4/.

The specimens in KORA were all examined at 800 °C and generally first at low moisture (1 kPa) followed by high moisture (50 kPa). The temperature of 800 °C was selected for this first test series because it is an HTR operating temperature and, moreover, a threshold temperature at which the

diffusion of moisture into the matrix graphite is still high and graphite corrosion low. At higher temperatures, chemical interaction with carbon impedes moisture penetration.

Spherical fuel elements with UO_2-TRISO particles can contain one fabrication-related defective particle in two fuel element spheres on average, as was shown by burn leach examinations. No damaged particles were found in the majority of fuel elements, but three in individual fuel elements.

For the 3 heated AVR-GLE3 fuel elements with UO_2-TRISO particles with about 9% FIMA. Moisture-induced ^{85}Kr releases were measured in two cases, while no release was detectable at all for one fuel element. Fig. 10 shows the measured releases and release rates relative to the total fuel element inventory from one of these tests. Since reactor experiments have proved for this fuel element variety that irradiation-induced particle defects do not occur, the ^{85}Kr releases are attributed to particle failure due to fabrication. The kernels of these defective particles can also have been carburized during manufacture in the final 1950 heat treatment, which may lead to changed release behaviour under the influence of moisture.

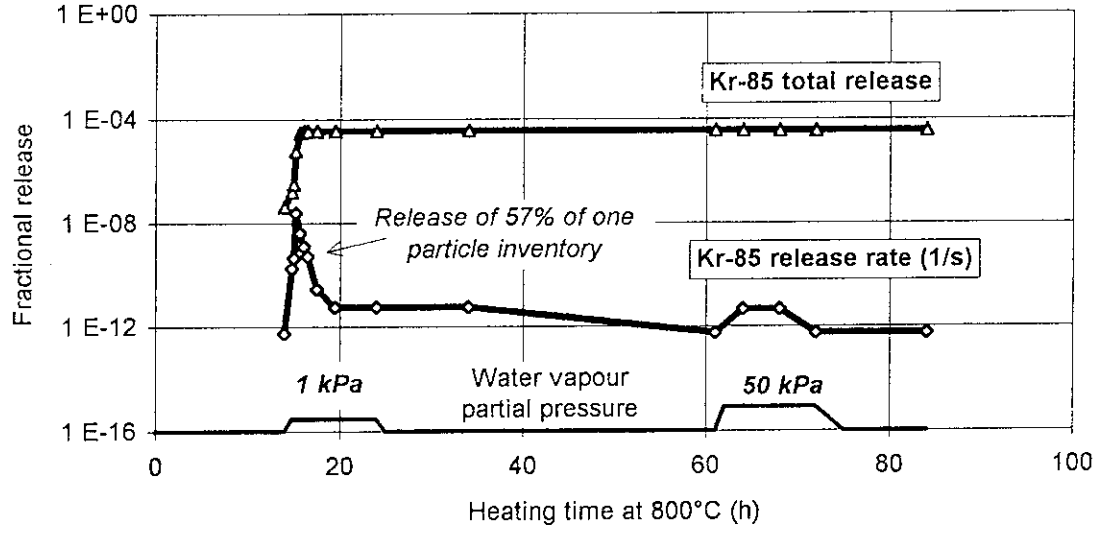


Fig. 10: Kr-85 release from a spherical fuel element (AVR-GLE3, 89/30; 9 % FIMA) during heating at 800 °C with intermittent water vapour injections

The typical curve for fission gas release from fuel kernels is obtained under the influence of water vapour. Initially, a strong release increase (burst) occurs after water vapour injection. The release rate then decreases to a lower equilibrium release which, however, is still clearly above the release prior to the water vapour phase. At the end of water vapour injection, the release rate decreases to the value prior to the addition of water vapour (Fig. 11). Water vapour thus has an effect on fission gas release similar to that of a temperature increase.

In the HFR-K6 irradiation experiment with four spherical fuel elements, water vapour with different partial pressure (0.2-2 kPa) was intermittently added in two capsules. In capsule 3 with fuel sphere 4,

the elevated R/B fission gas release rates were indicative of two fabrication-related particle defects. The moisture-induced release increases from this fuel element during the 22nd and 25th irradiation cycle (Fig. 11) rise with the water vapour partial pressure. The experiment was terminated after the 26th cycle when sphere 4 reached a burnup of 9.2 % FIMA.

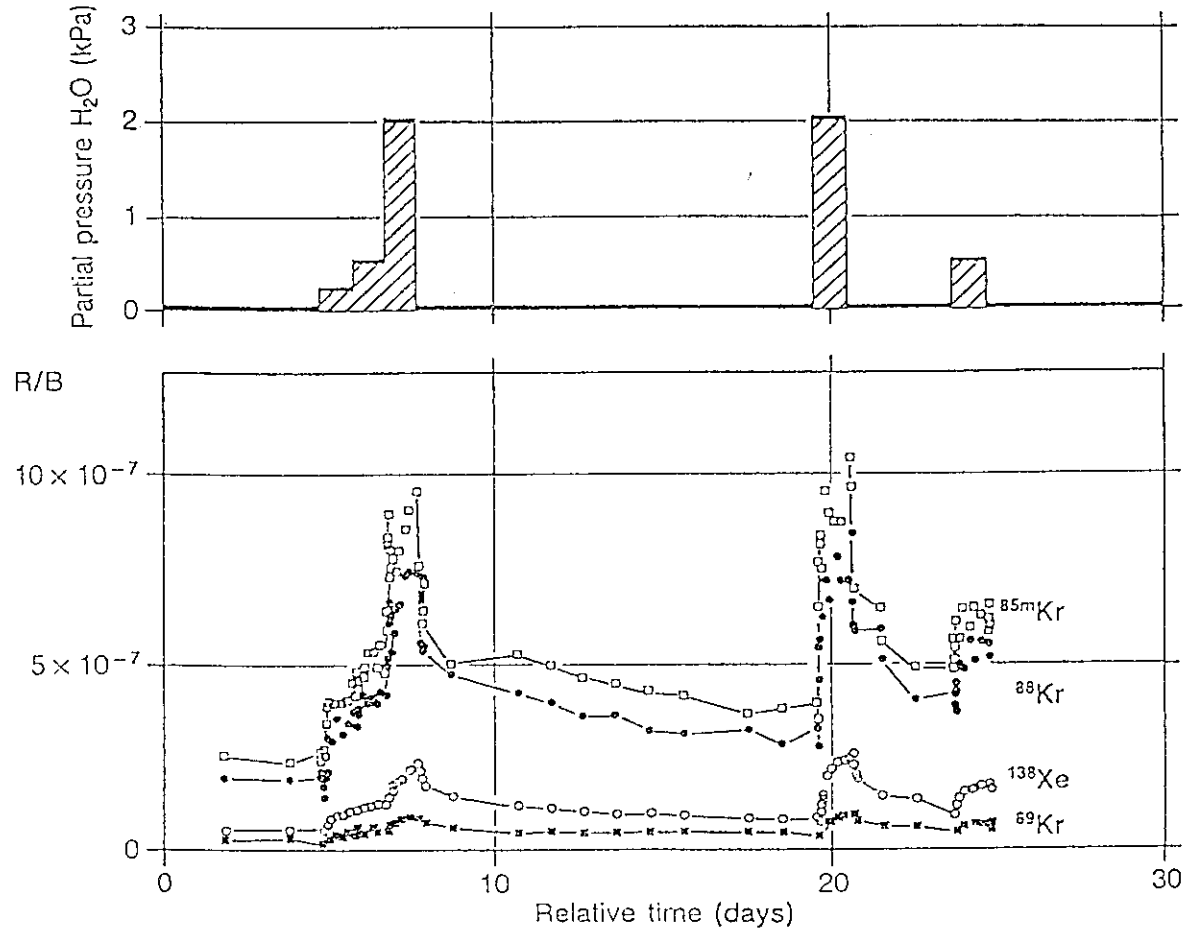


Fig. 11: Water vapour injections during irradiation of fuel element HFR-K6/4 result in an increase of measured krypton and xenon release rates (irradiation experiment HFR-K6 with German fuel, irradiation cycle 25)

Normalised to 800 °C, a release fraction of 23 % (HFR-K6, 25th cycle) from the defective particles was calculated at the highest water vapour pressure of 2 kPa. Assuming for the heating test on sphere 89/30 (Fig. 10) that two defective particles contributed to the measured Kr-85 release in this case, too, i.e. 29 % release per defective particle, good agreement is obtained between in-pile and out-of-pile experiments.

In order to better allocate the number and type of defects to moisture-induced fission gas release, UO_2 and UCO fuel kernels with different burnups were also examined. They were obtained by cracking particles from disintegrated fuel elements. The data and results of these experiments are

compiled in Tab. 3. The ^{85}Kr release profile from three experiments with different burnup kernels is shown in Fig. 12.

Table 3: Total ^{85}Kr release from five fuel kernels each: during fabrication by cracking particles, during the 800 °C heating test with water vapour injections and during subsequent high-temperature testing

Fuel kernels	*Fuel type*	*Burnup (% FIMA)*	*Kr-85 release fraction (%)*				
			Before test (internal release)	*At test before 1st injection*	*1st Injection 1 kPa w. v. at 800°C*	*2nd Injection 50 kPa w. v. at 800°C*	*A.-test at 2060°C*
AVR 73/8a	UO2	4.7	-	3.9	2.6	1	89.6
AVR 73/8b	UO2	4.7	-	4.7	0.4	0.6	94.2
AVR 92/29a	UO2	9.2	57	0.7	16.6	0.3	24.7
HFR, tr. 3-7a	UCO	19.5	-	29.1	65.6	1.6	2.5
HFR, tr. 3-7b	UCO	19.5	-	78.4	16.9	no inj.	2.1

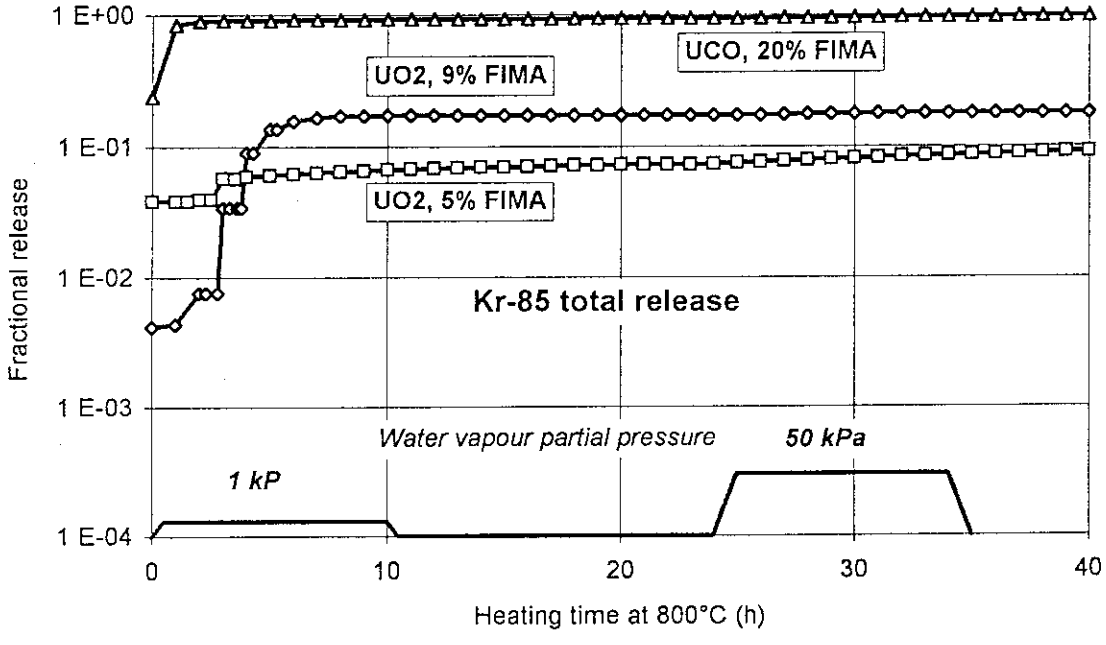


Fig. 12: ^{85}Kr release from specimens with five fuel kernels each during the 800 °C experiment with intermittent water vapour injections

Moisture-induced release clearly increases with burnup. The highest ^{85}Kr release for kernels with an average burnup of about 5 % FIMA (the MODULE target value is 9 % FIMA) was measured during heat-up and in the 800 °C starting phase, whereas the release increase influenced by water vapour is comparatively small. In the case of fuel kernels from the AVR fuel element 92/29, internal ^{85}Kr

release as a consequence of high possible irradiation temperatures in the AVR only left 43 % of the computational inventory in the kernel at the beginning of experiments. Release during the first water vapour injection is 16.6 instead of 38.6 % relative to this available ^{85}Kr. The significance of this value, however, has to be proved by further investigations. The significant releases from the UCO kernels, which were also obtained by cracking intact particles, are obviously attributable in all cases to the simultaneous bursting of kernels due to high internal gas pressure.

The burnup dependence of ^{85}Kr release under the influence of water vapour can be related to the appearance of different burnup fuel kernels (Fig. 13).

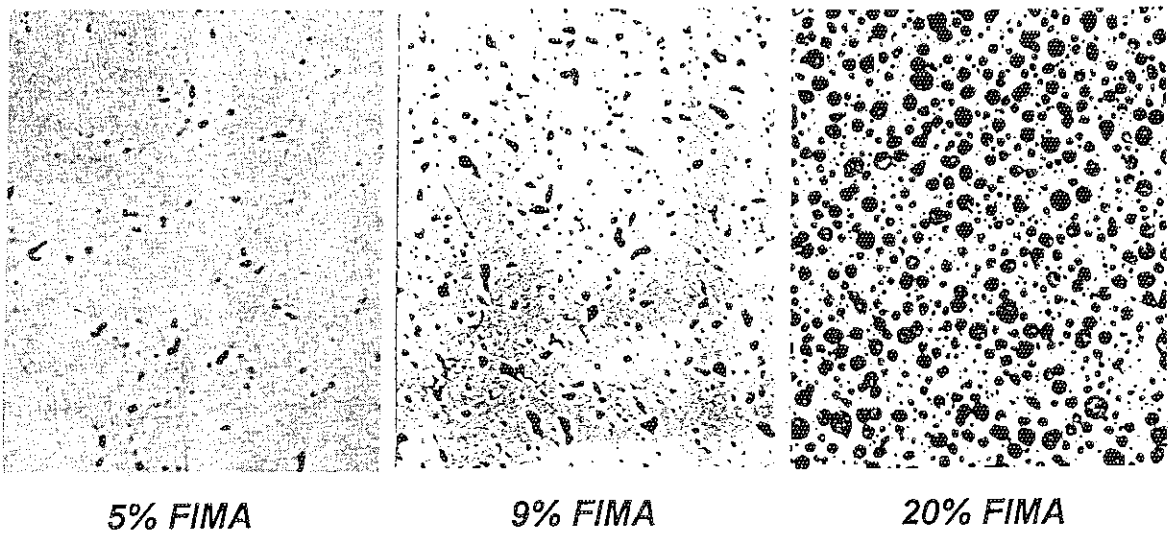


Fig. 13: Kernel sections from different burnup fuel particles

It can be seen that the kernel structure is significantly changed with increasing burnup; in particular, increased pore formation occurs as a consequence of growing fission gas inventory. The formation of gas pores and possibly also the changed chemical composition seem to basically cause almost complete fission gas release from the UCO(UO_2) kernels during irradiation and in the heating experiment at corresponding temperature and/or moisture.

Investigations with unirradiated UO_2 under water vapour did not indicate any structural changes that could lead to an increase in fission gas release. This is in conformity with the comparatively good ^{85}Kr retention in UO_2 kernels with 4.7 % burnup.

It has not been possible to demonstrate a similar burnup dependence with American in-pile experiments with UCO kernels /8/.

3.3. Fuel specimens in air

Experiments with UO_2-TRISO particle specimens and spherical fuel elements in air at a flow rate of 30 l/h and a pressure of about 1300 mbar were carried out in KORA (Tab. 4) /10/.
First of all, batches of ten UO_2-TRISO particles each from two disintegrated AVR fuel elements with differently high burnup were heated. Whereas only one particle was damaged after 397 hours at 1400 °C, defects occurred in all 10-particle batches at 1500 °C irrespective of burnup. When heated up to 1620 °C, damage began at 1613 °C. This shows that the oxidation of the SiC layer until destruction proceeds slowly at temperatures around 1400 °C and rapidly towards 1600 °C.

Table. 4: Heating tests with particles and fuel spheres in air (UO_2-TRISO)

Fuel sample	Number of particles	Burnup (% FIMA)	Test conditions			Kr-85 release		
			Heatup (h)	Max. temp. (°C)	Time (h)	1st failed particle after	Number of failed particles	Fraction of failed particles
92/29,12	10	9.2	14	1400	400	397 h	1	1.0E-1
73/8, 11	10	4.7	15	1500	25	8 h	10	1.0E+0
92/29,13	10	9.2	15	1500	25	3 h	10	1.0E+0
92/29,11	10	9.2	28	1620	1	at 1613°C	10	1.0E+0
AVR 89/12	16400	9.4	13	1300	410	258	4	2.4E-4
AVR 92/22	16400	8.8	14	1400	140	1	20	1.2E-3
AVR 89/14	16400	9.0	14	1400	70	2	12	7.3E-4

Table 4 also shows the results from tests with three spherical fuel elements. At 1300 °C, only one of the 16,400 particles of the fuel sphere was damaged after 258 hours, followed by three further particle failures in the period up to 410 hours. In the 1400 °C experiments, individual defects begin shortly after the heat-up phase, but it is remarkable in this case, too, that only about 0.1 % of the particles were damaged in the further course of the experiments.
Fig. 14 shows the release of the gas activity and of the ^{85}Kr fraction during heating a fuel sphere in air. A temperature of 1100 °C was first selected at which particle defects can be ruled out, but corrosion of the matrix graphite and outer pyrocarbon coating of the particles proceeds rather rapidly. Increased initial release is first observed, which is essentially attributed to tritium contamination on the sphere surface from the sweep gas circuit of the experimental AVR reactor. Subsequent equilibrium release from ^{3}H and ^{14}C results from graphite combustion at an air flow rate of 30 l/h. This combustion is completed after about 100 hours. Following this experimental phase, the particles, which were all intact, i.e. gastight up to then, were heated to 1400 °C. During the 140-hour treatment at 1400 °C about 20 of the 16,400 particles were damaged.

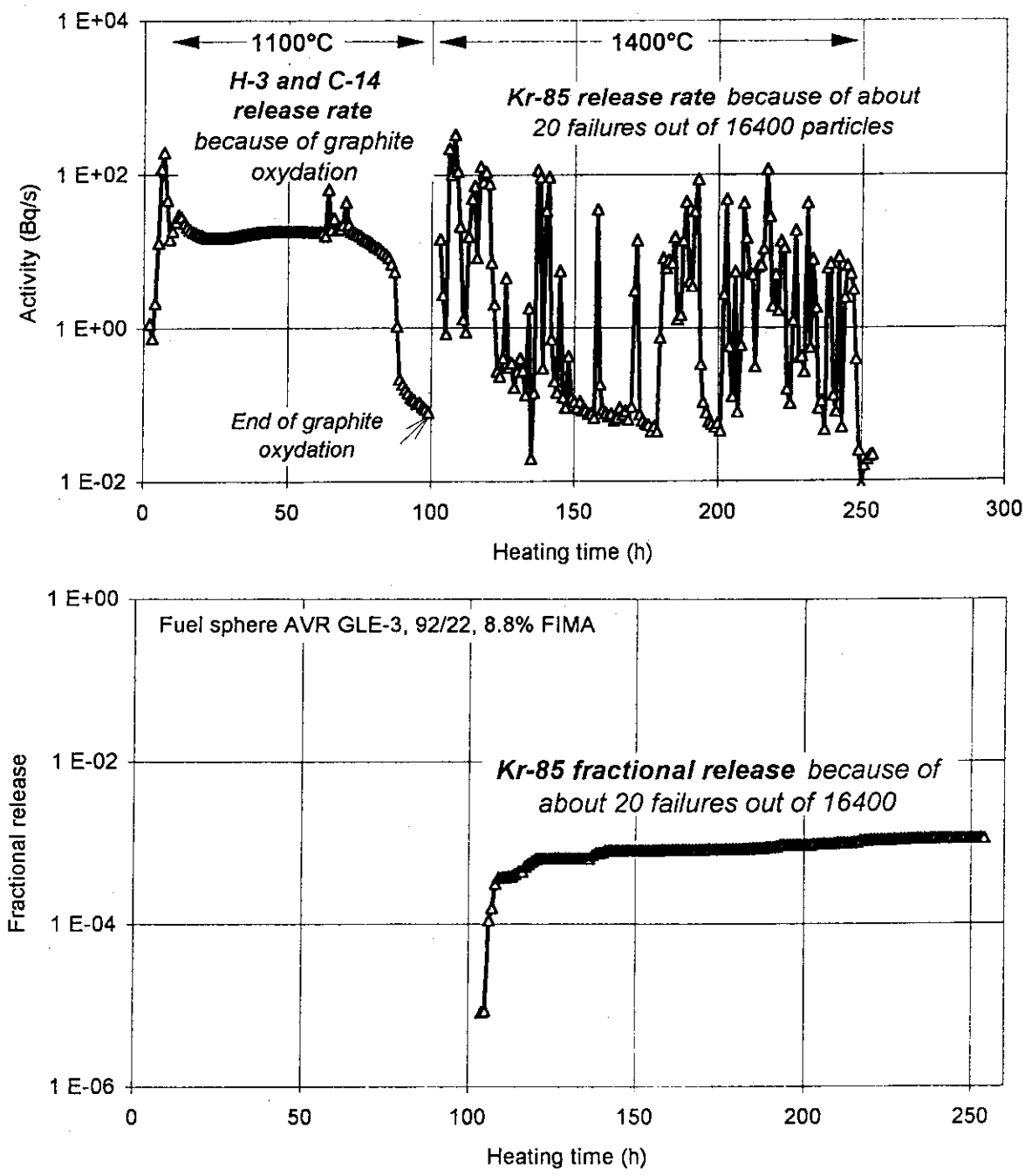


Fig. 14: Oxidation of a fuel sphere in air (AVR 92/8, 9 % FIMA)

5. References

/ 1/ W. Schenk
Untersuchungen zum Verhalten von beschichteten Brennstoffteilchen und Kugelbrennelementen bei Störfalltemperaturen
KFA Report Jül-1490, Mai 1978

/ 2/ G. Lohnert
Technical design features and essential safety-related propeties of the HTR-module
Nucl. Eng. Des. 121 (1990), 259

/ 3/ W. Schenk, D. Pitzer and H. Nabielek
Fission product release profiles from spherical HTR fuel elements at accident temperatures
Report Jül-2234, Research Centre Jülich (1988) (Jül-2091 in German)

/ 4/ W. Schenk, H. Nabielk
Simulation of Steam Ingress Accidents with Irradiated Fuel Elements
IAEA Technical Committee Meeting, Beijing, China, 25-27 October 1993,
IAEA-TECDOC-784, p. 37

/ 5/ H. Nabielek, W. Schenk, W. Heit, A.-W. Mehner and D.T. Goodin
The Performance of HTR Fuel Particles at Extreme Temperatures
Nucl. Techn. 84 (1989), 62

/ 6/ H. Nabielek, W. Rehm, W. Schenk, K. Verfondern and K. Krüger
Validation of predictive methods for thermal behaviour and fission product retention during accidents in small modular HTRs
Post-Smirt Seminar on Small and Medium-Sized Nuclear Reactors, New Delhi, August 1981

/ 7/ W. Schenk, R. Gontard, H. Nabielek
Performance of Fuel Samples under High-Irradiation and Accident Simulation Conditions, with Emphasis on Test Capsules HFR-P4 and SL-P1
KFA Report Jül-2992, November 1994

/ 8/ Myers, B.F.
Effect of Water Vapor on the Release of Fission Gases from Uranium Oxycarbide in High-Temperature, Gas-Cooled Reactor Coated Fuel Particles
J. Am. Ceram. Soc., 75, 686-693 (1992)

/ 9/ H. Nabielek, R. Conrad, K. Röllig, B.F. Myers
Fuel Irradiation Experiments HFR-K6 and HFR-B1 with Intermittent Water Vapor Injections
IAEA Technical Comittee Meeting, Beijing, China, 25-27 Octobe 1993

/10/ W. Schenk, G. Pott
Brennelemente mit hochabgebrannten beschichteten UO_2-Brennstoffpartikeln in Luft
Jahrestagung Kerntechnik '95 in Nürnberg, 16. - 18.5.95, Tagungsbericht S. 348

STATUS OF THE RESEARCH AND DEVELOPMENT AT JAERI ON THE C/C COMPOSITE CONTROL ROD FOR HTGR

M. Eto and S. Ishiyama
Japan Atomic Energy Research Institute
Tokai-mura, Ibaraki-ken 319-11 Japan

It is widely recognized that the control rod made of the C/C composite material would show the better performance for the HTGR than that of a metallic alloy. In the case of the High Temperature Engineering Test Reactor, HTTR, the control rod is made of Alloy 800H for which a particular process is imposed when the reactor needs to be shut down. The process rises from the limited heat resistance of the metallic alloy. The less restricted operation of the reactor as well as the even more reliable integrity of the core structure would be attained if there would be the control rod more resitant to high temperature environment.

In this respect the use of C/C composite for the control rod for HTGR is believed to be aspired, though there still remain a few difficulties to be overcome towards the actual use of the material in the reactor: evaluation of the effect of neutron irradiation on its properties, fabrication of the elements, structural integrity of the elements, etc. The present paper summarizes the present status of the R & D on the C/C composite control rod at JAERI.

Materials used were pitch- or PAN-based fiber-reinforced 2-dimensional carbon composites, from which preforms of the elements of a cotrol rod were fabricated. The preforms were carbonized at 1000°C after being impregnated with pitch. Then they were graphitized at 3000°C, followed by a purification treatment with halogen. The elements included the pellet holder to accommodate boron carbide pellets, lace track and pin. The pellet holder and lace track were preformed through the combination of cross-nitting and filament winding techniques. The pin was fabricated by the fiber laminating technique. A control rod is to consist of pellet holders which are connected by the lace tracks with pins.

Various strength tests were carried out on these elements uaing a screw-driven test machine at room temperature. An irradiation of the elements made of PAN-based material was performed in JRR-3 at JAERI at 900+50°C to a neutron fluence of 1×10^{25} n/m^2 (E>29fJ). As for the strength tests on

the elements, there were some differences between PAN- and pitch-based composites: In general, elements made of PAN-based composite showed the more plastic behavior before they fractured, whereas those of pitch-based material behaved in the more brittle manner.

Fracture tests of the irradiated elements showed that frature load and fracture displacement enough for assuring the integrity of the control rod structure were maintained even after the irradiaion. It was also found that if the applied load was parallel to the fiber felt plane both fracture load and strain increased, whereas the load increase and strain decrease were observed for the applied load was against the plane.

3.3 RESEARCH AND DEVELOPMENT ON C/C COMPOSITE CONTROL ROD FOR HTGR

M. Eto, S. Ishiyama and H. Ugachi
Japan Atomic Energy Research Institute
JAPAN

ABSTRACT

For the High Temperature Engineering Test Reactor, HTTR, the control rod sleeve is made of Alloy 800H for which a particular process is imposed when the reactor needs to be scrammed. The process rises from the limited heat resistance of the metallic alloy. The less restricted operation of the reactor as well as the even more reliable integrity of the core structure would be attained if there would be the control rod more resitant to high temperature and neutron irradiation.

In this respect the use of C/C composite for the control rod for HTGR is believed to be aspired, though there still remain a few difficulties to be overcome towards the actual use of the material in the reactor: evaluation of the effect of neutron irradiation on its properties, fabrication of the elements, structural integrity of the elements, etc. The present paper summarizes the present status of the R & D on the C/C composite control rod at JAERI.

Materials used were pitch- or PAN-based fiber-reinforced 2-dimensional carbon composites, from which preforms of the elements of a cotrol rod were fabricated. The preforms were carbonized at 1000°C after being impregnated with pitch. Then they were graphitized at 3000°C, followed by a purification treatment with halogen. The elements included the pellet holder, lace truck and pin. The pin was fabricated by the fiber laminating technique. A control rod is to consist of pellet holders which are connected by the lace trucks with pins.

Various strength tests were carried out on these elements. An irradiation of the elements made of PAN-based material was performed in JRR-3 at 900±50°C to a neutron fluence of 1×10^{25} n/m^2 (E>29fJ). As for the strength tests on the elements, there were some differences between PAN- and pitch-based composites: In general, elements made of PAN-based composite showed the more plastic behavior before they fractured, whereas those of pitch-based material behaved in the more brittle manner.

Fracture tests of the irradiated elements showed that frature load and fracture displacement enough for assuring the integrity of the control rod structure were maintained even after the irradiaion. It was also found that if the applied load was parallel to the fiber felt plane both fracture load and strain increased, whereas the load increase and strain decrease were observed for the applied load was against the plane.

1. Introduction

An HTGR named High Temperature Engineering Test Reactor(HTTR) has been under construction at JAERI, Oarai Research Establishment since 1990 and is supposed to attain criticality in 1997. As is shown in Fig. 1 the core of the reactor consists of arrays of stacked fuel or replaceable reflector blocks made of graphite. In the normal operation conditon the maximum temperature of the graphite blocks will be around 1300°C when the temperature of the helium coolant at the outlet is 950°C [1]. To control the reactivity control rods are to be inserted into appropriate holes in the core and reflector blocks. In the event of a scram the control rods are inserted into the core taking advantage of the gravity. Nine out of 16 pairs of control rods in the reflector region are inserted immediately at the time of scram, while the other seven pairs in the core region are to be inserted 40 minutes later when the tempeature of the outlet coolant becomes lower than 750°C. The two step inserting method is employed mainly for the purpose of preventing the control rod sleeves in the core region from overheating. Fig. 2 shows an overview of the present control rod system to be applied for the HTTR. In the system the control rod sleeve will be made of Alloy 800H.

Since the carbon-carbon (C/C) composite material is believed to be the more heat resistant than Alloy 800H, it would be lessen the restriction imposed on the reactor control procedure, if the control rod sleeve which accommodates boron carbide/carbon pellets is to be made of the material. The prominence of the C/C composite has been widely recognized as a high strength heat resistant structural material. Effect of neutron irradiation on thermal, mechanical and other properties of the composite has been fairly extensively examined by a number of investigators[2-9] so that the data on the material have been accumulated much enough to think about its application to high temperature components of nuclear facilities.

In consideration of this situation a concept of control rod to be made of C/C composites has been proposed at JAERI in quest of the even better performance of the control rod for the HTTR. On the basis of the concept several elements for the control rod have been prepared from C/C composites and their mechanical strengths have been tested both before and after neutron irradiation. This paper summarizes the results of fracture tests of the elements to evaluate the applicability of the material to the control rod, aiming at the further development of the more heat-resitant control rod.

2. Experimental

PAN(polyacrylonytrile)-based or pitch-based carbon fibers were used for the preparation of elements for the control rod. These elements were shown in Fig. 3. The

textile preforms were enforced two-dimensionally. After being impregnated with pitch, the preforms were carbonized at 1000°C and graphitized at 3000°C. Then they were purified with halogen gas. The pellet holder and the lace truck were preformed by the combination of the cross-knitting and filament winding techniques. The fiber lamination technique was employed for the fabrication of pins. Fig. 4 shows a schematic for the control rod when these elements are assembled.

The strength of these elements was measured at room temperature in air using a screw-driven tensile test machine. Compressive tests of the pellet holder were carried out in its radial direction or axial one, as shown in Fig. 5(a). The lace truck was tensile-tested in a manner shown in Fig. 5(b). Bending strength of the pins was measured by three point method in either the across or parallel direction, as is shown in Fig. 5(c). Cross-head speed for these tests was 0.5 mm/min. Some of these elements were irradiated at 900± 50°C in JRR-3 to a maximum fluence of 1×10^{25} n/m^2(E>29fJ).

3. Results and Discussion

3.1 Comparison between the PAN- and pitch-based materials

Fig. 6 shows the results of the bending test of pins made of PAN- or pitch-based material. The fracture strain for each material in the present case is several times larger than that for most materials which have been examined before[8-10]. The strength is also larger or comparable to that of the materials previously investigated. The fracture strength and strain of the materials in the present study seem to be comparable to those of PAN-based materials examined by other researchers who prepared hybrid C/C composites with surface treated fibers[11]. Comparing the present materials with each other, the pitch-based material showed the less brittle behavior, though the fracture strain seemed to be large enough even for the PAN-based material. The parallel specimens, which imply that their felt plane was parallel to the applied load, endured fairly larger stress comparing with the against specimens, whereas the fracture strain seems to be larger for the latter. This suggests that the felt plane bends more readily when the load is applied against itself.

Fig. 7 shows the results of the fracture test of pellet holders. Here, the ordinate and abscissa represent the load and displacement of the cross-head, respectively. It is seen in Fig. 7(a) that the axial fracture load does not differ much between the two materials, whereas the amount of deformation seems to be a little larger for PAN-based material than for the pitch-based one. The radial fracture load is much larger for the PAN-based material than for the pitch-based, which is seen in Fig. 7(b). On the basis of its larger fracture load and deformability observed in the case of radial fracture test, only PAN-based material was chosen for the irradiation experiment, since the space which was to accommodate the element specimens was limited in the reactor.

3.2 Results of the irradiation experiment on the PAN-based material

(1) Pins

Fig. 8 shows stress-strain curves obtained from the bending test of pins made of PAN-based material. Loads were applied to the specimens either (a)parallel to or (b)against the felt plane. It is to be noted that the strength increased very pronouncedly when the load was parallel to the plane. This is probably because the strength of the specimen parallel to the felt plane would be less influenced by the weakening of the bond between the felt planes which might be caused by the irradiation. Though there was no large difference in the bending strength and fracture strain between the parallel and the against specimens before irradiation, they behaved diferently after irradiation. As is seen in Fig. 8(b) for the against specimens, the bending strength increased after irradiation, whereas the fracture strain decreased, which seems to be characteristic of irradiated carbon materials. In fact, the most materials examined in the previous experimant showed this general trend[8,9].

Peak stress(bending strength) versus fracture strain is plotted in Fig. 9 for both irradiated and unirradiated pins of PAN-based material. It is to be noted in this figure that the strength of parallel specimens increases with increasing fracture strain, whereas that of against specimens decreases with increasing fracture starain. It is interesting to find that the solid lines drawn in the figure fit to the data points for both irradiated and unirradiated specimens.

(2) Lace trucks

The results of the fracture test of lace trucks are shown in Fig. 10, where one can see that both strength and displacement, which was estimated from the movement of the cross-head, are larger for the irradiated specimens than for the unirradiated. A tendency similar to that observed for the pin was also found for the lace truck, which is shown in Fig. 11, since the felt plane of the lace truck was parallel to the loading axis, i.e., the strength increases with increasing fracture starain, though in this case the strain is not the one derived from the strain gage but from the displacement of the cross-head of the tensile test machine.

(3) Pellet holder

Load versus displacement curves for pellet holders in the cases of axial and radial loadings are shown in Figs. 12 and 13, respectively. It is to be noted that the fracture load for the axial loading seems to increase after the irradiation, even though the curve is rather rugged, which is probably because of the inclination to the buckling during the test. In the case of radial loading, fairly large decrease in the fracture load as well as in the fracture displacement was observed after the irradiation, though the values of both load and displacement seem to be large enough to assure the integrity of the control rod.

(4) Dimensional changes caused by the irradiation

Results on the dimensional changes caused by the irradiation are shown in Fig. 14 for three kinds of elements. The dimensional changes of the control rod elements here are rather large comparing with those of the C/C composite materials, which have been reported in the references[8,9]. In an irradiation condition similar to the present case, dimensional reduction larger than 1 % was caused only for a uniaxial material and most materials showed reduction smaller than 0.3 %[8,9]. However, the dimensional reduction of about 2 % caused in the present irradiation conditon is believed to be tolerable for the design of the control rod of C/C composites. Moreover, it is very probable that the future modification or improvement of the material, of the preparation technique of preforms and/or of the heat treatment procedure would increase the stability of the irradiated elements. Along this line, the elements the concept of which is different from that for the ones tested in the present study were also considered and prepared for the future evaluation. This is shown in Fig. 15.

(5) Young's modulus

Fig. 16 shows changes in the Young's modulus of irradiated elements. Here, the data on the pin are derived from stress-strain curves obtained using strain gages during the bending test. The rest of the data are relative values calculated from the load-displacement curves.

The results on pins which indicate that there is a rather large difference in the modulus change between the parallel and the against specimens are reasonable if the fact that the against specimen can bend more readily than the parallel specimen is taken into account, i.e., the lower modulus of the against specimens. The apparent decrease in the modulus of the lace truck may be fortuitious in consideration of the method of calculation described above.

4. Conclusions

Elements for the control rod to be used in the HTTR were prepared from two kinds of carbon-carbon composites, pitch-based and PAN-based, aiming at the development of the more heat-resistant control rod which is believed to lessen the restriction on the operation and shut-down processes of the HTTR. The elements included pellet holder, lace truck and pin.

Main conclusions are;

(1) For the unirradiated elements those of PAN-based material showed the more deformable behavior than those of the pitch-based.

(2) Elements of PAN-based material irradiated at 900°C to a fluence of 1×10^{25} n/m^2 ($E>29fJ$) maintained the fracture load and fracture displacement which may well be believed to be enough to assure the integrity of the control rod made of the material.

(3) The dimensional changes of the elements were at most less than 2 % after the irradiation.

(4) The strength and fracture starain increased after the irradiation when the applied load was parallel to the felt plane, whereas the strength increase and strain decrease were observed for the load applied against the plane.

References

1) S. Saito et al., JAERI-1332, September 1994.
2) S. Sato et al., J. At. En. Soc. Japan 32(1990)1124-1132.
3) T.D. Burchell et al., Proc. 5th Int. Carbon Conf., Essen, Germany, June 22-26, 1992, pp.985-987.
4) T. Maruyama amd M. Harayama, J. Nucl. Mater. 195(1992)44-50.
5) F. Gao et al., Carbon 31(1993)103-108.
6) H. Matsuo amd T. Nagasaki, J. Nucl. Mater. 217(1994)340-343.
7) C.H. Wu et al, J. Nucl. Mater. 212-215(1994)1168-1173.
8) M. Eto et al., ibid., 1223-1227.
9) H. Ugachi et al., to be published.
10) S.-M. Oh and J.-Y. Lee, Carbon 27(1989)423-430.
11)L.O.Pardini and B. MacEnaney, Carbon 32(1994)815-824.

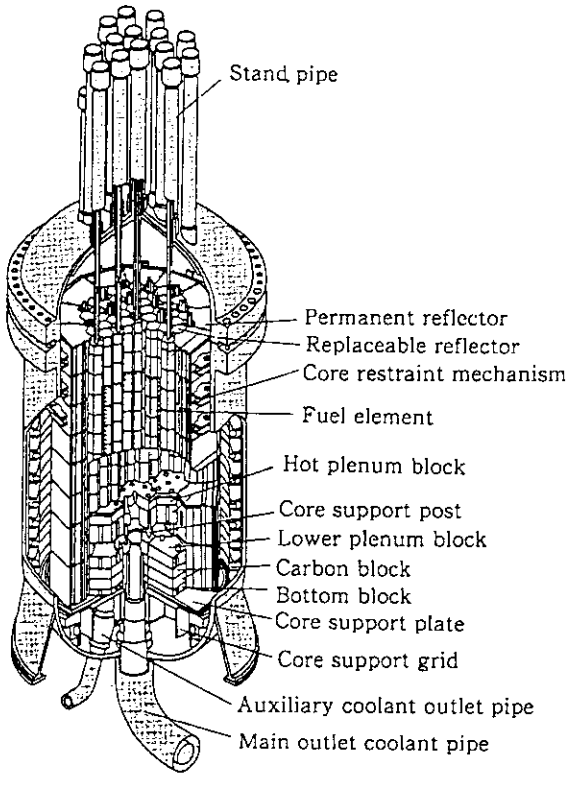


Fig. 1 A schematic for the HTTR pressure vessel and core.

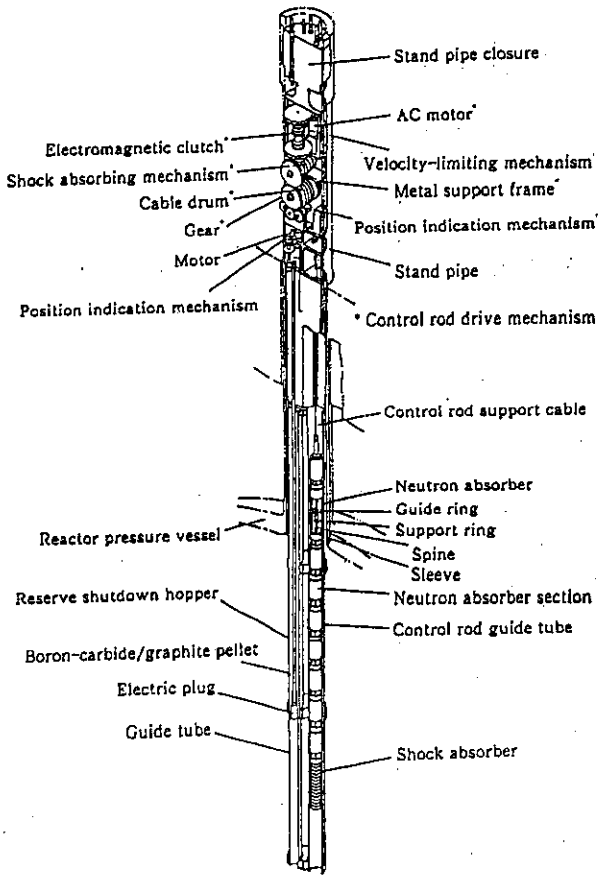


Fig. 2 Reactivity control system of the HTTR.

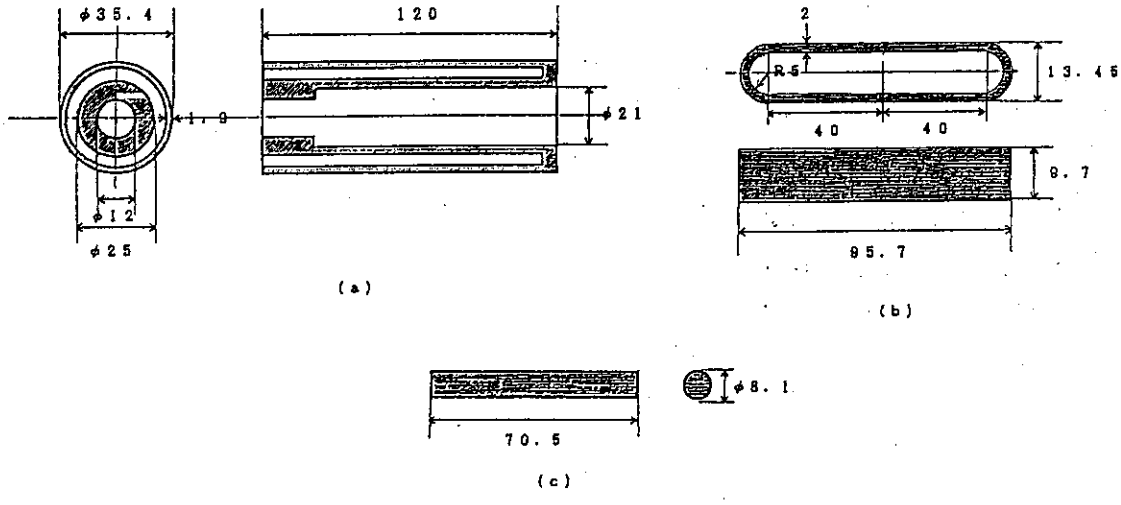


Fig. 3 Control rod elements prepared and tested in the present study.

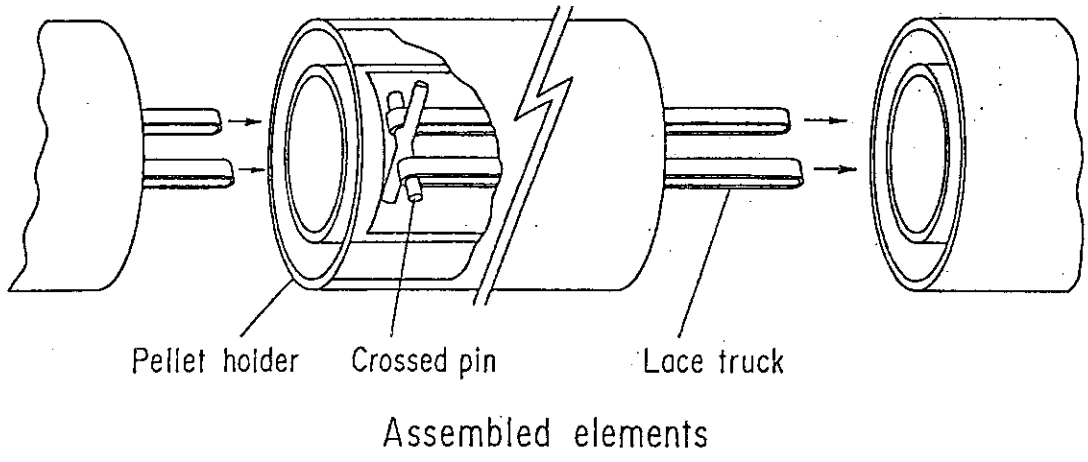


Fig. 4 A schematic for the control rod consisting of the elements.

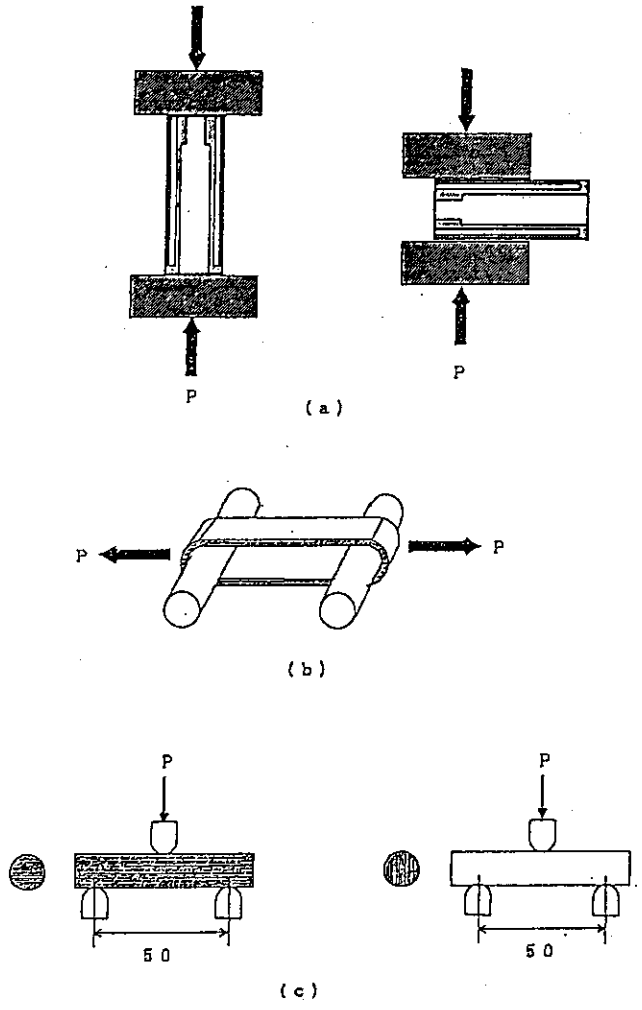


Fig. 5 Method of mechanical strength tests.

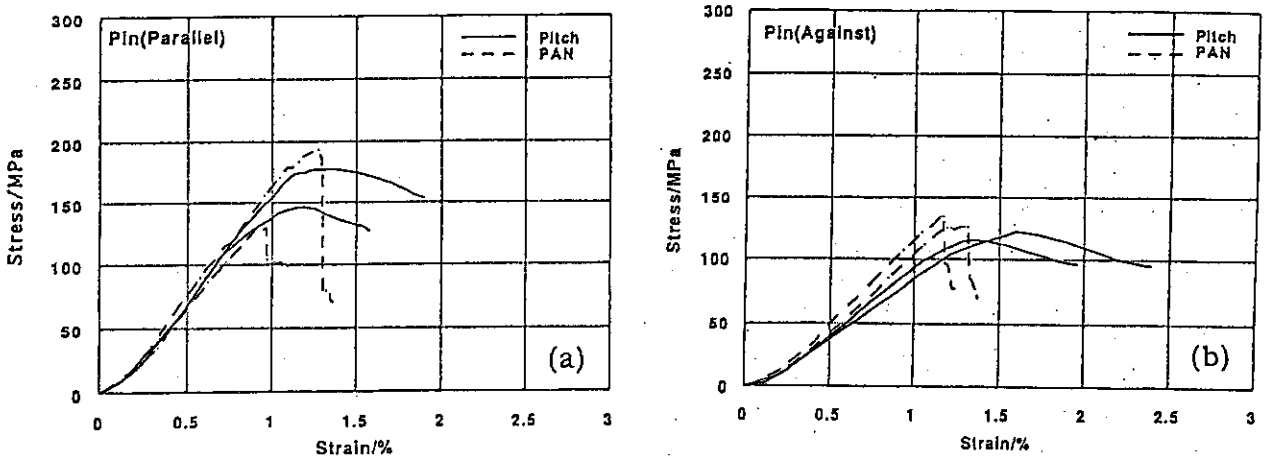


Fig. 6 Stress-strain curves obtained during the bending test of pins of pitch- or PAN-based material (a)parallel to or (b)against the felt plane.

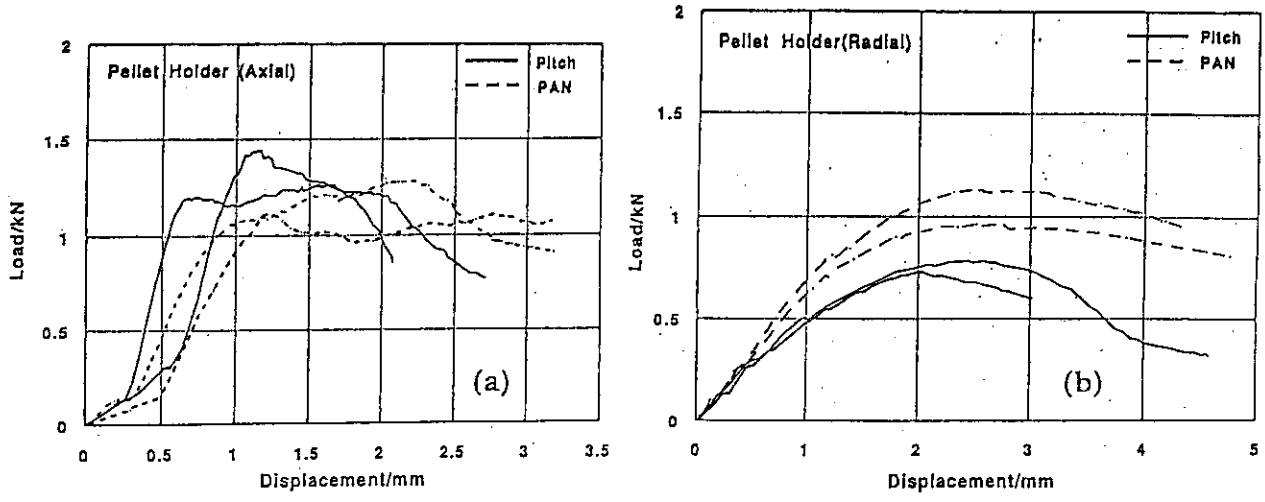


Fig. 7 Load-displacement curves obtained during the strength tests of pellet hoders of pitch- or PAN-based material with the load applied (a)axial or (b)radial.

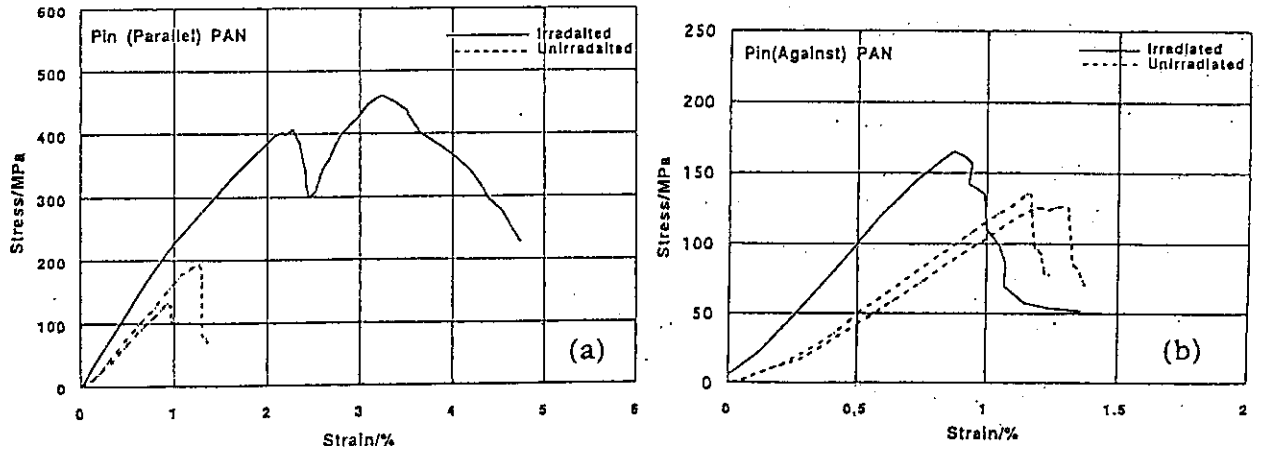


Fig. 8 Stress-strain curves for irradiated or unirradiated pins of PAN-based material with the applied load (a)parallel to or (b)against the felt plane.

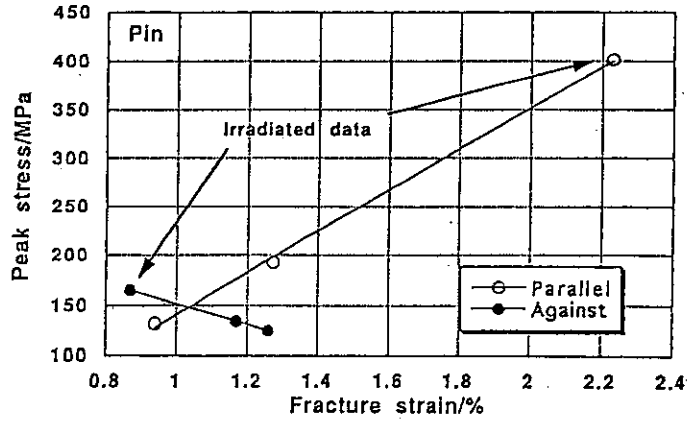


Fig. 9 Peak stress(bending strength) versus fracture strain curves for irradiated or unirradiated pins of PAN-based material.

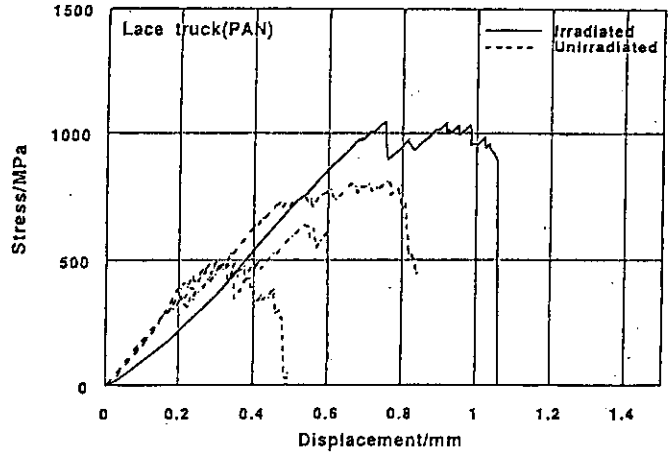


Fig.10 Stress-displacement curves for lace trucks of the PAN-based material irradiated or unirradiated.

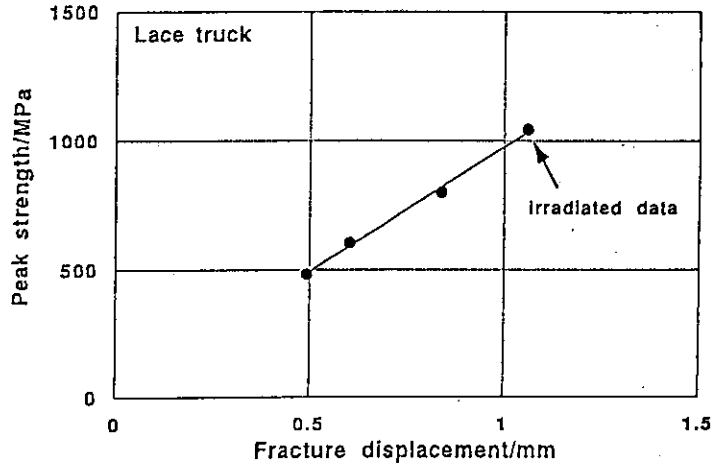


Fig.11 Peak stress(strength) versus fracture displacement plots for lace trucks.

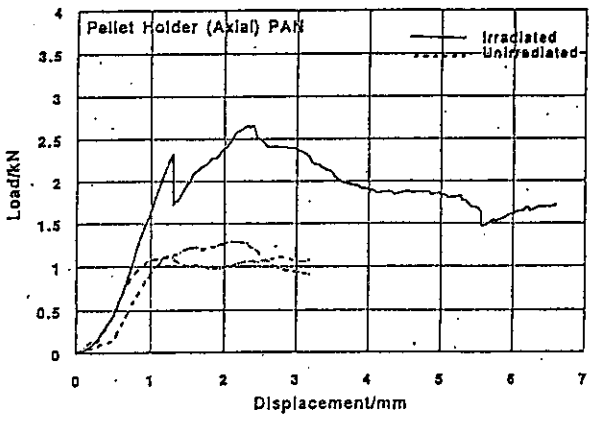


Fig.12 Load-displacement curves for pellet holders of PAN-based material loaded axially.

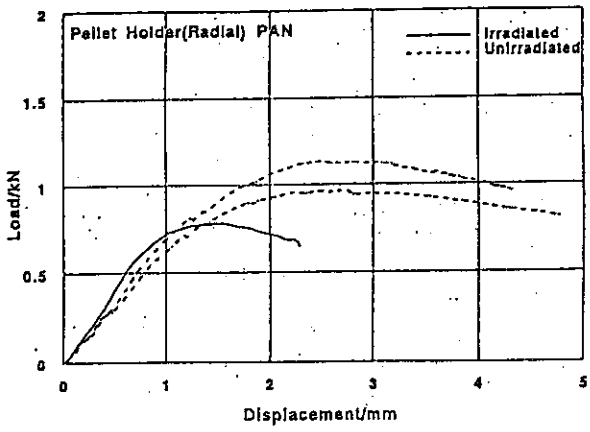


Fig.13 Load displacement curves for pellet holders of PAN-based material loaded radially.

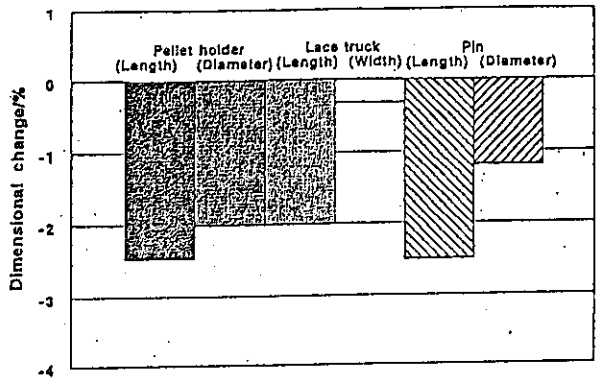


Fig.14 Dimensional changes of the elements after the neutron irradiation.

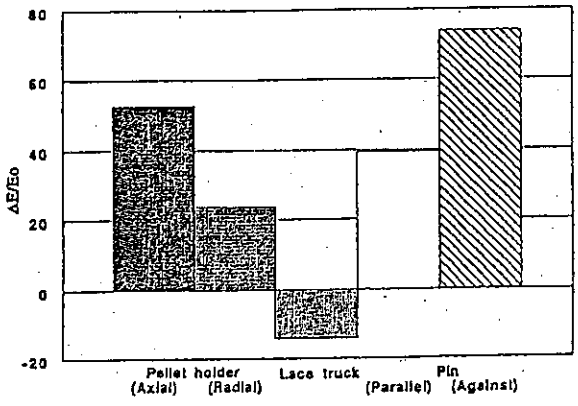
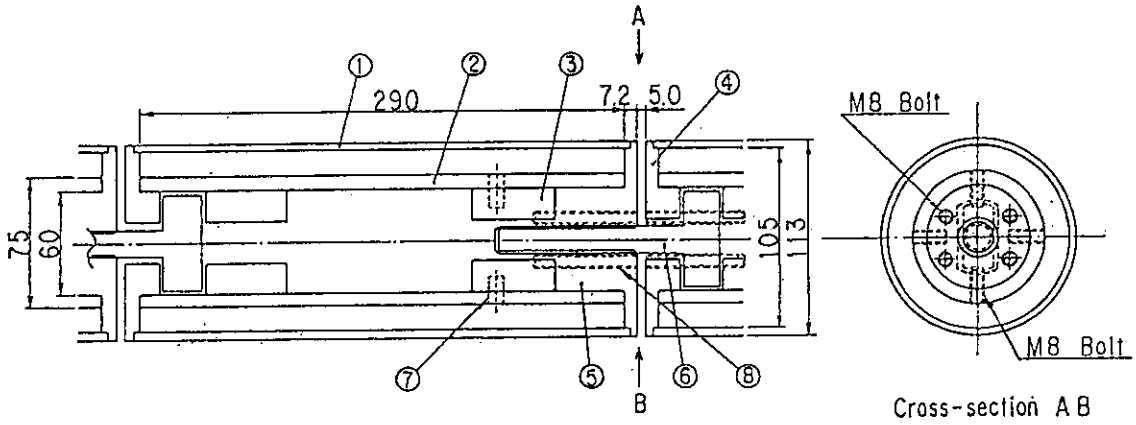


Fig.16 The modulus changes of the elements after the neutron irradiation.



① Holder outer tube
② Holder inner tube
③ Lid support plate
④ Upper lid
⑤ Lower lid
⑥ M16 Bolt
⑦ M8 Bolt
⑧ M8 Bolt

Fig.15 A new concept of the control rod.

To be presented at the 3rd JAERI Symposium on HTGR Technologies
Feb. 15-16, JAERI, Japan

3.4 General Design of the 10MW HTR

Zhenya Qin

Institute of Nuclear Energy Technology
Tsinghua University, Beijing, China

Abstract:

According to the development programme of advanced technologies in China, a 10MW side-by-side high temperature gas-cooled test module reactor with spherical fuel elements will be erected before the year 2000 by the Institute of Nuclear Energy Technology of Tsinghua University. The aims of this project are to demonstrate the inherent safety features of the HTGR modular design and to test the technologies of electricity generation, district heating as well as process heat application with modular HTGR.

At present, the 10MW HTR main building is being constructed and the principle large components have been ordered and are being fabricated.

The design philosophy and safety features, the reactor structure, the principle components, the design parameters, the general layout of principle systems in the nuclear island of the 10MW high temperature gas-cooled test module will be presented in this paper.

General Design of the 10MW HTR

Qin Zhenya
Institute of Nuclear Energy Technology
Tsinghua University, Beijing, China

Abstract

According to the plan of advanced technology development of our county, a 10MW High Temperature Gas cooled Test reactor (HTR-10) was designed by INET of Tsinghua University. At present, the reactor building is being constructed and the principal components are being fabricated or under goods. This paper describes the technical design of the HTR-10 test reactor.

1. General description

The Fig. 1 shows the HTR-10 primary system. The primary pressure boundary consists of reactor pressure vessel, steam generator pressure vessel and hot gas duct pressure vessel which connects the above two vessels. This arrangement can make the maintenance and inspection of the components easier and mitigate the accident result of water ingress into reactor core if the steam generator tubes were broken. We hope that the inherent safety features of side-by-side style HTR module can be demonstrated.

2. Reactor

The reactor core volume is $5m^3$, 1.8m in diameter and the mean height is 1.97m. About 27,000 spherical fuel elements with 60mm in diameter will be filled up in the reactor core, the enrichment of fuel is 17% and the mean burn up is 80,000MWd/T. At the funnel bottom of the reactor core, there is a fuel elements discharging tube, about 3.3m long and 500mm in diameter, at its end part through a special discharge facility the tube becomes a smaller one with 65mm in diameter only and penetrates the reactor pressure vessel. The fuel elements would be discharge one by one into the discharge system during the normal operation condition, therefor the shielding and cooling of the discharge tube will be easy. At the top of reactor core there is one loading tube, the internal diameter is 62mm.

Around the reactor core there are graphite reflectors, they can be divided into three parts: top reflector, side reflector and bottom reflector. In the outside of graphite reflector, there are carbon bricks containing thermal neutron absorber materials (B_4C), therefor they have thermal insulation and absorbing functions.

The whole graphite reflector consists of 20 layers of graphite bricks and carbon bricks. Each layer is divided into 20 segments, the graphite key and reactor core sleeve put them all together.

In the side reflector near the core there are 10 bore holes for control rods, the 10 control rods serve as the first shutdown system of HTR-10. According to our safety authority requirement there are 7 bore holes for small boron absorber balls as independent second shutdown system.

The reactor pressure vessel is more than 11m height and more than 4m in diameter, the reactor total weight is more than 300t.

3. Steam generator

The steam generator is once through modular helical tubes style. There are 30 small helical tubes modules which are installed in the annular space, each tube is 34m long, the total heat transfer area is $56m^2$ (See Fig. 2). The feed water temperature is 104℃, the temperature of outlet steam is 440℃, the steam pressure is 4MPa. At the center, a N_2-He intermediate heat exchanger (IHX) will be installed in the second experimental stage for gas-turbine and process heat application experiment and in this case the helium inlet and outlet temperature would be from first stage 250℃ and 700℃ increased to 300℃ and 900℃ respectively, but at the first stage the place for the IHX is empty. The pressure vessel is more than 11m height and 2.6m in diameter.

4. Hot gas duct

The hot gas duct pressure vessel connects the reactor and steam generator pressure vessels, the center tube with 300mm in diameter, the hot helium will flow from reactor core to steam generator through this tube, so between the inside tube and outside tube a thermal insulation will

be installed. The outside tube with 900mm in diameter, the annular space between those two tubes is for cold helium flow from helium circulator into the reactor core, so the inside tube operation under high temperature but low pressure conditions.

5. The flow of coolant

The flow of the primary helium coolant is as following: After through the helium circulator, the pressure of the cold helium would be increased about 0.6 bar and flow through the annular space between the steam generator pressure vessel and the sleeve, that location in the outside of outside thermal insulation, and then come into the annular tube of the hot gas duct and then through the space between the reactor pressure vessel and the reactor core sleeve into the bottom part of the reactor support structure, the reactor support structure will be cooled at first, about 2% of cold coolant will be flowed into the control rods holes and 1% into the outside of fuel elements discharge tube for cooling, most of them will be risen through the 20 cold Helium bore holes enters the top cold helium plenum, after through the pebble bed, the cold helium was heated and from the hot Helium bore holes flow down to the hot Helium plenum, after mixture the average temperature will be 700℃, then through the central tube of the hot gas duct into the steam generator. After heat exchange the helium is cooled down from 700℃ to 250℃, then through 6 tubes enters the inlet of the helium circulator to form a closed circulation (See Fig. 3).

6. HTR-10 Confinement

Because the ceramic coated particles of fuel are selected in HTR-10, in our case under the normal operation condition and all accident conditions, the maximum temperature of the fuel elements are much more lower than the 1600℃ maximum temperature limit, so the coated particles are a strong barrier against release of radioactivity, and the HTR-10 has a large negative reactivity temperature coefficient of both fuel and moderator, its value is about -8.5×10^{-5}/K. So under the normal operation condition, the maximum fuel elements temperature has a 700℃ margin to the limits of 1600℃. China nuclear safety authority agrees that for HTR-10 the containment is unnecessary, but we have a confinement design. The primary cavity is a principal part of confinement and the helium purification cavity is another part of confinement, therefor the primary system and all helium systems which are connected with primary system are covered by the confinement.

The primary cavity includes reactor cavity, steam generator cavity and fuel elements discharge system cavity. The wall thickness of reactor cavity is 2.3m mainly for shielding purpose. The design pressure of confinement is 1.3bar, during normal operation condition, the primary cavity is kept -150Pa lower other parts of reactor building through negative pressure system of the ventilation system, therefore the outside atmosphere can be released into the cavity, but the cavity inside gas couldn't release to the outside and only can be exhausted over 40m height chimney of ventilation center after filter.

If the primary lost pressure accident happened, for example, the helium purification system inlet and outlet tube or fuel elements discharge tube with 65mm in diameter one was damaged, the primary coolant will release very quickly and the pressure of primary cavity will be increased, when the pressure increased to 1.1 bar the flap or blast membrane will be opened, the gas will be exhausted form special chimney directly into atmosphere very quickly without filter (See Fig. 4).

In the reactor cavity a passive residual heat removal system is designed. It consists of reactor cavity coolers, air coolers and natural circulation loop. At normal shutdown condition the helium circulator and the steam generator can be operated, therefor the residual heat can be removed through the steam generator to the starting and shutdown loop, then to atmosphere. If above system was failed and at the starting and shutdown loop, then to atmosphere. If above system was failed and at the same time de pressurization accident was happened, the residual heat can be removed passively by means of conductivity of graphite reflector, reactor pressure vessel and then by means of radiation to the reactor cavity cooler, the residual heat will be removed passively over natural circulation, circulation loop, air cooler to the atmosphere.

Now the HTR-10 reactor building is being constructed. It consists of 6 floors, 3 of them are underground, the total height is 43m, the construction area is 6000 m^2. All 23 Nuclear inland systems will be installed in this building. The Fig. 5 and Fig. 6 show an example of systems layout. The Table 1 shows the general design parameters of HTR-10.

Table 1 General Design Parameters of HTR-10

1. Reactor Thermal Power	10MW
2. Design Life Time	20 years
3. Average Load Factor	50%
4. Reactor Core Volume	5 m^3
5. Reactor Core Diameter	180 cm
6. Equivalent Core Height at Equilibrium State	197cm
7. Fuel	UO2
8. Fresh Fuel U-235 Enrichment	17%
9. Diameter of Fuel element	6 cm
10. Heavy Metal Content of Each Ball	5 g
11. Fuel Loading Mode	multi-circulation (5 times)
12. Position of Control rods	side reflector
13. Control Rod Channels	10
14. Absorbing Ball Channels	7
15. Irradiation and Measuring Channels	3
16. Helium Inlet Temperature of Core	250℃
17. Helium Outlet Temperature of Core	700℃
18. Helium Mass Flow at 100% Power	4.3 kg/s
19. Primary Helium Pressure	3.0 MPa
20. Feed Water Temperature of SG	104℃
21. Feed Water Pressure of SG	6.1 MPa
22. Steam Outlet Temperature	440 ℃
23. Steam Outlet Pressure	4.0 MPa
24. Feed Water/Steam Mass Flow	3.49 kg/s
25. Residual Heal Removal Mode	natural circulation
26. Power of Residual Heat Removal System	250 kW

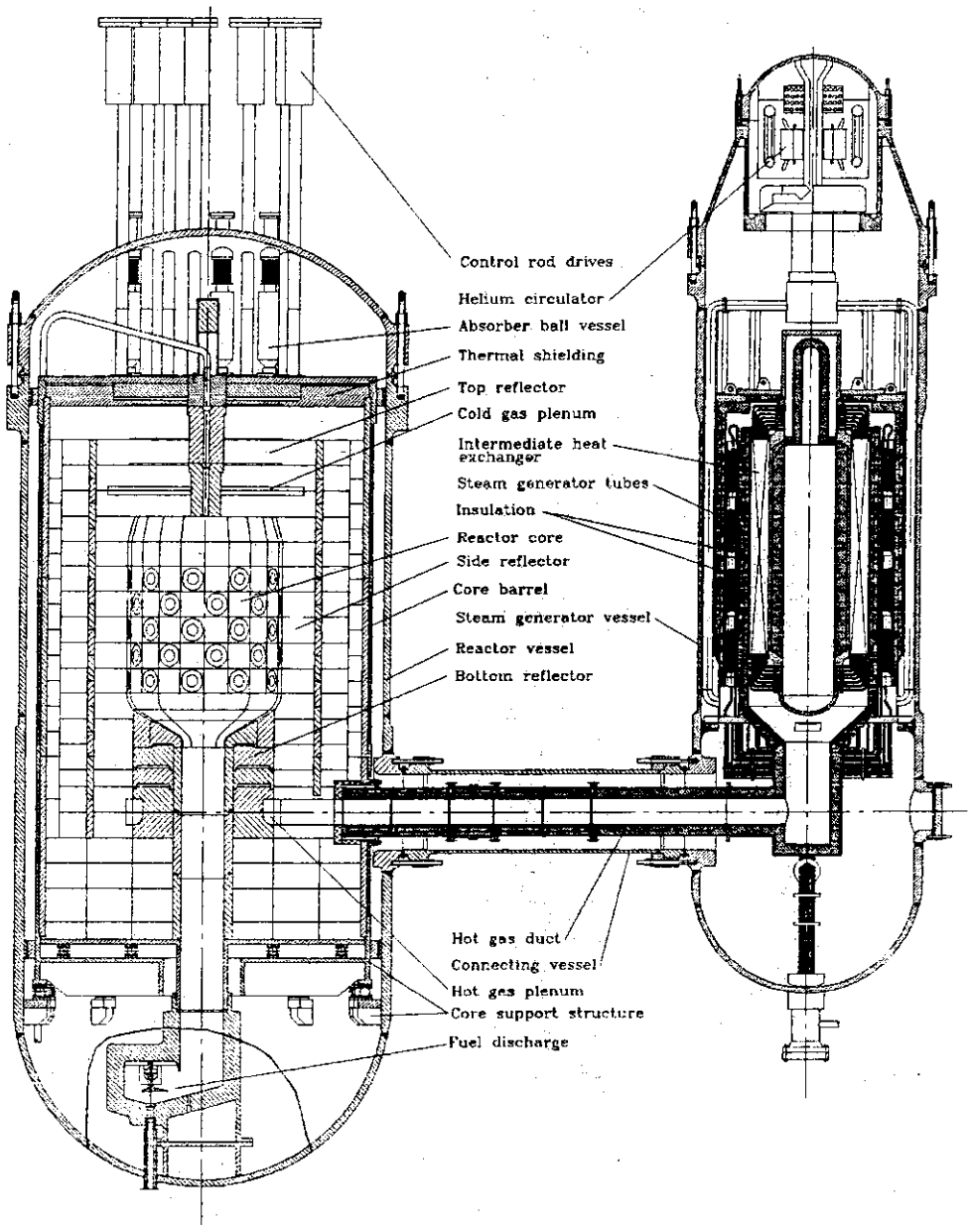


Fig.1 HTR−10 Primary System

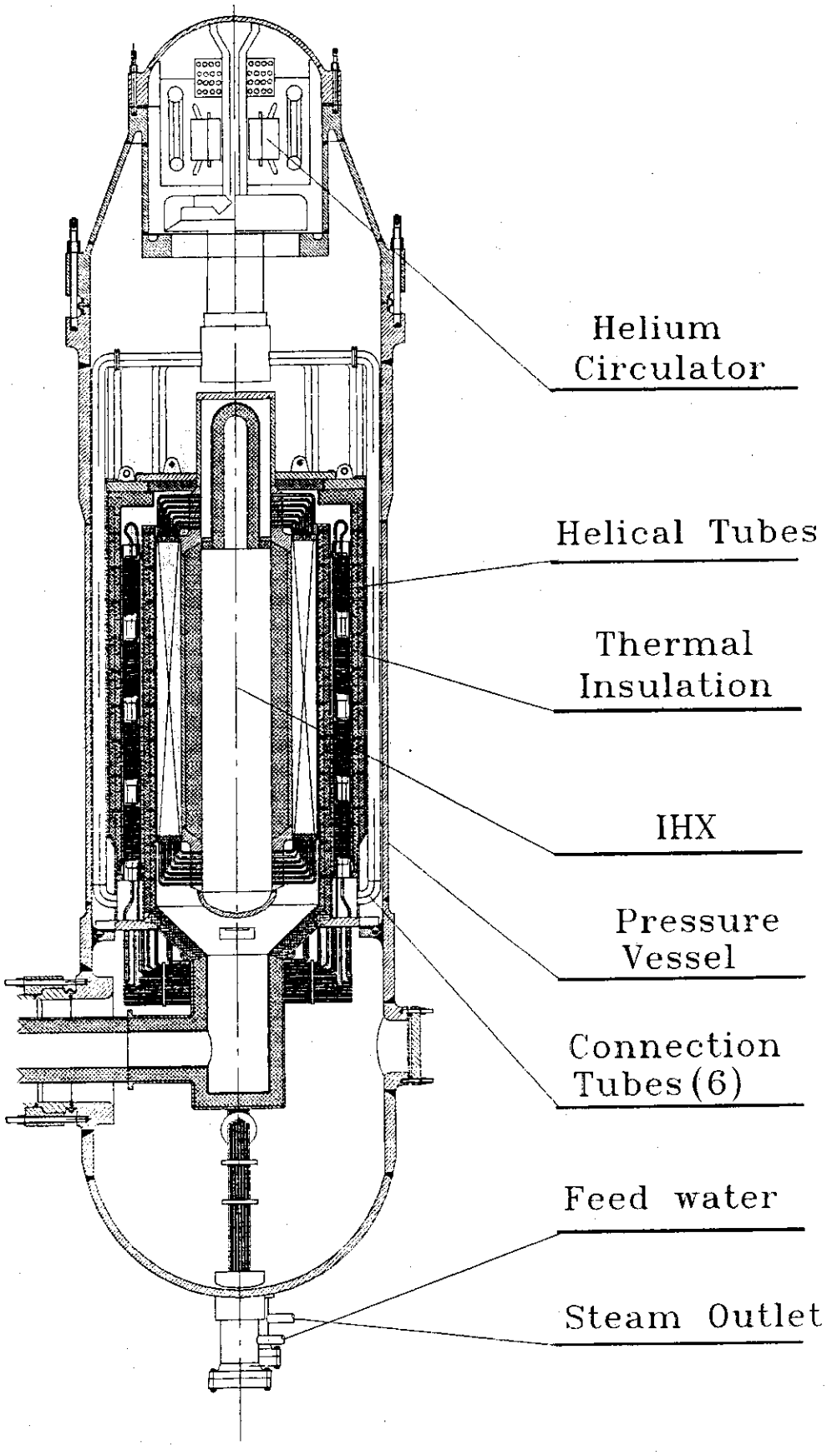


Fig. 2 HTR－10 Steam Generator

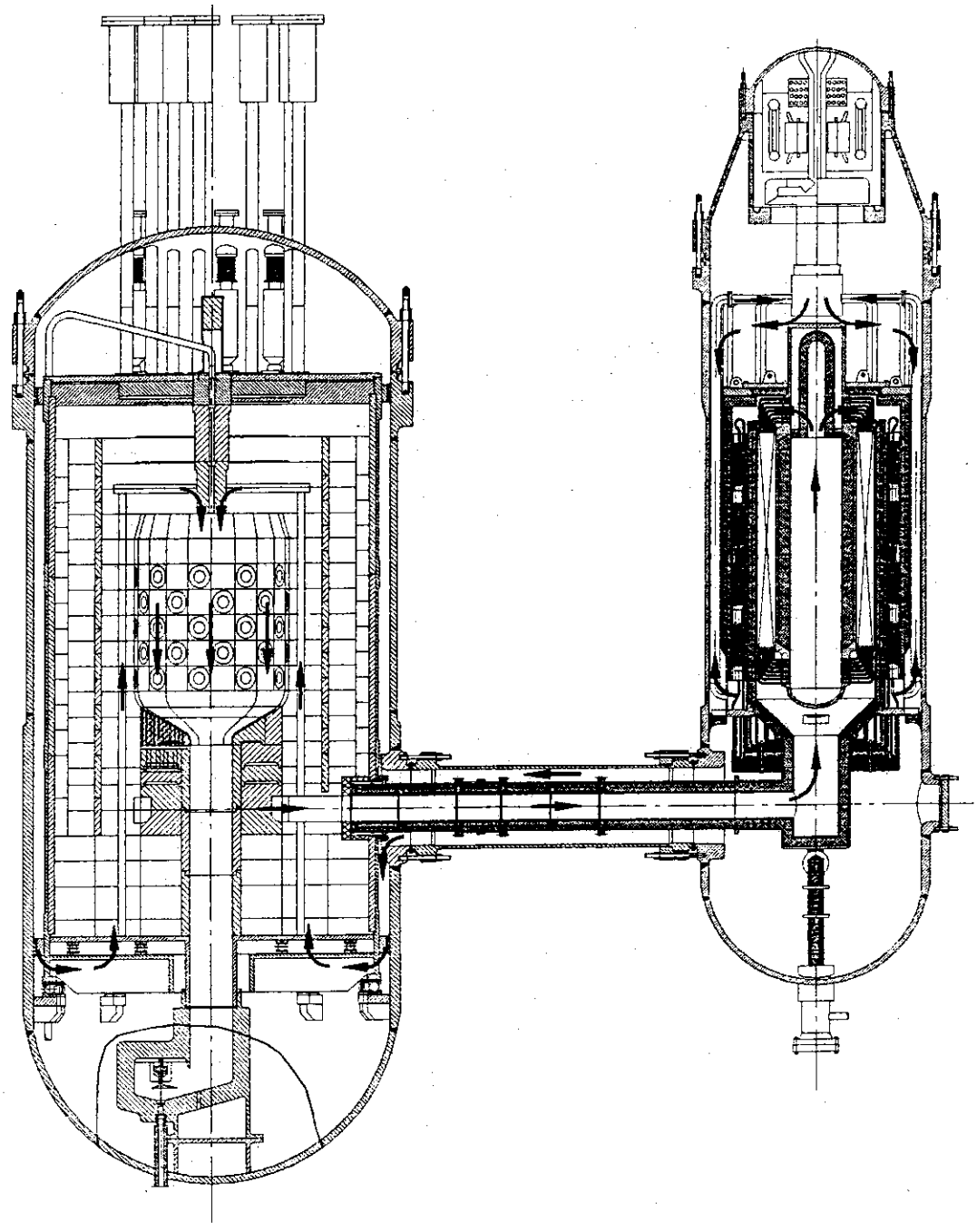


Fig3 The coolant flow of HTR－10

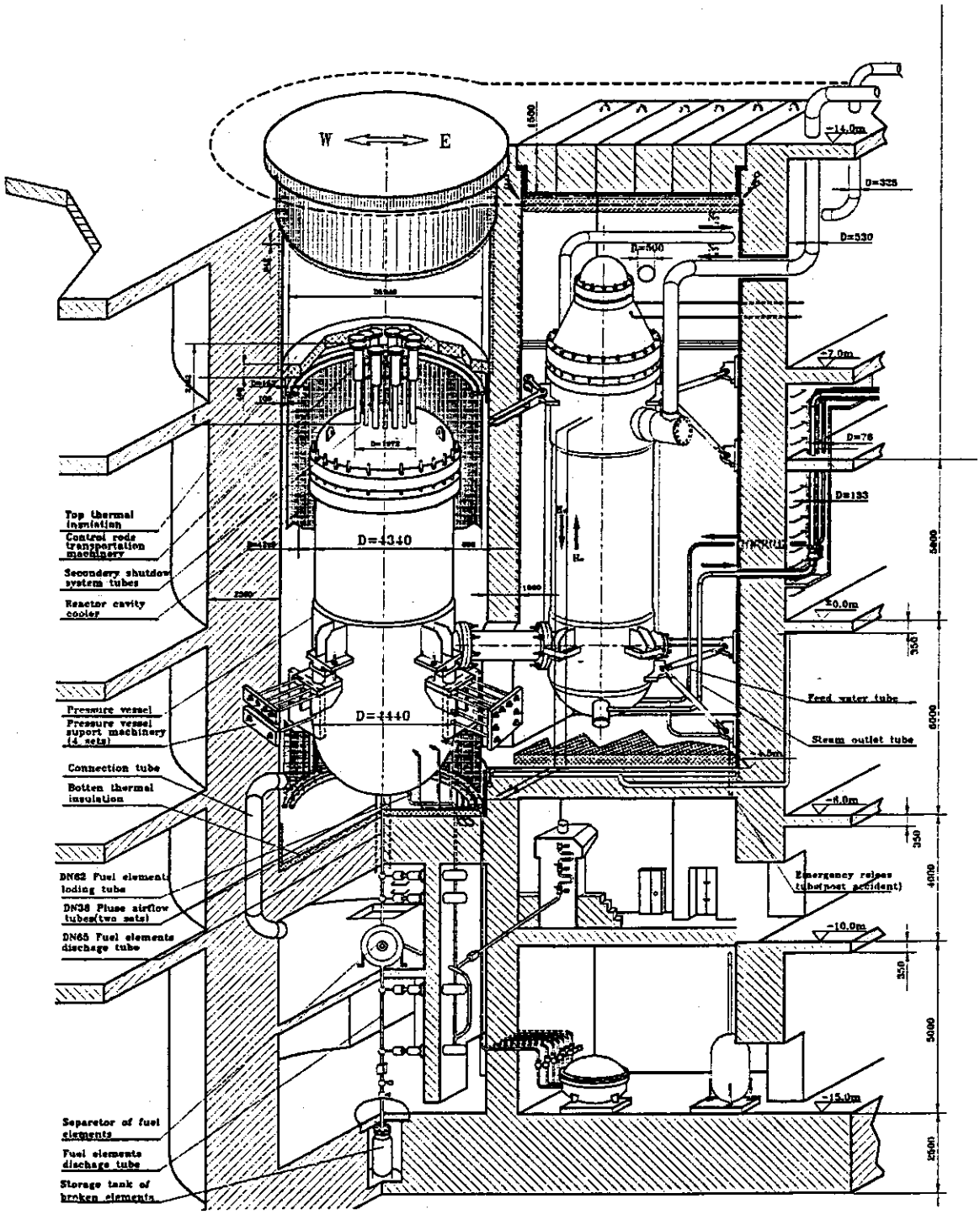


Fig4 THR－10 Confinement

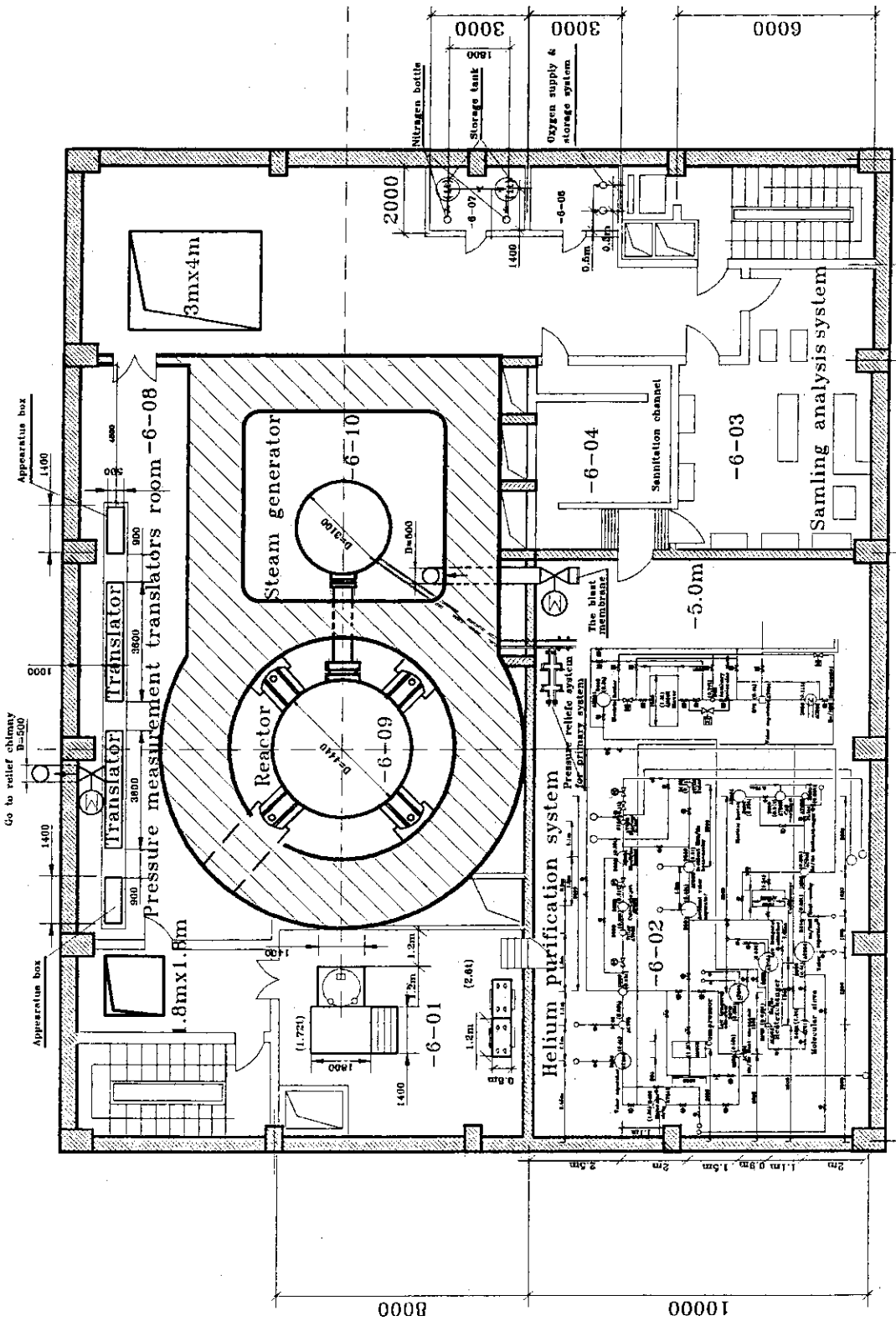


Fig.5 HTTR－10 Systems Layout in －6.0m Floor

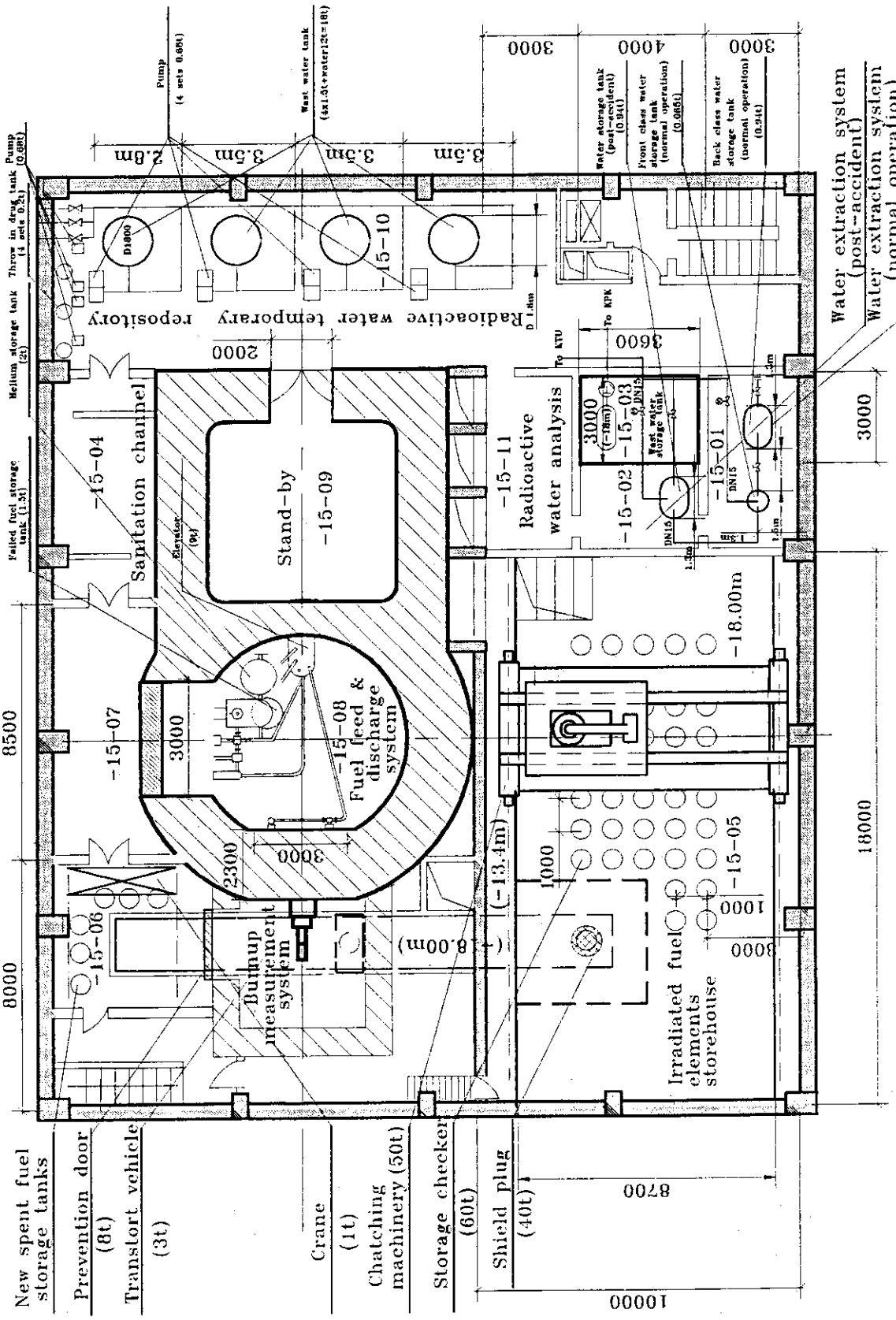


Fig. 6 HTR−10 Systems Layout in −15.0m Floor

3.5 Construction of the HTTR In-Core Components

S. Maruyama, A. Saikusa, S. Shiozawa
Japan Atomic Energy Research Institute, Japan
N. Tsuji, K. Jinza, T. Miki
Fuji Electric Co., Ltd., Japan

Abstract ; The reactor internals of HTTR consist of graphite and metallic core support structures and shielding blocks and are designed to support core elements and to shield neutron fluence. They also have functions to restrict by-pass flow for ensuring the core cooling performance and to maintain the temperature of metallic core support structures within their design limits.

The detailed design of the HTTR core support structure was approved by the government through safety review, 1990-1991. Machining of all graphite components, which consist of about 150 large blocks, was finished in September 1994 successfully. Machining and fabricating of the metallic components were also finished in September.

Prior to their installation in the reactor pressure vessel (RPV), the assembly test of actual reactor internals was performed at the works to confirm above mentioned functions. The assembly test was conducted by examining fabricating precision of each component and alignment of piled-up structures, measuring circumferential coolant velocity profile in the passage between the RPV and reactor internals as well as under the core support plates with respect to structural integrity, and measuring by-pass flow rate through gaps between graphite components which may degrade core performance. The another purpose of the assembly test was to confirm the installation procedure of those components.

All components were assembled at the works according to the planned procedure, and the tests were executed while assembling. As a result of the tests, measured level difference and gap width between reactor internals were negligible from core thermal and hydraulic performance point of view. Coolant flows uniformly in circumferential direction at any axial level in the RPV. By-pass flow rate was found to be suppressed sufficiently and far less than the design limit.

The assembly test was also conducted for the core restraint mechanism (CRM). The CRM is placed periphery of every layer of permanent reflector blocks (PRBs) to push them inward for restricting by-pass flow between PRBs. Binding force of the CRM should be set so as to keep stresses in PRBs and CRM within their stress limit during

not only normal operation but also transient condition. The peripheral distribution of binding force was measured to confirm that binding force was well adjusted at designed value and distributed uniformly.

After completion of the assembly test at the works, all components were disassembled and government inspection of those components was carried out. Installation of the reactor internals in the RPV was started at the construction site of HTTR in April 1995. Installation was proceeded with the procedure confirmed at the works. And in the installation process, main items of the assembly test at the works were conducted to investigate the reproducibility of assembling. The test results were equivalent and reproducibility was confirmed.

The installation was successfully completed in September 1995 and government inspection was also finished in September.

Construction of the HTTR In-Core Components

S. Maruyama, A.Saikusa, and S.Shiozawa
Japan Atomic Energy Research Institute,
Oarai-machi, Higashiibaraki-gun, Ibaraki-ken, Japan
N. Tsuji, K.Jinza, T.Miki
Fuji Electric Co., Kawasaki-shi,Kanagawa-ken, Japan

1. INTRODUCTION

The High Temperature Engineering Test Reactor(HTTR), being constructed by Japan Atomic Energy Research Institute(JAERI), is a helium gas-cooled and graphite-moderated thermal reactor with 950℃ in reactor outlet coolant temperature and 30 MW in thermal output[1]. The reactor internals of HTTR consist of graphite and metallic core support structures and shielding blocks; They are designed to support core elements and to shield neutron fluence.

The reactor internals of HTTR are also designed to restrict by-pass flow for ensuring the core cooling performance by sealing at surrounding graphite blocks of outer part of the core with tight binding, and also to maintain temperatures of metallic structures within their limit. The R&D works have been carried out to quantitatively asses the performance of these functions using partially simulated model and/or scale down mock-up[2].

The detailed design of the HTTR core support structures was approved by the government through the review, 1990-1991. Prior to their installation in the reactor pressure vessel(RPV) the assembly test of actual reactor internals at the works was conducted to demonstrate design required functions.

Installation of the reactor internals in the RPV was started at the construction site of HTTR in April 1995. Installation was proceeded with the procedure confirmed at works. And in the installation process, main items of the assembly test at works were conducted to investigate the reproducibility of assembling. The test results were equivalent and reproducibility was confirmed. The installation was successfully completed in September 1995 and government inspection was also finished in the same September.

2. OUTLINE OF REACTOR INTERNAL

The core of HTTR is an array of hexagonal graphite blocks which provides the physical structure for the arrangement and confinement of fissile materials, neutron moderation, heat

transfer and positioning of control/shielding absorber materials. The core is supported by the reactor internals such as permanent reflector blocks(PRBs), hot plenum blocks(HPBs), support posts, support plates, core restraint mechanisms (CRMs),etc. as shown in Fig.1 and Fig.2.

The reactor internals consist of the graphite core support structures, the metallic core support structures and the shielding blocks. The graphite core support structures mainly consist of PRBs, HPBs, support posts, and the core bottom insulation structures. PRBs consist of 8 axial layers of total height about 8m. In each layer, PRBs surround the core element blocks and consist of 12 circumferential segments with the keys on the adjacent surface as shown in Fig.3. PRBs in each layer are bound each other by CRMs, and by-pass flow between adjacent blocks is restricted by face contact and seal elements. HPBs, support posts and the core bottom insulation structures are illustrated in Fig.4. HPBs are composed of the sealed blocks and keyed blocks. These blocks are located underneath the core elements to support them directly and to form passages of coolant flow from the core to the hot plenum. The gaps between the sealed blocks are sealed by triangular seal elements to reduce gap flow between core element blocks which is ineffective for core cooling. The support posts are located below the keyed hot plenum blocks and form the hot plenum. The core bottom insulation structures are located beneath the hot plenum and are composed of the lower plenum blocks, the carbon blocks, and the bottom blocks. These structures have the function to prevent temperature rise of the lower metallic core support structures.

The metallic core support structures support above-mentioned graphite structures and transmit the vertical and horizontal loads to the RPV. The metallic core support structures consist of the support plates and CRMs. The support plates forms a plain foundation surface for the core components and the reactor internals. The support plates are set on steel support posts and are cooled by helium gas which flows radially outward between two parallel plates; upper plate is the support plates and lower plate cover plate of the core support grid. CRMs are located between RPV and the side shielding blocks as shown in Fig.5. CRMs surround and bind PRBs like hoops for a barrel with 10 axially distributed units to restrict excessive by-pass flow through gaps between blocks by preventing radially outward movement of PRBs. CRMs are cooled by inlet helium gas to prevent reduction of binding force caused by relaxation of the tensile element material under high temperature creep condition.

The shielding blocks consist of the upper shielding blocks and the side shielding blocks. The upper shielding blocks are placed on the top of columns of the core and form the entrance to control flow rate distribution into the core. The side shielding blocks form the coolant flow path to cool the metallic structures in the core side.

The coolant enters in RPV through the annular passage of concentric hot gas duct, then,

flows upward to the upper plenum via two side flow passages: one is an inner passage between the PRBs and side shielding blocks and the other an outer passage between side shielding blocks and the RPV. Finally, the coolant entering into the upper plenum flows downward to the hot plenum through the core via coolant channels in the fuel blocks and control rod guide blocks. Besides the bulk of the coolant flows through the core, small amount of the coolant flows through the gaps between adjacent graphite blocks. As the low temperature leakage flow is mixed with the bulk of the coolant in the hot plenum, the leakage flow brings the lower reactor outlet coolant temperature.

3. MANUFACTURING

The reactor internals of HTTR were manufactured according to the schedule shown in Fig.6.

At first, the graphite material procurement was started at the end of 1990. Those materials were machined mainly by large scale machining center. Then those graphite materials and machined components were inspected according to the acceptance standard, which include non-destructive inspection, developed by JAERI. Material procurement of metallic components were started in 1992. After that, machining and assembling to components were started in 1993.

Then assembly test at the work was started at the beginning of 1994.

4. ASSEMBLY TEST AT THE WORK[3]

4.1 TEST PROCEDURE

In the assembly test at the works, the support plates, which form a foundation of stack, were placed in the simulated RPV, then, the graphite core support structures of PRBs, HPBs, support posts and others were piled-up onto the plates. PRBs were bound in tight contact by the CRMs. The over view of assembly test and cross sectional view of the test apparatus is shown in Fig.7 and 8, respectively.

Following items of the assembly test were conducted at the works.

(1) fabrication precision of alignment of piled-up structures

(2) seal performance against by-pass flow

(3) cooling performance for metallic structures

(4) binding performance of CRMs

The test procedure of each test item is described below.

(1) fabrication precision of alignment of piled-up structures

Level differences and gaps between blocks, which affect by-pass flow or core cooling

performance, were measured each time one layer was assembled, and also checked for unexpected leakage flow passage.

(2) seal performance against by-pass flow

As shown in Fig.9, a sealing cap was set on top surface of PRBs to shut the open window, and pull air from cavity through the simulated concentric hot gas duct. In this configuration, leakage flow rate into the cavity through gaps of PRBs, the support plates and others were measured.

(3) cooling performance for metallic structures

The support plates and CRMs are cooled by helium gas of 400℃, so velocity profiles in the passage under the support plates and in the core side flow passage were measured by means of hot wire anemometers for evaluation of cooling performance.

(4) binding performance of CRMs

The restraining force of the CRM was loaded by means of specially developed hydraulic jack. The restraining force on each PRB was measured by load cells.

the another purpose of the test was to confirm the installation procedure of the reactor internals in actual RPV. This purpose was achieved by assembling the components with the same procedure which had been planned for site.

4.2 TEST RESULTS

(1) fabrication precision of alignment of piled-up structures

All measured data were in the range of design limit. For example, measured level difference between top surfaces of sealed block of HPBs are 0.7mm at maximum and this difference is sufficiently small compared with allowable limit of 4mm for triangular seal elements.

(2) seal performance against by-pass flow

The result of this test is shown in Fig.10. The solid line shows the upper limit of the leakage flow rate. It was confirmed that the assembly had sufficient seal performance against by-pass flow.

(3) cooling performance for metallic structures

Measured air velocity profile at outer edge of the support plates is shown in Fig.11. From this result, it can be said that the flow under the support plates is almost uniform from the view point of their temperature distribution, in other words, structural integrity. Figure12 shows the measured flow distribution in the core side passage. As a result of numerical

analysis, it was clarified that the flow ratio of 35% in the inner passage is necessary to maintain CRM adequate low temperature. The measured flow ratio satisfies the design limit at any level and agrees well with estimated value.

(4) binding performance of CRMs

Figure13 shows measured distribution of restraining force on PRBs by CRMs at bottom layer. Restraining force is loaded uniformly and fulfills its design value.

5. INSTALLATION

After completion of the assembly test at the works, installation of the reactor internals in actual RPV was started at the construction site of HTTR in April,1995. The installation was conducted under controlled air condition, which was achieved by covering the RPV opening with "clean room" and ventilating the space in the RPV, to prevent absorbing moisture in graphite components and to prevent rusting on steel structure. At first, the support plates were installed in the RPV. Then the graphite core support structures were placed and bound by the CRMs. The installation procedure was same as that of assembly test. Figure14 shows over view of installed components in RPV. In the installation process, test items of (1),(2),and(4) were conducted to investigate the reproducibility of assembling. The test results were equivalent and reproducibility was confirmed.

Then the installation was successfully completed in September 1995 and government inspection was finished in same September.

6. CONCLUSION

Concerning the reactor internals of HTTR, fabrication, assembly test and installation were successfully completed.

Especially by the assembly test conducted at the work, expected performances of sealing, cooling and binding function necessary to achieve high temperature reactor outlet coolant of 950℃ were demonstrated.

After completion of the assembly test at the works, the reactor internals were installed in actual RPV from April to September,1995. Among these test items of the assembly test at the works, tests of fabrication precision, seal performance, and binding performance were repeated in installation process. Test results, both at the works and at the construction site, were equivalent and reproducibility at the construction site was confirmed. Then installation of the reactor internals of HTTR was completed at September 1995.

REFERENCE

[1] Saito.S, et al. 1994. Design of High Temperature Engineering Test Reactor(HTTR). JAERI-1332.

[2] JAERI. 1992. Present Status of HTTR Research & Development.

[3] Maruyama.S, et al. 1995. Results of assembly test of HTTR reactor internals. IAEA SM. on Graphite Moderator Life Cycle Technologies

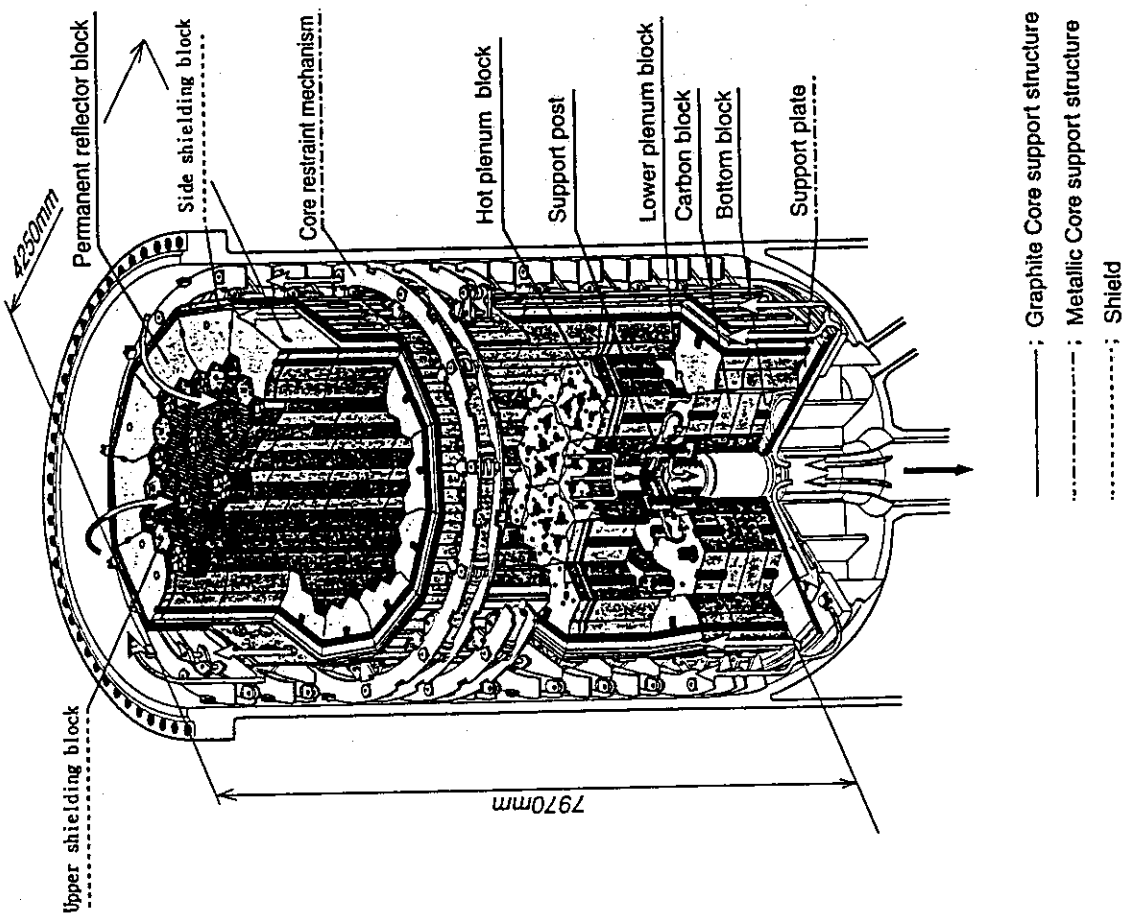


Fig.2 Bird's-eye view of the Reactor Internal Structure

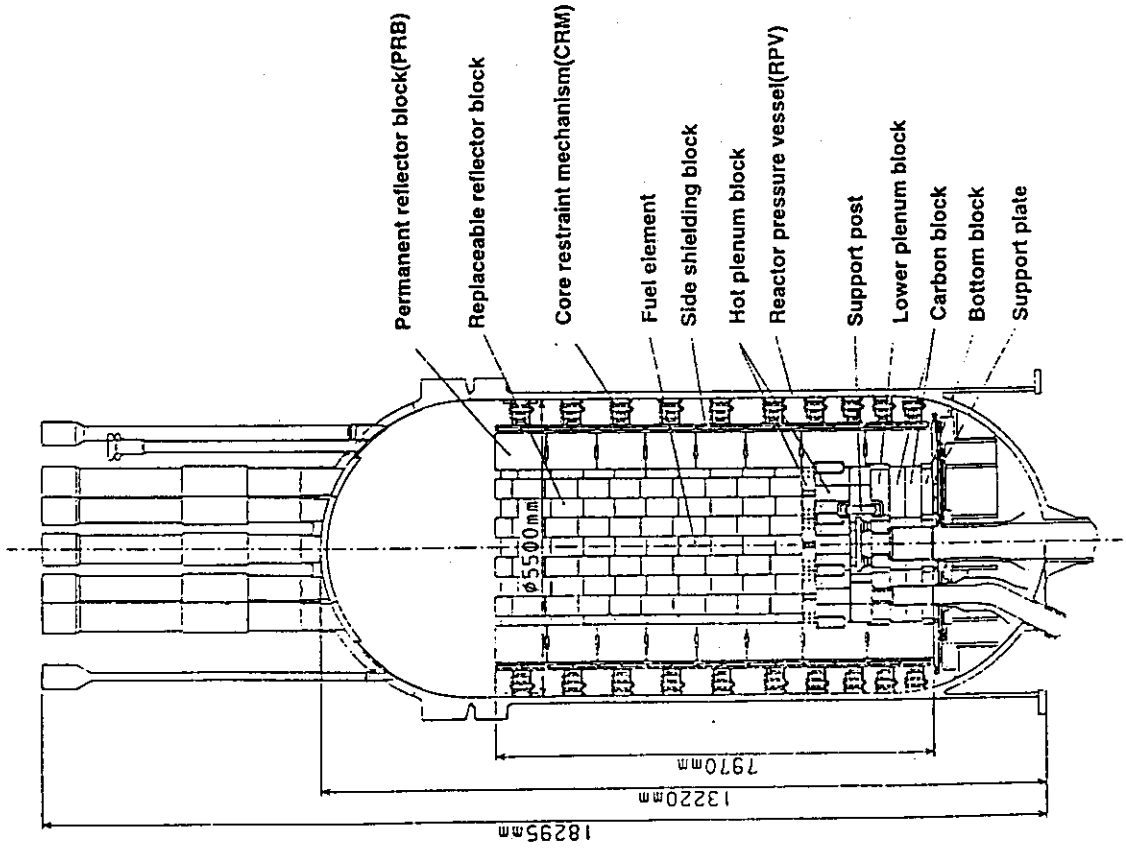


Fig.1 Cross section of HTTR

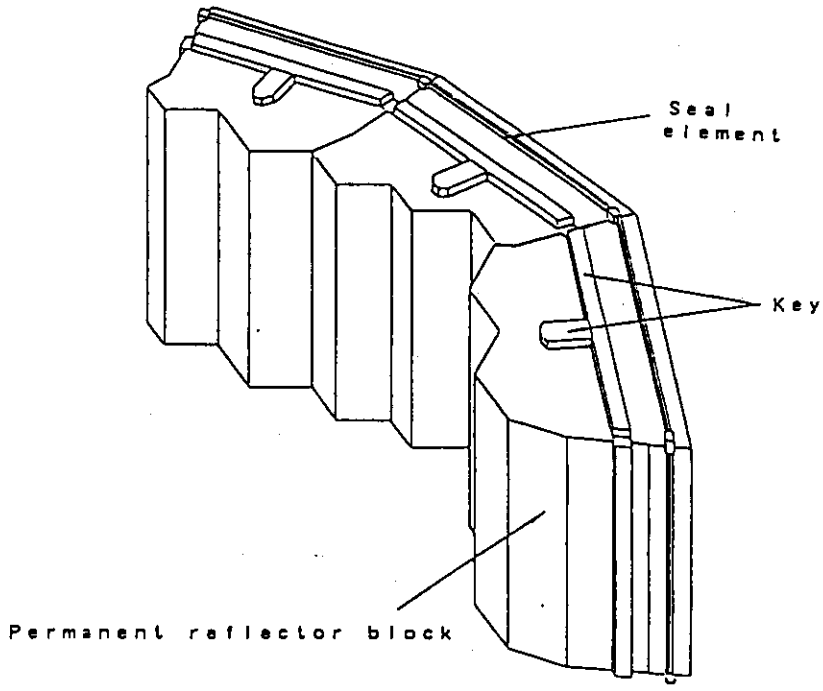


Fig.3 Schematic diagram of the Permanent Reflector Blocks

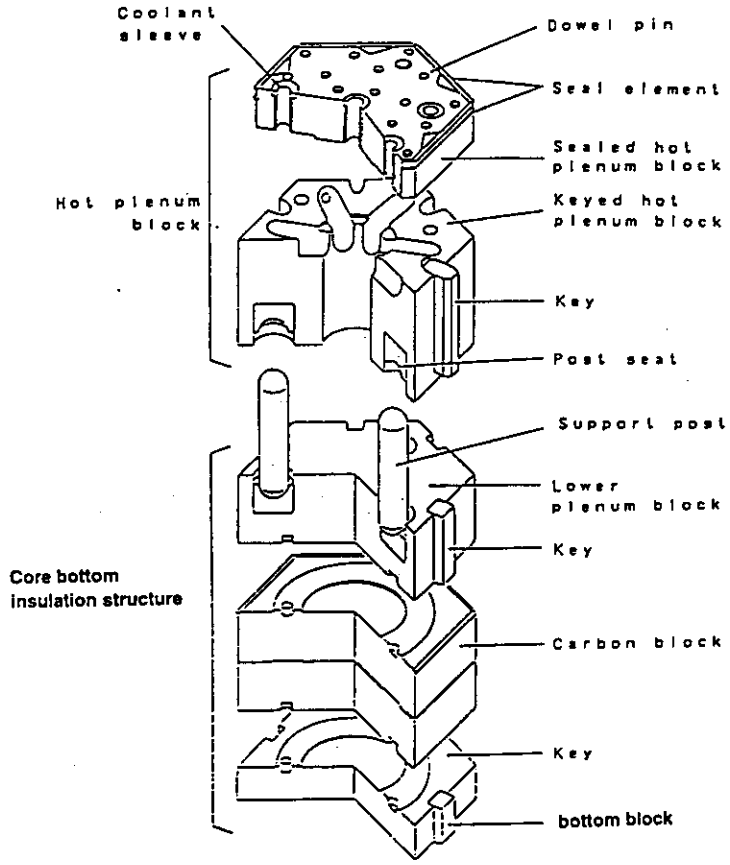


Fig.4 Schematic diagram of the Core Bottom Graphite Structures

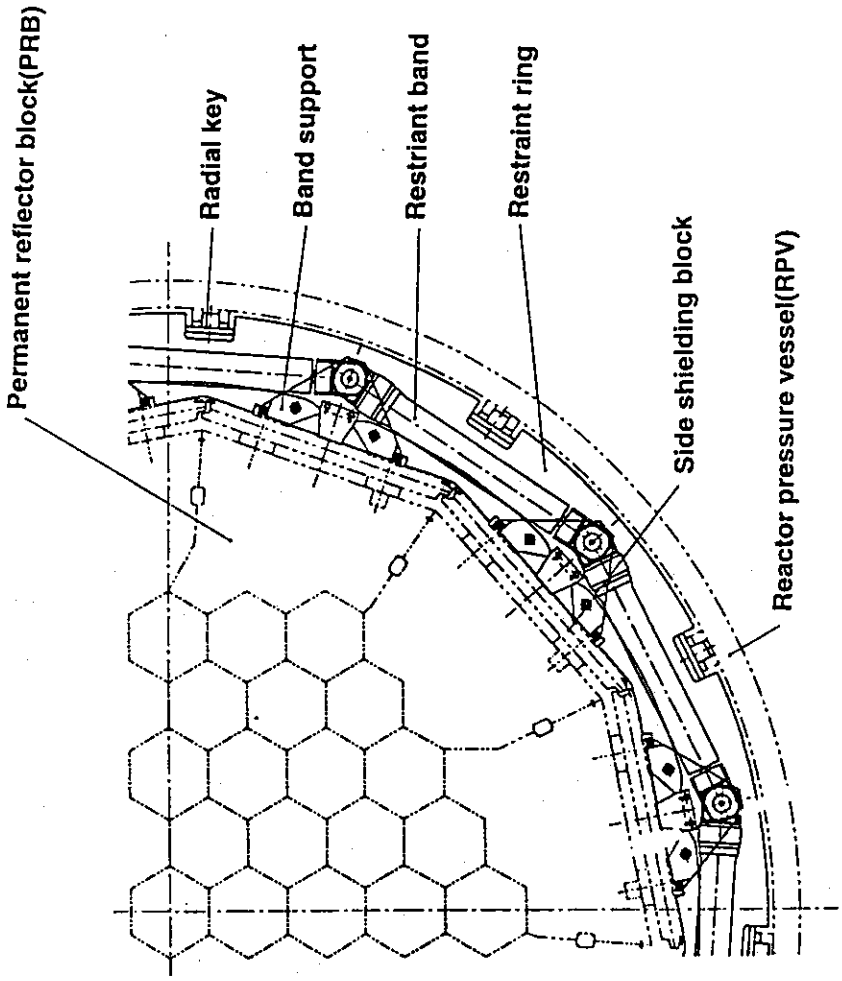


Fig.5 Schematic diagram of the Core Restraint Mechanism

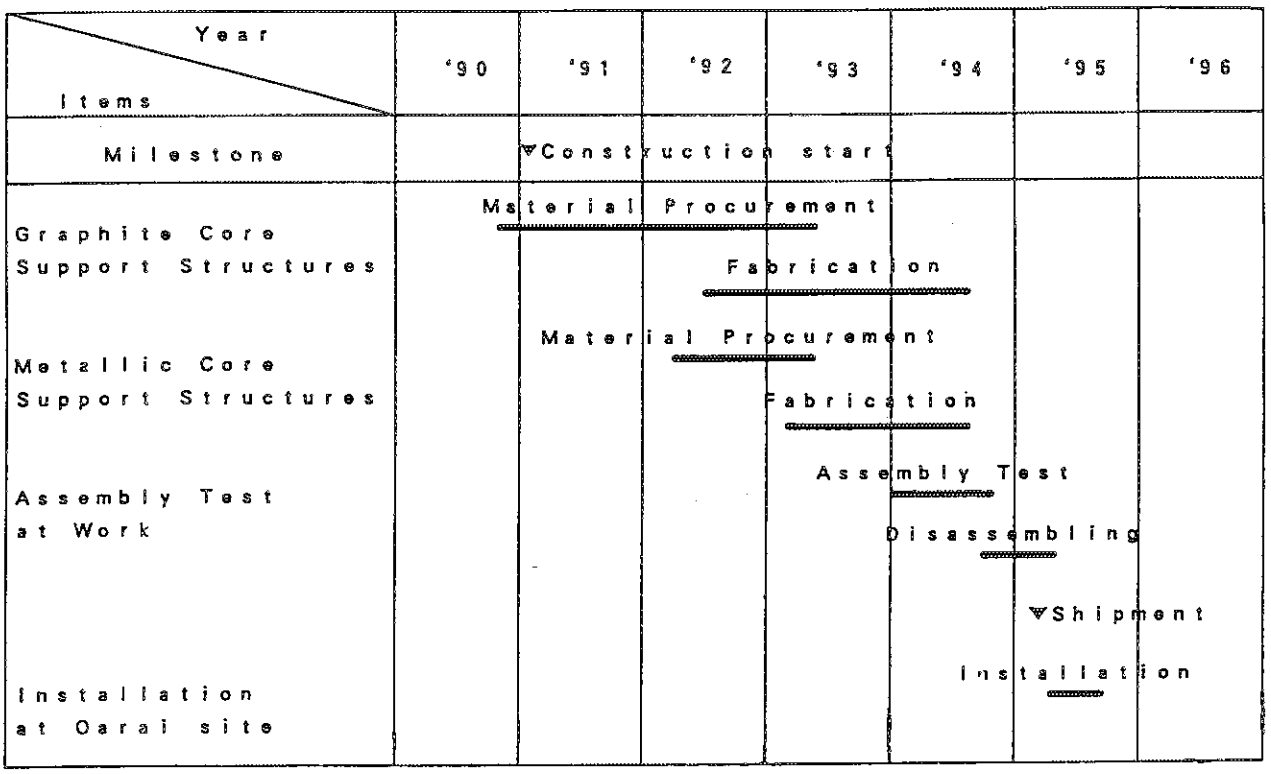


Fig.6 Construction schedule of the HTTR core internal structures

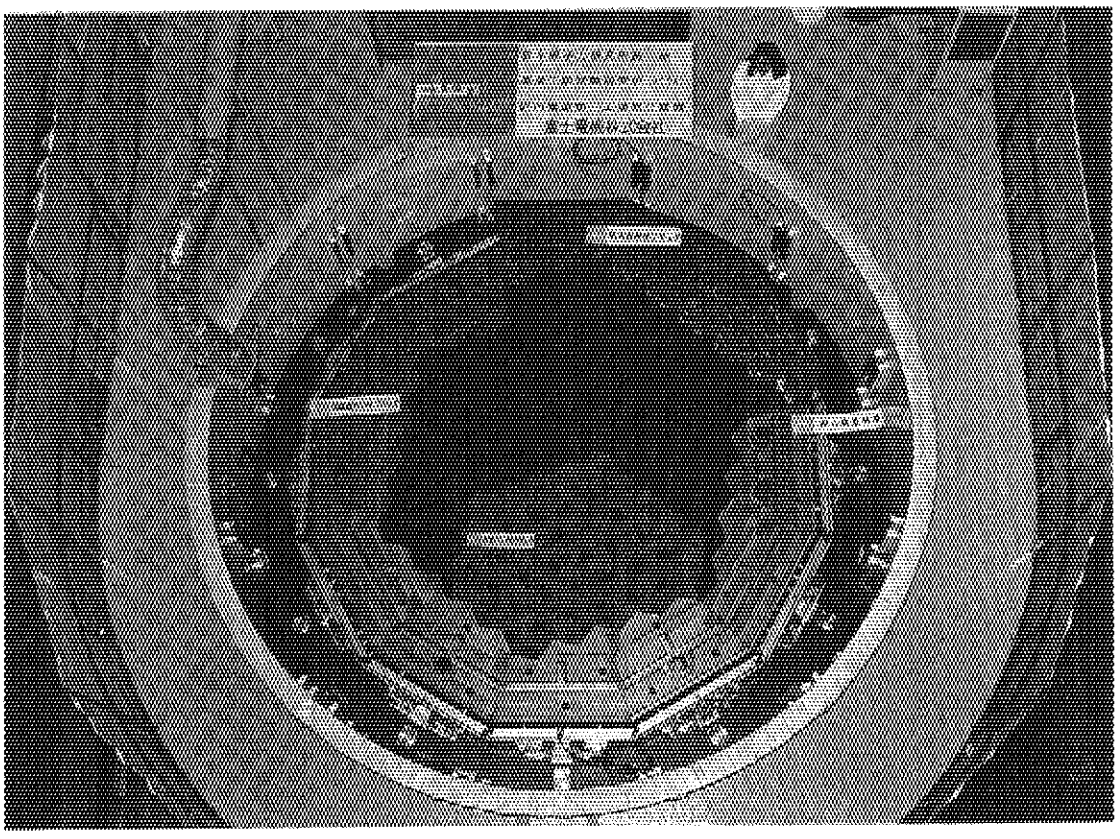


Fig.7 Over view of the assembly test

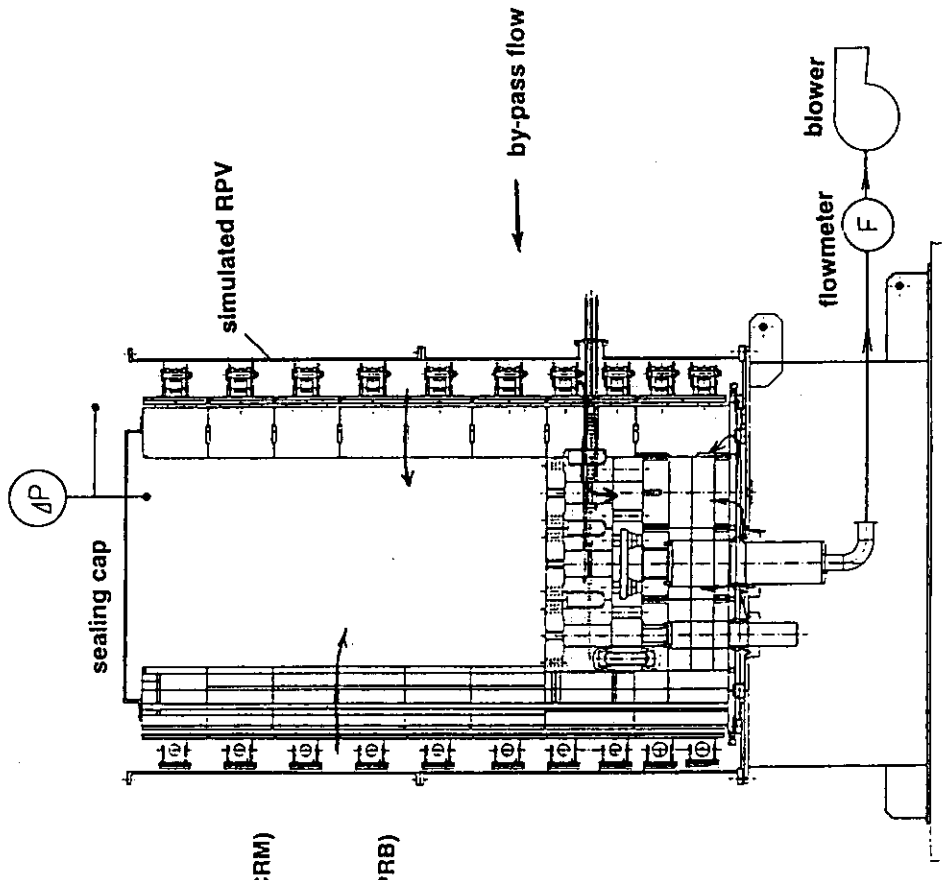


Fig.9 Schematic diagram of seal performance test

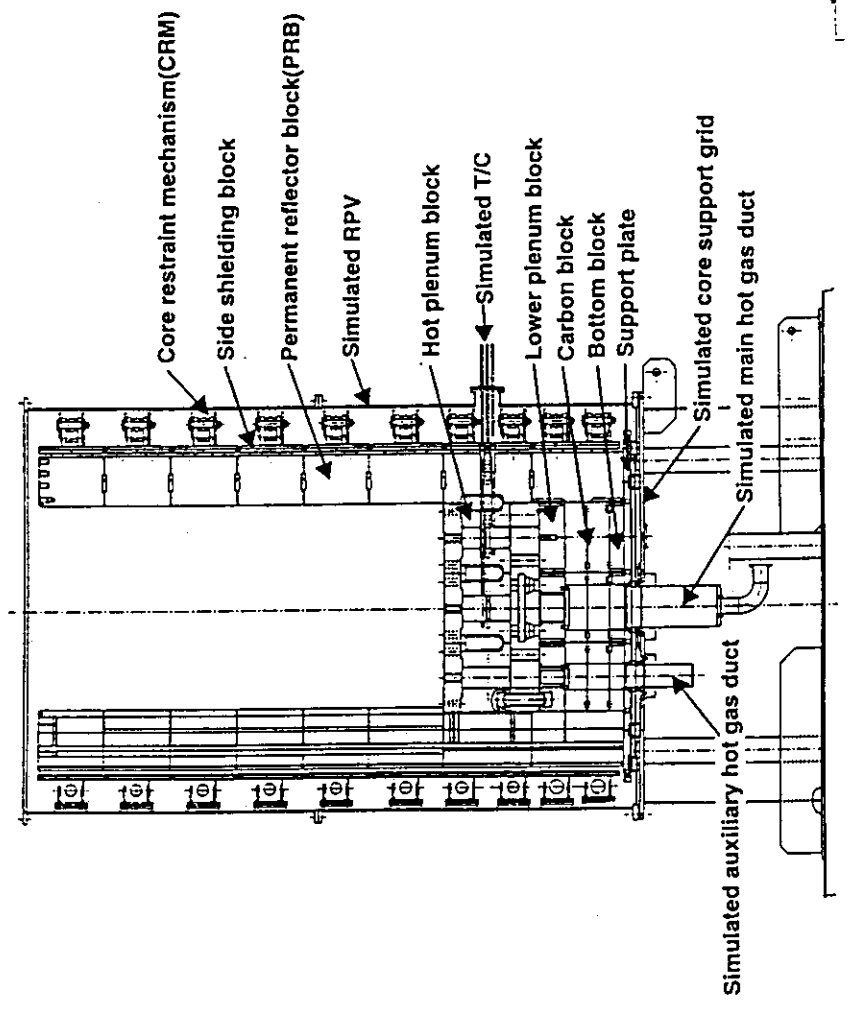


Fig.8 Cross sectional view of test apparatus -assembly test at works

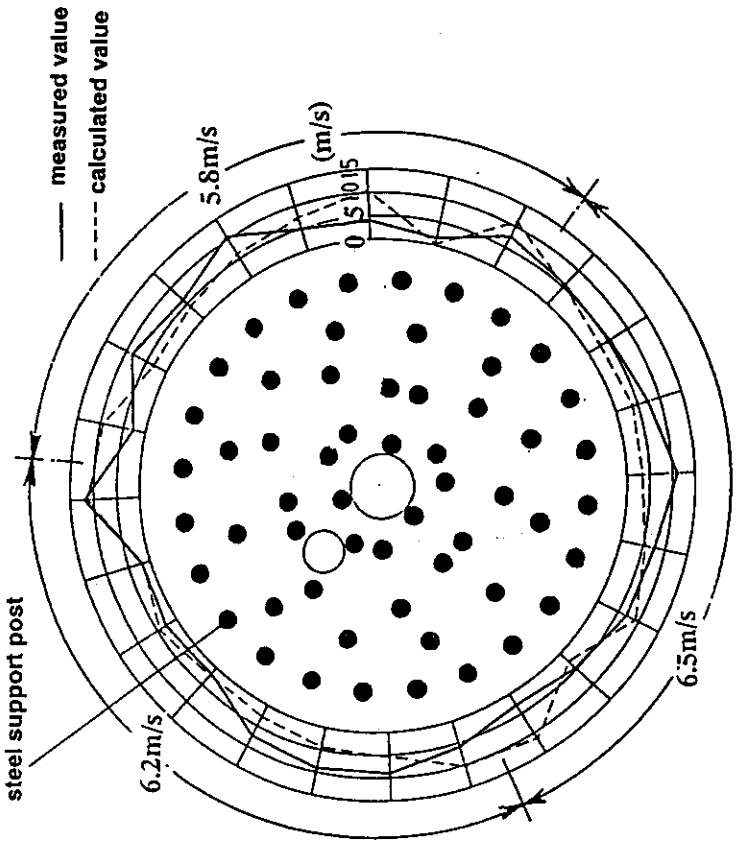


Fig.11 Result of cooling performance test
-velocity profile under support plates

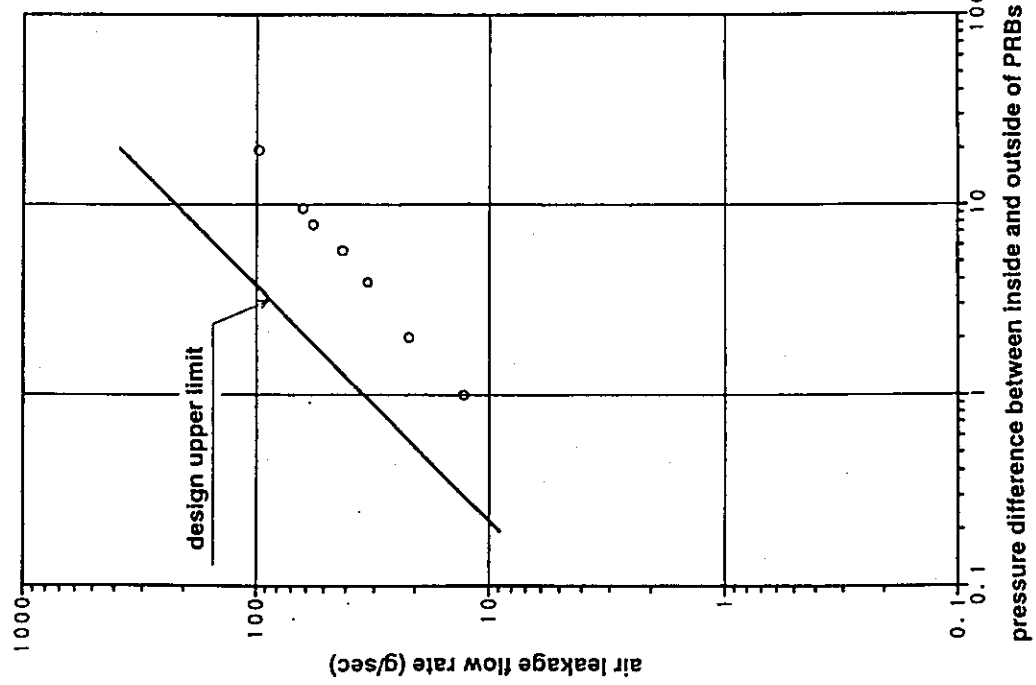


Fig.10 Result of seal performance test

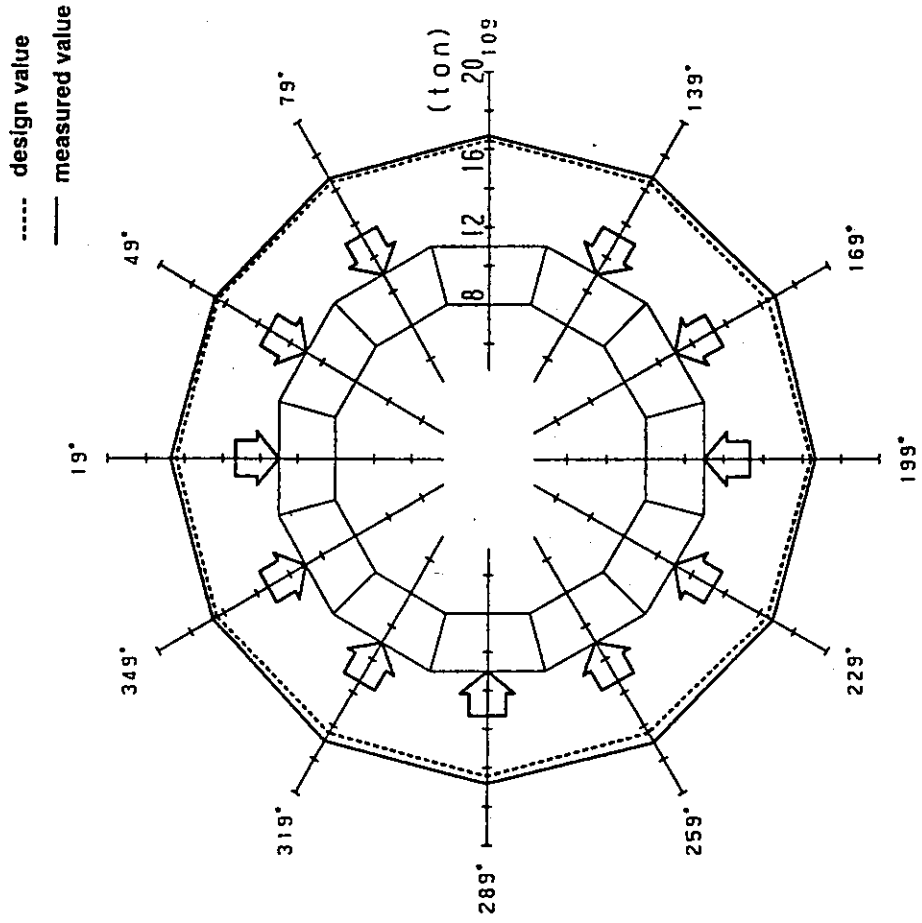


Fig.13 Result of binding performance test
-restraining force onPRBs of lowest layer

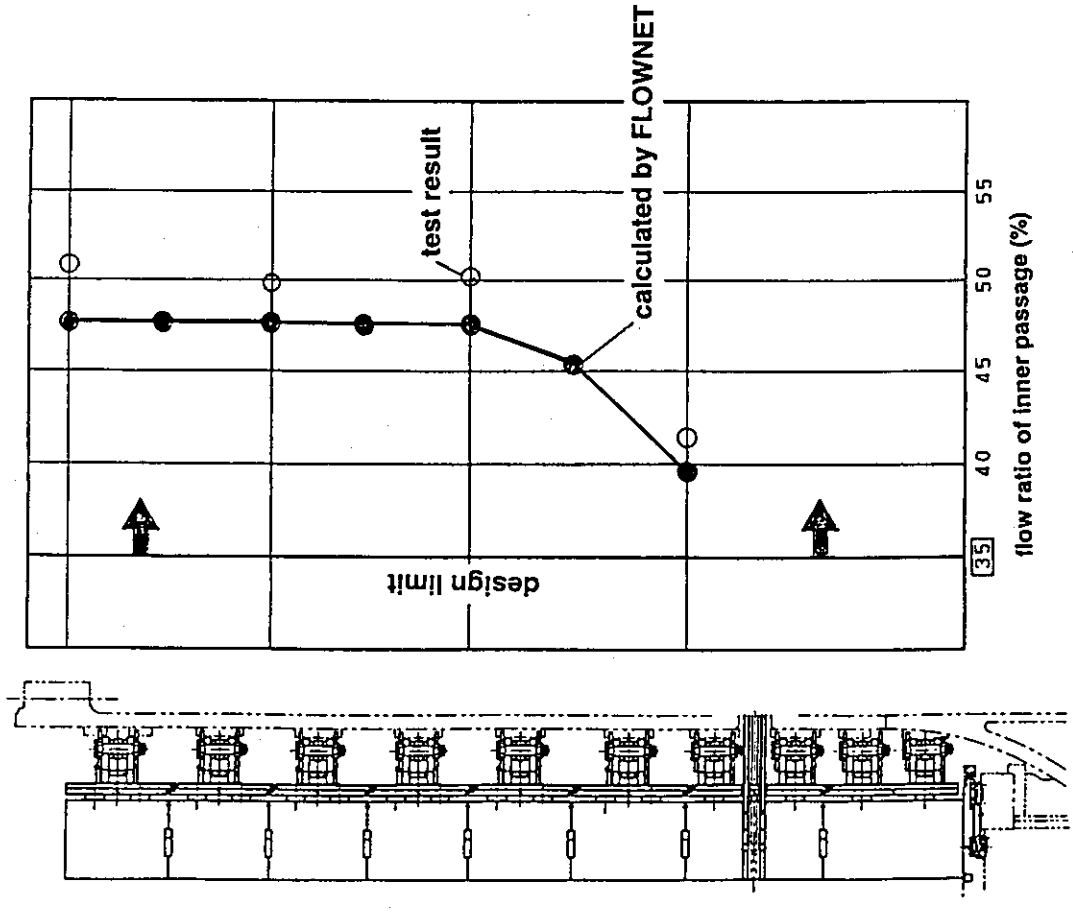


Fig.12 Result of cooling performance test
-flow ratio of inner passage in the core side passage

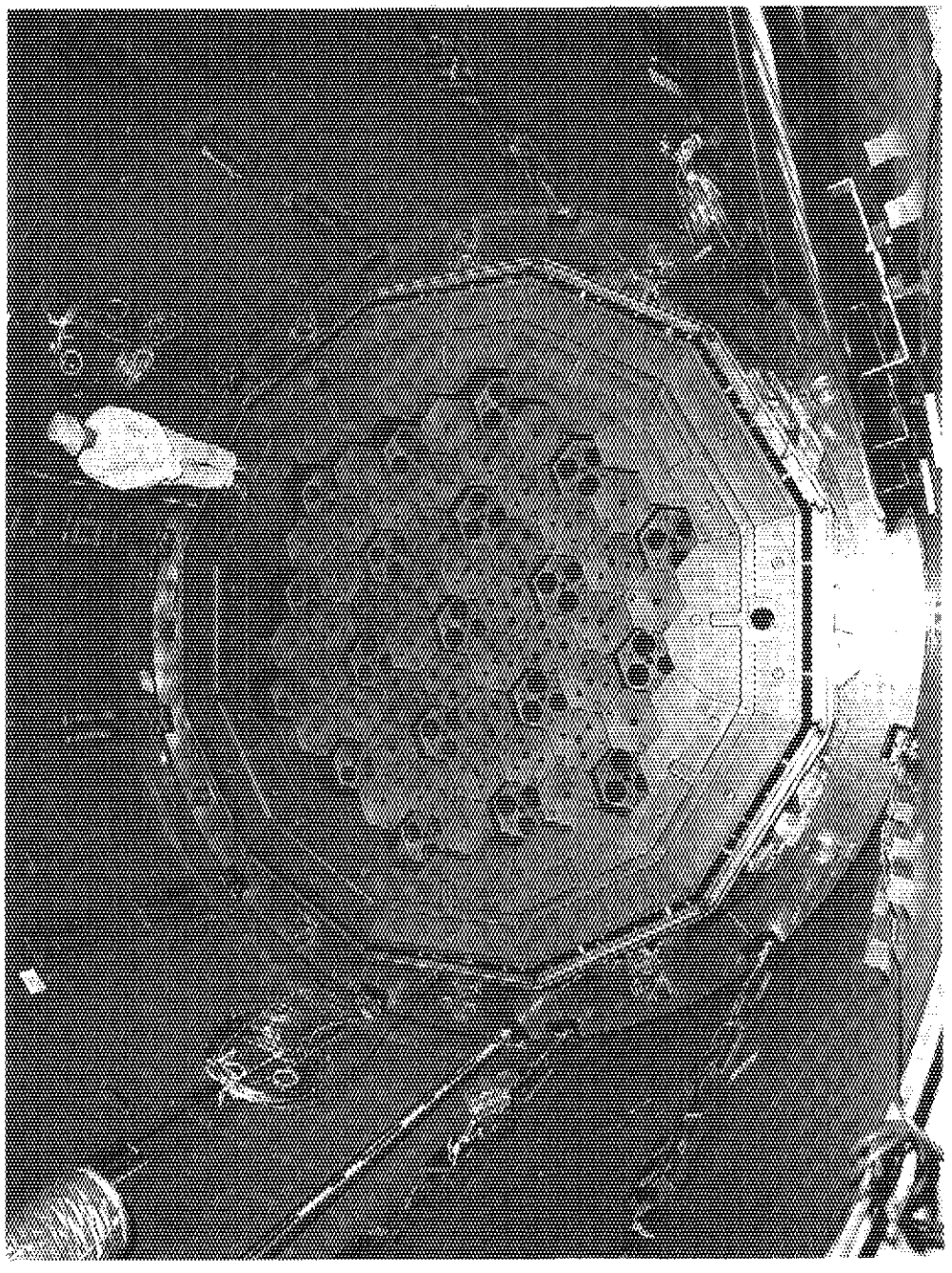


Fig.14 Over view installed In-Core Components in RPV

3.6 Experimental Reactivity Assessment During AVR Defuelling

by P. Pohl

Arbeitsgemeinschaft Versuchsreaktor AVR GmbH

Düsseldorf

Abstract

Defuelling is the first major step in decommissioning the AVR experimental nuclear power plant with high temperature gas-cooled reactor, shut down in 1988. Its about 100,000 ball-shaped fuel elements (pebbles, 6 cm diam) were cycled during reactor operation. At present (Jan. 1996), defuelling is 32 % completed.

In defuelling, the pebble bed surface transforms into a funnel-shaped form with pebbles from the outer core zones steadily rolling towards the core axis. Since the fuel concentration in the outer core is about 2 to 3 times higher than in the inner core, this means the build-up of an inner core richer in fuel and thus supplementary reactivity. To make sure the reactor would not become critical with defuelling, it was agreed in the licensing process to closely follow the development of subcriticality by measurements, so that countermeasures (feeding of absorber pebbles) could be initiated in time.

Up to the defuelling of 15,000 pebbles the subcriticality could be assessed by accurate period measurements which came then to a limit at a subcriticality of about 3.5 % Δk_{eff}. Higher values were determined in an approximation method in which the critical position of the control rod bank (all 4 rods in parallel) was determined and the subcriticality read from rod bank worth curves approximatively adapted to the respective advances in defuelling. The adaptation process takes into account that the upper rod ends with advancing defuelling move on a growing portion of their stroke in the upper void, and it led to the assumption of a slight loss of rod worth with defuelling.

The approximation method came to an end after the defuelling of 26,000 pebbles and a subcriticality of about 5.5 % Δk_{eff} when the reactor by full withdrawal of the rod bank could not be made critical any more.

Up to now, positive reactivity effects could not be expected since the pebbles with low enriched fuel (LEU) had to be returned to the reactor, thus avoiding the funnel-shaping of the pebble bed surface. The neighbouring Jülich Research Center (KFA), who receives the fuel, needed an extra licence to treat the LEU fuel.

Experimental Reactivity Assessment During AVR Defuelling

by P. Pohl

Arbeitsgemeinschaft Versuchsreaktor AVR GmbH
Düsseldorf

Synopsis

In defuelling the AVR experimental nuclear power plant with pebble bed high temperature gas-cooled reactor positive reactivity effects are to be considered. The development of subcriticality with defuelling was therefore monitored by measurement. At first, the subcriticality was assessed by accurate period measurements; later, when this method came to its limit, an approximation method was used that allowed the determination of subcriticality values of up to about 5.5 % Δk_{eff}.

1. Introduction

The AVR experimental nuclear power plant with high temperature gas-cooled reactor was successfully operated for 21 years /1/ and finally shut down at the end of 1988. Its decommissioning started in 1994 with defuelling and dismantling outside of the reactor building /2/.

AVR is a pebble bed reactor that contained about 100,000 ball-shaped fuel elements (pebbles, 6 cm diam) cycled during reactor operation. It had never been completely defuelled, so defuelling was part of the licensing process for decommissioning. At present (January 1996), defuelling is 32 % completed.

Having a two-zone core with a fuel concentration in the outer core zones that is about 2 to 3 times higher than in the inner core, AVR defuelling is in regard of reactor physics not a trivial process. In defuelling, the pebble bed surface transforms into a funnel-shaped form with outer core pebbles constantly rolling towards the core axis. By this, an inner core richer in fuel builds up from the top adding reactivity to the core. To make sure the reactor would not become critical with defuelling it was agreed in the licensing process to closely follow the development of subcriticality by measurements, so that countermeasures (feeding of absorber pebbles) could be initiated in time.

The measurement results are presented in Fig. 1. A measurement was made every 1000 discharged pebbles. The first measurements up to a defuelling of 15,000 pebbles and a subcriticality of about 3.5 % Δk_{eff} are based on the period measurement method. This method came to its limit and higher values were obtained in an approximative method using adapted control rod bank worth curves. This method and further measurements in general came to an end beyond a defuelling of 26,000 pebbles and a subcriticality of about 5.5 %

Δk_{eff} when the reactor even by full withdrawal of the rod bank could not be made critical any more. *

The methods used to determine subcriticality are regarded here in more detail, especially the approximation method.

2. Period measurement method

The period measurement method is a well-known procedure in reactor physics. At AVR, it is carried out using all 4 control rods. The two diagonally opposed rods 1 and 3 are taken as measurement rods, and the remaining diagonally opposed rods 2 and 4 act as reactivity compensators. The procedure starts with withdrawing the compensation rods until the reactor is just critical. In a first period measurement step, the measurement rods are then withdrawn so that the reactor is about 0.15 % Δk_{eff} supercritical. The real reactivity release by this withdrawal is determined, and thus a first point of the measurement rods worth curve is obtained. The supercritical position of the measurement rods becomes a critical position by appropriate insertion of the compensation rods, and the reactor is ready for the second period measurement step by further withdrawal of the measurement rods. In this stepwise procedure the compensation rods move counterwise to the measurement rods so that the procedure is also referred to as counter rod measurements.

All counter rod measurements accompanying AVR defuelling are presented in Fig. 2. As they are time consuming, these measurements were only carried out in defuelling intervals of 3000 pebbles; intermediate results (Fig. 1) were obtained by just determining the critical position of the measurement rods, taking readings of the subcriticality from the respective adjacent measurement rods worth curves, and by interpolating the readings according to the defuelling advance.

---

* Trials to make it critical are nevertheless continued every 1000 discharged pebbles because of the described positive reactivity effect.

Unfortunately, the counter rod method is subject to a systematical deviation leading to an underestimation of the determined reactivity and thus subcriticality values. It is due to the fact that the compensation rods are more or less withdrawn during the measurements (when they should be inserted!)' pulling away' neutron flux from the measurement rods and thus affecting their effectiveness. However, earlier experiments at AVR comparing various rod combinations proved the rod combination 1 and 3 against 2 and 4 as being the least affected, suggesting a deviation in the order of only 1 %. One reason certainly is that with this method the neutron flux is kept centered on the core axis keeping the deformation of the desired flux distribution small. In other experiments it was found that at AVR counter rod measurements can be reproduced with an accuracy of better than ± 1 %.

It should be reminded here that period measurements are, in principal, independent from the detector location in relation to the core. This is particularly advantageous in defuelling with the core constantly changing its form.

3. Rod Bank Worth Curve Approximation Method

This method was used when by full withdrawal of the two measurement rods of the counter rod method the reactor could not be made critical any more. The critical position of the rod bank (all 4 rods in parallel) was then determined and the subcriticality read from an approximated rod bank worth curve for the respective defuelling status.

The approximation procedure to obtain a bank curve for each defuelling status of interest starts from a given bank curve experimentally determined in 1986 (44 data pairs) and consists of two different approximation steps as can be seen in Fig. 3.

First step: Adaptation of the rod position data

This step takes into account that with defuelling the upper rod ends move on a growing part of their stroke length in the upper core void when withdrawn. Here, only little reactivity is released. The rod worth at the rod position of the initial average pebble bed height (1000 scale units, point A) is shifted to the appropriate lower pebble bed height after a certain defuelling (point A'), and all other rod positions of the curve are shifted proportionally. With the relation that in the prismatic part of the pebble bed 1000 pebbles mean 3 cm or 32 rod scale units of core height, and with a rod position of 4300 scale units at full withdrawal, the rod position data x of the initial curve were adapted using the formula

$$x' = 4300 - (4300-x)\,\frac{4300 - 1000 - 32n}{4300 - 1000}$$

with n meaning the number of discharged pebbles in units of 1000.

Second step: Adaptation of the reactivity data

In terms of the reactivity data of the rod bank worth curve two questions arise. Firstly, were the data of the 1986 curve still true for the start of defuelling, and secondly, did they change with defuelling. Both questions can be answered approximatively by using the counter rod measurement results. At each of the 6 counter rod measurements, the critical position of the rod bank was also determined. This means, that for the start of defuelling and for defuelling steps of 3000 pebbles up to a defuelling status of 15,000 one precise curve point of the respective rod bank curve is known (point C in Fig. 3), apart of course from the zero point of the curve which is trivial.

A sufficient approximation of the real rod bank worth curves, that is the curve for the start of defuelling and the curves for defuellings of up to 15,000 pebbles, can now be obtained by propor-

tional adaptation of the reactivity data, so that the respective precise curve point becomes part of the respective curve (Fig. 3).

The first question posed at the beginning of that chapter is answered. The approximate bank curve for the start of defuelling was found to be considerably flatter than the 1986 curve. However, the curves obtained in the described way, including that for the start of defuelling, are of no direct use since the subcriticality up to a defuelling of 15,000 pebbles could be determined by period measurements. The second question can now be posed more precisely: Can a change in rod bank worth with defuelling be seen and can a dependence be deduced which could then be extrapolated to obtain bank curves for defuellings beyond 15,000 pebbles?

Defuelling status	Measured point of control rod bank worth curve		Reactivity read from intermediate curves[1] at critical rod bank position	Deviation measurement/reading	
Number of pebbles discharged	Critical rod bank position	Reactivity from period measurements		absolute	relative
0(Start)	1668	1,444	1,444[2]	0[2]	0[2]
3000	1954	2,183	2,129	0,054	2,5 %
6000	2054	2,327	2,237	0,090	4,0 %
9000	2180	2,427	2,461	-0,034	-1,4 %
12000	2392	2,820	3,094	-0,274	-8,9 %
15000	2648	3,489	3,944	-0,455	-11,5 %

Reactivity in % Δk_{eff}
1) Rod bank position data already adapted (A →A', Fig 3).
2) Reactivity data of the 1986 curve already adapted.

TABLE 1 Test of a change in rod bank worth with defuelling by using period measurement results

Table 1 shows the data of the counter rod measurements as of interest here and the according reactivity readings from the respective bank curves as obtained after the first adaptation step (adaptation of rod position data). The deviations of the readings

from the measurements of Table 1 are plotted in Fig. 4. The course of the plotted values seems strange and not suitable to derive a real deviation function. For advanced defuelling, however, Fig. 4 strongly suggests a drop in rod worth with defuelling. For the necessary approximation process the simple linear relation of Fig. 4 was chosen, assuming a relative rod worth loss of 0.76 % for every 1000 pebbles discharged.

As an example, the approximated control rod bank worth curve that was used to determine the subcriticality after the defuelling of 20,000 pebbles is presented in Fig. 5.

4. Conclusions and Outlook

The task of closely following the subcriticality development of the AVR with defuelling could for a considerable portion of defuelling be successfully performed and, as Fig. 1 shows, with sufficient accuracy. These measurements are one more example of so far unique experiments that reactor is known for.

The steady rise of subcriticality (Fig. 1) is no surprise, since positive reactivity effects could not be expected so far. The neighbouring Jülich Research Center (KFA), who receives the fuel, needed an extra licence to treat the AVR low enriched fuel (LEU), about half of the core. Therefore, the LEU fuel had to be returned to the reactor, thus avoiding the funnel-shaping of the pebble bed surface. Furthermore, the LEU fuel has sufficient burn-up so that the fuel concentration in the inner core could be kept low.

The complete defuelling of AVR is bound to start soon, and in a later stadium of defuelling the described positive reactivity effects will no doubt occur. However, in regard of the consider-

able defuelling already achieved, a recriticality by withdrawal of the rod bank cannot be expected. The described measurement methods, nevertheless, are standing ready to be performed again, the approximation method of course with less accuracy. Should the subcriticality against expectations even drop into the measurement range of the period measurement method, it can be determined with the usual accuracy, and the approximation results can be reviewed.

References

/1/ Association of German Engineers (VDI)
AVR-Experimental High-Temperature Reactor,
21 Years of Successful Operation for a Future Energy Technology
VDI-Verlag, Düsseldorf, 1990

/2/ Wahlen, Wahl, Pohl
Decommissioning of the AVR experimental nuclear power plant,
Intern. Conf. on Nuclear Decommissioning, London, Nov. 1995,
IMechE Conf. Transaction 1995-7, p. 255

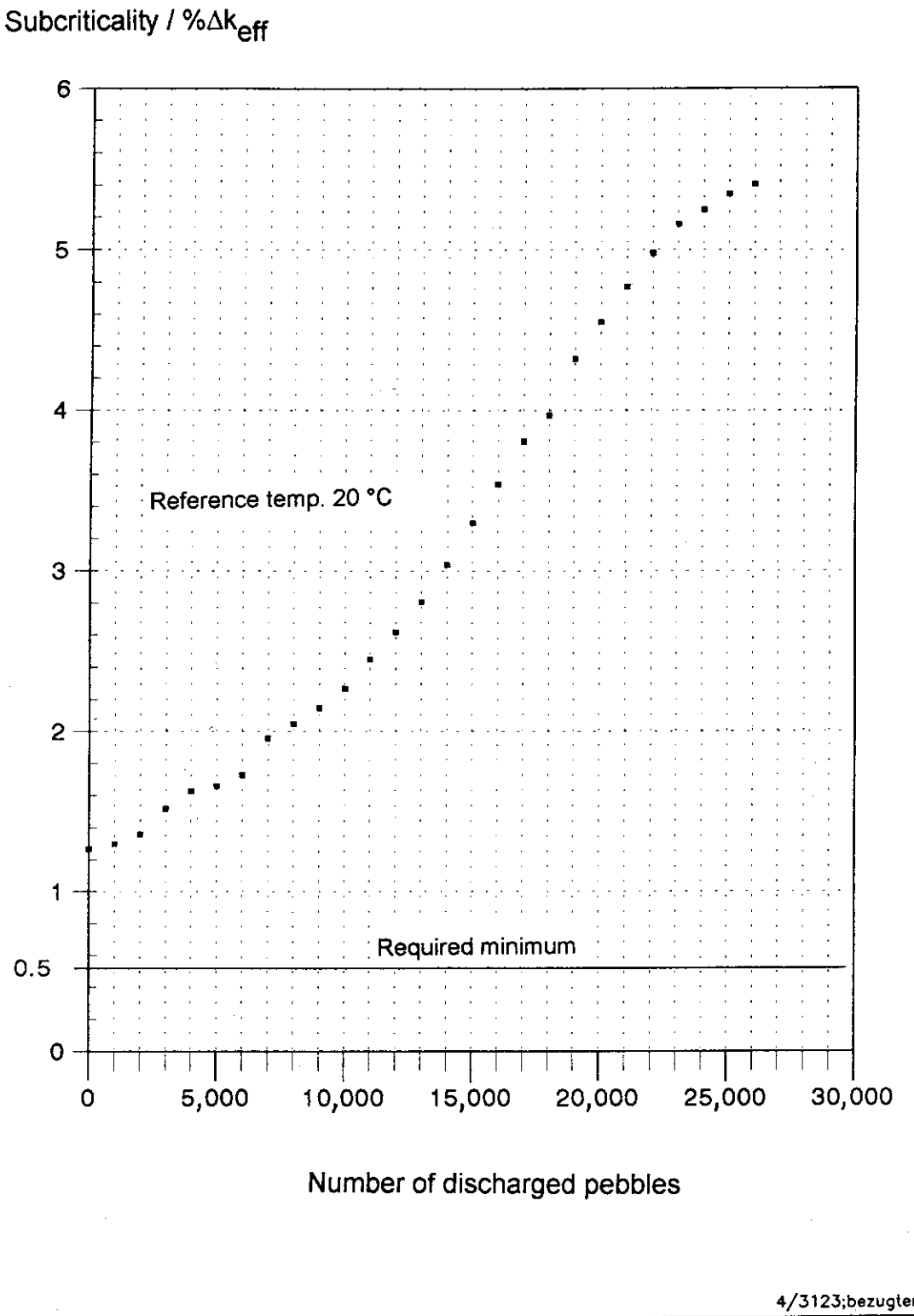


Fig.1 Measurement of Subcriticality During AVR Defuelling

AVR GmbH

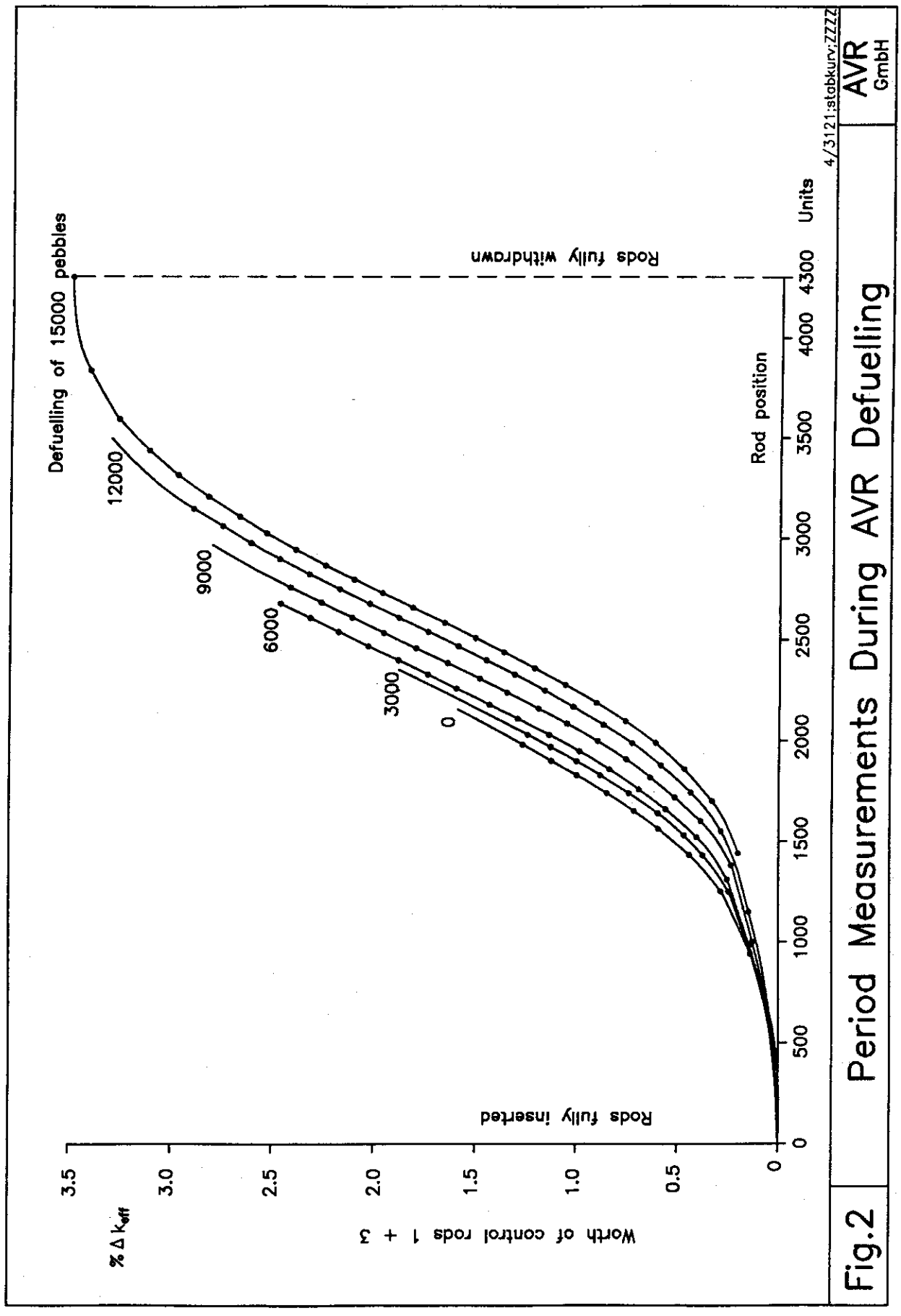


Fig.2 Period Measurements During AVR Defuelling

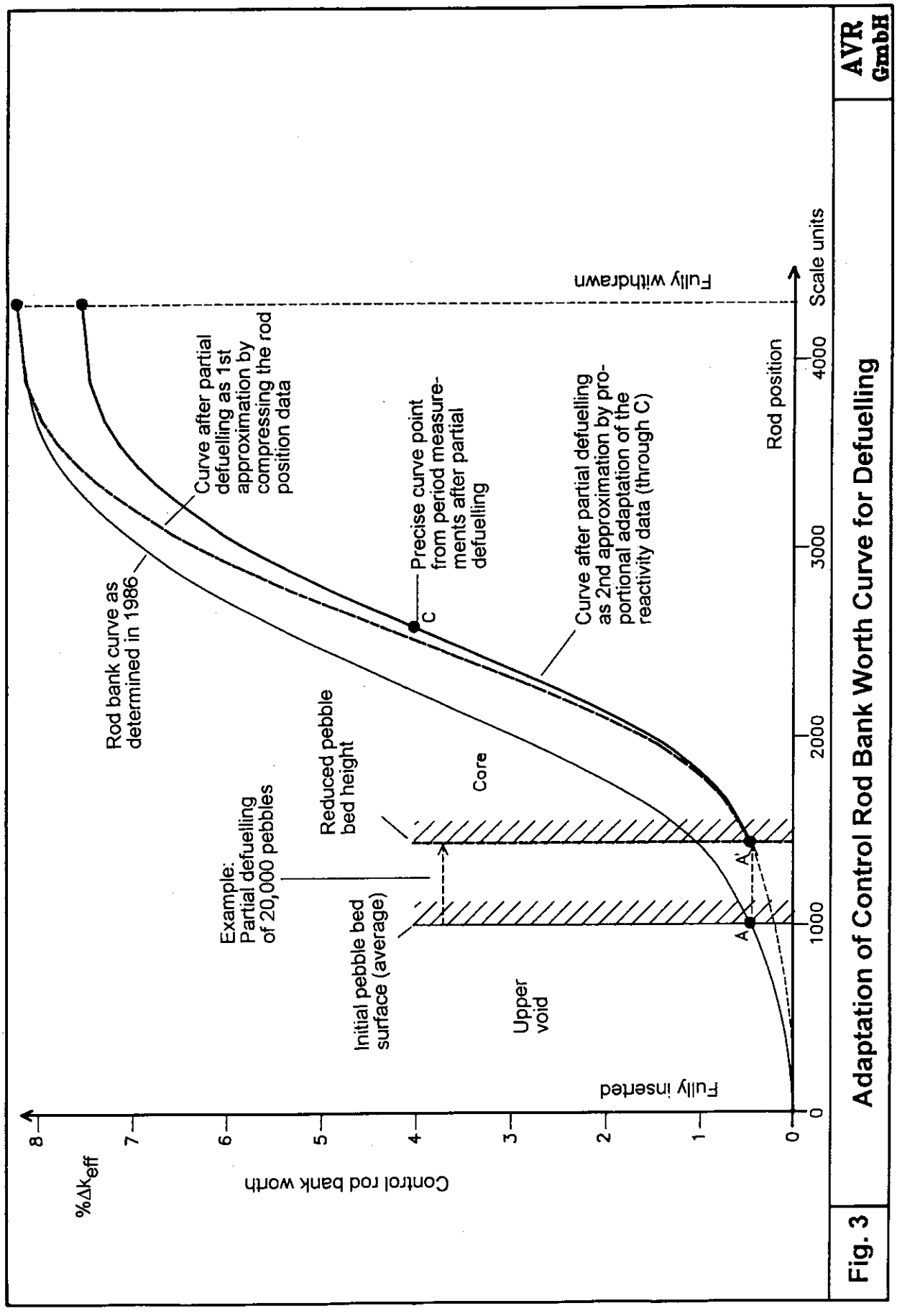
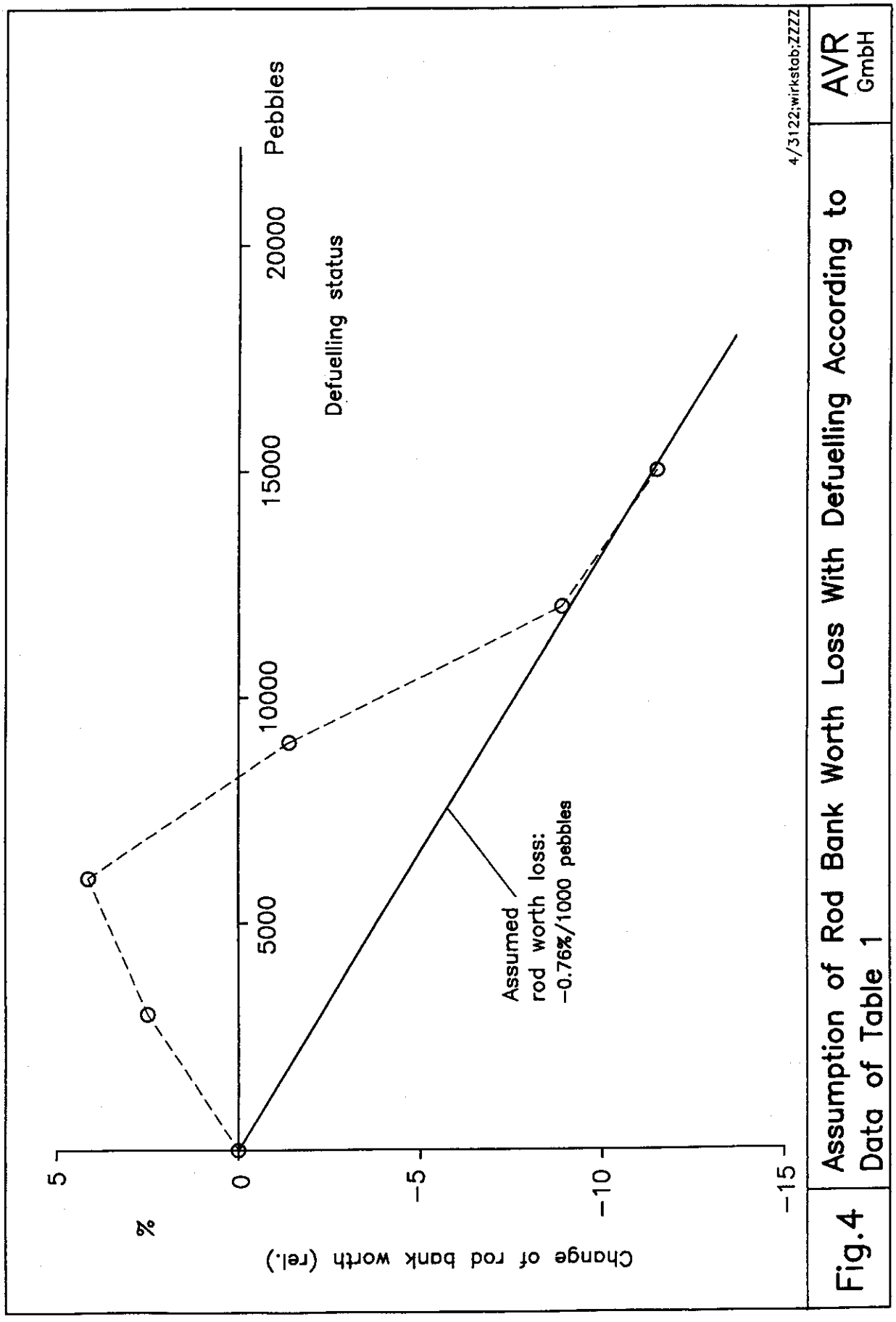


Fig. 3 Adaptation of Control Rod Bank Worth Curve for Defuelling


Change of rod bank worth (rel.)
%
5
0
−5
−10
−15
5000
10000
15000
20000
Pebbles
Defuelling status
Assumed
rod worth loss:
−0.76%/1000 pebbles
4/3122;wirkstab;ZZZZ
Fig.4
Assumption of Rod Bank Worth Loss With Defuelling According to
Data of Table 1
AVR
GmbH

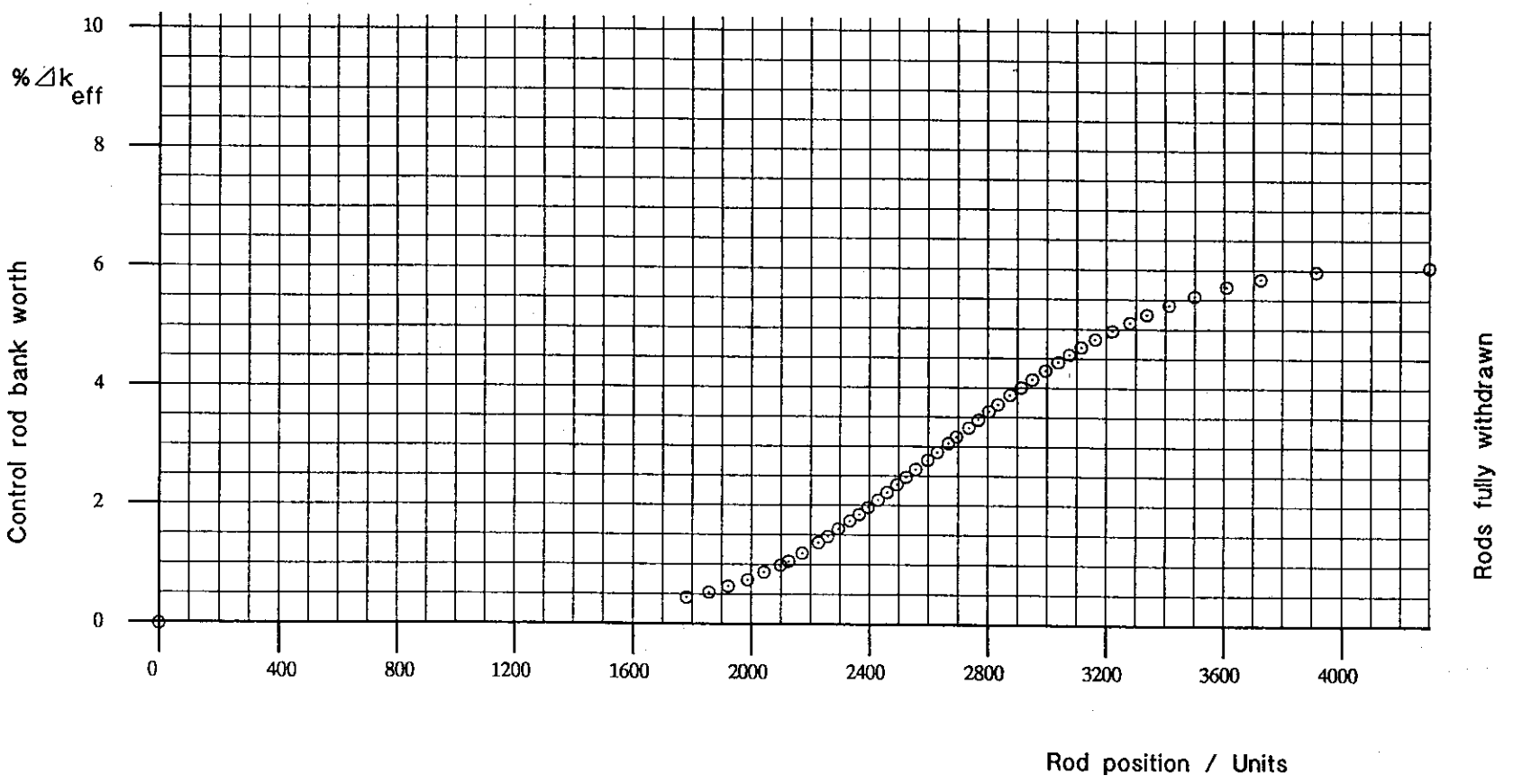


Fig.5 Control Rod Bank Worth Curve Approximation for a Defuelling of 20,000 Pebbles

AVR GmbH

4. Session Ⅳ

－Heat Utilization of HTGR－

4.1 Design and Evaluation of Heat Utilization Systems for the HTTR through International Cooperation

by Dr. Irene Lewkowicz

Abstract

The International Atomic Energy Agency (IAEA) has the statutory function to "foster the exchange of scientific and technical information", and "encourage and assist research on, and development and practical application of, atomic energy for peaceful uses throughout the world". The IAEA Co-ordinated Research Programmes (CRPs) are effective vehicles for implementing the above.

The CRP on Design and Evaluation of Heat Utilization Systems for HTTR has started in September 1994 and is aimed at promoting international co-operation to identify the most promising heat utilization system(s) to be demonstrated at the HTTR, for the benefit of current operators and future designers and constructors of HTGRs. Participating Member States are collaborating by exchanging existing technical information on the technology of heat utilization systems, by developing design concepts and by performing evaluations of candidate systems for potential demonstration with the HTTR.

The systems being assessed in the CRP for potential demonstration have been selected by the participants according to their own national interests and,n depending on the status of the technology chosen, its economic potential, and other factors such as safety and environmental considerations. The systems and/or processes are:

- steam reforming of methane for production of hydrogen and methanol
- CO_2 reforming of methane for production of hydrogen and methanol
- combined coal conversion and steam generation
- thermochemical water splitting for hydrogen production
- high temperature electrolysis of steam for hydrogen production
- gas turbine for generation of electricity

The key tasks of the CRP are to:

a. define the R&D requirements prior to coupling to the HTTR
b. define the goal of the demonstration at the HTTR
c. prepare design concepts for coupling selected systems to the HTTR and perform preliminary safety evaluations
d. check licensability of selected systems under Japanese conditions.

At the First Research Co-ordination Meeting (RCM) of the CRP held in October 1994 at Oarai (Japan), it was determined that based on evaluations of technology status until then, the first priority candidate systems that will very likely be selected for connection to the HTTR are: the steam (and/or CO_2) methane reforming and the gas turbine. R&D will continue on the other processes and/or systems until their development reaches a status where they can be considered feasible for demonstration at the HTTR.

CRP activities during the first two years have focussed on steps a and b, and with some progress in c and d. At the Second RCM to be held in February 1996, also at Oarai, the progress attained by the participants will be assessed in detail. The timing of initiating specific design of the Heat Utilization Plant (HUP) will be discussed.

It is believed that timely completion and successful operation of the HTTR and these heat utilization systems will be the major milestones in gas-cooled reactor development and in development of nuclear process heat applications.

Design and Evaluation of Heat Utilization Systems for the HTTR through International Cooperation

Irene Lewkowicz
Division of Physical and Chemical Sciences
Department of Research and Isotopes
Internasional Atomic Energy Agency
Vienna, Austria

John Cleveland
Division of Nuclear Power
Department of Nuclear Energy and Safety
International Atomic Energy Agency
Vienna, Austria

Presented
at the
3rd JAERI Symposium on HTGR Technologies
Oarai, Ibaraki, Japan, February 1996

1. Introduction

The International Atomic Energy Agency (IAEA) has the statutory function to "foster the exchange of scientific and technical information", and "encourage and assist research on, and development and practical application of, atomic energy for peaceful uses throughout the world".

Many IAEA Member States are concerned about global environmental problems which result from burning fossil fuels. Nuclear power provides a means to produce energy in all forms, i.e. as electricity, district heat, process steam and high temperature process heat, under environmentally acceptable conditions. Currently, nuclear energy produces approximately 17% of the world's total electricity generation at competitive costs. At present, about 30% of the world's primary energy consumption is used for electricity generation, about 15% is used for transportation and the remaining 55% is converted into hot water, steam and heat. This shows that the potential for applications of nuclear energy in the non-electric sector may be quite large, although currently only a few nuclear plants are used for non-electric applications.

The ultimate potential offered by HTGRs derives from their unique ability to provide heat at high-temperatures (e.g., in the range from about 550°C to 1000°C) for endothermic chemical processes and, at 850°C and above, for highly efficient generation of electricity with gas turbine technology. Heat from HTGRs could be used for production of synthesis gas and/or hydrogen and methanol by steam-methane reforming, production of hydrogen by high temperature electrolysis of steam and by thermochemical splitting of water, production of methanol by steam or hydrogasification of coal, and for processes requiring lower temperatures, such as petroleum refining, seawater desalination, district heating and generation of steam for heavy oil recovery. If the heat demand is not in the immediate vicinity of the reactor, a chemical heat pipe could be developed as a high temperature heat transporter. It is important to establish nuclear heat process application technology through research, development and demonstration.

In Japan an important milestone was reached in March 1991 with the start of construction of the High Temperature Engineering Test Reactor (HTTR) at the Oarai Research Establishment of the Japan Atomic Energy Research Institute (JAERI). This 30 MW(t) reactor will produce core outlet temperatures of up to 950°C. It is anticipated that the HTTR will be the first nuclear reactor in the world to be connected to a high temperature process heat utilization system. Criticality is expected in 1997. The timely completion and successful operation of the HTTR and its heat utilization system will be major milestones in gas-cooled reactor development and in development of nuclear process heat applications.

2. Coordinated Research Programme framework and goals

The early development of nuclear power was conducted to a large extent on a national basis. However, for advanced reactors, international co-operation is playing an increasingly greater role. The IAEA promotes international co-operation in advanced reactor development and application. Especially for designs incorporating innovative features, international co-operation allows a pooling of resources and expertise in areas of common interest to help to meet the high costs of developing the technology. Agency sponsored Co-ordinated Research Programmes (CRP's) are one method, of promoting international cooperation. These are typically 3 to 6 years in duration, and often involve experimental activities in selected technology areas of mutual interest to the participating countries. Such CRPs allow a sharing of efforts on an international basis and benefit from the experience and expertise of researchers from the participating institutes.

To foster international cooperation in HTGR applications, the IAEA has established a Coordinated Research Programme on Design and Evaluation of Heat Utilization Systems for the High Temperature Engineering Test Reactor (HTTR). This is a joint activity of the IAEA's Division of Nuclear Power and the Division of Physics and Chemistry. The CRP began in January 1994 and will last 5 years.

The most promising nuclear heat application systems in terms of feasibility, safety, size of market, the associated economics, and environmental considerations will be selected for demonstration at the HTTR. In order to establish and upgrade the HTGR technology basis, JAERI is willing to provide the HTTR for international use to promote R&D on HTGRs and their applications more efficiently.

The objective of this CRP is to identify the most promising heat utilization system(s) to be demonstrated at the HTTR. Participating Member States are collaborating by exchanging existing technical information on the technology of heat utilization systems, by developing design concepts and by performing evaluations of candidate systems for potential demonstration with the HTTR. The participating institutes are:

* JAERI, Oarai (Japan)
* Kurchatov Institute, Moscow (Russia)
* Institute of Nuclear Energy Technology, Beijing (China)
* KFA Jülich (Germany)
* National Atomic Energy Agency, Jakarta (Indonesia)
* Weizmann Institute of Science, Rehovot (Israel)
* General Atomics, San Diego (USA)

The systems being assessed for potential demonstration have been selected by CRP participants, during the 1st RCM in November 1994, [1] according to their own national interests depending on status of the technology, economic potential, safety and environmental considerations, and other factors.

The following systems are being examined:

- steam reforming of methane for production of hydrogen and methanol
- CO_2 reforming of methane for production of hydrogen and methanol
- combined coal conversion and steam generation
- thermochemical water splitting for hydrogen production
- high temperature electrolysis of steam for hydrogen production
- gas turbine for electricity generation

In addition, testing of advanced intermediate heat exchangers will be examined.

For the systems being examined key tasks of the CRP are to

a) define the R&D needs remaining prior to coupling to the HTTR
b) define the goal of the demonstration with the HTTR
c) prepare design concepts for coupling selected systems to the HTTR and perform preliminary safety evaluations
d) check licensability of selected systems under Japanese conditions

3. The HTTR and its heat utilization system

The HTTR is a high temperature gas cooled test reactor with thermal output of 30 MW and an outlet coolant temperature of 850°C at rated operation and 950°C at high temperature test operation. The HTTR consists of a reactor pressure vessel with a prismatic, graphite moderated core, a main cooling system with a helium-to-helium intermediate heat exchanger and a pressurized water cooler in parallel, an auxiliary cooling system, reactor vessel cooling system and related components (see Figure 1). The major technical parameters of the HTTR are given in Table 1. The construction schedule for the HTTR is shown in Table 2.

JAERI is proposing to construct the high temperature nuclear process heat utilization system close to the HTTR a few years after completion of the HTTR (Figure 2) and then to connect it to the helium-to-helium intermediate heat exchanger (IHX) at the first refuelling. The secondary helium from the IHX will transfer 10 MW to the heat utilization plant. The IHX is a counter-current and helically wound tube type shell-and-tube heat exchanger (Figure 3). Under high temperature test operation the IHX will provide a supply of compressed helium gas at a temperature of about 900°C with practically no contamination risk to the heat utilization plant.

As is shown in the schedule and test plan (Table 3) it is proposed to start the heat utilization system test at the end of fiscal year (FY) 2002, or 2001. To do this, construction of the heat utilization plant should be started in FY 2000.

4. Incentives, technical status and development needs of heat utilization systems being examined

As an energy source, nuclear energy provides a means to produce not only electricity but also other clean energy carriers. Hydrogen is a convenient medium for storing and transporting energy in chemical form and has a high energy density. Methanol is attractive as automobile fuel, is easy to transport and store, and is less CO_2 emissive than gasoline. Hydrogen and/or methanol production with nuclear energy could play a key role in resolving global warming and conserving fossil fuels. At the same time, it is important to bear in mind that the large scale use of hydrogen as an energy carrier would require changes in the energy infrastructure.

Hydrogen can be produced by several methods. The most important process used on an industrial scale is steam reforming of methane. Produced in this way it serves as feedstock for the ammonia and the fertilizer industries, for oil refining and for the synthesis of methanol. Another small scale industrial process is the electrolysis of water, which produces much purer but more expensive product. Integration of coal hydrogasification to produce methane together with steam reforming of methane leads to production of methanol from coal.

A number of other processes may also provide the link between the nuclear heat source and hydrogen. These are high temperature steam electrolysis and the various thermochemical cycles for splitting water. Presently at the R&D stage, these processes require extensive development and demonstration to establish their technical feasibility and their economic viability as candidate processes for thermal energy conversion.

4.1 Hydrogen and Methanol Production by Steam Reforming

Steam reforming of methane is a well known industrial process, often combined with hydrogasification of coal. The basic reactions involved in these processes are shown in Figure 4. The coal to methanol reaction requires substantial quantities of heat. For efficient reaction rates, the reformer requires heat at temperatures of 790°C and above. If the heat were supplied by coal about 80% more coal feedstock would be required along with oxygen for combustion and would produce 1 to 1.4 moles of CO_2 per mole of methanol produced.

In order to produce methanol from coal without CO_2, two process inputs in addition to coal and steam are required: a supplemental hydrocarbon feed with a H/C ratio higher than two, and a non-combustion source of high temperature heat. The ideal supplemental feed would be H_2. Although small quantities of inexpensive H_2 are available as process by-products, a large scale methanol economy would require enormous quantities of H_2. In lieu of a cheap H_2 source, CH_4 from natural gas can be an interim feedstock.

If a HTGR is the heat source, the principal challenge is the method of transporting heat to the process. Conventional coal conversion technologies introduce oxygen into the steam coal gasifier to provide the reaction heat via direct combustion. Nuclear heat must be generated separately and supplied indirectly to the process steam through a heat exchanger.

Although the full scheme presented in Figure 4 is sound on the economical basis for countries having large fossil energy reserves, principally in the form of coal and natural gas, it was decided to test individual parts of the scheme to establish the HTGR as a process heat source. Steam reforming of methane to produce hydrogen and methanol (or syngas) has been chosen as a first priority candidate nuclear process heat application to be demonstrated using the HTTR. The following reasons led to this decision:

- steam reforming for production of hydrogen and methanol is an endothermic reaction
- it is a well-experienced production process in non-nuclear industrial applications
- at present and in the near future, the most economical process to produce hydrogen is considered to be steam reforming of natural gas
- hydrogen and methanol are co-produced from the syngas. Hydrogen, as shown in Figure 4, can be used further for coal hydrogasification or liquefication.

When heat is supplied from an HTGR to the steam reforming process, the nuclear plant dictates the main design and operation parameters of the process. To attain similar heat fluxes and high conversion rates with helium heating despite the 50 to 100°C lower temperature than with flame heating, a different steam reformer design is required compared with existing commercial steam reformer plants.

Test module helium heated steam reformers have been successfully tested at the 10 MW(t) level in Germany in the 1980s, using 40 bar helium heated by electric heaters to 950°C and steam reforming temperature of ~820°C. Total operation included 13,000 hrs, of which 7,750 hr were above 900°C verifying the operation of reformers with convective helium heating [2].

The goal of testing at the HTTR is to demonstrate reliability, and the ability to operate and control the process effectively utilizing nuclear heat (10 MW). The flow diagram is shown in Figure 5. The reformer tubes are packed with catalyst (e.g. Ni on alumina) and are heated by helium gas flow outside the tubes (Figure 6). The reformer design developed by JAERI will produce 1390 Nm^3/h of hydrogen and 1930 Kg/h of methanol from 950 kg/h of methane [3].

4.2 CO_2 reforming of methane for production of hydrogen and methanol

While CO_2 reforming of methane is not commercially performed, it is currently experimentally investigated at the solar energy research facilities of the Weizmann Institute of Science, Rehovot, Israel. The system investigated involves a "solar chemical heat pipe". The CO_2 reformer could potentially be adapted for demonstration at the HTTR to produce syngas as feed for a methanol synthesis plant.

Figure 7 shows a solar heat pipe system which is based on the chemical heat pipe concept originally developed in connection with the HTGR at the KFA Research Center, Juelich, Germany, and adapted and modified to solar energy at the Weizmann Institute. The method, which involves conversion of solar energy to a chemical form

that can be stored and then transported at the time and to the place that energy is needed is based on the following reaction:

$$CH_4 + CO_2 \rightleftarrows 2\,(CO + H_2)$$

The reforming reaction is conducted in a solar furnace by passing methane and CO_2 through a catalyst (1% Ru on alumina) at 800 to 1000°C. In the chemical heat pipe process the stored solar energy is released in a methanator plant that reacts hydrogen and carbon monoxide to recover methane and release high temperature heat to generate steam, electric power or both. The methane is returned to the solar site, completing the cycle. CO_2 reforming is preferred to steam reforming for solar application because its gaseous phase simplifies the start up - shutdown cycle which occurs daily.

The cycle has been proven at a laboratory-scale facility using 5 to 10 KW of heat. The process has been scaled up to 480 KW and testing has started in 1994. The temperatures achieved in the solar heated reformer are similar to those produced by HTTR heat.

4.3 Combined coal conversion and steam generation

Hot water or steam injection to enhance oil recovery is commercially performed. However, if the hot water or steam is produced by burning oil, about 40% of the recovered oil is used. An alternative is to use HTGR heat to produce the steam.

The steam temperature and pressure conditions required for oil recovery are highly dependent on the geological conditions of the oil field and range up to about 550°C. Coal liquefaction processes need temperatures from 400-550°C, and, for the pyrolysis process, up to 870°C. Combined coal conversion and steam generation for oil recovery may be reasonable in special locations where there are dual needs such as in the Sumatra and Kalimatan Islands of Indonesia.

The feasibility of coupling a combined system to the HTTR will be examined.

4.4 Thermochemical water splitting for hydrogen production

The most extensively studied and promising thermochemical water splitting cycles are the ones based on the high temperature decomposition of sulfuric acid:

(i) $2H_2O + I_2 + SO_2 \rightarrow H_2SO_4 + 2HI$ Bunsen reaction ~100°C

(ii) $H_2SO_4 \rightarrow SO_2 + H_2O + \frac{1}{2}O_2$ 950°C and above (endothermic)

(iii) $2HI \rightarrow H_2 + I_2$ ~ 300°C - 370°C

Preliminary analytical studies showed the process thermal efficiency of ~ 40-50% can be expected under optimum operating conditions. Carlo Rubia CERN [4] predicts a thermal efficiency of 64%.

Experimental results reported by JRC Ispra in 1983 [5] point out that thermochemical production of hydrogen is feasible on a pilot plant scale ($10Nm^3/h$) using the above mentioned technology. The overall efficiency of the process has been assessed to be around 36-40%. However many difficulties remain in establishing the gaps in optimal engineering design including materials corrosion resistivity, coupling of the chemical plant to the nuclear heat source and safety problems. As a result JAERI has developed an improved process on the laboratory scale of 1-10 liter H_2/h in glass, quarz and teflon apparatus. Since the process utilizes corrosive chemicals the structural materials impose a serious problem and their proper selection constitutes an important part of the R&D. The main achievements are the demonstration of thermal efficiency higher than 40% and selection of better structural materials.

Further R&D will focus on optimization of the hydrogen iodide decomposition step with respect to structural materials and efficiency, and on the sulphuric acid decomposition step. The optimal engineering design is in progress including coupling to the helium loop. Mechanical properties of the selected structural materials will be investigated. The planned demonstrations are:

(i) laboratory scale to show continuous production of hydrogen in more efficient operation mode
(ii) process demonstration using metallic reactors to produce $1Nm^3$ H_2/h
(iii) scale-up process $100Nm^3$ H_2/h coupled to the 10 MW non nuclear HENDEL facility of JAERI.

Some critical items which must be addressed with the further development of thermochemical water splitting are:

a) materials appropriate for large industrial plants
b) engineering design to improve efficiency and decrease investment costs
c) coupling of the chemical plant to the nuclear heat source, and establishment of safety design criteria and procedures for the combined nuclear and chemical plant complex

4.5 High temperature electrolysis of steam for hydrogen production

Hydrogen production by high-temperature electrolysis of steam is also one of candidates of nuclear heat application. The process is the reverse of that used for solid oxide fuel cells (Figure 8). The process requires temperatures ranging from 900 to 1000°C. The high temperature electrolysis of steam, although very promising, is still at an early stage of technology. The main technology challenges are in development and low cost production of efficient, reliable and durable electrolysis cells. The cells technology is known from the ceramic fuel cells. This technology, however, is currently too expensive and not suitable for mass production. A fundamental study on material selection of solid electrolytes and ceramics electrodes for application to electrolysis of steam has been carried out by measurements of electrical conductivity and phase stability in the JAERI. A hydrogen production rate of 7 liters/hr has been attained at 950°C by the laboratory scale tests. For further development, the following tasks are planned by JAERI in cooperation with Fuji Electric Co.

(i) Improvement of electrolysis cell in order to reduce ohmic loss, and increase the working life of the cell. New construction materials such as Yterbia stabilized zirconia will be tried, together with new geometrics of the cell. The mechanical strength of the cell and its durability during heat cycles impose a problem especially when scale-up is planned.

(ii) Optimization of the full system will include auxiliary equipment such as steam generators, steam super heaters and heat exchangers.

The working plan includes demonstration of a system with hydrogen production rate 10 Nm^3/h. Based on the results obtained, a prototype system with a production capacity of 100 Nm^3/h will be tested to provide data for safety review for the possible coupling to HTTR.

4.6 Gas turbine for electricity generation

A promising approach for making good use of the high temperature capability of HTGRs is to use the primary helium coolant to drive a gas turbine in a direct closed cycle arrangement. In the seventies, this was extensively studied in the USA, in Germany, in Great Britain and in France. At that time, the concept was based on enclosing a large (2000 to 3000 MWt) reactor core and the gas turbine power conversion system within a prestressed concrete reactor vessel (PCRV). After nearly a decade of work, this concept was abandoned primarily because the system achieved only about 39% efficiency and would have required substantial development to resolve design and safety issues. It was concluded that the HTGR with a gas turbine offered little advantage over a steam cycle HTGR, which could be deployed with much less development.

However, recent advances in turbomachinery and heat exchanger technology, and the development of smaller modular reactor concepts, have resulted in renewed design and development activities in the USA and Russia for a gas turbine HTGR. Key technology developments have been achieved the last decade associated with large gas turbines, magnetic bearings and compact plate-fin heat exchangers. Turbine and compressor efficiencies have increased, and more compact recuperators with a higher effectiveness have been developed. Direct, indirect and combined cycles can be considered.

In the USA, activities have focused on design and development of a direct cycle modular HTGR gas turbine system of 600 MW(t) with a predicted 47% cycle efficiency at a turbine inlet helium temperature of 850°C. Natural gas combustion turbines are now commercially available in sizes up to 200 MW(e) and operate reliably at temperatures well above this 850°C level. Use of magnetic bearings would provide efficiency gains and eliminate the possibility of ingress of lubricating fluids into the reactor environment; performance of magnetic and thrust bearings of adequate capacity to support large-size turbo generators must be shown. In extending the open-cycle gas turbine recuperator experience to meet the requirements of a high pressure system, development is necessary to demonstrate that the compact surface geometries have structural integrity for long service life.

The helium turbine technology base includes a comprehensive programme conducted in Germany for a Brayton (closed) cycle power conversion system. The programme, which was initiated in 1968, was for electric power application with a high temperature gas cooled reactor heat source (the HHT project) using helium as the working fluid. The R&D program involved two experimental facilities. The first was an experimental cogeneration power plant (district heating and electricity generation) constructed and operated by the municiple utility, Energieversorgung Oberhausen (EVO), at Oberhausen, Germany. It consisted of a fossil fired heater, helium turbines, compressors and related equipment. The second facility was the High Temperature Helium Test Plant (HHV) for developing helium turbomachinery and components at the Research Center Jülich (KFA). The heat source for the HHV derived from an electric motor-driven helium compressor.

In both facilities negative and positive experiences were gained. At initial commissioning, operation difficulties were encountered with the EVO facility, including failure to meet fully the design power output of 50 MW. The reasons for these difficulties were identified and to a large extent were corrected. The EVO facility achieved an operation period of 24,000 hrs of which 11,500 were at 750°C [5].

Start-up problems also occurred, at the HHV, but these were subsequently corrected. The HHV achieved 1100 hrs of operation, of which 325 hrs were at 850°C [6].

The results of the research and development programmes at both facilities support the feasibility of the use of high temperature helium as a Brayton cycle working fluid for direct power conversion from a helium cooled nuclear reactor. Ultimately, the HHT project was terminated in Germany and both test facilities have been shut down. Except for information on life testing the facilities accomplished their missions.

Within the CRP activities, in the USA [7], two theoretical heat balances were developed for a Brayton cycle, coupled to HTTR, based on the interface conditions. The potential goals and benefits of a demonstration involving the coupling of a small helium turbine to the HTTR can be summarized as follows:

(I) Basic proof of concept
(II) System interactions and operational characteristics for power conversion system coupled to nuclear heat source
(III) Evaluation of integrated operation and control strategies including startup and shutdown
(IV) Power conversion system integration data on system interfaces, operation, reliability,and maintainability
(V) Additional confirmation of component technology in high temperature helium environment

In China [8] the thermodynamic calculations, preliminary design of the system configuration, and the accident analysis have been carried out for the indirect GT cycle of the 200 MW Modular HTGR, also Japan has evaluated conceptual designs of the direct cycle helium gas turbine for both a 450 MWt and 1200 MWt MHTGR [9].

4.7 Advanced intermediate heat exchangers

High temperature process heat utilization systems for HTGRs would operate in a circuit to which the nuclear heat is transferred through an intermediate heat exchanger. This serves the purpose of isolating the reactor from possibly explosive gases produced in the heat utilization plant, as well as, of providing a barrier to radioactivity circulating in the primary helium.

Major considerations for IHXs include fabricability, repair capability, flow induced vibration, thermal stress, cost and lifetime. Very significant IHX development and testing in the 1.5 to 10 MW range in Japan and Germany for primary helium gas temperatures of 950°C has been conducted.

The feasibility of testing advanced IHXs with the HTTR will also be considered in the CRP.

5. Status and plans for CRP

The steps in examining each of the processes/systems/components described in section 4 are:

a. Collect existing information (6 months)
b. Define boundary conditions for tests (6-12 months)
c. Define research and development work, testing requirements and demonstration goals (12-24 months)
d. Prepare design concept (parallel to step 3)
e. Perform preliminary safety evaluation (12 months)
f. Check licensability under Japanese conditions (12 months)

CRP activities during the first year have focused on steps a and b, also with progress in c and to a lesser extent, in d.

Based on evaluations up to now on technology status, the first priority candidate systems to be connected to the HTTR are (1) steam (and/or CO_2) methane reforming system and (2) gas-turbine system. For the other candidate systems the R&D shall be continued to bring them to the stage in their technology development when they will be considered feasible to be demonstrated at the HTTR.

6. Summary

IAEA Coordinated Research Programmes are an effective way of promoting international cooperation in gas-cooled reactor development and in development of high temperature applications.

The HTTR is a unique research facility from a viewpoint of supplying high temperature heat of about 900°C at the exit of the IHX, and could serve as an international joint research facility for nuclear heat utilization systems.

The timely completion and successful operation of the HTTR and its heat utilization system will be major milestones in gas-cooled reactor development and in development of nuclear process heat applications.

First priority candidate systems for demonstration with the HTTR have been determined to be the steam (and/or CO_2) reforming of methane and gas turbine systems. R&D is continuing for the other candidate systems towards the stage when they can be considered feasible for demonstration at the HTTR.

References

[1] First Research Coordination Meeting (RCM), Tokai, Japan, 9-11 November 1994

[2] R. Harth, et. al, Experience Gained from the EVA II and KVK Operation, *Nuclear Engineering and Design*, 121 (1990) 173-182.

[3] High Temperature Application of Nuclear Energy, Proceedings of a Technical Committee Meeting held in Oarai, Japan, 19-20 October 1992 (IAEA-TECDOC-761).

[4] C. Rubia, CERN/AT/95-12 (ET), June 1995

[5] Nuclear Heat Application, Proceedings of a Technical Committee Meeting and Workshop, Cracow, 5-9 December 1983 (IAEA, Vienna).

[6] Summary Report on Technical Experiences from High Temperature Helium Turbomachinery Testing in Germany (IAEA report, in publication).

[7] A. Shenoy, private information, November 1995

[8] Xu Yuanhui, Progress Report, September 1995

[9] Technical Committee Meeting on "Design and Development of Gas Cooled Reactors with Closed Cycle Gas Turbines, Beijing, People's Republic of China, 30 October - 2 November 1995 (IAEA TECDOC in preparation).

stathttr2
il/12 January 1996

Table 1 Major technical parameters of HTTR

Thermal power	30 MW
Core outlet coolant temperature	850°C / 950°C [a]
Core inlet coolant temperature	395°C
Primary coolant pressure	4 MPa
Fuel	Low enriched UO_2
Fuel element type	Prismatic block
Pressure vessel	Steel
Number of main cooling system	1
Heat removal	Pressurized water cooler and IHX, parallel loaded
Hot helium temperature (secondary side of IHX)	905°C [a]
Intermediate loop helium flow rate	9.07 t/h
Intermediate loop pressure	4.1 MPa
Targeted temperature at inlet/outlet of heat utilization plant	880 [a] / 144°C
Plant lifetime	20 years (load factor = 60%)

[a] at high temperature test operation

Table 2 Construction Schedule of HTTR

ITEM \ FY*1	1990	1991	1992	1993	1994	1995	1996	1997	1998
MILESTONE	Construction start		C/V installation		RPV installation			Fueling ▽ Criticality	
Safety review									
Approval of design and construction method									
Site renovation									
Excavation of reactor building									
Reactor building									
Containment vessel									
Cooling system									
Reactor pressure vessel and core internals									
Fuel fabrication									

*1 Fiscal year of Japan starts in April and ends in March

Table 3 Operation schedule and test plan of the HTTR

Development objective	FY'98	'99	'00	'01	'02	'03	'04～
(1) To establish HTGR basic technologies though operating the HTTR	Reactor performance tests at ascent to power		Rated power operation (30MW) at T_{out}=850～950°C*		Re-fueling	Rated power T_{out}=950°C	
(2) To upgrade HTGR basic technologies though the following test							
1)Irradiation test			at T_{out}=850°C				
2)Safety demonstration tests							
3)Nuclear heat utilization demonstration test				Construction of a heat utilization system		Demonstration test	
(3) To serve as an irradiation facility for innovative and basic researches							

(*)T_{out} : Reactor outlet coolant temperature

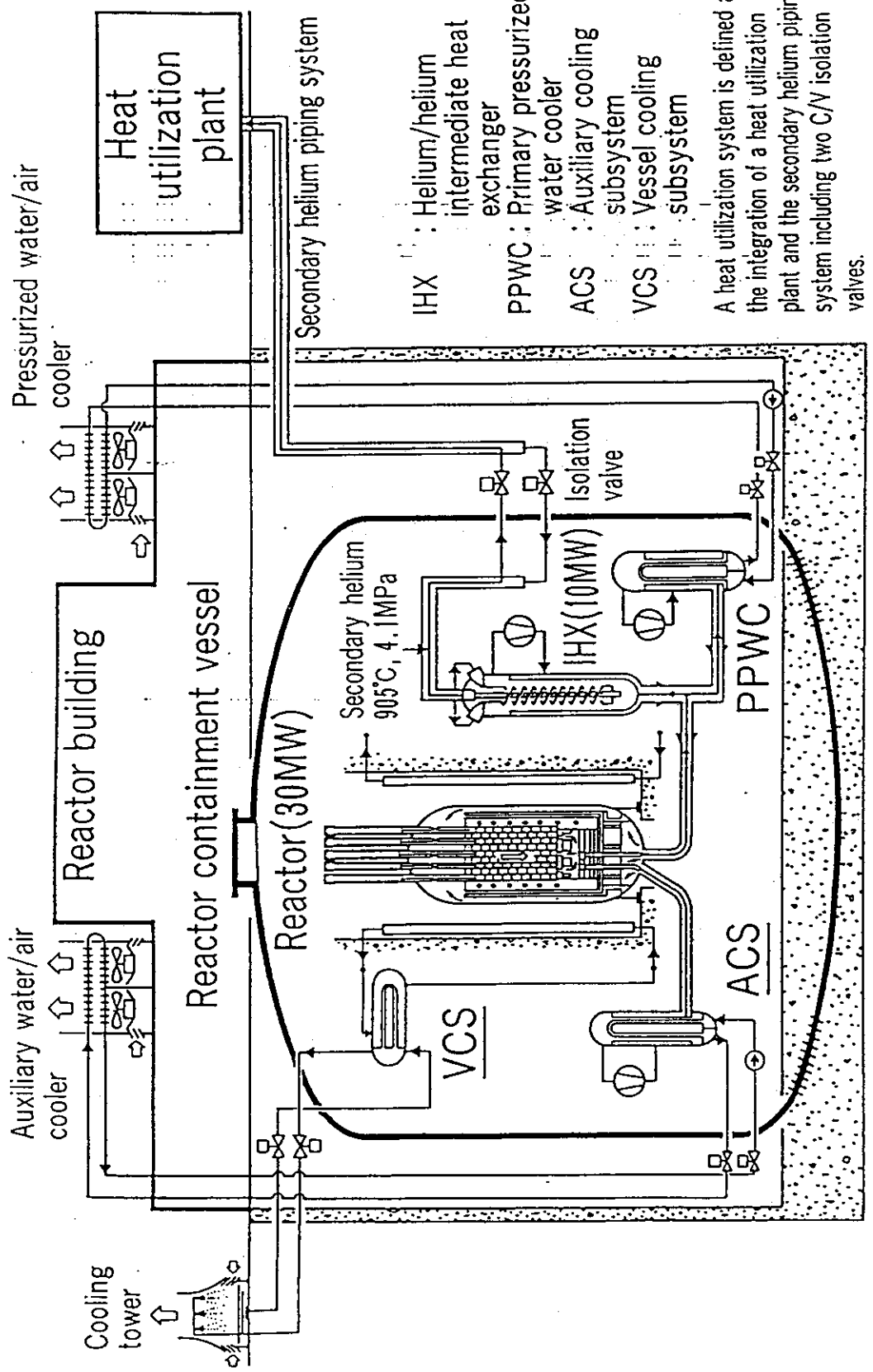


Fig. 1 Simplified diagram of the HTTR plant with a heat utilization system

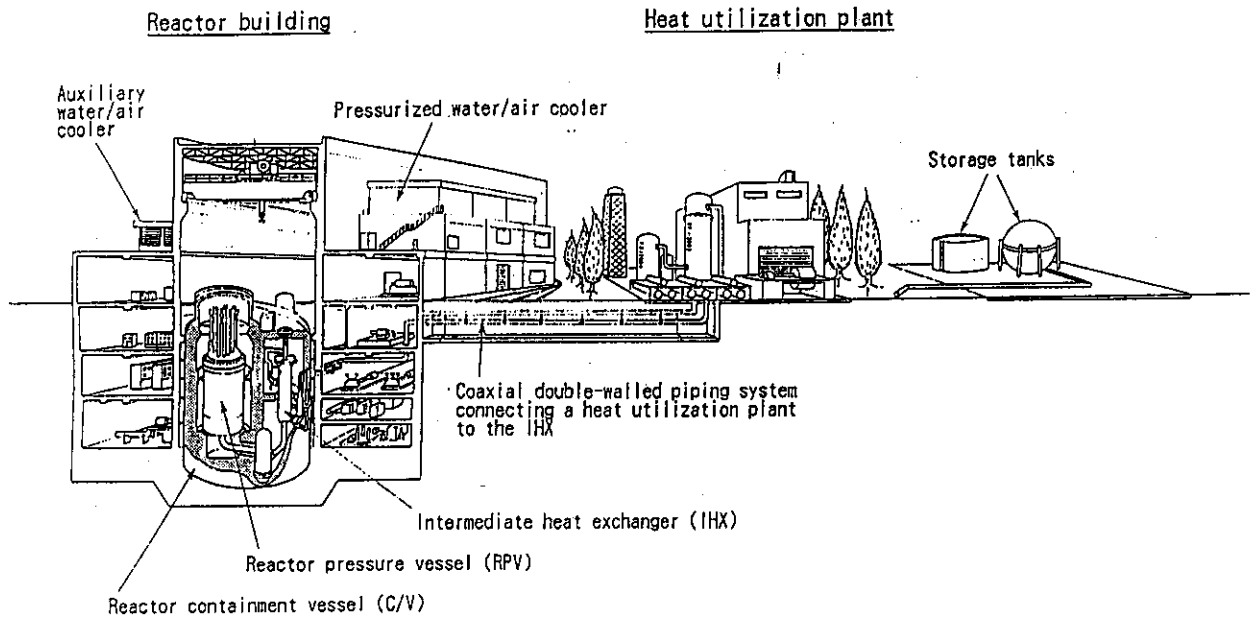


Fig. 2 Cutaway drawing of the HTTR plant with a heat utilization system

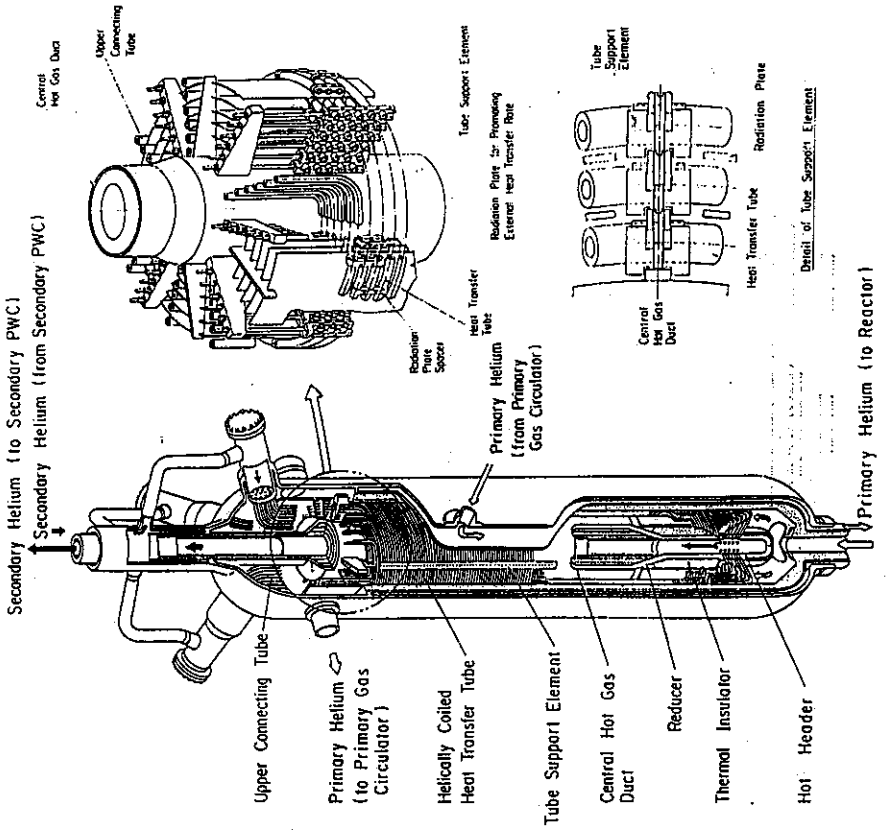


Fig. 3 View of the He/He intermediate heat exchanger of HTTR

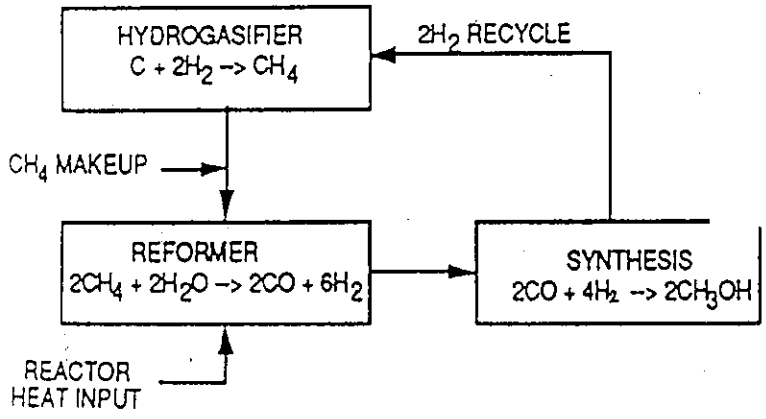


Fig. 4 **Reactions for coal to methanol by hydrogasification**

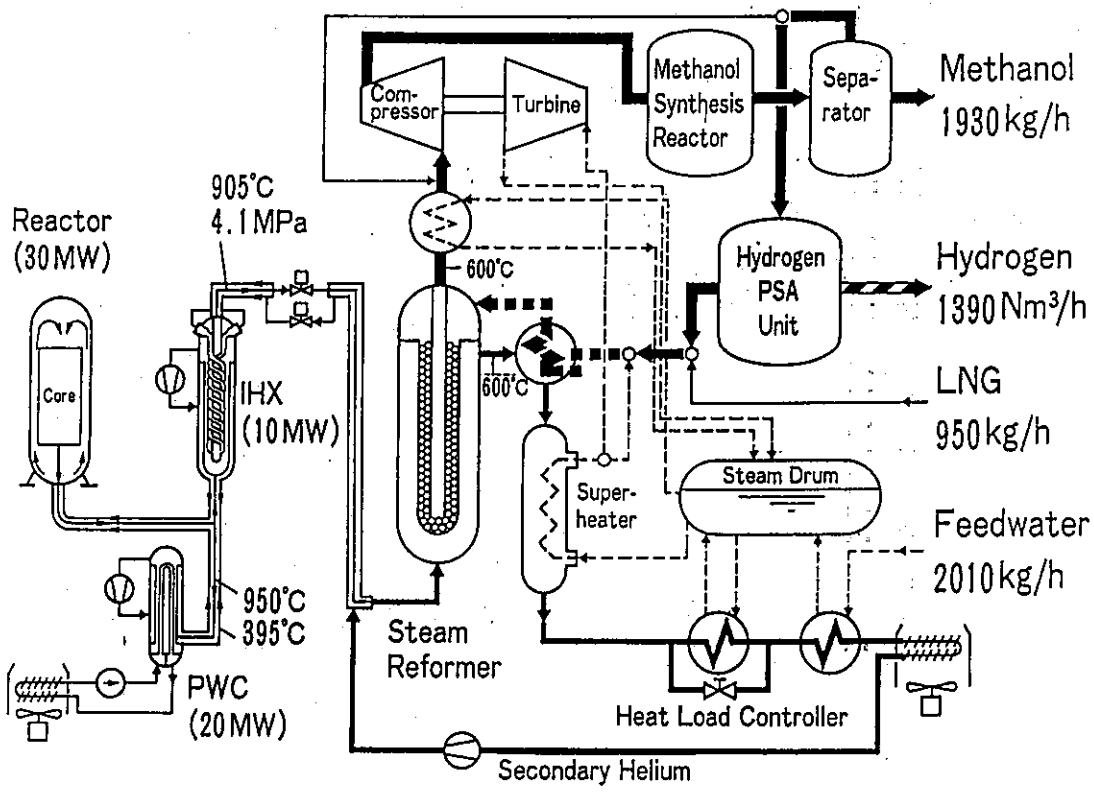


Fig. 5 **Schematic Illustration of HTTR steam reforming hydrogen/methanol co-production system**

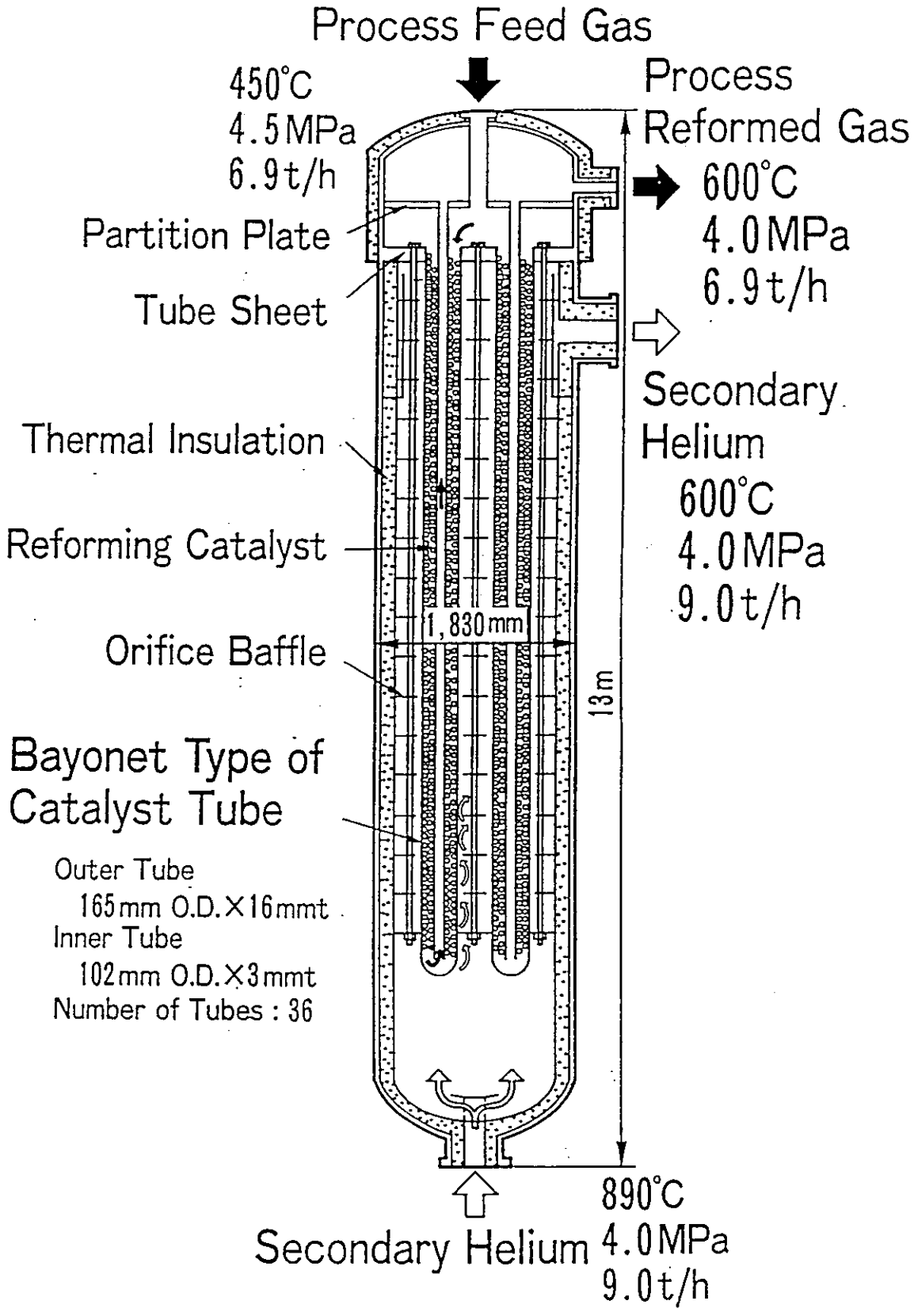


Fig. 6 Sectional view of steam reformer

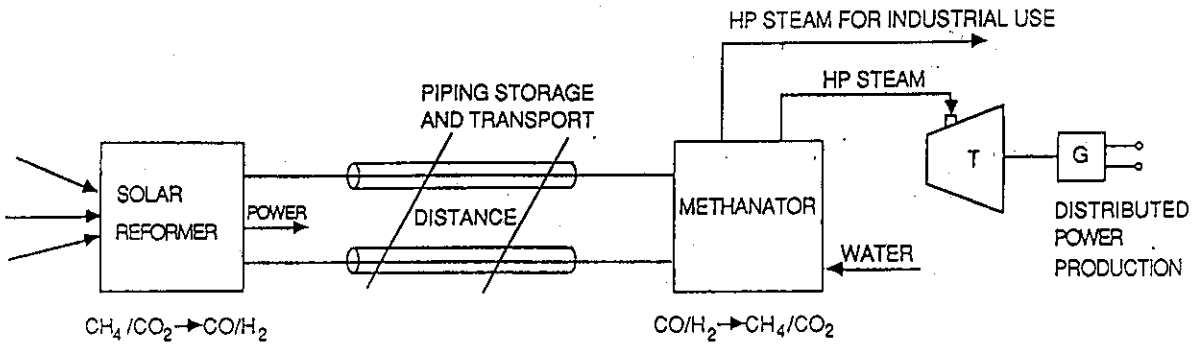
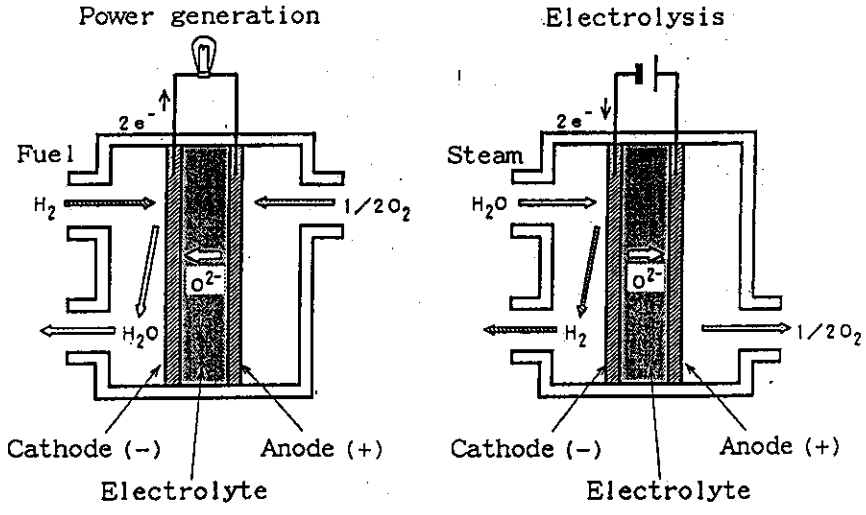


Fig. 7 Solar thermochemical concept reference system



Cathodic reaction	$H_2+O^{2-} \rightarrow H_2O+2e^-$	$H_2O+2e^- \rightarrow H_2+O^{2-}$
Anodic reaction	$1/2O_2+2e^- \rightarrow O^{2-}$	$O^{2-} \rightarrow 2e^-+1/2O_2$
Total reaction	$H_2+1/2O_2 \rightarrow H_2O$	$H_2O \rightarrow H_2+1/2O_2$

Fig. 8 Principle of high-temperature electrolysis of steam (Reverse reaction of solid oxide fuel cell)

4.2 DESIGN PROCEDURES OF SMALL PEBBLE BED HTGR FOR ELECTRIC GENERATION IN ISOLATED ISLANDS[1]

Peng Hong **LIEM**

National Atomic Energy Agency (BATAN), Center for Multipurpose Reactor,
Puspiptek Complex, Serpong, Tangerang, Indonesia

ABSTRACT

Design procedures for modularized, small-size pebble-bed high temperature gas-cooled reactors (HTGRs) have been proposed for electric generation in isolated islands. The design procedures cover the existing fueling schemes, i.e. the multipass, Once-Through-Then-Out (OTTO) and peu a peu fueling schemes. The well-established HTR-Module (200 MWth) is taken as the starting point in designing the small-size pebble bed reactors (PBRs), and its inherent safety features are maintained in the design procedures by imposing the safety related key design constraints derived from the HTR-Module. The burn-up characteristics of both uranium and thorium fuel cycles, with fissile enrichment and heavy metal loading identical with the HTR-Module fuel composition are investigated for the small pebble bed reactor design.

Under the proposed design procedure for multipass and OTTO fueling schemes, small-sized PBRs with fuel burn-up performance competitive to HTR-Module and meet the safety constraints can be satisfactorily designed. However, although the proposed design for peu a peu fueling scheme can produce a safe small-size PBR design, the burn-up performance in general is less superior to the HTR-Module design which has a larger reactor/core dimension.

The analysis results show that small-size PBRs with multipass and OTTO fueling schemes have better performances than those with peu a peu fueling scheme in term of fuel burn-up and fuel utilization although they require complex refueling mechanism and devices. On the other hand, besides its simplicity small-size PBRs with peu a peu fueling scheme show relatively higher power peaking at its beginning of life so that the reactor power which can be designed is limited to low power range. This characteristic indicates that peu a peu fueling scheme is a suitable option for small-size PBRs located in the remote or isolated islands where minimum maintenance and surveillance are required. The analysis results also prove that the thorium fuel cycle for all fueling schemes considered has superior burn-up performance than the uranium fuel cycle.

---

[1] The 3-rd JAERI Symposium on HTGR Technologies, 1996, Japan

1. INTRODUCTION

Presently, the High Temperature Reactor (HTR) team of the Agency is conducting assessment and prefeasibility study on the utilization of high temperature gas reactors (HTGRs) for future industrialization programs, particularly in the fields of: (1) process heat applications, (2) process steam and electricity co-generation, and (3) electric generation for isolated or remote islands (Subki *et al.*, 1992).

The modularized, small-size HTGR is yet considered since it could reduce the construction time and cost of manufacturing. Another reason for going to modularized, small-size HTGRs is that while the country has many major islands that need electric power for their economic development, integrating the electric grid might prove to be impractical. On top of that, islands far from the energy resources are burdened with high cost of fuel transportation and management. Several design basic requirements have been proposed such as 10 year continuous operation, small power, maintenance free and remote operation. The power scale is anticipated to be up to 50 MWe (or about 200 MWth) for each module and the reactors are planned for the eastern regions of the country which consist of many small islands.

In the early phase of the assessment and prefeasibility study, intensive studies were conducted to investigate the behaviors of several important design parameters as the power and core go to small scale or dimension, respectively. The well-known and yet established design of HTR-Module (200 MWth) (Reutler and Lohnert, 1983) was used as the starting point to design small-size pebble-bed reactors (PBRs).

Proper design procedures followed by systematic neutronic, fuel burn-up, and in-core thermal-hydraulic analyses are required in this phase of the study (1) to ensure that these small-size PBRs still possess an acceptable neutron economic condition, good fuel burn-up performance and fuel utilization, and (2) to maintain the inherent safety features inherited from the HTR-Module design. Along with these efforts, computer code development was also conducted to support these quantitative analyses (Liem, 1994a and Liem, 1995).

This paper gives the summary report on the results[2] of the study mentioned above. Two conventional fueling strategies for PBRs, that is, the multipass and the Once-Through-Then-Out (OTTO) fueling schemes were investigated, although the HTR-Module design adopts the multipass scheme. In addition to the two fueling schemes, the recently proposed peu a peu fueling scheme (Teuchert *et al.*, 1991) was also included in the study since it simplifies significantly the fueling

[2] The report has been published in *Ann. Nucl. Energy* **23**, 207, 1996

mechanism and devices of the reactors. Furthermore, despite the HTR-Module design uses only uranium fuel cycles, for sake of completion of the work, both uranium and thorium fuel cycles were considered for each fueling scheme in the present work.

The objective of the present work is to provide comprehensive neutronic, fuel burn-up and thermal-hydraulic information required for further prefeasibility study on the safety and economic aspects of the design.

2. SMALL-SIZE PEBBLE-BED HTGR DESIGN PROCEDURES

In the present work, the pebble type modular HTGR, first proposed by Reutler and Lohnert (1983) and developed into the so-called HTR-Module concept (Reutler and Lohnert, 1984), is taken as the starting point to design small-size PBRs. This concept was launched to meet the growing demands for inherently safe reactors in the past decade. The main reactor data are reproduced in Table 1. As it can be observed, a low thermal power (200 MWth) as well as average power density (3 W/cc) and a slender core geometry (3 m in diameter and about 9 m in height) are the key design parameters related to the inherent safety. A small core radius guarantees that the decay heat generated during the primary system depressurization accident (which is considered as one of the severest accident for the design) can be well transported to the graphite reflector and then to the surrounding. Hence, the maximum fuel temperature attained during the accident is below the fuel failure temperature (1600 °C) (Verfondern *et al.*, 1989).

In designing the small-size PBRs, these safety related, key design parameters will be maintained in order to ensure that the inherent safety features of the HTR-Module are still valid. First, the core dimension will be reduced by decreasing the core height but keeping the core radius to be identical with the HTR-Module. Second, the average core power density of 3 W/cc will also be used as the design constraint for the small-size PBRs. These two parameters ensure that during the depressurization accident the intensity of the decay heat is limited and the heat can be conducted effectively to the surroundings as in the case of HTR-Module. The maximum power which can be generated per ball is limited to 4.5 kW/ball (Teuchert *et al.*, 1992) (which is equivalent to 24.3 W/cc core power density). Thirdly, the heavy metal loading and enrichment are also kept to their original values in order to provide enough negative reactivity feedback during water ingress accident. Using the same composition also enables direct comparison on the burn-up performance between the HTR-Module design and the small-size PBR design. Thermal data also follow the HTR-Module design. The design parameters used in the small-size PBRs are summarized in Table 1.

2.1. Design Procedures for OTTO and Multipass Fueling Schemes

Two steps for down-sizing the reactor with OTTO and multipass fueling schemes are proposed (Liem, 1994a):

Step 1

Reducing the reactor power and core dimension (simultaneously) with constant core average power density until unacceptable neutron economic condition is reached.

Step 2

Reducing the reactor power to desired level while maintaining the minimum core dimension obtained in Step 1.

Step 1 guarantees that the average power density is maintained to be identical with the original HTR-Module so that its inherent safety features are still valid. Since the core radius will be fixed then as the reactor power goes from 200 MWth to small scale, the core height becomes proportionally smaller. A direct consequence of a smaller core is that neutron leakage will be enhanced so that a worse neutron economic condition is unavoidable. However, smaller core height increases the neutronic coupling between the upper part of the core which contains more fissile fuel and the lower part of the core with higher fertile fuel. To some extent the power peaking factor will be relaxed and fissile production at the lower part of the core increases. All of these effects, in turn, significantly influence the burn-up characteristic of the reactor. On the other hand, conducting design procedure Step 2 results in a lower average power density, hence, increasing the safety margin of the design.

2.2. Design Procedure for Peu a Peu Fueling Scheme

The following steps for down-sizing the reactor with peu a peu fueling scheme are proposed:

Step 1

Determine the critical core dimension at beginning of life (BOL) with a specified fuel composition for initial loading. Using the obtained core dimension, specify the maximum allowable power density to obtain the maximum reactor power which can be designed.

Step 2

Reduce the power to desire level, and determine the core dimension at end of life (EOL) by specifying the core life time.

In Step 1, the core dimension at BOL is determined mainly by the fuel enrichment of the initial loading (and is independent of power). Introducing the constraint of average power density yields the highest reactor power which can be

designed. This suggests that high fissile enrichment for initial loading is not preferable since the average power density will increase significantly, and at the same time, the highest reactor power which can be designed will be limited.

On the other hand, in Step 2, for a specified fuel composition for refueling, the difference of the core dimension at EOL and BOL (or equivalent to the additional core height because of refueling operation) is determined mostly by the product of reactor power and core life time (which commonly expressed in GWD unit). Smaller reactor power produces longer core life time. If in Step 1, too high fissile enrichment is unfavorable, then in Step 2, in the contrary, fissile enrichment can be freely used to control the core dimension at EOL. This is because of the core average power density is no longer a constraint. As the core dimension increases from BOL to EOL with constant reactor power, the average power density must decrease.

As in the former two schemes, the HTR−Module will be taken as the starting point in designing the small−size PBRs with peu a peu fueling scheme. Since, we aim at reactors with relatively lower power then the same low fissile enrichment of the HTR−Module still can be used for both initial loading and refueling.

From the thermal aspects, the primary cooling system of reactor with peu a peu fueling scheme has to accommodate a wide range of core pressure drop as the core dimension (height) changes from BOL to EOL. Furthermore, comparing to the other two schemes, the power peaking factor for this scheme is much higher, particularly at BOL.

3. CALCULATIONAL METHOD

A computer code, Batan−MPASS (Liem, 1994b) is used extensively to analyze both neutronic, pebble fuel flow and burn−up, as well as in−core thermal−hydraulic aspects of the small−size PBR design. The code is a general fuel management code for calculating the core equilibrium condition of pebble−bed high temperature reactors with multipass and OTTO schemes. For the peu a peu scheme, a similar code, Batan−PEU, was developed (Liem, 1995). This code is almost identical with Batan−MPASS except for the fuel burn−up calculation. The fueling operation which increases the core height is simulated in the code by moving the boundary between core and upper core void regions.

Since numerous cases have to be solved, four group neutron diffusion theory with direct coupled scattering law in 1−D geometry (axial direction) is used for approximating the neutron transport in the reactor. The radial leakage is considered in the calculations with radial buckling correction.

4. RESULTS AND DISCUSSIONS

4.1. OTTO and Multipass Fueling Schemes

First, the proposed design procedure for OTTO and multipass schemes is now applied to design small-size PBRs. The result is shown in Fig.1 for multipass fueling scheme, uranium fuel cycle. Design procedure Step 1 is conducted along the isoline of power density (about 3 W/cc), starting from point A, which represents the HTR-Module design (thermal power of 200 MWth and normalized core dimension of 1). In the calculation, the fresh fuel composition follows the one of the HTR-Module, that is, 8 % fissile enrichment and 7 gram heavy metal per pebble fuel element (cf. Table 1). The moderation ratio (carbon to heavy metal atomic density ratio) is found to be 537 for this composition (for thorium fuel cycle the ratio is found to be 525). The figures in the parentheses denotes two important parameters of fuel burn-up characteristics, i.e. the fissile loading requirement (in kg/GWD) and discharged fuel burn-up (GWD/THM). A break point (point B) in the isoline of power density indicates where the minimum core dimension is attained.

Figs.2 and 3 show several important design parameters as the reactor scale and core dimension are reduced from the HTR-Module (point A) toward point B in Step 1 for multipass and OTTO schemes, respectively. Five calculations for reactor thermal power of 200, 150, 100, 50 and 40 MWth are carried out. Although they are not shown in the figure, similar calculations are also conducted for thorium fuel cycle. As the core dimension decreases, the neutron economic condition becomes worse since neutron leakage is enhanced. This behavior is observed for both multipass and OTTO fueling schemes. Below reactor power level of 100 MWth (point B), the conversion ratio, fuel burn-up and fuel residence time decrease sharply so that the rate of fissile loading has to be significantly increased. Furthermore, it is found that criticality can not be achieved for reactor power and core dimension below 40 MWth and 1/5 of HTR-Module, respectively, since the core dimension becomes very small (cf. Fig.1).

The axial distributions of the thermal neutron flux and power density are depicted in Figs.4 and 5 for reactor power of 100 and 50 MWth, respectively. The thermal neutron flux and power density of OTTO fueling scheme show an upward tilted distribution since the upper part of the core contains higher fissile atomic densities while the lower part of the core contains higher atomic densities of depleted fuel and fission products. In case of the multipass scheme the fuel elements are recycled 15 times before being discarded so that the old (recycled) fuel elements are mixed with the fresh ones. Then, the thermal neutron flux and power density distributions show much lower peaking factor. However, even for the OTTO scheme, the maximum power density in all cases is much lower than the permissible values (22.3 W/cc).

The conversion ratio, fuel burn-up and residence time of the OTTO scheme are slightly lower than those of the multipass. Furthermore, as the reactor power and core height decrease, the power peaking factor is reduced since the neutronic coupling between the upper and lower parts of the core is stronger. Below 50 MWth the maximum power density for both schemes are practically the same.

It can be concluded from the analysis results of Step 1 that the core dimension should not be decreased lower than half of the HTR-Module since the neutron economic condition becomes unacceptable. This is the main argument to choose point B.

Now, in Step 2 of the design procedure the reactor power is reduced. Three additional calculations for reactor power of 50, 30 and 10 MWth are conducted. In this case, the average power density is proportionally reduced as a result of decreasing the reactor power. The calculation results are shown in Figs. 6 and 7 for multipass and OTTO schemes, respectively. The neutron economic condition in terms of neutron leakage for the present case is expected to be independent of the reactor power since the core dimension is fixed. Smaller reactor power (and power density) means that the fissile materials are burnt more slowly so that the fuel residence time in the core is proportionally longer. It can be observed from the figures that for both fueling schemes, slowly burning the fissile materials gives a slightly better burn-up performance. This is indicated by higher values of fuel burn-up and conversion ratio as the power decreases. The maximum power density shows a linear behavior as the reactor power decreases.

If we follow the design procedure Step 1 and 2, it can be found that the fissile loading requirements and the discharged fuel burn-up are still considerably close to the larger-size HTR-Module design. This proved that the proposed design procedure works satisfactorily.

4.2. Peu a Peu Fueling Scheme

The result of the parametric survey for small-size PBR design with peu a peu fueling scheme is shown in Fig.8. The result corresponds to uranium fuel cycle where for both initial loading and refueling the HTR-Module fuel composition is used (8 % fissile enrichment, 7 gram heavy metals per ball).

In order to bring the reactor critical at BOL the core has to be filled for initial loading up to its height of about 12 % of the HTR-Module. At this point, as indicated by Step 1 of the design procedure, the core average power density constraint will be applied. Since the HTR-Module's power density (3 W/cc) is used as the constraint then it can be found from the figure that the maximum reactor

thermal power which can be designed is 25 MWth (the hatched area in the graph).

In the figure, the isolines (solid lines) for several values of core life (BOL to EOL) are drawn. With help of these isolines, the core dimension at EOL can be readily determined if the reactor power and core life time are specified (Step 2 of the design procedure). For a specified value of core life time, the height of the core cavity required increases almost proportionally with power. For ease of operation and higher reactor availability (capacity factor) then higher core life times are in general preferable.

The burn−up simulation results for reactor thermal power and core life time of 25 MWth and 10 years, respectively, for both uranium and thorium fuel cycles are summarized in Table 2. For both fuel cycles, large reduction (about 40 %) of neutron leakage can be obtain as the core height increases from BOL to EOL. Howeve., although the core volume increases to more than 5 times of its BOL volume, the maximum power density at EOL only reduces to 1/3 of its BOL value. The core pressure drop at EOL is roughly one order of magnitude of its BOL value.

If we compare the burn−up performance of this particular case with the original HTR−Module design, it is found out that the fissile loading requirement is 60 % higher and the average fuel burn−up at EOL is 40 % lower. This result indicates that in general the peu a peu fueling scheme are not competitive to their counterpart, the multipass and OTTO fueling schemes.

It turns out that the thorium fuel cycle is superior to uranium fuel cycle. This is attributed to the higher η value of ^{233}U in the thermal energy region compared to ^{235}U or ^{239}Pu. This, in turn, results in higher conversion ratio and fuel burn−up, lower fissile inventory and fissile loading requirements. Using more reactive ^{233}U enables one to design smaller−size PBRs as can be observed from the table. The thorium cycle only requires 60 % core volume of the uranium cycle, which is a considerable large gain in down−sizing effort. With smaller core dimension, the thorium cycle shows higher power density and produces higher fuel temperature. Although not shown here, the superiority of thorium cycle is also observed in the multipass and OTTO schemes.

The axial distributions of power density and thermal neutron flux at BOL, 5 years operation, and EOL are shown in Fig.9. At EOL, the profile of the thermal neutron flux is significantly tilted toward the bottom graphite reflector and this produces similar power density profile. This is a consequence of large upward neutron streaming attributed to the existence of large upper core cavity. Since the helium flow in the core in downward then it is not advantageous to have high power peaking at the bottom of the core where the helium coolant has already been hot. However, even for this severe condition, the maximum power density of about 5

W/cc is still much lower than the permissible value (24.3 W/cc), which indicates that infact the average power density constraint of 3 W/cc is too conservative. Then, it is very possible to increase the maximum reactor power which can be designed to more than 25 MWth.

At its mid-life and EOL, these profiles to some extent resemble the OTTO scheme previously discussed due to its similar distribution of fissile-fertile material in the core. The upper part of the core contains higher density of fissile material while the lower part of the core contains higher fertile material added with fission products. This in turn will shift the power peaking from the bottom of the core to the upper parts of the core. It can be concluded that for peu a peu scheme if the in-core thermal design requirements at BOL are fulfilled then the rest of the core life will be less conservative.

4.3. Comparison between Fueling Schemes

The comparison of burn-up performances of the peu a peu, OTTO and multipass fueling schemes is shown in Table 3. For both uranium and thorium fuel cycles, the peu a peu scheme burn-up performances are in general worse than the other two schemes. This is due to the relatively larger neutron leakage for peu a peu scheme especially at BOL when the core dimension is small. The multipass scheme seems to be the best available method to burn fuel in PBRs. The low neutron leakage combined with the effect of recycling the old fuel elements, so that pebbles containing higher fissile material (low burn-up) are mixed with ones containing fertile material (high burn-up), yields a better burn-up performance and fuel utilization. However, much simpler fueling devices needed in the peu a peu compared to the other schemes make the peu a peu scheme still an attractive and feasible option particularly for very small, low thermal power PBRs where the OTTO or multipass schemes can not attain their equilibrium core conditions.

5. CONCLUDING REMARKS

Design procedures for modularized, small-size PBRs have been proposed for the existing fueling schemes, i.e. the multipass, OTTO and peu a peu fueling schemes. The well-established HTR-Module (200 MWth) is taken as the starting point in designing the small-size PBRs, and its inherent safety features are maintained in the design procedures by imposing safety related, key design constraints derived from the HTR-Module. The burn-up characteristics of both uranium and thorium fuel cycles, with fissile enrichment and heavy metal loading identical with the HTR-Module fuel composition, are investigated for the small pebble-bed reactor design.

Under the proposed design procedure for multipass and OTTO fueling

schemes, small-sized PBRs with fuel burn-up performance competitive to HTR-Module and meet the safety constraints can be satisfactorily designed. However, although the proposed design procedure for peu a peu fueling scheme can produce a safe small-size PBR design, the burn-up performance in general is inferior to the HTR-Module design which has a larger reactor/core dimension.

The analyses results show that small-size PBRs with multipass and OTTO fueling schemes have better performances than those with peu a peu scheme in term of fuel burn-up and fuel utilization although they require complex refueling mechanism and devices. On the other hand, besides its simplest refueling mechanism and devices, small-size PBRs with peu a peu fueling scheme show relatively higher power peaking at its BOL so that the reactor power which can be designed is limited to low power range. This characteristic indicates that the peu a peu fueling scheme is a suitable option for small-size PBRs located in the remote/isolated islands where minimum maintenance and surveillance are required. The analysis results also prove that the thorium fuel cycle for all fueling schemes considered has superior burn-up performance than the uranium fuel cycle.

REFERENCES

Gerwin H. and Scherer W. (1979) Jul-1599.
Liem P.H. and Sekimoto H. (1993a) *Nucl. Engng Des.* **139**, 221.
Liem P.H. and Sekimoto H. (1993b) *J. Nucl. Sci. Technol.* **30**, 648.
Liem P.H. (1994a) *Ann. Nucl. Energy* **21**, 281.
Liem P.H. (1994b) *Atom Indonesia* **20**, 1.
Liem P.H. (1995) *Batan-PEU: Fuel Management Code for Pebble Bed HTGR with Peu A Peu Fueling Scheme*, Batan Seminar on HTR Technology and Application II, Jakarta.
Reutler H. and Lohnert G.H. (1983) *Nucl. Technol.* **62**, 22.
Reutler H. and Lohnert G.H. (1984) *Nucl. Technol.* **78**, 129.
Subki I.R. *et al.* (1992) JAERI-M 92-215.
Teuchert E. *et al.* (1980) Jul-1649.
Teuchert E. *et al.* (1991) *Simplification of the Pebble Bed High Temperature Reactor*, International Specialists' Meeting on Potential of Small Nuclear Reactors for Future Clean and Safe Energy Sources, Tokyo Institute of Technology, Tokyo.
Teuchert E. *et al.* (1992) Jul-2618.
Verfondern K. *et al.* (1989) *Nucl. Technol.* **91**, 235.

Table 1. HTR-Module and small-size PBRs data

Design parameters	HTR-Module	Small-size PBRs
Power (MWth)	200	< 200
Ave. pow. dens. (W/cc)	3	3
Core diameter (m)	3	3
Core height (m)	9.6	< 9.6
HM loading/ball (g)	7	7
Fissile enrich. (%)	8	8
Coated fuel particle	TRISO	TRISO
Fuel cycle	U	U or Th
Fuel loading scheme	Multipass	Multipass OTTO Peu a Peu
Multiplication factor	1.005	1.005
He temperature (^{o}C)	250/700	250/700
He pressure (MPa)	6	6
He gas flow (kg/s)	76	76
Burn-up (GWD/THM)	80	-
Fuel resid. time (day)	1020	-
Conversion ratio	0.47	-

Table 2. Burn-up simulation results for peu a peu feuling scheme

Fuel Cycle	Uranium (BOL/EOL)	Thorium (BOL/EOL)
Reactor Power (MWth)	25	25
Core height (m)	1.20/6.86	0.80/4.01
Core volume (m^3)	8.50/48.5	5.67/28.3
Fiss. inventory (kg/GW)	1027/5859	685/3423
Neutron leakage (%)	28.1/16.5	39.1/22.3
Max. pow. dens. (W/cc)	4.78/1.50	7.33/2.11
Max. fuel temp. (^{o}C)	871/750	934/751
Core press. drop (%)	0.003/0.020	0.002/0.014
Core life (a)	10	10
Ave. fueling rate (ball/month)	1774	703
^{235}U or ^{233}U loading/ disloading (kg/GWD)	1.606 0.688	0.938 0.469
Pu-fiss or ^{235}U disloading (kg/GWD)	0.140	0.015
Conversion ratio	0.471	0.488
Ave. burn-up (GWD/THM)	49.8	71.1
Max. burn-up (GWD/THM)	69.2	98.2

Table 3. Effect of fueling scheme on burn-up characteristics (reactor power 25 MWth; first and second rows represent U and Th fuel cycles, respectively)

Fueling scheme	Peu a Peu	OTTO	Multipass
Core volume (m^3)	46	34	34
	30	34	34
Core height (m)	6.86	4.50	4.50
	4.01	4.50	4.50
Leakage (%)	28.1/16.5	16.0	13.8
	39.1/22.3	22.6	17.7
Core life time (a)/	10.0	9.41	11.0
residence time (a)	10.0	14.0	16.5
Ball velocity (cm/day)/	1774	0.140	1.802
fueling rate (ball/month)	703	0.094	1.200
Conversion ratio	0.471	0.468	0.486
	0.488	0.490	0.549
Fissile loading	1.606	1.197	1.026
(kg/GWD)	0.938	0.805	0.684
Ave. burn-up	49.8	67.2	78.5
(GWD/THM)	71.1	99.4	117.0
Max. pow. dens.	4.78	1.53	0.99
(W/cc)	7.33	2.11	1.02

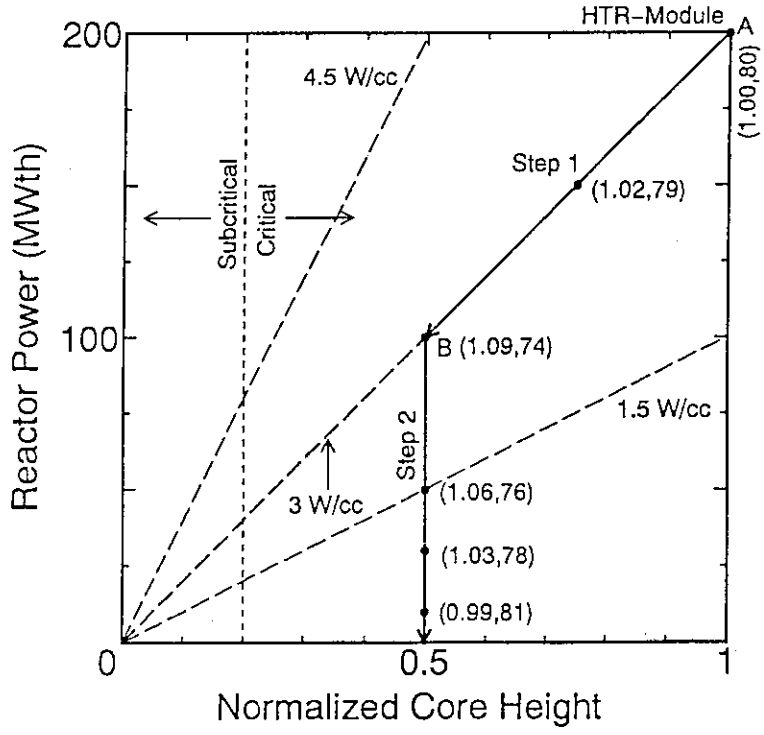


Fig.1. Results of the design procedure for multipass fueling scheme and uranium cycle (the figures in the parentheses denote the fissile loading requirement, kg/GWD and fuel burn-up, GWD/THM).

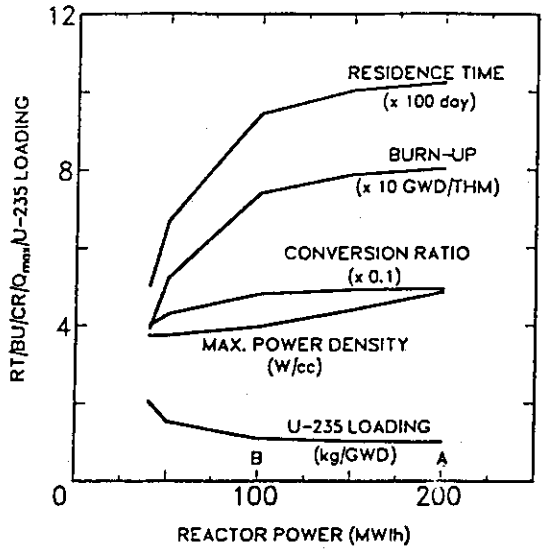


Fig.2. Calculation results for design procedure Step 1 (multipass fueling scheme, uranium cycle).

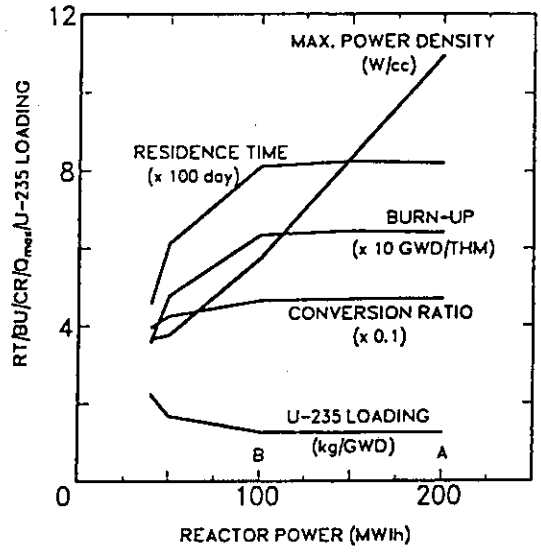


Fig.3. Calculation results for design procedure Step 1 (OTTO fueling scheme, uranium cycle).

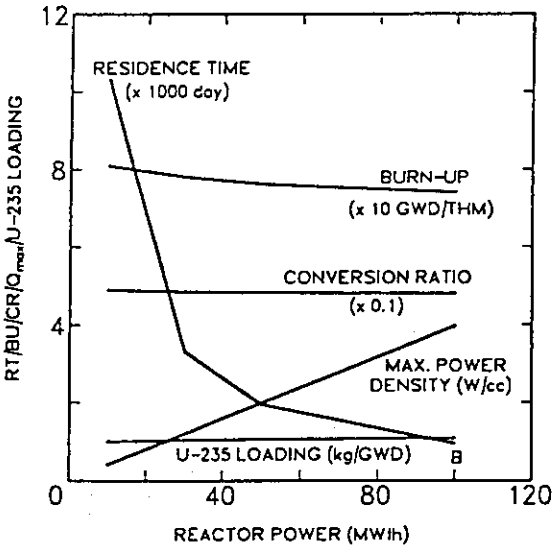


Fig.6. Calculation results for design procedure Step 2 (multipass fueling scheme, uranium cycle).

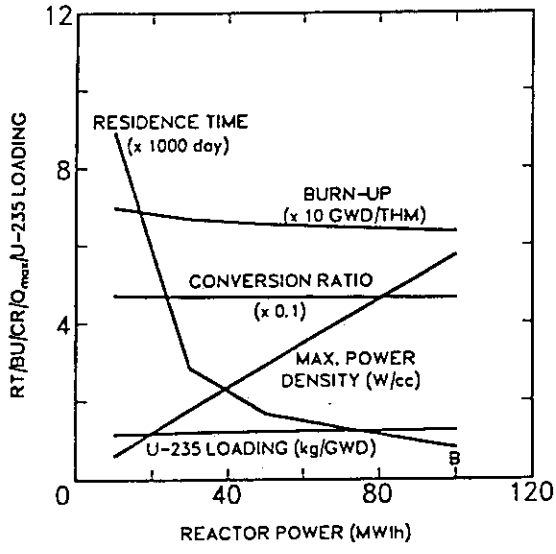


Fig.7. Calculation results for design procedure Step 2 (OTTO fueling scheme, uranium cycle).

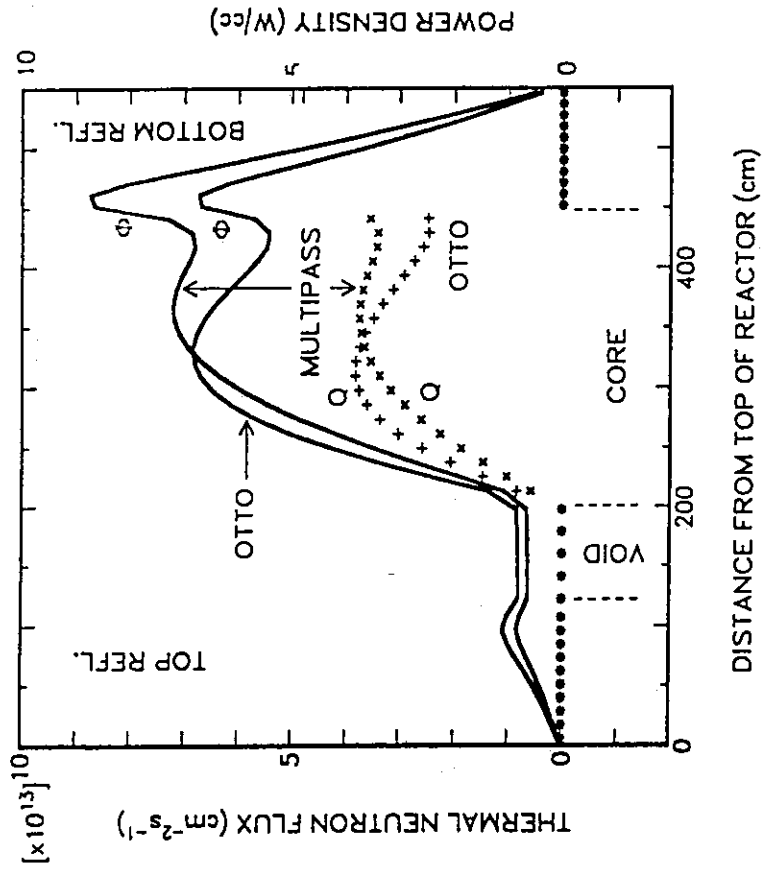


Fig.5. The axial distributions of thermal neutron flux and power density for reactor power of 50 MWth (uranium cycle).

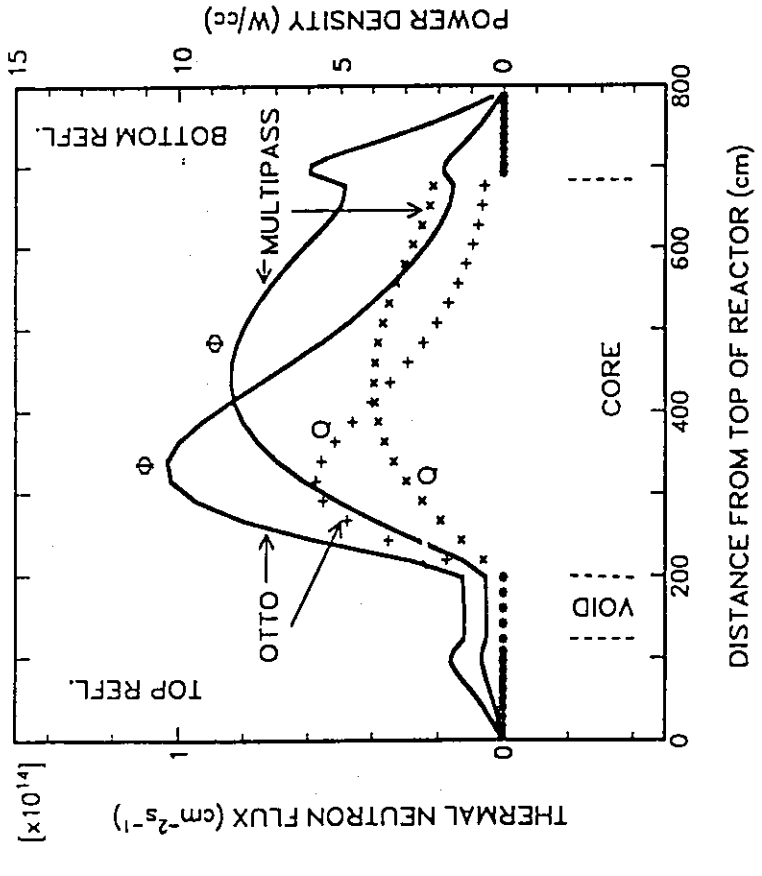


Fig.4. The axial distributions of thermal neutron flux and power density for reactor power of 100 MWth (uranium cycle).

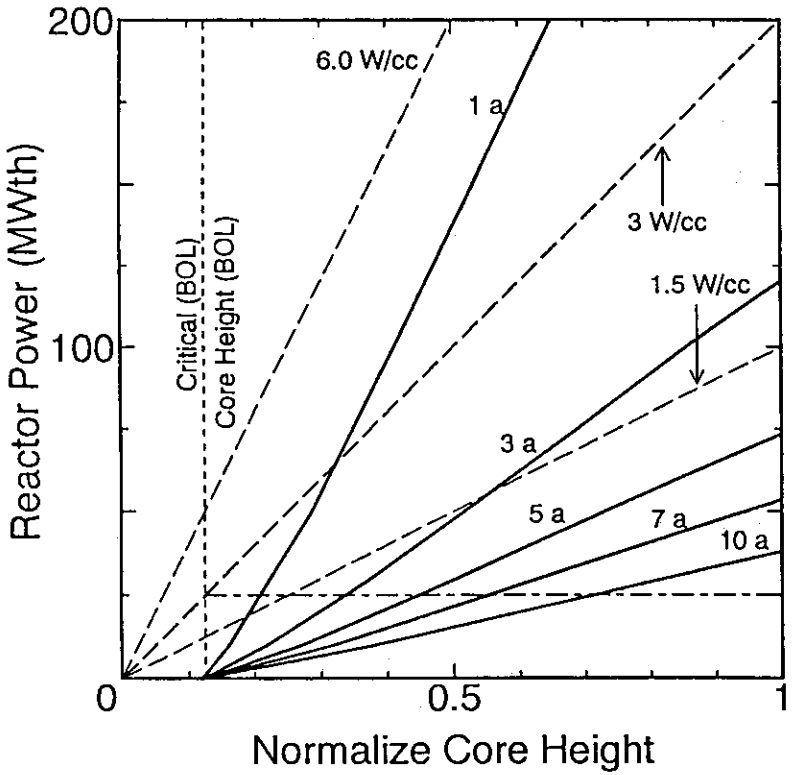


Fig.8. Results of the design procedure for peu a peu fueling scheme (uranium cycle)

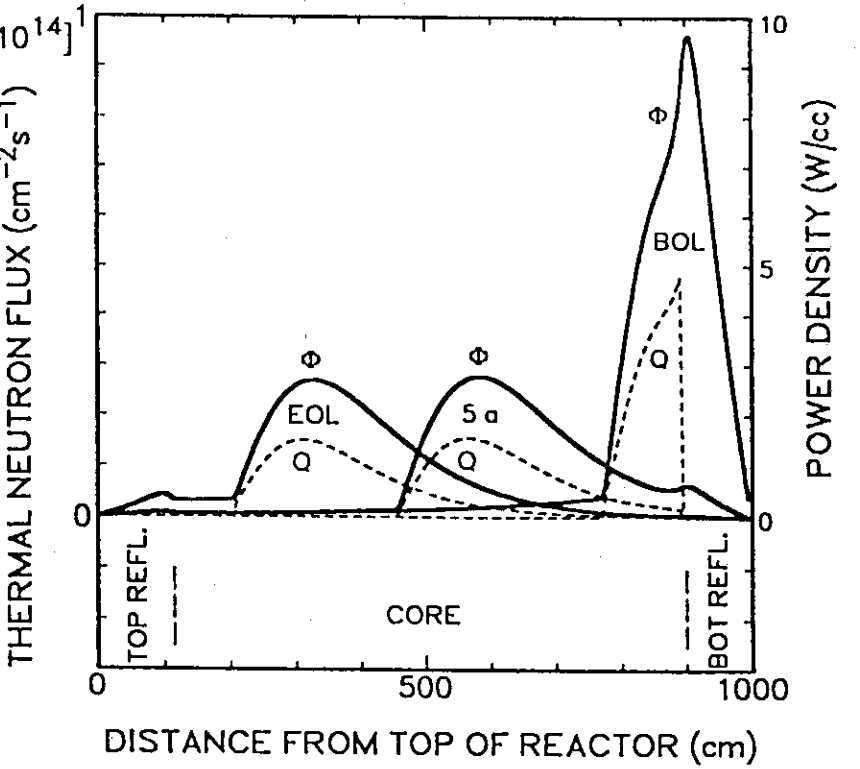


Fig.9. The axial distributions of thermal neutron flux and power density for peu a peu fueling scheme at BOL, 5 year, and EOL (uranium cycle, 25 MWth).

4.3 Recent Test Results of CO_2 Reforming of Methane in a Closed Loop

Michael Epstein
Solar Research Facilities Unit
The Weizmann Institute of Science
Rehovot, Israel

Presented at the 3rd JAERI Symposium on HTGR Technologies,
February 1996
Oarai, Ibaraki, Japan

Abstract

Ruthenium metal on an alumina support was found to be suitable catalyst for reforming of methane with CO_2 or steam and for the reverse reaction, methanation of synthesis gas. These reactions are currently under testing in a Solar Chemical Heat Pipe for the purpose of storage and transport of solar energy. The system is designed for 480 kW heat input to the reforming reaction and 350 kW heat output at the methanator plant as saturated steam at 30 bars.

The system which has been in operation for more than two years has so far accumulated about 150 cycles of startup-shutdown, because of the intermittent nature of operation with solar energy as a heat source. Recent results of the testing are reported on. The system performs well and startup time has been substantially reduced, especially if the methanator and the reformer are maintained warm at a stand-by mode.

In the reformer 1% ruthenium has been used. In the methanator 2 and 4% Ru catalyst has been used. The 4% Ru/Al_2O_3 was used as the top layer in each methanator stage to reduce the ignition temperature and the rest was 2% Ru/Al_2O_3 catalyst. In the final stage of the methanator Ni/SiO_2 catalyst was used to suppress the water gas shift. Detailed kinetic data for both catalysts is reported.

A computer code for the chemical and thermal analysis of a commercial cycle working both with CO_2 or steam reforming of methane was developed. The process diagram of these cycles and results of sample calculations are reported on.

4.4 *DESIGN OF A STEAM REFORMING SYSTEM TO BE CONNECTED TO THE HTTR*

K. Hada, T. Nishihara, T. Shibata and S. Shiozawa
Japan Atomic Energy Research Institute
Japan

ABSTRACT

Top priority objective for developing the first heat utilization system to be connected to the HTTR is to demonstrate technical feasibility of a nuclear process heat utilization system for production of hydrogen for the first time in the world. Major issues to be resolved for coupling the heat utilization system to the HTTR are 1)to develop safety philosophy for reasonably and reliably ensuring safety of the nuclear reactor, 2)to develop control design concept for the total system of the nuclear reactor and heat utilization system because thermal dynamics of endothermic chemical reactor to be heated by nuclear heat is much different from the nuclear reactor, 3)to develop helium－heated components and 4)to develop enhanced hydrogen production technoligies for achieving competitiveness to a fossil－fired plant.

A steam reforming hydrogen production system was studied as one of the first priority candidates for an HTTR－heat utilization system due to matured technology in fossil－fired plants and since technical solutions demonstrated by the coupling of the steam reforming system to the HTTR will contribute to all other hydrogen production systems.

Basic design philosophy for the HTTR－steam reforming system is that the steam reforming plant downstream of an intermediate secondary helium loop is designed at the same safety level as fossil－fired plants and therefore the secondary helium loop was selected as a safety barrier to the HTTR nuclear reactor.

JAERI has been conducting several studies to develop a framework of the HTTR－steam reforming system. Key design achievements were as follows.

1) Hydrogen production performance was improved to achieve the competitiveness to the fossil－fired by applying new concepts of steam reformer and optimizing heat and material balance conditions of the system.

2) A natural convection type of steam generator was allocated downstream the steam reformer in the secondary helium loop to achieve sufficient system controllability with accomodating the large difference in thermal dynamics as mentioned above, and to form the safety barrier by the secondary helium loop.

3) Basic safety design criteria for fire and explosion originated at the steam reforming plant were developed.

1. Introduction

Consumption of a huge amount of fossil fuels resulted from human activities since the industrial revolution, in addition to deforestation, causes an enhanced global warming. In order to relax the global warming issue and to sustain our future development, new energy resource/carrier or energy technology to meet the following requirements may be needed to develop as early as possible;

1) freedom from resource constraint, especially stable and unlimited supply of resource,
2) environmentally friendly energy use,
3) high efficiency energy use, and
4) concentrated energy use for industries.

Such an energy technology includes to reform fossil fuels to new energy carrier.

Hydrogen is one of key energy carriers to meet the above requirements. The Ministry of International Trade and Industry has started the New Sunshine Program(R&D Program on Energy and Environmental Technologies) in April 1993, with focusing on development of hydrogen production and utilization technology[1]. A High Temperature Gas−cooled Reactor(HTGR) supplies a high temperature nuclear heat enabling us to attain a high efficiency heat utilization without any emission of CO_2 gas. Therefore, hydrogen production by the use of nuclear heat generated from an HTGR as a heat source has the high possibility to meet the above requirements.

JAERI has been studying a possibility of developing nuclear−heated hydrogen production technologies and of demonstrating technical feasibility of nuclear−heated hydrogen production at an engineering testing HTGR, called HTTR(High Temperature engineering Test Reactor) since 1990. A steam−methane reforming system is under study as a hydrogen production system to be connected to the HTTR due to its advantages as described below:

1) It is highly possible to couple it to the HTTR in the early 2000's because a fossil−fired steam reforming of natural gas or naphta is an economical and mature technology for production of hydrogen.
2) Technical solutions demonstrated by coupling the steam reforming system to the HTTR will contribute to other nuclear−heated hydrogen production systems.
3) The nuclear−heated steam reforming is a practicable means for producing hydrogen by pre−combustion removal of CO_2 from hydrocarbon resources such as natural gas and coal and has great potential as a means to facilitate the transition from fossil fuels to future hydrogen energy systems[2].

At a preliminary design conducted from fiscal 1990 through 1995, JAERI has developed a framework of the HTTR−steam reforming system. Key design achievements were as follows.

1) By applying a new concept of steam reformer heated by helium gas from nuclear reactor(precisely, from IHX) and by optimizing arrangement of helium−heated components and related heat and material balance conditions of the system, hydrogen production performance was improved to achieve the competitiveness to the fossil−fired.
2) A natural convection type of steam generator was allocated downstream the steam reformer in the secondary helium loop to achieve sufficient system controllability with accomodating a large differnece in thermal dynamics between nuclear reactor and steam reformer, and to form a safety barrier at the secondary helium loop.

3) Basic safety design criteria for fire and axplosion originated at the steam reforming plant were developed.

In the next fiscal year, JAERI is planning to start a conceptual design in consignment of the Science and Technology Agency, aiming at a start of test for developing nuclear－heated hydrogen production technologies by the steam reforming process at the HTTR in fiscal 2002.

In the following, key technologies to be developed for coupling an HTGR and hydrogen production system are discussed first, and then design philosophy and concept of the HTTR－steam reforming system for providing the capability to develop these technologies are proposed. Finally, achievements of design studies so far are presented.

2. Design philosophy and basic concept of HTTR－steam reforming system

The first HTGR in Japan, namely HTTR, is under construction at the Oarai Research Establishment of JAERI. Key technologies for assuring reasonable reliability and safety of an HTGR at malfunction or accident of the HTGR itself have been developed through a design and construction of the HTTR. For coupling a process heat utilization system for production of hydrogen to an HTGR, the following key technologies remain to be developed.

1) Enhanced hydrogen production to achieve its competitiveness to an economical fossil－fired hydrogen production plant.

2) Helium－heated components, especially helium－heated endothermic chemical reactor:

A hot helium gas which provides the nuclear generated heat to an endothermic reactor is pressurized to cool the nuclear reactor core. A heat exchanger type of chemical reactor is suitable to contain the pressurized helium.

3) Control of the total system connectiong an HTGR to a process heat utilization system with an endothermic chemical reactor which has a quite different thermal dynamics from an HTGR reactor:

In an HTGR core, a nuclear generated heat is transformed to a sensible heat of helium gas, the reactor coolant, resulting in a proportional relationship of reactor power and helium temperature. On the other hand, in an endothermic chemical reactor where an endothermic reaction occurs for production of hydrogen, a heat input enough to cause the reaction dramatically increases with increasing reaction temperature due to the Arrenhius type temperature dependence of reaction rate. A new control technology needs to be developed to balance such a quite difference in thermal dynamics between the nuclear reactor and the chemical reactor.

4) Safety measures for ensuring reasonable reliability and safety of HTGR against malfunction or failure of a hydrogen production system:

A higher probability of malfunction or failure of a hydrogen production system than a power generation system is expected to result from a severe environment of chemical reactors for production of hydrogen. A safety measures needs to prevent frequent reactor scrams triggered by such a malfunction or failure for ensuring a reasonable reliability and safety of an HTGR.

5) Safety measures against a fire/explosion caused by a combustible/explosive gas in storage at a hydrogen production system because of integration arrangement of an HTGR and hydrogen production system:

Two different potential origins of fire/explosion should be taken into account. One origin is the hydrogen production system outside the nuclear reactor building and the other is the inside of the reactor building if it is possible to form a route of explosive gas ingress from chemical reactor with the explosive gas feed to the inside of the reactor

building.

6) Safety measures for transportation of fission products released from the reactor to the product hydrogen at a normal operation and for preventing uncontrolled release of fission products to environment at a accident of the steam reforming system.

Tritium has a possibility to be transported from the reactor to the product hydrogen through a hot tube walls of helium−heated heat exchangers such as a helium−to−helium intermediate heat exchanger(IHX) and an endothermic chemical reactor in service at a high temperature. Tritium concentration of the product hydrogen should be limited as low as reasonably achievable.

The top−priority objective for coupling a steam reforming hydrogen production system to the HTTR is to develop these technologies and then to demonstrate technical feasibility of a nuclear process heat utilization system for production of hydrogen for the first time in the world. Taking into consideration the importance of the objective, the authors have defined the following design philosophy for establishing a design concept of the HTTR−steam reforming system for providing the capability to develop those key technologies.

1) Techinical solutions demonstrated by coupling the steam reforming system to the HTTR should contribute to all other hydrogen production systems.

2) The steam reforming system is designed at the same safety level as a fossil−fired plant under a strict requirement of assuring the safety and reliability as a nuclear reactor sytem.

3) Simplicity and operator friendly methodologies are pursued.

Several design studies have been conducted to develop a design concept of the HTTR−steam reforming system for developing the key technologies of an HTGR−hydrogen production system under the design philosophy. Finally, the authors propose the following basic design concept which incorporates new ideas of passive safety features.

1) An innovative design concept of helium−heated steam reformer is developed to improve hydrogen production performance, with optimizing heat and material balance conditions of the whole steam reforming system.

2) A steam generator is installed in the helium loop(the secondary helium loop for the HTTR) for providing the stable controllability against any disturbance triggered in the steam reforming system.

3) A passive safety barrier as shown in Table 1, separating the HTTR reactor and the steam reforming system, is adopted to ensure the reactor safety passively against any transient or accident triggered at the steam reforming system.

4) Tritium transportation is limited as low as reasonably achievable primarily by purification systems of the reactor coolant helium and the secondary helium which flows in the intermediate cooling loop(named the secondary helium loop) separating the reactor cooling loop and the steam reforming loop. Both of IHX and a pair of isolation valves in the secondary helium loop provide a safety barrier for preventing uncontrolled release of fission products at the accident of secondary helium pipe rupture according to the HTTR safety design guideline.

The detail of the design concept for the items 1) to 3) is presented in the following chapter.

3. Design concept of HTTR−steam reforming system arrangement and key system components

The steam reforming system is arranged to connect to the IHX as schematically illustrated in Fig. 1. A cut−away view of the whole total system is shown in Fig. 2. The HTTR reactor supplies nuclear generated heat of 30MW to parallel−loaded two heat exchangers in

the reactor cooling loop, namely the IHX of 10MW at the rated heat exchanging rate and a pressurized water cooler of the remaining 20MW. The thermal energy of 10MW transfered at the IHX to the secondary helium loop is utilized for production of hydrogen. Heat and material balance conditions at the IHX are given in Table 2 for the maximum secondary helium temperature of 905 °C at the outlet of IHX. Due to a heat loss along a secondary helium piping from the IHX to a steam reformer, the secondary helium temperature is reduced to 880 °C at the inlet of the reformer for the IHX outlet temperature of 905 °C.

JAERI has been conducting several design studies to develop a design concept of the HTTR−steam reforming system under the boundary conditions as defined above.

3.1 Improvement of hydrogen production performance

In the HTTR−steam reforming system, the secondary helium at the temperature of 880 °C and at the high pressure of 4MPa flows into a heat exchanger type of steam reformer, and supplies the thermal energy enough to cause a steam reforming reaction to a reforming process gas flowing inside catalyst tubes. With a conventional type of heat exchanger and for similar process gas feed conditions to a fossil−fired plant, lower hydrogen production performance of the HTTR−steam reforming system is predicted than a fossil−fired system. A comparison of operational conditions between HTTR− and fossil−fired reforming system is shown in Table 3.

Since a hydrogen production rate is expressed as the product of a reforming process gas feed rate and a reforming rate, the following improvements are found to provide higher hydrogen production performance.

1) Increasing heat input to the reforming process gas which flows in catalyst tubes
2) Increasing a reaction temperature, that is a process gas temperature at the outlet of catalyst zone in the catalyst tube
3) Optimizing reforming gas composition so as to enhance the reforming rate

Reduction in process gas pressure is one of effective improvements, but depends on the helium pressure. Survey of improved types of heat exchangers and an analytical study on enhancement of hydrogen production rate lead to the proposal shown in Fig. 3. The proposed type of helium−heated reformer as shown in Fig. 4 and its optimized operating conditions has the possibility to attain a competitive hydrogen production performance(by comparing a thermal energy utilization, 78% is competitive to 80−85% for a fossil−fired plant).

These improvements are applicable not only to HTGR−steam reforming system but also to other HTGR−hydrogen production systems because a heat exchanger type of endothermic chemical reactor is an essential technology for production of hydrogen by utilizing the nuclear heat.

3.2 Steam generator in the secondary helium loop for stable controllability and as a safety barrier

The authors have found that installation of a steam generator(SG) at the downstream of the steam reformer in the secondary loop provides the stable controllability for any disturbance at the steam reformer due to a larde capacity of heat sink. For example, for such a thermal transient that a helium temperature at the steam reformer outlet and then at the SG inlet goes up by a disturbance in the reforming process gas feed line, a helium temperature at the SG outlet can remain constant at the saturation temperature of steam. A transient analysis result is shown in Fig. 5 for a stepwise decrease in process gas flow rate by 20%. System arrangement is shown in Fig. 6. This is phenominologically explained that an increased heat input to SG due to increasing SG inlet helium temperature is possible to result in only an increased steam quality at the saturation temperature due to boiling, but not

in an increased steam temperature.

Such an advantage of SG is utilized to prevent a reactor scram due to a malfunction or accident at the steam reforming system and therefore the secondary helium loop with SG can be functioned as a safety barrier as mentioned above. For preventing a reactor scram due to a loss of water feed to SG by a loss－of－on－site－power accident at the reforming system and by a malfunction of feed water flow rate control system for example, a natural convection type of SG with a sufficient capacity of water holdup and with a passive SG cooling system is selected as the safety barrier SG and is now under design to specify a reasonable safety requirements and reasonable configuration.

A comparison of system arrangement among candidate nuclear－heated hydrogen production processes has revealed that the technical solution to achieve stable controllability and to meet the safety requirement to the steam reforming system of designing it at the same safety level of a fossil－fired plant contributes to other hydrogen production systems.

Accordingly, the arrangement of the HTTR－steam reforming system is specified as shown in Fig. 6.

3.3 Safety barrier agaist fire/explosion

Safety barrier(functional or physical) is required to assure the safety of nuclear system and public. In the HTTR－steam reforming system has a potential possibility of two types of origins of fire/explosion, namely outside of the nuclear reactor building(R/B) and inside of the R/B. The safety design concept is schematically illustrated in Fig. 7.

Against the fire/explosion outside the R/B, it is reasonable to assure safety integrity of safety－related items as the nuclear system against a potential fire/explosion because a low possibility of fire/explosion should be assumed. However, against fire/explosion inside the R/B, it is the principle to take a safety measures to prevent occurrence of fire/explosion. In detail, the secondary helium piping system is designed to prevent the formation of route of explosive gas ingress from the steam reformer into the R/B. For the HTTR－steam reforming system, a possibility of pipe rupture of the secondary helium loop does not seem to completely exclude and therefore, the basic design concept is to limit ingress amount of explosive gas within an allowable limit to prevent any hazard to safety－related items such as the reactor containment vessel. A combination of the C/V isolation valves and emergengy shut－off valve in the process gas feed line is effective to restrict the amount of ingress gas.

4. Concluding remarks

Based on the defined design philosophy, the authors have conducted design studies to develop a design concept of the HTTR－steam reforming system. The framework of the system arrangement and the helium－heated steam reformer concept have been specified for achieving a competitive hydrogen production performance to a fossil－fired plant and for ensuring a stable controllability and safety barrier.

A heat transfer enhancement, an increased heat input to the process gas and others contribute to a competitive hydrogen production performance, in detail, the thermal energy utilization of around 80%.

A steam generator is designed to install at the downstream of the steam reformer in the secondary helium loop, providing the stable controllability and the safety barrier against malfunctions or accidents in the process gas and feed water lines.

A safety design concept is developed for explosion/fire due to explosive gas, taking

into account difference of safety requirements depending upon the origins of fire/explosion.

These technical solutions will contribute to other hydrogen production systems.

In consignment of the Science and Technology Agency, JAERI is plannning to establish the design concept of the HTTR－steam reforming system and the related R&Ds, aiming at a start of test operation of the steam reforming system in fiscal 2002.

References

[1] C.Watanabe, "MITI's new comprehensive approach to energy and environmental technologies: the New Sunshine Program", presented at the 7th Japanese－French Expert Meeting on Energy and Environmental Technologies, May 31－June 1, 1993, Tokyo, Japan.

[2] Y.Mori et al., "Pre－combuction removal of carbon dioxide from natural gas power plants and the transition to hydrogen energy systems", J. of Energy Resources Technology, vol.114(Sept. 1992), p.221－226.

Table 1 Passive safety barrier for ensuring the reactor safety against transient/accident triggered at the steam reforming system

Transient / accident		Safety barrier
Thermal-hydraulic transients triggered at the steam reforming system		Physical barrier of the secondary helium loop installing a natural convection type of steam generator for preventing a reactor scram
Fire and explosion accident	Originated outside the HTTR reactor building	Functional barrier of safe distance for preventing damage at the reactor building and components important to safety
	Within the reactor building	Physical barrier of the secondary helium loop and emergency shut-off valves (or isolation valve) for preventing occurrence of explosion or for preventing damage at componets important to safety

Table 2 Heat and material balance conditions at the IHX and key design parameters of the IHX

Rated heat exchanging rate	9.94MW
Primary helium	
Temperature at the inlet/outlet	950℃/389℃
Pressure at the inlet	4.02MPa
Mass flow rate	12.2t/h
Secondary helium (for the maximum design allowable temperature at the outlet of 905℃)	
Temperature at the inlet/outlet	158℃/905℃
Pressure at the inlet	4.14MPa
Mass flow rate	9.07t/h
Type	Counter-current and helically wound tube type of shell-and-tube heat exchanger
Design condition of heat transfer tubes	
Design temperature	955℃
Design pressure	0.29MPa
Design pressure drop through IHX (for maximum flow rate at the normal operation)	
Primary helium	9.2kPa
Secondary helium	50.2kPa

Table 3 Comparison of operational conditions and performance of steam reformers

Reformer type	Fossil-fired	Helium-heated without improvements	Improved helium-heated
Process gas pressure	1～3MPa depending upon final products	＞Helium pressure P_{He} of 4.0MPa	Balanced presure ($\cong P_{He}$) ➡ 4.5MPa at the inlet of steam reformer
Maximum process gas temperature	850～900℃	≦750℃	800℃
Maximum heat flux to catalyst zone	50～80 kW/m²	10～20 kW/m²	40 kW/m²
Thermal energy utilization of steam reformer	80～85%	(～50%)*	78%
CO_2emission from heat source for heat source power	3t-CO_2/h／10MW	0	

(＊) Based on JAERI's design data

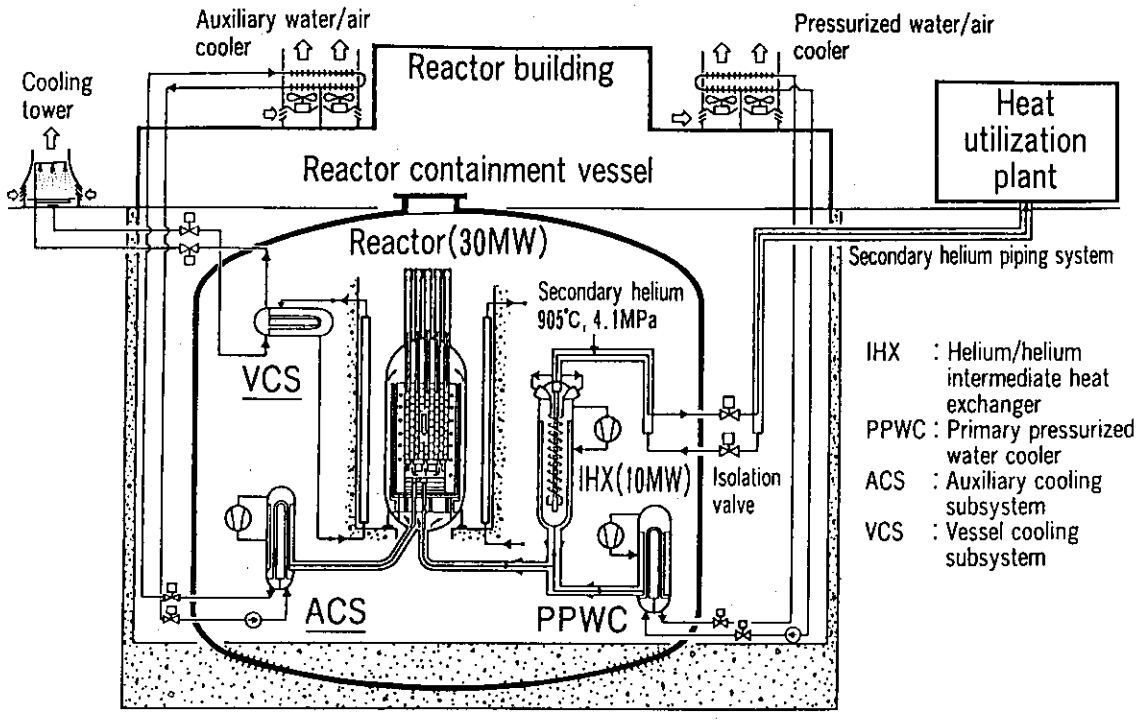


Fig.1 Simplified diagram of the HTTR plant with a heat utilization system.

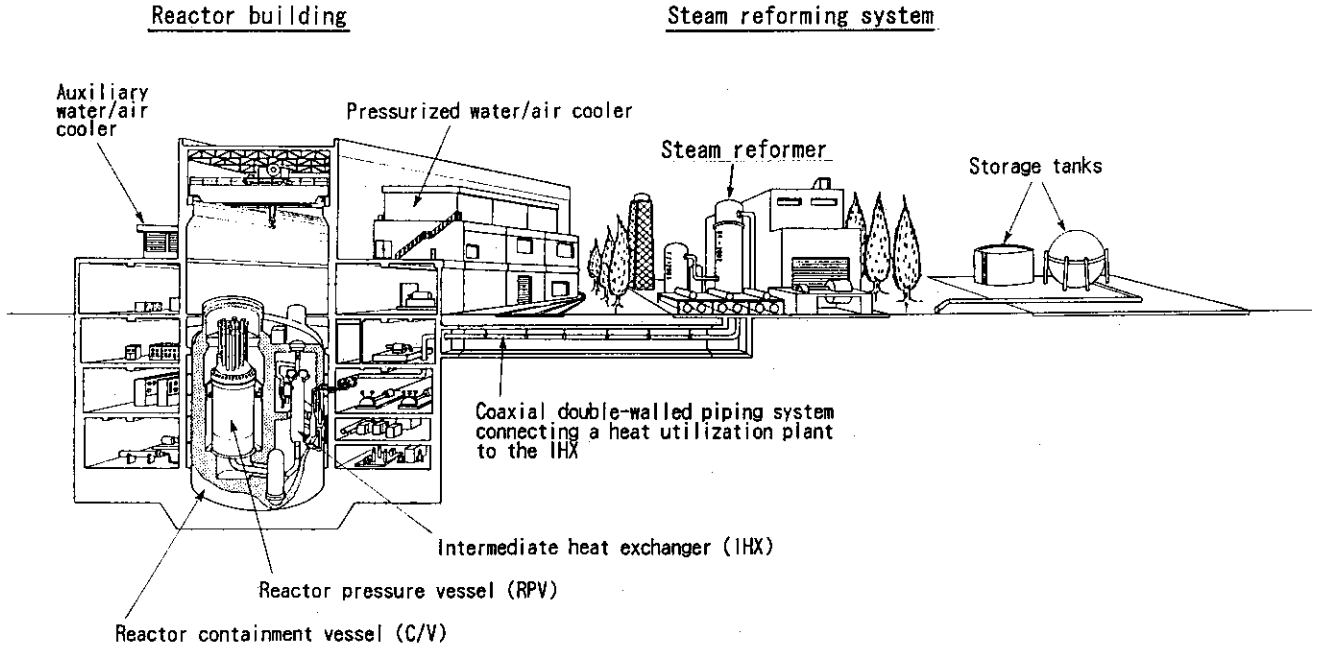


Fig.2 Cutaway drawing of the HTTR-steam reforming system.

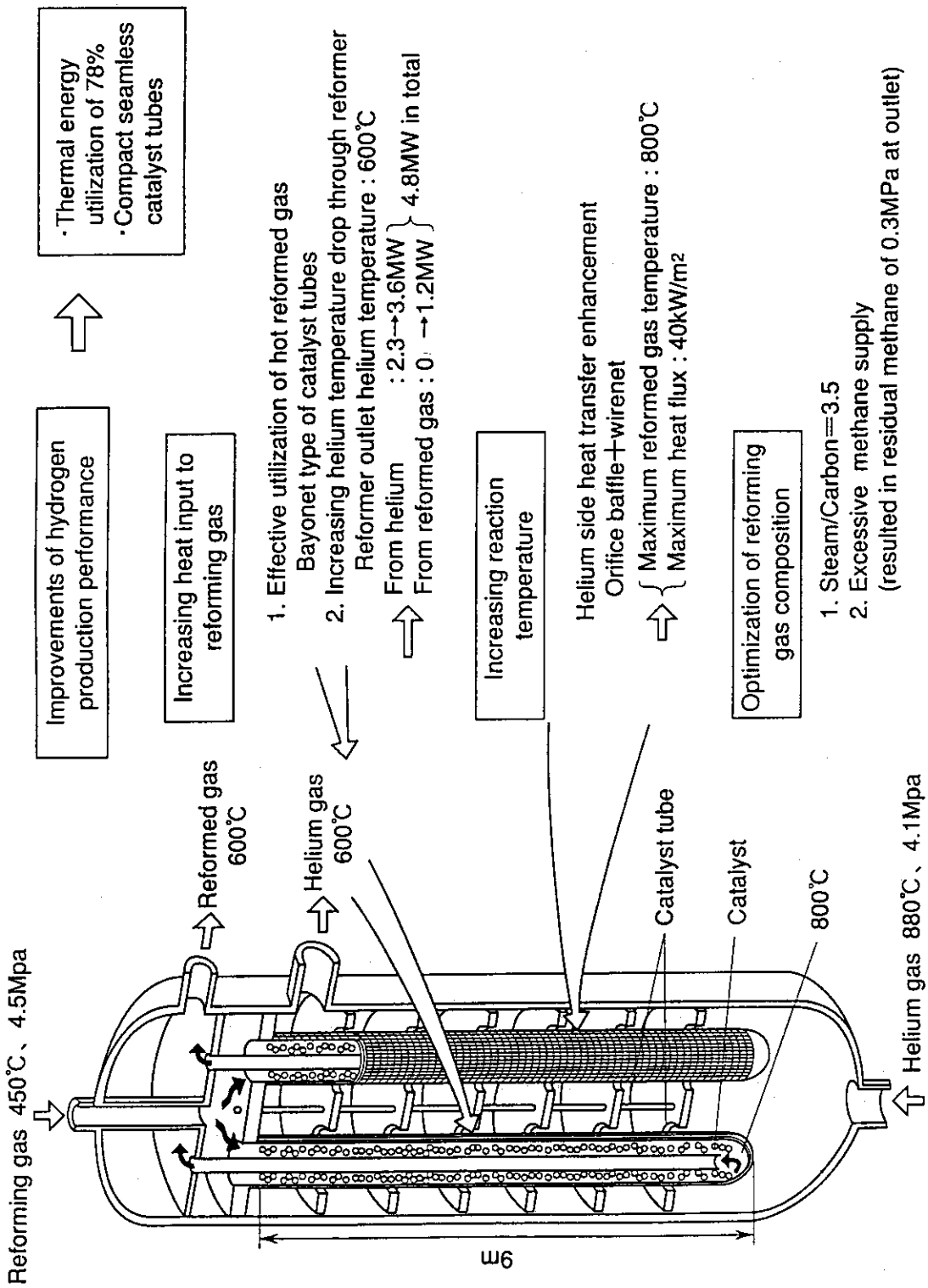


Fig.3 Improvements of helium-heated steam reformer performance.

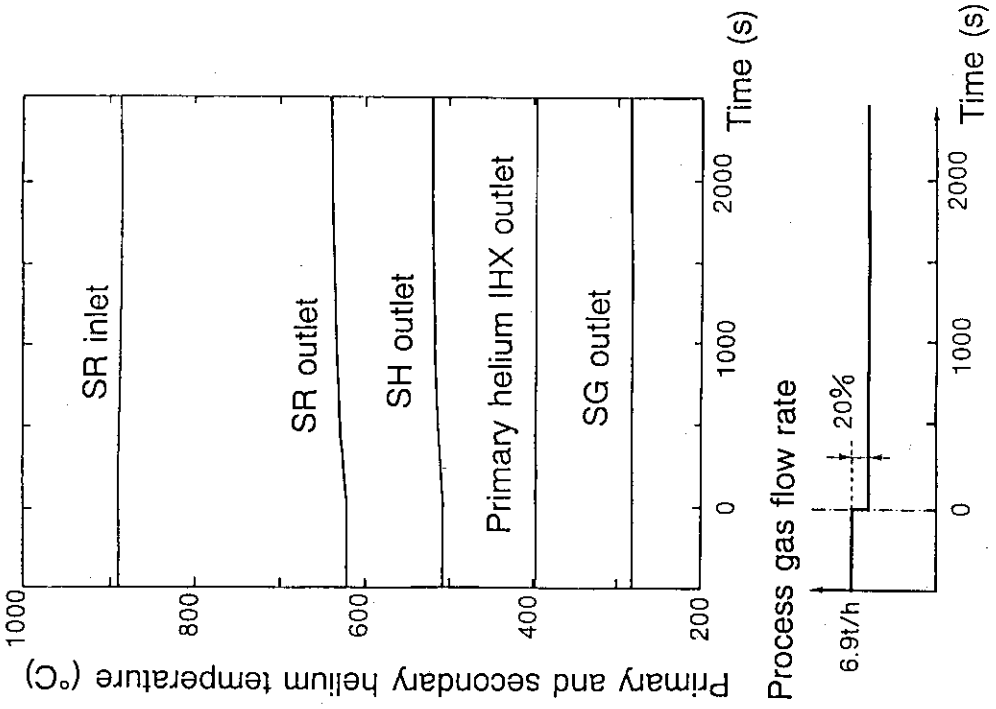


Fig.5 Helium gas temperatures at the HTTR-steam reforming hydrogen production system by transient thermal hydraulic analysis.

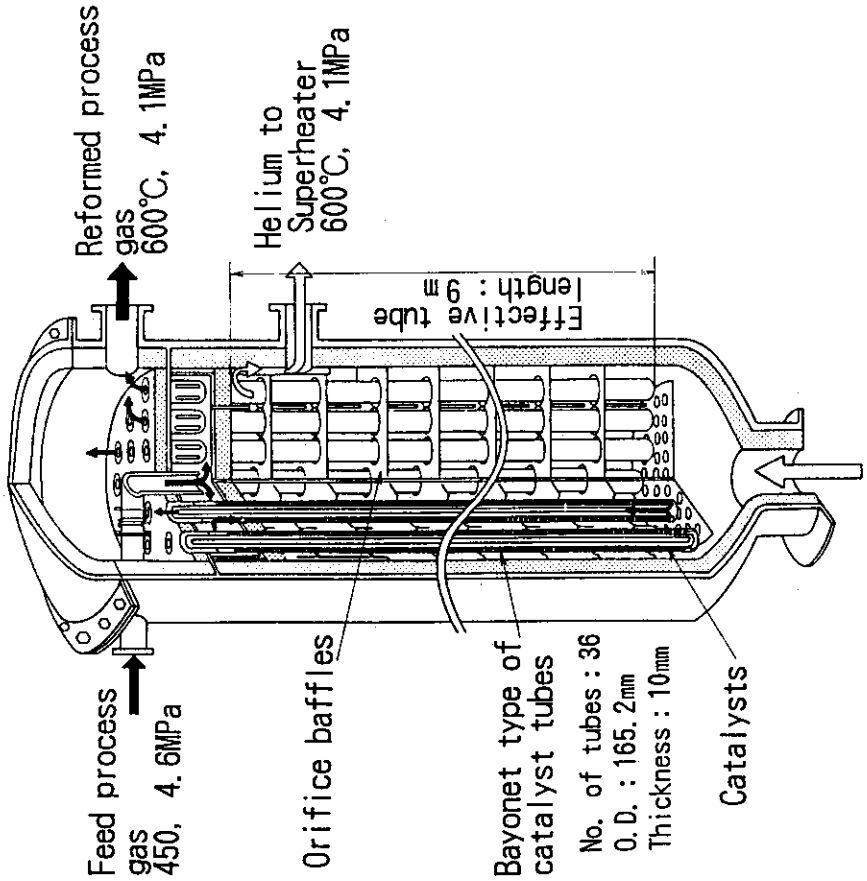


Fig. 4 Schematic illustration of HTTR-steam reformer

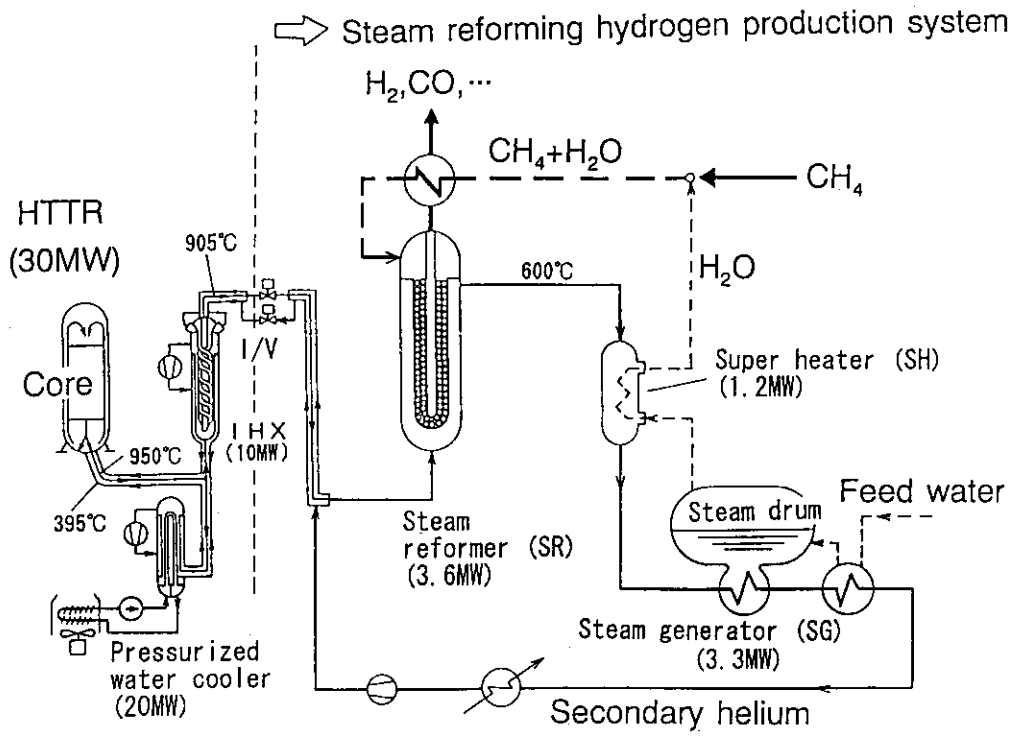


Fig.6 Flow scheme of the HTTR-steam reforming hydrogen production system.

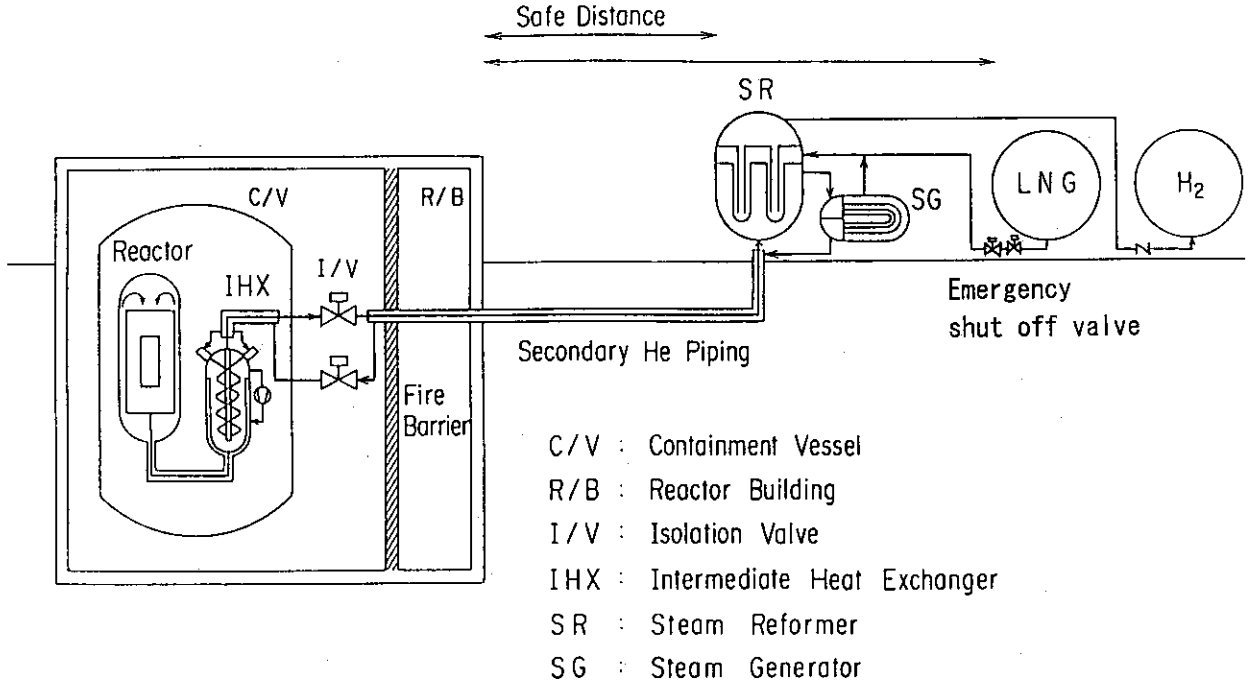


Fig.7 Safety design concept against fire and explosion.

5. Session V

－Panel Discussion－
"Future Perspectives of Nuclear Energy Utilization and Expected Role of HTGR"

5.1 FUTURE PERSPECTIVE OF NUCLEAR ENERGY UTILIZATION AND EXPECTED ROLE OF HTGR − JAERI'S ENERGY SYSTEMS ANALYSIS RESEARCH −

Osamu SATO
Japan Atomic Energy Research Institute

ABSTRACT

Since the beginning of the industrial revolution mankind's activity has expanded so substantially that we are now facing the limit of the earth's environmental capacity. Although our knowledge is not yet sufficient to explain all of the scientific processes involved, the greenhouse effect, which is primarily caused by the combustion of huge amounts of fossil fuels, is thought to cause serious and irreversible damage to the environment of the earth. Future energy strategies must be established within the context of minimizing the further man−made global warming.

Japan experienced rapid economic growth during the 1960s by using petroleum which was cheap and abundant. The era of this high economic growth ceased with the oil crisis in 1973. After that time, the dependence on imported oil has been substantially lowered by promoting utilization of alternative energy such as nuclear energy or natural gas, and by improving efficiency of final energy consumption. Japan is now one of the countries with the highest energy utilization efficiency.

In the future, the demand for electricity will continue to increase rapidly due to structural changes in the industry sector and further electrification in the residential and commercial sector. On the other hand convenient liquid fuels will be necessary for industrial boilers and furnaces and for transportation vehicles. In meeting such future energy demands we must make appropriate choices of energy sources and energy technologies that can stably provide required forms of energy at low cost and in a manner compatible with the environment.

Studies have been made in JAERI in order to assess the possibility of using nuclear energy symbiotically with fossil and biomass fuels, and to evaluate its implications for the environment. The application system of high temperature nuclear heat has been designed for this purpose with various technology options. The core of the system is a set of technologies for hydrogen production and its application to produce clean and convenient fuels from fossil or biomass sources.

The results of analytical studies using the MARKAL model have indicated sufficient possibilities of combining nuclear energy effectively with fossil or biomass fuels via hydrogen produced by high temperature nuclear heat. In addition to providing clean and convenient liquid fuels on a large scale, the combined system will contribute to the substantial reduction of long−term CO_2 emissions. The relatively high cost of this system will be well justified when CO_2 emission penalties are taken into account.

1. Introduction

The progress of science and technology has enabled rapid development of material civilization since the beginning of the industrial revolution. During these two hundred years energy utilization by mankind has increased so much that we now face the limit of the earth's capacity in both natural resources and living environment. Yet, the present circumstances have been created primarily by the developed countries. It is expected that with rapidly growing population the social and economic activity by the developing countries will expand significantly in the next century.

According to the study by IPCC, global CO_2 emissions must be reduced immediately by more than 60% in order to stabilize its atmospheric concentration at the present day level, or it must be reduced at the annual rate of approximately 1% in order to stabilize it to the level of 50% higher than the pre−industrial concentrations. Although there exist a lot of unknown factors in the processes involved between emissions and their ultimate consequences, the developed countries will have to make substantial efforts to reduce their emissions. Future energy strategies must be established within the context of minimizing further possible man−made global warming.

2. Past and Present Energy Consumption

2.1 World Energy Supply and Demand

The total population in the OECD countries was 20% of the entire world in 1975, but it decreased to 17% in 1990 as shown in Fig. 1. During these 15 years the population in the rest of the world increased at the annual rate of 2%, although it was almost stagnant in the OECD countries. On the other hand, approximately two thirds of annual GWP (gross world production) came from the OECD region throughout the same time period. See Fig. 2. Some developing countries achieved significant economic growth, however the GNP growth rates are comparable between the OECD region and the rest of the world despite rapid population increases in the developing countries.

From the viewpoint of energy consumption, the share of OECD countries in the entire world declined from 61% in 1975 to 52% in 1990. See Fig. 3. This was caused by two different factors in the OECD countries; successful energy conservation and economic recession. At the same time, the primary energy consumption in the developing countries increased very rapidly reflecting the progress of their industrialization in recent years. However, as shown in Fig. 4, the difference in per capita energy consumption is still quite large between the OECD countries and the developing countries.

In line with the primary energy consumption, the share of CO_2 emissions from the developing countries increased rapidly during these years. The world growth rate excluding the OECD region and the former USSR was 5.2% per annum, while that of the OECD regions was only 0.8% per annum. According to the energy projection by the Energy and Industry Subgroup of IPCC, with further progress of industrialization in the developing world, the portion of its contribution to global CO_2 emission will increase rapidly from 26% in 1985 to 44% in 2025. It seems evident that the global warming problem will become more serious with rapidly growing energy consumption by the developing countries in the next century.

2.2 Energy Utilization in Japan

Japan achieved high economic growth during the 1960s by using petroleum which was cheap and abundant in those years. This high economic growth ceased with the oil crisis in 1973. After that time total primary energy consumption remained at an almost constant level until the late 1980s. However, oil's share in that consumption was successfully lowered from 77% in 1973 to 56% in 1985. See Fig. 5. Although the economic boom in the late 1980s pushed up the energy consumption, the share of oil was quite stable in recent years.

In reducing the share of oil, the main alternatives were nuclear energy and natural gas. Nuclear energy gradually expanded its share in the primary energy consumption to 11% in 1993. The electricity generated by nuclear energy was 34% of total generation by utilities in 1993 as shown in Fig. 6. With expanding capacity of gas-fired power stations and increased demand for town gas, natural gas has also increased its share in the primary energy consumption. Since these alternatives have reduced particularly the consumption of heavy fuel oil, transportation fuels have largely increased their shares in oil products as indicated in Fig. 7.

Coal, a major energy source in the past, reduced its share during the period of high economic growth. However, it was reevaluated after the oil crisis as a cheap and abundant alternative to oil, although it was only recently that the consumption of coal other than for iron and steel making increased significantly. See Fig. 8. Renewable energy is also an important alternative to oil. In spite of people's expectations, however, the contribution of renewable energy remains quite small with the exception of hydropower.

Energy conservation efforts have been very successful in Japan. The energy intensity of manufacturing industry was reduced by more than 40% since the oil crisis, as shown in Fig. 9, through improvements of efficiency, rational uses of energy, or recycling of wastes. Including the significant effect of the changes in industrial structure, the GDP elasticity of energy consumption after the oil crisis was 0.36, as compared with 1.08 between 1953 to 1973. Now Japan is one of the countries with the highest energy efficiency.

3. Long-term Energy Perspective in Japan

3.1 Evolution of Energy Demand

There are many factors that will directly or indirectly affect future energy consumption in Japan; GDP, industrial structure, energy prices, population, life style, modal structure of transportation, environmental constraints, technological progress, and so on. One appropriate method for estimating future consumption of energy would be to divide it according to the purpose of consumption and to examine the future growth of each component taking historical changes into account.

The total energy consumption by industry is strongly related to its structure. During the long-term growth of an economy major industry products typically change from raw materials to machines, and then to services. Main products in the Japanese economy have now already shifted substantially to services with the share of the tertiary industry being 55% of GDP in 1993. In the future growth of the economy a larger portion of the GDP will be shared by the tertiary industry.

The raw materials and machinery industries will gradually reduce their contribution to GDP. Nevertheless, the absolute amount of their production will not decrease so much. Comparing the stock of social capital or per capita stock of raw materials, Japan is still far behind the European countries. Therefore the production of raw materials will not substantially decrease from the current level during the next a few decades. This implies that the demand for large amount of fuels for industrial boilers and furnaces will continue in order to produce these materials.

The modes of transportation have largely shifted from railways to automobiles despite the well developed railway systems in Japan. Railways are used for inter-city long distance travel, and for inner-city transportation in large cities. In the future, it is expected that the population currently in large cities will be redistributed to local areas. This will enhance the use of automobiles, even though railway transportation is much more efficient.

Gasoline and diesel oil are currently used as major fuels for automobiles. In order to reduce dependence on oil and its products, various new fuels from other energy sources are being developed. Electric vehicles are also being developed. Although they have excellent characteristics for road transportation and technical problems should be solved in the foreseeable future, it will be a long time before they can compete economically with conventional automobiles. For the time being, a more realistic option will be to use synthetic fuels that do not require major changes in current automobile technologies.

With increases of income people demand higher grades of products, more convenience, and more comfort. Energy consumption by the residential and commercial sector has increased more rapidly than that of other sectors. Particularly, electricity consumption has increased very rapidly. Such tendencies in recent history will likely continue in the future. The demand for electricity will grow further with increasing size and capacity of such appliances as TV sets or refrigerators, with development of new electric appliances, and with people's preference of electricity for space heating and water heating as well.

In summary, when assuming stable and continuous economic growth, the demand for energy will increase further in the future even at the decreasing energy intensity of GDP. In particular the demand for electricity will increase more rapidly than other forms of energy. Liquid fuels, now contributing a major portion of energy consumption, will reduce its relative importance. Nevertheless, the demand for convenient liquid fuels will still continue. Accordingly, we need to discuss how to meet growing demands for electricity and how to provide liquid fuels at low cost and in a manner compatible with the environment.

3.2 Energy and Technology Options

While meeting growing demands for electricity and ever continuing requirements for liquid fuels, future energy systems must also comply with various social, economical, or environmental requirements. Particularly important requirements are ensuring overall stability in energy supply and reducing environmental emissions, particularly of carbon dioxide. In order to increase stability, energy sources must be diversified by avoiding excessive dependence on a single source. In this sense the dependence on oil should be further reduced by enhancing the development of alternative energy sources for liquid fuels.

Since the first oil crisis, the development of synthetic fuels from coal or other sources has

been actively carried out. However, the R&D activities are sluggish in recent years due to the unfavored conditions of the international oil market for such development. Moreover the situation is becoming worse since threat of the global warming makes it unattractive to promote the development of coal conversion technologies. We need to establish new strategies for providing liquid fuels from alternative sources.

The second requirement, reduction of CO_2 emissions, should be discussed in a broad context. CO_2 emissions can be disaggregated into several components according to the Kaya's Formula:

CO2 = GDP * (PE/GDP) * (FE/PE) * (CO2/FE), or

GR(CO2) = GR(GDP) + GR(PE/GDP) + GR(FE/PE) + GR(CO2/FE)

where PE is primary energy, FE is fossil energy, and GR(X) is a growth rate of X. PE/GDP, energy intensity of GDP, is determined by two factors; a social and economic framework and an overall efficiency of energy systems. In the future, the former factor will contribute to lowering PE/GDP through the continuing shift of industrial structure to machinery and services, and of product mix to higher value added products. The latter factor should be discussed by dividing it into the efficiency of final consumption and that of conversion.

As explained above, Japan has achieved a remarkable record in energy conservation. This successful experience makes some people overly optimistic about its future potential. In reality, most of the effective and economically attractive conservation measures have already been implemented in the industry sector. The average energy efficiency of vehicles might become even worse as a result of modifications to meet environmental regulations. The efficiency of some of the household appliances might be improved significantly, however this would be more than offset by shifting to a larger unit capacity of each appliance. The efficiency of energy consumption would be improved, rather through changes in social service systems such as transportation systems or waste recycling systems.

On the other hand, efficiency of energy conversion will probably be improved particularly in the field of electric power generation. Combined cycle technologies using natural gas are already commercialized. IGCC (integrated coal gasification and combined cycle) is expected to substantially improve the efficiency of coal−fired power stations. In addition, cogeneration of electricity and heat is now widely used for district heating in large cities in Japan.

FE/PE indicates the share of fossil energy in the total primary energy. This figure can be reduced by introducing more nuclear and/or renewable energy. Nuclear energy has a large potential to meet the growing demand for electricity, if sufficient sites are acquired together with social acceptance of its expansion program. There are many different sources of renewable energy. Among them, hydropower is already well developed, and further development would be expensive for the unit of electricity produced. There is a large potential resource of geothermal energy in Japan. Although its development is behind schedule due to the environmental regulations for development, we expect gradual increases of its contribution to electric power generation. Solar energy is also a large potential resource, but because of high equipment costs, the application is currently limited to residential water heating. However PV systems will be economically attractive by early next century.

CO2/PE, CO_2 emission per unit of fossil energy consumed, is determined in principle by relative shares of coal, oil, and natural gas used as primary energy. It can be reduced by shifting

from coal to oil, and further from oil to natural gas. Natural gas is the most attractive among fossil energy source. However its price is expected to rise significantly when developed countries depend too much on it in order to achieve their emission reduction goals. For countries without a domestic supply like Japan, switching to natural gas might not be an economically feasible option for reducing CO_2 emissions.

An example of analysis on the potential effects of implementing above measures[1] is given in Fig. 10. In this example, the measures are sequentially applied in the order of energy conservation, fuel switching, expansion of nuclear and renewable energy, and CO_2 recovery and disposal (applied only to CO_2 from power boilers). Therefore it should be noted that relative contributions by any individual measure will change with a different order of application. This figure still indicates that through energy conservation and switching among fossil fuels CO_2 emissions will at best be stabilized at the current level until 2030, and nuclear and renewable energy application must be expanded in order to reduce them further.

4. Application of High temperature Nuclear Heat

As mentioned above, we need to propose new technology options to produce liquid fuels in a manner compatible with the environment. Nuclear energy can be also applied for this purpose. In particular, high temperature nuclear heat from HTGRs (high temperature gas−cooled reactors) has a variety of potential application areas. Studies using the MARKAL model have been made in JAERI in order to examine the market potential of high temperature nuclear heat, and to assess environmental implications of its application in the future energy systems of Japan.

Based on the conception of IES (Integrated Energy System), the structure of high temperature nuclear heat application systems has been designed, as shown in Fig. 11, so as to integrate three different energy sources; nuclear, fossil, and biomass energy. The core of the high temperature nuclear heat application system is hydrogen production by methane steam reforming, thermochemical water splitting, or high temperature electrolysis. Hydrogen produced by these processes will be used for desulfurization of fossil fuels, for producing clean and convenient synthetic fuels from low grade fossil or biomass fuels, or as a fuel for transportation and/or electric power generation.

The analysis was made on the long−term energy demand and supply with the above technology options[2]. Fig. 12 gives a projection of primary energy supply in the maximum CO_2 reduction case where penalties are assessed for the emission in terms of carbon tax. In this analytical case HTGRs are introduced up to the externally given upper limits, i.e. 180GWt in 2050, although they are not in the least cost case. Fig. 13 gives the possible contribution of nuclear energy to the reduction of CO_2 emissions. CO_2 emissions in 2050 will be significantly reduced by using nuclear energy for both electric power generation and synthetic fuel production. Taking the contribution by HTGRs alone, the emission level in 2050 will be reduced to 40% of the 1990 level by using HTGRs, as compared with 60% without HTGRs.

Fig. 14 illustrates the application of high temperature nuclear heat provided by HTGRs. In addition to hydrogen production, it is applied for the liquefaction of biomass, for the supply of process heat, and for electric power generation. The production and consumption of hydrogen are shown in Fig. 15. Hydrogen is currently produced by steam reforming of naphtha, and is

used for desulfurization and hydrocracking processes in oil refineries. This figure indicates the large potential demand for hydrogen produced by using high temperature nuclear heat.

In this example it is assumed that hydrogen can be used for automobiles either directly or via conversion to methanol. In the result, hydrogen automobiles are introduced up to their upper limits indicating better contribution to the emission reduction than methanol automobiles with assumed characteristics of relevant technologies. Since the development of hydrogen automobiles is at an early stage as compared with methanol automobiles, further investigation will be required to identify appropriate methods of using hydrogen for transportation.

It should be also noted that, in this projection, methane steam reforming produces most of hydrogen by using high temperature nuclear heat. High temperature electrolysis depends too much on expensive electricity. Thermochemical water splitting is less efficient in hydrogen produced per unit of high temperature heat. The latter option is selected in this analytical example only because a large amount of its waste heat can be used for electric power generation. The improvement in efficiency of these non−fossil hydrogen production technologies is the most important subject for the future development of this system.

5. Concluding Remarks

Nuclear energy can be produced stably on a large scale. It can be used not only for generating electricity but also for producing clean and convenient fuels through integration with fossil and biomass energy sources. Its economy in generating electricity is well demonstrated in many countries. It emits no CO_2 during operation and only a little throughout the lifetime of its production facilities.

We need effective and inexpensive measures for coping with the global warming problem. At the same time, we need large amounts of low cost energy for future economic growth and improvements of living standards in developing countries. Nuclear energy is one the most realistic and effective solutions to these problems. The global warming problem is now presenting an issue of fair distribution of costs and benefits between generations. The investment on the necessary R&D to minimize possible damage in the future is the responsibility of the current generation.

References

1) Yasukawa S., Sato O., Tadokoro Y., Kajiyama T., Shiraki H., Konta M., Ohkawa Y., Shimoyamada Y., and Iizuka T. : "Fuel and Technology Mix Toward CO_2 Emission Reduction −OECD/IEA/ETSAP Annex−IV Summary Country Report of Japan −", in Kram T. (Editor) : "National Energy Options for Reducing CO_2 emissions, Volume II : Country Studies" (1994).

2) Yasukawa S., Sato O., Tadokoro Y., Konta M. : "Potential of CO_2 Emission Reduction by High Temperature Nuclear Heat", in Executive Committee of The 2nd JAERI Symposium on HTGR Technologies (Editors) : "Proceedings of The 2nd JAERI Symposium on HTGR Technologies, October 21−23, 1992, Oarai, Japan", JAERI−M 92−215 (1993).

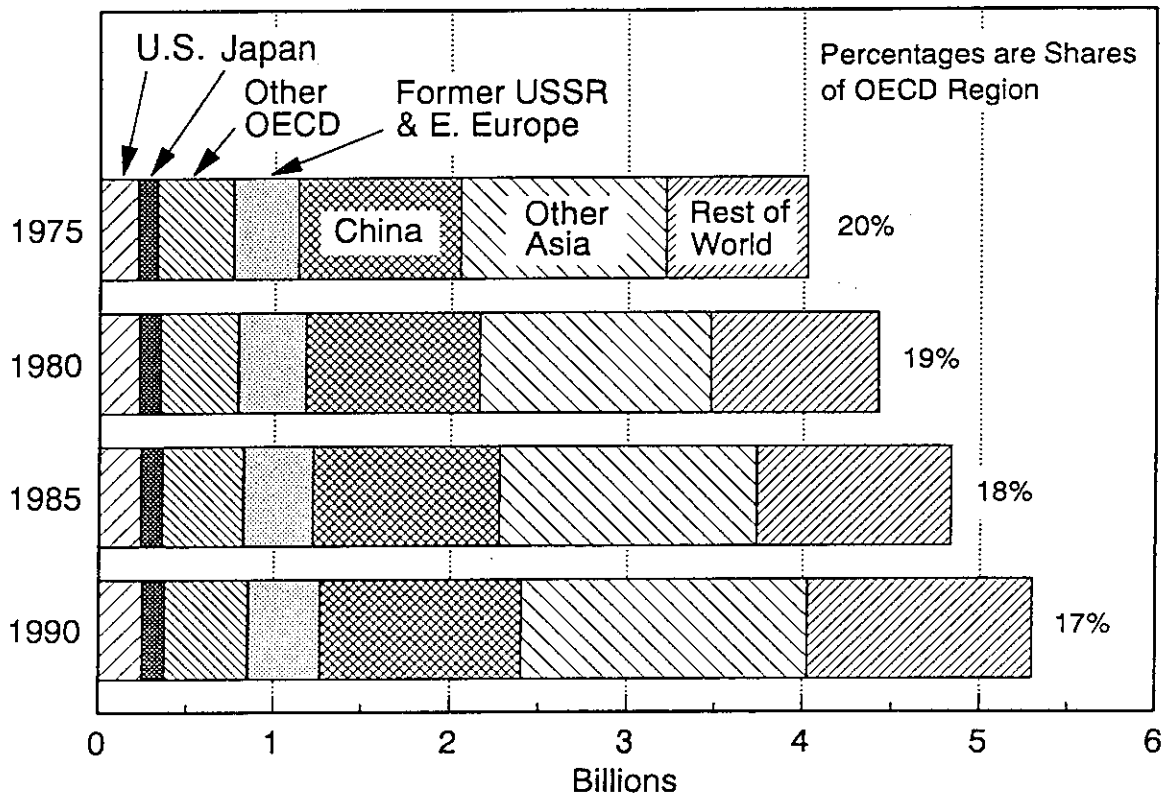


Fig. 1 World Population

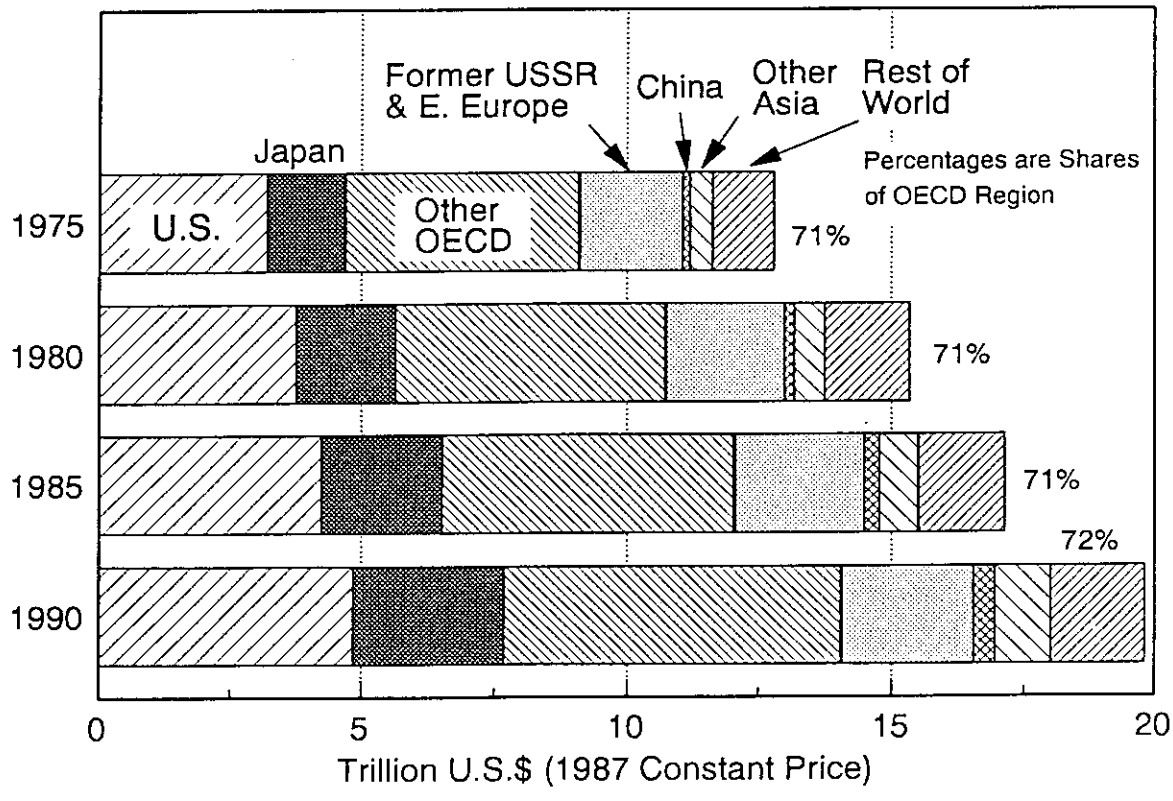


Fig. 2 Gross National Production

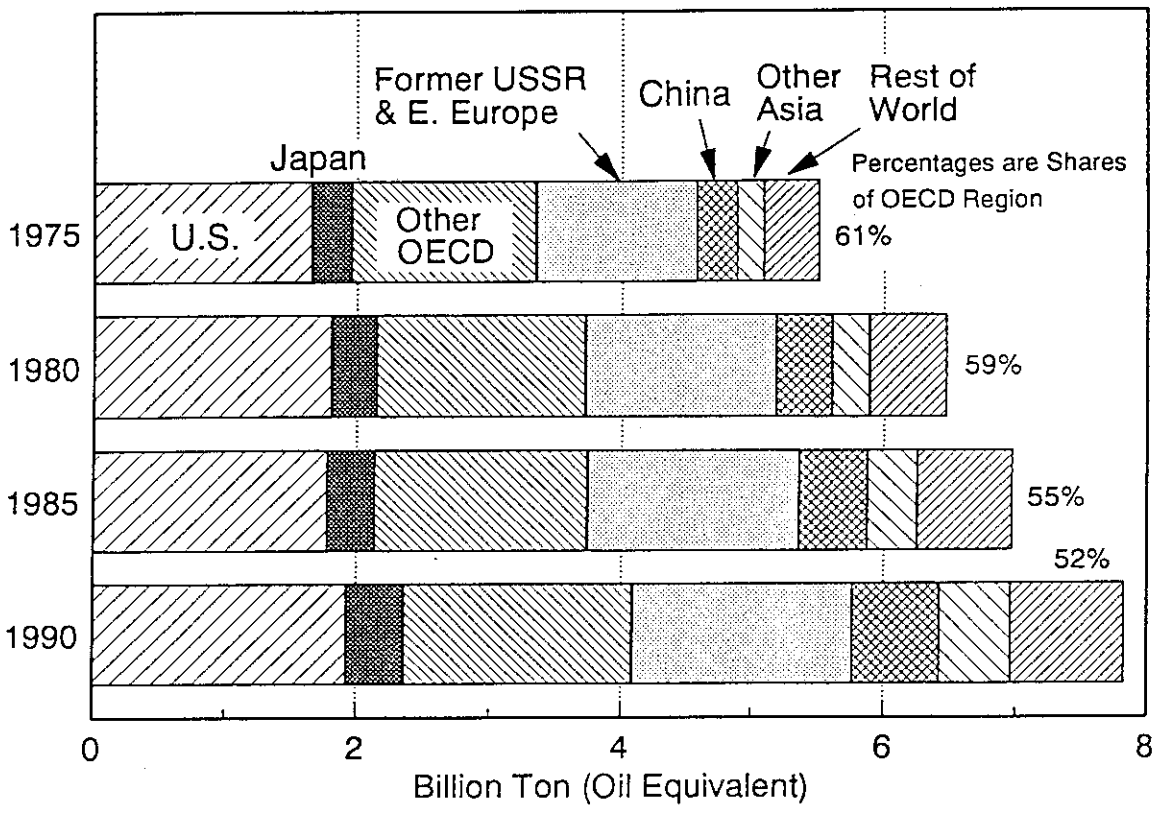


Fig. 3 World Primary Energy Consumption

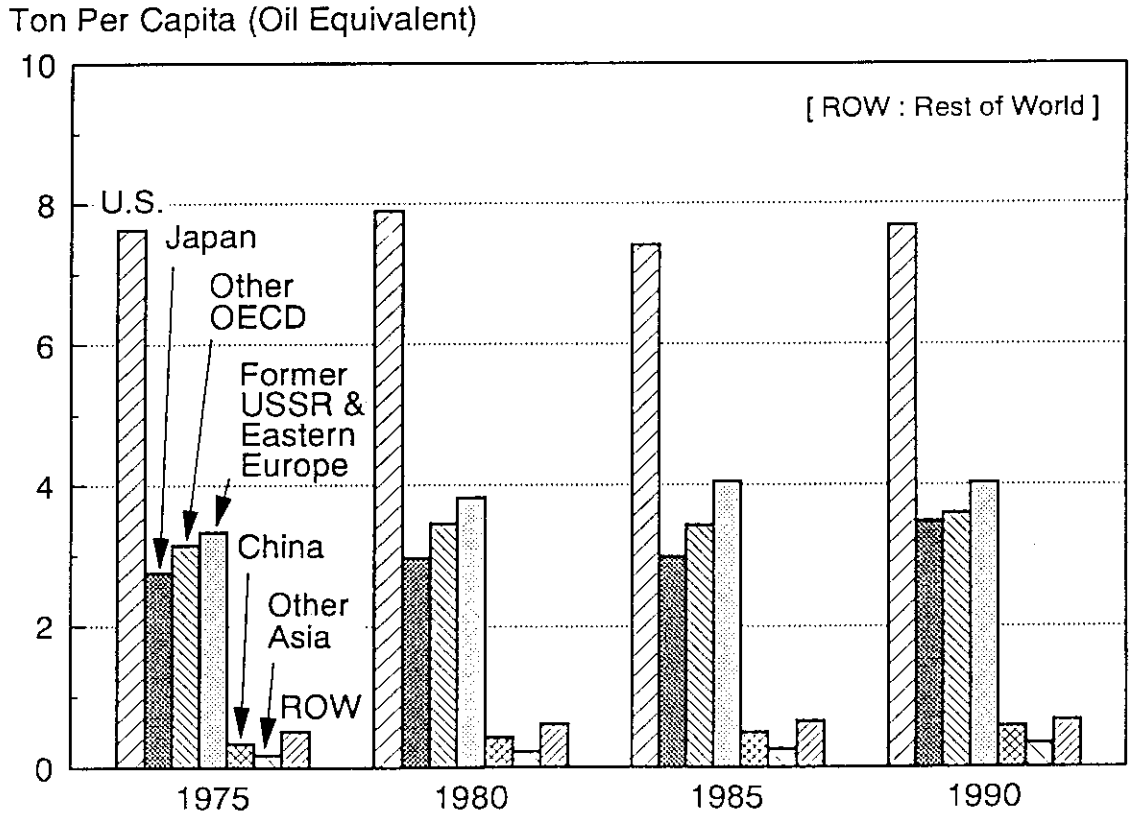


Fig. 4 Primary Energy Consumption Per Capita

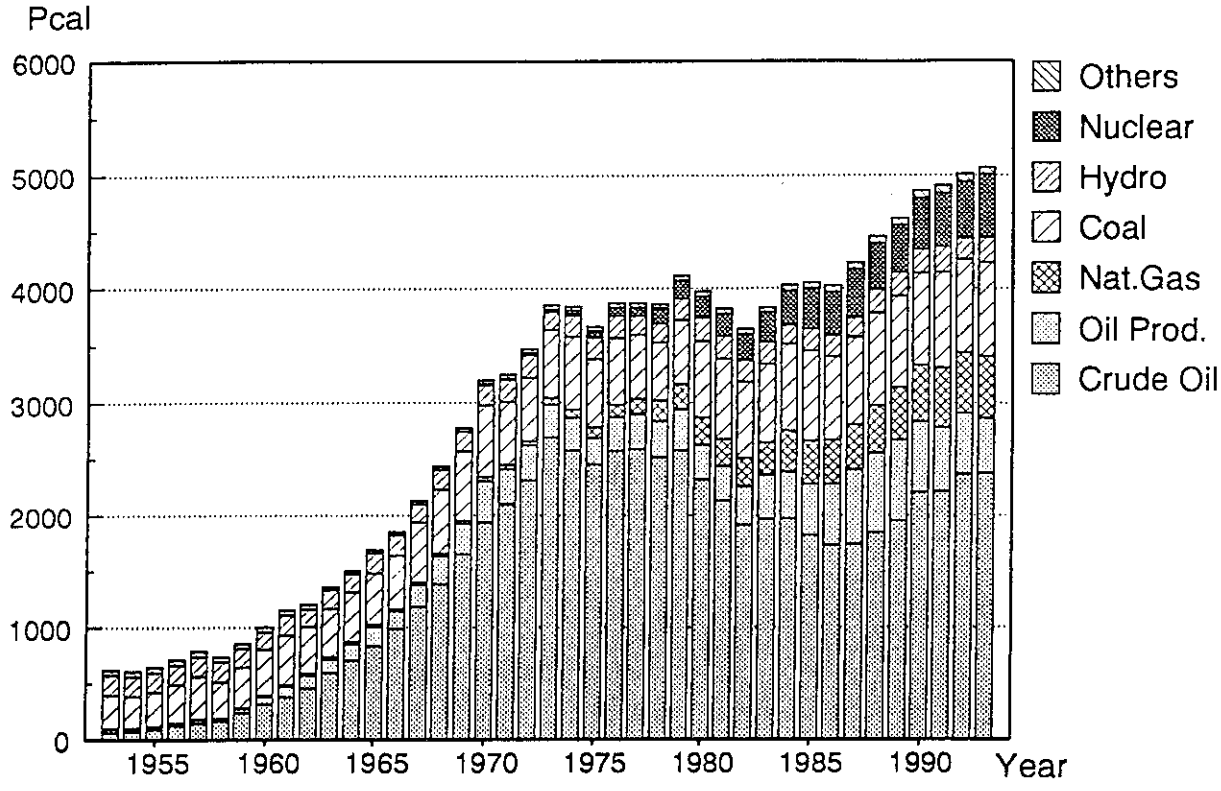


Fig. 5 Primary Energy Consumption in Japan

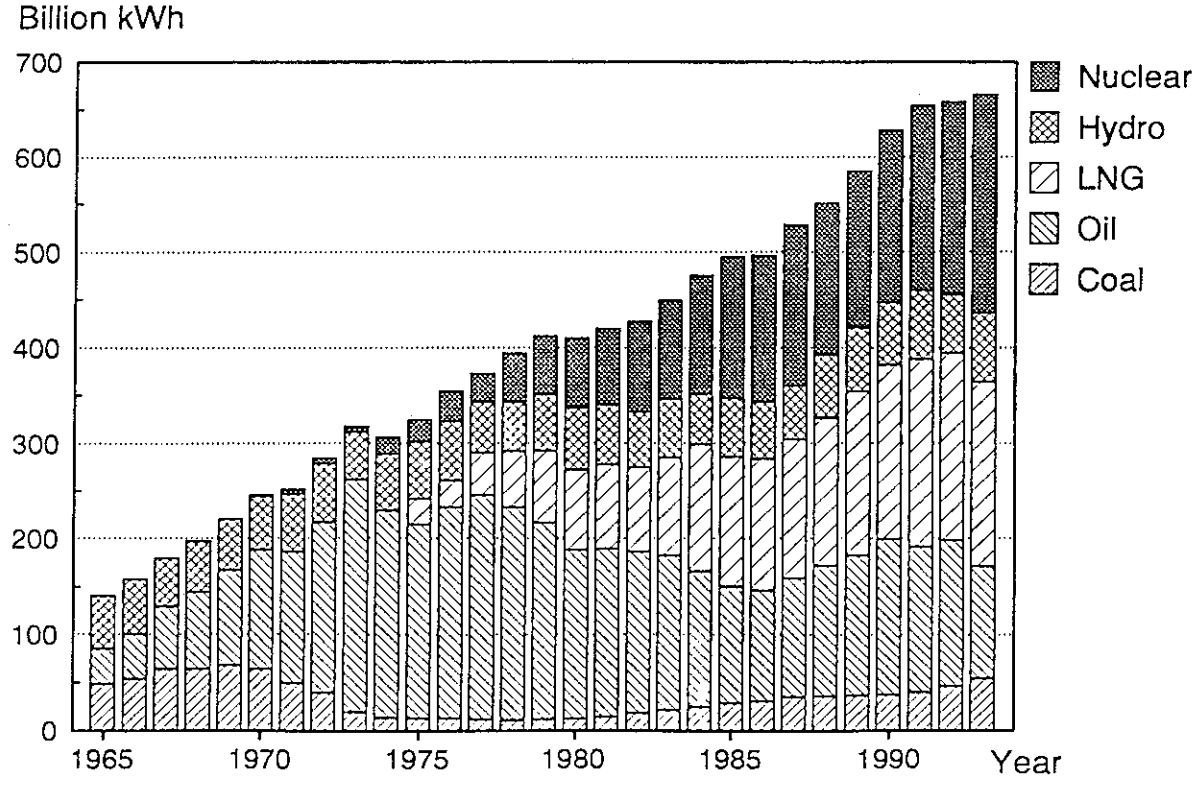


Fig. 6 Electric Power Generation

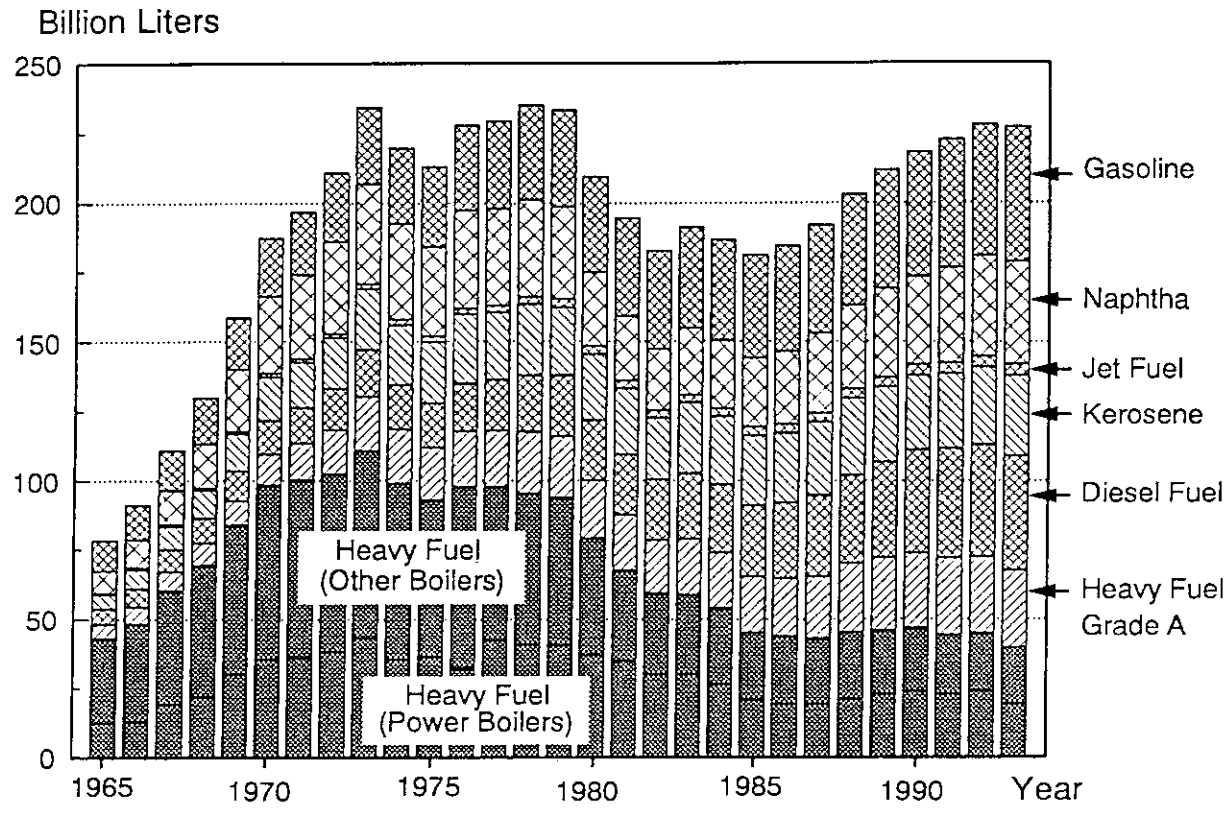


Fig. 7 Consumption of Oil Products

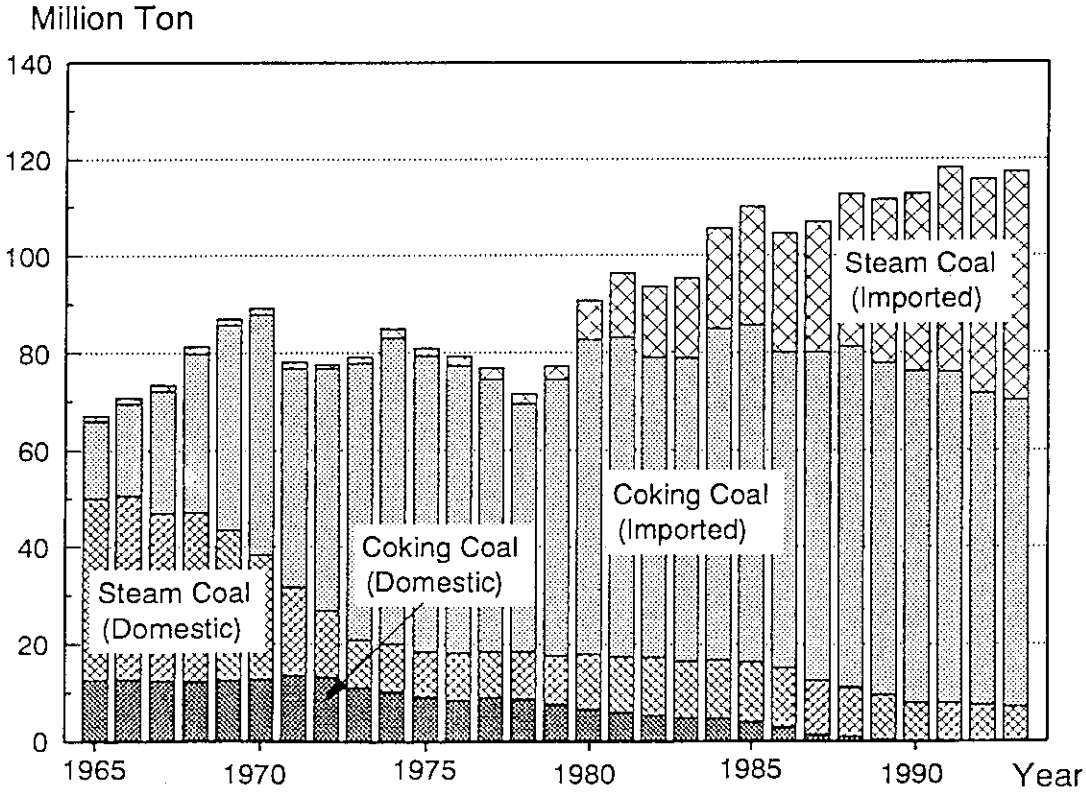


Fig. 8 Consumption of Coal

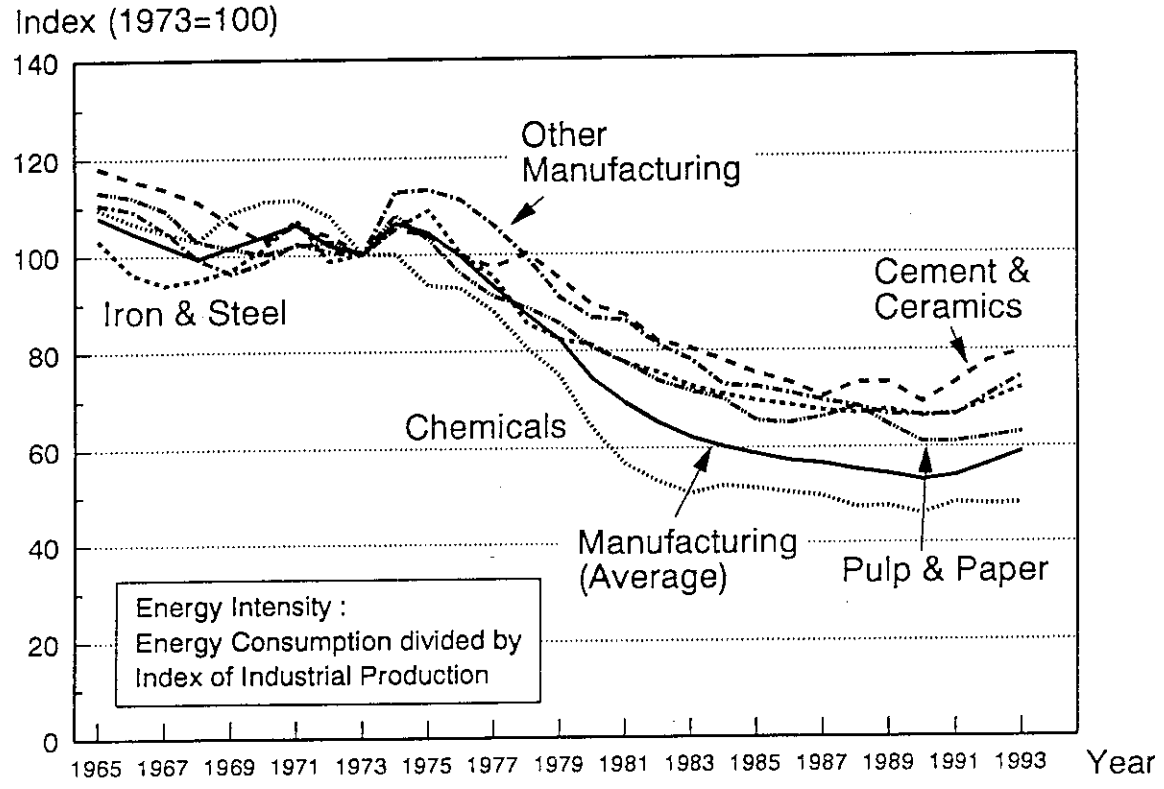


Fig. 9 Energy Intensity of Manufacturing Industry

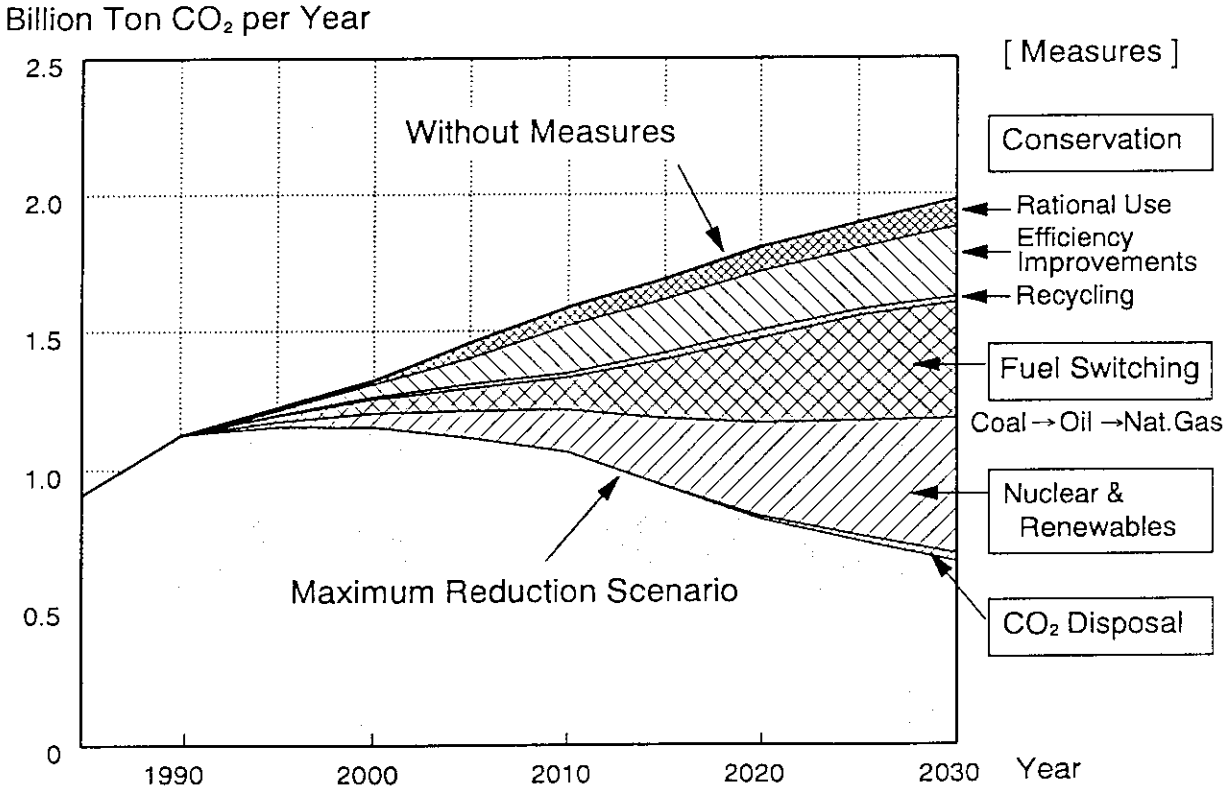


Fig. 10 CO_2 Emission Reduction by Measures

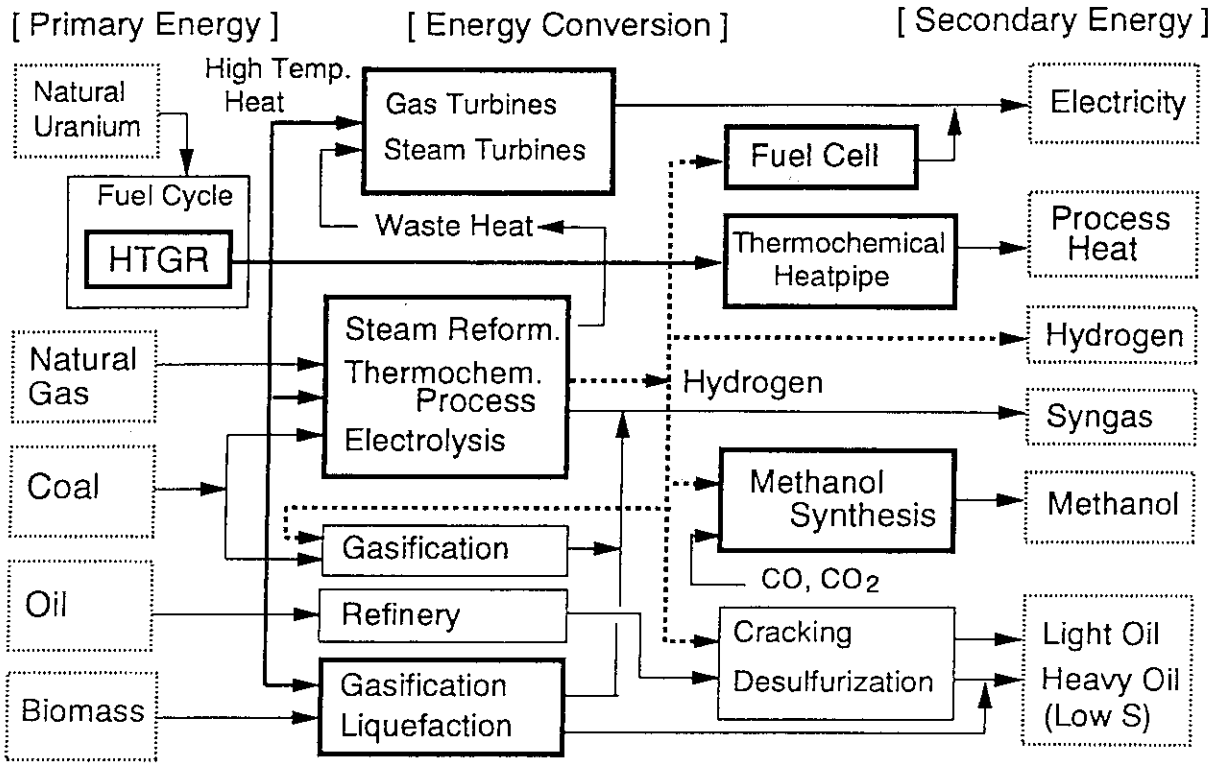


Fig. 11 Application System of High Temperature Nuclear Heat

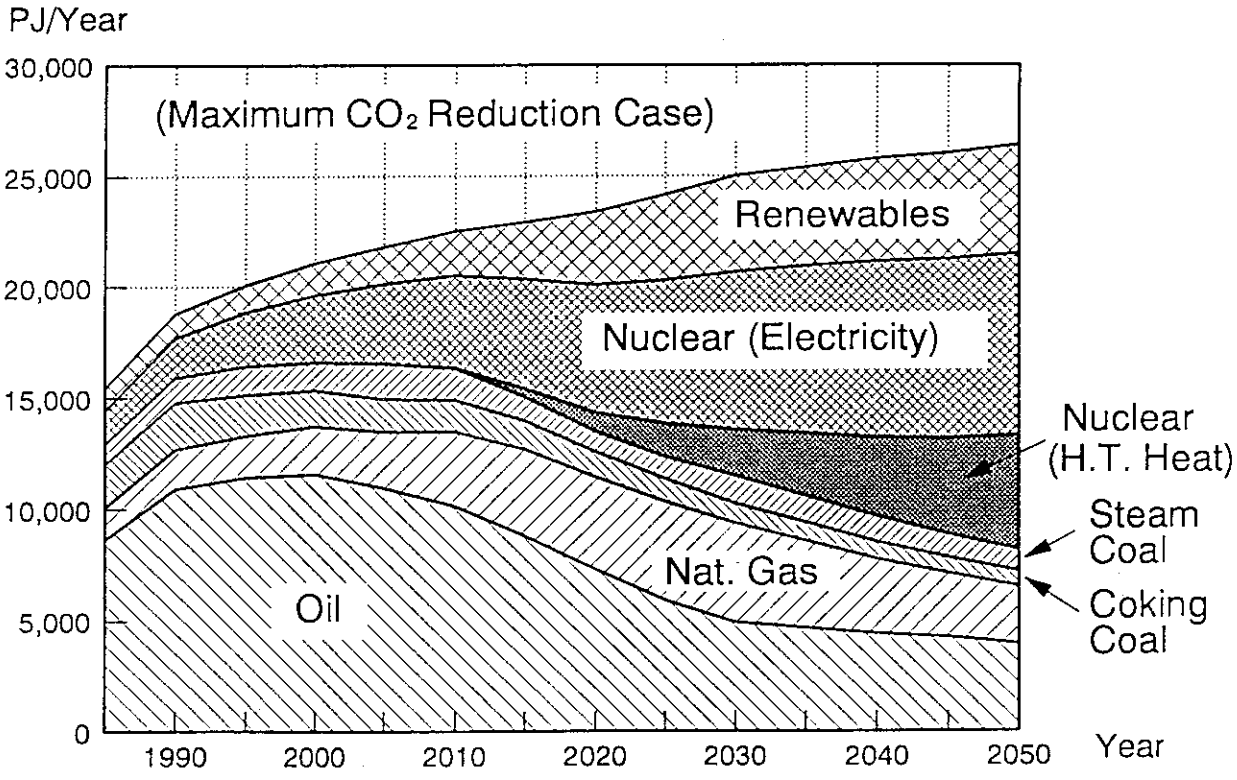


Fig. 12 Projection of Primary Energy Supply

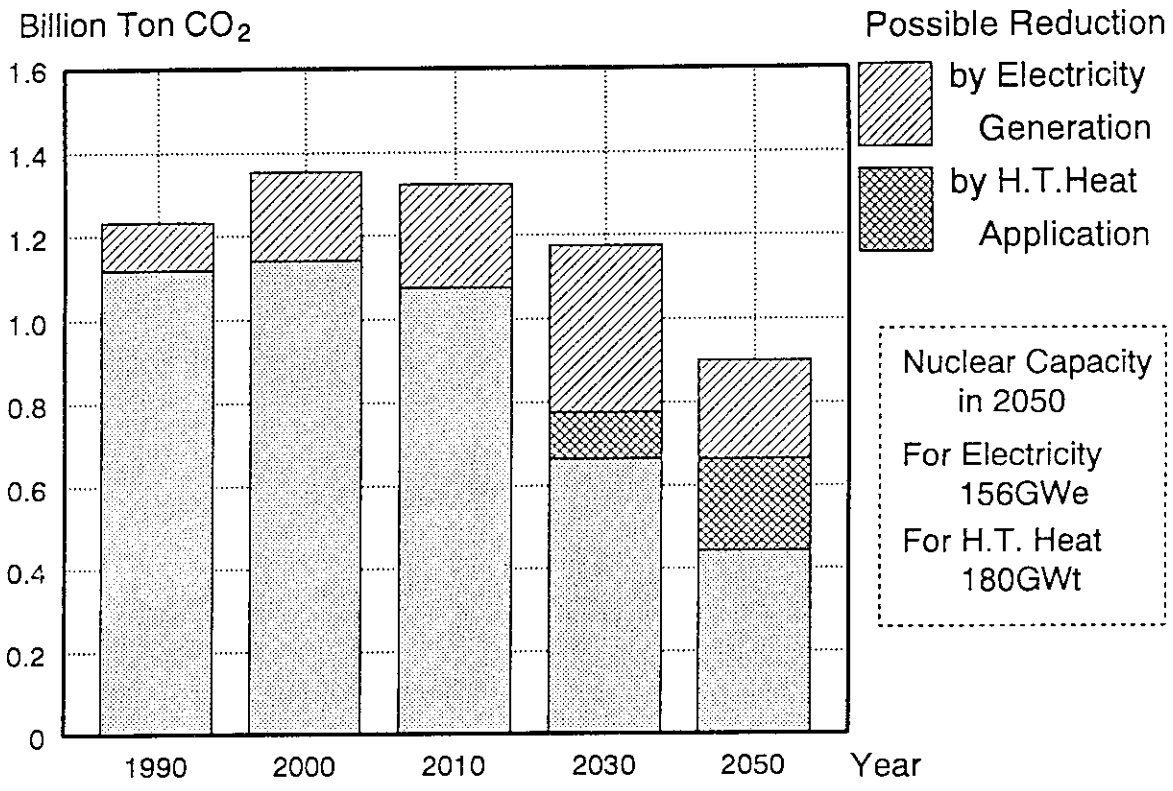


Fig. 13 Potential of CO_2 Reduction by Nuclear Energy

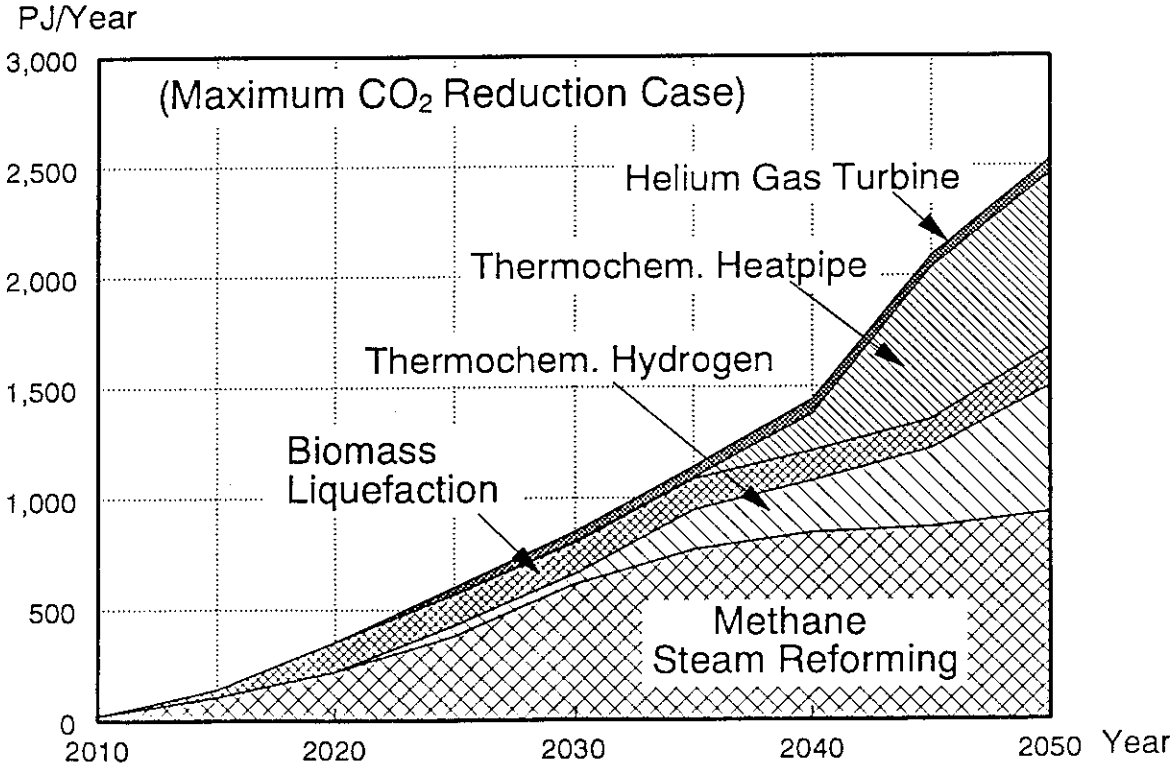


Fig. 14 Utilization of High Temperature Nuclear Heat

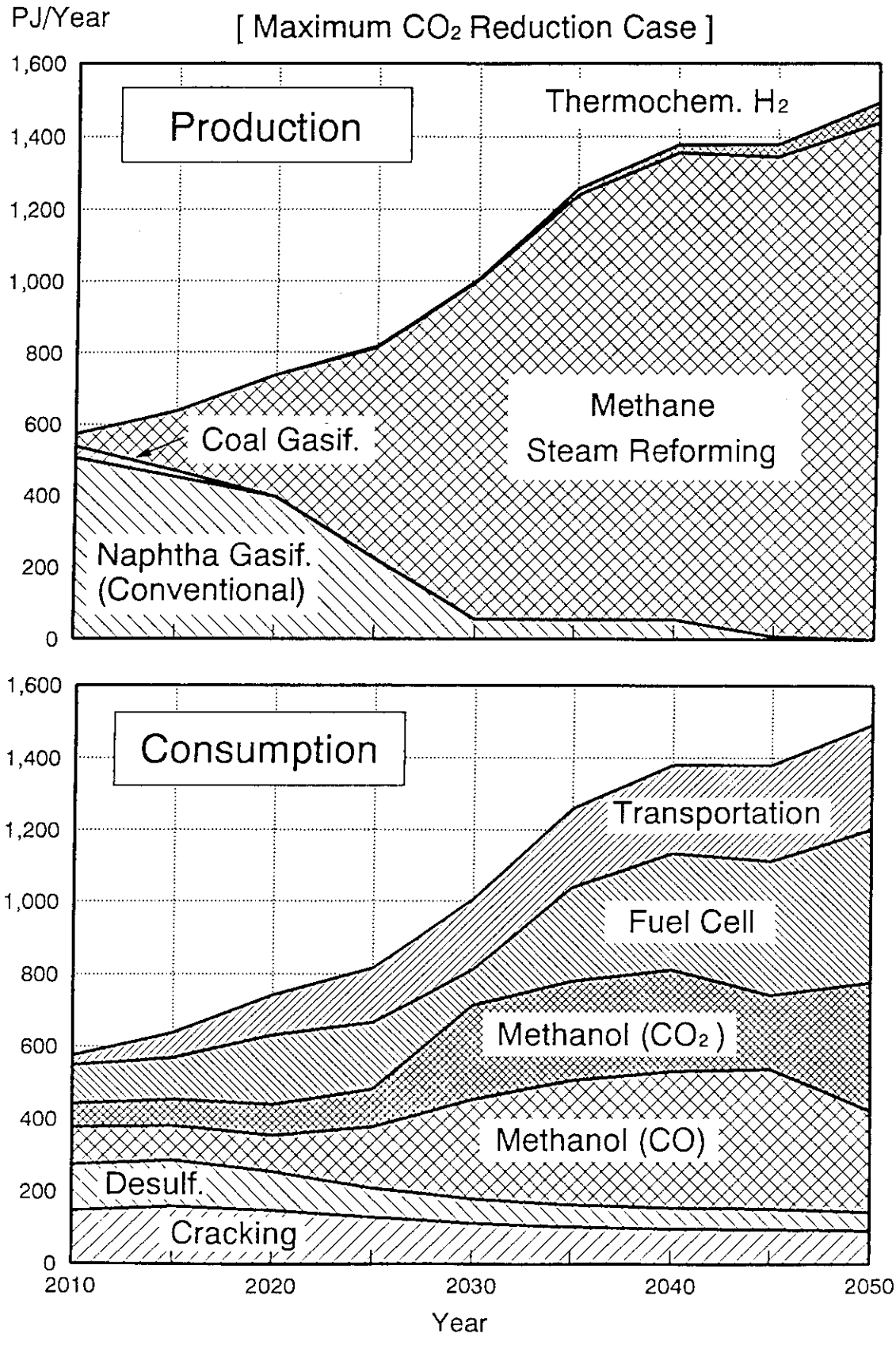


Fig. 15 Hydrogen Production and Consumption

6. Poster Session

6.1 Preliminary study on the use of the heat pipe to the passive decay heat removal system of the modular HTR

Kazutaka OHASHI, Hitoshi HAYAKAWA, Masao YAMADA
Nuclear Power Promotion Division, Fuji Electric Co.,Ltd.
Takao HAYASHI
Nuclear Engineering Department, Tokai University

ABSTRACT

Passive decay heat removal (DHR) is one of the most important features of the modular HTR. It is performed by the cooling system installed outside the reactor pressure vessel. Decay heat of the core is transferred to the reactor pressure vessel and then to the decay heat removal system passively by conduction, radiation and convection.

The purpose of our study is to establish the concept of the fully passive and highly reliable decay heat removal system utilizing the separated type of heat pipe, which has the self-regulation characteristics to minimize the heat loss under the normal operation with maintaining the sufficient heat removal capability during the accidents.

As the first step of the preliminary study, the system concept of the Heat Pipe DHR system was studied and the core heatup behaviour during the depressurization accident was calculated. These results show that the Heat Pipe DHR System is applicable to the modular HTRs and its heat removal capability is sufficient. Especially, by applying the variable conductance heat pipe, possibility of the self-regulation characteristics to reduce the normal heat loss is suggested.

The experiments to obtain the fundamental characteristics data of the separated type of the variable conductance heat pipe were carried out under various conditions such as heat removal rate, cooling mode and initial pressure of the non-condensible gas. These results show that the variable conductance heat pipe has sufficient self-regulation characteristics. The numerical model for the experiments was developed and the numerical results were compared with the experimental results.

These studies show that, by utilizing the variable conductance heat pipe, it is possible to design a fully passive DHR system with the self-regulation characteristics which can reduce the heat loss under the normal operation and can be sufficiently capable to remove large decay heat during accidents.

This paper provides the outline of our study mentioned above.

Preliminary Study on the Use of the Heat Pipe to the Passive Decay Heat Removal System of the Modular HTR

Kazutaka Ohashi, Hitoshi Hayakawa, Masao Yamada (Fuji Electric)
Takao Hayashi (Tokai University)

1. Purpose of the study

- Decay Heat Removal (DHR) system which is fully passive, highly reliable, and applicable to the modular HTR.
- DHR system which is able to have sufficiently heat removal capacity while the heat loss during normal operation is minimized.

2. Preliminary study of the VCHP DHR System

- Concept of the VCHP DHR System : Fig. 1
  (VCHP ; Variable Conductance Heat Pipe)
- Temperature analysis under depressurization accident : Fig. 2

3. Fundamental experiment

- Experimental apparatus : Fig.
- Experimental results : Fig. 4 (typical example)

Experiments have been done under various conditions and parametric changes in combination of the following parameters.

- With and without nitrogen gas
- Air flow rate on the cross flow fan (including fan stoppage)
- Initial N2 gas pressure P0 (including vacuum)
- Heat input Q

4. Conclusion

- By adopting VCHP, it is possible to design a fully passive DHR system which can minimize the normal heat loss and can remove a large heat during accidents without significant changes of the temperature and pressure in the system.
- Basic data of DHR behavior by the separated-type heat pipe were obtained and its self-control characteristics to keep the working temperature nearly constant by adding non-condensable gas was confirmed by fundamental experiment.

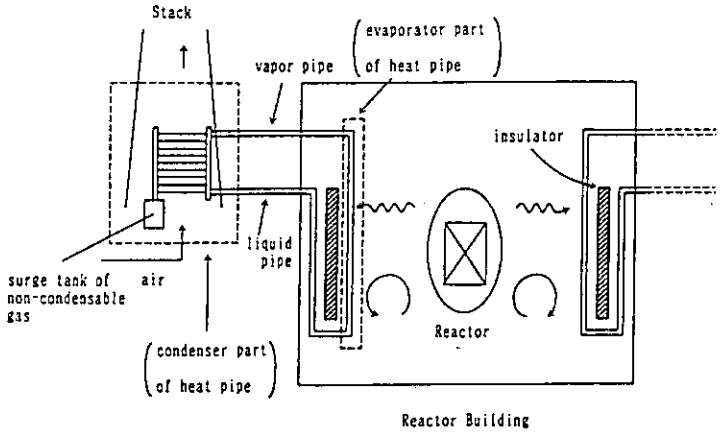


Fig. 1. Concept of Variable Conductance Heat Pipe (VCHP) Decay Heat Removal System for Modular HTR

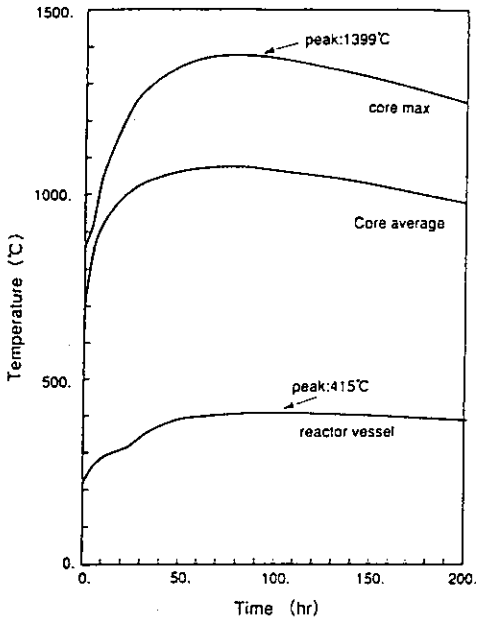


Fig.2. Temperature Behavior under Depressurization Accident

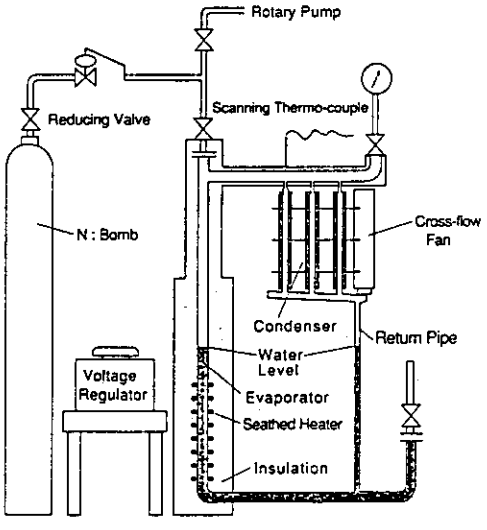


Fig.3. Vertical Condenser Type Apparatus With Forced Air Cooling

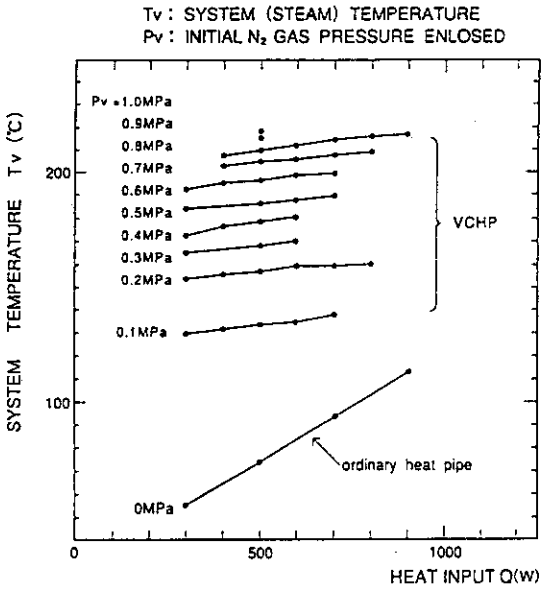


Fig.4. System Temperature Behaviors in Response to the Parametric Changes of Heat Input

6.2 Safety considerations and countermeasures against fire and explosion at an HTGR-hydrogen production system (Proposal of safety design concept)

T.Nishihara, K.Hada, T.Shibata and S.Shiozawa
Department of HTTR project, JAERI
Oarai, Ibaraki, Japan

Abstract

Establishment of safety design concept and countermeasures against fire and explosion accidents is among key safety-related issues in an HTGR-hydrogen production system. We propose the different safety design concepts depending upon the origin of fire and explosion which may happen in the HTGR-hydrogen production plant.

Against fire and explosion originated outside the reactor building (R/B), namely in the area of hydrogen production plant, the safety design concept is primarily to take a safe distance for preventing the damage on safety-related items or a proof wall if necessary. Because the hydrogen production plant is designed in the same safety level as a conventional chemical plant. The safe distance is proposed to limit an incident overpressure to 10kPa so as not to suffer any damage on the items and to limit a wall-averaged temperature of concrete structures of the R/B to 175°C according to the current regulation.

On the other hand, against a potential possibility of explosion originated inside the R/B, the safety design concept is to minimize the possibility of explosion low enough to assume no occurrence inside the R/B. That is, the measure is to exclude a simultaneous failure of a secondary helium piping and an endothermic chemical reactor. Furthermore, in severe accident condition in which the explosion may be postulated a priori, an incidental overpressure of explosion inside the reactor containment vessel (C/V) should be limited so as not to fail the C/V through restricting the amount of combustible gas ingress into the C/V by means of a combination of C/V isolation valve installed in the helium piping and emergency shut off valve in the process feed gas line.

1. Introduction

The nuclear plant should be designed to ensure the safety function, such as reactor shut down, residual heat removal and FP containment, against any postulated accident. Ensuring the function of safety-related items against fire and explosion accidents is among key issues in design of the nuclear plant. In particular, an HTGR-hydrogen production system has a potential possibility of fire and explosion due to a large amount of combustibles produced and/or stored in this system.

In this paper we propose safety design concept against fire and explosion happening in the hydrogen production plant which is designed in the same safety level as a conventional chemical plant without any further safety requirement for an economical reason.

2. Safety design concept for fire and explosion

The safety design concept of nuclear plant to ensure the safety function is usually based on the defense-in-depth concept that has three principal objectives, such as prevention of occurrence, prevention of spread and mitigation of effect. According to the above philosophy, the safety design concept against fire and explosion happening in the hydrogen production plant should be established.

At the HTGR-hydrogen production system, two quite different origins of fire and explosion are expected to occur and the accident scenarios differ by the origin. We categorize fire and explosion happening in the hydrogen production plant into two groupes, that are outside the reactor building (R/B) and inside the R/B .

In this discussion of the safety design concepts for both origins, we assume that the HTGR-hydrogen production system has an intermediate heat exchanger (IHX), therefore an endothermic chemical reactor is installed in the same secondary helium circuit as the HTTR steam reforming system. (Fig. 1) [1]

2.1 Outside the R/B

Outside the R/B, namely in the area of hydrogen production plant, the following phenomena may occur as a consequence of fire and explosion. (Fig. 2)

(1) radiation heat by fire on the ground and fireball
(2) blast by explosion
(3) radiation heat and blast explosion of explosive gas cloud

We discuss on the safety design concept taking into account two phenomena of (1) and (2) in this paper. The remaining phenomenon of (3) will be discussed elsewhere next.

Design of the hydrogen production plant for preventing the occurrence of accident and the spread of it outside the R/B can be implemented according to the domestic regulation for chemical plant. Because the hydrogen production plant is not to be requested any futher safety requirement for an economical reason. This regulation is on the basis of the same defense-in-depth concept as the design concept of nuclear plant and provides adequate measures for preventing the occurrence of accident and the spread of it, such as pressure resistance design, combustible gas leak detection system, fire extinguish system, emergency shut off system. This design seems to achieve no hazard to the nuclear plant in the case of small and middle scale of accident by the above countermeasures. So, in discussion on the safety design concept we take into account mitigation of effect of the maximum postulated fire and explosion so as to protect the safety-related items. The basic philosophy is no damage to the safety-related items in nuclear plant and the safety design concept is to take a safe distance from the hydrogen production plant to the nuclear plant. (Table 1) And if the safe distance is not taken, the proof wall is available to reduce the safe distance. (Fig. 3)

2.2 Inside the R/B

Key issue in developing the accident scenario of inside the R/B is the ingress of combustible gas into the R/B, especially into the C/V, through the helium piping due to the simultaneous failure of a helium piping and an endothermic chemical reactor. The explosion inside the R/B has a possibility to suffer heavy damage on the safety-related items. So, against fire and explosion inside the R/B, the safety design concept is to minimize the possibility of explosion to assume no occurrence inside the R/B due to the gas ingress through the hilium piping. For preventing the gas ingress, the helium piping and the chemical reactor should be designed as highest grade reliability to prevent the abnormal condition and aseismic design against extreme design earthquake.

Furthermore, in taking into account the severe accident condition, a combination of the C/V isolation valve installed in the helium piping and the emergency shut off valve in the process

feed gas line is available for restricting the amount of gas ingress. And this countermeasure mitigate the effect of explosion inside the C/V so as not to fail the C/V even if the combustible gas ingress through the helium piping into the C/V.(Fig. 3) Then the incidental overpressure of explosion can be limited to lower than acceptable design pressure of the C/V.

3. Design criteria for radiation heat and blast

Damage on the safety-related concrete structure and steel frame components in the nuclear plant should be avoided so as to maintain the safety function against fire and explosion outside the R/B. We propose safety design allowable limits of these items for preventing the loss of safety function.

Based on experimental data [2], mechanical properties of concrete make no significant change for the period of 24 hours at temperature of 175°C. And similar value is provided as the acceptable upper temperature of concrete in ASME Section Ⅲ Division 2. We propose that the wall-averaged temperature of concrete structure of the R/B by the radiation heat due to the fire is limited to 175°C so as to maintain the stractual strength of concrete.

we propose the incidental overpressure on the safety-related items by the blast due to the explosion is limited to 10kPa. Aithough the U.S.NRC recommends the incidental overpressure of explosion on the items in nuclear plant at 1 psi (approximately 7kPa) conservatively[3], this level of overpressure is realized to induce no failure of the reinforced concrete and the steel frame components. (Table 2)[4]

4. Conclusion

We propose the following safety design concept based on the defense-in-depth concept against fire and explosion in an HTGR-hydrogen production system so as to ensure the function of the safety-related items in nuclear plant.

(1) Against the fire and explosion originated outside the R/B, the safety design concept is to take the safe distance for preventing the damage on the safety-related items or the proof wall if necessary. Measures to prevent the occurrence of accident and the spread of it are implemented according to the regulation for

conventional chemical plant.
(2) The safe distance should meet the safety requirements of the wall-averaged temperature of the concrete structure of the R/B at 175°C and of the incidental overpressure on the nuclear safety-related items at 10kPa.
(3) Against potential possibility of explosion inside the R/B, especially inside the C/V, the safety design concept is to minimize the possibility of explosion low enough to assume no occurrence inside the R/B.
(4) The secondary helium piping and the endothermic chemical reactor are designed as the highest grade reliability to prevent abnormal condition and the aseismic design against extreme design earthquake to exclude simultaneous failure.
(5) In case of severe accident condition, the effect of explosion inside the C/V should be mitigated through restricting the amount of ingressed combustible gas by means of a combination of the C/V isolation valve installed in the helium piping and the emergency shut off valve in the process feed gas line.

Reference

[1] K.Hada et al,"Design of steam reforming hydrogen and methanol co-production system to be connected to the HTTR",IAEA-TECDOC-761,High temperature applications of nuclear energy, October 1992.
[2] K.Nagao et al,"Experimental studies on characteristics of concrete members subjected to high temperature",Annual Meeting of architecture Society of Japan, October 1988.(in Japanese)
[3] Clancey,V.J."Diagnostic features of explosion damage", Sith Int. Mtg. of Forensic Science, Edinburgh, 1972.
[4] U.S.Nuclear regulatory commission,"Evaluation of explosions postulated to occur on transportation routes near nuclear power plants", February 1978.

Table 1 Safety requirement against fire and explosion

Event		Basic Philosophy	Safety design concept
Fire and explosion	Outside the R/B	No significant damage to reactor safety • Reactor shut down • Residual heat removal • FP containment	No damage to safety related items • Safe distance • Proof wall if necessary
	Inside the R/B		Prevention of occurrence • No simultaneous failure of 2ry He piping and hydrogen production reactor tube • Aseismic design against extreme design earthquake • Limiting amount of gas ingress into the C/V

Table 2 Relationship between peak pressure and damage effects

Pressure kPa(psig)	Damage
0.21(0.03)	Occasional breaking of large glass windows already under strain
0.7 (0.1)	Breakage of windows, small, under strain
1.0 (0.15)	Typical pressure for glass failure
2.1 (0.3)	"Safe Distance"(probability 0.05 no serious damage beyond this value) Missile limit Some damage to house ceilings, 10% window glass broken
3.5-7.0 (0.5-1.0)	Large and small windows usually shattered occasional damage to window frames
5.0 (0.7)	Minor damage to house structure
5.3 (0.75)	Breakage of small windows, not under strain
7.0 (1.0)	Partial demolition of house, made uninhabitable
7-14 (1-2)	Corrugated asbestos shattered Corrugated steel or aluminum panels, fastenings fail, followed by buckling Wood panels(standard housing) fastenings fail, panels blown in
9.0 (1.3)	Steel frame of clad building slightly distorted
14 (2)	Partial collapse of walls and roofs of houses
14-21(2-3)	Concrete or cinder block walls, not reinforced, shattered
16 (2.3)	Lower limit of serious structural damage
21 (3)	Heavy machine(1300kg) in industrial building suffered little damage Frameless, self-framing steel panel building demolished Steel frame building distorted and pulled away form foundations
21-28(3-4)	Frameless, self-framing steel panel building demolished
28 (4)	Cladding of light industrial buildings ruptured
35 (5)	Wooden utilities poles(telegraph etc) snapped Tall hydraulic press(18,000kg) in building slightly damaged
35-49(5-7)	Nearly complete destruction of house
49 (7)	Loaded train wagons overturned
49-56(7-8)	Brick panels, 20-30cm not reinforced fail by shearing or flexure
63 (9)	Loaded train box-cars completely demolished
70 (10)	Probable total destruction buildings Heavy(3,000kg) machine tools moved and badly damaged Very heavy(5,500kg) machine tools survived.

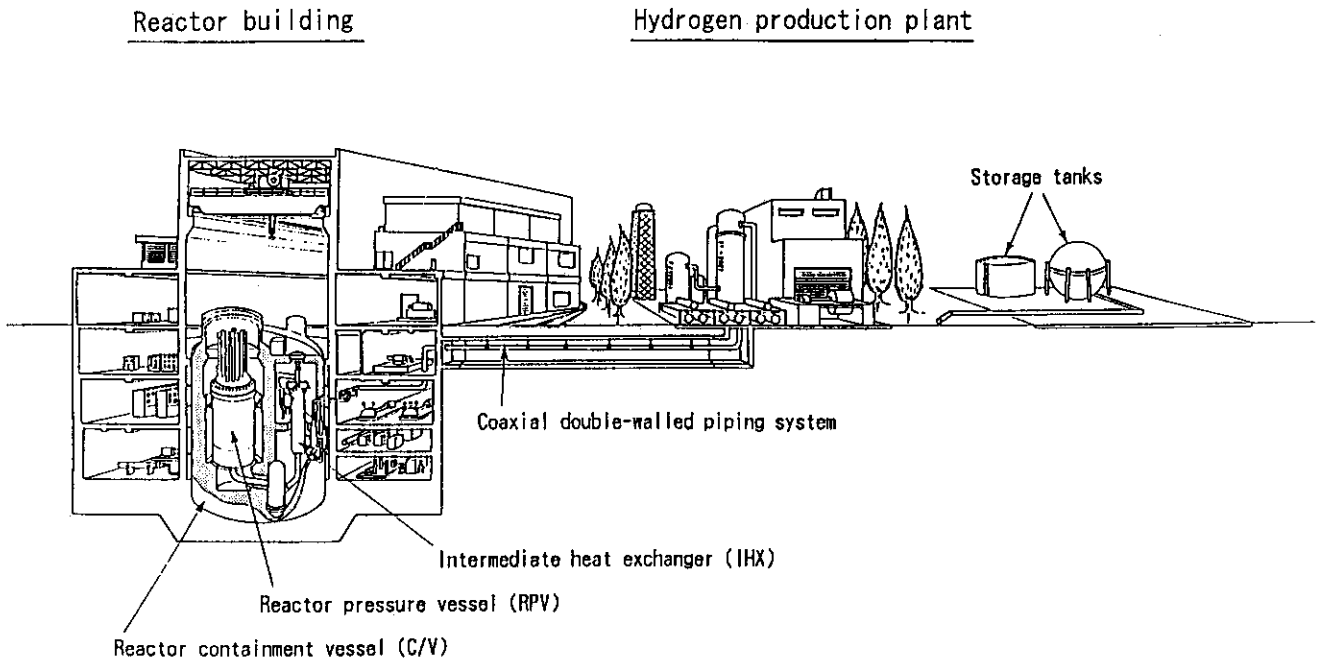


Fig. 1 Cutaway drawing of the HTGR-hydrogen production system

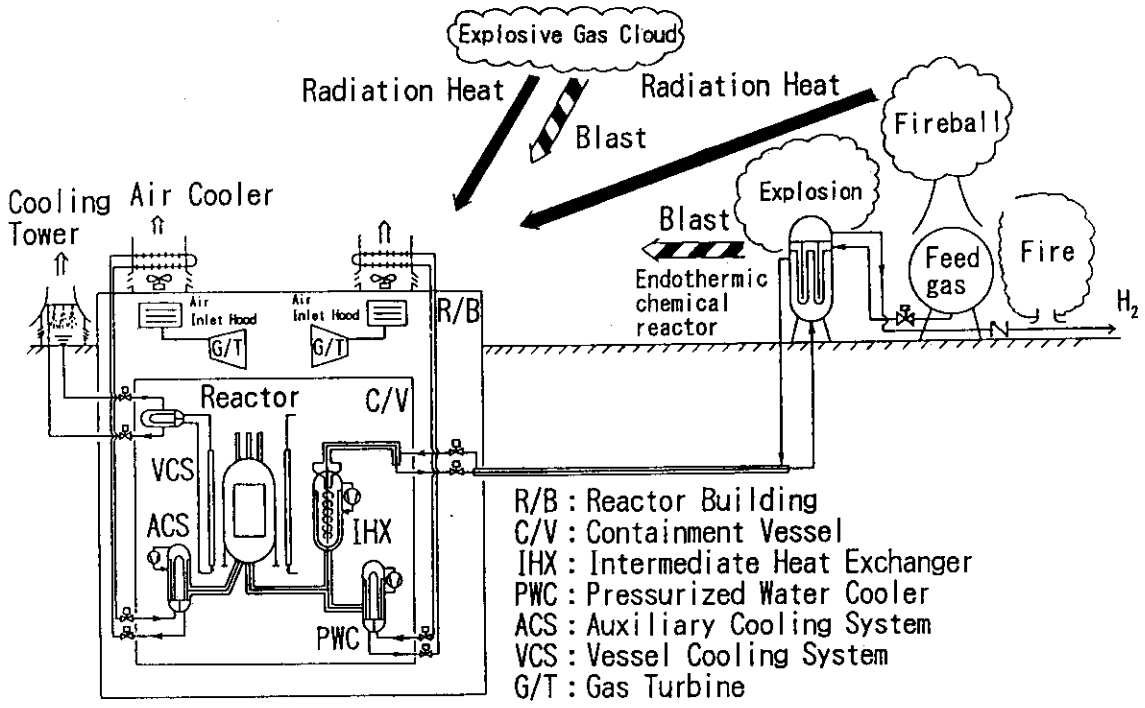


Fig. 2 Possible effect of fire and explosion outside the R/B

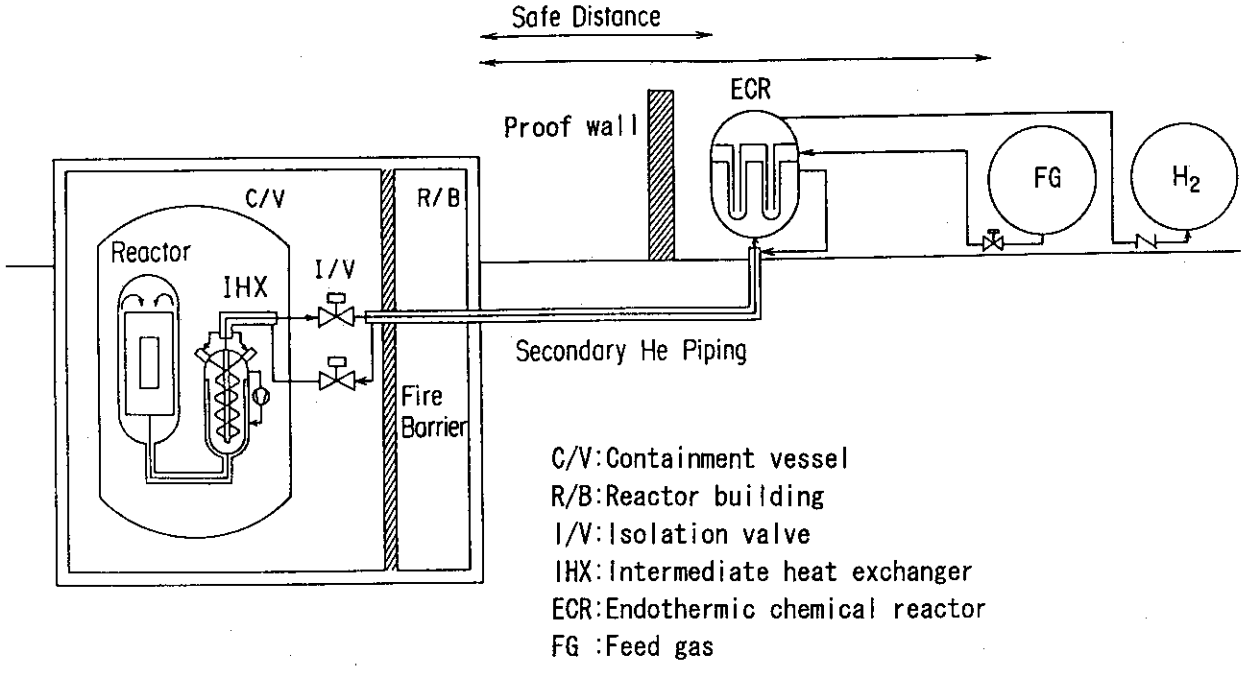


Fig. 3 Safety design concept against fire and explosion

6.3 Analysis of air ingress process during the primary-pipe rupture accident of the HTGR

Tetsuaki TAKEDA[*1], Makoto HISHIDA[*1], Shiryu IMANISHI[*2], and Satsuki TAKENAKA[*3]

[*1)]Nuclear Heat Application System Laboratory, JAERI

[*2)]Fujitsu Facom Information Processing Corporation

[*3)]Kawasaki Heavy Industries, Ltd.

ABSTRACT

A primary-pipe rupture accident is one of the most common of accidents related to the basic design regarding the High Temperature Gas-cooled Reactor (HTGR). It is a guillotine type break of the main pipe of coaxial double tube at the nozzle part connecting to the bottom of the reactor vessel. When the primary-pipe rupture accident happens, one may consider that air entering into a reactor vessel reacts with high temperature graphite structures and causes temperature rise of the reactor core and corrosion of graphite components. Therefore, it is very important to make sure that the air ingress accident cannot seriously oxidize the graphite fuel elements to release the radioactive materials from the reactor core to the environment nor severely damage the graphite components to loose the integrity of the reactor internals.

A high-temperature engineering test reactor (HTTR) is now in its developmental stage at JAERI[1]. It is a graphite-moderated high-temperature gas-cooled thermal reactor. A hot leg consists of an inner passage of a coaxial duct, a high-temperature outlet duct, a high-temperature plenum and fuel cooling channels. A cold leg consists of an annular passage of the coaxial duct, a bottom cover and an annular passage between the reactor vessel and permanent reflector. As the hot and cold legs are connected at the top cover, they make a kind of reverse U-shaped tube. When the primary-pipe rupture accident occurs, the high-pressure helium gas coolant in the reactor is forced out into the reactor container through the breach. Gas pressure should become balanced between the inside and outside of the reactor vessel after a few minutes. During this stage, called the depressurization stage, air is not able to enter the

reactor core from the breach. After the depressurization stage, it is supposed that air enters the reactor core from the breach due to molecular diffusion and natural convection of a multicomponent gas mixture induced by the distribution of gas temperature and the resulting concentrations in the reactor. Density of the gas mixture in the reactor gradually increases as air enters by the molecular diffusion and natural convection of the gas mixture in the first stage of the accident. Finally, the second stage of the accident starts after natural circulation of the air occurs suddenly throughout the entire reactor[2].

Previous studies focused mostly on molecular diffusion and natural convection of the two-component gas mixture in a reverse U-shaped tube and in a simple test model of the HTTR[3,4]. Moreover, to investigate the basic features of the flow behavior of the multicomponent gas mixture, consisting of He, N2, O2, CO2, CO, etc., experimental and numerical studies were performed on the combined phenomena of the molecular diffusion and the natural convection of the multicomponent gas mixture with the graphite oxidation reaction in the reverse U-shaped tube[5]. The numerical results of the density change of the gas mixture, the mole fraction changes of each type of gas species and the onset time of the natural circulation of air agree well with the experimental results.

In order to predict or analyze the sequence of the air ingress accident of HTGRs, it is very important to develop computer programs and to validate them by experiments. This paper describes a computer program, which is named FLOWGR, developed to analyze the thermal and hydraulic behavior of the HTGR during the first stage of the primary-pipe rupture accident. FLOWGR provides a numerical method for analyzing the transient thermal hydraulic behavior of the HTGR by solving the one-dimensional basic equations for continuity, momentum conservation, energy conservation of the gas mixture, and the mass conservation of gas species. It predicts the velocity, temperature, density, pressure and mole fractions of each gas species at user-defined control volumes.

FLOWGR treats the gas mixture consisting of arbitrary components and takes into account the graphite oxidation reaction. The production and dissipation terms in the mass conservation equations resulting from these chemical reactions are expressed by the temperature dependent Arrhenius formula having rate constants which are specified by the user. The reactor system to be analyzed by FLOWGR is modeled as a network of one-dimensional stream-tubes which represent components of the system such as a piping, plenum and reactor core. Each stream-tube is further divided into fluid volumes (control volume or cells). There are three types of tube-ends: a normal, break, and closed end. The normal end connects

with adjacent stream-tubes, the closed end has no adjacent stream-tube and the break end represents the breach connected to the open air.

The numerical results are compared with the experimental ones regarding the density of the gas mixture, the concentration of each gas species produced by the graphite oxidation reaction and the onset time of the natural circulation of air. The experimental results showed that air entered the test model due to the molecular diffusion and the very week natural convection of the multicomponent gas mixed prior to the onset of the natural circulation of air. The calculated results are in good agreement with the experimental ones regarding the concentration changes in the gas species and the onset of the natural circulation of air.

References

[1] S. Saito, et al., Design of High Temperature Engineering Test Reactor (HTTR), Japan Atomic Energy Research Institute, JAERI-1332 (1994).

[2] M. Hishida, M. Fumizawa, T. Takeda, M. Ogawa and S. Takenaka, Researches on air ingress accidents of the HTGR, Nucl. Engng. Des. 144, 317-325 (1993).

[3] M. Hishida and T. Takeda, Study on air ingress during an early stage of a primary-pipe rupture accident of a high-temperature gas-cooled reactor, Nucl. Engng. Des. 126, 175-187 (1991).

[4] T. Takeda and M. Hishida, Studies on diffusion and natural convection of two-component gases, Nucl. Engng. Des. 135, 341-354 (1992).

[5] T. Takeda and M. Hishida, Studies on molecular diffusion and natural convection of multi-component gases, to be publiched in Int. J. of Heat and Mass Transfer.

ANALYSIS OF AIR INGRESS PROCESS DURING THE PRIMARY-PIPE RUPTURE ACCIDENT OF THE HTGR

Tetsuaki TAKEDA[*1], Makoto HISHIDA[*1], Shiryu IMANISHI[*2], and Satsuki TAKENAKA[*3]

[*1)] Nuclear Heat Application System Laboratory, JAERI

[*2)] Fujitsu Facom Information Processing Corporation

[*3)] Kawasaki Heavy Industries, Ltd.

ABSTRACT

In order to predict or analyze the process of air ingress during the primary-pipe rupture accident of HTGRs, it is very important to develop computer programs and to validate them by experiments. This paper describes a computer program, which is named FLOWGR, developed to analyze the process of air ingress during the first stage of the primary-pipe rupture accident. FLOWGR provides a numerical method for analyzing the transient thermal hydraulic behavior by solving the one-dimensional basic equations for continuity, momentum conservation, energy conservation of the gas mixture, and mass conservation of each gas species. The numerical results are in good agreement with the experimental ones regarding the density of the gas mixture, the concentration of each gas species produced by the graphite oxidation reaction and the onset time of the natural circulation of air.

1. INTRODUCTION

A primary-pipe rupture accident is one of the most common of accidents related to the basic design regarding the High Temperature Gas-cooled Reactor (HTGR). It is a guillotine type break of the main pipe of coaxial double tube at the nozzle part connecting to the bottom of the reactor vessel. When the primary-pipe rupture accident happens, one may consider that air entering into a reactor vessel reacts with high temperature graphite structures and causes temperature rise of the reactor core and corrosion of graphite components. Therefore, it is very important to make sure that the air ingress accident cannot seriously oxidize the graphite fuel elements to release the radioactive materials from the reactor core to the environment nor severely damage the graphite components to loose the integrity of the reactor internals.

A high-temperature engineering test reactor (HTTR) is now in its developmental stage at JAERI[1]. It is a graphite-moderated high-temperature gas-cooled thermal reactor. A schematic drawing of the HTTR and the coolant passages in the reactor are provided in Fig.1. A hot leg consists of an inner passage of a coaxial duct, a high-temperature outlet duct, a high-temperature plenum and fuel cooling channels. A cold leg consists of an annular passage of the coaxial duct, a bottom cover and an annular passage between the reactor vessel and permanent reflector. As the hot and cold legs are connected at the top cover, they make a kind of reverse U-shaped tube. When the primary-pipe rupture accident occurs, the high-pressure helium gas coolant in the reactor is forced out into the reactor container through the breach. Gas pressure should become balanced between the inside and outside of the reactor vessel after a few minutes. During this stage, called the depressurization stage, air is not able to enter the reactor core from the breach. After the depressurization stage, it is supposed that air enters the reactor core from the breach due to molecular diffusion and natural convection of a multicomponent gas mixture induced by the distribution of gas temperature and the resulting concentrations in the reactor. Density of the gas mixture in the reactor gradually increases as air enters by the molecular diffusion and natural convection of the gas mixture in the first stage of the accident. Finally, the second stage of the accident starts after natural circulation of the air occurs suddenly throughout the entire reactor[2].

Previous studies focused mostly on molecular diffusion and natural convection of the two-component gas mixture in a reverse U-shaped tube and in a simple test model of the HTTR[3,4]. Moreover, to investigate the basic features of the flow behavior of the multicomponent gas mixture, consisting of He, N_2, O_2, CO_2, CO, etc., experimental and numerical studies were performed on the combined phenomena of the molecular diffusion and the natural convection of the multicomponent gas mixture with the graphite oxidation reaction in the reverse U-shaped tube[5]. The numerical results of the density change of the gas mixture, the mole fraction changes of each type of gas species and the onset time of the natural circulation of air agree well with the experimental results.

To predict or analyze the process of air ingress during the accident, it is very important to develop computer programs and to validate them by experiments. This paper describes a computer program, which is named FLOWGR[6], developed to analyze the process of air ingress during the first stage of the primary-pipe rupture accident.

2. NUMERICAL ANALYSIS

2.1 Features of the program

FLOWGR provides a numerical method for analyzing the transient thermal hydraulic behavior by solving the one-dimensional basic equations for continuity, momentum conservation, energy conservation of the gas mixture, and the mass conservation of each gas species. The main features of FLOWGR are explained in the following:

(1) FLOWGR treats the gas mixture consisting of arbitrary components and takes into account the graphite oxidation and CO combustion reactions. The source and sink terms in the mass conservation equations resulting from these chemical reactions are expressed by the temperature dependent Arrhenius formula having rate constants which are specified by the user.

(2) The reactor system to be analyzed by FLOWGR is modeled as a network of one dimensional stream-tubes which represent components of the system such as a piping, plenum and reactor core. Each stream-tube is further divided into fluid volumes (control volumes or cells). There are three types of tube-ends: a normal, break and closed end. The normal end connects with adjacent stream-tubes, the closed end has no adjacent stream-tube and the break end represents the breach connected to the open air.

2.2 Basic equations

The basic equations (mass-based formulation) are as follows.

The equation of continuity for the gas mixture:

$$\frac{\partial \rho}{\partial t}+\frac{\partial(\rho u)}{\partial x}=\sum_{i=1}^{n} Q_i \quad . \tag{1}$$

The equation of mass conservation for each gas species:

$$\frac{\partial(\rho \omega_i)}{\partial t}+\frac{\partial(\rho u \omega_i)}{\partial x}=\frac{\partial}{\partial x}\left(\rho D_{i-m}\frac{\partial \omega_i}{\partial x}\right)+Q_i \quad , \tag{2}$$

for i=1 to n-1, and $\omega_n = 1-\sum_{k=1}^{n-1}\omega_k$.

The equation of energy conservation:

$$\frac{\partial(\rho c_p T)}{\partial t}+\frac{\partial(\rho u c_p T)}{\partial x}=\frac{\partial}{\partial x}\left(\lambda\frac{\partial T}{\partial x}\right)+\alpha\frac{L_h}{A_e}(T_w-T) \quad . \tag{3}$$

The equation of momentum conservation:

$$\frac{\partial(\rho u)}{\partial t}+\frac{\partial(\rho u^2)}{\partial x}=-\frac{\partial p}{\partial x}-\rho g\cos\theta-\frac{1}{2}\rho u|u|\left(\frac{f}{D_e}\right) \quad . \tag{4}$$

The equation of state for the gas:

$$pM_m=\rho RT \quad \text{or} \quad p=CRT \quad . \tag{5}$$

Here, t = time, x = path length co-ordinate, ρ = density, u = velocity, ω_i = mass fraction, n = number of component gases, $D_{i\text{-}m}$ = effective diffusion coefficient in the multicomponent gas mixture, Q_i = production or dissipation term of the mass conservation equation, p = fluid static pressure, T = gas temperature, T_w = wall temperature, C = molar density, g = acceleration of gravity, θ = inclination of flow direction, c_p = specific heat capacity at constant pressure, λ = thermal conductivity, R = gas constant, M_m = molecular weight of the gas mixture, D_e = effective diameter of the stream-tube, f = friction factor, α = heat transfer coefficient, A_e = flow area and L_h = length of heated periphery of the stream-tube. Friction factor (f) and heat transfer coefficient (α) corresponding to the fully developed laminar flow are used[7]. Viscosity (μ) and thermal conductivity (λ) of each gas species and the gas mixture is obtained using the Wilke method[8] and by the Eucken correlation[9], respectively.

The other set of the basic equations (molecule-based formulation) includes the equations of continuity (Eq.(6)) and of number of molecules conservation for each gas species (Eq.(7)) instead of Eq.(1) and Eq.(2). The equation of continuity for the gas mixture:

$$\frac{\partial C}{\partial t}+\frac{\partial (Cu)}{\partial x}=\sum_{i=1}^{n}\left(Q_i/M_i\right) \qquad (6)$$

The equation of number of molecules conservation for each gas species:

$$\frac{\partial (CX_i)}{\partial t}+\frac{\partial (CuX_i)}{\partial x}=\frac{\partial}{\partial x}\left(CD_{i-m}\frac{\partial X_i}{\partial x}\right)+Q_i/M_i \qquad (7)$$

for i=1 to n-1, and $X_n=1-\sum_{k=1}^{n-1}X_k$.

where X_i = mole fraction for the component gas i, M_i = molecular weight. In this set of equations, the conservation equation of momentum (Eq.(4)) and the equation of state for the gas (Eq.(5)) are used. However, the equation of energy conservation (Eq.(3)) is omitted based on the assumption that the gas temperature is equal to the wall temperature.

The diffusion coefficients $D_{i\text{-}m}$ for the multicomponent gas system are obtained from the diffusion coefficients for the binary gas system and the mole fractions of each gas species.

$$D_{i-m}=\frac{1-X_i}{\sum_{j=1}^{n}\frac{X_j}{D_{i-j}}} \qquad (8)$$

This coefficient is called the effective diffusion coefficient in the multicomponent gas mixture, which is provided by references [10,11,12].

In the present analysis, the graphite oxidation reaction (C-O_2 reaction) and the carbon monoxide combustion (CO-O_2 reaction) are taken into account. The dissipation or generation terms Q_i of the mass

conservation equations for O_2, CO and CO_2 are written as:

$$Q_i = Q_i^{(1)} + Q_i^{(2)}, \tag{9}$$

where $Q_i^{(1)}$ is the term for the graphite oxidation reaction and $Q_i^{(2)}$ the one for the CO combustion. Using the arrhenius formula, these terms are

$$Q_i^{(1)} = K_i^{(1)} \exp\left(-\frac{E_1}{RT}\right), \tag{10}$$

$$Q_i^{(2)} = K_i^{(2)} \exp\left(-\frac{E_2}{RT}\right), \tag{11}$$

where $K_i^{(1)}$ and $K_i^{(2)}$ are constants, E_1 and E_2 the activation energies. Details of these constants and activation energies are explained in reference[5].

2.3 Numerical methods

The numerical methods are based on replacing the system of differential equations with a system of finite-difference equations fully implicit in time except the convection term for the momentum equation which is treated explicitly. This results in a set of discretized nonlinear equations are solved by iteration procedure. In each iteration the implicit terms are formulated to be linear in the dependent variables at new time. The resulting linear systems are solved by direct inversion or Gauss-Seidel iteration.

The finite-difference equations used in FLOWGR can be obtained by integrating the conservation equations over a fixed fluid volume. The fluid volumes are connected by the junctions used to transfer fluid into and out of the fluid volumes. A general flow path description is shown in Fig.2. The scalar properties (pressure, temperature, etc.) of the flow are defined at the volume centers, while vector quantity (velocity) is defined at the junctions. The equations of continuity and mass conservation (Eqs.(1) and (2)), and the equation of energy conservation (Eq.(3)) for the mass-based formulation as well as the equations (Eqs.(6) and (7)) for the molecule-based formulation are integrated with respect to the spatial variable x from the junction at x_j to the junction at x_{j+1}. The equation of momentum conservation (Eq.(4)) is integrated with respect to the spatial variable from the volume center at $x_{j+1/2}$ to the adjacent volume center at $x_{j+3/2}$. In this integration loss of pressure is taken into account at the volume boundary with abrupt area change. The fluxes due to convection and diffusion which appear in the integrated equations are approximated using the Hybrid difference scheme according to D.B.Spalding[13,14].

The finite-difference equations thus obtained can be solved by setting the initial and boundary conditions. The initial conditions for the temperature, pressure and mole fractions for each component gas are specified at the volume centers and those for velocities at the junctions. It is assumed that the gas

velocities are zero for the initial condition. As for the boundary conditions, the pressure, temperature, mole fractions of each gas species are specified at the end of the stream-tube which has the break end. The wall temperature of the stream tubes is also specified for each control volume as a function of time. At the closed ends of the stream-tubes, the boundary conditions are that the flow velocity and fluxes due to convection and diffusion are zero.

In order to obtain stable and fast convergence of the nonlinear equations, the equations of continuity and of momentum conservation for the gas mixture linearized by the pressure and velocity are solved using the SIMPLER method proposed by S.V.Patankar[13] along with the other conservation equations linearized by the mass (mole) fractions and temperature. In this iteration procedure numerical relaxation is applied for the production and dissipation terms as well as for the dependent variables in such a way that

$$\Gamma_{new} = \delta\Gamma_{cal} + (1-\delta)\Gamma_{old} \qquad (12)$$

where Γ_{new} is a new value, Γ_{cal} a calculated value without the relaxation, Γ_{old} an old value and δ is a relaxation parameter, the value of which is chosen in a range $0<\delta<1$.

3. COMPARISON WITH EXPERIMENTS

In order to investigate the effect of the graphite oxidation reaction on the air ingress behavior in the first stage of the accident, the simulation test of the primary-pipe rupture accident was performed. Figure 3 shows an experimental apparatus, which consists of a reactor core simulator, a high-temperature plenum, a water-cooled jacket corresponding to the reactor vessel and simulated inlet and outlet pipes corresponding to the coaxial tube. A gas flow loop is equipped with this test model, which simulates the primary cooling system of the HTTR. The reactor core simulator has 4 graphite tubes and a ceramic plenum. The graphite tube has an inner diameter of 40mm and a length of 800mm. Three graphite support posts can be inserted into the high-temperature plenum. To measure an ingress velocity of air, an ultrasonic anemometer is equipped with the lower end of the outlet pipe. The temperatures of the gas mixture, the reactor core simulator and other structures were measured by 124 thermocouples. Density of the gas mixture, concentrations of O_2, CO and CO_2 were continuously measured at the inlet and outlet pipes, the high-temperature plenum, the top space and the annular passage between the inner barrel and the water cooled jacket.

We analyzed the experimental results of the density and mole fraction changes in the apparatus. The apparatus is modeled as a network consisting of one dimensional stream-tubes. Figure 4 shows the network model of the apparatus. At the beginning of the experiment, the experimental apparatus was filled with helium gas. When the temperature of the gas and the reactor core simulator reached a steady-state,

the valves located at the ends of the inlet and outlet pipe were opened at the same time to simulate the pipe rupture accident condition.

The parameters of the stream-tubes are listed in table 1. To analyze the experimental result by FLOWGR, we employed the molecule-based formulation instead of the mass-based formulation. In the preliminary calculations, we calculated the process of air ingress in a reverse-U-shaped tube model with the graphite oxidation reaction by the two sets of formulations. It has been revealed that fairly good agreements are obtained between the calculated results of the two sets of formulations with respect to the concentration changes of each gas species and the onset time of the natural circulation of air. It has also been revealed that the computations by the mass-based formulation take two to three times as much time as those by the molecule-based formulation. A typical computation time for a system having 88 cells is 23 minutes for the molecule-based formulation and 63 minutes for the mass-based formulation. In case of the reverse-U-shaped tube model, the matrix structure of the simultaneous linear systems is of simple tridiagonal type. In this case the linear systems are efficiently solved by direct inversion. For the model which has a complex network with many stream branches as shown in Fig. 4, discretized equations are expressed by sparse matrices having a large band width. In this case much more computation time is expected to be required. So we decided to analyze the experimental model by the molecule-based formulation and to use Gauss-Seidel iteration which is suitable to solve the linear systems with such matrices.

Figures 5,6,7 and 8 show an example of the measured density and mole fraction changes of O_2, CO_2 and CO at various measuring points. The average temperature of the reactor core simulator is 700℃. The mole fractions of CO and CO_2 in the plenum and the top cover gradually increase by molecular diffusion and the very weak natural circulation until the onset of the natural circulation of air. The first stage of the accident lasted for about 7 days. From this study, it became clear that air ingress process is completely different in the first and second stages. The important mechanisms of the air ingress in the first stage of the accident are molecular diffusion and the very weak natural circulation of the gas mixture. It also became clear that the duration of the first stage period is fairly long.

The numerical results compared with the experimental ones are also shown in Figs. 5,6,7 and 8. As can been seen from these figures, the onset time of the natural circulation of air is fairly well reproduced and considerable agreements between the experiment and calculation are obtained for the density of the gas mixture and the mole fractions of each gas species. In the present analysis, the CO combustion reaction was neglected in the low temperature condition (T<700℃).

4. CONCLUDING REMARKS

A computer program has been developed to analyze thermal-hydraulic behavior during the first stage of the primary-pipe rupture accident of the HTGR. It has been revealed the program is sufficiently versatile to analyze transient behavior during the accident. The program was validated with the simulation experiment.

However, it is important to find the efficient computational algorithms, taking into account the use of vector or parallel computers, in order to get even faster computation. Transient calculations for the primary-pipe rupture accident require a time period spanning many hours or days. The computation time was about 20 hours in the present calculation.

REFERENCES

[1] S. Saito, et al., Design of High Temperature Engineering Test Reactor (HTTR), Japan Atomic Energy Research Institute, JAERI-1332 (1994).

[2] M. Hishida, M. Fumizawa, T. Takeda, M. Ogawa and S. Takenaka, Researches on air ingress accidents of the HTGR, Nucl. Engng. Des. 144, 317-325 (1993).

[3] M. Hishida and T. Takeda, Study on air ingress during an early stage of a primary-pipe rupture accident of a high-temperature gas-cooled reactor, Nucl. Engng. Des. 126, 175-187 (1991).

[4] T. Takeda and M. Hishida, Studies on diffusion and natural convection of two-component gases, Nucl. Engng. Des. 135, 341-354 (1992).

[5] T. Takeda and M. Hishida, Studies on molecular diffusion and natural convection in a multicomponent gas system, Int. J. of Heat and Mass Transfer 39-3(1996) 527-536.

[6] M. Hishida, S. Imanishi, T. Takeda, and S. Takenaka, A Computer Program for Analyzing Air Ingress Process During the First Stage of the Primary Pipe Rupture Accident of the HTGR, Proc. of the 9th Power Plant Dynamics, Control & Testing Symposium, (1995)

[7] R. K. Shah and A. L. London, Advances in Heat Transfer : Laminar Flow Forced Convection in Ducts (Academic, New York, 1978) pp. 78.

[8] C. R. Wilke, J.Chem. Phys. 18 (1950) 517.

[9] R. C. Reid, J. M. Prausnitz and T. K. Sherwood, The Properties of Gases and Liquids, 3rd Edn. (McGraw-Hill, New York, 1977) pp. 37-40, 226, 410-414, 470-474, 548-565.

[10] C. R. Wilke, Diffusional properties of multicomponent gases, Chem. Eng. Prog. 46 (1950) 95-104.

[11] D. F. Fairbanks and C. R. Wilke, Diffusion coefficients in multicomonent gas mixture, Ind. Eng. Chem. 42 (1950) 471-475.

[12] R. E. Walker, N. de Haas and A. A. Westenberg, Measurements of multicomponent diffusion coefficients for the CO2-He-N2 system using the point source technique, J. Chem. Phys. 32(1960) 1314-1316.

[13] S. V. Patankar, Numerical Heat Transfer and Fluid Flow, (McGraw-Hill, New York, 1980).

[14] D. B. Spalding, A novel finite-difference formulation for differential expressions involving both first and second derivatives, Int. J. Num. Methods Eng., vol 4, 551.

Table 1 Parameters of the stream-tubes

Path number	Path name	Length (m)	Diameter (m)	Vertical angle (deg.)	Number of cells	Wall temp.(℃)	Graphite oxidation
1	Outlet pipe	1.431	0.0763	0	9	19.8	no
2	Plenum	0.15	0.4	0	3	685	no
3	Central graphite pipe	0.8	0.04	0	8	700	yes
4	Central ceramic pipe	0.535	0.04	0	2	462.7	no
5	Peripheral graphite pipe	0.8	0.0693	0	2	700	yes
6	Peripheral ceramic pipe	0.535	0.0693	0	2	462.7	no
7	Thermal insulator	1.471	0.736	0	2	700	no
8	Top cover	0.46	0.733	90	2	88.2	no
9	Annular passage	1.471	0.454	180	15	200	no
10	Bottom cover	0.46	0.413	90	3	35.2	no
11	Coaxial pipe	0.406	0.163	180	2	20.6	no
12	Inlet pipe	0.543	0.0693	90	3	21.2	no
13	Inlet pipe	0.5	0.0693	180	3	21.2	no

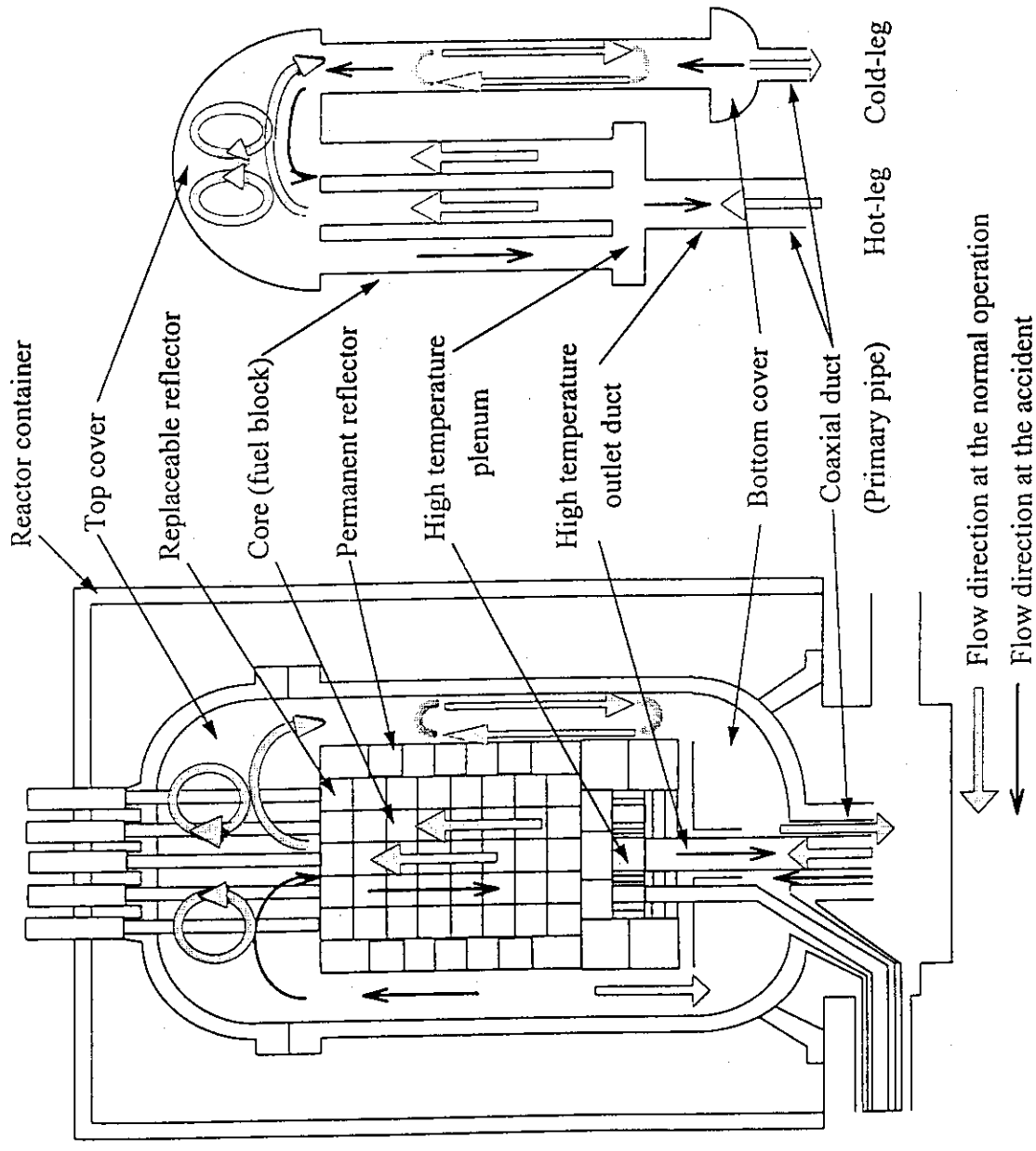


Fig.1 Schematic drawing of the HTTR and the coolant passages in the reactor.

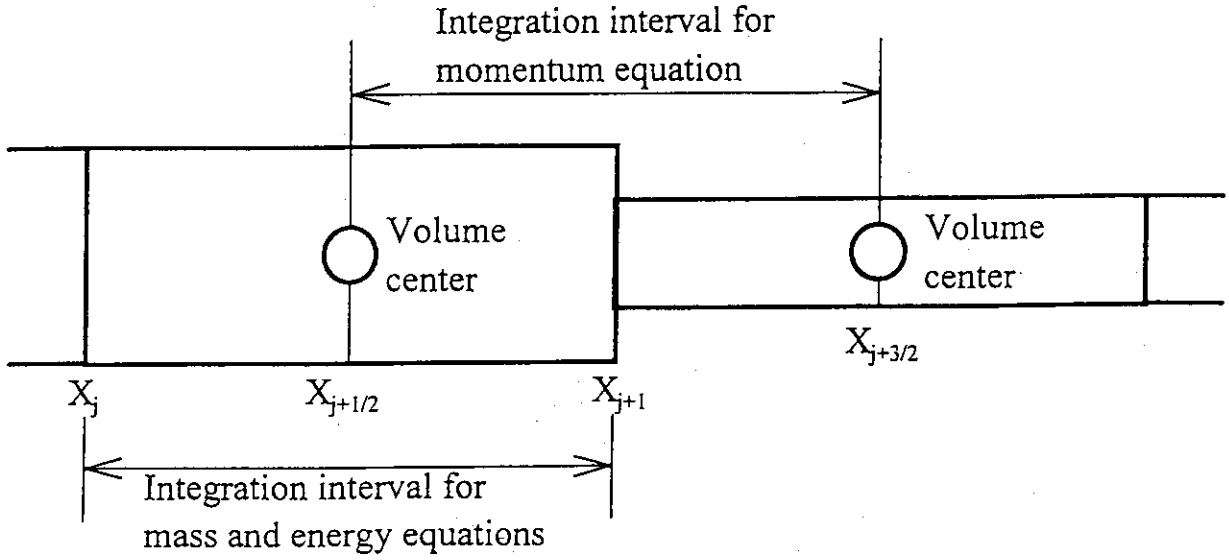


Fig.2 Flow path control volume

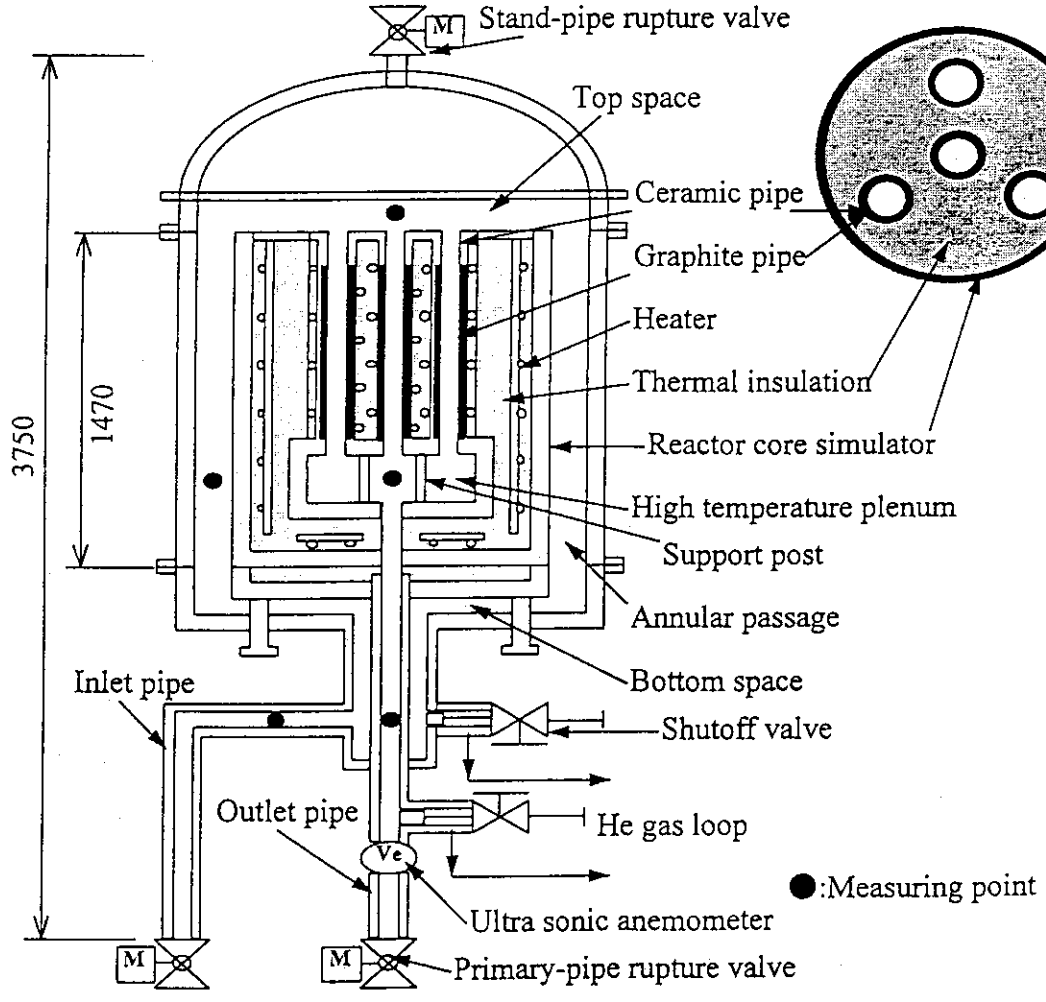
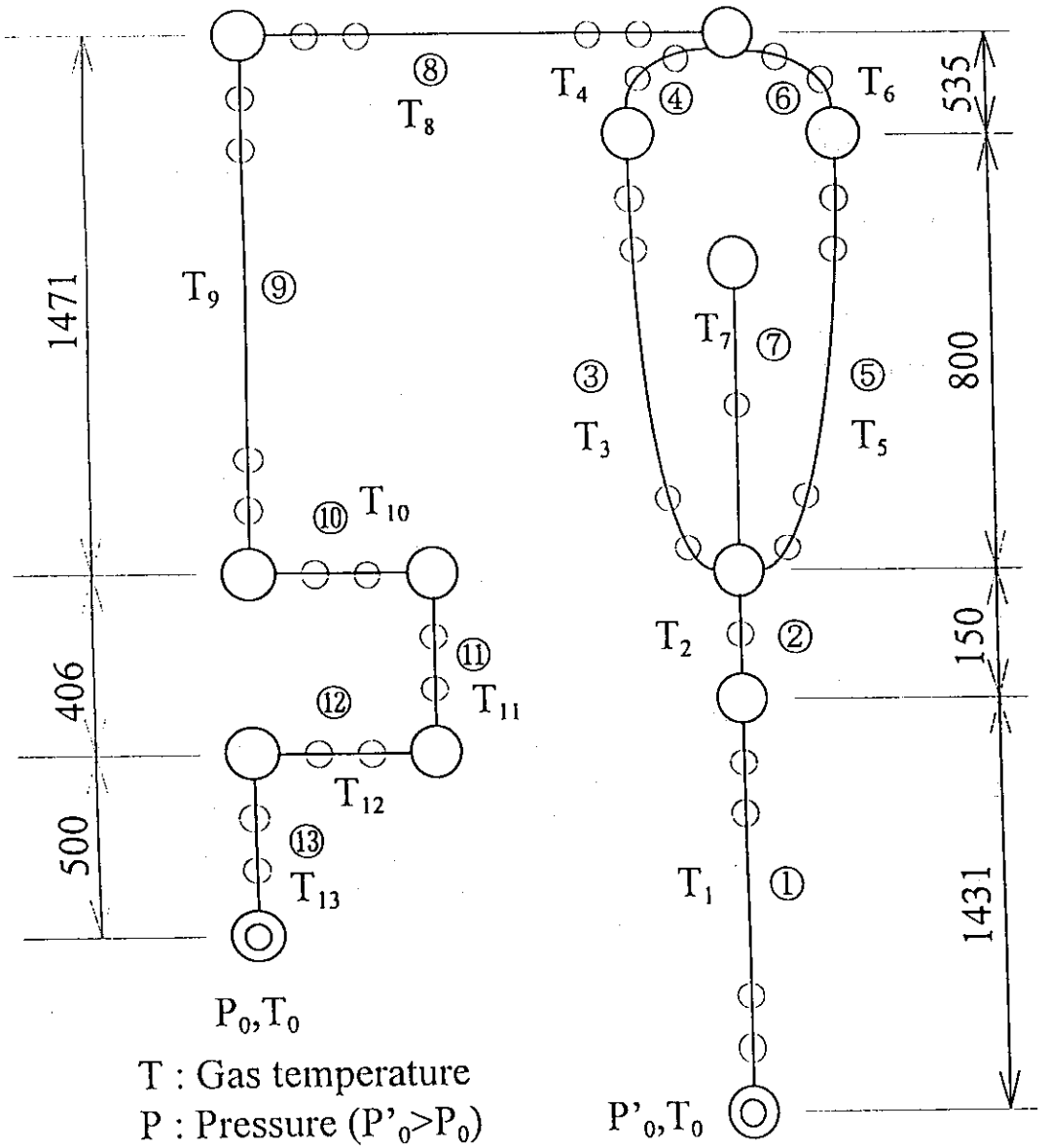


Fig.3 Schematic drawing of the experimental apparatus



Flow paths

① Middle temperature outlet pipe
② High temperature plenum
③ Central graphite pipe
④ Central ceramic pipe
⑤ Peripheral graphite pipe
⑥ Peripheral ceramic pipe
⑦ Thermal insulator (dead end)
⑧ Top cover
⑨ Annular passage
⑩ Bottom cover
⑪ Coaxial pipe
⑫ Inlet pipe (horizontal)
⑬ Inlet pipe (vertical)

Fig.4 Network model of the experimental apparatus

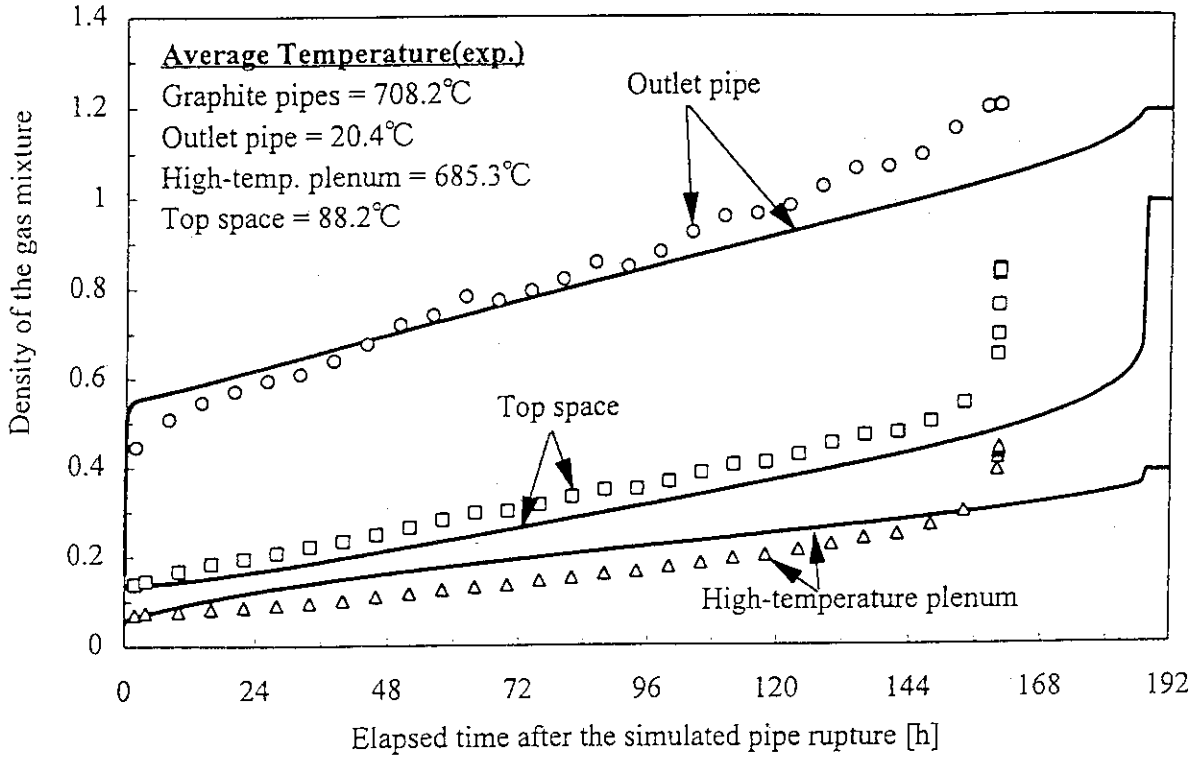


Fig.5 Density change of the gas mixture

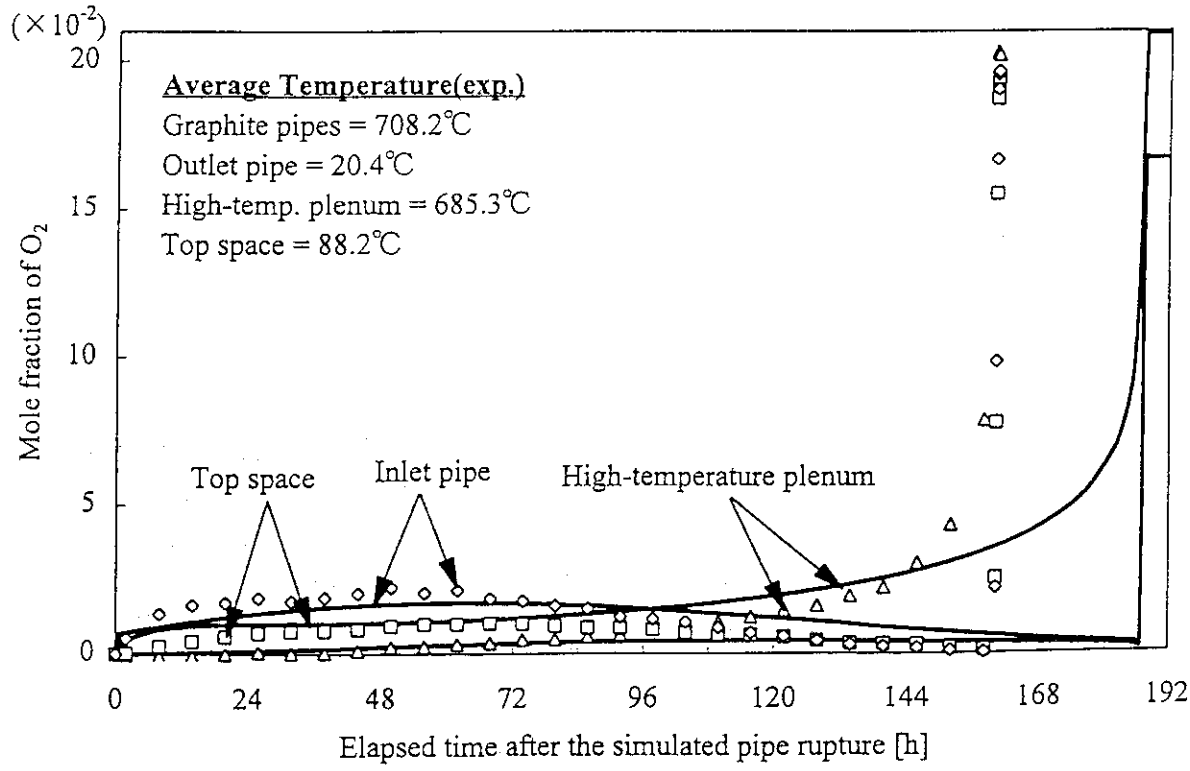


Fig.6 Mole fraction change of O_2

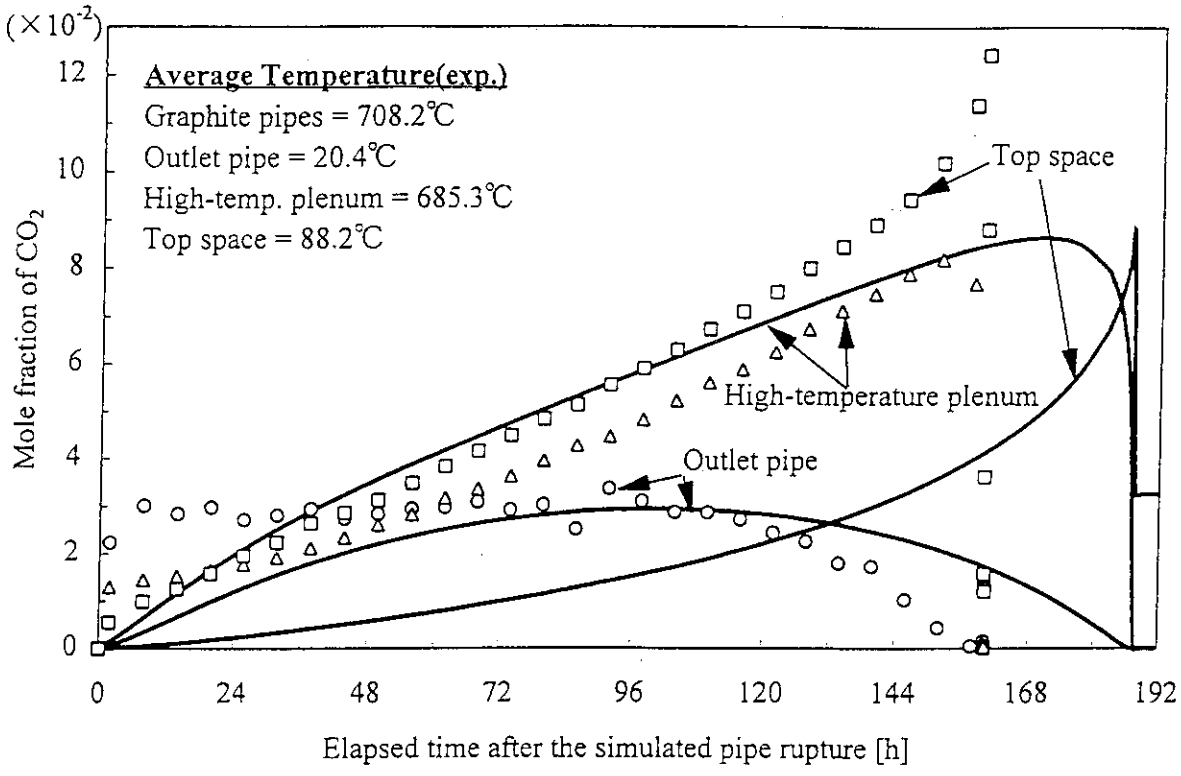


Fig.7 mole fraction change of CO_2

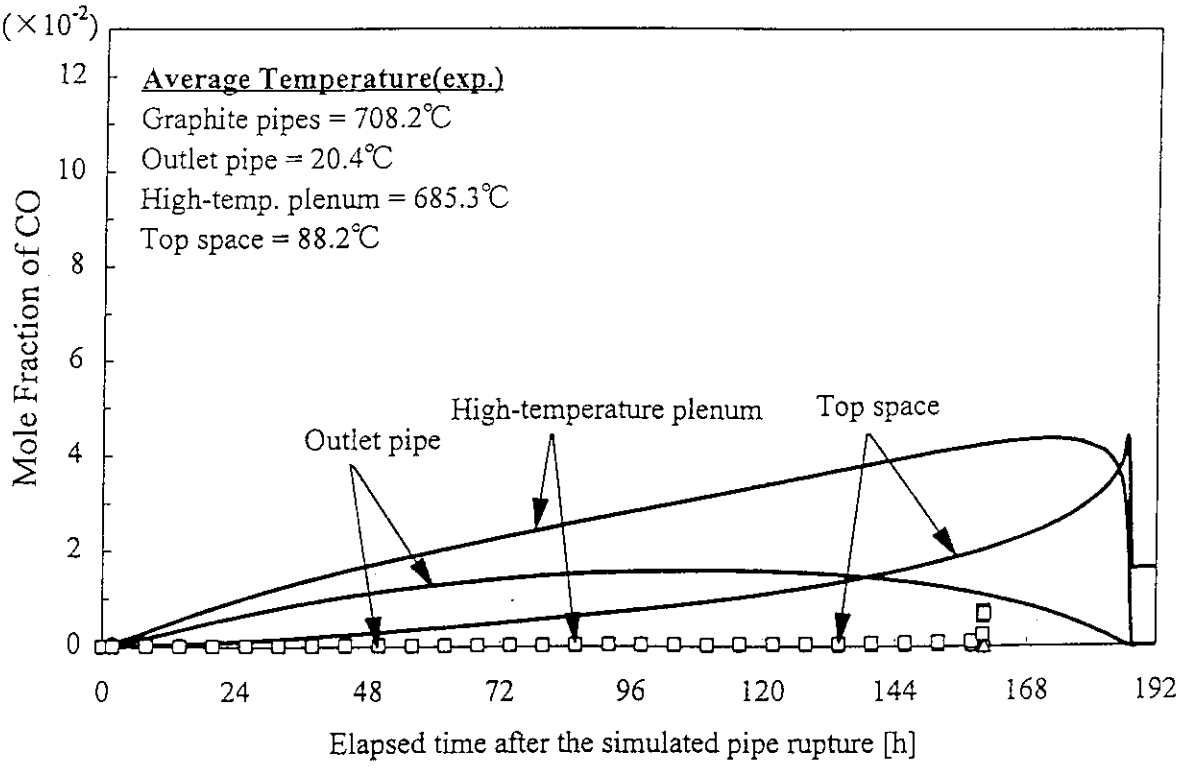


Fig.8 Mole fraction change of CO

6.4 Availability of steam generator against thermal disturbance of hydrogen production system coupled to HTGR

Taiju SHIBATA, Tetsuo NISHIHARA,
Kazuhiko HADA and Shusaku SHIOZAWA

Japan Atomic Energy Research Institute
JAPAN

ABSTRACT

One of the safety issues to couple a hydrogen production system to an HTGR is how the reactor coolability can be maintained against anticipated abnormal reduction of heat removal (thermal disturbance) of the hydrogen production system. Since such a thermal disturbance is thought to frequently occur, it is desired against the thermal disturbance to keep reactor coolability by means other than reactor scram. Also, it is thought that the development of a passive cooling system for such a thermal disturbance will be necessary from a public acceptance point of view in a future HTGR-hydrogen production system.

We propose a SG as the passive cooling system which can keep the reactor coolability during a thermal disturbance of a hydrogen production system.

This paper describes the proposed steam generator (SG) for the HTGR-hydrogen production system and a result of transient thermal-hydraulic analysis of the total system, showing availability of the SG against a thermal disturbance of the hydrogen production system in case of the HTTR-steam reforming hydrogen production system.

Availability of steam generator against thermal disturbance of hydrogen production system coupled to HTGR

Taiju SHIBATA, Tetsuo NISHIHARA
Kazuhiko HADA and Shusaku SHIOZAWA

Japan Atomic Energy Research Institute
JAPAN

1. Introduction

High temperature heat of about 1000°C offered by an HTGR is expected to be available for industrial chemical process such as a hydrogen production. HTGR-hydrogen production system would play an important roll to resolve global CO_2 emission problem, because the system can produce hydrogen as a clean energy source without CO_2 emission, which is different from the conventional fossil burning system.

Nuclear heat from the HTGR will be transferred to the hydrogen production system by helium gas. This heat will be utilized at a hydrogen production high temperature chemical reactor at first, and then at heat exchangers such as a steam generator (SG), installed in series in the helium loop.

One of the safety issues to couple the hydrogen production system to the HTGR is how the reactor coolability can be maintained against anticipated abnormal reduction of heat removal (thermal disturbance) of the hydrogen production system. Since such a thermal disturbance is thought to frequently occur, it is desired against the thermal disturbance to keep reactor coolability by means other than reactor scram. Also, it is thought that the development of the passive cooling system for such a thermal disturbance will be necessary from a public acceptance point of view in a future HTGR-hydrogen production system.

2. System arrangement and SG

Japan Atomic Energy Research Institute (JAERI) has been constructing the High Temperature Engineering Test Reactor (HTTR) at the Oarai Research Establishment. The HTTR will attain its first criticality in 1997. The HTTR is the first HTGR in Japan

with thermal output of 30MW and a reactor outlet coolant temperature of 950°C at high temperature test operation.

JAERI is planning to couple a steam reforming hydrogen production system to the HTTR through helium-to-helium intermediate heat exchanger (IHX). Figure 1 shows flow scheme of the HTTR-steam reforming hydrogen production system. The hydrogen production system comprises a steam reformer (SR), a super heater (SH), a SG, etc..

The IHX is designed to transfer 10MW of a part of the reactor thermal output to the hydrogen production system. The secondary helium heat will be removed by the SR, the SH and the SG in sequence. At the SR, approximately 4MW of the secondary helium heat will be utilized for steam reforming reaction to produce hydrogen from process gas which is a mixture of steam and methane. Steam reforming reaction is an endothermic chemical reaction and occurs at 600°C or above. Downstream the SR in the helium loop, the rest of the secondary helium heat will be utilized to generate superheated steam through the SH and the SG. Then, the secondary helium gas will be returned to the IHX after 10MW of heat removal at steady state in normal operation.

Regardless of the SG inlet helium temperature, the SG outlet helium temperature will be a saturation temperature of steam because of large latent heat of steam. If the SG inlet helium temperature increases, the quality of steam increases naturally under constant pressure, and therefore the SG outlet helium temperature remains constant. As can be understand, this SG has a feature that its outlet helium temperature is controlled in passive manner in normal operation.

JAERI has been conducting a study about the SG to be a passive safety system in order to mitigate a thermal disturbance of the hydrogen production system. In our design, the SG has a large volume steam drum so as not to lose storage water to keep reactor coolability. We are trying to realize this cooling function of the SG in passive manner by making use of natural circulation of water and natural convection of air.

3.Transient analysis of the HTTR-hydrogen production system

Figure 2 exemplifies a transient response of helium gas temperatures at abnormal decrease of process gas flow rate at the

HTTR-steam reforming hydrogen production system shown in Fig.1. The analysis was made by the IRIS (Integrated tRansient thermal-hydraulIcs computer code System for HTGR with heat utilization system) code developed by the authors[1]. At the SR feed process gas flow rate 20% stepwise decrease, the SR and the SH outlet helium temperatures increase about 10°C slowly, as expected. However, the SG outlet helium temperature remains almost constant. Therefore, the IHX outlet primary helium temperature is found to remain almost constant. This result suggests that the SG has an availability to keep the reactor coolability without causing reactor scram during thermal disturbance of the hydrogen production system.

Therefore we propose that thermal disturbance of the hydrogen production system to be connected to the future HTGR should be mitigated by the SG so as to keep reactor coolability, passively.

4.Conclusions

The following conclusions were delivered from the present study.

(1) Thermal-hydraulics analysis of the HTTR-steam reforming hydrogen production system using the IRIS code shows that the SG has an availability to keep reactor coolability without causing reactor scram during a thermal disturbance of the hydrogen production system.

(2) Therefore, we propose that reactor coolability should be maintained during a thermal disturbance by the SG in passive manner in the future HTGR-hydrogen production system.

Reference

1) HIRANO, M. and HADA, K., JAERI-M 90-071, (1990).

The IRIS code was developed by the authors based on the THYDE-HTGR code described in reference 1).

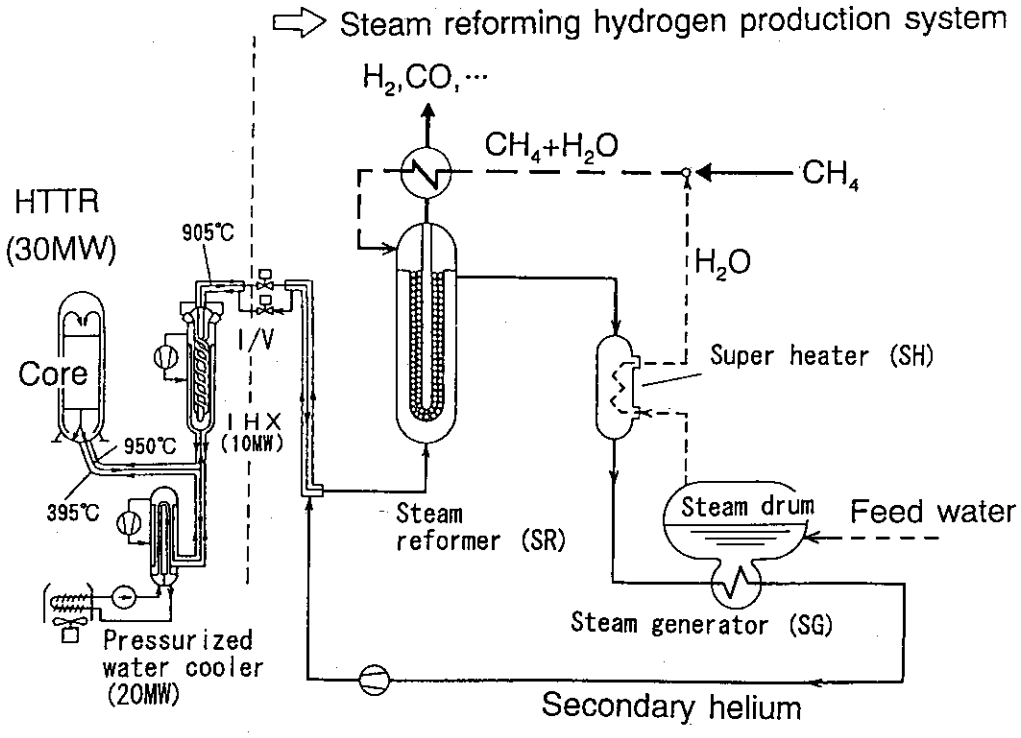


Fig.1 Flow scheme of the HTTR-steam reforming hydrogen production system.

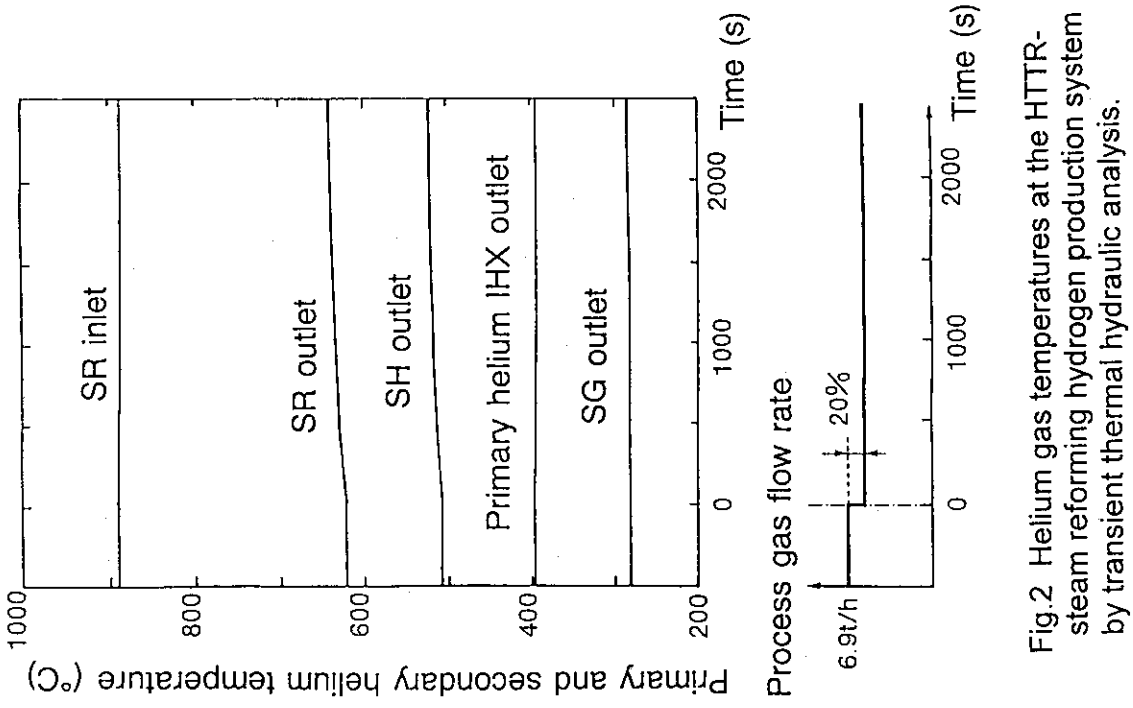


Fig.2 Helium gas temperatures at the HTTR-steam reforming hydrogen production system by transient thermal hydraulic analysis.

6.5 ON THE IMPROVEMENT OF HTGR FUEL ELEMENTS CORROSION RESISTANCE

Chernikov A.S. and Kurbakov S.D.

State Scientific and Industrial Association LUTCH, Russia

ABSTRACT

One of the main HTGR safety factor is the reliability of uranium-graphite fuel elements provided on the one hand by the manufacturing technology and quality of the used materials, and on the other hand by the fuel element design (multistage barrier on the path of radionuclides migration). Combination of this features makes it possible to retain fission products inside the fuel element and to preserve the required level of mechanical, physical, irradiation and other characteristics during the operation.

At the same time various accidents (failure of coolant circuit, failure of steam generator pipeline, unsealing of protective cladding, etc.), including hypothetical, e.g. ingress of large amounts of air into reactor core and reaction of air with fuel elements matrix graphite causing as a result possible failure of fuel elements.

Two approaches proposed to improve fuel elements corrosion resistance are discussed in the paper. The first one is based on a purification of fuel elements matrix graphite from impurities, for example iron being a catalyzer of corrosion process. The other is coating of outer surface of fuel element by protective layers. Two types of ceramic materials are considered in the paper for practical realization of the second approach - silicon carbide and aluminum phosphate. Silicon carbide layer is deposited by pyrolysis of methylthreeclorinesilane or by carbonization of polycarbosilanes.

The results of comparative corrosion tests at the air during 1 h at the temperature 1600 C are presented. It was shown that silicon carbide coating deposited by pyrolysis of methyl-threeclorinesilane has more corrosion resistance at the air and are preferable for protection of fuel elements.

CORROSION RESISTANCE OF HTGR FUEL ELEMENTS

A.S. Chernikov, S.D. Kurbakov, A.I. Vavilin

Scientific and Industrial Association LUTCH

Russia

ABSTRACT

The results of corrosion tests of matrix graphite based on calcinated (30PG graphite) and non-calcinated (MPG graphite) petroleum cokes in helium containing 0.01-1 vol.% water vapour in the temperature range 600-1200°C are presented.

The results of investigation of matrix graphite components reactivity are considered. It is shown that the filler graphite 30PG has the minimum activity towards the water vapour.

The influence of impurities content on the oxidation rate are considered.

The results of corrosion tests of matrix graphite coated with protective layers (silicon carbide and aluminium phosphates) in the air environment at 1600°C, 1 h, are given.

1. INTRODUCTION

One of the main HTGR safety factor is the reliability of uranium-graphite fuel elements provided, on the one side, by the manufacture technology level and quality of raw materials, and, on the other side, by fuel elements design (multi-layer barrier on the path of migration of radionuclides). Combination of these factors provides fission products retention inside the fuel element volume and the possibility to keep the required level of fuel element mechanical, thermophysical, radiation and other characteristics.

At the same time designing of HTGR includes into consideration various accident situations (failure of coolant circuit, of steam generator pipe line, of containment etc.) including hypothetical, such as the possibility of water or air ingress into the core of reactor resulting in the essential interaction with matrix graphite of fuel elements. Therefore especial attention during the development of HTGR fuel elements (FE) is paid to the investigations of matrix graphite corrosion in helium containing water vapours and at the air. Some results of these investigations are considered in the paper.

II. EXPERIMENTAL DETAILS

Cylindrical matrix graphite specimens (D = 6 mm, L = 20 mm) used for experiments were cut of fuel element imitator on the basis of calcinated (30PG graphite) and non-calcinated (MPG graphite) petroleum cokes. Some characteristics of the tested specimens are given in Table 1.

Table I.

Characteristics of matrix graphite specimens for corrosion tests

Properties / Material	30PG-matrix graphite	MPG - matrix graphite
Filler	Calcinated petroleum coke	Non-calcinated petroleum coke
Binder	Coal-tar pitch,20%	Coal-tar pitch, 20%
Method of ball manufacture	Compacting and sintering	Compacting and sintering
Temperature of final heat treatment, °C	1800	1800
Density, g/cm^3	1,9	1,9
Total ash content, %	≤ 0,03	≤ 0,03
Bending strength, MPa	24	34

Corrosion rate was measured by thermogravimetry method at TAG 24 Setaram with automatic balance continuously recording the change of specimen mass, accuracy of temperature stability was ±0.5 K and mass change error ± 10 μg.

Investigations of corrosion were performed in a gas mixture flow at pressure 0.12 MPa, gas flow was laminar with Reynolds numbers in the range of 0.1 - 1.0, temperature range was 600-1200 °C, water vapour content (C_{H_2O}) was in the range of 0.01 - 1.0 vol.%. RMS error of corrosion rate measurement was not greater than 10%.

Besides these tests the estimation of corrosion resistance of matrix graphite specimens coated by silicon carbide or by aluminium phosphate was carried out in the air environment at 1600 °C during 1 h.

Specimens were coated using gas-phase pyrolisis of CH_3SiCl_3-H_2-Ar mixture at 1600 °C and by pyrolisis of solution of polycarbosilane in toluene as well, samples of matrix graphite on the base of non-calcinated petroleum coke were impregnated beforehand by this solution. Specimens coated by aluminium phosphate were prepared by impregnation with

mixture of aluminium hydroxide and phosphoric acid solution and heat treated. Thickness of layers was in the range of 10-30 μm.

Besides the above-mentioned thermogravimetry method, the standard techniques such as measurement of specific magnetic susceptibility (Faraday method), specific free surface (BET-method, low-temperature krypton adsorption), pore size distribution (mercury porometry), electrical resistivity (four point method), density (hydrostatic weighing) were used to determine matrix graphite components reactivity as well as the influence of porous material structure on corrosion rate.

III. RESULTS AND DISCUSSION

Typical curves of reaction rate of water vapour with matrix graphite vs. burn-off are presented in Fig. 1. The unstationary process of oxidation in a wide range of burn-off results in a significant inaccuracy of corrosion rate measurements. It is seems that the full characteristic of material corrosion resistance is given perhaps by maximum value of corrosion rate attainable due to stabilisation of reacting porous graphite layer. At the same time this value is conservative because it is obtained at high material burn-off accompanied by reacting layer crumbling. The conservative values of corrosion rate are given below. Experimental curves of matrix graphite corrosion rate vs. temperature are given in Fig. 2. The peculiar feature of the attained relationships is their two-stage character. The experimental data were processed according to well-known macrokinetics equations primarily derived by Ya.B.Zeldovich [1]:

$$W = \beta (Co-Cs) \quad (1)$$

$$W = \sqrt{((2/(n+1)) Di\ KiCs^{n+1}} \quad (2)$$

where W - corrosion rate, $kg/m^2.s$;

Co - oxidant concentration (C_{H2O})in a volume;

Cs - oxidant concentration on the specimen surface;

β - mass transfer coefficient, β=NuD/d, where Nu-Nusselt number; D- interdiffusion coefficient, d -specimen typical size;

Di - oxidant effective diffusion coefficient in a specimen volume (considered to be constant);

Ki - reaction rate constant;

n - reaction order.

Experimental data analysis in accordance with equations (I) and (2) shows that the first range (T ≤ 960°C) in Fig. 3 corresponds to kinetics determined by the chemical interaction rate. In this range the corrosion rate is satisfactorily approximated by the equations:

$$W_{3OPG} = 5.5 \times 10^{7} \exp(-33600/T) \times C^{0.65}$$
$$W_{MPG} = 7.2 \times 10^{6} \exp(-30800/T) \times C^{0.65} \quad (3)$$

The second temperature range 960° < T ≤ 1200°C corresponds to kinetics determined by water vapour diffusion transfer through matrix graphite pores. In this range the corrosion rate is expressed by the equation:

$$W_{3OPG} = 123.\exp(-14344/T)C$$
$$W_{MPG} = 36.\exp(-12530/T)C \quad (4)$$

In the investigated temperature range (600-1200°C) the variation of apparent activation energy takes place from 267 kJ/mole down to 115 kJ/mole for 30PG matrix graphite and from 244 kJ/mole down to 104 kJ/mole for MPG matrix graphite.

Boundaries of corrosion mechanisms realization and corrosion rates are determined not only by test conditions but physical and chemical properties of the initial material as well. It is known that corrosion rate of carbon-graphite materials depends, for example, on the graphitization degree. Thus, poorly graphitized binder coke residue is subjected to corrosion in the first place [2]. The investigation of filler and binder reactivity of 30PG and MPG matrix graphites was carried out. Magnetic susceptibility was chosen as a characteristic of matrix graphite. The magnetic susceptibility is an additive value of material phase components [3] and submits to the equation:

$$\chi_{mg} = (1-x)\chi_f + x\chi_b \quad (5)$$

where χ_{mg}, χ_f, χ_b are specific magnetic susceptibility of matrix graphite, filler and binder, respectively;

x - coke yield from the binder.

The results shows (Table 2) that 3OPG filler graphite has a minimum reactivity towards the water vapor. MPG phase components have approximately the same reactivity.

As it was shown above, matrix graphite corrosion under these conditions has the volume character. Consequently corrosion rate of matrix graphite should depend on their porous structure. The porous structure of these matrix graphites has bimodal pore distribution. Both materials have approximately the same pore volume of 0.065-0.066 cm^3/g and specific free surface of 0.3-0.4 m^2/g. Oxidation leads to significant changes of the porous structure. For example, oxidation of 30PG matrix graphite specimen to 3 mass % burn-off pore resulted in volume increase by 50%, and free surface increase by 1.5 order.

Table 2

Average values of specific magnetic susceptibility of matrix graphites and their phase components at the temperature 20°C

Material	Specific magnetic susceptibility, GGS/g x10^6	
	Initial	Oxidized, T=1000 °C, C_{H_2O}=1.0 vol.%
30PG filler graphite	-6,1	-6,1
MPG filler graphite	-5,6	-5,6
Binder coke	-3,6	-3,6
30PG matrix graphite	-5,82	-5,95
MPG matrix graphite	-5,4	-5,42

Increase of matrix graphite specimen porosity as a result of corrosion leads to their mechanical strength decrease. Thus, bending tests of MPG matrix graphite specimens after corrosion at T = 1000 °C, C_{H_2O} = 1 vol.% and burn-off of 10 mass % showed 2 time strength decrease.

The most peculiar difference of corrosion behaviour of tested materials is the oxidation isotropy of MPG matrix graphite and the oxidation anisotropy of 30PG matrix graphite. 30PG matrix graphite in the initial state is an anisotropy material that is follow from the electrical resistivity of specimens cut of the spherical fuel element imitator parallel and perpendicular to the compacting directions (Table 3). Corrosion test results showed that the specimens cut out in the parallel direction were oxidized more actively and the corrosion rates relationships were approximately proportional to the degree of anisotropy. One can also observe the interconnection of corrosion rate with density and specific volume of pores in specimen (Table 3). When specimen density increases from 1.80 g/cm^3 up to 1.90 g/cm^3 and

related pore volume decreases, the corrosion rate of 30PG matrix graphite decreases by a factor of 1.5.

Table 3

The results of corrosion tests of 30PG matrix graphite specimens (T = 1000°C, C_{H_2O}=1 vol. %, 10 h) in parallel and perpendicular to the compacting directions

Density, g/cm^3	Electric resistivity, μohm.cm		Specific surface, m^2/g		Specific pore volulme, cm^3/g		Cutting direction	Corrosion rate, g/cm^2 h x 10^3
	initial	oxidized	initial	oxidized	initial	oxidized		
1,80	1820	2690	0,29	3,55	0,099	0,155	∥	3,76
	1480	2070	0,29	3,36	0,096	0,143	⊥	3,26
1,88	1500	1870	0,44	2,93	0,075	0,101	∥	2,47
	1250	1470	0,32	2,28	0,068	0,097	⊥	2,1
1,90	1510	1920	0,4	3,15	0,066	0,096	∥	2,3
	1200	1450	0,4	2,1	0,064	0,089	⊥	1,9

Impurities content essentially influences on corrosion resistance of matrix graphite. Impurities content in graphite is characterized by such parameter as ash residue. According to the data of X-ray spectral analysis the iron constitutes the main mass of the ash residue of MPG matrix graphite ($1x10^{-3}$ - $5x10^{-3}$ mass %). The analysis of the up-to-date results makes it possible to obtain partial dependencies of corrosion rate on iron and ash contents at the constant volume of the open porosity (~ 0.066 cm^3/g). The dependencies of corrosion rate on iron content at the constant ash content (0.03 mass %) and on ash content are given in Fig. 3. The corrosion rate increases with the increase of iron content and ash residue.

The testing at 1600 °C of specimens coated by silicon carbide and aluminium phosphate protective layers at the air showed different results. The best ones were obtained for specimens with silicon carbide coating deposited by gas phase pyrolisis and with thickness 30 μm. They had no defects, no mass changes, but thin (1 μm) film of silicon oxide was appeared. Specimens coated by silicon carbide prepared by pyrolisis of polycarbosilane had single defects - crack and chipping.

After testing of specimens with aluminium phosphate coating white spots were observed consisting of Al_2O_3 as it was analysed. Matrix graphite burn-off took place near such spots in some specimens .

IV. CONCLUSION

Summarizing the results of the corrosion tests of matrix graphite on the base of 30PG and MPG graphite fillers one can note the following:

- in the tested ranges of temperature and water vapour concentrations in helium and pressure 0.12 MPa corrosion has a volumetric character;
- corrosion resistance of 30PG matrix graphite is higher than that of MPG but this difference decreases with test temperature increase;
- corrosion of 30PG matrix graphite is accompanied by a primary burn-off of the coke-binder.has anisotropy character, whereas the same characteristic of MPG matrix graphite has isotropic and non-selective character;
- the corrosion rate of matrix graphite increases with increase of metallic impurities, in particular, iron;
- the corrosion resistance of matrix graphite with protective coating at the air at 1600 °C increases in the following order:

$$nAl2O3mP_2O_5 > SiC_{polycarbosilane} > SiC_{\text{gas phase}}(CH_3SiCl_3)$$

REFERENCES

1. Zeldovich Ya.B. Journal of physical chemistry, 1939, V. 13, N 2, pp. 163-168.

2 Virgiliev Yu.S., Cherednik E.M., Ostrovsky V.S. Chemistry of solid fuel, 1974, N 3, p. 25.

3. Fialkov A.S. Formation of the structure and properties of carbon-graphite materials, 1965,.Metallurgy, pp. 58-61.

The list of figure captions

Fig. 1. Dependence of a corrosion rate of matrix graphites on burn-off (T=1000°C, C_{H2O}=1 vol.%)

1 - MPG matrix graphite;

2 - 30PG matrix graphite

Fig.2. Dependence of a corrosion rate of matrix graphites on temperature:

a - 30PG matrix graphite; b - MPG matrix graphite;

1 - 1 vol.% H_2O; 2 - 0.08 vol.% H_2O;

3 - 0.04 vol.% H_2O; 4 - 0.02 vol.% H2O;

Fig. 3. Dependence of a corrosion rate of MPG matrix graphite on impurities content:

1 - iron concentration (ash content ~ 0.03 mass %)

2 - ash content

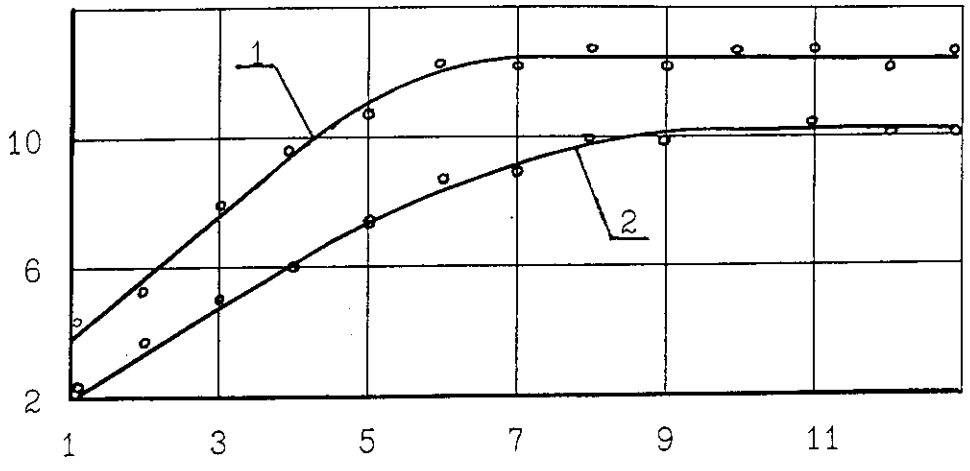
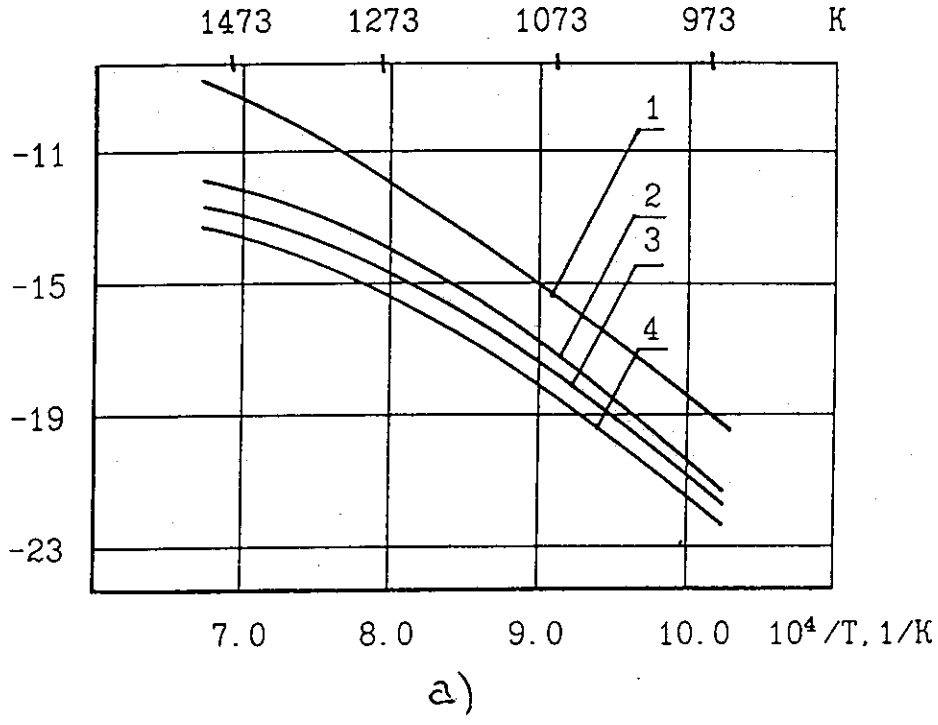


Fig. 1. Dependence of a corrosion rate of matrix graphite on burn-off (T=1000°C, C_{H2O}=1 vol. %)

1 - MPG matrix graphite;

2 - 30PG matrix graphite



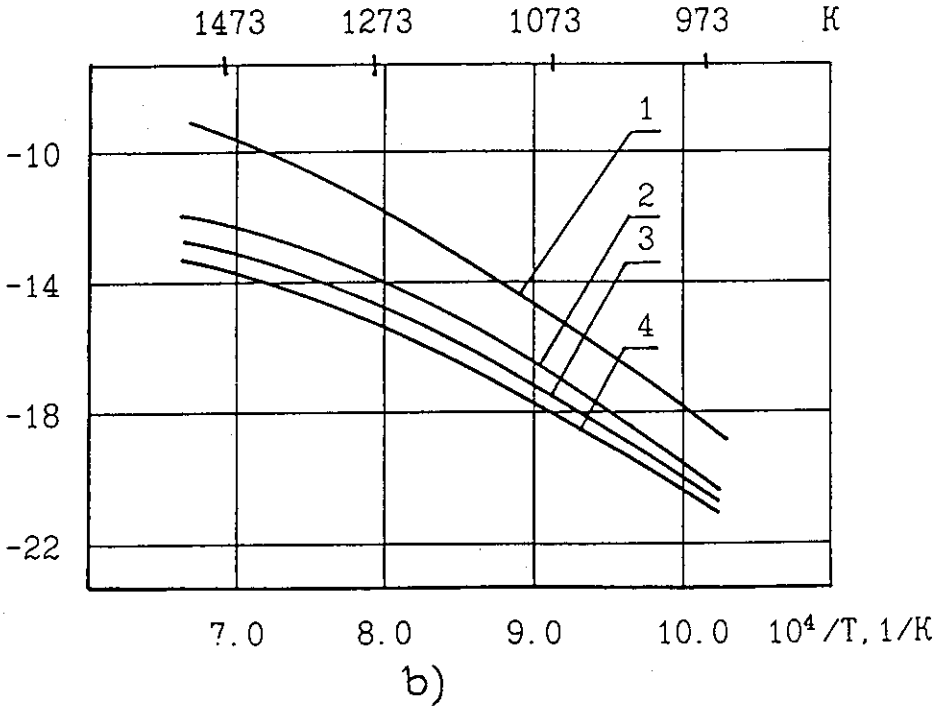


Fig.2. Dependence of a corrosion rate of matrix graphites on temperature:
a - 30PG matrix graphite; b - MPG matrix graphite; 1 - 1 vol. % H_20; 2 -0.08 vol. % H_2O; 3 - 0.04 vol. % H_2O; 4 - 0.02 vol. % H2O;

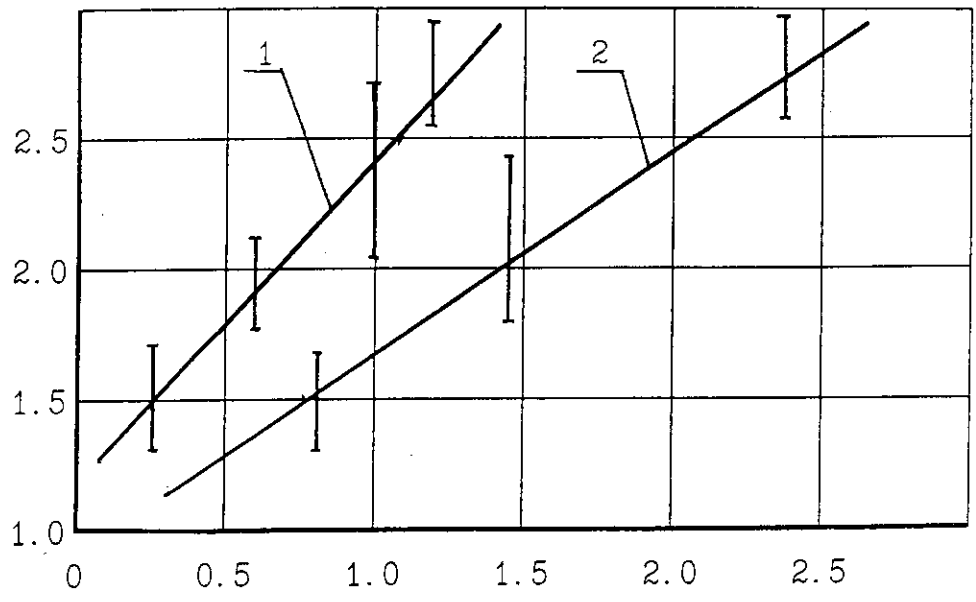


Fig. 3. Dependence of a corrosion rate of MPG matrix graphite on impurities content:

1 - iron concentration (ash content ~ 0.03 mass %)

2 - ash content

6.6 Design and Fabrication of He-He Intermediate Heat Exchanger for HTTR

Hajime KOIKEGAMI
Ishikawajima-Harima Heavy Industries Company, Ltd.
JAPAN

Shigeki MARUYAMA
Toshiba Corporation
JAPAN

Kazuhiko KUNITOMI, Minoru OHKUBO
Japan Atomic Energy Research Institute
JAPAN

The High Temperature Engineering Test Reactor (HTTR) being constructed by JAERI has a helium-helium intermediate heat exchanger (IHX) with approximately 10MW thermal rating in a primary cooling system.

The IHX is a vertical helically coil counter flow type heat exchanger operated at a very high temperature above 900°C. It transports the nuclear heat energy of primary helium gas to secondary helium gas, which is to be used in heat utilization system in future. The IHX has to meet the requirement on structural integrity as class 1 component for nuclear use during the service life, so it is one of the most important component in HTTR. As a member of the HTTR project, TOSHIBA/IHI has been responsible for the IHX. Our scope covers the design, fabrication, inspection and testing, installation, quality assurance, research and development.

The helical coil tube bundle is composed of 96 heat transfer tubes with six layers of helical coils. The outer diameter and thickness of the heat transfer tube are 31.8mm and 3.5mm respectively. Heat transfer tube material is Ni-base superalloy Hastelloy XR with high resistance for high temperature and corrosion in helium atmosphere. In case of internal structures, such as the heat transfer tubes, it is difficult to meet the elevated temperature structural design criteria based on the simplified elastic analysis, especially the creep damage criteria and the limitation of the accumulated

inelastic strain. So their structural integrity have been evaluated by inelastic creep analysis approach.

To increase the heat transfer by radiation, the radiation plates are installed between the helical coil tube layers. The formulas of heat transfer coefficient include the effects of the tube arrangement and geometry, such as eccentricity, inclination, flatness, and effect of radiation plates.

The outer diameter and total height of the outer shell is approximately 2.0m and 10.0m respectively. Inner surface of the inner shell is covered with thermal insulation to maintain the metal temperature of the inner shell at the lower level. Material of the inner shell and the outer shell is commercial low alloy steel, that is 2•1/4Cr-1Mo steel. Total weight of the IHX is 65,000kgf.

In order to fabricate the reliable IHX, research and development has been performed. Main items are as follows:

(1)Making a reliable thick welded joint of Hastelloy XR and developing a reliable tube-to-tube automatic welder.

(2)Making a precise helical coil to keep the tolerance of the tube bundle and assembling the six layers of the helical coil tube bundle precisely.

To assure the integrity of the IHX for nuclear use, very severe inspections and testings, such as radiographic test, ultrasonic test, creep rupture test, pneumatic test, helium leak test, are required.

Fabrication of the IHX was successfully completed in September 1994, and the IHX was installed in the containment vessel in the reactor building in February 1995.

Design and Fabrication of He-He Intermediate Heat Exchanger for HTTR

Hajime KOIKEGAMI
Ishikawajima-Harima Heavy Industries Company, Ltd.
JAPAN

Shigeki MARUYAMA
Toshiba Corporation
JAPAN

Kazuhiko KUNITOMI, Minoru OHKUBO
Japan Atomic Energy Research Institute
JAPAN

ABSTRACT

The High Temperature Engineering Test Reactor (HTTR) being constructed by JAERI has a helium-helium intermediate heat exchanger (IHX) with approximately 10MW heat capacity in a primary cooling system.

The IHX is a vertical helical coil counter flow type heat exchanger operated at a very high temperature above 900℃. It transports the nuclear heat energy of primary helium gas to secondary helium gas, which is to be used in heat utilization system in future. The IHX has to meet the requirement on structural integrity as class 1 component for nuclear use during the service life, so it is one of the most important component in HTTR. As a member of the HTTR project, TOSHIBA and IHI has been responsible for the IHX. Our scope covers the design, fabrication, inspection and testing, installation, quality assurance, research and development.

The detailed design and construction method of the IHX were approved by the government in April 1992. Fabrication of the IHX was started in July 1992, and was successfully completed in September 1994. The IHX was transported from works to HTTR site and was installed in the containment vessel in the reactor building in February 1995.

This paper describes the design and fabrication of the IHX.

1. Introduction

The HTTR is a helium-cooled and graphite-moderated reactor with outlet coolant temperature of 950℃ and thermal output of 30MW. It is being constructed at Oarai Research Establishment in Japan Atomic Energy Research Institute (JAERI). As a member of the HTTR project, TOSHIBA and IHI has been responsible for the IHX. Our scope covers the design, fabrication, inspection and testing, installation, quality assurance, research and development of it.

The detailed design and construction method of the IHX were approved by the government in April 1992. Fabrication of the IHX was started in July 1992, and was successfully completed in September 1994. The IHX was transported from works to HTTR site and was installed in the containment vessel in the reactor building in February 1995. The design and construction schedule of IHX is shown in Table 1.

From 1973 to 1980, the research and development of direct steelmaking using high temperature reducing gas, which was taken up as a large-scale national project by the Agency of Industrial Science and Technology of the Ministry of International Trade and Industry (MITI), was performed by the Engineering Research Association of Nuclear Steel-making (ERANS).

As one member of ERANS, IHI was engaged in the research and development of 1.5MW He-He IHX. In this project, IHI designed and fabricated the IHX. Moreover, the IHX was operated in the high temperature helium test loop over 5000h.

The experiences obtained from this previous project are effectively utilized for the HTTR project, and contribute to the design and fabrication of the IHX for HTTR.

2. Outline of IHX

The IHX is employed under extremely severe conditions with the primary helium temperature of 950℃ and pressure of 4.1MPa(gauge), secondary helium temperature of maximum 905℃ and pressure of 4.2MPa(gauge). It transports the nuclear heat energy of primary helium gas to secondary helium gas, which is to be used in heat utilization system in future. The IHX has to meet the requirement on structural integrity as class 1 component for nuclear use during the service life, so it is one of the most important

components in HTTR. The basic design condition of the IHX is shown in Table 2. The configuration and the principal specification of the IHX are shown in Fig. 1 and Table 3 respectively.

The IHX is a vertical helical coil counter flow type heat exchanger with approximately 10MW heat capacity. The design pressure of the outer shell is 4.7MPa[gauge] and that of the heat transfer tubes is 0.29MPa. The design temperature of the outer shell is 430℃ and that of the heat transfer tubes is 955℃.

There are two ways of operation. One is the rating operation mode and the other is the high temperature operation mode. In case of the high temperature operation mode, the primary inlet helium temperature is 950℃ and maximum of the secondary outlet helium temperature is 905℃.

The primary helium gas at 950℃ enters at the inlet nozzle located at the bottom center of the vessel and flows upwards through the outer of helical coil tube bundles. After transferring heat to secondary helium, the primary helium is led into the primary circulator and flows down the outer annular flow path provided between the inner shell and the outer shell in order to cool the outer shell of pressure boundary.

On the other hand, the secondary helium gas at 300℃ separates at tubesheet located at the upper part of the vessel and flows into the heat transfer tubes. It is heated up to maximum 905℃ by the primary helium and collected into the hot manifold header. Then the heated secondary helium flows upwards inside the central hot gas duct in the center pipe.

3. Design of IHX

Concerning the thermal and hydraulic performance of the IHX, we adopted the formulas obtained from our previous work of the large-scale national project performed in 1973-1980. The formulas of heat transfer coefficient include the effects of the tube arrangement and geometry, such as eccentricity, inclination, flatness, and effect of radiation plates.

The overall structure of the IHX was designed to form the axial symmetrical arrangement in order to decrease the thermal stress and keep the thermal expansion uniformly. In designing the IHX, careful studies for the thermal stress and thermal expansion had been made for each part of structure exposed high temperature and many of experiences obtained from

the previous project had been employed.

The helical coil tube bundle is composed of 96 heat transfer tubes with six layers of helical coils. Maximum coil diameter is 1310mm and effective height of coils is 4870mm. The outer diameter and thickness of the heat transfer tube are 31.8mm and 3.5mm respectively. To determine the tube thickness, the differential pressure between the primary helium and the secondary helium was adopted. The pressure of the secondary helium is controlled a little higher than that of the primary helium in order to prevent the fission products from releasing to the secondary helium boundary.

The heat transfer tubes are supported by the tube support assemblies and the center pipe is hung with the tube support assemblies for the purpose of decreasing the thermal expansion difference between the center pipe and the tubes. The helical coil tubes are connected with the hot manifold header and the cold tubesheets by the lower and upper connecting tubes. Material of the heat transfer tubes, the hot manifold header and the cold tubesheets is Ni-base superalloy Hastelloy XR with high resistance for high temperature and corrosion in helium atmosphere, which is developed by JAERI. The geometry of lower connecting tubes and hot manifold header is shown in Fig.2

To increase the heat transfer by radiation, the radiation plates, which are thin curved plates, are installed between the helical coil tube layers. Moreover these radiation plates inserted between the layers of helical coil tube bundle are also effective on restraining the flow induced vibrations of the heat transfer tubes.

To evaluate the structural integrity of the HTTR components, including the IHX, "Elevated Temperature Structural Design Guide for the HTTR components (HTTR ETSDG)" was prepared by JAERI. HTTR ETSDG is composed of the simplified elastic analysis approach and the inelastic analysis approach.

In case of internal structures, such as the heat transfer tubes and the hot manifold header, the metal temperature is over 900℃ during the steady state operation. Though the primary stresses are limited within the lower level, it is difficult to meet the elevated temperature structural design criteria based on the simplified elastic analysis approach,

especially the creep damage criteria and the limitation of the accumulated inelastic strain. To estimate the creep damage and the creep strain reasonably, more detailed creep analysis approach, which includes the stress relaxation and effects of load histories, have been performed.

The example of creep analysis results of the hot manifold header is shown in Fig.3 and Fig.4. The analytical model of the hot manifold header is shown in Fig.3 and Fig.4 shows the equivalent creep strain versus time. Creep strains at evaluation point increase in the first thermal load cycle and the increment of creep strain are limited small in the second or third thermal load cycle.

The outer diameter and total height of the outer shell is approximately 2.0m and 10.0m respectively. Inner surface of the inner shell is covered with thermal insulation to maintain the metal temperature of the inner shell at the lower level. Material of the inner shell and the outer shell is commercial low alloy steel, that is 2•1/4Cr-1Mo steel.

4. Fabrication of IHX

The fabrication sequence of IHX is shown in Fig.5. Four parts of IHX, tube bundle, center pipe with thermal insulation, outer shell and inner shell, were fabricated in parallel and were assembled in order.

To fabricate the reliable IHX, many of technical investigations and preparations were conducted. Development of the IHX manufacturing process is shown in Table 4. The major investigations are as follows:

(1) Establishing a reliable thick welded joint of Hastelloy XR with high resistance for cracking and high temperature creep strength same as the base metal.

(2) Developing a reliable tube-to-tube automatic welder at narrow space.

(3) Developing a precise helical coil bending method to keep the tolerance of the tube bundle.

(4) Establishing a reliable assembling process of six layers of the helical coil tube bundle precisely.

(5) Establishing a reliable assembling process and examination method of thermal insulation structure.

To make the reliable thick welded joint of Hastelloy XR with not only low cracking susceptibility but also high creep strength similar to the

base metal, IHI cooperated with JAERI in the development of the filler metal. On the other hand, we investigated the best welding method and condition for thick welded joint and the narrow-gap TIG welding procedure was established.

The weldments of tube-to-tube joints at narrow space were performed by the automatic orbital-bore-welder and the weldments of tube-to-manifold joints and the curved connecting tube weldments were performed by manual TIG welding method. Tube-to-tubesheet welded joints were welded by the automatic internal-bore-welder. The automatic welders were newly developed for the fabrication of the IHX. Appearance of automatic TIG welding of tube-to-tube is shown in Fig. 6.

The heat transfer tubes were helically coiled by the coil bender and the bending conditions were examined by trial fabrication of a mock-up. To assemble the six layers of the helical coil tube bundle, helical coils are required the high precision. They are constrained by the working implements. Fig. 7 shows the helical coil tube bundle of third and fourth layer.

The tube bundle was assembled in vertical position. The completed appearance of tube bundles is shown in Fig. 8 and Fig. 9.

Though the hot manifold header and the cold tubesheets had a complicated geometry, they were machined from Hastelloy XR forging by the numerical controlled machining center. Fig. 10 shows the appearance of the machined hot manifold header.

The thermal insulation structure of inner shell is composed of thermal insulation and inner liner. Thermal insulation was installed inside of inner shell. To absorb the thermal expansion, inner liner is separated five parts of vertical direction and six parts of circumferential direction. The space between tube bundles and thermal insulation structure of inner shell was controlled precisely. Fig. 11 shows the appearance of thermal insulation structure inside of the inner shell.

The outer shell, inner shell, top head and bottom head were cold rolled or hot pressed, then assembled as the welding structures. Concerning the low alloy steel weldments, pre-heating and post weld heat treatment were done for stress relief of the welded joints.

To assure the integrity of the IHX for nuclear use, very severe inspections and testings are required. For example, radiographic test,

ultrasonic test, liquid penetrant test, magnetic particle test for base metal and welded joint, creep rupture test for Hastelloy XR material, fracture toughness test for reactor pressure boundary material, hydrostatic test, pneumatic test, helium leak test for pressure boundary.

The completed appearance of the IHX waiting for shipping is shown in Fig.12 and Fig.13 shows the installation of the IHX in the reactor building.

5. Conclusions

(1) The IHX, which is one of the most important component in HTTR, was successfully constructed in January 1995.

(2) To increase the heat transfer, the radiation plates, which are also effective on restraining the flow induced vibration, were installed between the helical coil tube layers.

(3) To evaluate the structural integrity of the IHX, detailed creep analysis was performed and creep strain and creep damage were estimated reasonably.

(4) To fabricate the reliable IHX, many of technical investigations were conducted and manufacturing process of the IHX was developed.

6. Acknowledgments

The design and fabrication of IHX for HTTR was conducted by TOSHIBA and IHI under contract with JAERI as a member of HTTR project. Permission to publish this work is gratefully acknowledged. The authors would like to take this opportunity to thank the members of the technical staff of JAERI.

7. References

(1) S.saito, Present Status of HTTR Project and Associated International Cooperation, The 2nd JAERI Symposium on HTGR Technologies, Oct. 21-23(1992)

(2) JAERI, Proceedings of Third JAERI Seminar on HTGR Technologies, Nov. 7-8(1994), JAERI-Conf 95-009, (1995.3)

(3) K.Kunitomi, H.Koikegami et al., Structural Design for an Intermediate Heat Exchanger of the HTTR, J. At. Energy Soc. Japan, Vol.37, No.4, pp.316-326, (1995.4)

Table 1 IHX construction schedule

YEAR	1991	1992	1993	1994	1995	1996
HTTR MILESTONE	Construction Start ▽			RPV ON ▽		Pressure Test ▽
Approval of design and construction method						
Design						
Production of material						
Fabrication						
Installation						

Table 2 IHX basic design condition

Number of unit	1	
Heat capacity	10MW	
Design pressure		
Outer shell	4.7MPa[gauge]	
Heat transfer tube	0.29MPa	
Design temperature		
Outer shell	430℃	
Heat transfer tube	955℃	
Operating condition	Rating operation	High temperature operation
Fluid		
Primary	Helium gas	Helium gas
Secondary	Helium gas	Helium gas
Flow rate		
Primary	Max. 15ton/h	Max. 12ton/h
Secondary	Max. 14ton/h	Max. 12ton/h
Pressure		
Primary	4.1MPa[gauge]	4.1MPa[gauge]
Secondary	4.2MPa[gauge]	4.2MPa[gauge]
Temperature		
Primary		
Inlet	850℃	950℃
Outlet	390℃	390℃
Secondary		
Inlet	300℃	300℃
Outlet	775℃	860℃ (Max. 905℃)

Table 3 IHX principal specification

Type	Helical coil counter flow
Number of unit	1
Heat capacity	10MW
Design temperature (Heat transfer tube)	955℃
Heat transfer tube	
Outer diameter	31.8mm
Thickness	3.5mm
Material	Hastelloy XR
Number	96
Pitch	47mm
Number of coil layers	6
Radiation plate	
Thickness	5mm
Material	Hastelloy XR
Shell	
Material	2·1/4Cr-1Mo
Outer diameter	Approx. 2.0m
Height	Approx. 10.0m

Table 4 Development of IHX manufacturing process

ITEMS	CONTENTS
Reliable welded joint of Hastelloy XR	(1) Development of filler metal with high creep strength (2) Accumulation of creep test data on welded joint (3) Establishment of reliable high efficient welding process
Reliable automatic welder at narrow space	(1) Development of automatic orbital-bore-welder for tube-to-tube welding (2) Development of automatic internal-bore-welder for tube-to-tubesheet welding
Precise helical coil tube bundles	(1) Design of reliable tube support structure (2) Development of helical coil tube bender (3) Establishment of assembling process to make the precise tube bundles
Reliable thermal insulation system	(1) Design of reliable thermal insulation structure (2) Establishment of assembling process to install thermal insulation (3) Establishment of examination method of thermal insulation structure

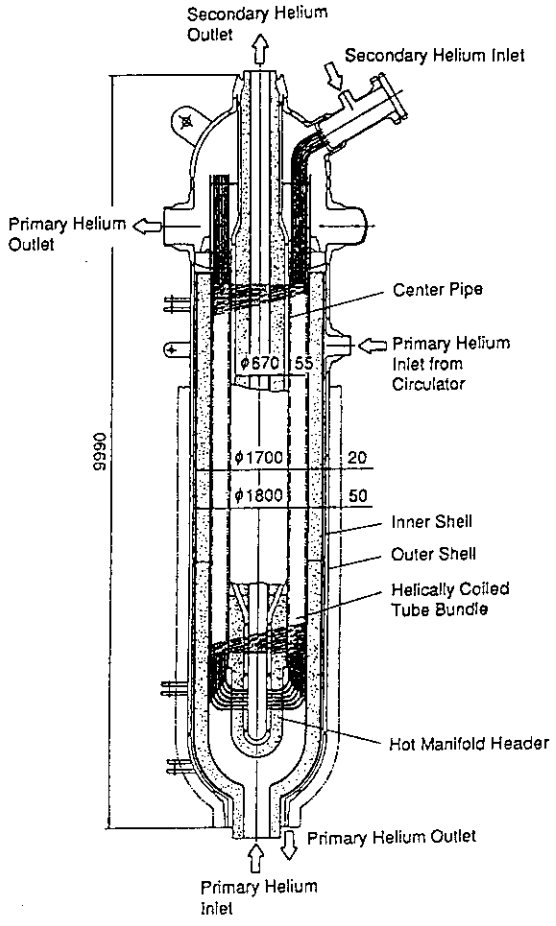


Fig.1 Configuration of IHX

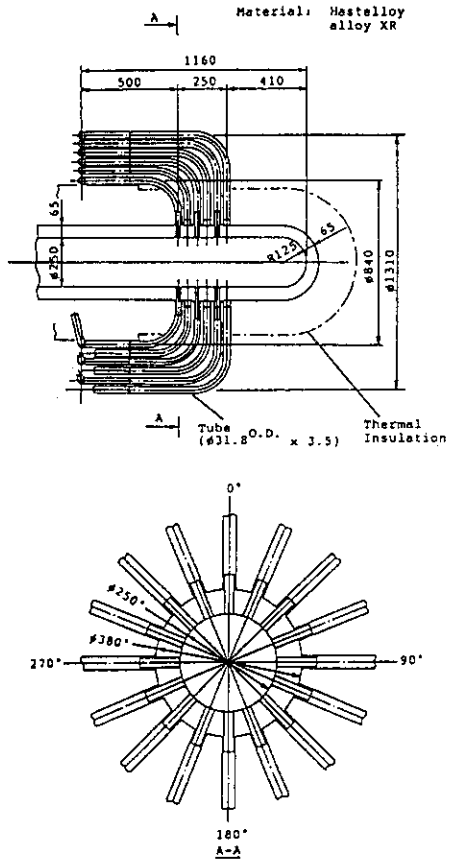


Fig.2 Geometry of hot manifold header

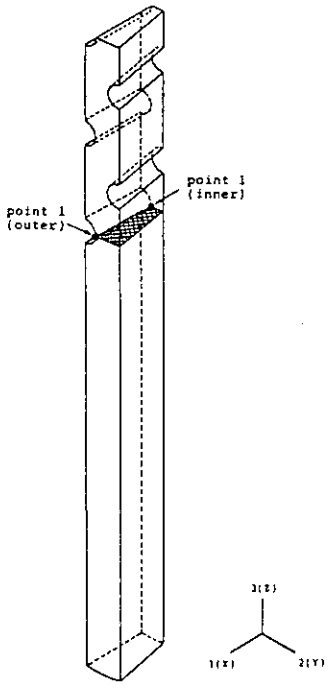


Fig.3 Analytical model of hot manifold header

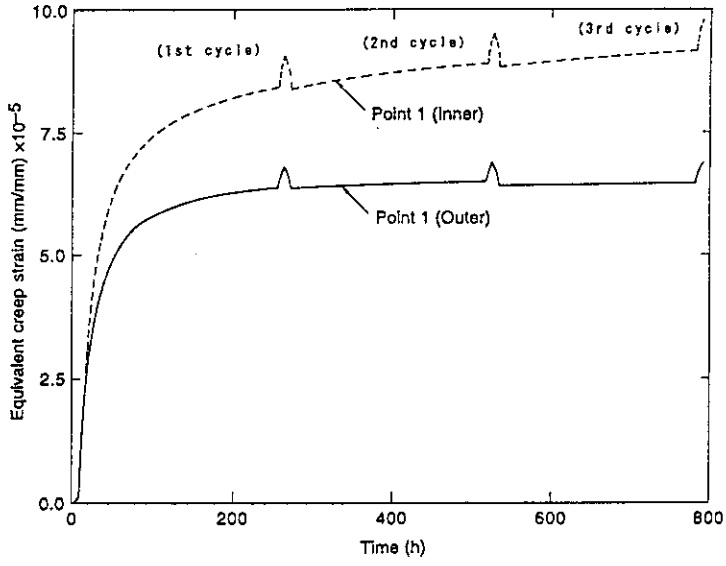


Fig.4 Example of creep analysis results of hot manifold header

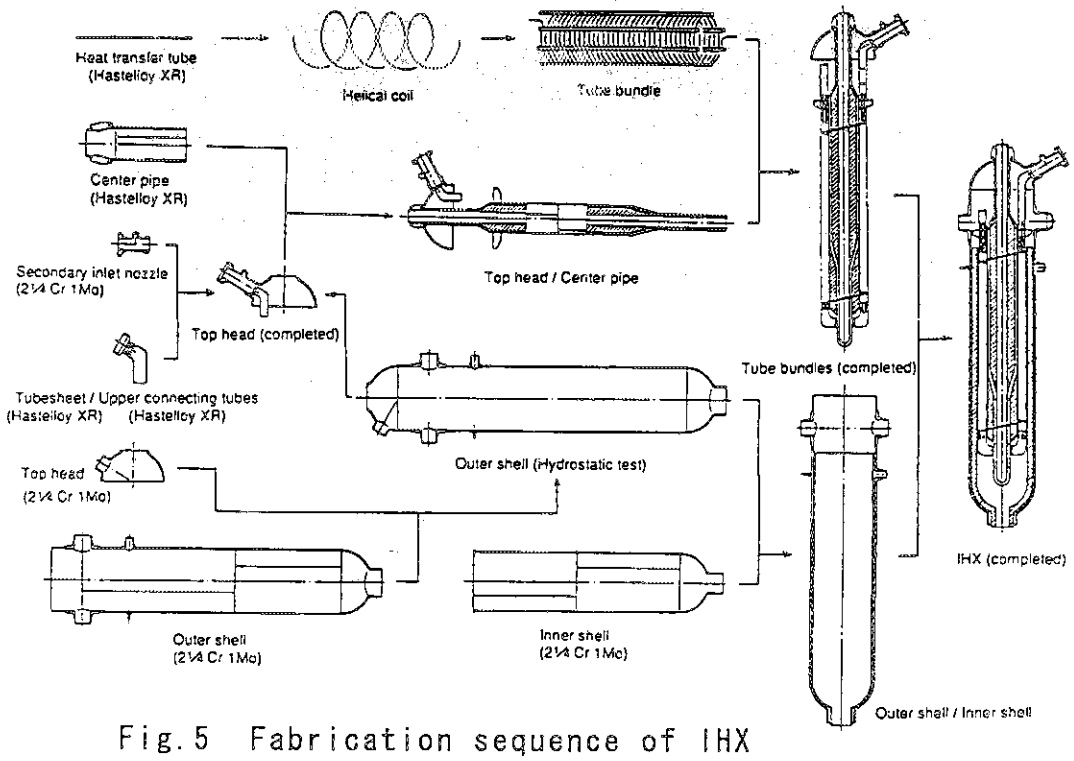


Fig.5 Fabrication sequence of IHX

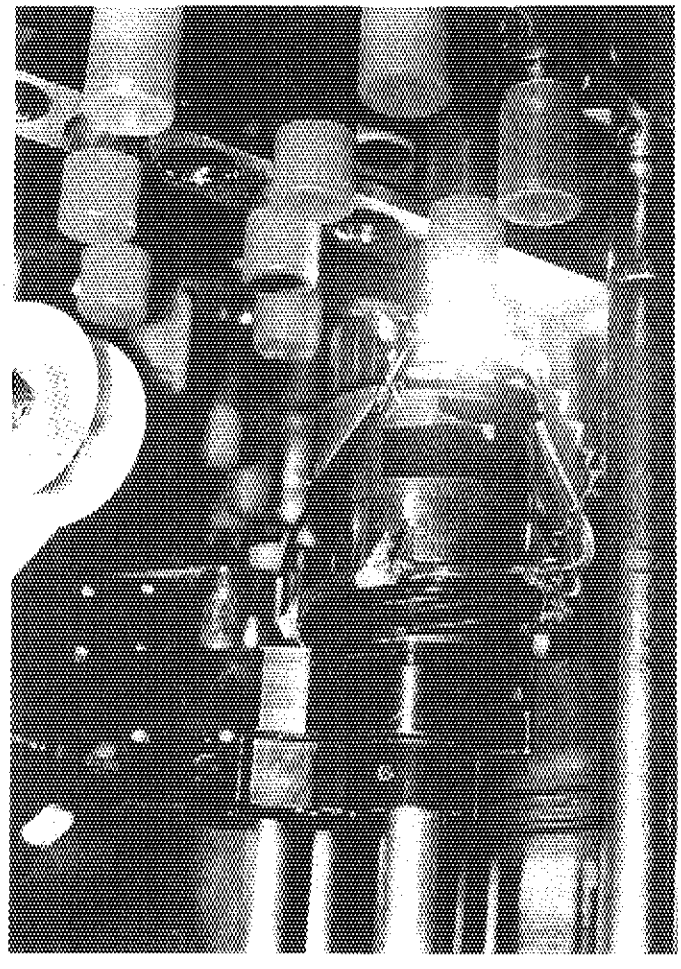


Fig.6 Automatic TIG welding of tube-to-tube

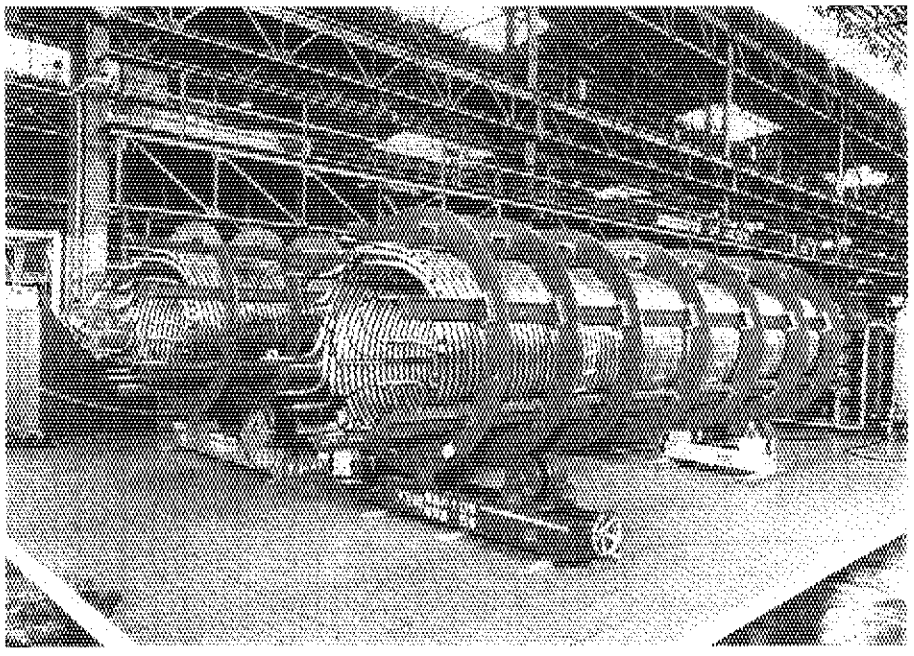


Fig.7 Helical coil tube bundle



Fig.8 Tube bundles (General view)

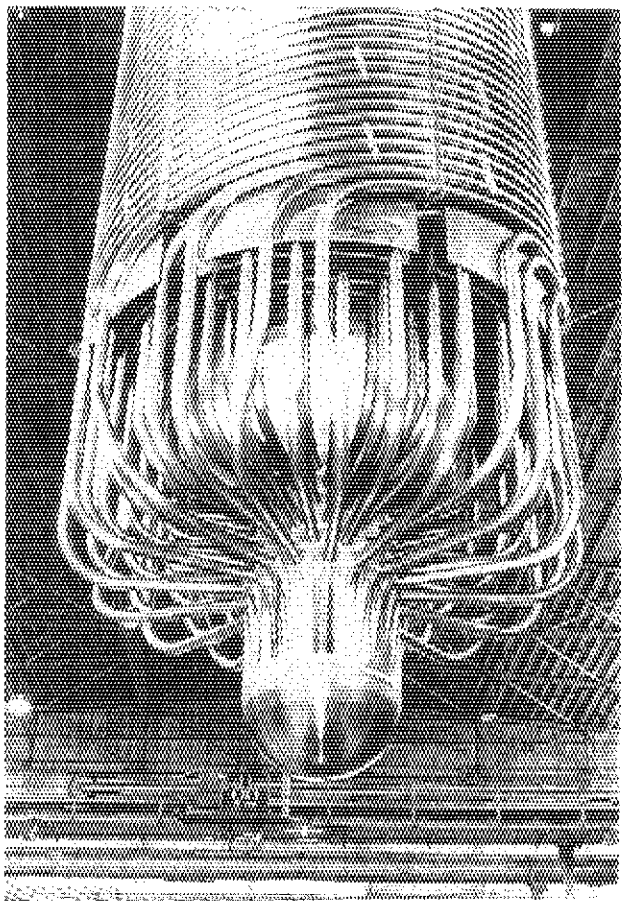


Fig.9 Tube bundles (Lower connecting tubes)

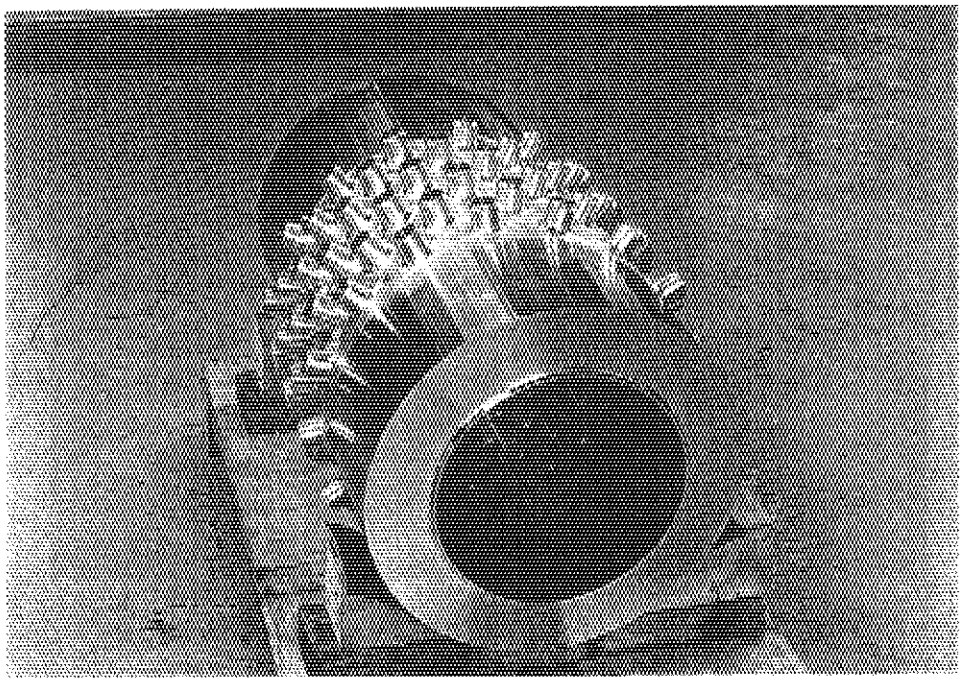


Fig.10 Machined hot manifold header

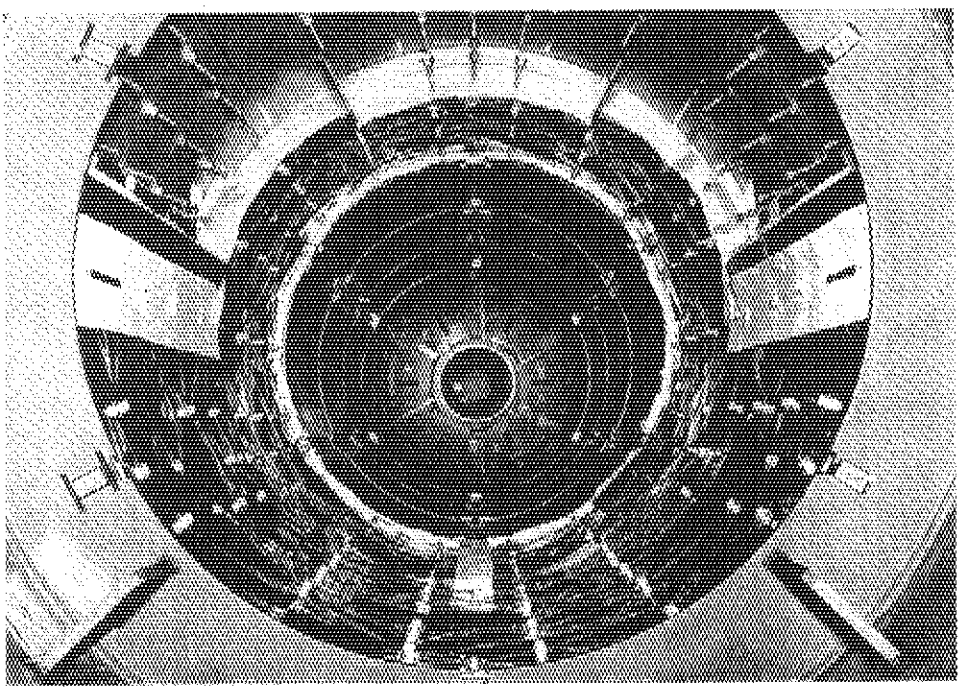


Fig.11 Thermal insulation inside of inner shell

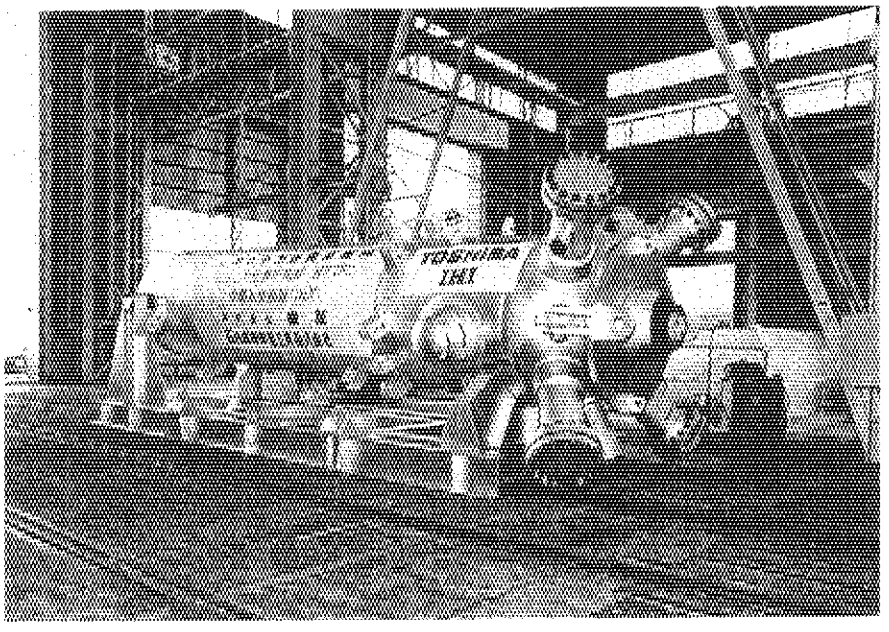


Fig.12 General view of IHX (Completed)

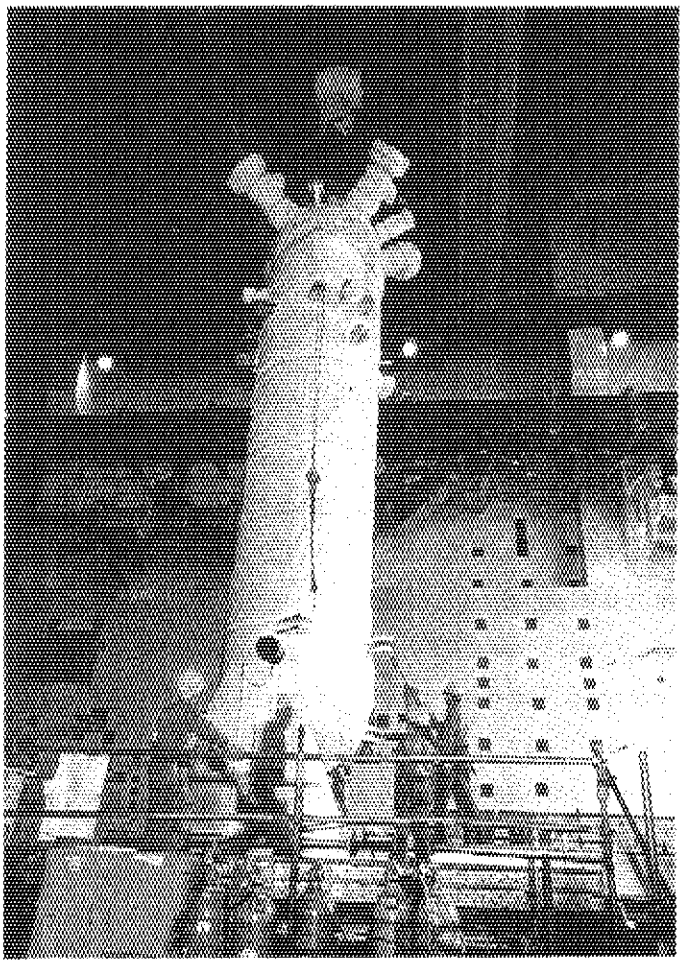


Fig.13 Installation of IHX

6.7 Design and Fabrication of the Reactor Vessel Cooling System (VCS) in HTTR

Kazuhiko Kunitomi*, Masayuki Shinozaki*,
Hiroshi Kodama**, Masayuki Yamamoto**,
Kouji Hontani**

* Japan Atomic Energy Research Institute,
Oarai, Ibaraki-ken, 311-13, Japan
** Kure Works, Babcock-Hitachi K.K.,
6-9 Takara-machi, Kure-shi, Hiroshima-ken, 737, Japan

ABSTRACT

The reactor vessel cooling system (VCS) is an engineered safety device that is used as a decay and a residual heat removal system when forced circulation in both the primary and the auxiliary cooling systems cannot be performed. The VCS consists of a Cooling Water Panel (CWP) and a water circulation system supplying a coolant. The CWP is separated into 3 parts with the upper, middle and lower panels for the vertical RPV region and this is installed on the surface of the concrete wall of the reactor vessel room. The water circulation system consists of two circulation pumps, a heat exchanger, pipes and valves. In view of the multiple safety countermeasure necessary for the VCS, the CWP and the cooling water circulation system employ dual system. The limited temperature of the RPV and the fuel at the loss-of-coolant accident are regulated by the stipulated requirements of the VCS which are:

(1) Limited heat removal value

above 0.3MW using only one system in case of accidents,

below 0.6MW using two systems under normal operations.

(2)Limited temperature of the concrete

below 65℃ for the concrete surface using two systems under normal operations.

The basic structure of the CWP is designed in accordance with calculations of heat distribution for the concrete wall of the reactor vessel room and the analysis of heat removal values in order to comply with their given specifications. Ratio tests for the metallic surfaces were performed initially as the objectives of heat removal values of CWP were to control radiation. Based on the tests the radiation ratios from minimum 0.6 to maximum 0.85 of metallic surfaces were employed for the analysis. In the results above, the structure of the CWP was a panel structure with cooling water pipes welded separately with fin plates. This structure satisfied the limited heat removal values for the VCS. As a result it was found that the heat removal ability of the structure was more than 0.6MW which was too big to keep the core outlet temperature of the primary coolant, thus additional structures based

on the structure that 4 heat reflector panels between the RPV and the CWP were added to decrease heat removal values into the limits. On the other hand, concerning the minimum heat removal values for the minimum radiation ratios, the cooling water pipes ran cooling water to the innermost reflector panel to increase the heat removal value. From the results above, the VCS-panel has arranged the structure with the CWP on the concrete wall of the reactor vessel room, 4 reflector panels inside it and cooling water pipes on the innermost panel. As a result of the heat distribution analysis based on the heat removal ability for the practical structure of the CWP at the loss-of-coolant accident, the VCS-panel can meet the requirements of both the limited temperature of the RPV and the fuel.

Fabrication of VCS-panel has been completed and installed into the reactor vessel room completely. The piping systems of VCS will be flushed and a pressure test for the system will be performed. As of Mar. 1996 a component test of the circulation pumps for the VCS will be carried out. The heat removal value will be measured to confirm the results of analysis and the field data during the start up test in 1998.

P-07 Design and Fabrication of the Reactor Vessel Cooling System (VCS) in HTTR

Hiroshi Kodama*, Masayuki Yamamoto*,
Kouji Hontani*, Kazuhiko Kunitomi**,
Masayuki Shinozaki**

* Kure Works, Babcock-Hitachi K.K.,
6-9 Takara-machi, Kure-shi, Hiroshima-ken, 737, Japan
** Japan Atomic Energy Research Institute,
Oarai, Ibaraki-ken, 311-13, Japan

ABSTRACT

The reactor Vessel Cooling System (VCS) is one of the engineered safety features used as a residual heat removal system when forced circulation in both the primary and auxiliary cooling systems cannot be performed simultaneously. The VCS consists of a Cooling Water Panel (CWP) and a water circulation system supplying a coolant. The CWP is installed on the surface of the concrete wall of the Reactor Pressure Vessel (RPV) room to remove heat from the RPV by thermal radiation. The water circulation system is installed in the reactor building and transfers heat, removed by CWP to a cooling tower.

In view of the limited temperatures of the RPV and fuel at the loss-of-coolant accident, it is necessary to design a VCS in accordance with stipulated requirements, limited heat removal values and limited temperature of the concrete. We will describe the Design and Fabrication of the water circulation system, especially for the CWP in the present paper giving conclusive evidence to support the results which met the stipulated requirements.

Fabrication of the VCS-panel was completed and the VCS-panel was installed into the RPV room last year. The piping systems of VCS are flushed and a pressure test for the system will be performed shortly. A component test of the circulation pumps for the VCS will be carried out in March, this year. Heat removal values will be measured to confirm the results of analysis along with collecting field data for the start up test in 1998.

1. Introduction

The CWP is separated into 3 parts with upper, side and lower panels for the vertical RPV region and is installed on the surface of the concrete wall of the RPV room. The water circulation system consists of two circulation pumps, a heat exchanger, pipes

and valves. A dual-type system has been adopted in view of the multiple safety countermeasures necessary for the CWP and the cooling water circulation system of the VCS. To satisfy the limited temperature of the RPV and the fuel at the loss-of-coolant accident, the following requirements of the VCS were stipulated.

(1) Limited heat removal values

above 0.3MW using only one system in the case of accidents,

below 0.6MW using two systems under normal operations.

(2)Limited temperature of the concrete

below 65℃ for the concrete surface using two systems under normal operations.

The basic structure of the CWP is designed in accordance with calculations of heat distribution for the concrete wall of the RPV room and the analysis of heat removal values to comply with their given specifications. Heat removal of CWP is mainly thermal radiation. Based on reports, the emissivity from minimum 0.6 to a maximum 0.85 of metallic surfaces was designated for analysis. In the above results, the structure of the CWP was a panel-type with cooling water pipes welded separately with fin plates. This structure satisfied limited heat removal values for the VCS. As a result, it was found that the heat removal capacity of the structure was more than 0.6MW which was too big to maintain the core outlet temperature of the primary coolant. Thus in order to decrease heat removal values into the limits, 4 heat reflectors between the RPV and the CWP were added to the basic structure. On the other hand, concerning the minimum heat removal values for the minimum emissivity, the cooling water pipes were added to the innermost reflector to increase heat removal values. Thermal radiation tests for metallic surfaces and heat removal tests for the cooling water pipes on the innermost reflector were performed to confirm the CWP performance.

Given these results, the VCS-panel has been arranged with a CWP, 4 interior reflectors and cooling water pipes on the innermost reflector of the concrete wall of the RPV room.

2. Specification of the VCS

The VCS employs a dual system because it is one of the engineered safety features requiring multiple safety countermeasures, normally operated for cooling the concrete wall of the RPV room as well as maintaining operation during accidents. The VCS stipulates two limited heat removal values that satisfy both maximum and minimum values. The minimum limited heat removal value is above 0.3MW using only one system required to stop the reactor safely in the case of accidents and the maximum limited heat removal value is below 0.6MW using both systems under normal operations to keep the coolant temperature above 950℃ at the outlet of the RPV.

A flow diagram is shown in Fig.1 and specifications for the VCS are listed in Table 1. The VCS employs a dual system, each system consists of a CWP, two circulation pumps, a heat exchanger, surgetank, pipes and valves. The CWP occupies the upper, side, lower part, door and adjustable panel. Each circulation pump has complete capacity to cope with design specifications. The heat exchanger is a Shell-and-Tube type(water to water), and auxiliary coolant flow inside the tube. The capacity of the surgetank is designed on the basis of heat expansion of the coolant.

3. Design of CWP

The VCS has to satisfy two stipulated requirements, removal of heat from the RPV and cooling the concrete wall of the RPV room. The basic structure of the CWP is designed in accordance with the calculations of heat distribution for the concrete wall of the reactor vessel room and the analysis of heat removal values in order to comply with their given specifications.

3.1 Concrete cooling structure

The structure of the CWP is a panel structure with cooling water pipes welded separately with fin plates, to make the cool surface remove heat. The pipes of the both systems are arranged by turns to keep the heat removal equal. The relation between the separation pitch of the cooling water pipes and concrete temperature is shown in Fig.2. Here it is found that the pitch to make the concrete temperature below 65℃ is below 170mm. For practical reasons we adopted a 120mm pitch for its advantages in cooling ability.

3.2 Structure to satisfy the limited heat removal values

The analysis of heat removal values was performed on the CWP considering the distribution of emissivity on the surface of the cooling water pipes.

(1) Design emissivity

It is known that emissivity has its distribution factors in surface conditions and temperatures. Design emissivity values were decided based on several data[1~6]. This data is shown in Fig.3.

Design emissivity was decided at 0.85 as a maximum and 0.6 as a minimum and 0.79 as a nominal value for surface conditions in operation. These designs agreed well with the aforesaid data.

(2)Heat removal value

Regarding the CWP within 120mm as the pitch of the cooling water pipes, the analysis of heat removal values was performed with the design emissivity. The results are shown in Fig.4. It was found here that a structure which could decrease the heat removal values was required.

(3) Structure decreasing the heat removal value

To decrease the heat removal value into the limits, additional structures consisting of heat reflector panels between the RPV and the CWP were added to the structure, as they controlled heat removal value well and were easy to fabricate. The relation between the number of reflectors and heat removal values is shown in Fig.4.

It was found that heat removal value decreased in relation to the increase in the number of reflectors. When 4 reflectors were added, heat removal value was sustained below the maximum limit at the maximum emissivity value. On the other hand, at the minimum emissivity value, it was 0.29MW and unable to maintain a level above minimum values.

(4)Adjustable-panel

Minimum heat removal values were satisfied by a modified CWP structure of 4 reflectors. To decrease temperatures of the reflectors, additional cooling water pipes were arranged on the innermost reflectors. In this case the coolant flow was controlled by operating valves outside the reactor vessel room. The relation between the number of added pipes in which the coolant flows and the heat removal value is shown in Fig.4. It was found that the heat removal value could be maintained at a minimum when the coolant was flown in the pipes.

4. Thermal radiation tests for CWP

Thermal radiation tests were carried out to verify both the design emissivity and the performance of adjustable panels.

4.1 Basic test for thermal radiation

The design emissivity was verified comparing measured heat removal values with calculated values. The test equipment is composed of thermal reflectors arranged in concentric circles, and electric heaters centered in thermal reflectors inside a water cooling jacket. Schematic representation of the test equipment is shown in Fig.5. The temperature and flow rates of cooling water were measured to calculate the heat removal values. The following surface conditions for reflectors were prepared in this test:keeping in air after the shot blast (simulating before operation) and keeping at high temperature after the shot

blast (simulating after operation) . The metal as received was also tested for reference.

The results of the thermal radiation test are shown in Fig.6, comparing measured values with calculated value. As shown in Fig.6, the measured values are inside the both lines, calculated by means of emissivity 0.6 and 0.85. As a result, it can be said that the design emissivity is reasonable. The measured value on the upper side of the calculation line at the temperature range of lossage, however is no problem because active cooling is requested at the time of lossage.

4.2 Heat removal test

Performance verification of adjusting panels was performed by comparing measured heat removal values of the test with calculated values. These tests were carried out by means of the test equipment in Fig.7, and replacing the innermost reflector in Fig.5 by a reflector with water cooling tubes.

The results of the heat removal test are shown in Fig.8, comparing measured values with the calculation values. As shown in Fig.8, the measured heat removal values increase when running cooling water to the adjustable panel, and measured values are inside the both lines, calculated by means of emissivity 0.6 and 0.85. As a result, we can verify the performance of the adjustable panel and the calculated methods. The calculation was carried out by means of the temperature distribution analysis, FEM. The calculation model is shown in Fig.9. Heat transfer roots by way of the water cooling tube and the thermal reflector are considered in this model.

5. Analysis of heat removal values for the practical structure of the VCS

The analysis of heat removal values took into account design emissivity and property confirmation test results to evaluate practicability of the VCS structure.

5.1 Analysis of heat removal value

The analysis of heat removal value was calculated with parameters in the nominal, maximum and minimum heat removal conditions. The maximum heat removal condition was confirmed that the real heat removal value was lower than the calculated one. For instance, the effects of natural convection were considered at the time of maximum condition. The minimum heat removal conditions confirmed that the real value was over the calculated values. For instance, the minimum emissivity without natural convection was adopted. These conditions are arranged in Table 2.

These results of the analysis by the above three conditions are shown in Fig.10. The results satisfied the limited maximum heat removal value as 0.49MW under nominal conditions 0.58MW under maximum conditions but the limited minimum heat removal

value was 0.29MW nominal conditions.

5.2 Heat removal Value adjustment

In view of maintaining the heat removal capacity in the case of lossage, when the real heat removal value is below the limited minimum, adjustment was carried out assuming that the objective is over 0.45MW as shown below.

If the heat removal value is 0.29MW,100 pipes of the adjustable panel's must run coolant in order to increase levels up to the designated objective. If the heat removal value is in region Ⅱ, using the adjustable panel makes the heat removal value surpass the limited maximum value. Therefore it was decided that the adjustable panel be a separated dual system and operation.

As a result, if the heat removal value is in region Ⅰ no adjustable panel is used, if in region Ⅱ one of adjustable panels is used and if in region Ⅲ both of them are used. Therefore, the actual heat removal value is able to cope with fluctuations in the region of 0.45MW to 0.6MW despite the actual heat removal value distribution.

6. Fabrication of the VCS

Specifications of the VCS were decided by calculations of heat distribution for the concrete and the analysis of heat removal value considered above. A structural design of the VCS is given in Fig.11. The CWP consists of the upper side, sides, lower side, door and adjusting panel. The upper panel has a round shape with penetrations for stand-pipes fitting into the upper barrier block covered on the RPV room. The side panel parts and side parts of the lower panel consist of 12 panels each fitting to dodecagon shape of the RPV room. Fig.12 shows parts from 30 to 150 degrees of the overall picture of the 12 panels. Specifications of the CWP are listed in Table 3.

A sectional plan of the side panel is shown in Fig.13. Water cooling pipes and fins are joined by welds and installed by bolts set on the concrete wall by nuts. Reflectors and the adjustable panels are supported by bolts set on fins of the side panel.(Due to prevention of over-heating the concrete wall the number of bolts were minimized.) Each of the side panel parts and side parts of the lower panel are fabricated in the works separately, and then transported to the HTTR site and installed in the RPV room.

7. Conclusion

The CWP structure of thermal radiation cooling method was established for the VCS-panel of the HTTR. Heat removal value limits as well as temperature limits of concrete were satisfied through the thermal radiation cooling process which brought about the following features.

(1) A lower limit for heat removal values was established by additional reflectors to the cooling water pipes.

(2) Heat removal values could be controlled by the addition of adjustable cooling panels at the location of the innermost reflector. A lack of heat can be rectified by the flow of water in the pipes.

(3)The compatibility of emissivity and analysis methods were confirmed through thermal radiation and heat removal tests, which agreed well with the calculated values.

References

1. JSME Data Book : Heat Transfer 4th Edition.
2. William H. MacAdams : Heat transmission : Appendix, Asian Students' Edition, McGRAW-HILL BOOK COMPANY INC.
3. James. R Welty : Engineering Heat Transfer : Appendix, D John Wiley & Sons (1974)
4. Siegel and Howel : Thermal Radiation Heat Transfer
5. G Neuens : Influence of Surface Properties on the Total Emittance of Steel
6. E.M.Sparrow, R. D. Cess : Radiation Heat Transfer : Chapter 2, McGRAW-HILL BOOK COMPANY INC. (1978)

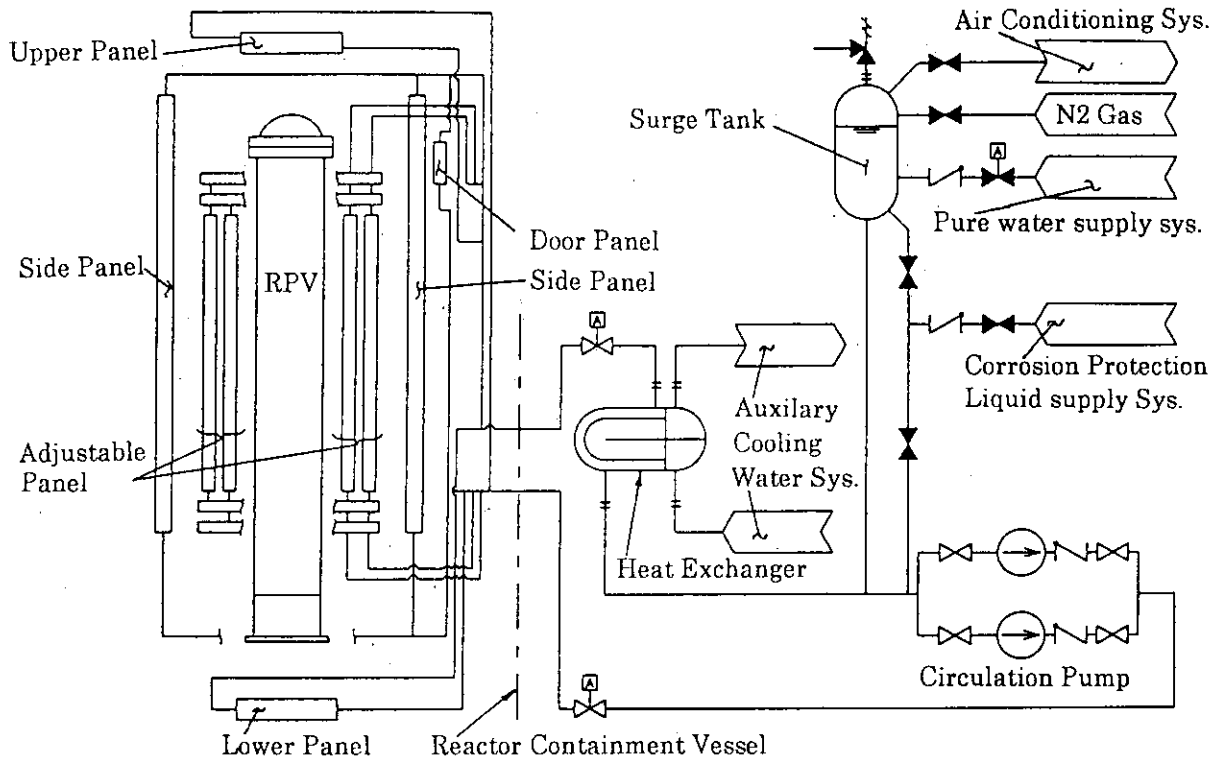


Fig.1 Flow diagram of the VCS (Showing one of the two systems)

Table 1 Design specifications of the VCS

Items	Specifications	
Number of systems	2	
Limited heat removal value	0.3～0.6MW	
Limited temperature of the concrete	65℃	
Coolant	Pure water	
Flow rate	86 metric ton per hour	
Maximum operating temperature	90℃	
Maximum operating pressure	0.98MPa	
Class of aseismic design	As	
Main components and number of each components	Circulation pumps	2 per a system
	Heat exchanger	1 per a system
	Surge tank	1 per a system
Arrangement of the Water Cooling Panel	Upper panel Side panel Door panel Adjustable Panel Lower panel	

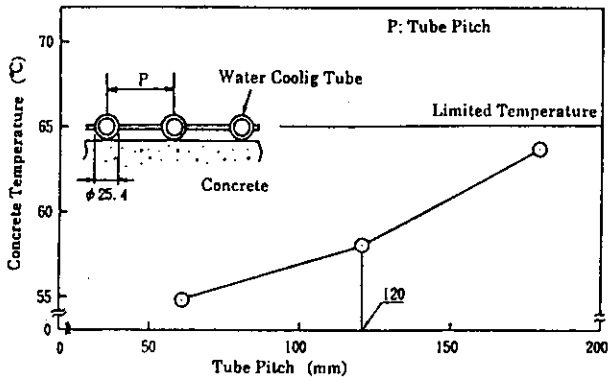


Fig.2 Effect of tube pitch on the concrete temperature

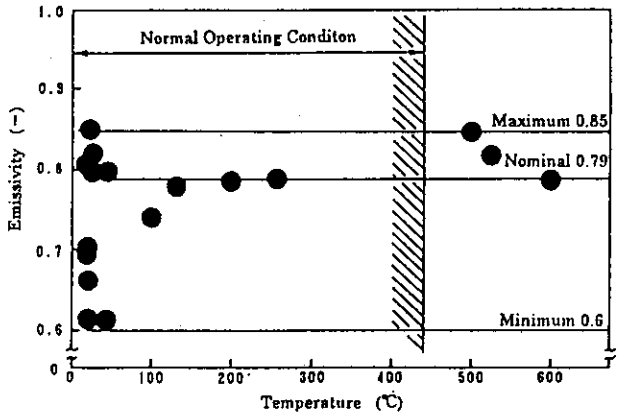


Fig.3 Emissivity data of carbon steel by public issue

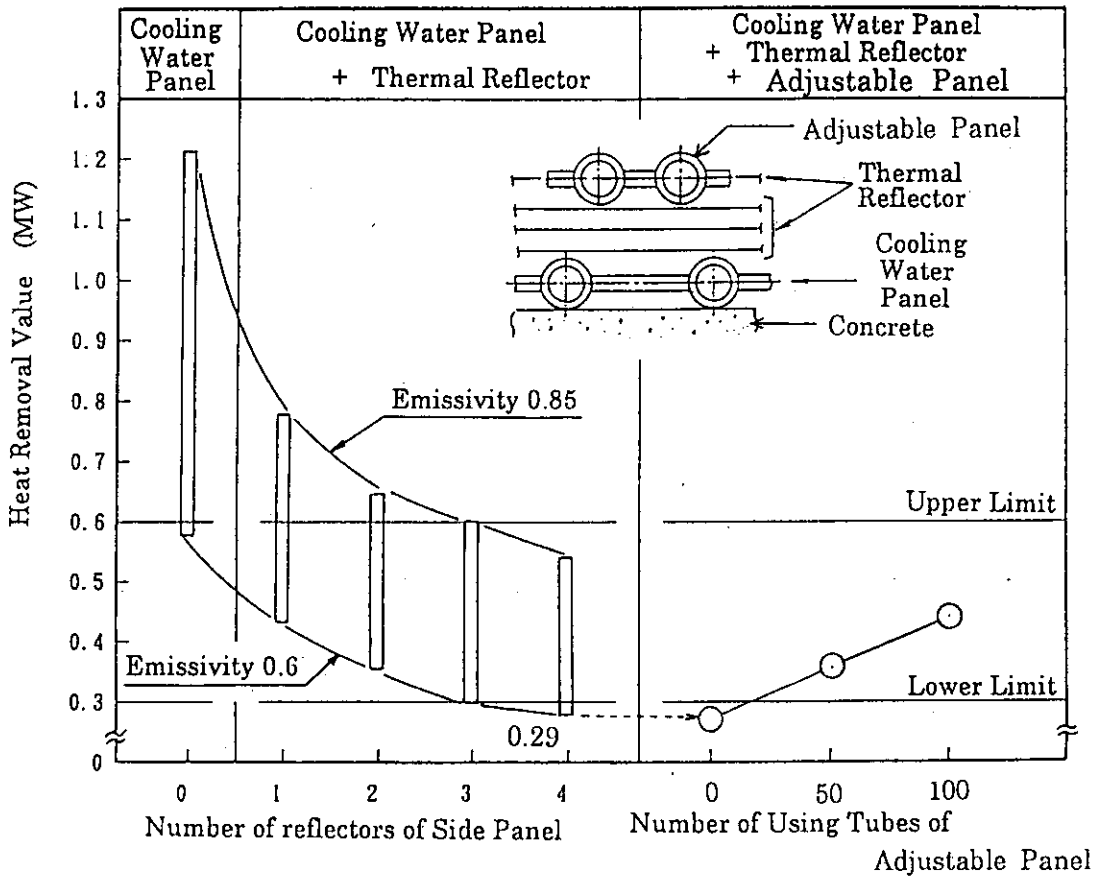


Fig.4 Calculation results of heat removal value

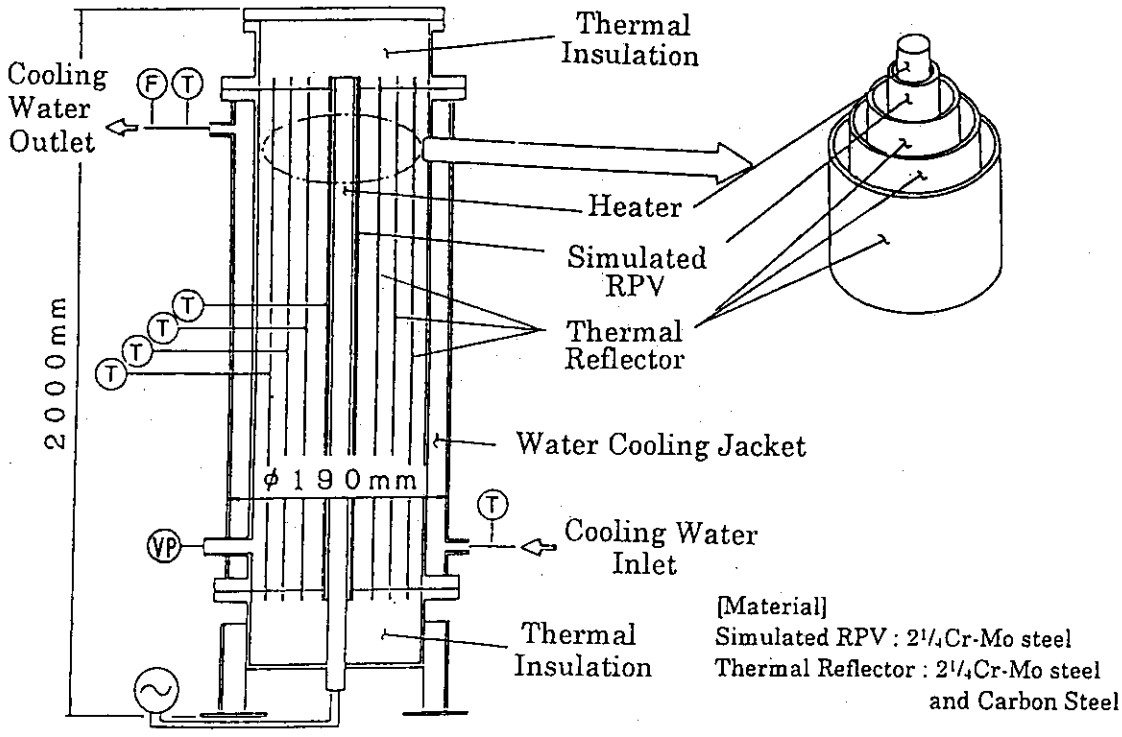


Fig.5 Equipment of basic test for thermal radiation

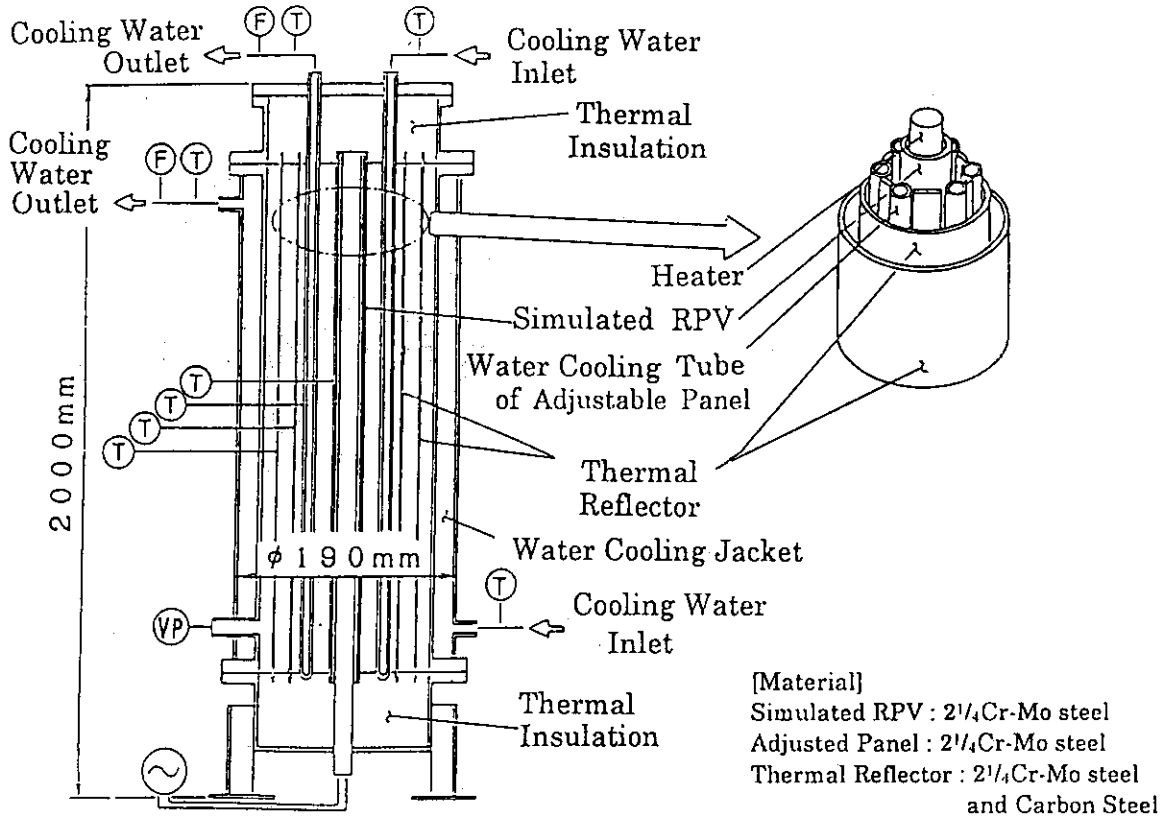


Fig.6 Equipment of heat removal test

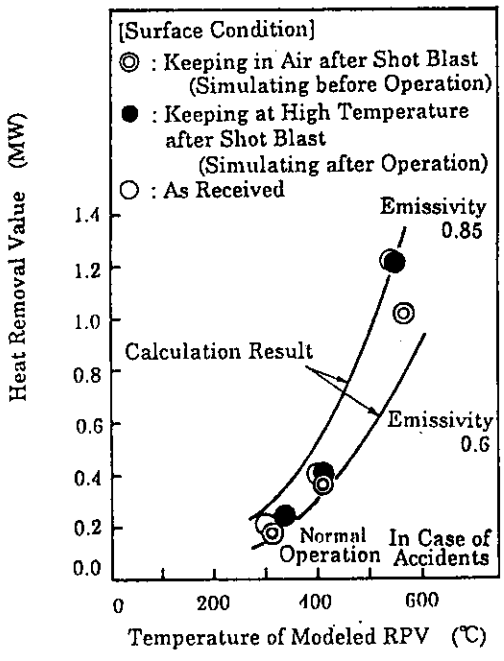


Fig.7 Results of thermal radiation test

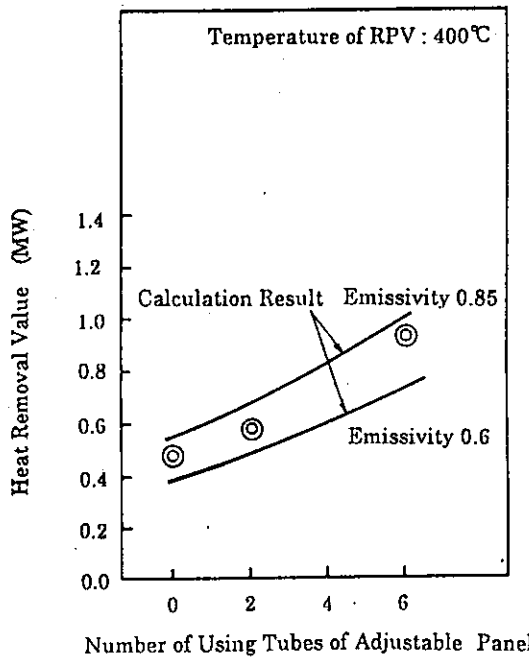


Fig.8 Results of heat removal value test

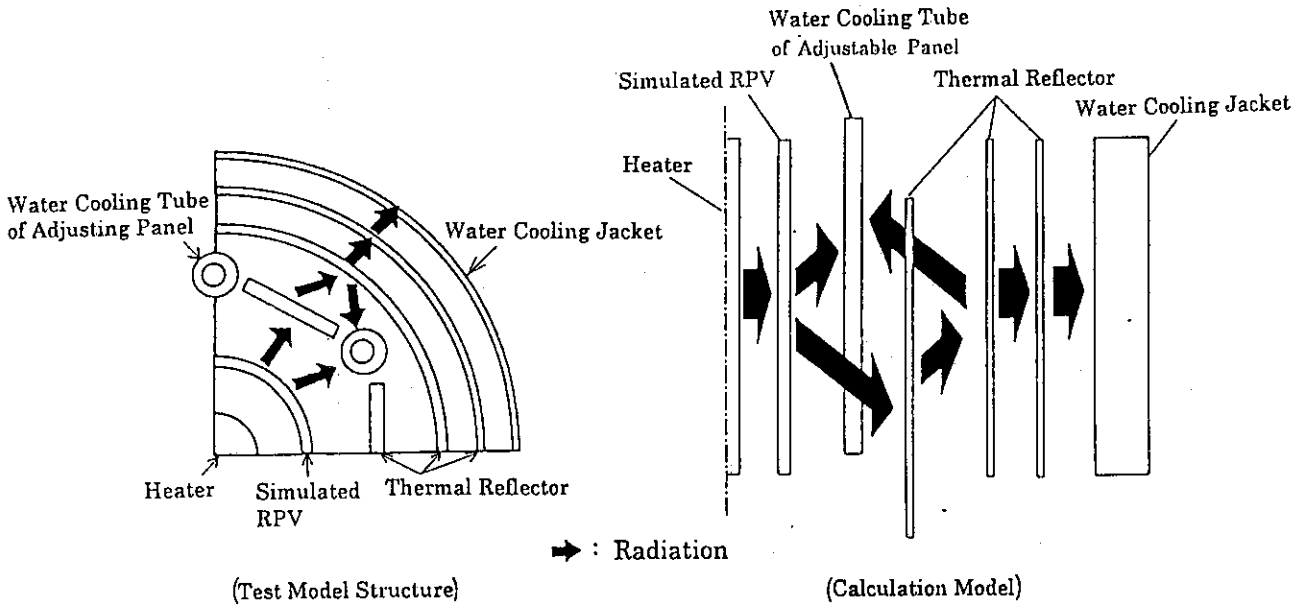


Fig.9 Calculation model for heat removal test

Table 2 Calculation conditions on heat removal value of the practical Cooling Water Panel(CWP)

Items		Maximum value	Nominal value	Minimum value
Panel condition	Emissivity	0.85	0.79	0.6
	Radiation configuration factors (between the RPV and the CWP)	1.0	0.96	0.9
	Surface area of the CWP	All surface area without penetrations for piping	All surface area without penetrations for piping	All surface area without penetrations for piping and the stand pipes surface
	Temperature of the CWP	17℃	35℃	60℃
Room condition	Heat transfer through the CWP's support	considering	considering	not considering
	Heat transfer through the RPV's stabilizer	considering	considering	not considering
	Natural convection	considering	considering	not considering
Inner condition of the RPV	Power level of the core	0.75MW	30MW	29.25MW
	Heat transfer of the core	40.0W/m·K	16.7W/m·K	13.5W/m·K
	Emissivity Graphite block of the core	1.0	1.0	0.8
	Inner surface of the RPV	1.0	1.0	0.6

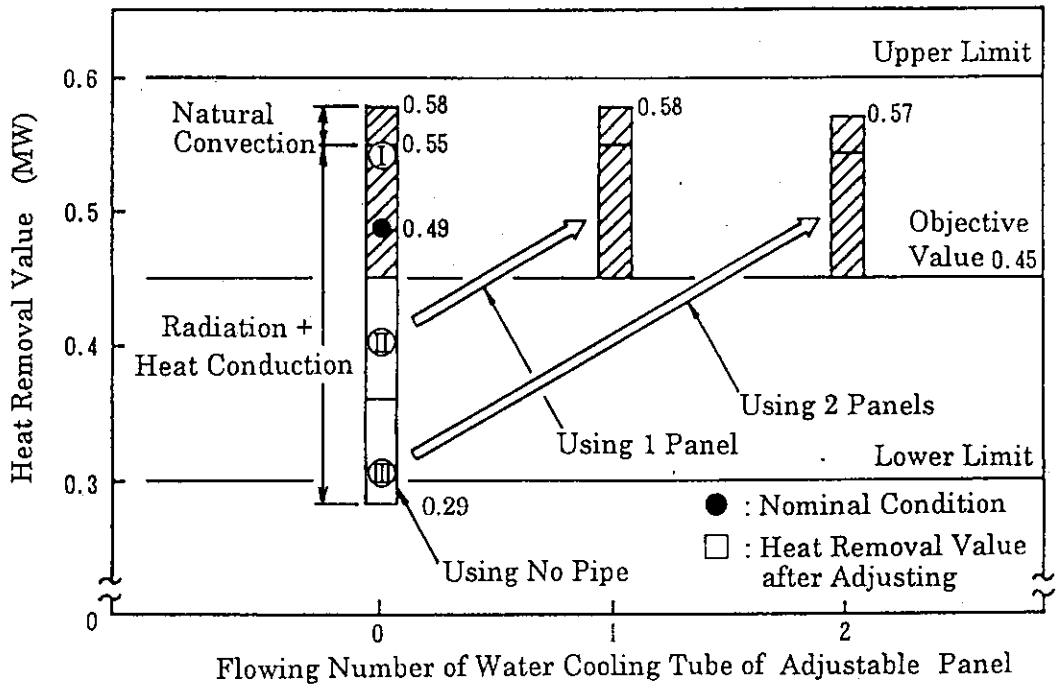


Fig.10 Results of calculation of heat removal value

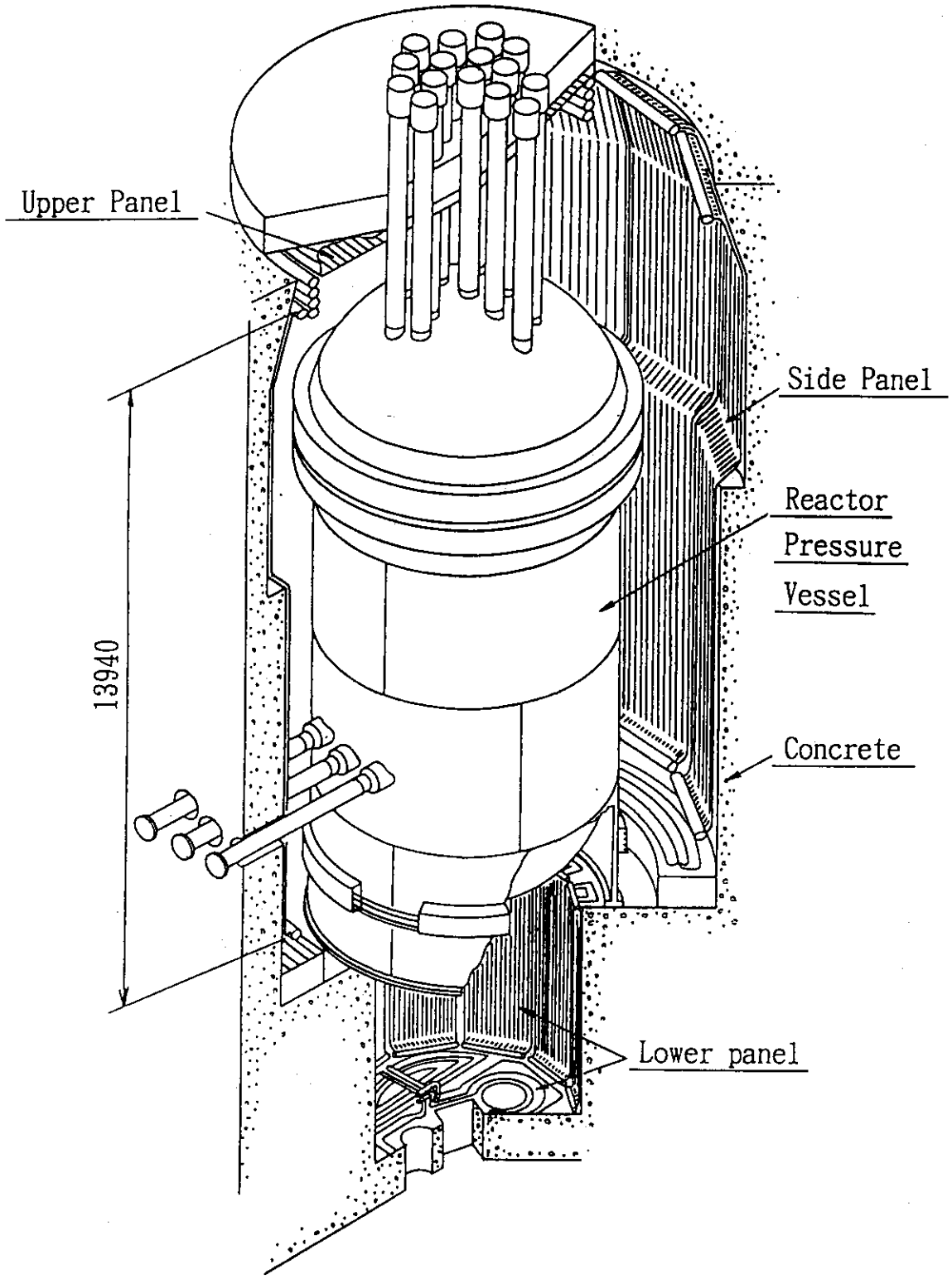


Fig.11 Structure view of water cooling panel of the VCS

Table 3 Design data of the Cooling Water Panel

Upper panel	Tube material	STB410
	Tube O.D., mm	15.9
	Tube thickness, mm	3.2
	No. of tubes	48 per a system
Side panel	Tube material	STB410
	Tube O.D., mm	25.4
	Tube thickness, mm	3.5
	No. of tubes	108 per a system
	Thermal reflector plates' material and No. of plates	one plate made of SUS304 and 3 plates made of SPHC
Adjustable panel	Tube material	STBA24
	Tube O.D., mm	25.4
	Tube thickness, mm	3.5
	No. of tubes	48 per a system
Lower panel	Tube material	STB410
	Tube O.D., mm	25.4
	Tube thickness, mm	3.5
	No. of tubes	120 per a system
	Thermal reflector plates' material and No. of plates	one plate made of SUS304 and 3 plates made of SPHC
Door panel	Tube material	STB410
	Tube O.D., mm	25.4
	Tube thickness, mm	3.5
	No. of tubes	6 per a system

STB410:Carbon steel boiler and heat exchanger tubes
SUS304:Cold rolled stainless plates
SPHC :Hot-rolled mild steel plates
STBA24:Alloy steel boiler and heat exchanger tubes

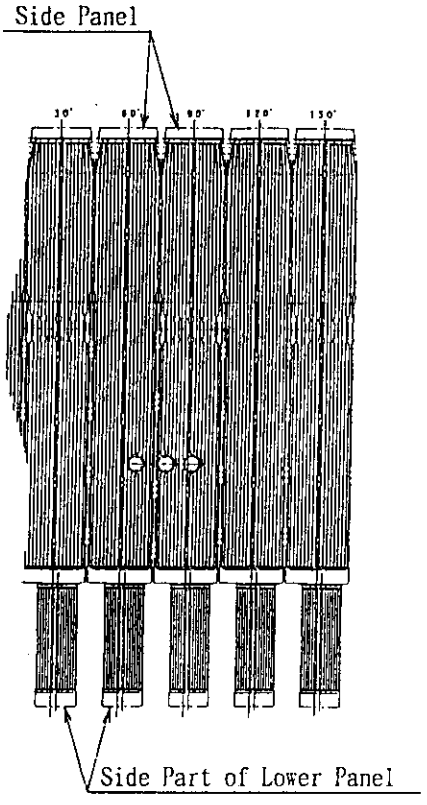


Fig. 12 Developed view of the side panel and the lower panel (from 30° to 150°)

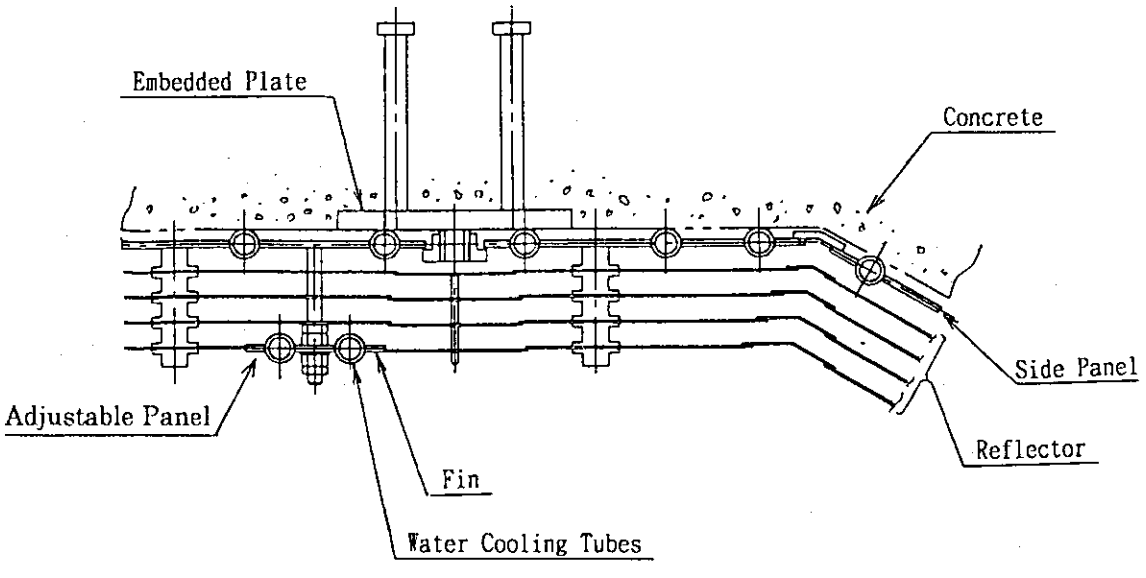


Fig. 13 Cross section of the side panel

6.8 EVALUATION OF LONG-TERM CREEP PROPERTIES OF HASTELLOY XR IN SIMULATED HIGH-TEMPERATURE GAS-COOLED REACTOR HELIUM

Yuji KURATA, Yutaka OGAWA*, Tomio SUZUKI,
Masami SHINDO, Hajime NAKAJIMA and Tatsuo KONDO**

Japan Atomic Energy Research Institute,JAPAN
* now Research Institute for Metals, Tohoku University,JAPAN
** now Faculty of Engineering, Tohoku University,JAPAN

ABSTRACT

Creep properties are among the important basic items of material performance for design of high temperature components of high-temperature gas-cooled reactors(HTGRs). In order to evaluate creep properties of Hastelloy XR (a modified version of the conventional Hastelloy X) developed for the High-Temperature Engineering Test Reactor(HTTR), long-term creep tests were carried out in simulated HTGR helium at 800, 900 and 1000℃. The test results up to about 50,000h showed no significant degradation in creep properties. The creep-rupture strength obtained through the long-term tests was above the level corresponding to the design allowable creep-rupture stress of the HTTR. Rupture lives could be estimated with sufficient accuracy using Larson-Miller parameter. The values of the stress exponent were 4.5 to 5.7 when the stress dependence of the steady-state creep rate was expressed in terms of the Norton equation. It was judged that dominant creep process was dislocation creep. The relationship between the steady-state creep rate and the rupture life was expressed in terms of the Monkman-Grant equation. Carburization during creep in simulated HTGR helium did not degrade creep properties of this alloy. Internally formed cavities and cracks were initiated at sites of precipitates at grain boundaries, growing nearly perpendicular to the stress axis. Creep fracture was caused by the nucleation, growth and link-up of grain boundary cavities in long-term tests. Two phases, Cr-rich carbide and Mo-rich carbide, co-existed in specimens after long-term creep tests.

1. Introduction

The HTTR, which uses helium gas as the primary coolant, is currently under construction as the first HTGR in Japan[1]. Creep properties are among the important basic items of material performance to be considered in high-temperature structural design of the HTTR. Although pure helium gas is inert, the primary coolant helium, which passes through the large mass of hot graphite core structure, cannot avoid containing slight amount of impurity gases, i. e., H_2, H_2O, CO, CO_2 and CH_4. It is considered that these impurities can cause oxidation and carburization or decarburization of heat-resistant alloys and possible effects upon creep properties are suspected. For this reason many research works on creep tests in flowing helium containing a small amount of impurities have been carried out. We have also conducted creep tests in simulated HTGR helium with special care on impurity control in helium.

An intermediate heat exchanger(IHX) of the HTTR is being manufactured using Hastelloy XR. High temperature components such as the IHX were designed using High-Temperature Structural Design Code[2] and Design Allowable Limits[3]. At the time of the design of the HTTR a lot of creep data were used to generate the Design Allowable Limits for which the allowable stress for long-time service was determined through some reasonable extent of extrapolation from the test data obtained up to that time. The allowable stress up to 10^5 h was determined using data up to about 25,000 h[3]. Therefore, it is necessary to confirm whether the allowable stress is sufficiently marginal or not when creep data in longer tests are obtained.

We reported that there was no significant difference between helium and air in the creep rupture lives at 800 to 1000℃ up to about 10,000h and that the test results showed no significant degradation in creep properties[4,5]. Since a series of creep tests for Hastelloy XR in simulated HTGR helium have been accomplished, all results including creep data up to about 50,000 h are analyzed in this study in conjunction with carburization behaviour, microstructure observation and mechanism estimation of creep deformation and fracture.

2. Experimental procedure

2.1 Specimens

The material tested in this study is Hastelloy XR developed for high temperature components of the HTTR. Hastelloy XR is an improved version of Hastelloy X. Table 1 shows the chemical composition of Hastelloy XR together with the specification of Hastelloy X(ASTM B435). Hastelloy XR has a basal composition for the major constituents common with that of Hastelloy X (i.e., nominally Ni-22Cr-18Fe-9Mo in mass %), while contents of specific minor elements are optimized: Mn and Si are adjusted in the optimum ranges and Al, Ti and Co are reduced to the possible lowest levels[6]. The material was supplied in the form of bars of 15 mm in diameter. The solution treatment temperature of the bars was 1180℃ and the grain size was ASTM No.3-4. Specimens of 6 mm in diameter and 30 mm in gauge length were used for creep tests.

2.2 Test methods

Creep tests were carried out in helium environment designated as JAERI Type B helium, which was one of the experimental specifications of the simulated HTGR primary coolant environments. Impurity composition of JAERI Type B helium is shown in Table 2. The chemical characteristic of this impure helium environment is low oxidizing and slight carburizing for Hastelloy XR.

Single specimen type uniaxial creep machines[7] designed for a helium environment were used. Special care was exercised in avoiding undesirable perturbation of the local impurity composition at the test section due either to degassing from or to reaction with the machine components.

Creep tests in the helium environment were carried out at 800, 900 and 1000℃, and under 6.9 to 98.1 MPa. During the test, the temperature was monitored by platinum/ platinum-rhodium thermocouples attached along the specimen gauge section. Microstructure observation was made for ruptured specimens using optical microscope , scanning electron microscope and EPMA.

3. Results and discussion

3.1 Creep rupture properties

Figure 1 shows the relationship between stress and time to rupture for Hastelloy XR in JAERI Type B helium. The solid lines are the regression curves obtained from analysis in terms of Larson-Miller parameter, and the broken lines the design allowable creep-rupture stress (S_R) of the Design Allowable Limits[3]. The design allowable creep rupture stress was determined from the minimum creep rupture time which was one tenth of the mean values obtained by applying the time-temperature parameter (TTP) method to available creep rupture data in air and in simulated HTGR helium[3]. The strength level of the creep-rupture data including results of creep tests up to 48,557.5h is above S_R at each test temperature, and the long-term data above 10,000 h show no significant degradation in creep rupture lives.

The TTP method is often used to analyze creep-rupture data and to predict rupture life and stress[8,9]. In the present study, the following parameters were investigated.

Larson-Miller: $LMP=T(C+\log t_R)$, (1)

Orr-Sherby-Dorn: $OSDP=\log t_R - Q/19.1425T$, (2)

where t_R is time to rupture, T the absolute temperature, and C and Q parameter constants. Equation $f(\sigma)$, which represents stress dependence of TTP, is approximated using polynomials of logarithmic of stress, σ, as

$$f(\sigma)=b_0+b_1\log(\sigma)+b_2(\log(\sigma))^2+\cdots+b_k(\log(\sigma))^k, \quad (3)$$

where $b_0, b_1, b_2, \cdots, b_k$ are regression constants. Parameter constants in equations (1)-(3) are optimized to minimize standard error of estimate (SEE) of $\log t_R$.

$$SEE=\sqrt{\Sigma(Yi - \hat{Y}i)^2/(n_d - n_p-k-1)}, \quad (4)$$

where Yi is a measured value of $\log t_R$, $\hat{Y}i$ an estimated value of $\log t_R$, n_d the number of

data points, n_p the number of parameter constant in TTP and k the degree of equation (3). The optimization procedure was carried out following the study on standardization of creep-rupture data evaluation of metals [9]. Table 3 shows results of TTP analysis for Hastelloy XR. It is found that the degree of polynomials is 2 for LMP and OSDP to have good approximation. Furthermore, the application of LMP results in better fit than that of OSDP since the SEE value of LMP is smaller than that of OSDP. On this basis, the results obtained from analysis in terms of LMP are shown in Fig.1. These regression curves fit experimental results containing long-term data. The final Larson-Miller equation is shown as follows:

$$T(13.545293+\log t_R)$$

$$=23556.529+155.41729\log(\sigma)-1837.2623(\log(\sigma))^2, \quad (5)$$

The relationship between reduction of area and time to rupture at 800, 900 and 1000℃ is shown in Fig.2. While rupture ductility generally decreases with increasing rupture time, the results shown in Fig.2 have a tendency of leveling off in the decrease of rupture ductility after a few thousand hours.

3.2 Creep curve and steady-state creep rate

Creep curves in long-term tests are shown in Fig.3. It was reported that normal type creep curves consisting of transient, steady-state and accelerated stages were observed at 800℃ and that, for Hastelloy XR at 1000℃, some irregular creep curves were often observed [10]. In the present case, while long-term creep curves at 800 and 900℃ are normal type curves as shown in Fig.3, the creep curve at 1000℃ is the irregular creep curve where the transient stage is hardly recognized. Figure 4 shows the relationship between the steady-state creep rate and stress. The creep rate at 3% strain was adopted as the steady-state creep rate when the steady-state region was not recognized clearly in the irregular creep curves.

The relationship between the steady-state creep rate, $\dot{\varepsilon}_s$, and stress, σ, is generally expressed as a power law, often called Norton's Law.

$$\dot{\varepsilon}_S = A\,\sigma^n \ , \qquad (6)$$

where n is the stress exponent and A a constant. The stress exponent, n, obtained by applying the least squares method to data at each temperature is 5.745 at 800℃, 4.686 at 900℃ and 4.527 at 1000℃, respectively. The n value at each temperature does not change within this experimental condition even if the stress decreases. It was reported that n would be unity under the diffusional creep mechanism and that n would be greater than 3 under the dislocation creep mechanism[11]. The creep process of Hastelloy XR within this experimental condition is interpreted to be dominated by the dislocation creep mechanism since n values are above 3. Generally n value is about 5 for solution-strengthened alloys, and it is often above 5 for precipitation-strengthened alloys[12]. Hastelloy XR is strengthened mainly by solution and additionally by precipitation. The facts that the n value is above 5 at 800℃ and that it decreases with increasing temperature are explained by the decrease in the function of precipitation strengthening due to the coarsening of precipitates at high temperatures.

An activation energy for creep, Qc can be derived from a plot of log $\dot{\varepsilon}_S$ against (1/T) at constant stress. The Qc values obtained were 340-450 kJ/mol. These values are larger than the activation energy value, 285 kJ/mol[13], of lattice diffusion of Ni in Ni-20 at %Cr alloy. By these approaches, we can say that dislocation creep with n values of about 5 and with Qc values larger than the activation energy for lattice diffusion of Ni in Ni-20 at %Cr alloy is predominant under conditions applied in this study.

The following Monkman-Grant equation is useful to perform the prediction of life or residual-life of high-temperature component.

$$\log t_R = c - m \log \dot{\varepsilon}_S \ , \qquad (7)$$

where c and m are constants. Figure 5 shows the relationship between the time to rupture and the steady-state creep rate for Hastelloy XR. The regression curves at each temperature or at all temperatures are also shown in this figure. Creep rupture lives for Hastelloy XR can be predicted using the Monkman-Grant equation.

3.3 Carbon analysis and microstructure observation

Since decarburization and carburization have appreciable effects on creep behaviour [14,15], carbon analysis was carried out for ruptured specimens. Furthermore, microstructure observation for surface and cross sections of ruptured specimens was performed.

Figure 6 shows results of carbon analysis. Carbon content was analyzed for section including rupture portion where there are many cracks and for 8-mm-diameter section where there is little creep deformation. Carbon content in the former is high as shown in Fig.6. This tendency becomes significant with higher temperatures and longer times. On the other hand, there is only a little carburization in 8-mm-diameter section even after long-term exposure to the impure helium. It can be pointed out that carbon intrusion during the steady-state creep stage was limited to a negligible level. No specimen experienced decarburization which caused significant decrease in rupture lives[14]. Carburization during creep in simulated HTGR helium did not substantially degrade creep properties of Hastelloy XR.

The following characteristic of microstructures of specimens ruptured in long-term creep tests can be described from Fig. 7. The depth of the surface crack was about 100-150 μm at 800 and 900℃, and about 200 μm at 1000℃. It was found that creep fracture was caused by the growth and link-up of cavities nucleated at sites of precipitates at grain boundaries, growing nearly perpendicular to the stress axis. Grain boundaries perpendicular to the stress axis are under tensile stress. Precipitates at grain boundaries under tensile stress coarsened as shown in Fig.7. In order to obtain information on precipitates, EPMA analysis was carried out. Figure 8 shows the results of EPMA analysis for the specimen ruptured at 900℃ in 48,587.5 h. It is clear that bright precipitates co-exist with dark precipitates in both secondary and backscattered electron images. The bright precipitates have high molybdenum, silicon and comparatively low chromium contents, while the dark precipitates have high chromium, carbon and molybdenum, and low silicon contents. Table 4 shows quantitative analysis of precipitates and matrix by EPMA. The dark phase is Cr-rich carbide presumed to be

$M_{23}C_6$ type carbide[16,17]. The bright phase has high molybdenum and comparatively low chromium contents. This bright phase enriched with Mo is presumed to be M_6C type carbide[17].

4. Conclusions

Creep tests of Hastelloy XR were carried out in simulated HTGR helium up to about 50,000 h at 800, 900 and 1000℃. The main results obtained are as follows:

(1)The test results up to about 50,000 h showed no significant degradation in creep properties such as the rupture life, rupture ductility and the steady-state creep rate. Creep-rupture stress is substantially above S_R of the Design Allowable Limits.

(2)The stress dependence of the steady-state creep rate is expressed in terms of the Norton equation. The values of the stress exponent is 4.5 to 5.7. On this basis, it is judged that dominant creep process is dislocation creep.

(3) Rupture lives of Hastelloy XR can be estimated with sufficient accuracy using a Larson-Miller parameter. The relationship between the steady-state creep rate and time to rupture is expressed in terms of the Monkman-Grant equation.

(4)Some appreciable carburization was recognized in the specimens ruptured after creep tests in simulated HTGR helium. Carburization during creep in the helium did not substantially degrade creep properties of Hastelloy-XR.

(5)Creep fracture was caused by the growth and link-up of cavities nucleated at sites of precipitates at grain boundaries, growing nearly perpendicular to the stress axis. There were two phases, Cr-rich carbide presumed to be $M_{23}C_6$ and Mo-rich carbide presumed to be M_6C in specimens after long-term creep tests.

Acknowledgements

Authors are very grateful to staffs of Material Performance and Testing Laboratory for their assistance during this long-term study.

References

(1)Japan Atomic Energy Research Institute : Present Status of HTGR Research and Development (1996).

(2)HTTR Designing Laboratory, Department of Fuels and Materials Research and Department of High-Temperature Engineering : JAERI-M 89-005 (1989) [in Japanese].

(3)HADA, K., MOTOKI, Y., and BABA, O. : JAERI-M 90-148(1990) [in Japanese].

(4)KURATA,Y., OGAWA, Y. and KONDO, T. :Nucl. Technol.., 66, 250(1984).

(5)OGAWA, Y., KURATA, Y. ,SUZUKI, T., NAKAJIMA, H. and KONDO, T. : Nihon-Genshiryoku-Gakkai Shi (J. At. Energy Soc. Japan), 36, 967 (1994) [in Japanese].

(6)SHINDO, M. and KONDO, T. : Proc. Conf. on Gas-Cooled Reactors Today, Bristol/UK, 1982(British Nuclear Energy Society) Vol.2, p.179.

(7)OGAWA,Y. and KONDO, T. : JAERI-M 8801 (1980) [in Japanese].

(8)VISWANATHAN, R. : Damage Mechanism and Life Assessment of High-Temperature Components, ASM International, Metals Park, Ohio, (1989).

(9)VAMAS Data Evaluation Committee : Study on Standardization of Creep-Rupture Data Evaluation of Metals, The Iron and Steel Institute of Japan, (1994) [in Japanese].

(10)YOKOI, S., MONMA, Y., KONDO, T,., OGAWA, Y. and KURATA, Y. : JAERI-M 83-138 (1983) [in Japanese].

(11)FROST, H.J. and ASHBY, M.F. : Deformation Mechanism Maps, Pergamon Press, London, (1982).

(12)SIDEY, D. and WILSHIRE, B. : Met. Sci. J., 3, 56 (1969).

(13)MONMA, K., SUDO, H. and OIKAWA, H. : Nihon-Kinzoku-Gakkai Shi (J. Jpn. Inst. Met.), 28, 188 (1964) [in Japanese].

(14)KURATA, Y., OGAWA, Y. and NAKAJIMA, H. : Tetsu-to-Hagane (J. Iron Steel Inst. Jpn.), 74, 380 (1988) [in Japanese].

(15)idem. : ibid., 74, 2185 (1988) [in Japanese].

(16)SABOL, G.P. and STICKLER, R. : Phys. Stat. Sol., 35, 11(1969).

(17)TANABE, T., ABE, F., SAKAI, Y. and OKADA, M. : Transactions ISIJ (J. Iron Steel Inst. Jpn.), 26, 968 (1986) .

Table 1 Chemical composition of Hastelloy XR (mass%)

	Cr	Fe	C	Si	Co	Mn	B
Hastelloy X (ASTM B435)	20.5～23.0	17.0～20.0	0.05～0.15	max. 1.00	0.5～2.5	max. 1.00	—
Hastelloy XR	21.90	18.23	0.07	0.27	0.04	0.88	0.0003
	Mo	P	S	W	Al	Ti	Ni
Hastelloy X (ASTM B435)	8.0～10.0	max. 0.04	0.030	0.2～1.0	—	—	Remainder
Hastelloy XR	9.13	0.005	0.005	0.47	0.03	0.02	Remainder

Table 2 Impurity levels of JAERI Type B helium (vol ppm)

H_2	H_2O	CO	CO_2	CH_4
200～210	0.8～1.2	100～110	2～3	5～6

Table 3 Comparison of standard TTP (time-temperature parameter) fit for rupture lives of Hastelloy XR

Degree of Polynomals	SEE(standard error of estimate)	
	Larson-Miller Parameter	Orr-Sherby-Dorn Parameter
1	0.223	0.278
2	0.160	0.173
3	0.164	0.175
4	0.159	0.171
5	0.156	0.168

Table 4 Quantitative analysis of precipitates and matrix of Hastelloy XR ruptured at 1000℃ and 6.9 MPa in 13,014 h (mass%)

	Ni	Cr	Fe	Mo	Mn	W
Precipitate (Dark)	4.7	71.6	3.6	18.7	0.36	0.99
Precipitate (Bright)	20.2	16.1	6.4	53.8	0.16	3.3
Matrix	49.6	22.8	18.5	7.7	0.93	0.40

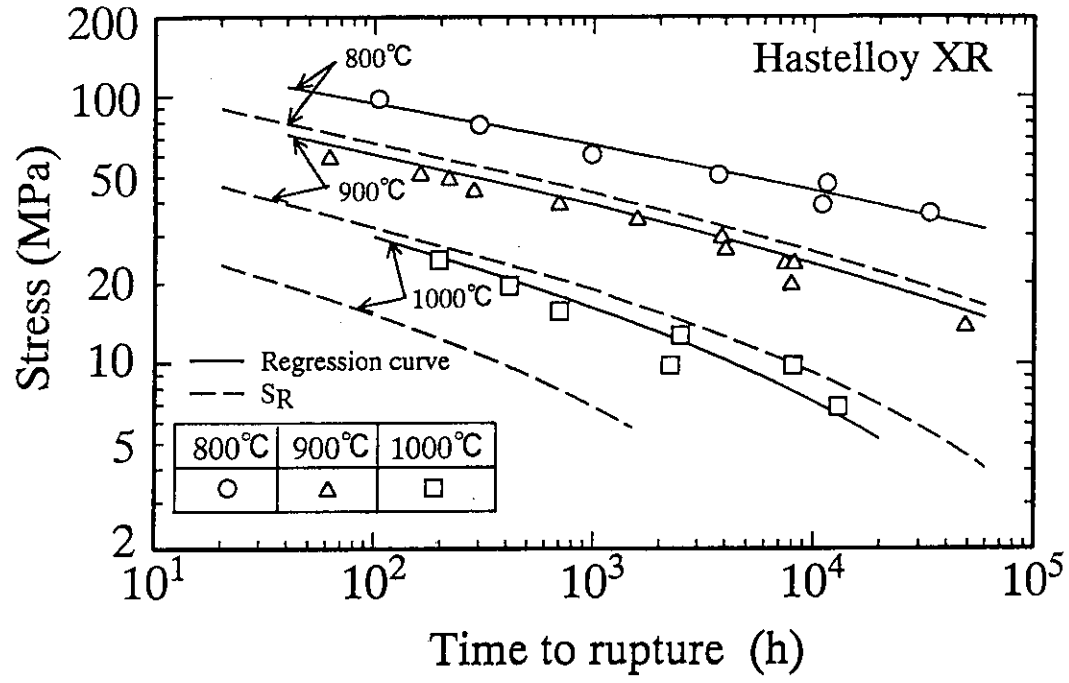


Fig. 1 Stress vs. time to rupture for Hastelloy XR in JAERI Type B helium. The solid lines are the regression curves obtained from application of Larson-Miller parameter, and the broken lines the design allowable creep-rupture stress (S_R) of the Design Allowable Limits [3].

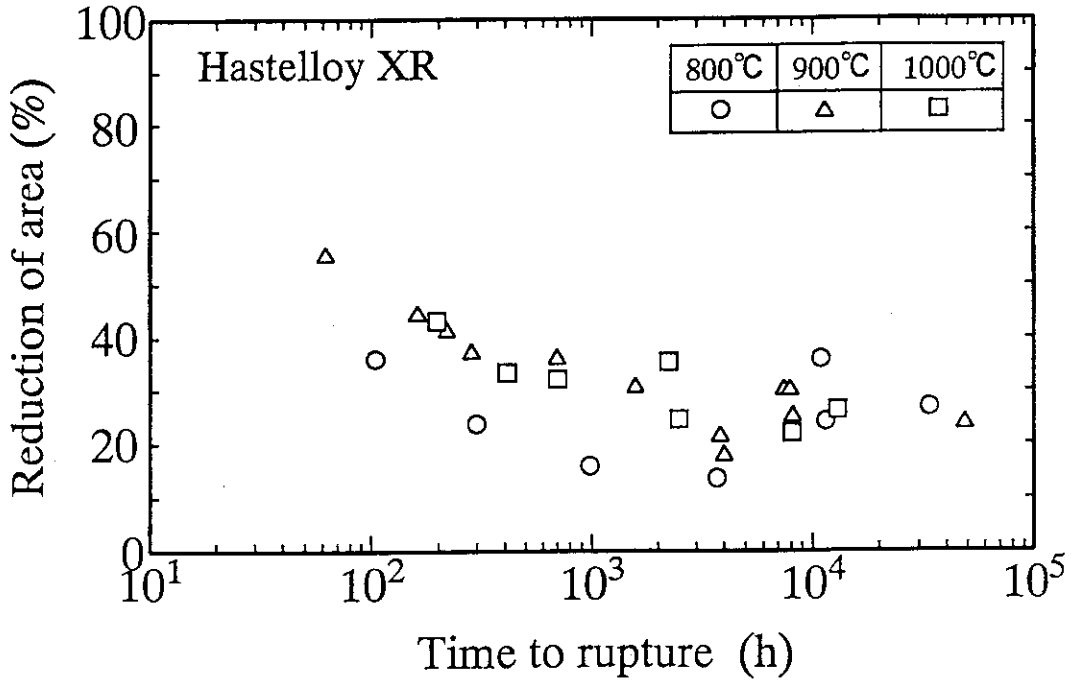


Fig. 2 Reduction of area vs. time to rupture for Hastelloy XR in JAERI Type B helium.

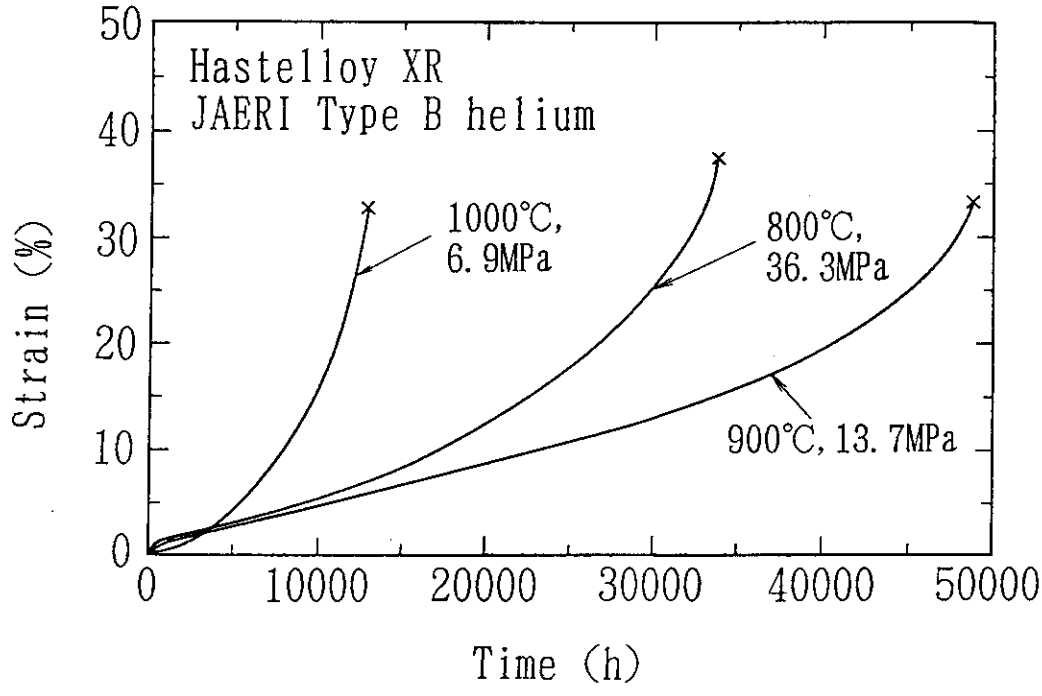


Fig. 3 Long-term creep curves of Hastelloy XR in JAERI Type B helium.

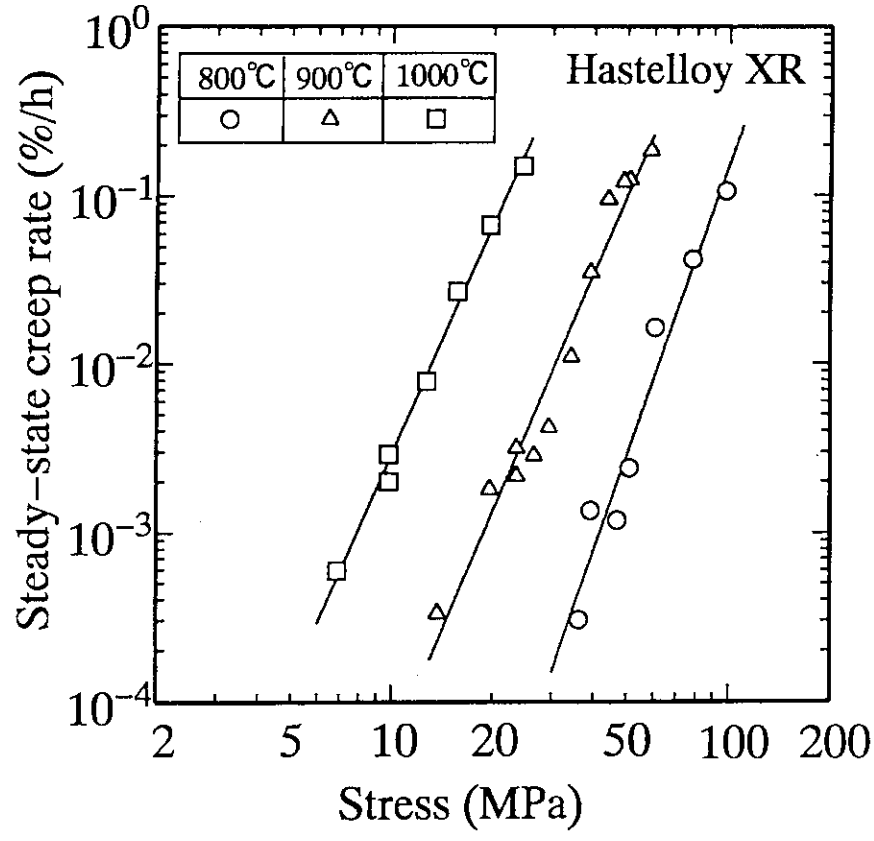


Fig. 4 Relationship between steady-state creep rate and stress for Hastelloy XR in JAERI Type B helium.

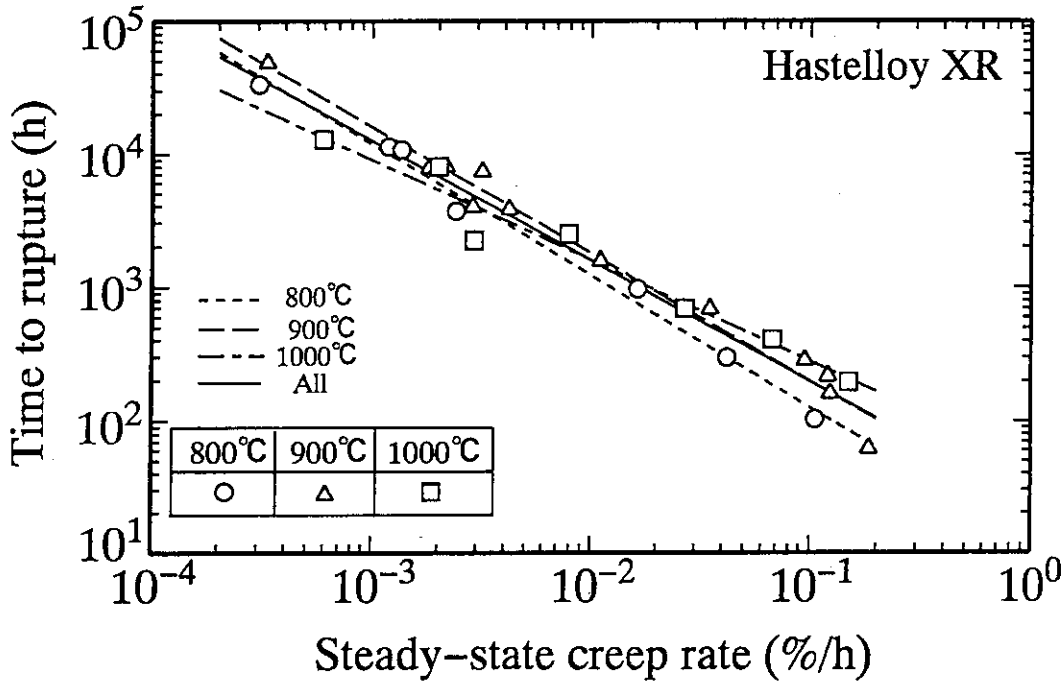


Fig. 5 Relationship between time to rupture and steady-state creep rate (Monkman-Grant relationship) for Hastelloy XR in JAERI Type B helium.

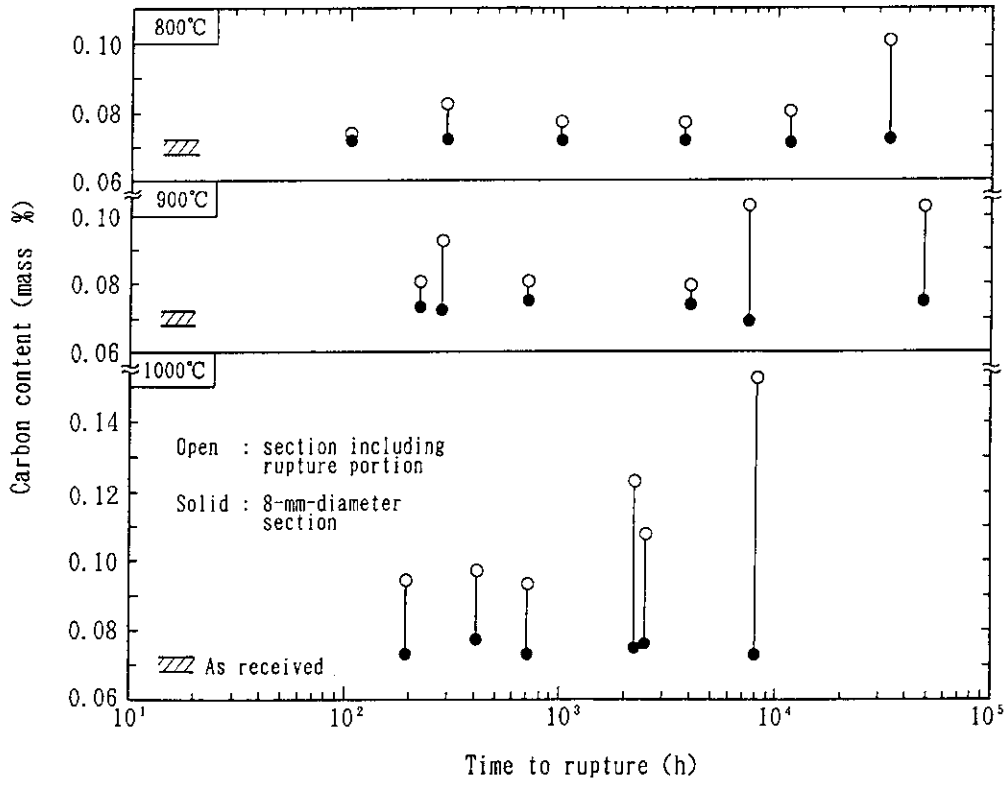
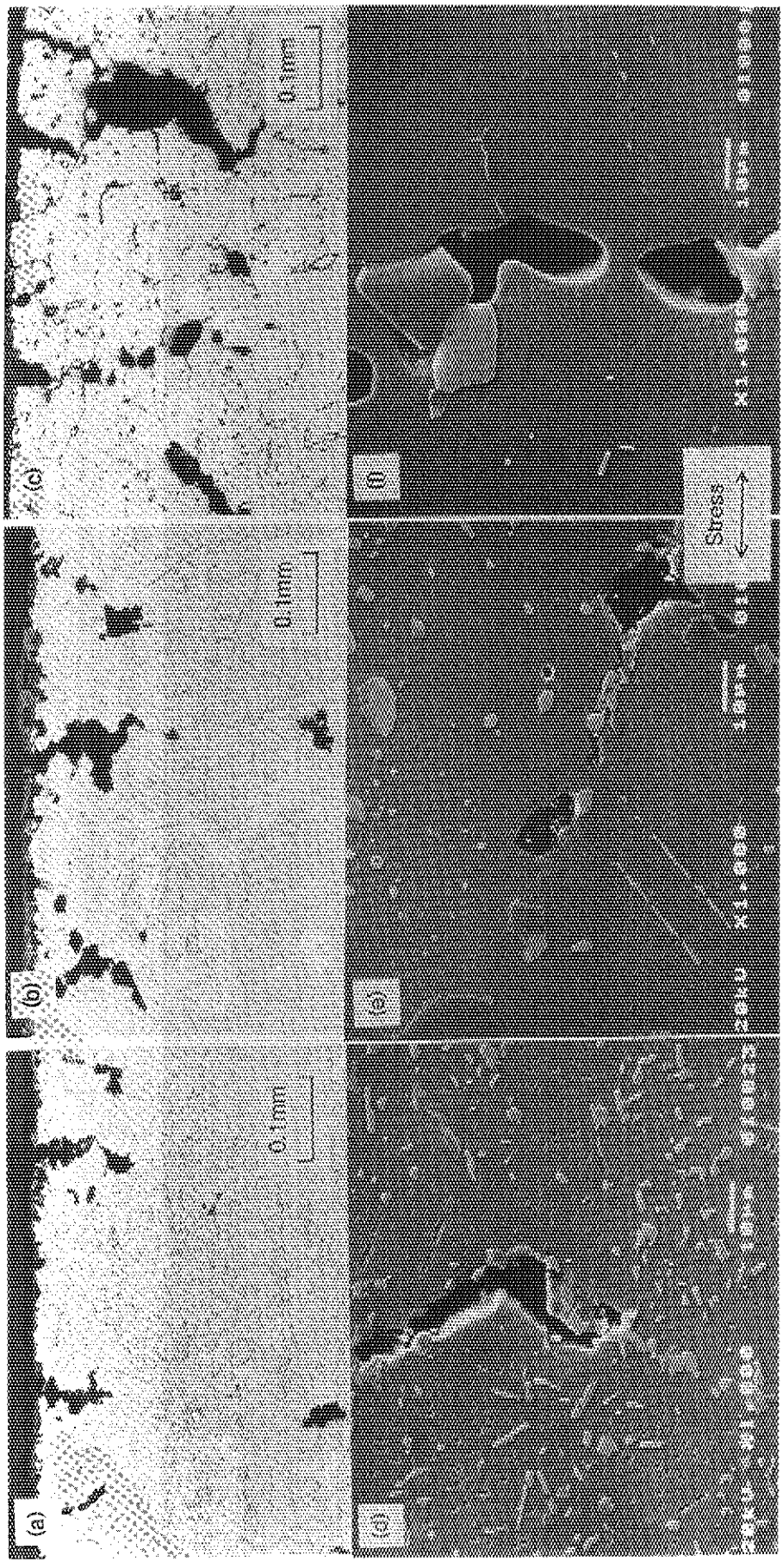


Fig. 6 Results of carbon analysis on the specimens of Hastelloy XR creep-ruptured in JAERI Type B helium.

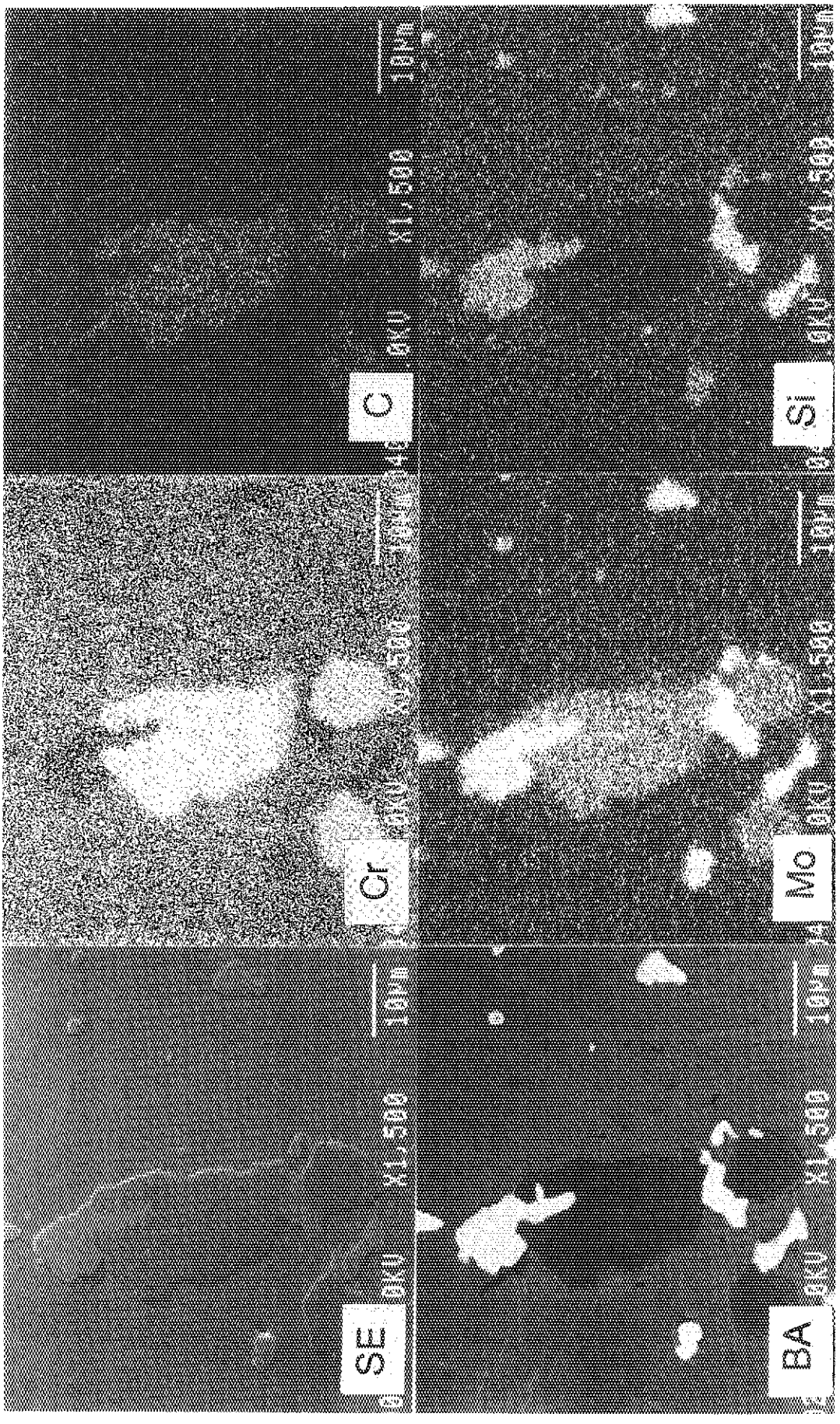


(a),(d) 800℃, Stress : 36.3 MPa, Time to rupture : 33,521.0h

(b),(e) 900℃, Stress : 13.7 MPa, Time to rupture : 48,587.5h

(c),(f) 1000℃, Stress : 6.9 MPa, Time to rupture : 13,014.0h

Fig. 7 Microstructures of Hastelloy XR after long-term creep tests in JAERI Type B helium.



SE ; Secondary electron image,
BA ; Backscattered electron image

Fig. 8 Characteristic X-ray images of Hastelloy XR creep-ruptured at 900℃ and 13.7 MPa in 48,587.5 h.

6.9 DEVELOPMENT OF A NI-CR-W SUPERALLOY FOR APPLICATION TO HIGH-TEMPERATURE GAS-COOLED REACTOR SYSTEMS -CREEP PROPERTIES AND WELDABILITY-

Yuji KURATA, Teiichiro SAITO*, Hirokazu TSUJI, Tamao TAKATSU*,
Masami SHINDO and Hajime NAKAJIMA

Japan Atomic Energy Research Institute, JAPAN
*Nippon Welding Rod Co., Ltd., JAPAN

ABSTRACT

Creep tests in air and weldability tests were carried out in a research program on development of the new Ni-Cr-W superalloy as a component material for high-temperature gas-cooled reactors(HTGRs) with coolant outlet temperatures up to 1000℃. The optimum chemical composition has already been proposed on the basis of a series of experiments. Creep tests were performed at 900, 1000 and 1050℃ using the new Ni-Cr-W superalloy manufactured in an industrial scale, i. e. 2000 kg. Creep rupture lives of the Ni-Cr-W superalloy were dependent on grain size. It was confirmed that the creep rupture strength of the Ni-Cr-W superalloy with grain sizes above ASTM No. 2 was above 9.8 MPa for a $1x10^5$ h life at 1000℃, which was the final target of the program. Creep rupture lives of this superalloy could be estimated in terms of Larson-Miller parameter. Weldability tests were carried out using several heats of the Ni-Cr-W superalloy with different content levels of minor alloying elements as filler metals on the TIG welding process. Although most of heats showed high susceptibility to cracking in the weldments, some heats showed good weldability. According to the weldability tests, it was estimated that minor alloying elements such as Zr, B, Y and Ti influenced susceptibility to cracking in the weldments.Two heats of the Ni-Cr-W superalloy showing good weldability were used to fabricate trial welded joints. Creep rupture strength of the trial welded joints was a little lower than that of the base metal with grain size of ASTM No.2.

1. Introduction

Ni-Cr-W superalloys were recognized as one of the best materials for intermediate heat exchangers in the national research project concerning nuclear steel-making in Japan, where some superalloys possessing high creep strength were developed [1-3]. In Japan Atomic Energy Research Institute (JAERI), study on material behaviour in high temperature gas-cooled reactor [HTGR] system was carried out, and as a result Hastelloy XR possessing high corrosion resistance in HTGR helium environment was developed [4]. Succeeding to these research activities, research and development of new heavy duty Ni-Cr-W superalloys for use at service temperatures around 1000℃ have been promoted by JAERI in cooperation with experienced authorities of industrial and academic organizations [5,6].

The program had set the following targets;

①creep rupture strength over 7.8 MPa for a $1x10^5$ h life at 1000℃, with the final target being 9.8 MPa for the same life and temperature,

②no substantial susceptibility to intergranular attack or internal oxidation after exposure to the simulated HTGR helium at 1000℃ for $1x10^5$ h,

③formability to 32-mm-outer dia., 4- to 5-mm-thick, 7-m-long seamless tubes, and

④enough capacity for the secondary cold-forming and welding.

The optimum chemical composition of the base metal, which can be expected to attain the targets of creep rupture strength and corrosion resistance, has been already proposed as a result of a series of experiments in this program [6]. Furthermore, it was shown that the Ni-Cr-W superalloy fabricated in an industrial scale possessed sufficient formability to seamless tubes [7]. The items to be solved in order to put the developed Ni-Cr-W superalloy to practical use are estimation of long-term creep strength and development of weldments.

In this paper, estimation of creep properties of the base metal fabricated in an industrial scale, development of the filler metal for welding and creep properties of trial welded joints are described.

2. Alloy development

2.1 Creep properties of base metal

(1)Specimen and experimental procedure

The material tested is Ni-18～19mass%Cr-20～22mass%W alloy manufactured in

an industrial scale, i. e. 2000kg. Table 1 shows aimed and analyzed values of chemical composition of the alloy. Chemical composition was analyzed for six specimens sampled from the top position to the bottom position of the ingot. Homogeneous material could be fabricated because the analyzed value of each element was almost same for any samples as shown in this table. Creep specimens were sampled from bars manufactured in an industrial scale. Heat treatment shown in Table 2 was conducted to study effect of heat treatment condition on creep properties. Grain size increased with increase in heat treatment temperature. Heating at 1190℃ for 2h was conducted after water quenching following heating at 1215℃ for 1h in heat treatment B. During this treatment, α_2-W precipitated at grain boundaries.

Creep tests were performed at 900, 1000 and 1050 ℃ in air. Specimens of 6 mm in diameter and 30 mm in gauge length were used for creep tests.

(2)Experimental results and discussion

Figure 1 shows the relationship between stress and time to rupture. Although time to rupture at 900℃ is almost independent on heat treatment, time to rupture for specimens with high heat treatment temperature and large grain size becomes long at 1000 and 1050℃. Significant difference in time to rupture for specimens between heat treatment A and B was not found. The relationship between rupture elongation and time to rupture is shown in Fig. 2. Rupture elongation seems to decrease with increase in grain size. Rupture elongation for the Ni-18～19mass%Cr-20～22mass%W alloy was above 20% after long-term creep tests.

Figure 3 shows creep curves at 1000℃ under 19.6 MPa for specimens with heat treatment A and D. For the specimen with heat treatment D, abnormal creep[8], where creep rate decreased again after accelerated creep stage, was observed. It was reported that oxidation and/or nitrization which occurred through surface cracks of specimens caused abnormal creep observed in long-term creep tests at high temperatures in air [9]. Therefore, rupture time for the specimen with abnormal creep overestimates inherent rupture time of the metallic material. As shown in Fig. 1, rupture time at 1000℃ under 19.6 MPa for the specimen with heat treatment D is very long compared with that with heat treatment C. An example which corrected abnormal creep was shown for the creep curve of heat treatment D in Fig. 3.

Rupture time can be analyzed using the time-temperature parameter method [10,11]. We applied Larson-Miller and Orr-Sherby-Dorn parameters to data of heat treatment A to D. The optimization procedure of parameter constants was carried out following the study on standardization of creep-rupture data evaluation of metals[11]. As a result, it was found that rupture time of the Ni-Cr-W alloy could be estimated with sufficient accuracy using Larson-Miller parameter. The creep rupture strength for a $1x10^5$h life at 1000℃ predicted in terms of Larson-Miller parameter is the following:

8.5 MPa for heat treatment A

9.1 MPa for heat treatment B

10.8 MPa for heat treatment C

12.2 MPa for heat treatment D

The creep rupture strength of the material with heat treatment D was calculated after correction as mentioned above because obvious abnormal creep was recognized for this material. The relationship between stress and Larson-Miller parameter for the material with heat treatment C is shown in Fig.4. Creep rupture strength of the Ni-Cr-W alloy with grain sizes above ASTM No.2 is above 9.8 MPa for a $1x10^5$ h life at 1000℃, which is the final target of the program.

(3)Conclusions

①Creep rupture lives of the Ni-18～19mass%Cr-20～22mass%W alloy become long at 1000 and 1050℃ with increase in grain size although they are independent on grain size at 900℃.

②Rupture lives can be predicted with sufficient accuracy using Larson-Miller parameter. Creep rupture strength of the Ni-Cr-W alloy with grain sizes above ASTM No.2 is above 9.8 MPa for a $1x10^5$ h life at 1000℃, which is the final target of the program.

2.2 Weldability

(1)Specimen and experimental procedure

Totally, twenty-one heats of Ni-18～19mass%Cr-20～22mass%W alloys controlling contents of minor alloying elements were prepared to conduct weldability tests. Table 3 shows the range of chemical composition of the alloys tested. Weldability tests for tungsten inert gas (TIG) welding were performed. Rectangular rods with a base

3mm x 3mm and a length of about 230mm cut from a 15mm-thick plate were used as a filler metal for manual TIG welding. Some filler wires with 1.2mm in diameter were used for automatic TIG welding. Tables 4 and 5 show condition of manual and automatic TIG welding, respectively. Furthermore, welding procedure and groove geometries for weldability tests are shown in Fig. 5. At first the following tests ①～④, were conducted to estimate susceptibility to cracking. In addition, the following tests ⑤～⑧, were performed for alloys needed detail inspection. In this paper, mainly results of the tests ①, ③,⑤ and ⑧ are described.

① bead-on-plate weldability test
② FISCO test
③ overlaying test
④ bend test of welded joints
⑤ microstructure observation
⑥ hardness test
⑦ chemical analysis of weld metal
⑧ electron probe micro analyzer (EPMA) observation

(2)Experimental results and discussion

It was found from a series of weldability tests that susceptibility to cracking in the weldments of Ni-18～19mass%Cr-20～22mass%W alloys was very high. Hence effort was made to lower susceptibility to cracking of the Ni-Cr-W alloy. For example, Fig.6 shows examples of bead-on-plate weldability tests. As shown in this figure, addition of Ti clearly made susceptibility to cracking low. Furthermore, the alloy with Ti addition produced in an industrial scale exhibited excellent weldability. However, cracking was observed for this alloy as shown in Fig. 7 when the alloy heat-treated at higher temperature was used in weldability tests. In this way, good weldability could not constantly obtained using the alloy with the same chemical composition as that of the base metal.

Effect of Mn, Si, Mg, and Y on susceptibility to cracking was investigated because addition of Ti improved weldability as mentioned above and because it was reported that such elements as Ti, Al and Mg improved weldability owing to effect of deoxidation and desulphuration in Ni-base superalloys[12]. However, addition of Mn, Si, Mg and Y did not result in significant improvement on weldability as shown in Fig. 8. On the other hand, localization of Zr and Y was recognized in EPMA observation of weld metals as shown in Fig. 9. It is considered that these elements make susceptibility to cracking high owing to formation of compounds with low melting points in welding. It was found that weldability was extremely improved in the alloy with low contents of these elements.

Quantitative estimation of effect of minor elements on susceptibility to cracking was carried out using results of overlaying tests for twenty one heats of the Ni-Cr-W alloys. We performed multiple regression analysis on the relation between the area ratio of indication in liquid penetration tests to a cross-sectional area of the overlay weld metal and the amount of each alloying element. The indication in liquid penetration tests of the overlay weld metal represents cracking during re-heating by multipass. Figure 10 shows the measured examples of the area ratio of the indication in liquid penetration tests by means of image processing. It was found that such elements as Zr, B,and Y made susceptibility to cracking high because the partial regression coefficients of these alloying elements were positive and high. Comparison between experimental values and ones predicted using the multiple regression analysis is shown in Fig.11. Both experimental and predicted values agree considerably well as can be seen in this figure. Table 6 shows examples of chemical compositions of the alloys which exhibited good weldability. Filler metals of P3 and P67 were worked to filler wires for automatic TIG welding. Creep properties of trial welded joints fabricated using F and P5 alloys as a filler metal are described later. At present creep properties in air and corrosion properties in simulated HTGR helium are being investigated for welded joints produced using P3 and P67 wires.

(3)Conclusions

①Since susceptibility to cracking in the weldments of the Ni-Cr-W alloy is very high, good weldability cannot constantly obtained using the alloy with the same chemical composition as that of the base metal.

②Effect of minor alloying elements on susceptibility to cracking was clarified in terms of a series of weldability tests and the multiple regression analysis for the overlay test.

③Decrease in contents of Zr, B and Y is effective on decrease in susceptibility to cracking. It is necessary to optimize contents of these minor alloying elements so as not to deteriorate hot-workability, corrosion resistance and creep properties.

2.3 Creep properties of trial welded joints

(1)Specimen and experimental procedure

Welded joints were prepared by means of manual TIG welding using F alloy and P5 alloy which exhibited good weldability as mentioned in 2.2. The plate produced in an

industrial scale as mentioned in 2.1 was used as a base metal for filler metal F. The plate of P5 alloy was used as a base metal for filler metal P5. Welded condition is shown in Table 4, and groove geometry is shown in Fig.5(d). Creep specimens of welded joints were sampled so that loading direction might be perpendicular to the weld line.

Creep tests were performed at 900, 1000 and 1050 ℃ in air. Specimens of 6 mm in diameter and 30 mm in gauge length were used for creep tests.

(2)Experimental results and discussion

Figure 12 shows time to rupture of trial welded joints F in comparison with that of base metals with heat treatment A to D. The result for trial welded joints P5 is also shown in Fig.13. Rupture time of welded joints P5 is a little longer than that of welded joints F. At 900℃, creep rupture strength of welded joints F and P5 is the same as or above that of base metals with heat treatment A to D. At 1000 and 1050℃, it almost lies between creep rupture strength of base metals with heat treatment A or B and C. Namely, creep rupture strength of trial welded joints F and P5 is a little lower than that of the base metal with grain size of ASTM No.2.

Reduction of area of trial welded joints F and P5 is shown in Fig. 14. Although rupture location of welded joints was mostly the base metal, rupture at the weld metal occurred frequently in creep tests at 1050℃. It was observed more frequently for welded joints P5 than for welded joints F. Reduction of area was small in case rupture at the weld metal occurred .

(3)Conclusions

①Creep rupture strength of trial welded joints F and P5 of Ni-18～19mass%Cr-20～22 mass%W alloy is a little lower than that of the base metal with grain size of ASTM No.2.

②Most of trial welded joints ruptured at the base metal although rupture at the weld metal was observed in creep tests at 1050℃.

3. Summary

Creep properties in air and weldability were studied in a research program on development of the new Ni-Cr-W superalloy as a component material for HTGRs with coolant outlet temperatures up to 1000℃.

Creep rupture strength of the Ni-Cr-W alloy with grain sizes above ASTM No.2 is

above 9.8 MPa for a $1x10^5$ h life at 1000℃, which is the final target of the program. Since susceptibility to cracking in the weldments of the Ni-Cr-W alloy is very high, good weldability cannot constantly obtained using the alloy with the same chemical composition as that of the base metal. Effect of minor alloying elements on susceptibility to cracking was clarified in terms of a series of weldability tests and the multiple regression analysis for the overlay test. Decrease in contents of Zr, B and Y is effective on decrease in susceptibility to cracking. Creep rupture strength of the trial welded joints was a little lower than that of the base metal with grain size of ASTM No.2.

It is necessary to optimize contents of such minor alloying elements as Zr, B, Y and Ti so as not to deteriorate creep properties and corrosion resistance in HTGR helium.

Acknowledgment

The authors are grateful to the members of the JAERI Subcommittee on Advanced Superalloys (Chairman: R.Tanaka, Prof. emeritus of Tokyo Institute of Technology) for their assistance and useful discussion. The authors also appreciate National Research Institute for Metals, and Tokyo Institute of Technology for creep experiments.

References

[1] Agency of Industrial Science and Technology - Ministry of International Trade and Industry and the Engineering Research Association of Nuclear Steelmaking (Japan) : Summary Report of R and D Project on Direct Steelmaking Technology with High Temperature Reducing Gas - Nuclear Steelmaking, 1981.

[2] R. Tanaka and T. Matsuo : J. Iron Steel Inst. Japan., 68(1982), 226.

[3] R. Tanaka and T. Kondo : Nuclear Technology, 66(1984), 75.

[4] M. Shindo and T. Kondo : Proc. Conf. on Gas-cooled Reactors Today, Bristol/UK, BNES, Vol.2, (1982), 179.

[5] Ad Hoc Committee on Advanced Superalloys, Technical Expert Committee on HTGR, Japan Atomic Energy Research Institute : Development of Ni-Cr-W Superalloys for High Temperature Components in High Temperature Gas-cooled Reactors (Interim Report), JAERI-M 88-270 (1989).

[6] Subcommittee on Advanced Superalloys, Technical Expert Committee on HTGR, Japan Atomic Energy Research Institute : Development of Ni-Cr-W Superalloys for

High Temperature Components in High Temperature Gas-cooled Reactors (Second Report : Examination of Effects of Minor Alloying Elements and Proposal of Optimum Chemical Composition), JAERI-M 92-137 (1992).

[7] H.Tsuji, M. Ohashi, M. Takemura and H. Nakajima : Examination of Formability to Seamless Tubes on Ni-Cr-W Superalloy, JAERI-M 92-148 (1992).

[8] T. Itagaki, T. Watanabe and R. Yoda : J. Japan. Inst. Met., 40(1976)914.

[9] M. Kikuchi, S. Wakita and R. Tanaka : Trans. Iron and Steel Inst. Japan., 13(1973)226.

[10] R. Viswanathan : Damage mechanism and life assessment of High-Temperature Components, ASM Int., Metals Park, Ohio (1989).

[11] VAMAS Data Evaluation Committee : Study on Standardization of Creep-Rupture Data Evaluation of Metals, Iron and Steel Inst. Japan, (1994).

[12] W. F. Savage, E. F. Nippes and G. M. Goodwin : Welding Journal, 56(1977)No.8, p.245s.

Table 1 Chemical composition of a Ni-Cr-W alloy fabricated in an industrial scale (mass%)

		C	Si	Mn	P	S	Cr	W	Ti	Zr	Y	B	Co	Al	N	O	Fe	Nb	Ni
Aim		0.03	LAP	LAP	LAP	LAP	18.5	21.5	0.07	0.04	0.008	0.005	——	LAP	------	------	----	----	Bal.
Top	1	0.029	0.06	0.02	0.003	0.001	18.68	21.40	0.06	0.02	0.008	0.006	0.02	0.04	0.0010	0.0008	0.08	0.02	Bal.
	2	0.030	0.06	0.02	0.003	0.001	18.70	21.46	0.06	0.02	0.008	0.006	0.03	0.03	0.0012	0.0009	0.08	0.02	Bal.
	3	0.029	0.06	0.02	0.003	0.001	18.75	21.79	0.07	0.02	0.008	0.006	0.02	0.04	0.0012	0.0007	0.09	0.02	Bal.
	4	0.028	0.06	0.02	0.003	0.001	18.70	21.83	0.06	0.02	0.009	0.006	0.02	0.04	0.0013	0.0008	0.08	0.02	Bal.
	5	0.029	0.06	0.02	0.003	0.001	18.76	21.43	0.06	0.02	0.008	0.006	0.02	0.04	0.0011	0.0005	0.07	0.02	Bal.
Bottom	6	0.031	0.06	0.02	0.003	0.001	18.74	21.44	0.06	0.02	0.009	0.006	0.02	0.04	0.0012	0.0007	0.07	0.02	Bal.

LAP : Low as possible

Table 2 Heat treatment condition and grain size for bars of a Ni-Cr-W alloy

	Heat treatment condition	Grain size
A	at 1215℃ for 1h WQ	ASTM No.3
B	at 1215℃ for 1h WQ + at 1190℃ for 2h AC	ASTM No.3
C	at 1250℃ for 1h WQ	ASTM No.2
D	at 1250℃ for 1h WQ	ASTM No.0

Table 3 Range of chemical composition of alloys used for weldability tests (mass%)

C	Mn	Si	P	S	Cr	W	Ti	Zr	Y	B	Al	Mg	Nb
0.010 ～ 0.040	0.010 ～ 0.060	0.002 ～ 0.10	0.001 ～ 0.01	max. 0.002	18.2 ～ 18.8	21.0 ～ 21.83	0.002 ～ 0.20	max. 0.04	max. 0.022	0.0008 ～ 0.006	0.005 ～ 0.06	max. 0.01	0.003 ～ 0.034

Table 4 Condition of hand-operated TIG welding

Shape and size of filler metal (mm)	Diameter of electrode (mm)	Welding current (A)	Arc voltage (V)	Ar flow rate (ℓ / min)	Travel speed (mm / min)
Rectangular rod with a base 3x3 and a length of about 230	φ3.2	100～200	11～17	10～15	80～200

Table 5 Condition of automatic TIG welding

Shape and size of filler metal (mm)	Diameter of electrode (mm)	Welding current (A)		Arc voltage (V)	Ar flow rate (ℓ / min)	Travel speed (mm / min)
		base	peak			
Wire with φ1.2	φ3.2	150	170	8～10	15～20	100

Table 6 Examples of chemical composition of the alloy exhibiting good weldability (mass%)

	C	Mn	Si	P	S	Cr	W	Ti	Zr	Y	B	Al	Mg	Nb
F	0.031	0.010	0.002	0.010	0.0010	18.5	21.41	0.070	0.020	0.005	0.0045	0.005	<0.0001	0.032
P5	0.020	0.030	0.060	0.003	0.0010	18.5	21.10	0.050	0.020	0.009	0.0016	0.005	0.0020	0.020
P3	0.020	0.030	0.050	0.001	0.0002	18.5	21.40	0.070	0.010	0.008	0.0008	0.040	0.0010	0.020
P67	0.030	0.020	0.050	0.001	0.0004	18.4	21.50	0.080	<0.001	<0.001	0.0020	0.040	0.0020	0.020

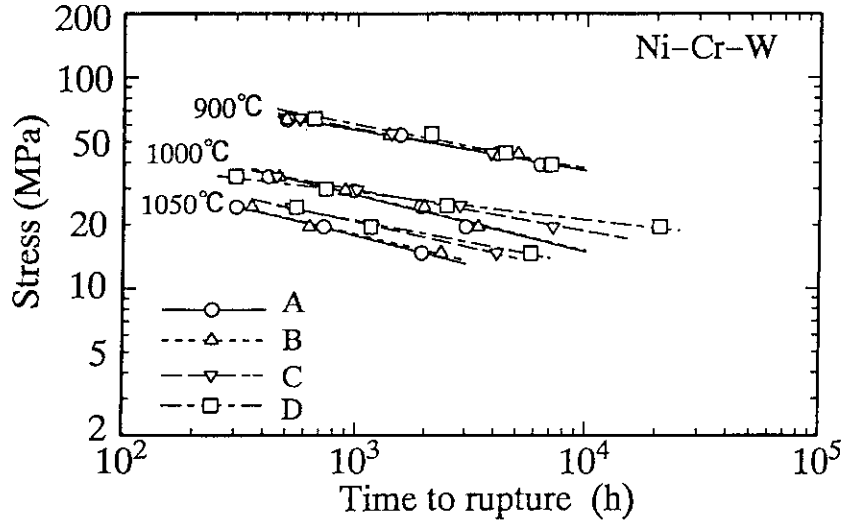


Fig. 1 Relationship between stress and time to rupture for a Ni-Cr-W alloy with heat treatment A to D.

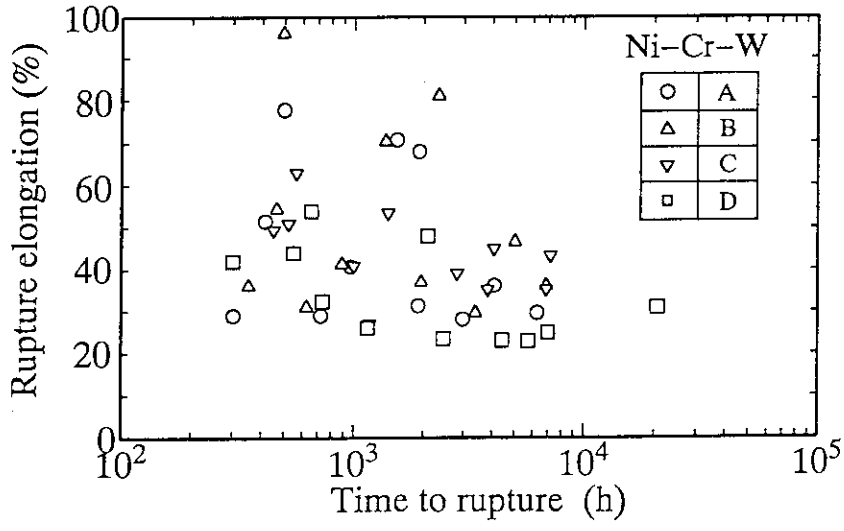


Fig. 2 Rupture elongation vs. time to rupture for a Ni-Cr-W alloy with heat treatment A to D.

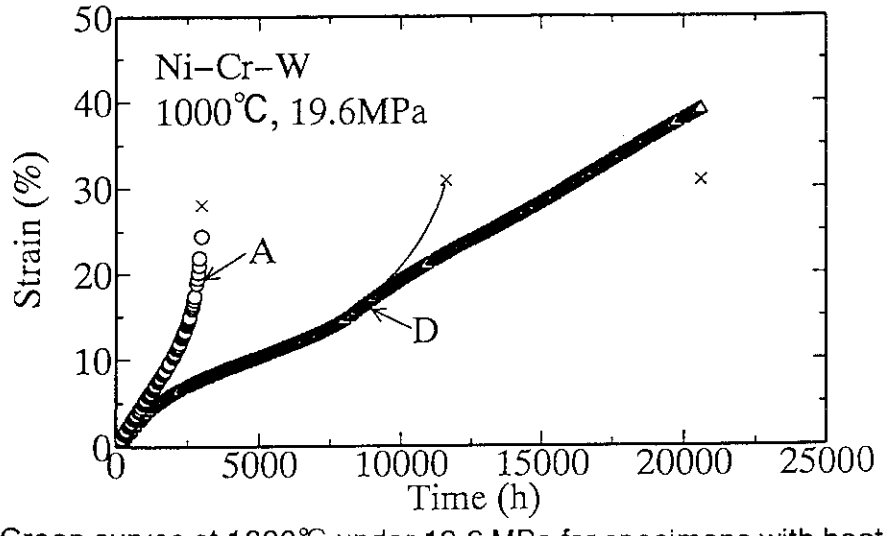


Fig. 3 Creep curves at 1000℃ under 19.6 MPa for specimens with heat treatment A and D.

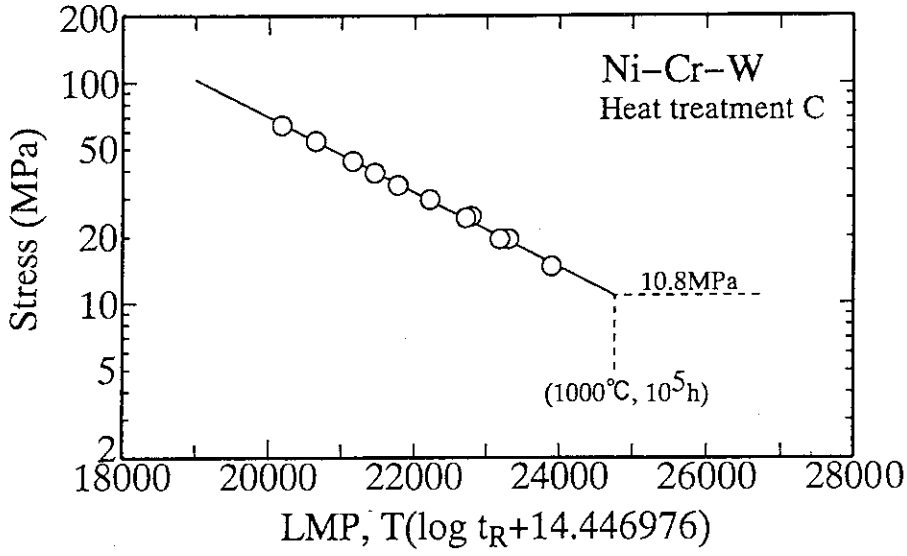


Fig. 4 Relationship between stress and Larson-Miller parameter (LMP) for a Ni-Cr-W alloy with heat treatment C.

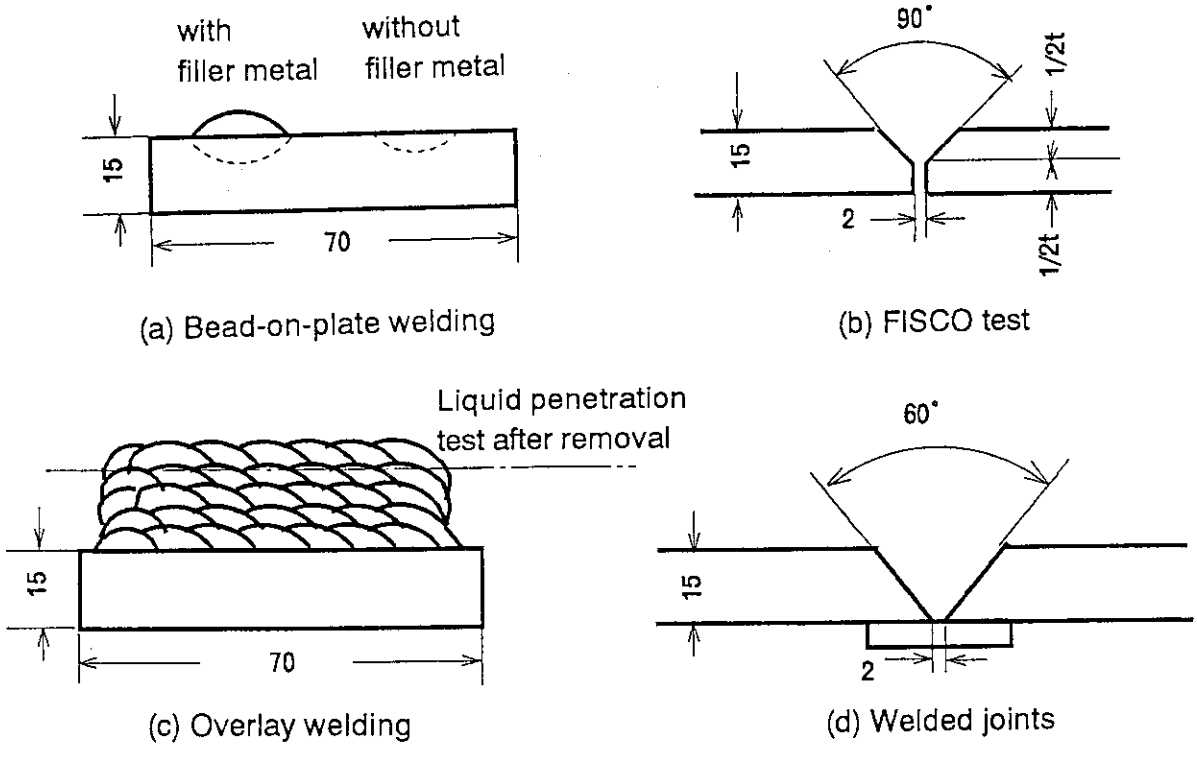


Fig. 5 Welding procedure and groove geometries for welding tests.

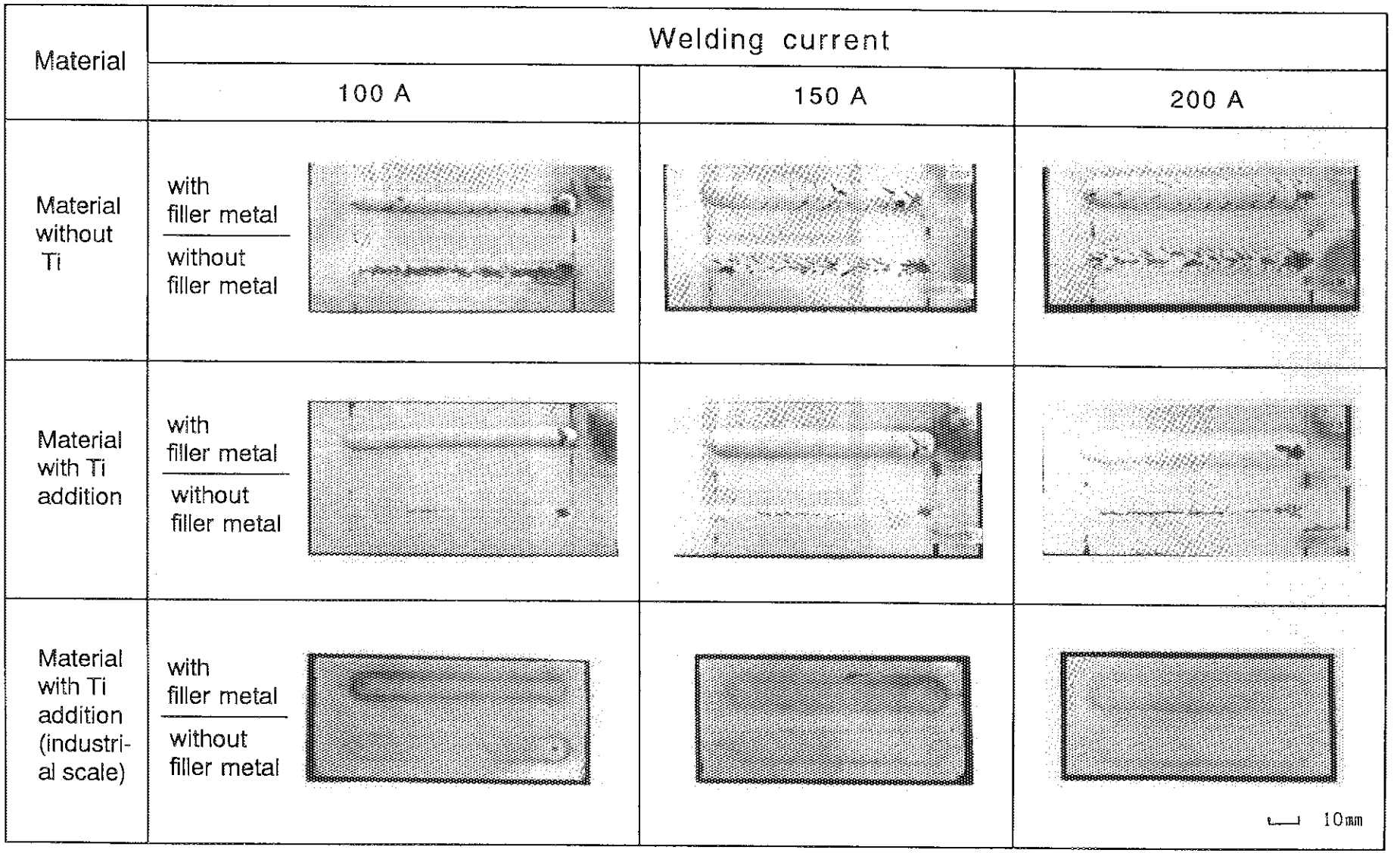
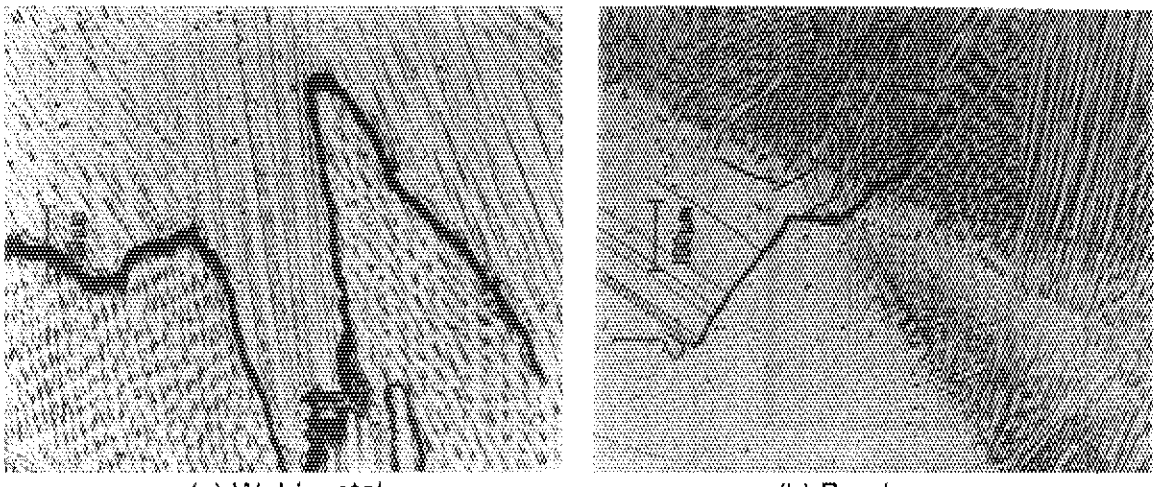
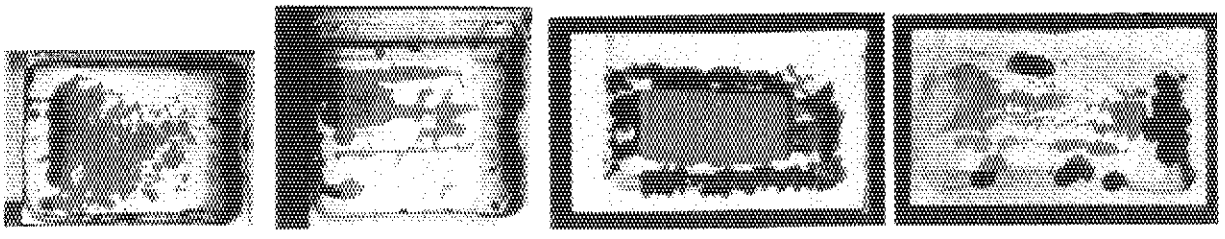


Fig. 6 Results of liquid penetration tests for the specimens after bead-on-plate welding.



(a) Weld metal (b) Bond

Fig. 7 Microstructures of weldments of the alloy with Ti addition produced in an industrial scale. Re-solution heat treatment was made for the alloy at higher temperature.



(a) high Y (b) high Mg (c) high Mn (d) high Mn and Si

Fig. 8 Results of liquid penetration tests for specimens after overlay welding using filler metals with Y, Mg, Mn and Si addition.

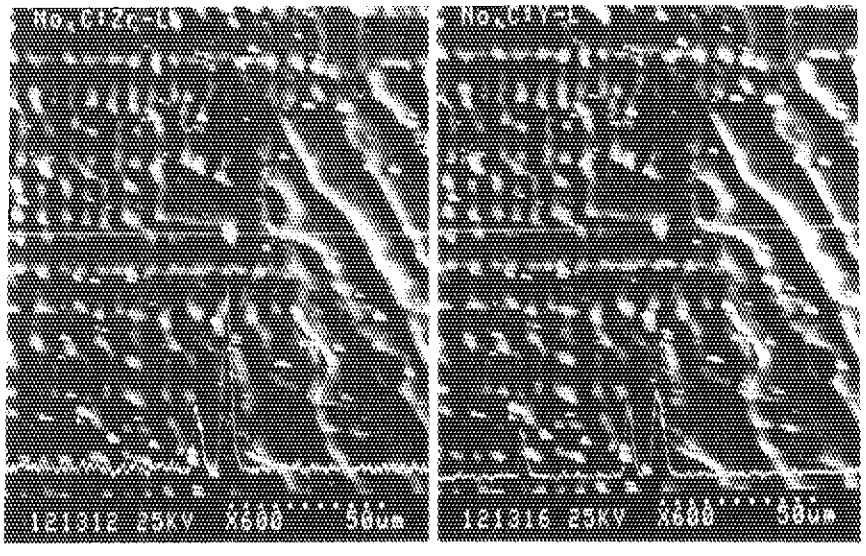
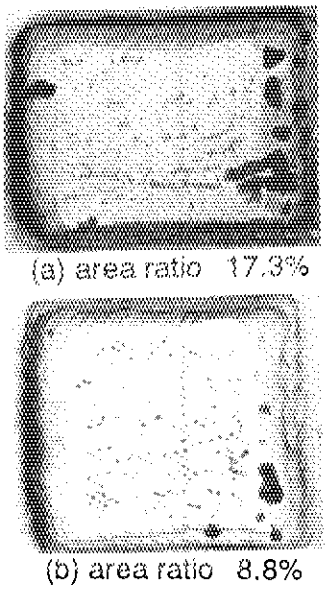


Fig. 9 Concentration profiles of Zr and Y for weld metal.



(a) area ratio 17.3%

(b) area ratio 8.8%

Fig. 10 Measured examples of the area ratio of indication in liquid penetration tests of overlay weld metal.

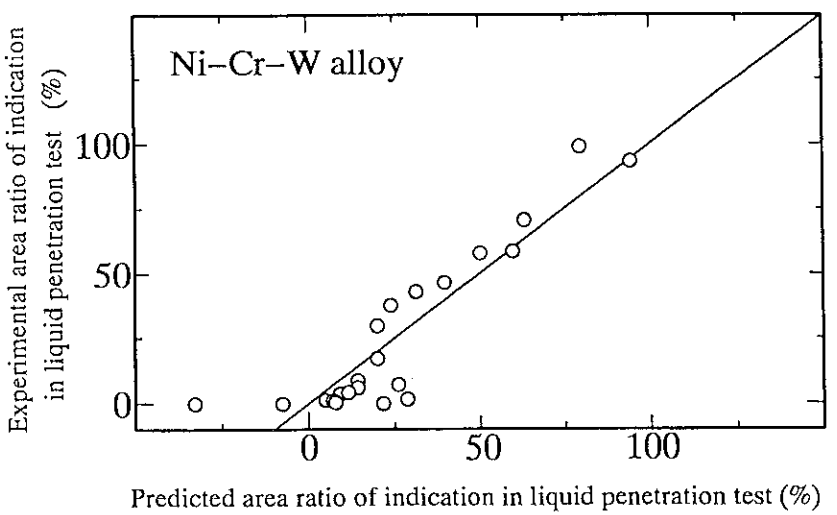


Fig. 11 Comparison between experimental and predicted area ratio of indication in liquid penetration tests of overlay weld metal. Multiple correlation coefficient, R=0.90.

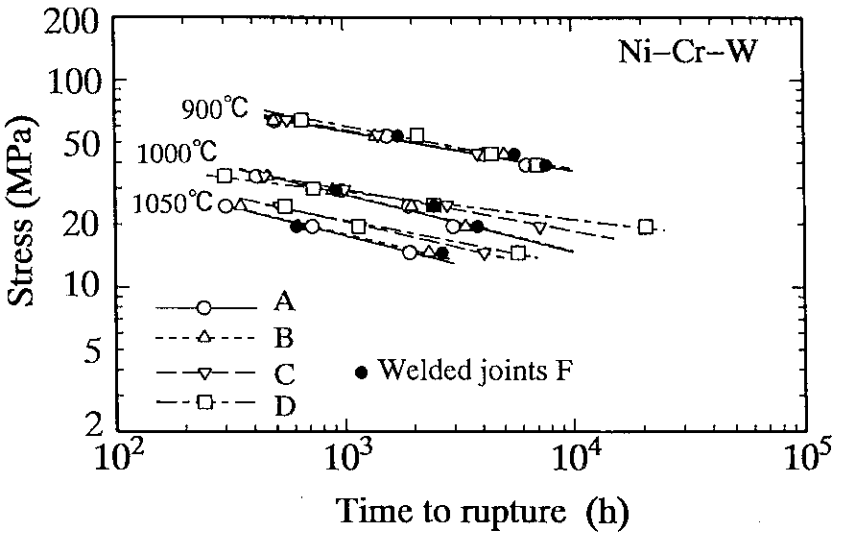


Fig. 12 Time to rupture of trial welded joints F in comparison with that of base metals with heat treatment A to D.

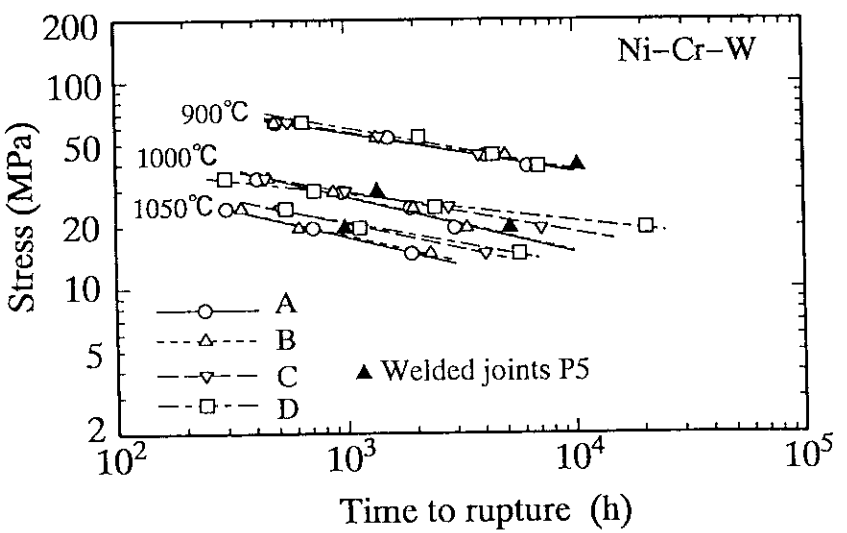


Fig. 13 Time to rupture of trial welded joints P5 in comparison with that of base metals with heat treatment A to D.

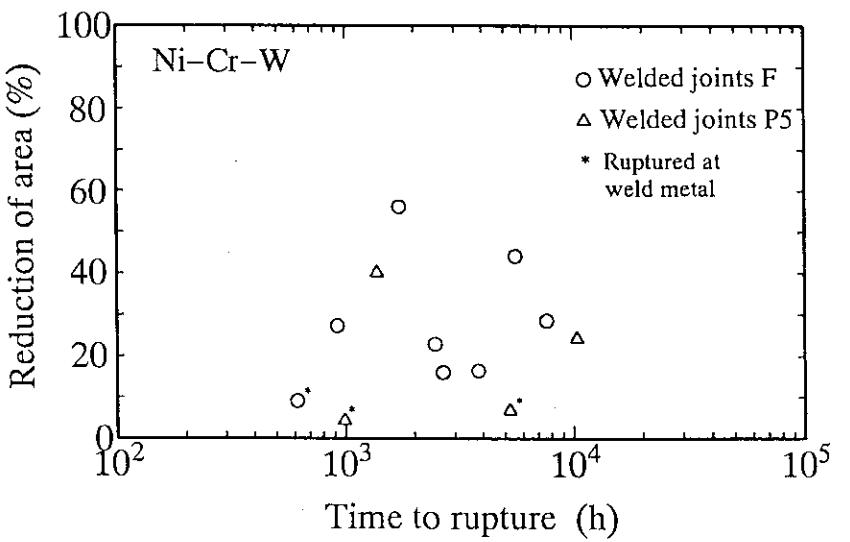


Fig. 14 Reduction of area of trial welded joints F and P5.

6.10 Evaluation on Materials Performance of Hastelloy Alloy XR for the High Temperatere Engineering Test Reactor Components -Weldability and high temperatute strength properties-

Katsutoshi Watanabe[a], Masami Shindo[a], Hajime Nakajima[a], Hajime Koikegami[b], Makoto Higuchi[b], Teiichiro Saitoh[c], Tamao Takatsu[c], Tsuneo Nakanishi[d], Kensho Sahira[e], Kouki Marushichi[e] and Toshiki Takeiri[e]

[a]Japan Atomic Energy Research Institute, Japan

[b]Ishikawajima-Harima Heavy Industries Co. Ltd., Japan

[c]Nippon Welding Rod Co. Ltd., Japan

[d]Fuji Electric Corporate Research and Development, Ltd., Japan

[e]Mitsubishi Materials Corporation, Japan

ABSTRACT

Weldability and high temperature strength properties of Hastelloy Alloy XR were investigated in order to evaluate the materials performance of base metal and filler metal for the High Temperature Engineering Test Reactor (HTTR) uses. The weldability was examined by means of the chemical analysis in the deposited metals, optical microscopy, FISCO test, hardness measurements and bend test. The high temperature strength properties were investigated through tensile tests at R.T., 800, 900 and 950℃ in air, and creep and creep rupture tests at 900 and 950℃ in air. The results obtained by each test showed favarable performance. In particular, the bend test which is considered to be critical pass demonstrated low susceptibility to weld cracking through the optimization of B and C contents in the filler metal and by narrowing the groove. Creep rupture strength was nearly equal or higher than those of Hastelloy Alloy XR master curve and was much higher than design creep rupture strength [SR]. Therefore, it is concluded that weldability, tensile and creep properties with these base metals and filler metals for the HTTR components are entirely satisfactory.

1. Introduction

The High Temperature Engineering Test Reactor (HTTR) is currently under construction at the Japan Atomic Energy Research Institute at Oarai towards the attainment of first criticality in 1997 [1]. Hastelloy Alloy XR has been developed as the high temperature-structural material for the HTTR

intermediate heat exchanger(IHX), and afterwards improved with respect to the material properties through a series of research and development.

The IHX is the welded-structures, which are used at outlet coolant temperature of 850℃ for rated operation and 950℃ for elevated temperatures test operation. Therefore, it has been often pointed out that the weldability specified in high nickel alloy [2] and high temperature strength properties of weldments are the most important problems to be solved. A series of research and development has progressively been performed on such subjects.

In the first phase of R&D [3-5], the filler metals were made by way of trial on the basis of alloy design in terms of multiple regression analysis and have been found to possess favourable properties through a series of materials evaluation tests.

In the second phase of R&D [6], it was demonstrated that both weldability and high temperature strength properties of weldments with the filler metals developed are to be satisfactory through performance evaluation tests for the welded-structures with thin-wall. However, the problems of the suitability of the developed filler metal to the welded-structures with thick-wall have remained not to be solved.

In the third phase of R&D [7-8], the development of the filler metal for the ones with thick-wall was conducted in addition to the results obtained previously. Through optimizing the content of minor elements based on the alloy design in terms of multiple regression analysis, the filler metals were made by way of trial, and their properties were examined by means of performance evaluation tests. It was found from these results that the filler metal developed has favourable properties because of lowering the high weld cracking susceptibility characterized by welded-structures with thick wall without degrading high temperature strength properties. At present these filler metals have been used for the manufacture of the IHX in the HTTR.

The present paper describes the results of weldability and high temperature strength properties on Hastelloy Alloy XR base metal and filler metal for the HTTR uses in order to investigate the materials performance from the viewpoint of the reliability evaluation for welded-structures.

2.Experimental procedures

2.1 Materials

(1) Base metal

The base metal was nuclear-grade Hastelloy Alloy XR. The ingot was fabricated by vacuum induction melting and electro-slag remelting procedures. Plates with 15 and 60 mm in thickness were prepared by hot-forging and hot-rolling, and sequentially solution-annealed at 1190℃. The chemical composition of the base metal is given in Table 1.

(2) Filler metal

The chemical composition of the filler metal is presented in Table 2. This heat was melted by using the vacuum induction melting procedure and worked by hot-forging, hot-rolling and cold-

drawing, followed repeatedly by intermediate annealing and cold-drawing. The final diameter of the filler metal was 1.2mm.

2.2 Welding

One-side welding with tungsten inert gas arc-welding(TIG) procedure made in the present work is the same as that used in the HTTR components. The welding conditions of the plates with 60 and 15mm in thickness are summarized in Tables 3 and 4, respectively. The weld groove geometry of the plates with 60 and 15mm in thickness is presented in Figs.1 and 2, respectively. In the case of the plate having a thickness of 60mm, the groove is U-type geometry without insert-metal, and is the narrow one with 10 degrees in groove angle, which is expected to lower the susceptibility to weld cracking in the bend tests. Furthermore, the build-up was roughly 29 layers with 54 passes. In this case, the number of layer and pass was significantly decreased as compared with the case of the conventional groove roughly with 40 layers and 140 passes. After welding, it was confirmed that the presence of weld-flaws were not observed by means of the penetrating inspection and radiant-ray inspection.

2.3 Weldability test

Weldability was examined by chemical analysis of the deposited metals, bend test, FISCO test, optical microscopy and hardness measurement. The fissure bend test, as described in JIS Z3122 [9], was performed by face and side bend using specimens with 10.0 mm in thickness. The susceptibility to hot cracking was examined by the FISCO test, which is described in JIS Z3155 [10].

2.4 High temperature strength property tests

The specimens were machined from the test plates. After welding, all the specimens were examined by X-ray radiography and found to be free of weld-flaws. The specimen size for tensile testing was 6 mm in diameter with a 30 mm gauge length. The tensile testing procedure was as described in JIS Z2241 [11] and JIS G0567 [12] both at room temperature and at elevated temperatures, respectively. Tests were made in air at room temperature, 800, 900 and 950℃. The specimen size for creep test was 6 mm in diameter and 20 and 30 mm in parallel part length. Tests were conducted under stress of 38.0, 47.0 and 58.0 MPa, and 22.0, 30.0 and 48.0 MPa at 900 and 950℃, respectively.

3. Results and discussion

3.1 Weldability

Table 5 shows the results of chemical analysis in the deposited metal and weld metal with the filler metal. Based on the comparison with the chemical composition between filler metal, and the deposited metal and weld metal, the decrease in Mg content due to welding was nearly one-fourths while B and the other elements remained nearly unchangeable. However, such decrease in Mg is considered not to have a severe problem in TIG welding since the materials properties in the weldments at elevated temperatures are little influenced with Mg addition.

Figs.3 and 4 show the representative macro-and micro-structures in the welded joint specimens made from the test plates with15 mm in thickness. The macro-structures were found to have the integrity because of being free of weld-flaws. In the micro-structures, the weld-flaws such as micro-cracks and so on were not observed in the weld metal and bond region. The coarsening of the grains due to the welding heat input did not occur in the heat-affected zone.

Fig. 5 shows the hardness distribution in the welded joint specimen made from 60mm-thick test plate. The hardness value was approximately Hv 210-300 and Hv200-260 in the weld metal and base metal region, respectively. The reason why the weld metal is higher in hardness value than the base metal is inferred to originate from strain accumulation due to the stacking of beads during welding since both weld metal and base metal are found to be free of weld-defects, as mentioned above.

The results of FISCO test is given in Table 6. It was found that cracks were present in the crater alone and entirely absent in the weld bead. Crack ratio was in the range of 13.6 to 16.2 %. This indicates that the resistance to hot cracking in the weldments is relatively high. Fig. 6 shows the comparison of the present filler metal with the other ones in crack ratio. It is pointed out from these results that the present filler is in the favourable level in the susceptibility to weld cracking since the present one is lower in crack ratio than the others. Based on the alloy design with the aim of obtaining the excellent weldability, the content as low as possible for the impurities such as P, S and O, and the slight reduction of B and C content is considered to be effective for lowering weld cracking susceptibility. Fig. 7 shows the effects of B and C content on the total number of cracks. The total number of cracks, which were measured by bend test, are the effective index to evaluate the weld cracking susceptibility. This indicates that the present filler metal possesses a good performance as compared with the previous ones. The reason seems to be that B and C content were reduced to lower level and that the narrowing in the groove was performed with the aim of lowering weld cracking susceptibility in bend test.

3.2 High temperature strength properties

As for tensile properties, stress, total elongation and reduction in area as a function of each test temperature are given on the comparison of the present filler metal with the previous ones in Figs. 8, 9 and 10, respectively. As shown in Fig. 8, strength properties on both the present base metal and weldment are not in the significant differences in comparison to those of the previous ones. From Fig. 9 and 10, it is shown that the values of total elongation and reduction in area on both the present base metal and weldment are in the data band obtained from those of the previuos ones.

The relationship between applied stress and time to rupture at 900 and 950℃ is given in Figs.11 and 12, respectively. In connection with these results, the plots of elongation to rupture versus time to rupture at the same temperatures are presented in Figs. 13 and 14, respectively. As seen in Figs.11 and 12, it is shown that the creep rupture strength of all of base metal, weld metal and welded joint specimens made from 60 and 15 mm-thick plates is nearly equal or higher than those of Hastelloy

Alloy XR master curve [13] and is much higher than design creep rupture strength [Sr]. As for ductility as shown in Figs.13 and 14, elongation to rupture and reduction in area tend to decrease with increasing time to rupture. In the case of weld metal, the ductility values of the specimens made from 60 mm-thick plate are inclined to be slightly lower than those of the ones made from 15 mm-thick plate. However, these values of weld metal were comparable to those of the previous ones. As for base metal, it was found that the differences in plate thickness did not result in creep rupture elongation. Figs.15 and 16 show the microstructures of crept specimens of weld metal. In the near-fracture surface region, the voids were continuously formed along the coarsened dendritic structures and their morphologies differed from those of base metal. The tendency for void formation appears to be slightly much remarkable at 950℃ than at 900℃. The fracture surface region of weld metal showed the microstructures, like grain boundary exfoliation in the dendrites, which is assumed to initiate it in the linked- voids formed in the grain boundary. The differences between base metal and weld metal were observed at the microstructures in their fracture surface.This suggests that it is reflected that creep ductility of weld metal is lower than that of base metal.

From the viewpoint of the comparison of the present filler metals with the previous ones [3, 6-7, 14] on creep properties of weld metal, the relationship between applied stress and time to rupture at 900 and 950℃, and the relationship between rupture elongation and time to rupture at the same temperatures are illustrated in Figs.17 and 18, and Figs.19 and 20, respectively. It was found that both creep rupture strength and rupture elongation in the weldments with the present filler metals manufactured in an industrial scale are in the data band with those of the previous ones containing 20-50ppm of B. Therefore, it was confirmed that the present filler metals is sufficiently enable to be applicable to Hastelloy Alloy XR welded-structures with the thick wall such as the HTTR intermediate heat exchanger.

4. Conclusions

Weldability and high temperature strength properties on Hastelloy Alloy XR base metal and filler metal for the HTTRuses were examined, and the followings were concluded:

(1) It was found that weldability is favourable in practical uses because of lower weld cracking susceptibility.

(2) On high temperature strength properties, the present base metal and filler metal are fully in the required level of strength and ductility in practical uses.

(3) The present base metal and filler metal are sufficiently enable to be applicable to the welded-structures in the HTTR.

Acknowledgement

The authors wish to express their thanks to the staffs of Ishikawajima-Harima Heavy Industries Co. Ltd., Nippon Welding Rod Co. Ltd., Fuji Electric Corporate Research and Development, Ltd., Mitsubishi Materials Corporation and Japan Atomic Energy Research Institute for their support and cooperation.

References

(1) For example: Japan Atomic Energy Research Institute, Present Status of HTGR Research and Development in JAERI (1995), in press.

(2) W. I. Hrivnak, Theory of Weldability of Metals and Alloys, (Elsevier, Amsterdam, 1992) p.307.

(3) K. Watanabe, H. Nakajima, K. Sahira, N. Kurauchi, T. Saitoh, T. Takatsu and T. Nakanishi, JAERI-M 89-206 (1989).

(4) K. Watanabe, T. Nakanishi, T. Takatsu. K. Sahira and H. Nakajima, J. High-Temp. Soc., 16 (1990) 368.

(5) K. Watanabe, H. Nakajima, K. Sahira, N. Kurauchi, T. Takeiri, T. Saitoh, T. Takatsu and T. Nakanishi, J. Nucl. Mater., 185 (1991) 8.

(6) K. Watanabe, H. Nakajima, K. Sahira, K. Marushichi, T. Takeiri, T. Saitoh, T. Nakanishi, H. Tsuji and T. Tsukada, JAERI-M 91-181 (1991).

(7) K. Watanabe, H. Nakajima, k. Sahira, K. Marushichi, T. Takeiri, T. Saitoh, T. Takatsu, H. Koikegami and M. Higuchi, JAERI-M 91-189 (1991).

(8) K. Watanabe, K. Sahira, T. Takatsu, T. Nakanishi, M. Higuchi and H. Nakajima, Proc. 2nd Inter. Conf. and Exhibition on Computer Applications to Materials and Molecular Science and Engineering - CAMSE '92, Elsevier Sci. Publishing Co. (1993) 1491.

(9) Japanese Industrial Standard, Methods of bend test for butt welded joint (JIS Z3122) (Japanese Standard Association, 1990).

(10) Japanese Industrial Standard, Method of FISCO cracking test (JIS Z3155) (Japanese Standard Association, 1979).

(11) Japanese Industrial Standard, Method of tensile test for metallic materials (JIS Z2241).

(12) Japanese Industrial Standard, Method of high temperature tensile test for steels and heat-resisting alloys (JIS G0567).

(13) K. Hada, Y. Motoki and O. Baba, JAERI-M 90-148 (1990).

(14) Japan Welding Engineering Society, A Study on Strength of Welded Joint of Hastelloy XR, JWES-AE-9005 (1990).

Table 1 Chemical composition of base metal (mass %).

element	C	Si	Mn	P	S	Cr	Fe	Mo	W	Cu	Al	Ti	Co	B	Ni	N
160mm plate	0.06	0.34	0.90	0.001	0.001	21.81	18.13	9.01	0.49	0.01	0.01	0.01	0.03	0.0030	Rem.	0.005
115mm plate														0.0029		

Table 2 Chemical composition of filler metal (mass %).

element	C	Si	Mn	P	S	Cr	Fe	Mo	W	Cu	Al	Ti	Mg	Co	B	Ni	N	O
φ5.5 mm	0.058	0.40	0.80	0.001	0.004	21.45	18.3	9.12	0.52	0.001	0.05	<0.001	0.015	0.004	0.0038	Rem.	0.0038	<0.0005
φ1.2 mm	0.052	0.39	0.82	0.001	0.003	21.41	18.1	9.38	0.49	0.003	0.05	<0.001	0.018	0.002	0.0032	Rem.	0.0032	0.0010

Table 3 Welding condition of plates with 60 mm in thickness.

Welding procedure	Diameter of filler (mm)	Welding current (A)	Arc voltage (V)	Welding speed (mm/min)	Wire feed rate (mm/min)	Ar gas flow rate (l/min)
GTAW	1.2	150-200	9-10	80	600-1000	25

Table 4 Welding condition of plates with 15 mm in thickness.

Welding procedure	Diameter of filler (mm)	Welding current (A)		Arc voltage (V)	Welding speed (mm/min)	Wire feed rate (mm/min)	Ar gas flow rate (l/min)
		Peak	Base				
GTAW	1.2	170	150	8-10	50-100	800	Torch :15-20 Trailing shield :15-20

Table 5 Results of chemical analysis in deposited and weld metal (mass %).

Element	C	Mg	B
φ1.2mm wire (Ch. No. 2-083)	0.052	0.016	0.0032
Deposited metal	0.051 0.052 0.052	0.004 0.003 0.004	0.0033 0.0037 0.0037
Weld metal (thickness : 15mm plate)	0.051	0.004	0.0034
Weld metal (thickness : 60mm plate)	0.040	0.003	0.003

Table 6 Results of FISCO test.

Repeat no.		Weld bead no. 1	2	3	Total length(mm)	Crack ratio(%)
1	Length of weld(mm)	47.50	44.65	48.30	140.45	16.2
	Length of crack(mm)	※ 8.60	※ 6.65	※ 7.50	22.75	
2	Length of weld(mm)	56.10	54.55	56.00	166.65	13.6
	Length of crack(mm)	※ 7.45	※ 6.00	※ 9.15	22.60	

※ Crack in crater

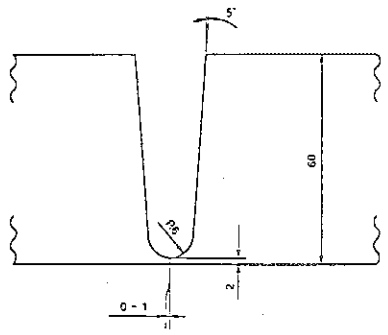


Fig. 1 Groove geometry of plates with 60 mm in thickness.

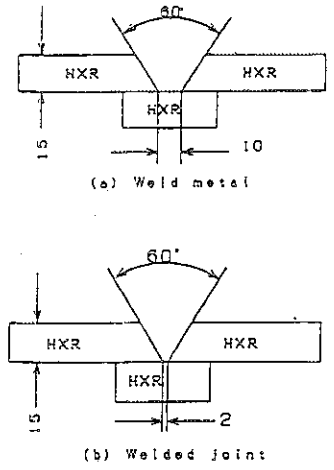


Fig. 2 Groove geometry of plates with 15 mm in thickness.

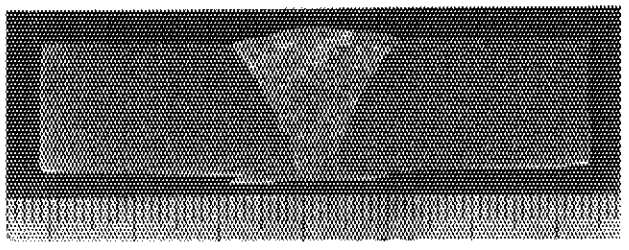


Fig. 3 Macro-structures of welded joint made from 15 mm-thick plate.

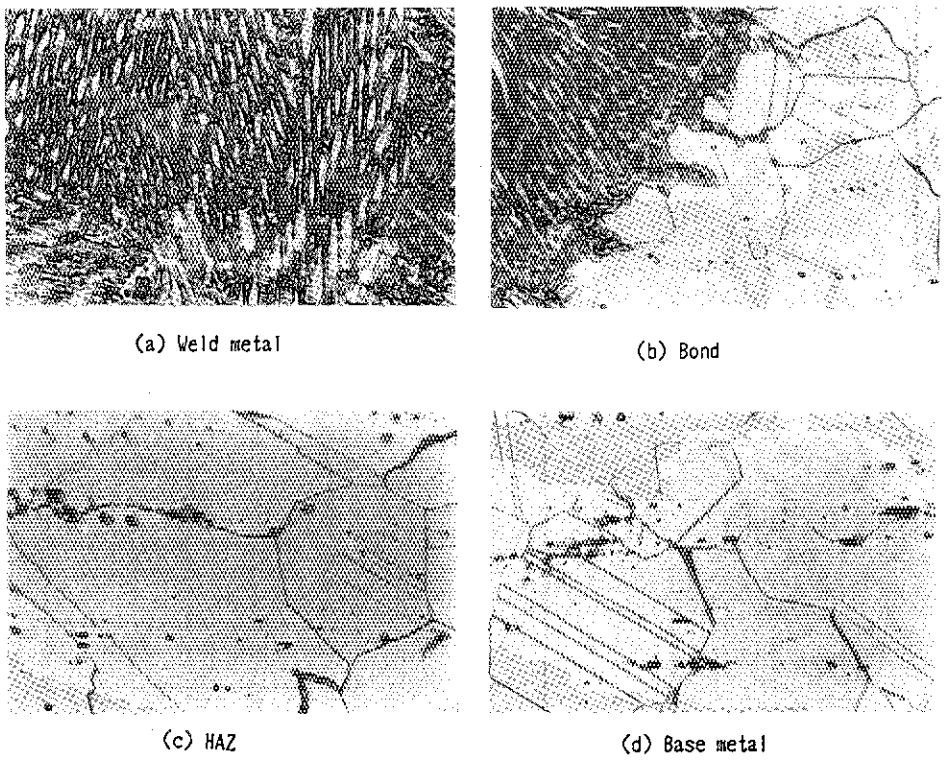


Fig. 4 Micro-structures of welded joint made from 15 mm-thick plate.

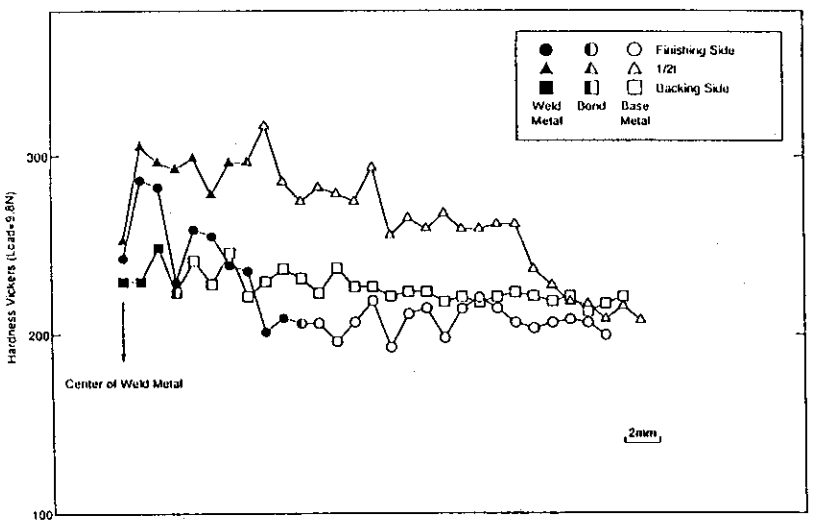


Fig. 5 Hardness distribution of welded joint made from 60 mm-thick plate.

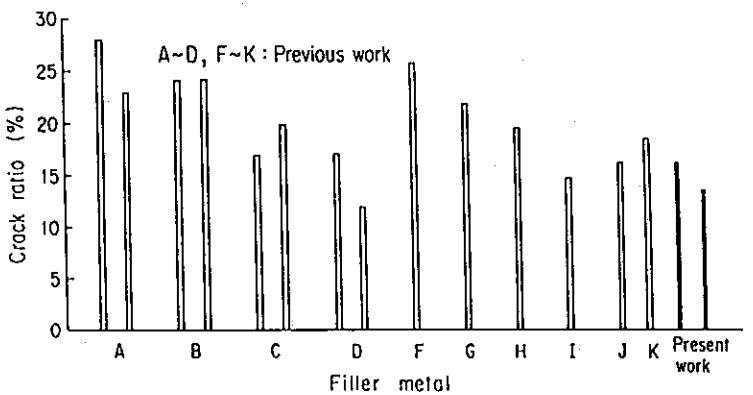


Fig. 6 Comparison of crack ratio in FISCO test.

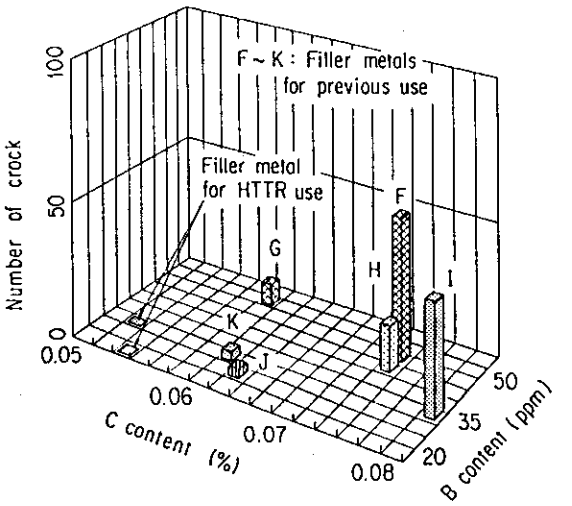


Fig. 7 C and B content of filler metal versus number of cracks.

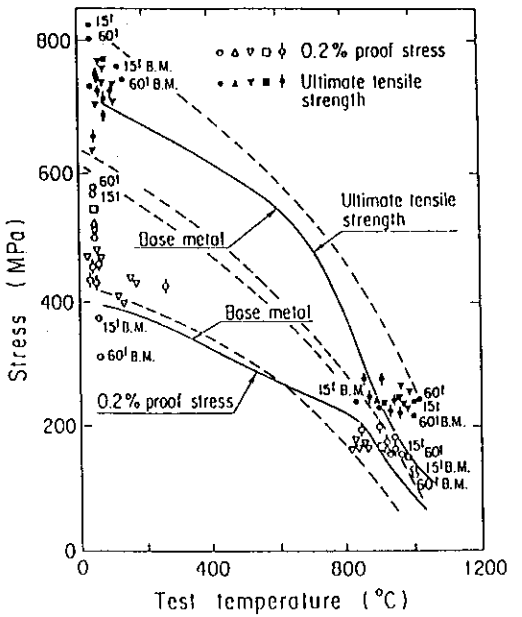


Fig. 8 Stress versus test temperature for weldments.

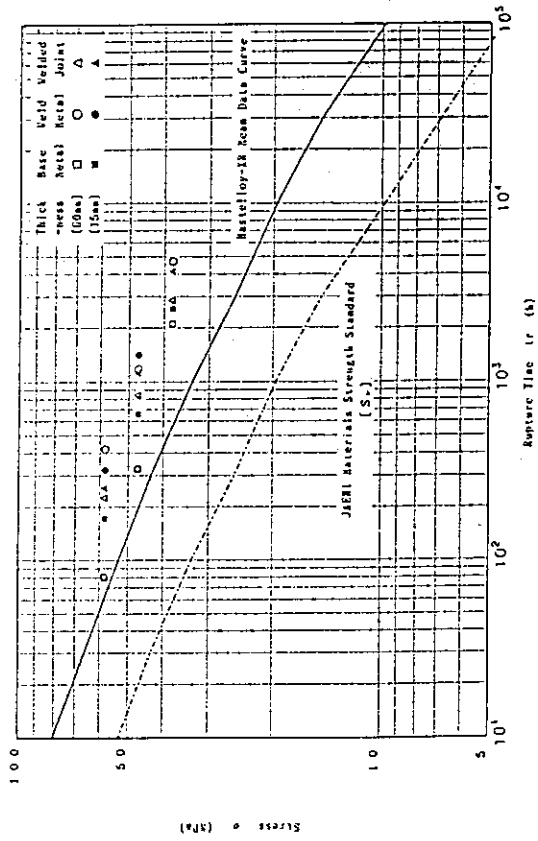


Fig. 11 Relation between applied stress and time to rupture at 900℃.

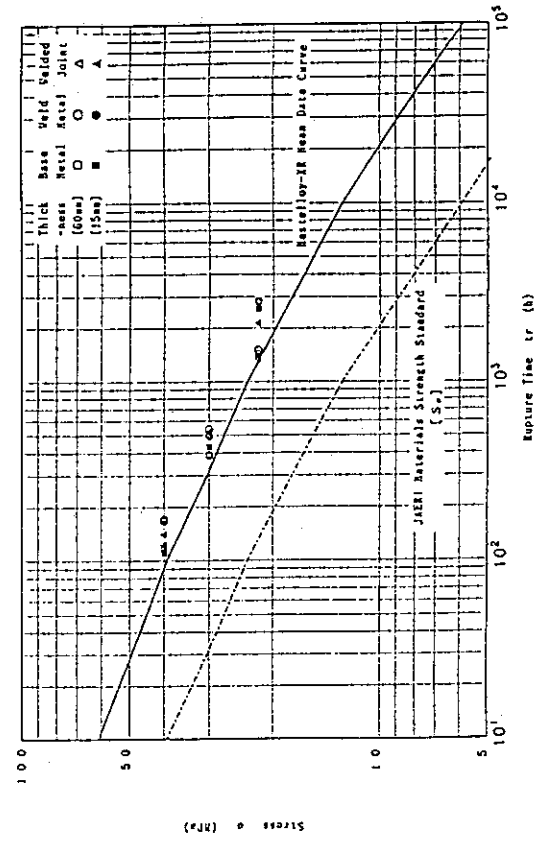


Fig. 12 Relation between applied stress and time to rupture at 950℃.

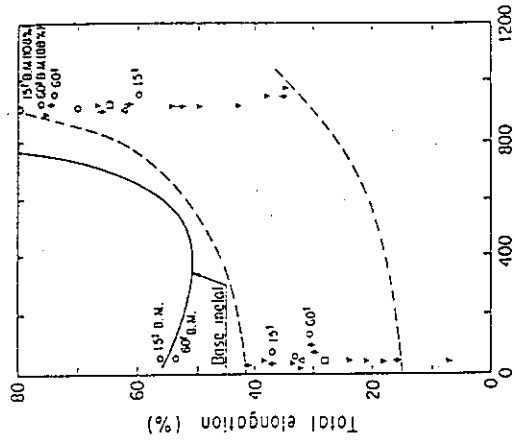


Fig. 9 Total elongation versus test temperature for weldments.

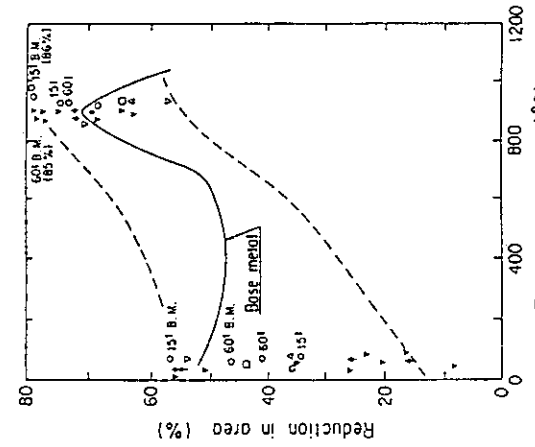


Fig. 10 Reduction in area versus test temperature for weldments.

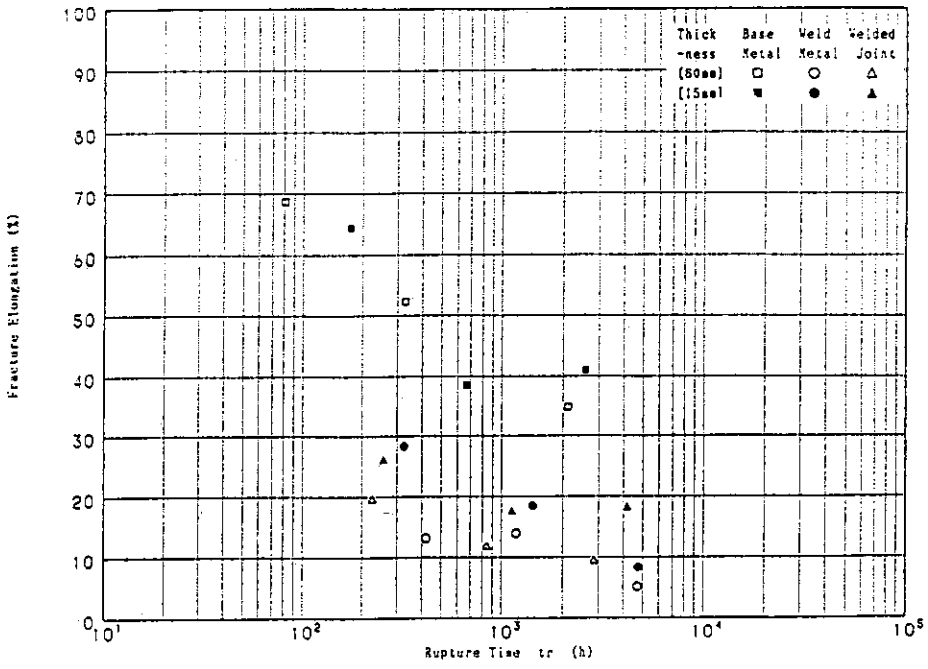


Fig. 13 Relation between rupture elongation and time to rupture at 900℃.

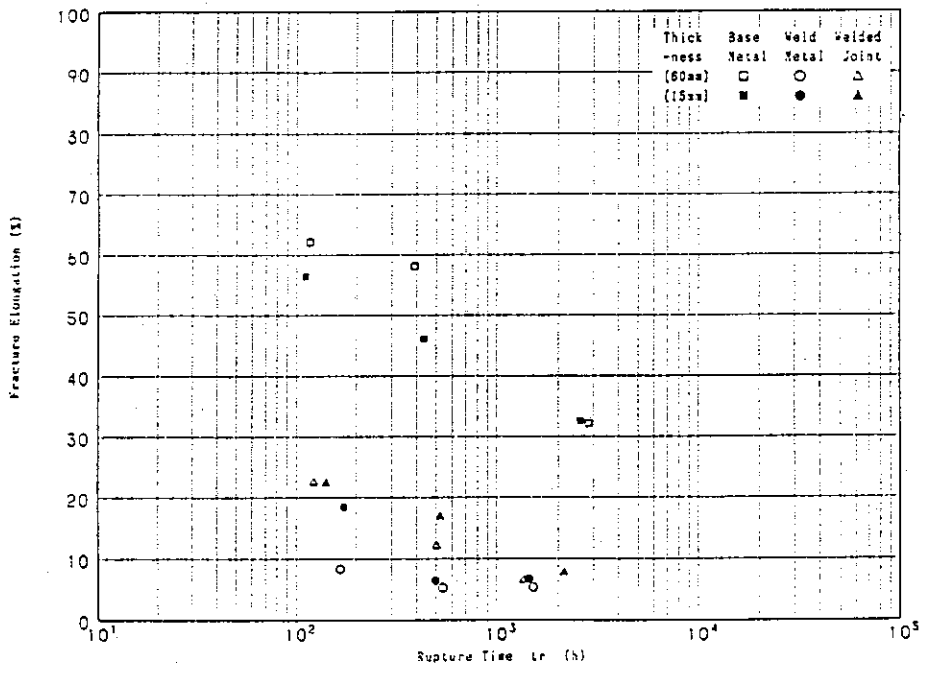


Fig. 14 Relation between rupture elongation and time to rupture at 950℃.

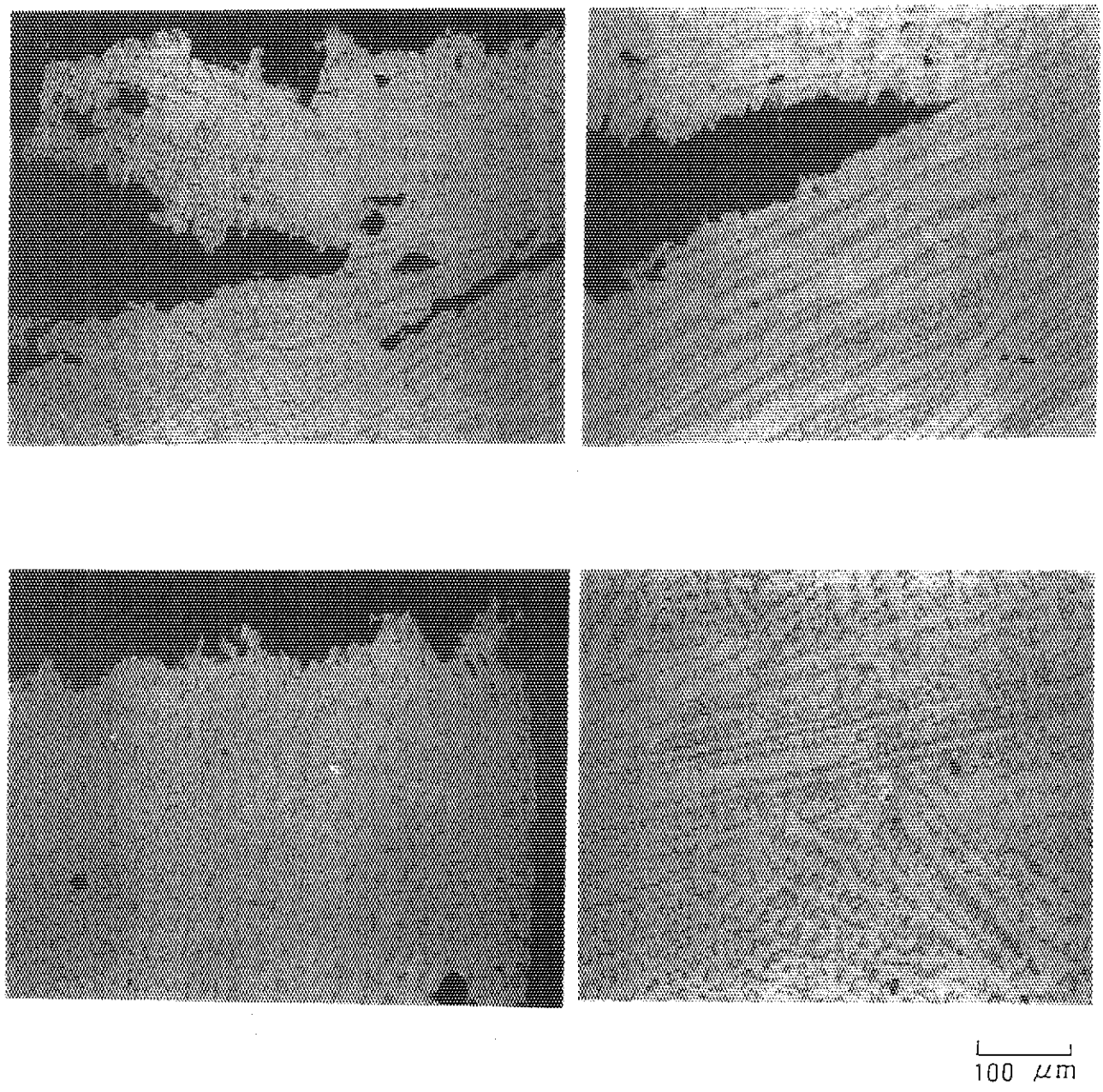


Fig. 15 Micro-structures of fracture surface for weld metal (900℃, 4686.9 h, 38.0 MPa).

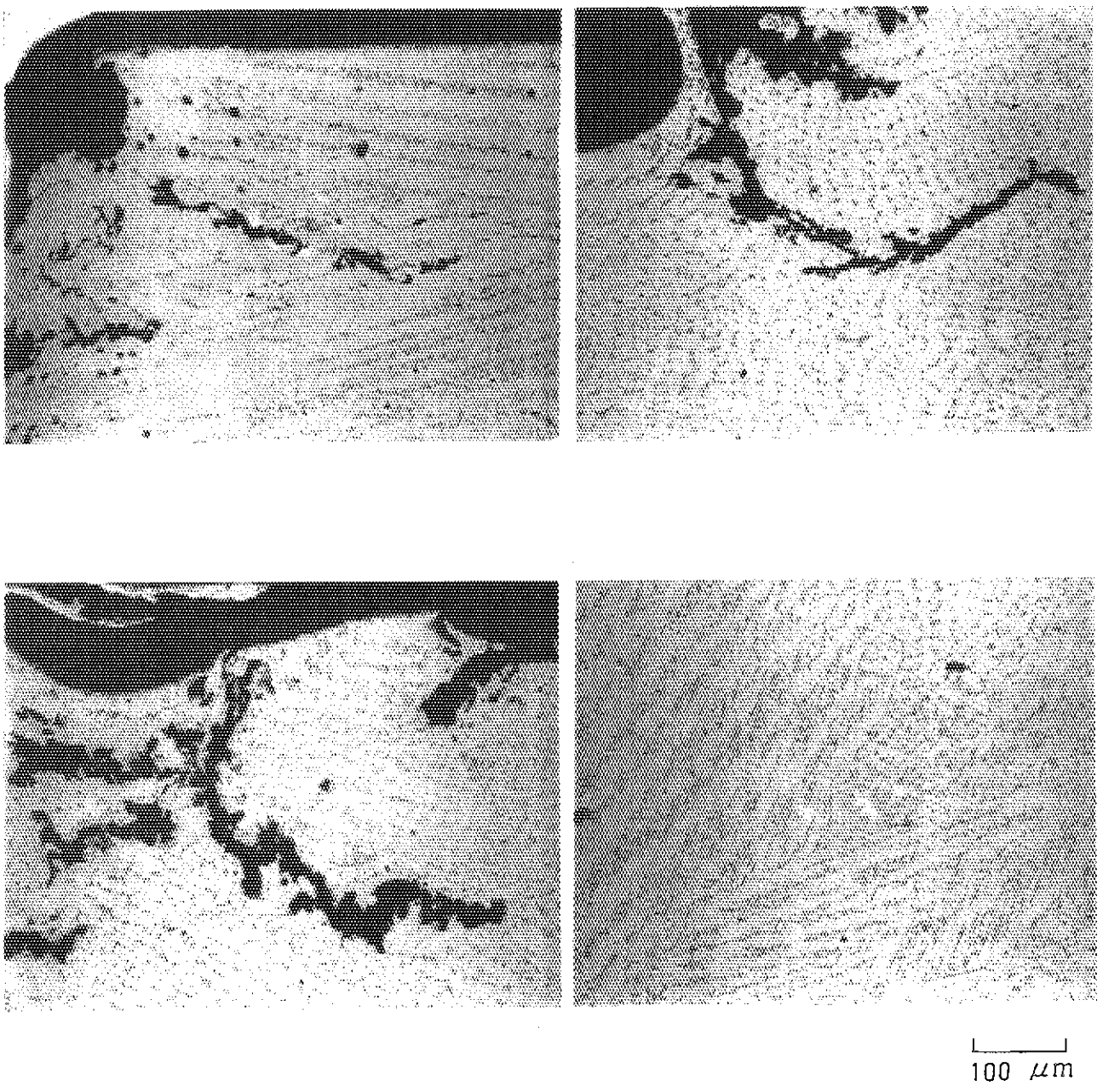


Fig. 16 Micro-structures of fracture surface for weld metal (950℃, 1508.6 h, 22.0 MPa).

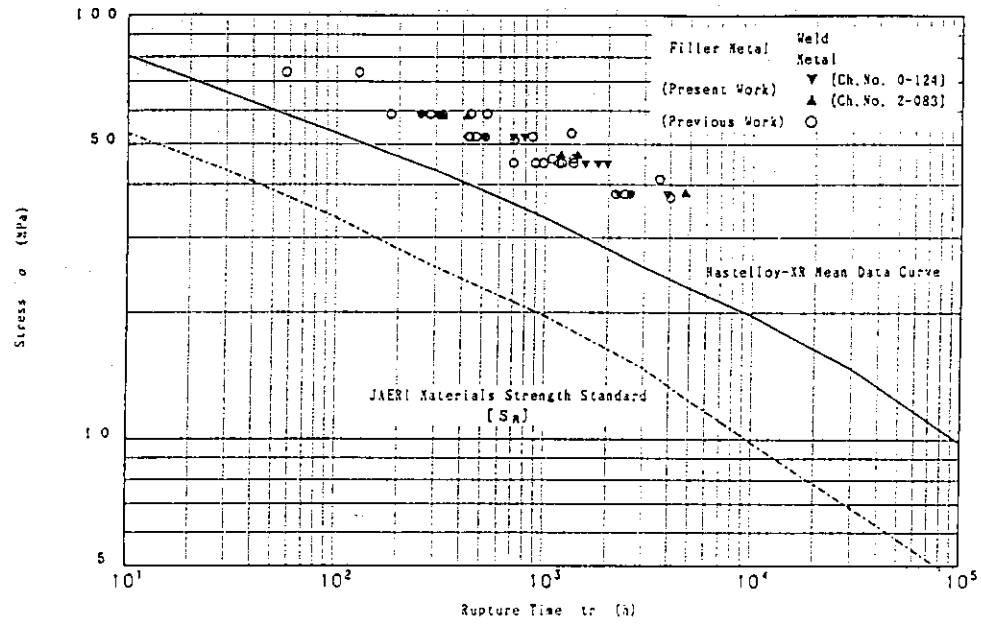


Fig. 17 Relation between applied stress and time to rupture at 900℃.

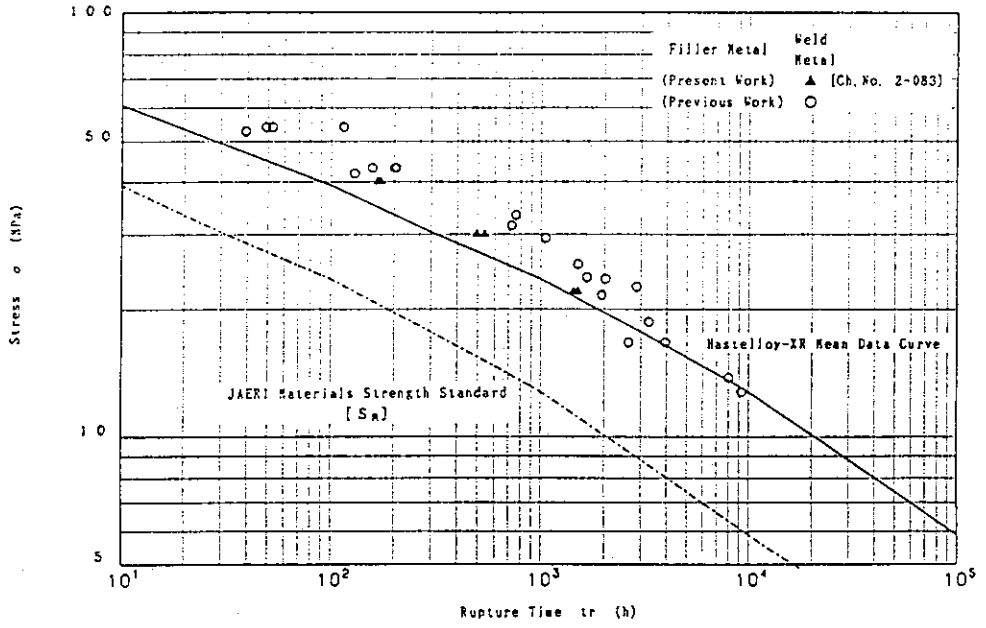


Fig. 18 Relation between applied stress and time to rupture at 950℃.

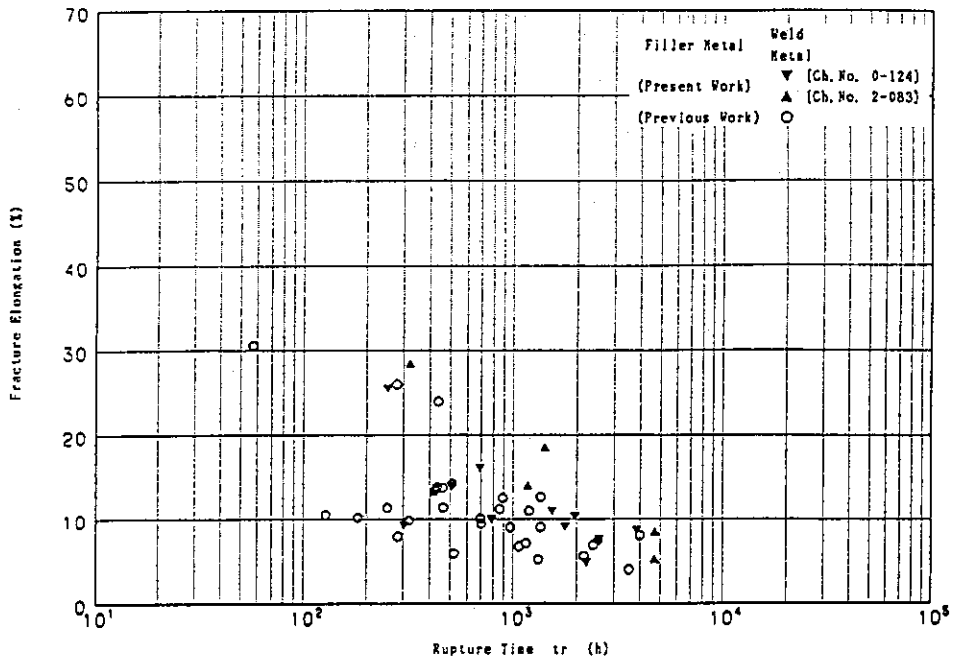


Fig. 19 Relation between rupture elongation and time to rupture at 900℃.

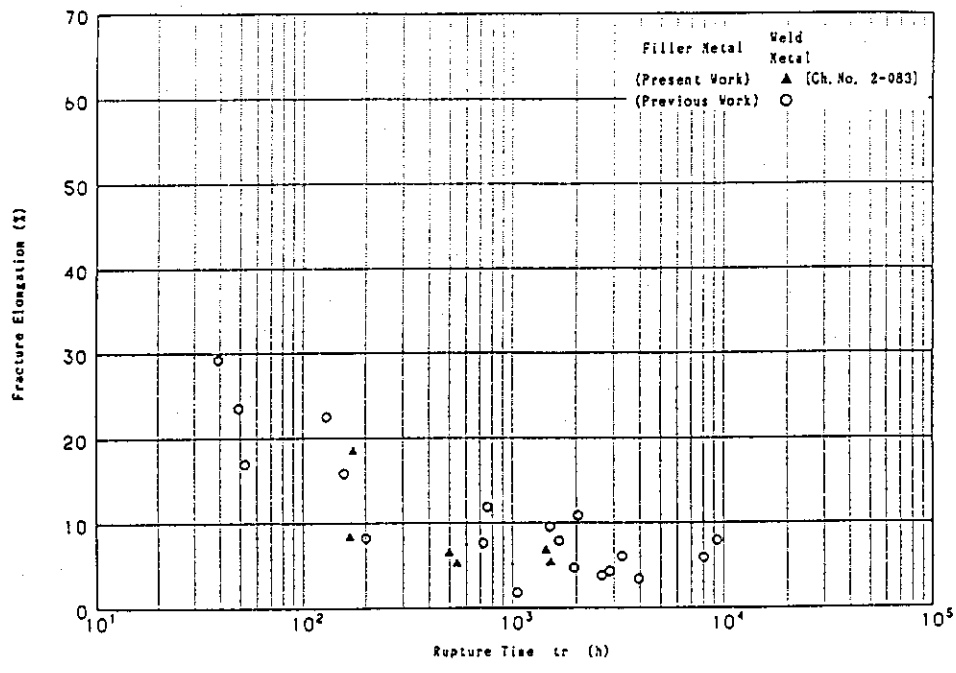


Fig. 20 Relation between rupture elongation and time to rupture at 950℃.

6.11 COMPARISON OF CREEP BEHAVIOR UNDER VARYING LOAD/TEMPERATURE CONDITIONS BETWEEN HASTELLOY XR ALLOYS WITH DIFFERENT BORON CONTENT LEVELS

Hirokazu TSUJI[*1], Tatsuhiko TANABE[*2], Yuji NAKASONE[*3],
Hajime NAKAJIMA[*1] and Masami SHINDO[*1]

*1 Japan Atomic Energy Research Institute
*2 National Research Institute for Metals
*3 Science University of Tokyo
JAPAN

ABSTRACT

In the course of Japanese research and development of high-temperature gas-cooled reactors (HTGRs), the High-Temperature Engineering Test Reactor (HTTR) was planned to be constructed as the first reactor, and it is currently under construction at Oarai Research Establishment of the Japan Atomic Energy Research Institute. A nickel-base heat-resistant alloy, Hastelloy XR was developed as the structural material for high-temperature components of the HTTR. Creep data of Hastelloy XR have been accumulated both in simulated HTGR helium gas and in air environments for the design and safety evaluation of the high-temperature components of the HTTR. The research on the creep behavior of Hastelloy XR has revealed that the creep properties of the alloy depend strongly on the boron content level. The boron content level is determined to be equal or less than 100 mass ppm in the specification of Hastelloy XR. Even within the range, Hastelloy XR shows the very different creep rupture strength according to the amount of boron content.

In the design of the high-temperature components, it is often required to predict the creep rupture life under conditions in which the stress and/or temperature may vary by using the data obtained with the constant load and temperature creep rupture tests. Some conventional

creep damage rules have been proposed to meet the above-mentioned requirement. The applicability of the proposed creep damage rules seems to depend strongly on materials. Currently only limited data are available on the behavior of Hastelloy XR under varying stress and/or temperature creep conditions.

Hence a series of constant load and temperature creep rupture tests as well as varying load and temperature creep rupture tests was carried out on two kinds of Hastelloy XR alloys whose boron content levels are different, i.e., below 10 and 60 mass ppm, in order to examine the behavior of the alloy under varying load and temperature conditions.

The life fraction rule completely fails in the prediction of the creep rupture life of Hastelloy XR with 60 mass ppm boron under varying load and temperature conditions though the rule shows good applicability for Hastelloy XR with below 10 mass ppm boron. The change of boron content level of the material during the tests is the most probable source of impairing the applicability of the life fraction rule to Hastelloy XR whose boron content level is 60 mass ppm. The modified life fraction rule has been proposed based on the dependence of the creep rupture strength on the boron content level of the alloy. The modified rule successfully predicts the creep rupture life under the two stage creep test conditions from 1000°C to 900°C. The trend observed in the two stage creep tests from 900°C to 1000°C can be qualitatively explained by the mechanism that the oxide film which is formed during the prior exposure to 900°C plays the role of the protective barrier against the boron dissipation into the environment.

COMPARISON OF CREEP BEHAVIOR UNDER VARYING LOAD/TEMPERATURE CONDITIONS BETWEEN HASTELLOY XR ALLOYS WITH DIFFERENT BORON CONTENT LEVELS

Hirokazu TSUJI*1, Tatsuhiko TANABE*2, Yuji NAKASONE*3,
Hajime NAKAJIMA*1 and Masami SHINDO*1

*1 Japan Atomic Energy Research Institute
*2 National Research Institute for Metals
*3 Science University of Tokyo

JAPAN

ABSTRACT

In the design of the high-temperature components, it is often required to predict the creep rupture life under the conditions in which the stress and/or temperature may vary by using the data obtained with the constant load and temperature creep rupture tests. Some conventional creep damage rules have been proposed to meet the above-mentioned requirement. The applicability of the proposed creep damage rules seems to depend strongly on materials. Currently only limited data are available on the behavior of Hastelloy XR, which is a developed alloy as the structural material for high-temperature components of the High-Temperature Engineering Test Reactor (HTTR), under varying stress and/or temperature creep conditions.

Hence a series of constant load and temperature creep rupture tests as well as varying load and temperature creep rupture tests was carried out on two kinds of Hastelloy XR alloys whose boron content levels are different, *i.e.*, below 10 and 60 mass ppm, in order to examine the behavior of the alloy under varying load and temperature conditions.

The life fraction rule completely fails in the prediction of the creep rupture life of Hastelloy XR with 60 mass ppm boron under varying load and temperature conditions though the rule shows good applicability for Hastelloy XR with below 10 mass ppm boron. The change of boron content level of the material during the tests is the most probable source of impairing the applicability of the life fraction rule to Hastelloy XR whose boron content level is 60 mass ppm. The modified life fraction rule has been proposed based on the dependence of the creep rupture strength on the boron content level of the alloy. The modified rule successfully predicts the creep rupture life under the two stage creep test conditions from 1000 to 900°C. The trend observed in the two stage creep tests from 900 to 1000°C can be qualitatively explained by the mechanism that the oxide film which is formed during the prior exposure to 900°C plays the role of the protective barrier against the boron dissipation into the environment.

1. Introduction

In the course of Japanese research and development of high-temperature gas-cooled reactors (HTGRs), the High-Temperature Engineering Test Reactor (HTTR) was planned to be constructed as the first reactor, and it is currently under construction at Oarai Research Establishment of the Japan Atomic Energy Research Institute. A nickel-base heat-resistant alloy, Hastelloy XR was developed as the structural material for the HTTR [1-3]. Hastelloy XR has a common basal composition for the major constituents with Hastelloy X (*i.e.*, nominally Ni - 22 mass% Cr - 18 mass% Fe - 9 mass% Mo), while minor elements such as Mn and Si are adjusted in the optimum ranges and Al, Ti and Co are eliminated to the lowest possible levels [1,3]. As the result of the above-mentioned modification, Hastelloy XR is known to have the substantially improved corrosion resistance in the simulated HTGR helium environment and the improved applicability to the HTTR relative to Hastelloy X [1-3].

Creep data for Hastelloy XR have been accumulated both in simulated HTGR helium and air environments for the design and safety evaluation of the high-temperature components of the HTTR. The research on the creep behavior of Hastelloy XR has revealed that the creep properties of the alloy depend strongly on the boron content level [4,5]. The boron content level is determined to be equal or less than 100 mass ppm in the specification of Hastelloy XR [1]. Even within the range, Hastelloy XR shows the very different creep rupture strength according to the amount of boron content as indicated in Fig. 1 [4].

In the design of the high-temperature components, it is often required to predict the creep rupture life under the conditions in which the stress and/or temperature may vary by using the data obtained with the constant load and temperature creep rupture tests. Some conventional creep damage rules have been proposed to meet the above-mentioned requirement. The applicability of the proposed creep damage rules seems to depend strongly on materials. Currently only limited data are available on the behavior of Hastelloy XR under varying stress and/or temperature creep conditions.

Hence a series of constant load and temperature creep rupture tests as well as varying load and temperature creep rupture tests was carried out on two kinds of Hastelloy XR alloys whose boron content levels are different, *i.e.*, below 10 and 60 mass ppm, in order to examine the behavior of the alloys under varying load and temperature conditions.

2. Experimental Procedures

2.1 Materials

The materials tested in this study are two kinds of commercially manufactured Hastelloy XR alloys whose boron content levels are different. The chemical compositions and the tensile properties of the materials are listed in Tables 1, 2 and 3. As shown in Table 1, the boron content levels of them are 1 to 2 mass ppm for Heat 1 and 60 mass ppm for Heat 2. The materials were solution annealed at 1190°C for 1 h followed by water quenching.

2.2 Creep rupture tests

Creep rupture tests were accomplished by using specimens with 6 mm in diameter and 30 mm in gauge length. The tests were performed with lever-type creep testers. Some tests were carried out in simulated HTGR helium gas environments, and others in air. The test section used for the tests in simulated HTGR helium gas environments was encased in a vacuum tight chamber connected to a circulating helium loop system. A series of constant load and temperature creep rupture tests as well as varying load and/or temperature creep rupture tests was conducted at 850, 900, 950 and 1000°C. Two types of simulated HTGR helium gas were employed, and the impurity contents in the gas are indicated in Table 4. The characterizations of these environments have been reported elsewhere [6], and they are essentially equivalent from the viewpoints of the chemical reactions between the material and the environment [6]. Test temperatures were chosen considering the outlet coolant temperatures of the HTTR which were 850°C at the rated operation and 950°C at the high temperature test operation. Stress levels were chosen with intention of the maximum rupture life being within 104 h.

3. Results and discussion

3.1 Constant load and temperature creep rupture tests

Figure 2 shows the relation between the applied stress, which is a nominal stress given by the load divided by the initial cross-sectional area, and the time to rupture obtained with the constant load and temperature creep rupture tests on Heat 1 whose boron content level is 1 to 2 mass ppm. The relation can be expressed as

$$t_R = 1.283 \times 10^{12} \sigma^{-5.458} \text{ at } 850°C, \quad (1)$$

$$t_R = 2.944 \times 10^{9} \sigma^{-4.272} \text{ at } 900°C, \quad (2)$$

$$t_R = 1.550 \times 10^8 \sigma^{-3.891} \text{ at } 950°C \quad (3)$$

and

$$t_R = 1.013 \times 10^7 \sigma^{-3.466} \text{ at } 1000°C, \quad (4)$$

where t_R is the time to rupture in hour and σ is the applied stress in MPa.

Figure 3 shows the relation between the applied stress, which is a nominal stress given by the load divided by the initial cross-sectional area, and the time to rupture obtained with the constant load and temperature creep rupture tests on Heat 2 whose boron content level is 60 mass ppm. In the figure, not only the data obtained in the present study but also those obtained for the same heat material in another work [7] are plotted. There is no significant difference in the creep rupture life among three test environments within the range tested. The relation between the applied stress and the time to rupture can be expressed as follows;

$$t_R = 3.849 \times 10^{13} \sigma^{-6.390} \text{ at } 900°C \quad (5)$$

and

$$t_R = 1.225 \times 10^8 \sigma^{-3.964} \text{ at } 1000°C, \quad (6)$$

where t_R is the time to rupture in hour and σ is the applied stress in MPa.

3.2 Creep damage rules

In the design of the high-temperature components, it is usually required to predict the creep rupture life under the conditions where the stress and/or temperature may vary from the data obtained with the constant load and temperature creep rupture tests. Some conventional creep damage rules have been proposed to meet such a requirement [8-13].

The life fraction rule, which has been widely utilized in the engineering design of high-temperature components, was proposed by Robinson [8,9]. According to the rule, creep rupture is predicted to occur when the summation of the life fractions is equal to unity, *i.e.,* the rule is expressed as

$$\sum_i \frac{\Delta t_i}{t_{Ri}} = 1, \quad (7)$$

where Δt_i is the period of time spent under a particular stress and temperature, and t_{Ri} is the rupture time corresponding to this stress and temperature. This rule has supported by several investigators

[14-17], while other investigators reported several cases where the prediction of this rule was unsatisfactory [10-13,18-20].

An analogous rule, which is known as the strain fraction rule, was proposed by Lieberman [10]. According to the rule, creep rupture is predicted to occur when the summation of the strain fractions is equal to unity, *i.e.* , the rule is expressed as

$$\sum_i \frac{\Delta\varepsilon_i}{\varepsilon_{Ri}} = 1, \tag{8}$$

where $\Delta\varepsilon_i$ is the strain under a given stress and temperature, and ε_{Ri} the strain at rupture under the same stress and temperature.

The mixed criterion of the two above-mentioned rules was proposed by Voorhees & Freeman [11,12]. In the criterion, the condition where creep rupture is predicted to occur is given as follows;

$$\sum_i \sqrt{\frac{\Delta t_i}{t_{Ri}} \cdot \frac{\Delta\varepsilon_i}{\varepsilon_{Ri}}} = 1. \tag{9}$$

Furthermore an attempt of modifying the mixed criterion was made by Abo El Ata & Finnie [13]. In the modified criterion, the condition where creep rupture is prediction to occur is given as follows;

$$K\sum_i \frac{\Delta t_i}{t_{Ri}} + (1-K)\sum_i \frac{\Delta\varepsilon_i}{\varepsilon_{Ri}} = 1, \tag{10}$$

where K is the material constant between zero and one which indicates the ability of the material to resist cracking during creep.

In the design of the high-temperature components of the HTTR, the life fraction rule was applied among the above-mentioned conventional creep damage rules from the viewpoints of actual experience and simplicity [1]. Applicability of the life fraction rule, therefore, was examined to the data obtained in the present study.

3.3 Results of application of life fraction rule

Figure 4 shows the results of application of the life fraction rule to the varying stress and/or temperature test results on Heat 1. In the figure, the life fraction $\Delta t_i / t_R$ was obtained using the

calculated values with Eqs. (1) to (4) as t_R. The summation of the life fractions ranges from 0.69 to 1.36, the average is 0.96, and the standard deviation is 0.19. These values suggest that the life fraction rule is applicable in engineering design of high-temperature components made of Hastelloy XR whose boron content level is below 10 mass ppm.

Figures 5 and 6 show the results of application of the life fraction rule to the varying stress and temperature test results on Heat 2. In these figures, the life fraction $\Delta t_i / t_R$ was obtained using the calculated values with Eqs. (5) and (6) as t_R. As can be seen in these figures, the life fraction rule completely fails in the prediction of the creep rupture life under varying load and temperature conditions in contrast with the result for Heat 1. The data tend to be located in the higher portion than the line which shows the summation of the life fraction is equal to unity in Fig. 5, *i.e.*, in the tests from 900 to 1000°C. On the contrary, all the data are located in the lower portion than the line which shows the summation of the life fractions is equal to unity in Fig. 6, *i.e.*, the tests from 1000 to 900°C.

3.4 Possible sources of changes in creep strength

In general, the life fraction rule shows good applicability to the material whose creep strength is not strongly affected by the change of the chemical composition and/or the microstructure of the material which occurs during exposure to the high-temperature environment. In the present study, the followings may be taken into consideration as the change of the chemical composition and/or the microstructure which may occur during exposure to the high-temperature environment, and may affect the creep strength;

(1) change of carbon content,

(2) change of chromium content,

(3) precipitation of carbides, and

(4) recrystallization, for both materials, and

(5) change of boron content, for Heat 2.

It is known that the creep strength of Hastelloy XR strongly depends on the carbon content level [21,22], and that carburization or decarburization may occur in the helium gas environment which contains specific levels of impurities for the alloy [21,22]. However in the environments employed in the present study, Hastelloy XR indicates protective corrosion behavior, and only mild carburization, which does not significantly affect the creep strength of the alloy [21,22], occurs [6].

It is also known that the chromium depleted zone is formed near the surface region of the material by exposure to the high-temperature simulated HTGR helium gas environments [3]. Such a

phenomenon might cause the creep strength reduction. The depth of the chromium depleted zone, however, is estimated below 200 μm even in the condition where Δt_1 is the longest at 1000°C [23]. The value is small relative to the diameter of the creep specimen, *i.e.*, 6 mm, employed in the present study. The phenomenon, therefore, does not affect the creep strength of Hastelloy XR significantly [24].

During exposure to the high-temperature test environment, carbides precipitate and may grow in Hastelloy XR. Precipitation of carbides is considered to contribute to the creep strength of the material, and there may be the most preferable amount and size of precipitates for the contribution. The amount and the size of precipitates are considered to depend on the exposed temperature more strongly than on the applied stress level. This may cause the tendency that the applicability of the life fraction rule under varying both stress and temperature conditions is slightly inferior to that under varying stress and constant temperature conditions as shown in Fig. 4.

Recrystallization might occur in Hastelloy XR crept at 1000°C [25]. Such a phenomenon might cause the creep strength reduction. Recrystallization occurs more easily in the material whose boron content level is below 10 mass ppm such as Heat 1 than the material with 50 to 60 mass ppm boron such as Heat 2 [26]. If this mechanism is dominant, the life fraction in the second stage becomes lower for Heat 1 under varying stress and temperature conditions from 1000 to 900°C, especially in the conditions where Δt_1 is long. Such a trend, however, cannot be observed in Fig. 4.

As already mentioned in section 1, the creep strength of Hastelloy XR depends strongly on the boron content level (see Fig. 1). If the amount of boron content decreases during exposure to the high-temperature environment, the creep strength of the alloy will reduce.

Among the above-mentioned five items, the items (1) to (4) are common to both of Heats 1 and 2, while the item (5) is specific to Heat 2. The item (5), therefore, is the most possible as the factor which caused the difference in the applicability of the life fraction rule between Heats 1 and 2 whose boron content levels are different.

3.5 Results of boron analyses

In order to examine the changes in the amount of boron content, boron analyses were made for the crept specimens of Heat 2. In some cases the specimens for boron analyses were separated into two portions, *i.e.*, the core and the surface portions as shown in Fig. 7, and in other cases the specimens were used for boron analyses in all. The specimens for boron analyses were selected from the crept ones indicated in Figs. 3, 5 and 6, and some specimens for boron analyses were newly prepared by conducting interruption creep tests under constant load and temperature

conditions.

Figures 8 and 9 show the results of boron analyses as a function of the exposure time to the high-temperature environments at 900 and 1000°C, respectively. In the figures only one stage test results are shown, and no results under varying load and temperature conditions are indicated. It is clearly recognized that the amount of boron content reduces with increasing the exposure time at 1000°C in Fig. 9. Even at 900°C such a tendency is observed in Fig. 8. The boron content reduction rate at 900°C, however, is much lower than that at 1000°C. The amount of boron content at the surface portion tends to be smaller than that at the core portion, *i.e.*, open symbols are generally located in the lower portion than solid ones in Figs. 8 and 9. The fact suggests that boron in the material dissipates from the surface as the result of the reaction with the high-temperature environments and that boron is supplied by the diffusion flow from the core portion to the surface.

Figure 9 suggests that the amount of boron content of the material crept at 1000°C in the first stage is lower than the original level at the point when the test conditions were changed from 1000 to 900°C. This mechanism may play the major role in impairing the reliability of the life fraction rule in Fig. 6, in which the creep lives in the second stage are extremely short.

3.6 Modification of life fraction rule

It is preferable to apply the evaluation method which takes account of the change of the chemical composition and/or the microstructure of the material which occurs during exposure to the high-temperature environment for the precise prediction of the creep rupture life under varying load and temperature conditions [19,20]. Since the above-mentioned mechanism seems to play the major role in impairing the reliability of the life fraction rule for Heat 2, the modification of the rule may be effective based on the dependence of the creep rupture strength on the boron content level of the alloy. In order to simplify the discussion, the followings are assumed:

(1) The boron content reduction at 900°C is negligible.

(2) There is no difference in the creep rupture life among three environments employed in the present study.

(3) The bulk boron content level is a mean value of the boron analyzed results of the core and the surface portions.

(4) The creep rupture life of the material whose boron content level is below 60 mass ppm becomes shorter along the line A linearly in a logarithm scale in Fig. 10.

By adding the results of boron analyses for the specimens crept under varying load and temperature conditions to Fig. 9 based on the assumption (1), Fig. 11 was obtained. According to

the assumption (1), the amount of boron content after creep rupture tests under the conditions from 1000 to 900°C can be regarded as the boron content level of the material at the point when the test conditions were changed from 1000 to 900°C. Consequently the creep rupture life of the material whose boron content level is equal to that of the material at the point when the test conditions were changed from 1000 to 900°C can be estimated based on the assumptions (2), (3) and (4).

Figure 12 shows the result of the application of the above-mentioned method. Comparison of Fig. 12 with Fig. 6 clearly shows that the creep rupture life under varying load and temperature conditions is predicted more successfully by the modified life fraction rule based on the dependence of the creep rupture strength on the boron content level than by the fraction rule.

By the way, the tendency is observed that the boron content reduction rate under the condition from 900 to 1000°C is low in Fig. 11. The tendency suggests that the prior exposure to 900°C could delay the phenomenon of boron dissipation during the following exposure to 1000°C. The oxide film which is formed on the surface of the specimen during the exposure to 900°C might play the role of the protective barrier against the boron dissipation into the environment. Since Eq. (6) expresses the relation between the applied stress and the time to rupture in the case where the amount of boron content of the material reduces gradually, the creep rupture life would be longer in the case where the boron content reduction rate is low than that calculated with Eq. (6). This mechanism can qualitatively explain the trend that the data are located in the higher portion than the line which shows the summation of the life fractions is equal to unity in Fig. 5, *i.e.*, in the tests from 900 to 1000°C.

4. Conclusions

A series of constant load and temperature creep rupture tests as well as varying load and temperature creep rupture tests was carried out on two kinds of Hastelloy XR alloys whose boron content levels are below 10 and 60 mass ppm at 850 to 1000°C in order to examine the behavior of the alloys under varying load and temperature conditions. Based on the results obtained the following conclusions are drawn:

(1) The life fraction rule shows good applicability for Hastelloy XR whose boron content level is below 10 mass ppm.

(2) The life fraction rule completely fails in the prediction of the creep rupture life under varying load and temperature conditions for Hastelloy XR whose boron content level is 60 mass ppm.

(3) The change of boron content level of the material during the tests is the most probable source

of impairing the reliability of the life fraction rule for the alloy with 60 mass ppm boron.

(4) The modified life fraction rule has been proposed based on the dependence of the creep rupture strength on the boron content level of the alloy. The modified rule successfully predicts the creep rupture life of the alloy with 60 mass ppm boron under the test condition from 1000 to 900°C.

(5) The trend observed in the tests from 900 to 1000°C for the alloy with 60 mass ppm boron can be qualitatively explained by the mechanism that the oxide film which is formed during the prior exposure to 900°C plays the role of the protective barrier against the boron dissipation into the environment.

Acknowledgement

The authors are grateful to Dr. H. Shiraishi of the National Research Institute for Metals and Dr. T. Kondo of Tohoku University for their advice and encouragement.

References

[1] K. Hada, I. Nishiguchi, Y. Muto and H. Tsuji, Nucl. Eng. Des. 132(1991) 1.
[2] Japan Atomic Energy Research Institute, Present Status of HTGR Research and Development (1992).
[3] M. Shindo and T. Kondo, Proc. Conf. on Gas-Cooled Reactors Today, Bristol/UK, British Nuclear Engineering Society vol. 2 (1982) 179.
[4] T. Kondo, K. Watanabe, K. Sato, T. Nakanishi, K. Sahira, H. Tsuji, Y. Kurata, T.Tsukada and K. Ozawa, JAERI-M 86-003 (1986).
[5] Y. Kurata, K. Sato, T. Nakanishi, K. Sahira and T. Kondo, Proc. Conf. on Creep, Tokyo /Japan, Japan Society of Mechanical Engineers (1986) 97.
[6] M. Okada, T. Tanabe, F. Abe, Y. Sakai, T. Kondo, H. Nakajima, Y. Ogawa, H. Tsuji and Y. Kurata, JAERI-M 87-193 (1987).
[7] H.Yoshizu, Y. Monma, E. Baba, Y. Kurata, H. Nakajima and T. Suzuki, JAERI-M 93-231 (1993).
[8] E.L. Robinson, Trans. ASME 60 (1938) 253.
[9] E.L. Robinson, Trans. ASME 74 (1952) 777.
[10] Y. Lieberman, Mettaloved, Term. Obrabotka Metal 4 (1962) 6.
[11] H.R. Voorhees and J.W. Freeman, ASTIA Document No. 118 (1957) 289.
[12] H.R. Voorhees and J.W. Freeman, ASTIA Document No. 207 (1959) 850.
[13] M.M. Abo El Ata and I. Finnie, Trans. ASME Series D, J. Basic Eng. 94 (1972) 533.
[14] J. Miller, ASTM STP 165 (1954) 53.
[15] P.N. Randall, Trans. ASME Series D, J. Basic Eng. 84 (1962) 239.
[16] H.R. Voorhees, Ph. D. Thesis, The University of Michigan (1956).
[17] R.M. Goldhoff and D.A. Woodford, ASTM STP 515 (1972) 89.
[18] J.W. Freeman and H.R. Voorhees, ASTM STP 391 (1965).
[19] L. Schäfer, J. Nucl. Mater. 138 (1986) 162.
[20] L. Schäfer, J. Nucl. Mater. 138 (1986) 170.
[21] Y. Kurata, Y. Ogawa and H. Nakajima, J. Iron Steel Inst. Japan 74 (1988) 380.

[22] Y. Kurata, Y. Ogawa and H. Nakajima, J. Iron Steel Inst. Japan 74 (1988) 2185.
[23] T. Tsukada, M. Shindo, T. Suzuki, H. Nakajima and T. Kondo, Proc. of Workshop on High Temperature Corrosion of Advanced Materials and Protective Coatings, Tokyo/Japan, Elsevier Sci. Publ. B.V. (1992) 233.
[24] M. Tamura, Y. Ogawa, Y. Kurata and T. Kondo, JAERI-M 82-036 (1982).
[25] S. Yokoi, Y. Monma, T. Kondo, Y. Ogawa and Y. Kurata, JAERI-M 83-138 (1983).
[26] T. Kihara, Y. Ogawa, Y. Kurata and H. Nakajima, unpublished work.

Table 1 Chemical compositions of the materials tested (mass%).

		C	Si	Mn	P	S	Cr	Co	Mo	W	Fe	B	Al	Ti	N	Ni
Heat 1	T	0.07	0.32	0.96	<0.001	<0.001	22.00	0.02	9.11	0.49	18.59	0.0002	0.01	0.01	0.007	Bal.
	B	0.07	0.33	0.93	<0.001	<0.001	21.96	0.03	9.11	0.49	18.62	0.0001	0.02	<0.01	0.006	Bal.
Heat 2		0.07	0.33	0.88	<0.001	0.001	21.99	0.06	8.73	0.63	17.80	0.006	0.03	0.01	0.006	Bal.

T : Top side of the ingot, B : Bottom side of the ingot

Table 2 Tensile properties of Heat 1 at room temperature and at temperatures where creep rupture tests were conducted.

Test temp. (℃)	Strain rate (%/s)	0.2% Proof stress (MPa)	Ultimate tensile strength (MPa)	Total elongation (%)	Reduction of area (%)
RT	5×10^{-3} (first stage) 1.25×10^{-1} (second stage)	301 - 323	688 - 697	57.1 - 62.8	62.8 - 64.6
Strain rate was changed at a strain of 1.5%.			Frequency was four.		
850	5×10^{-3}	188	203	116.3	75.2
	1.25×10^{-1}	155	250	108.9	80.2
	2.5×10^{-1}	147	274	84.6	74.3
900	5×10^{-3}	153	172	126.2	69.2
	1.25×10^{-1}	149	195	101.1	82.5
	2.5×10^{-1}	146	217	101.5	78.5
950	5×10^{-3}	117	137	94.6	67.2
	1.25×10^{-1}	136	172	122.3	83.8
	2.5×10^{-1}	143	171	101.7	80.7
1000	5×10^{-3}	81	103	86.7	64.1
	1.25×10^{-1}	123	136	132.7	84.0
	2.5×10^{-1}	129	145	100.4	79.6

Table 3 Tensile properties of Heat 2 at room temperature and at temperatures where creep rupture tests were conducted.

Test temp. (℃)	Strain rate (%/s)	0.2% Proof stress (MPa)	Ultimate tensile strength (MPa)	Total elongation (%)	Reduction of area (%)
RT	5×10^{-3} (first stage) 1.25×10^{-1} (second stage)	289	685	56.9	60.9
Strain rate was changed at a strain of 3%.					
900	5×10^{-3}	127	133	109.7	78.1
	1.25×10^{-1}	160	161	91.3	81.4
	2.5×10^{-1}	175	204	120.7	89.8
1000	5×10^{-3}	72	75	93.0	66.6
	1.25×10^{-1}	89	109	119.3	79.3
	2.5×10^{-1}	116	145	104.2	82.1

Table 4 Impurity levels in simulated HTGR helium gas environments (vol ppm).

	H_2	H_2O	CO	CO_2	CH_4
He-1	200	1	100	2	5
He-2	300	3	100	1	15

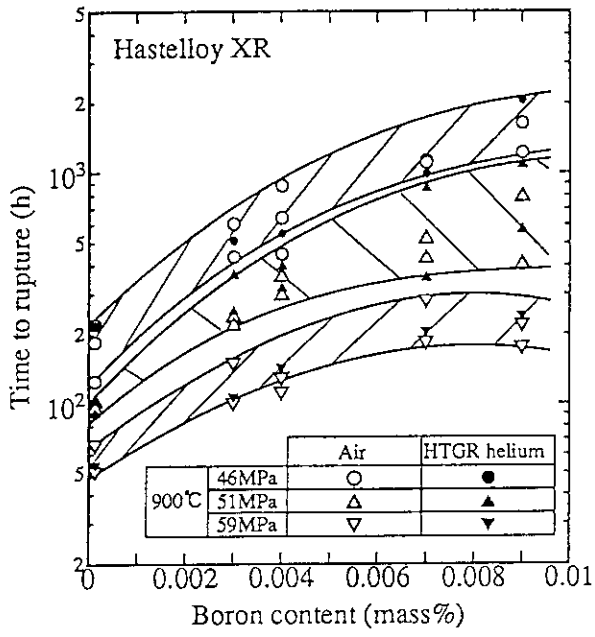


Fig. 1 Effect of the boron content level on the creep rupture life of Hastelloy XR [4].

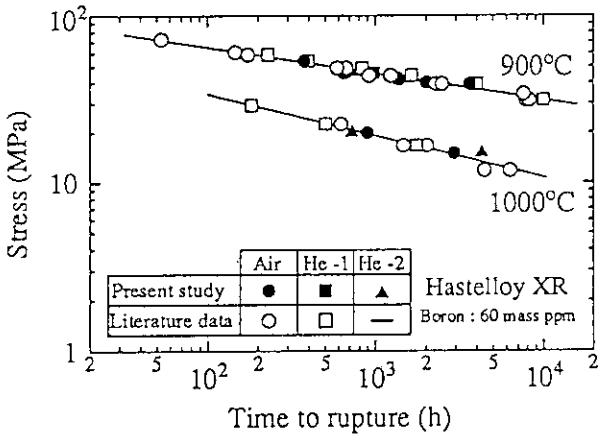


Fig. 3 Relation between applied stress and time to rupture obtained with constant load and temperature creep rupture tests for Hastelloy XR with 60 mass ppm boron. The figure includes both of the data obtained in the present study and in another work [7] for the same heat material.

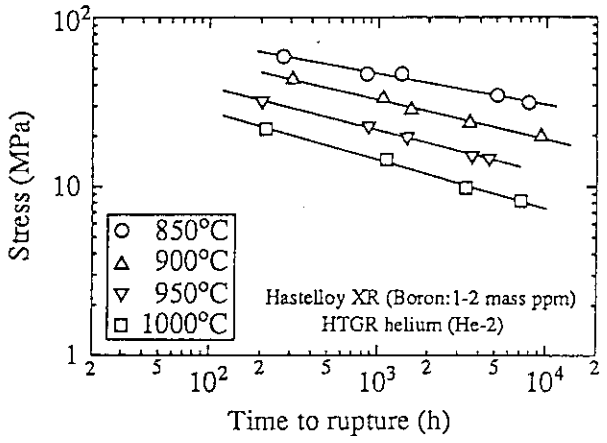


Fig. 2 Relation between applied stress and time to rupture obtained with constant load and temperature creep rupture tests for Hastelloy XR with 1 to 2 mass ppm boron.

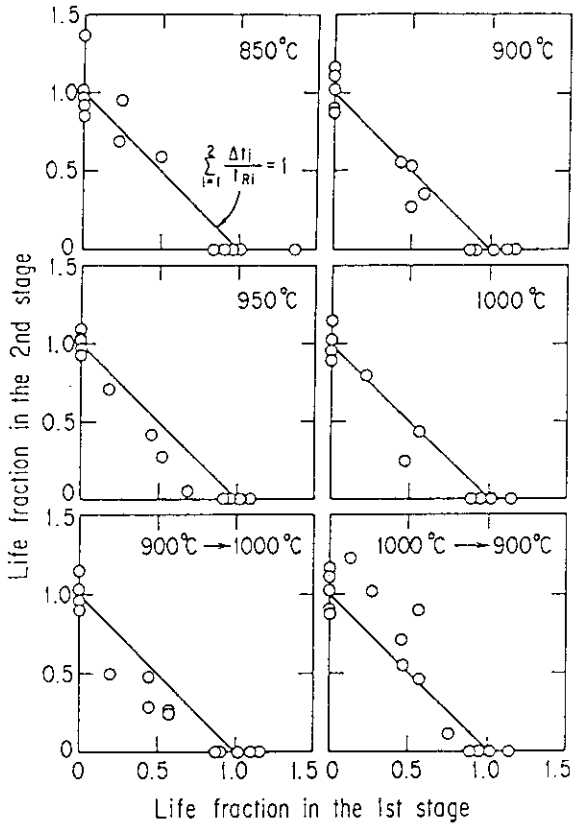


Fig. 4 Result of application of the life fraction rule to the varying stress and/or temperature test results for Hastelloy XR with 1 to 2 mass ppm boron.

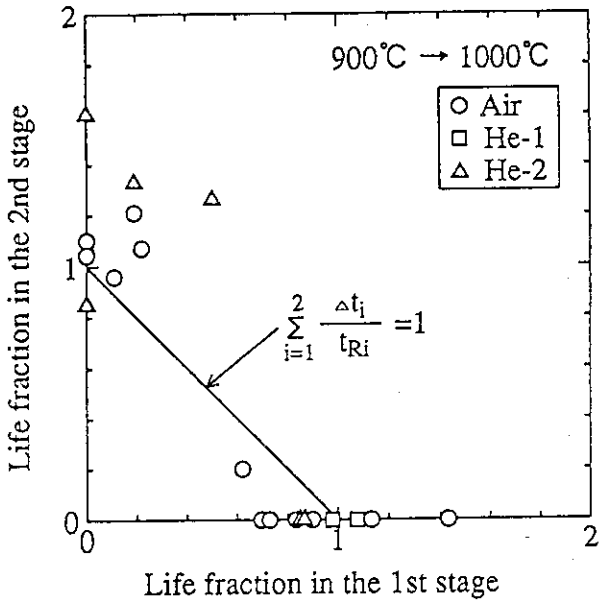


Fig. 5 Result of application of the life fraction rule to the test results under the conditions from 900 to 1000°C for Hastelloy XR with 60 mass ppm boron.

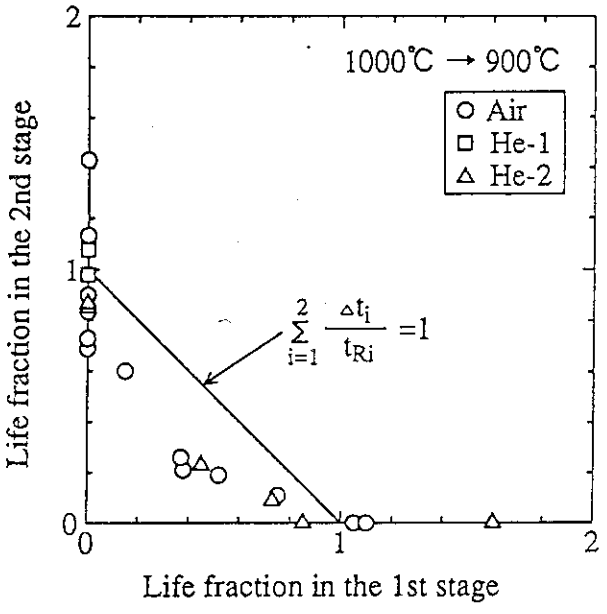


Fig. 6 Result of application of the life fraction rule to the test results under the conditions from 1000 to 900°C for Hastelloy XR with 60 mass ppm boron.

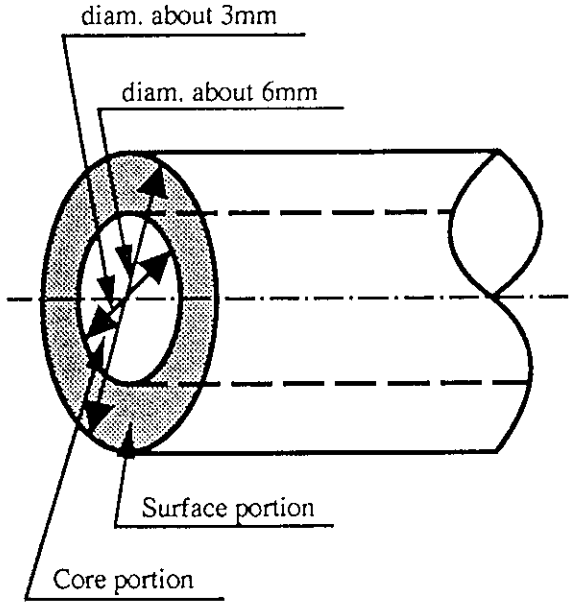


Fig. 7 Schematic illustration of the sampling method of specimens for boron analyses.

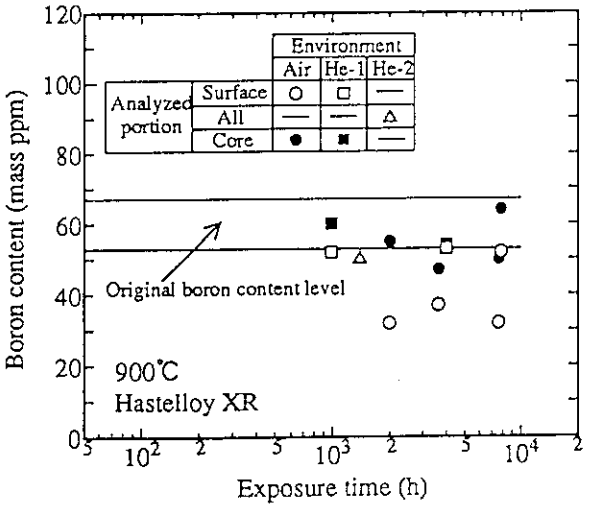


Fig. 8 Results of boron analyses as a function of the exposure time to the high-temperature environments at 900°C. The figure does not include the results under varying load and temperature conditions.

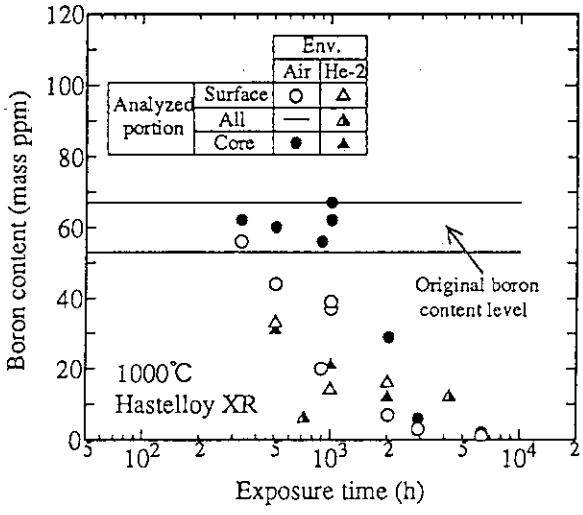


Fig. 9 Results of boron analyses as a function of the exposure time to the high-temperature environments at 1000°C. The figure does not include the results under varying load and temperature conditions.

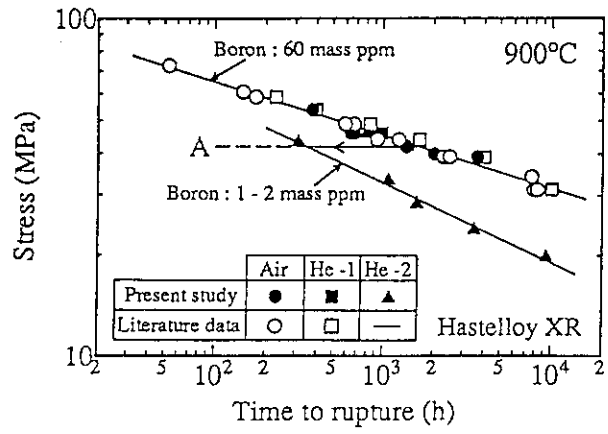


Fig. 10 Relation between applied stress and time to rupture obtained with constant load and temperature creep rupture tests for Hastelloy XR whose boron content levels are different . The figure includes the data obtained in another work [7] for the same heat material.

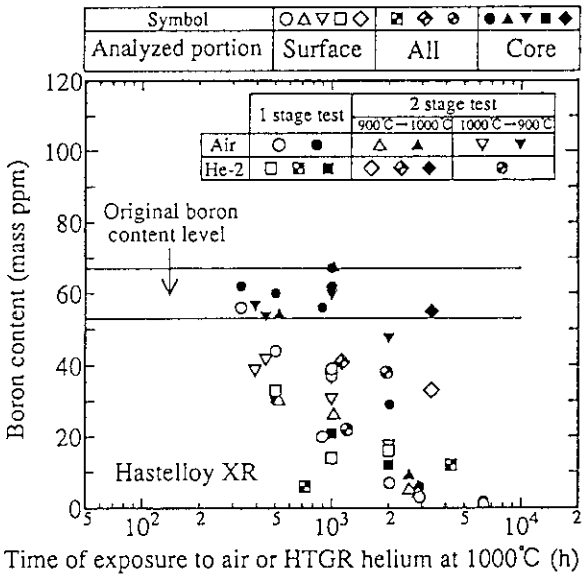


Fig. 11 Results of boron analyses as a function of the exposure time to high-temperature environments at 1000°C. The figure includes the results under varying load and temperature conditions.

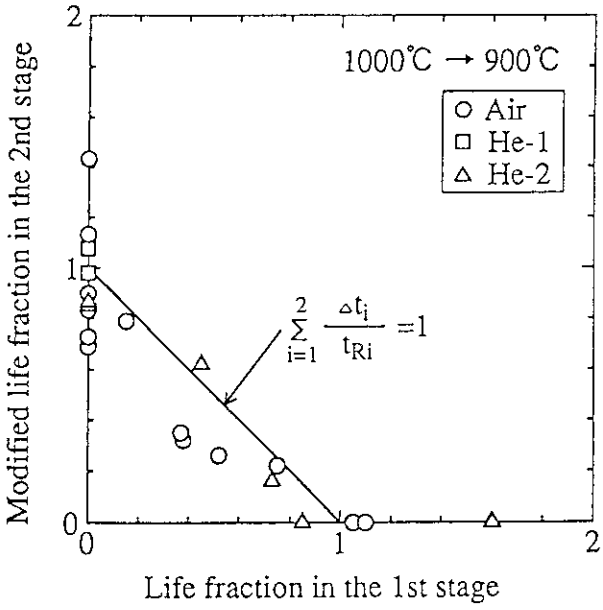


Fig. 12 Result of application of the modified life fraction rule to the test results under the conditions from 1000 to 900°C for Hastelloy XR with 60 mass ppm boron.

6.12 Operation Experience with In-pile Gas Loop OGL-1 for HTTR Fuels and Materials Irradiation

Tadahiko ISHII, Tohru SARUTA,
Isao ARASE and Toshisada NIIHO

Department of JMTR, Oarai Research Establishment
Japan Atomic Energy Research Institute

Abstract

The OGL-1 was the in-pile gas loop which was installed at the JMTR in 1976 to perform irradiation tests for the HTTR fuels and materials under condition similar to those of the HTTR coolant. Since 1977, various kinds of tests such as a series of irradiation test for the HTTR fuels, measurements of FP plated out behavior in the OGL-1, compatibility tests of structural materials, FP lift-off experiment, etc., were successfully conducted in the loop with total operation time of 38,200 hours. Irradiation utilization was completed in 1995, and the OGL-1 was removed from the JMTR.

This paper describes an outline of the operation experience with the OGL-1.

Operation Experience with In-pile Gas Loop OGL-1 for HTTR Fuels and Materials Irradiation

Tadahiko ISHII, Tohru SARUTA* ,
Isao ARASE and Toshisada NIIBO

Department of JMTR, Department of HTTR Project *
Oarai Research Establishment
Japan Atomic Energy Research Institute

1. Description of OGL-1

The OGL-1,Oarai Gas Loop No.1, was the in-pile gas loop which was installed at the JMTR in 1976 to perform irradiation tests for the HTTR fuels and materials under condition similar to those of the HTTR coolant. The OGL-1 was a high temperature and high pressure helium gas loop installed in a reflector region of the JMTR core. Major characteristics of the OGL-1 are summarized in Table 1.

Figure 1 shows a flow diagram of the OGL-1 schematically. The OGL-1 consists of an in-pile tube and out-of-pile equipments which are composed primary circuit system, secondary circuit system and purification system.

As shown in Fig. 2, the in-pile tube is composed of four coaxial tubes (outer tube, pressure tube, inner tube and flow tube) to prevent boiling in the JMTR core, and to protect the reactor core in the event of a potential pipe rupture incident. Materials of the in-pile section are mainly 316 stainless steel for the pressure boundary and Hastelloy-X for the high temperature boundary. The outer tube and the pressure tube are made of 316 stainless steel, and Hastelloy-X is used for the inner tube and the flow tube.

The primary circuit system consists of circulator, heater, re-generative heat exchanger, cooler, etc.. Direct electric resistance heating of primary piping is used as the heater. A cooling gas pressurized at 3 MPa is heated at about 670 ℃ by both the re-generative heat exchanger and the heater, thereafter flowing into the in-pile tube, where gas is further heated up to about 1000℃ by fission heating of a fuel element. Maximum heat generation of

the fuel element is 135 kW. The outlet gas from the in-pile tube is cooled down to about 710℃ by heat rejection from the inlet gas to the in-pile tube, and down to about 130℃ by the re-generative heat exchanger and the cooler, then forced back toward the in-pile tube by the circulator. Temperature distribution in the circuit is shown in Fig. 1.

Approximately one percent of the circulating gas is by-passed from the main stream and flows into the purification system to remove gaseous activities and impurities from the primary circuit. The purification system has capability of removal efficiency of 99 % for fission gas and 60-85 % for tritium.

2. Operation and maintenance experiences

2.1 Operation

Table 2 shows the experiences of utilization, operation and maintenance for the whole life of the OGL-1. Various kinds of tests such as the series of irradiation test for the HTTR fuel development, measurements of FP plate-out behaviour in the OGL-1 including the FP filter experiment in corporation with Germany, the compatibility tests for control rod materials, the experiment for development of gaseous FP monitoring system, the measurement of efficiency of the pre-charcoal trap, and the FP lift-off experiment to study the behaviour at the hypothetical depressurization accident of the HTTR, were successfully conducted in the loop with total operation time of 38,200 hours. Totally fifteen irradiation test assemblies on various kinds of fuels were performed as shown in Table 3 .

During operation of the OGL-1, concentrations of impurities, such as oxygen, nitrogen and moisture which affect on integrity and life of fuels and structural materials, were monitored continuously. Total concentrations of impurities were kept well below 10 vpm. This showed the purification system, which consisted of a charcoal trap, a helium purification dryer(MS) using molecular sieves, a cold charcoal trap and a titanium sponge trap, was operated with good function. Gaseous fission products which were released into the helium gas from fuel during irradiation, were also monitored successfully through the all irradiation tests.

The OGL-1 was successfully operated with only minor troubles such as blowing out of rupture disc for the primary coolant and failure of electric power supply unit for the circulator of primary circuit system, which both resulted in the reactor scram.

The OGL-1 had a limitation of temperature elevation speed to ease stress in the structural components cased by thermal expansion, such as the piping of

primary circuit, the heater, the re-generative heat exchanger, etc.. For that purpose it was needed to keep constantly both power levels of 30 MW and 40 MW for 90 minutes respectively at starting up of the JMTR.

2.2 Maintenance

The OGL-1 components have each design lives such as 6900 hours for the flow tube due to creep rupture time of Hastelloy-X under irradiation, 22000 hours for the in-pile tube (pressure tube and outer tube) due to neutron dose. Therefore, the exchanging works of both the flow tube and the in-pile tube were carried out periodically as shown in Table 2. The flow tube was replaced four times, and the in-pile tube including the flow tube was replaced one time. In addition, most of the alarm devices and instruments for indication on the control panel were replaced with new one due to aging.

The annual in-service inspections on the out-of-pile section of the primary circuit system were carried out as shown in Table-4. A visual inspection using a bore-scope was applied to the heater to observe a deformation of outside of the heating pipe. Both a radiography and a dye penetration test were used to detect defects in the welding parts of the high temperature piping. Functioning tests on main equipments, such as the cooler, the circulator, were conducted. A leak test, which kept the primary circuit system for 24 hours with pressurized helium gas at 3 MPa of operating pressure, was carried out. The allowable leak rate of the test was 3 %/day of the inventory in the primary circuit system. In the in-service inspection, any defect, deformation and abnormal function were not observed. The annual inspection by Scientific and Technology Agency (STA) of government was also conducted on the OGL-1 as shown in Table-4.

3. Removal of OGL-1

After completion of the irradiation utilization, the OGL-1 was removed from the JMTR in 1995. The outline of the removal procedure of the OGL-1 is shown in Fig. 3. The in-pile section transported to the canal at the JMTR will be cut in the canal as the disposal of radioactive waste after cooling. The out-pile section which consists of the primary circuit system, the secondary circuit system and the purification system is stored as the remains of the OGL-1 until the site is utilized for new irradiation apparatus. The inside of the primary circuit contained fresh helium gas of ambient pressure after evacuation by a vacuum pump. The coaxial tube for connection between the in-pile and out-pile section had been already disposed as the radioactive waste.

Table 1 Major Characteristics of OGL-1

Coolant Material		Helium Gas
Coolant Temperature		Max. 1000 ℃
Coolant Pressure		30 kg/cm² G
Fast Neutron Flux		Ave. 8.7×10¹³n/cm² s
Thermal Neutron Flux		Ave. 4.2×10¹³n/cm² s
Maximum Heat Generation		135 kW
Max. Dimension of Specimen		82 mm dia.×750 mm long
Design Life Time	In-pile Tube	22000 hrs.
	Flow Tube	6900 hrs.
	Primary Circuit System	44000 hrs.

Table 2 Experiences of Utilization, Operation and Maintenance of OGL-1

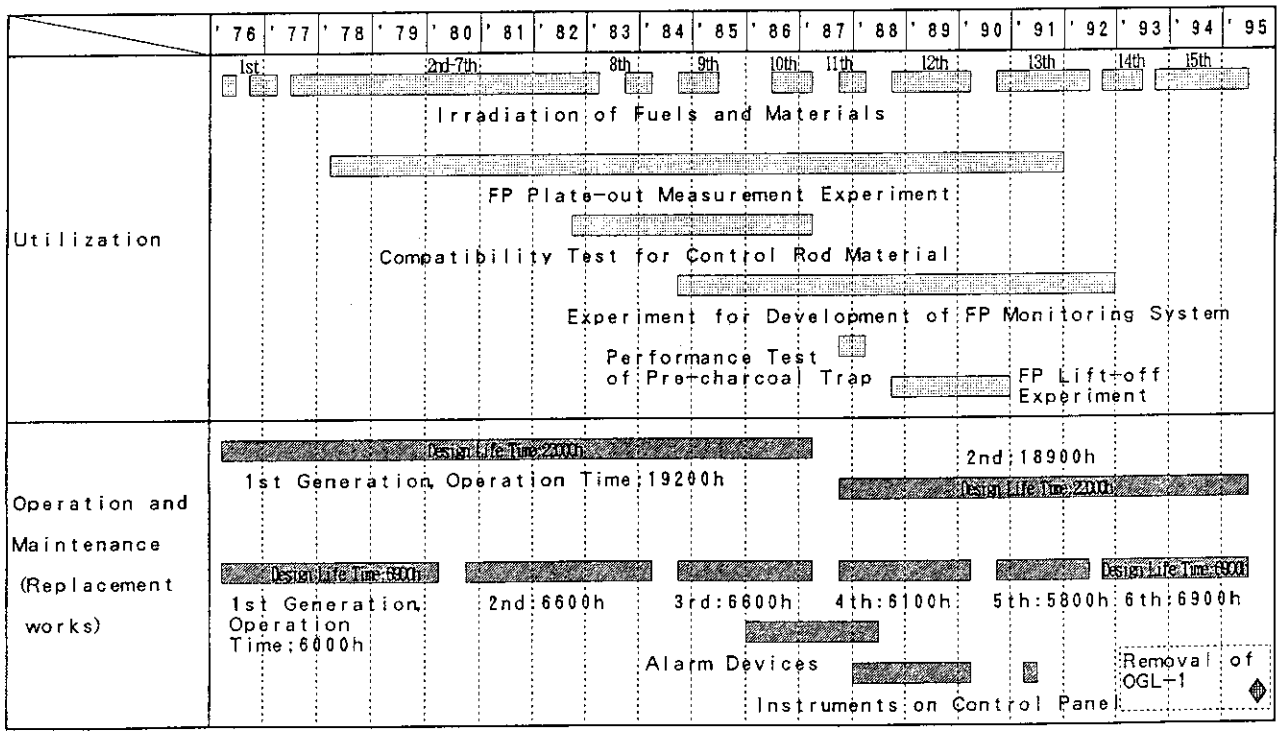


Table 3 Purpose of Irradiation Tests for Various Fuels Using OGL-1

Tests No.	Purpose of Irradiation Tests
1st	Functional Test of OGL-1
2nd-7th	Integrity Confirmation of Small Scale Test Fuel
8th	Study on FP Release Behaviour of Fuel
9nd-11th	Integrity Confirmation of Mass-produced Fuel
12th	Performance Test of High Burn-up Fuel
13th	Performance Test of High Burn-up Fuel
14th	Performance Test of Modern Fuel
15th	HTTR Driver Fuel Test

Table 4 Annual In-service Inspections Including Annual Inspections by STA on Primary Circuit System

Equipments or Devices	Items of Inspection	by STA	Remarks
Status of Operation	Saturation Values	○	
Reactor Scrum Devices	Functional Test	○	
Primary Circuit System	Leak Test	○	※1 Every
Gas Circulators	Performance Test ※1	○	10 Years
Re-generative Heat Exchangers	Non-destructive Examinations ※2	○	※2 Every 2 Years
Safety Valves	Dismantle and Functional Test	○	
Heater	Visual Test ※3	○	※3 Every
Flow Control Valves	Functional Test	○	5 Years
Primary Piping	Non-destructive Examinations ※1	○	
Blower	Functional Test	○	
Damper	Functional Test	○	
Power Supplying Panel	Insulation Test		
Instruments	Calibration Test		
Radiation Monitors	Calibration Test		
Rupture Discs	Replacement and Leak Test		
Cubicle Cooler	Leak Test and Functional Test		
Helium Gas Supply System	Leak Test		
De-humidifier	Functional Test		
Liquid N_2 Supply System	Leak Test		
Vacuum Pump	Functional Test		
Secondary Blower	Functional Test		
Piping Supports	Visual Test		

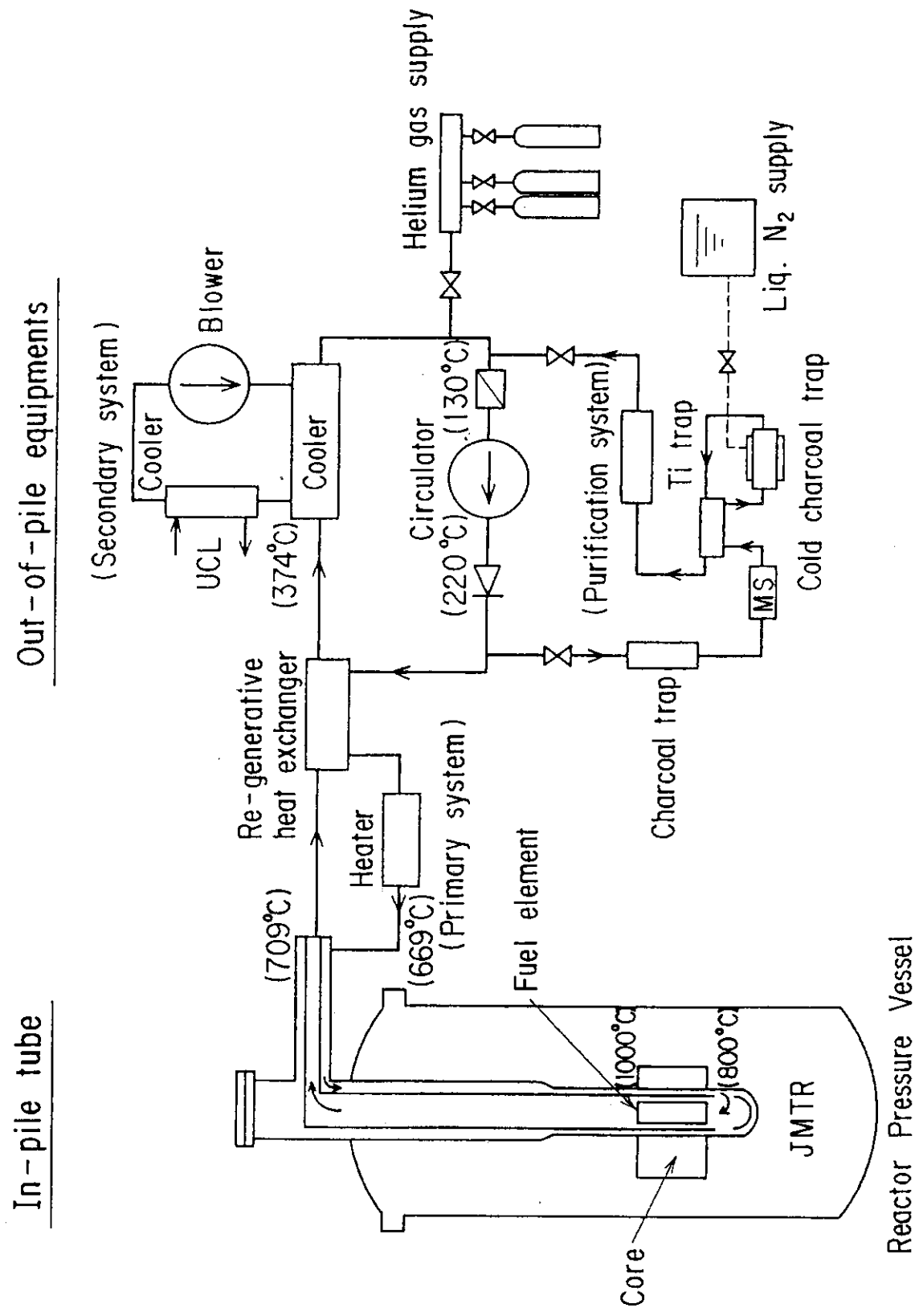


Fig. 1 Simplified Flow Diagram of OGL-1

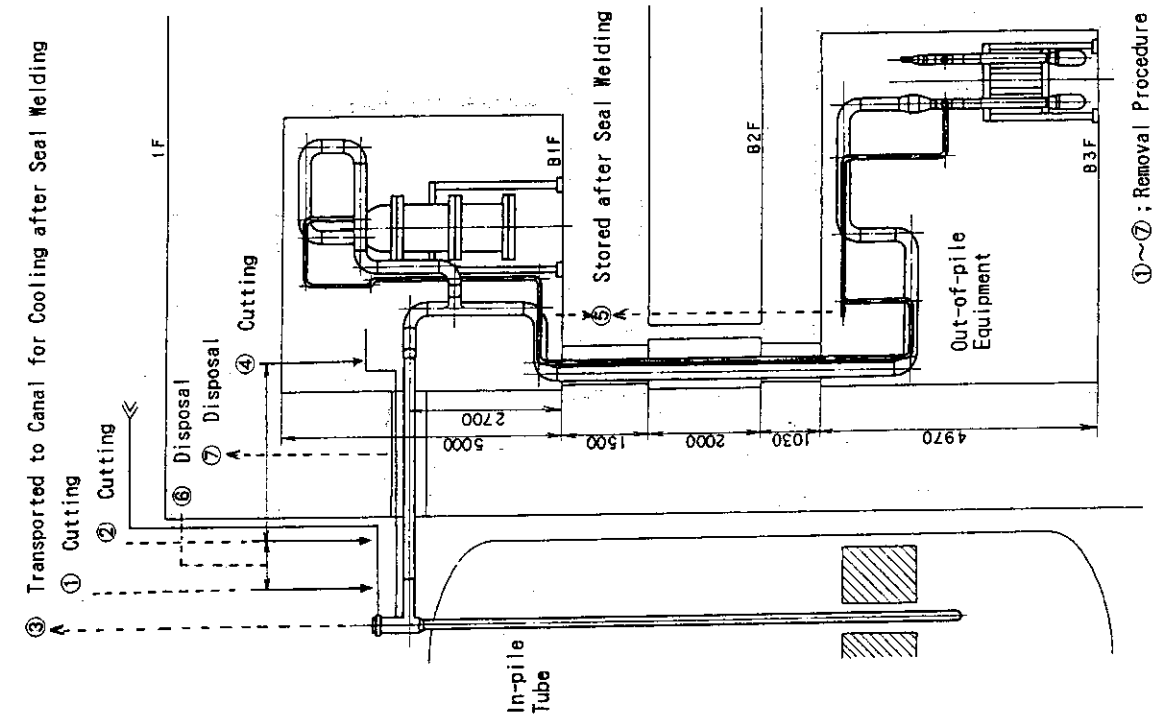
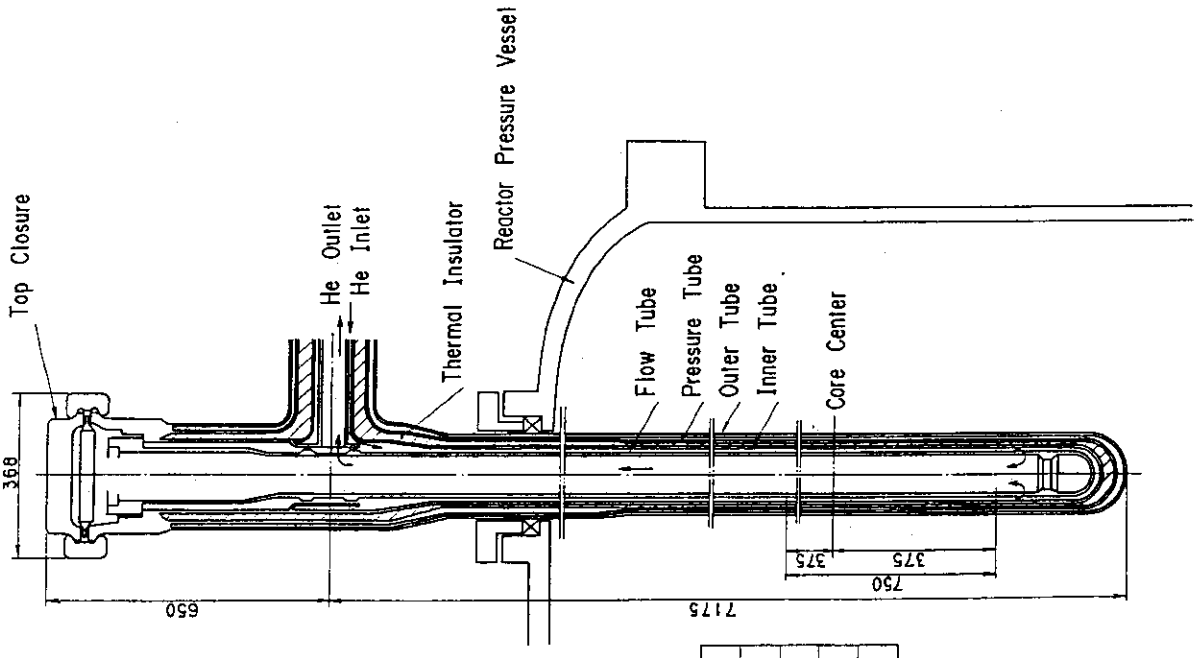


Fig. 3 Removal Procedure of OGL-1



	I.D	O.D
Outer Tube	ø137	ø146
Pressure Tube	ø126	ø132
Inner Tube	ø 92	ø 96
Flow Tube	ø 84	ø 88

(mm)

Fig. 2 Structure of OGL-1 In-pile Tube

6.13 Applicability Of Carbonation/Decarbonation Reactions For Storing Thermal Energy From Nuclear Reactors

Kyaw Kyaw, Hitoki Matsuda and Masanobu Hasatani
Dept. of Energy Engineering and Science
Faculty of Engineering, Nagoya University
Chikusa-ku, Nagoya 464-01, Japan
Tel: 052-789-3383, Fax: 052-789-3842

Abstract

Heat energy extracted from nuclear reactors so far has been used only for power generation. As it is known, there are industrial processes such as iron manufacturing, coal gasification and so on, which mainly consist of thermal energy process. Recently, cleaner fuels such as hydrogen and methanol are highly expected to resolve global warming and oil shortage problems. From the view point of best energy mixing or highly developed energy system, it is important to study the possibility of making effective use of thermal energy from the nuclear reactors for different kinds of industrial applications and for producing cleaner fuels.

In order to realize the usage of high temperature heat (around 1023-1273 K) from the nuclear reactors, development of thermal energy utilization system like heat storage, heat transportation, heat pump, etc. are essential. However, it is very difficult to store large amount of heat energy at very high temperatures. Among the thermal energy storage methods, thermochemical energy storage seems very appropriate for storing high temperature heat since chemical energy storage, in principle, needs a minimum of thermal insulation as the thermal energy is converted into chemical bonds and is stored as chemical bonding energy. Moreover thermochemical storage can store large amount of energy per unit mass and can also perform as a heat transformer.

As research works on the chemical reactions for heat energy storage are rather scant, simple thermal dissociation reactions have been investigated for energy storage and are compared in terms of their thermodynamic, reaction equilibrium and physical properties of the involved reactants.

Among them CaO/CO_2 reaction system seems very promising because (i) its energy storage density is very high (~0.42 kcal/kg) (ii) $CaCO_3$ dissociates at 1123 K under 101 kPa of CO_2 pressure (iii) the reaction products are free from toxicity and corrosiveness (iv) the $CaO-CO_2$ reversible reaction has no side reaction and (v) the $CaCO_3$ raw material is abundantly available.

Dissociation of $CaCO_3$ produces CO_2 gas which has to be stored (1) as compressed gas (2) in the form of other metal carbonates by letting the CO_2 gas reacts with other metal oxides or (3) as adsorbed CO_2 by adsorbing the CO_2 gas with appropriate adsorbents like zeolite. Each corresponding exergy values, COP (coefficient of performance) and the upgraded temperature in heat upgrading

configuration was evaluated.

Repeated carbonation/decarbonation of CaO was carried out by TGA (thermogravimetric analysis technique) to study the reactivity of CaO when it underwent repeated heat absorbing/releasing processes. It is found that under 101 kPa of CO_2 pressure, $CaCO_3$ completely decomposes at 1123 K and that reactivity and conversion of CaO is faster and higher with increase in temperature for temperatures lower than that of the decomposition temperature.

The ability to generate high temperature heat around 1273 K by CaO-CO_2 reaction is confirmed by means of carbonating CaO in a lab-scale adiabatic reactor. During these carbonation experiments, pseudo-steady state conditions prevailed in which the reactant bed temperatures are, e.g. about 1220 K for loaded CO_2 pressure of 200 kPa and about 1300 K for CO_2 pressure of 600 kPa, etc. From this, it is concluded that the CaO-CO_2 reversible reaction can be used not only for energy storage but also for transforming heat at a certain temperature to a relatively higher temperature; e.g. heat at 1123 K will be used for decomposing $CaCO_3$ at 101 kPa pressure, whereas, heat at about 1220 K will be generated when CaO is made to react with CO_2 of 200 kPa.

Such issues as the enhancement of reactivity of CaO, heat and mass transfer in the reactor packed with CaO particles are now being studied for realizing this CaO/CO_2 heat storage system from a practical point of view.

1. Introduction

It is well known that demand for energy had again restarted to expand at a significant rate. Moreover, it has been predicted that the demands will grow enormously also in developing countries in the near future. Hence, in order to establish a secure total energy system for our future needs, it is essentially important to re-organize current energy utilization systems.

There are various types of primary energy resources, such as fossil fuels, nuclear fuels and natural energy, etc. For most cases, energy included in these fuels is extracted at first as thermal energy in the form of steam or hot gases through boilers, combustors, nuclear reactors, etc. The generated steam or hot gases are subsequently transported and then used in heating processes and other applications, or are converted into electrical energy by means of steam or gas turbines. Thus, it is noticed that energy is used through the combination of the conversion among heat, electricity, substances, motion and light. In particular, heat energy is not only the first form being converted from fuels, but also is one of the energy forms that participated in all energy conversions that appear in the systems. This fact implies that an innovative advancement of conversion technology between heat and other forms of energy may be a breakthrough for the ultimate energy utilization.

So far, heat energy extracted from nuclear reactors has been used only for power generation. As it is known, there are industrial processes such as iron manufacturing, coal gasification, etc. which mainly consist of thermal energy processes and also recently, cleaner fuels such as hydrogen and

methanol are highly expected to resolve global warming and oil shortage problems. From the view point of ultimate energy utilization or highly developed energy system and of broadening the nuclear energy utilization, it is important to study the possibility of making effective use of thermal energy from the nuclear reactors for different kinds of industrial applications and for producing cleaner fuels.

In order to realize the usage of high temperature heat (around 1023-1273 K) from the nuclear reactors, development of thermal energy utilization system like heat storage, heat transportation, heat pump, etc. are essential. However, it is very difficult to store large amount of heat energy at very high temperatures. Among the thermal energy storage methods, thermochemical energy storage seems very appropriate for storing high temperature heat since chemical energy storage, in principle, needs a minimum of thermal insulation as the thermal energy is converted into chemical bonds and is stored as chemical bonding energy. Moreover thermochemical storage can store large amount of energy per unit mass and can also perform as a heat transformer.

Many candidate reaction systems have been reviewed [1] and the CaO/CO_2 systems very promising because of its high energy storage density, absence of toxic reactants, etc. Thermal operation efficiency of some of the heat storage systems employing CaO/CO_2 reaction are evaluated. The kinetics of the $CaO-CO_2$ reaction in the region 773-1273 K has been studied and the ability to generate heat at temperatures aroung 1273 K by the $CaO-CO_2$ reaction is verified by means of carbonating CaO particles in a lab-scale adiabatic reactor.

2. Operating principle of a CaO/CO_2 heat storage system

Reversible chemical reactions can absorb large amount of energy during their endothermic decomposition reaction and this absorbed energy can be extracted at any time by letting the decomposed products to react and form back into the original substance again. **Table 1** lists some of the candidate reactions and the respective turning temperature T* (the temperature at which the formation of reaction products is favorable), and the reaction enthalpy. Among these reversible thermochemical reactions, carbonate and hydroxide types are the only reaction types that are free from toxic reactants. However, hydroxide system is subjected at very high temperatures (above 773 K) where the steam pressure is excessively high. In carbonate type reactions, CaO/CO_2 reversible reaction seems very attractive, because

(i) its energy storage density is very high (~0.42 kcal/kg)

(ii) $CaCO_3$ dissociates at 1123 K under 101 kPa of CO_2 pressure

(iii) energy can be stored for a very long time as the reaction products can be readily stored separately

(iv) the reaction products are free from toxicity and corrosiveness (v) the $CaO-CO_2$ reversible reaction has no side reaction

(vi) the $CaCO_3$ raw material is abundantly available.

The operating principle of CaO/CO_2 heat storage system can be expressed by a box diagram as shown in **Fig. 1**. In each vessel a substance with the different pressure-temperature equilibrium

Table 1. ΔH^o and T* of some thermochemical energy storage systems

No	System	ΔH^o [kJ/mol]	T* [K]
1	Ammonia + Ammonium salts system		
	$2\,NH_3\,(g) \Longleftrightarrow N_2\,(g) + 3\,H_2\,(g)$	59	468
	$NH_4HSO_4\,(l) \Longleftrightarrow H_2O\,(g) + NH_3\,(g) + SO_3\,(g)$	335	740
2	Carbonate system		
	$ZnCO_3\,(s) \Longleftrightarrow ZnO\,(s) + CO_2\,(g)$	67	406
	$MgCO_3\,(s) \Longleftrightarrow MgO\,(s) + CO_2\,(g)$	125	670
	$CaCO_3\,(s) \Longleftrightarrow CaO\,(s) + CO_2\,(g)$	176	1110
	$SrCO_3\,(s) \Longleftrightarrow SrO\,(s) + CO_2\,(g)$	234	1381
3	Fluoride system		
	$KBF_4\,(s) \Longleftrightarrow KF\,(s) + BF_3\,(g)$	109	978
	$2\,NF_3\,(s) \Longleftrightarrow N_2\,(g) + 3\,F_2\,(g)$	130	945
4	Hydride system		
	$LiH\,(s) \Longleftrightarrow Li\,(s) + 1/2\,H_2\,(g)$	88	1220
	$NaH\,(s) \Longleftrightarrow Na\,(s) + 1/2\,H_2\,(g)$	88	735
5	Hydroxide system		
	$Mg(OH)_2\,(s) \Longleftrightarrow MgO\,(s) + H_2O\,(g)$	84	531
	$Ca(OH)_2\,(s) \Longleftrightarrow CaO\,(s) + H_2O\,(g)$	109	752
	$Sr(OH)_2\,(s) \Longleftrightarrow SrO\,(s) + H_2O\,(g)$	126	852
	$LiOH\,(l) \Longleftrightarrow {}^1/_2\,Li_2O\,(s) + H_2O\,(g)$	59	1004
6	NO2 system		
	$Ca(NO_3)_2\,(s) \Longleftrightarrow CaO\,(s) + 2\,NO_2\,(g) + 1/2\,O_2$	109	740
	$LiNO_2\,(s) + LiNO_3\,(s) \Longleftrightarrow 2\,LiO\,(s) + 2\,NO_2\,(g)$	109	1089
7	Oxide, peroxide systems		
	$BaO_2\,(s) \Longleftrightarrow 2\,BaO\,(s) + 1/2\,O_2\,(g)$	75	1029
8	Sulfate system		
	$MgSO_4\,(s) \Longleftrightarrow MgO\,(s) + SO_3\,(g)$	280	1470
	$CaSO_4\,(s) \Longleftrightarrow CaO\,(s) + SO_3\,(g)$	402	2145
9	SO3 system		
	$SO_3\,(g) \Longleftrightarrow SO_2\,(g) + 1/2\,O_2\,(g)$	109	1055
10	Organic systems		
	$C_2H_6\,(g) \Longleftrightarrow C_2H_4\,(g) + H_2\,(g)$	138	1136
	$C_6H_{12}\,(g) \Longleftrightarrow C_6H_6\,(g) + 3\,H_2\,(g)$	205	568
	$CH_4\,(g) + H_2O\,(g) \Longleftrightarrow CO\,(g) + 3\,H_2\,(g)$	205	961
	$CH_4\,(g) + CO_2\,(g) \Longleftrightarrow 2\,CO\,(g) + 2\,H_2\,(g)$	247	959

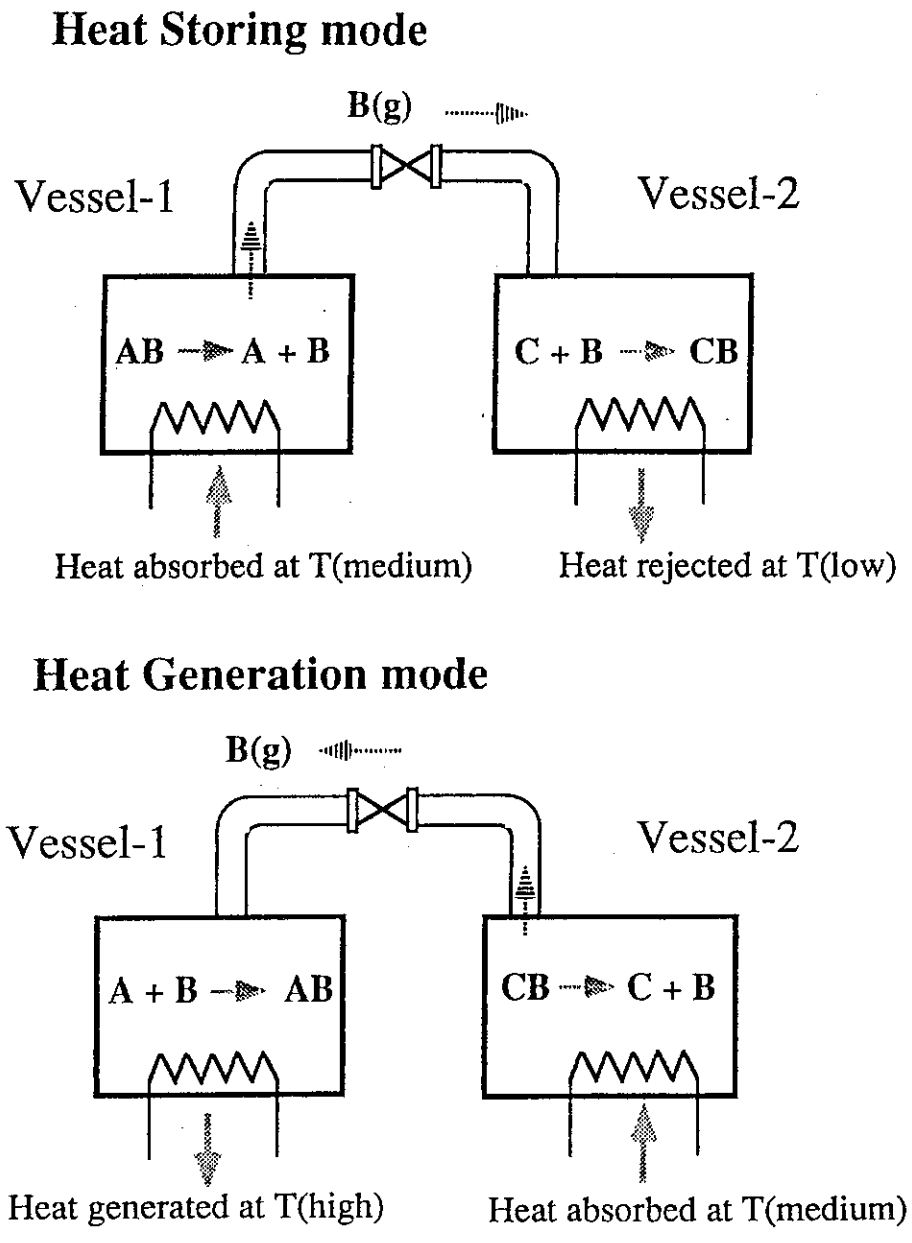


Fig. 1 Conceptual operation diagram of chemical heat pump

relationship for the working fluid CO_2 is packed. In heat storing mode, when vessel-1 is heated at a temperature T_M (773-1073 K), the decomposition of $CaCO_3$ takes place and the working fluid CO_2 gas is released. This CO_2 gas is absorbed or condensed in the other vessel. The process mentioned corresponds to the heat storage into the substance CaO. In heat generating mode, vessel-2 is sealed off and is heated at T_M and the pressure of CO_2 in this vessel will become higher than that of CO_2 in the vessel-1. By opening the connecting valve, CO_2 gas will move to vessel-1 and will react with CaO. As the reacting gas pressure is much higher than the CO_2 pressure during decomposition at T_M, the reaction heat will be obtained at a higher temperature T_H. The above processes can be conveniently expressed by means of temperature and pressure parameters in the form of log P vs. log 1/T employing the equilibrium temperature-pressure relationships as in Fig. 3(a-c).

Three cases are considered with regard to vessel-2 that functions as a storage for the decomposition product CO_2 gas and that regulates the pressure of the working fluid CO_2 gas in the system:

2.1 Case 1: CaO-CO_2-compressor system

Vessel-2 is composed of a compressor and the decomposition product CO_2 gas from $CaCO_3$ is compressed and sotred as a compressed gas (**Figs. 2a** and **3a**). In these figures, heat source at T_M (773 K) is used for decomposing the $CaCO_3$ in vessel-1 under 0.01 kPa CO_2 pressure. The product CO_2 is cooled down to T_L (373 K) where it is compressed and stored at P_H (1100 kPa). The stored CO_2 gas under high pressure is heated to T_M (773 K) and is made to react with the CaO in vessel-1 and the carbonation reaction will occur at the temperature T_H (~1273 K) which is in equilibrium with the loaded CO_2 pressure of 1100 kPa.

2.2 Case 2: CaO-CO_2-MgO system

Vessel-2 is packed with an inorganic oxide such as MgO, $CaMgO_2$, ZnO, etc. The decomposition product CO_2 from vessel-1 is made to react with the oxide at temperature T_L and is stored as a chemical substance in the form of another carbonate (**Figs. 2b** and **3b**). In the figures, the product CO_2 is cooled down to T_L (478 K) where it reacts with MgO and forms into $MgCO_3$. In heat generating mode, $MgCO_3$ is first heated to T_M (773 K) where it decomposes and releases CO_2 at pressure P_H. The released CO_2 is then let to react with CaO in vessel-1 and the reaction heat will be generated at temperature T_H.

2.3 Case 3: CaO-CO_2-zeolite system

Vessel-2 is packed with an appropriate CO_2 adsorbent material such as zeolite, activated carbon, etc. Since the adsorptivity at lower temperatures is very much higher than that at higher temperatures, large amount of CO_2 gas can be stored by this way (**Figs. 2c** and **3c**).

When evaluated, it is found that the thermal operation efficiencies of the above three systems are quite comparable to one another (**Fig. 4**).

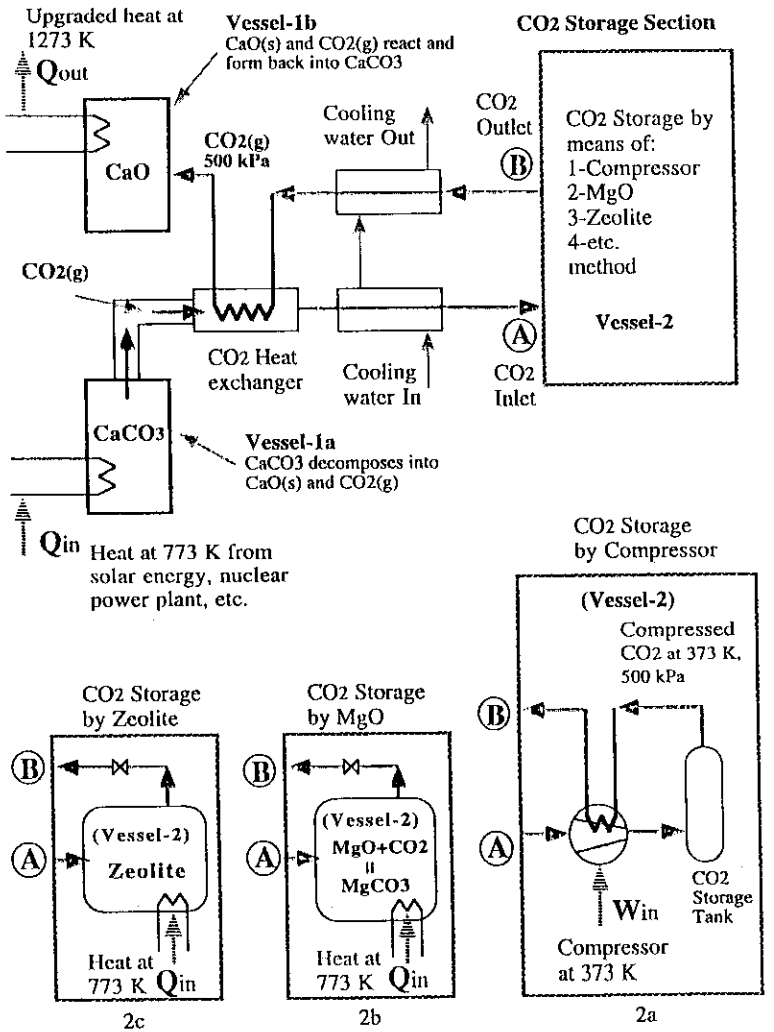


Fig. 2 Conceptual flow diagrams of CaO-CO_2 energy storage system in a heat upgrading mode. Some CO_2 storage methods are shown in the boxes.

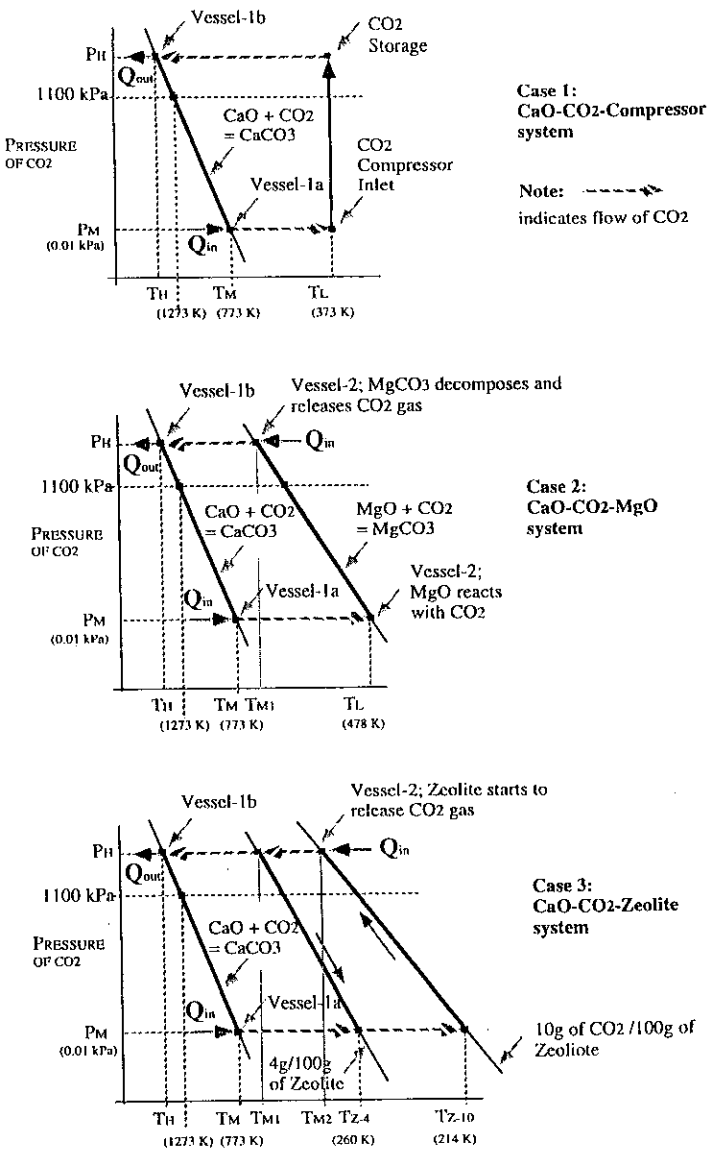


Fig. 3 Schematic diagrams of CaO-CO_2 energy storage systems with three different CO_2 gas storage methods.

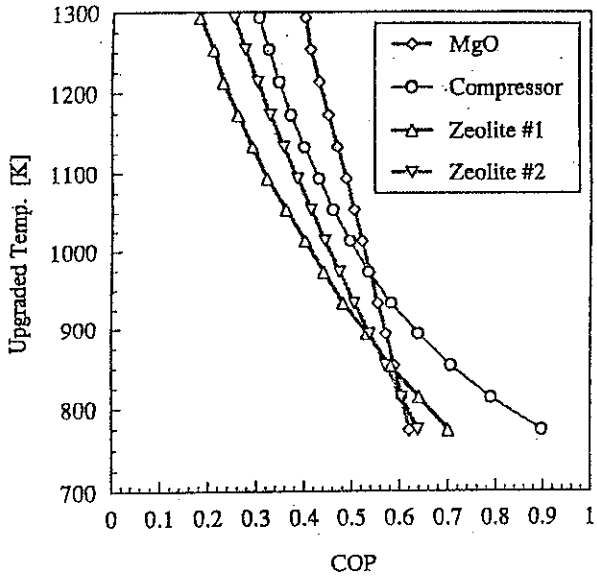


Fig. 4 COP vs. upgraded temperature of $CaO-CO_2$ energy storage systems with various $CaO-CO_2$ storage systems. Note: in Zeolite#1 system, it is assumed that adsorption of CO_2 by zeolite occurs within (4g of CO_2/100g of zeolite) to (10g/100g), whereas in Zeolite#2 system it is within (4g/100g) to (16g/100g).

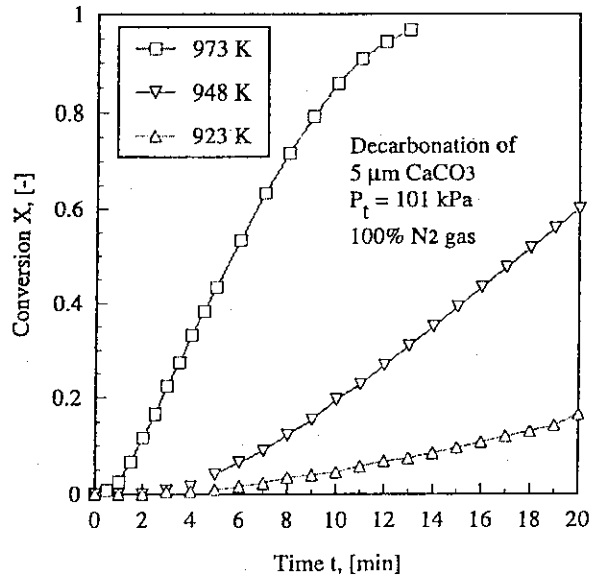


Fig. 5 Conversion of 5 µm $CaCO_3$ to CaO when decarbonated under various temperature and 101 kPa N_2. Note: no loss in weight is observed for decarbonation under 973 K and 1 kPa CO_2.

3. Experimental

3.1 Study of decarbonation reaction of $CaCO_3$

Experiments are carried out with 5 µm particles of limetsone (99.5% $CaCO_3$) in a Shimadzu TG-50H thermogravimetric apparatus.

The sample is placed in the TGA and is heated with a heating rate of 50 K.min^{-1} under 101 kPa CO_2 atmosphere. At a predetermined temperature, the CO_2 gas is shut off and pure N_2 gas or N_2-CO_2 gas mixture is introduced.

3.1.1 Result and discussion

It is observed that dissociation of $CaCO_3$ started to occur around 823 K under 100% N_2 gas atmosphere. The rate of dissociation increases with the increase in temperature and the conversion rate became quite significant around 873 K. **Fig. 5** shows the conversion of $CaCO_3$ to CaO when decarbonated at 923-973 K under 100% N_2 atmosphere. It can be seen that decomposition is almost complete for decarbonation at 973 K within a few minutes whereas the conversion reached only a mere 10% for 20 minutes of decarbonation at 923 K. **Fig. 6** shows the conversion for the decarbonation of $CaCO_3$ at 1073 K under various partial pressures of CO_2 gas. It can be seen that for a certain temperature, the rate of decomposition is strongly suppressed by the presence of CO_2 gas molecules: the higher the CO_2 partial pressure, the slower is the decomposition rate.

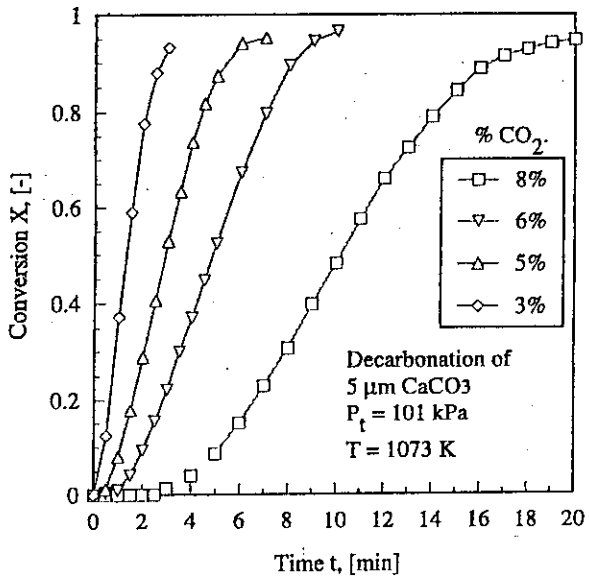


Fig. 6 Conversion of 5 µm $CaCO_3$ to CaO when decarbonated under 1073 K and various CO_2 partial pressures. Note: no loss in weight is observed for decarbonation under 10 kPa CO_2.

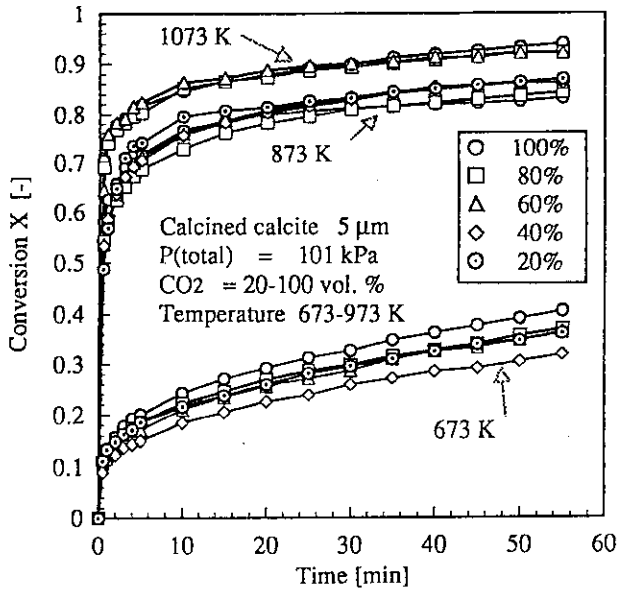


Fig. 7 Conversion of 5 µm CaO to $CaCO_3$ when carbonated under 673-1073 K and 20-101 kPa of CO_2 partial pressure for 1 hr.

It is concluded that the decomposition reaction of $CaCO_3$ can be used for absorbing thermal energy at temperatures around 823 K and higher and it is required that the heat storing mode (Figs. 1, 3) should be carried out at CO_2 partial pressures lower than the eqilibrium dissociation pressure of $CaCO_3$ related to the temperature of heat source.

3.2 Study of carbonation reaction of CaO

In these experiments, about 5 mg of $CaCO_3$ sample is placed in the TG and is heated with a heating rate of 50 $K.min^{-1}$ under 100% N_2 atmosphere. The sample is calcined at 1123 K for 15 min. Then it is cooled down to a predetermined temperature. When the temperature is reached, N_2 gas is shut off and carbonation reaction is started by introducing the CO_2 gas.

3.2.1 Result and discussion

Fig. 7 shows the conversion of CaO to $CaCO_3$ when carbonated under various temperature and pressure. It can be seen that although the initial reaction rate and final conversion increases with the increase in temperature, the initial reaction rate for a certain temperature is almost independent of the CO_2 partial pressure in the 40-100 kPa range.

It is concluded that the heat energy stored in the substance CaO can be extracted by letting it react with CO_2 gas (Vessel-1b in Fig. 2).

3.3 Verification of heat upgrading ability of CaO/CO_2 reaction

3.3.1 Sample preparation

Limestone of 1 mm are calcined at 1123 K for 3 hr under atmospheric condition in a muffle furnace. When the furnace has been cooled down to 773 K, the calcined sample is withdrawn and is placed in a dessicator where it is cooled down to room temperature.

3.3.2 Apparatus

Reactor of 50 mmϕ x 230 mmH is placed in a molten salt bath which is kept at 773 K. Schematic diagram of the reactor is shown in **Fig. 8**. Three thermocouple leads are placed along the central axis at 35, 70 and 105 mm points from the bottom of the reactor. The reactor is provided with vacuum pump, pressure recorder and a CO_2 supply.

3.3.3 Procedure

Calcined sample is filled into the reactor to a height about 120 mm. Then the reactor is sealed off and the air trapped inside the reactor is removced by vacuum pump. Pressure inside the reactor is maintained at 0.1 kPa until the temperature inside the reactor is equal to that of the molten salt bath. Then CO_2 gas is slowly introduced into the reactor to a certain desired pressure where it is kept throughout the experiment.

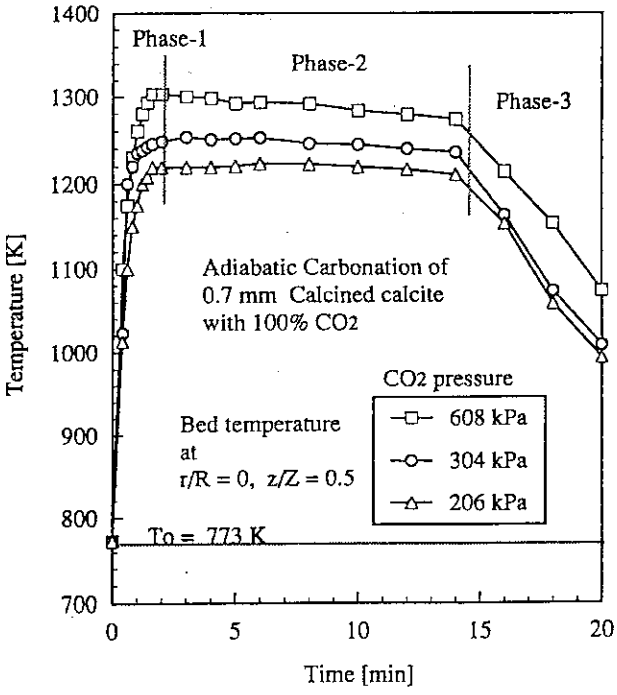


Fig. 9 Temperature profiles of the CaO reactant bed when it is carbonated adiabatically under CO_2 pressures of 200-700 kPa.

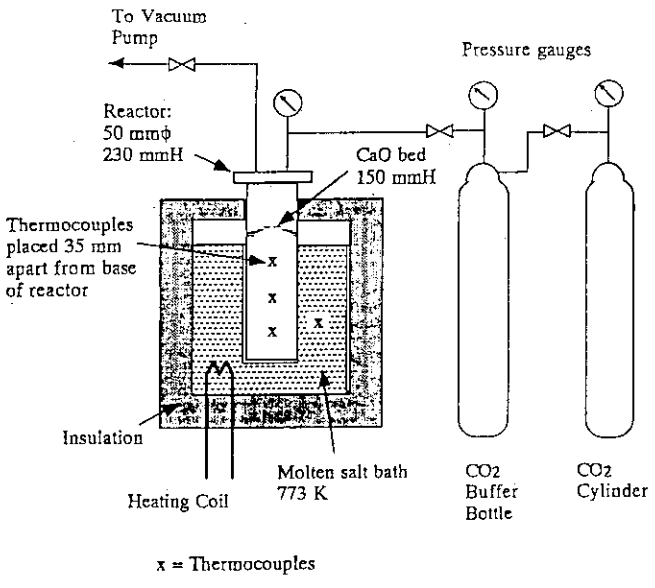


Fig. 8 Schematic diagram of the lab-scale adiabatic packed bed reactor used for verification of the temperature upgrading ability of the $CaO-CO_2$ reaction.

3.3.4 Results and Discussion

The temperature profile of the reactant bed for the adiabatic carbonation experiments with 206, 304 and 608 kPa CO_2 pressures are shown in **Fig. 9**. It can be seen that the temperature of the bed is raised from 773 K to about 1273 K within the first one two minutes (phase-1) due to heat generated during the fast initial reaction between CaO and CO_2. For the CO_2 pressure of 206 kPa, the temperature of the bed is upgraded to about 1200 K, whereas, if the CO_2 pressure is at 608 kPa, the temperature of the bed reaches 1300 K. It is estimated that about 40% conversion has to be attained so that the amount of reaction heat generated will be sufficient to elevate the temperature of the whole reaction medium to 1273 K.

The temperature of the reactant bed remains almost constant at the elevated temperature for about 15 minutes (phase-2). As the 'pseudo-steady state' exists for a certain period, the temperature and pressure prevail during phase-2 are considered to be in pseudo-equilibrium. The temperature of the reactant bed later falls gradually (phase-3) to that of the molten salt bath at 773 K.

In this way, heat energy at 773 K of the reactant bed is transformed to high temperatures during phase-1 and phase-2 of the reaction.

4. Conclusion

It has been pointed out that in order to broaden the use of nuclear energy, development of high temperature thermal energy utilization system like heat storage, heat pump, etc. are essential.

For storing large amount of heat energy at high temperatures, CaO-CO_2 reversible seems very attractive. In this paper, three energy storage methods employing CaO-CO_2 reaction has been proposed and their respective thermal operation efficiency are evaluated.

From the decarbonation/carbonation experiments carried out by thermogravimetric technique, it is found that:

- heat energy can be stored in the substance CaO by heating the carbonate material $CaCO_3$ under appropriate temperature-pressure conditions
- the heat energy stored in the substance CaO can be extracted again by letting it react with CO_2.

By lab-scale adiabatic carbonation experiments, it has been verified that the temperature of the reactant bed can be transformed from 773 K to temperatures around 1273 K by carbonating with CO_2 of 200-600 kPa pressures.

5. Literature

1) Kyaw Kyaw, H. Matsuda and M. Hasatani; Applicability of carbonation/decarbonation reactions to high-temperature energy storage and temperature upgrading system, J. of Chemical Engineering of Japan (1995) (to be published)

ABSTRACT

FUNDAMENTAL STUDY OF FISSION PRODUCT BEHAVIOR IN HTGR; EFFECT OF GRAPHITE ENVIRONMENT ON VAPORIZATION OF STRONTIUM URANIUM OXIDE ($SrUO_3$)

Michio YAMAWAKI [1], Jintao HUANG [1], Kenji YAMAGUCHI [1]
Masaru YASUMOTO [2], Hiroshi SAKURAI [3], Yasufumi SUZUKI [4]

1. Nuclear Engineering Research Lab., The Univ. of Tokyo
2. Res. Cent. for Nucl. Sci. & Tech., The Univ. of Tokyo
3. Nippon Nucl. Fuel Development Co., Ltd.
4. Dept. of Chem. & Fuel Research , JAERI

As fundamental study of fission product behaviors in HTGR cores, vaporization of strontium uranium oxide $SrUO_3$ (perovskite structure) has been studied both in platinum Knudsen cell and in graphite Knudsen cell. The vaporization study of $SrUO_3$ has been made for the first time by means of Knudsen effusion mass spectrometry in the temperature range of 1240−1610°C.

At first, a platinum Knudsen cell with ϕ 0.5mm orifice was utilized for vaporization study. Then the similar experiment was repeated by using a graphite cell in order to simulate HTGR coated particle environment. The temperature and absolute pressure were calibrated by using silver as the standard reference material. The modified Nuclide 12-90-HT type magnetic focusing 90° sector instrument was employed for the present research. The electron acceleration voltage was set as 22 V, corresponding to the maximum cross section of Sr.

It was found that Sr^+, UO_2^+ and SrO^+ were the main ions species that can be detected in Pt cell, while in graphite cell, the intensity of SrO^+ was much smaller. It was noticed that the signal of CO^+ originated from the Knudsen assembly housing outside of the Knudsen cell.

The possible reactions to occur were assumed as the following equations (1),(2) and (3) for Pt cell, as well as (4) and (5) for graphite cell:

$$2SrUO_3(s)=2Sr(g)+2UO_2(s)+O_2(g) \quad \text{..... (1)}$$

$$2Sr(g)+ O_2(g)=2SrO(g) \quad \text{..... (2)}$$

$$UO_2(s)=UO_2(g) \quad \text{..... (3)}$$

$$2C(s)+O_2(g)=2CO(g) \quad \text{.....(4)}$$

$$SrO(g)+C(s) = Sr(g) + CO(g) \quad \text{..... (5)}$$

The pressures over $SrUO_3+UO_2$ were plotted in the figure below. The partial pressure of Sr in the graphite cell was observed to be about 2 times larger compared to that in Pt cell. It suggested that carbon, simulated HTGR circumstance, decreased the oxygen potential so that the partial pressure of Sr increased. Furthermore, it also reduced SrO into Sr so that the SrO pressure in graphite cell decreased.

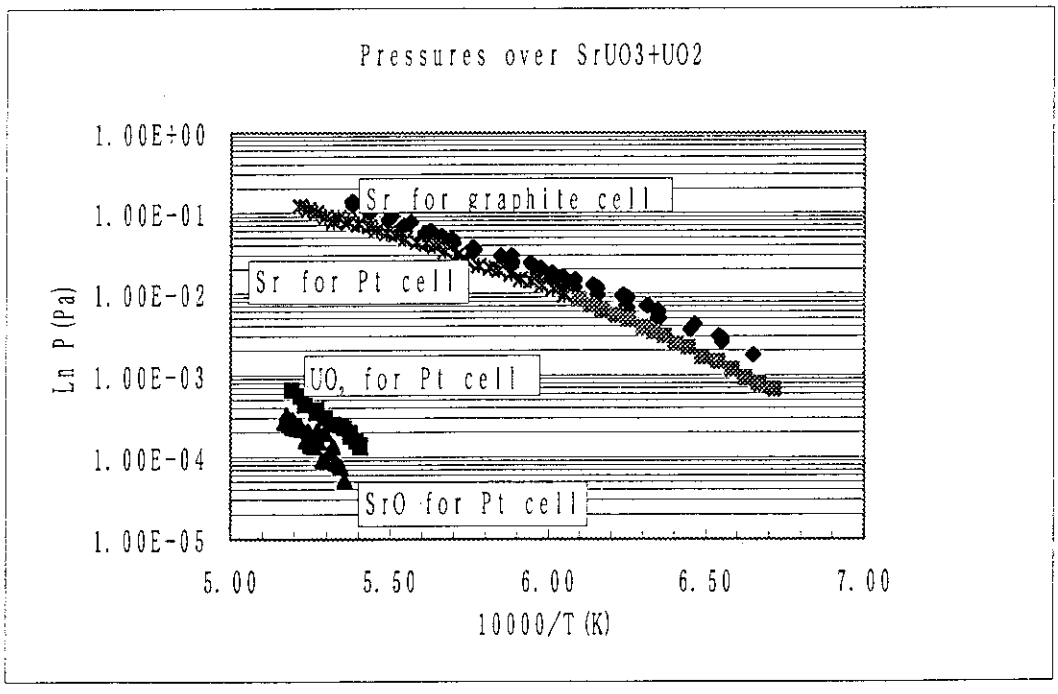


Figure. Partial Pressures observed over $SrUO_3+UO_2$

6.14 FUNDAMENTAL STUDY OF FISSION PRODUCT BEHAVIOR IN HTGR; EFFECT OF GRAPHITE ENVIRONMENT ON VAPORIZATION OF $SrUO_3$ AND $BaUO_3$

Jintao HUANG[1], Michio YAMAWAKI[1], Kenji YAMAGUCHI[1]
Masaru YASUMOTO[2] and Hiroshi SAKURAI[3]

1. Nuclear Engineering Research Laboratory, the University of Tokyo, 7-3-1 Hongo, Bunkyo-ku, Tokyo 113, Japan.
2. Research Center for Nuclear Science and Technology, the University of Tokyo, 7-3-1 Hongo, Bunkyo-ku, Tokyo 113, Japan.
3. Nippon Fuel Development Co. Ltd., 2163 Narita-cho, Oarai-machi, Higashi-Ibaraki-gun, Ibaraki-ken 311-13, Japan.

ABSTRACT

As fundamental study of fission product behaviors in the HTGR core, the vaporization properties of $SrUO_3$ and $BaUO_3$ have been investigated by Knudsen effusion mass spectrometry in the temperature range of 1510~1920K. The Knudsen cell was made of either platinum or graphite. The latter was employed to simulate the graphite environment in the HTGR. The pressure-temperature dependences of the main vapor species over either a mixture of $SrUO_3$+23wt%UO_2 or a pure $BaUO_3$ were obtained separately. It was found that Sr(g), UO_2(g) and SrO(g) were the main vapor species over the $SrUO_3$+23wt%UO_2 mixture in Pt cell while in graphite cell the vapor pressure of Sr(g) increased by about two times. On the other hand, the vapor species over $BaUO_3$ in Pt cell were BaO(g), Ba(g) and UO_2(g). In graphite cell, the partial vapor pressure of Ba(g) increased up to about three orders of magnitude higher than the pressure of whole Ba-containing vapor species in Pt cell. Compared to the case of the $SrUO_3$+23wt%UO_2 mixture, the effect of reducing graphite cell on the vaporization behavior of $BaUO_3$ was much more significant. In both cases, carbon acts to decrease oxygen potential so that the partial vapor pressures of Ba(g) and Sr(g) increase in graphite cell while those of oxides decrease. The difference in the effect of graphite cell between $SrUO_3$ and $BaUO_3$ can be attributed to the different ratios of vapor pressures of oxide-form and metallic-form vapor species. The result of this study is important in assessing the fission products behavior both in normal and accidental conditions in HTGR.

1. Introduction

The behavior of fission products in irradiated Triso-coated particles has being investigated continuously[1-4]. The chemical states of fission products are greatly dependent on temperature, oxygen potential and composition. Since the fission products are generated in such a large number that both experimental measurements and computer code calculations were employed to deal with this complicated multi-component multiphase system. For example, recently the thermodynamic analysis on the fission product-UO_2-C system was investigated by Minato et al.[5]. However, the ternary oxides such as (Ba, Sr)UO_3 were not taken into account in their study because of the absence of data at that moment, while those ternary oxides were often found to constitute so called gray phase in the irradiated oxide fuel [6].

This report will be concerned with the vaporization of $BaUO_3$ and $SrUO_3$ in different oxygen potentials to supply their high temperature properties data by means of Knudsen effusion mass spectrometry. A platinum Knudsen cell and a graphite Knudsen cell were utilized in the measurements. The graphite cell serves as a graphite environment simulating the graphite coating layers of the Triso-coated particles and the graphite block in the core of HTGR.

2. Experimental

The samples were prepared using a method similar to that described by Hinatsu [7]. Briefly the main processes can be expressed as follows,

$$UO_3(s) + (Ba \text{ or } Sr)CO_3(s) \longrightarrow (Ba \text{ or } Sr)UO_4(s) + CO_2(g), \quad (1053K, 8h) \quad (1)$$

$$(Ba \text{ or } Sr)UO_4(s) + H_2(s) \longrightarrow (Ba \text{ or } Sr)UO_3(s) + H_2O(g). \quad (1673K, 8h) \quad (2)$$

Formation of the pure phase of $BaUO_3$ was confirmed by X-ray diffraction analysis. Since it was difficult to obtain pure $SrUO_3$, a mixture of $SrUO_3$+23wt%UO_2 was prepared and employed for the vaporization study.

The modified Nuclide 12-90-HT type magnetic focusing 90° sector mass spectrometer employed in this study was described previously [8]. At first, a platinum Knudsen cell with an orifice of 0.5 mm in diameter was utilized in vaporization runs. Then similar experiments were repeated by using a graphite cell with an orifice of 0.5 mm in diameter held in a tantalum container. The temperature and absolute pressure were calibrated by using silver as the standard reference material.

3. Results

3.1 Vaporization characteristics of the $SrUO_3$+23wt%UO_2 mixture

The obtained ionization efficiency curves of Sr^+ and SrO^+ suggested that a simple ionization process occurs each with the electron impact energy up to 30 eV so that the impact energy of 22 eV was used for runs both in Pt cell and in graphite cell to obtain the maximum ion intensity. The molecular ionization cross sections σ_M of SrO and UO_2 were calculated by using the equation: $\sigma_M = 0.75\Sigma\sigma_A$ [9], where σ_A is the atomic ionization cross sections of the constituent atoms given by Mann [10].

It was found that Sr^+, UO_2^+ and SrO^+ were the main ion species that can be detected from Pt cell runs. In graphite cell, on the other hand, Sr^+ was the main ion specie. In the latter case, CO^+ was also observed, but it was attributed to the contribution from outside of the Knudsen cell on account of the shutter profile measurement. The intensity of SrO^+ decreased so rapidly that the partial vapor pressure of SrO(g) could not be measured in high accuracy. The possible reactions to occur were assumed as the following equations (3), (4) and (5) for Pt cell, while for graphite cell additionally equations (6) and (7),

$$2SrUO_3(s) = 2Sr(g) + 2UO_2(s) + O_2(g), \quad (3)$$

$$2Sr(g) + O_2(g) = 2SrO(g), \quad (4)$$

$$UO_2(s) = UO_2(g), \quad (5)$$

$$2C(s) + O_2(g) = 2CO(g), \quad (6)$$

$$SrO(g) + C(s) = Sr(g) + CO(g). \quad (7)$$

The pressure-temperature dependences for the vapors over the mixture of $SrUO_3$+23wt%UO_2 were plotted in Fig 1. The vapor pressure of Sr(g) increased by about 2 times in graphite cell compared with that in Pt cell. At the same time the vapor pressure of SrO(g) in graphite cell decreased down to lower than the detection limit of the mass spectrometer, where in platinum cell that remained in the range of the detection limit. These behaviors can be explained from the reducing atmosphere due to graphite cell.

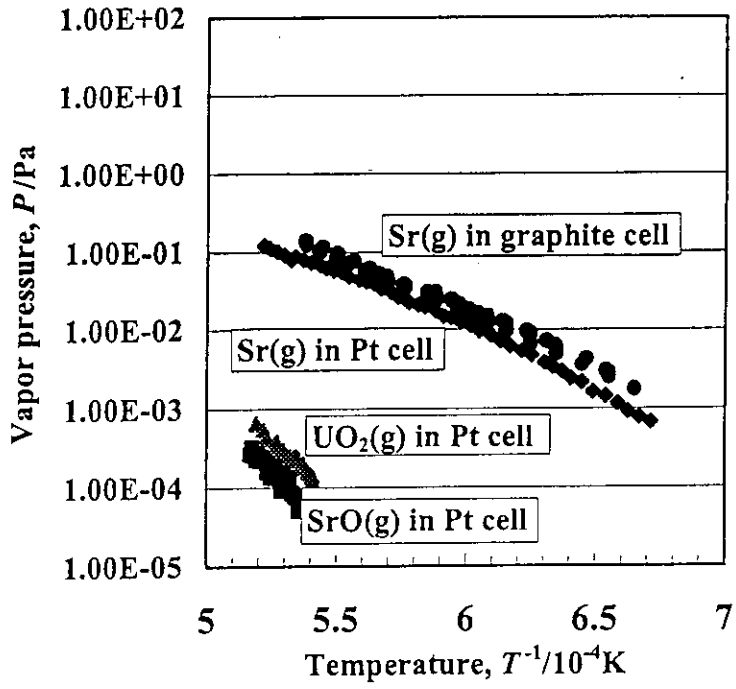


Fig. 1: Partial vapor pressures over $SrUO_3$+23wt%UO_2 mixture

3.2 Vaporization characteristics of $BaUO_3$

The ion identification showed that BaO(g), Ba(g) and UO_2(g) were the main vapor species over $BaUO_3$ in the decreasing order of vapor pressures. The ionization efficiency curves of Ba^+ and BaO^+ indicated that a simple ionization process each occurs only when the electron impact energy is less than 16 eV. Both fragmentation and simple ionization take place in the higher energy range. Thus 12 eV as the impact energy was chosen to avoid fragmentation in the measurement with Pt cell. While, with graphite cell, where the fragmentation of BaO(g) has little significance, 30 eV was adopted in addition to 12 eV. The ionization cross section of BaO at 12 eV was calculated by extrapolating the value at 22 eV given by Hilpert and Gerads [11].

The determination of vapor species allowed to estimate the equilibrium established in Pt cell as the reactions (8), (9) and (10), while in graphite cell additionally the reactions (11) and (12) such as,

$$BaUO_3(s) = BaO(g) + UO_2(s), \quad (8)$$

$$2BaO(g) = 2Ba(g) + O_2(g), \quad (9)$$

$$UO_2(s) = UO_2(g), \quad (10)$$

$$2C(s) + O_2(g) = 2CO(g), \quad (11)$$

$$BaO(g) + C(s) = Ba(g) + CO(g). \quad (12)$$

The pressure-temperature dependences for the vapors over $BaUO_3$ were plotted in Fig. 2. It is clearly seen that the partial vapor pressure of Ba(g) in graphite cell increased by almost 4 orders of magnitude compared with that in Pt cell. While, that of BaO(g) in graphite cell decreased to the undetectable level. The influence of graphite Knudsen cell on the vaporization of $BaUO_3$ was much more significant than that on the vaporization of $SrUO_3$.

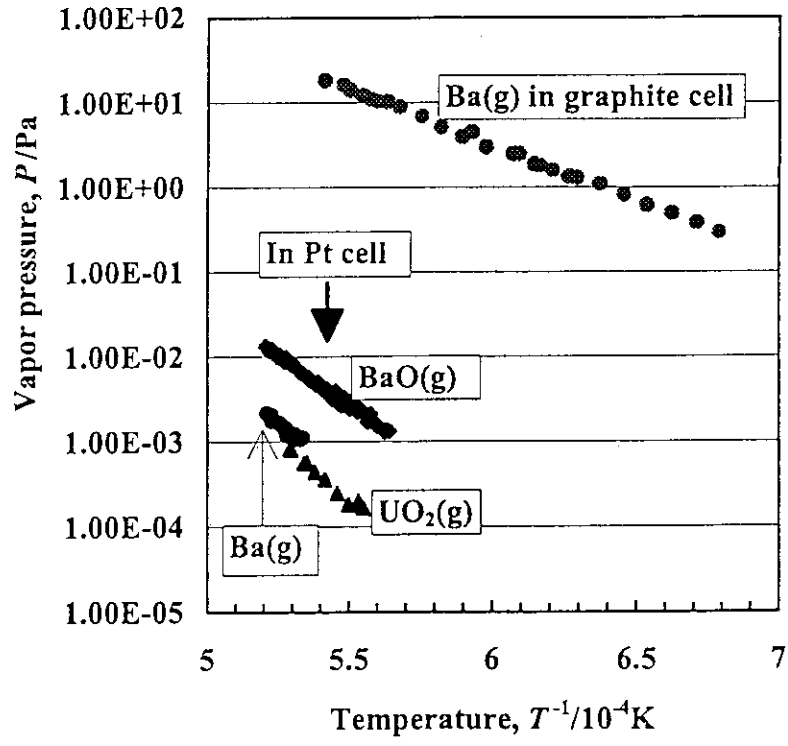


Fig. 2: Partial vapor pressures over $BaUO_3$

4. Discussion

Since the chemical state of each fission product and its equilibrium vapor pressure is dependent on oxygen potential as well as the chemical composition and temperature, it is necessary to determine the oxygen potential inside the Knudsen cell for discussing the vaporization behavior of fission products. In the present measurement, the oxygen potential was hard to be directly measured because of the low oxygen pressure. It was also difficult on account of the CO pressure due to the interference from outside of the Knudsen cell such as described before. So we had to calculate from either the reaction (4) or (9) to estimate the local oxygen potential although in most cases the vapor pressures of SrO(g) and Ba(g) were not as high to get precise enough values of oxygen potential.

The oxygen potentials were calculated as follows,

$$RT \log P_{O_2} = 2\times\{ RT \log (P_{SrO}/P_{Sr}) - \Delta r_4 G^\circ(T)\}, \quad (13)$$

$$RT \log P_{O_2} = 2\times\{ RT \log (P_{BaO}/P_{Ba}) - \Delta r_9 G^\circ(T)\}, \quad (14)$$

where $\Delta r_4 G^\circ(T)$ and $\Delta r_9 G^\circ(T)$ express the Gibbs energy change of the reaction (4) and that of reaction (9), respectively.

For the case of $SrUO_3$+23wt%UO_2 mixture, the oxygen potential in Pt cell from 1700 to 1900K was in the range of −474 ~ −392 kJ/mol. While that for $BaUO_3$ in Pt cell in the same temperature range was from −407 to −393 kJ/mol. Both of them fell in the actual oxygen potential range of −500 ~ −375 kJ/mol in the coated particles of HTGR reported by Lindemer and Nordwall [12]. Compared with the computer code values calculated by Minato et al. [5], the vapor pressures of BaO(g) and Ba(g) of this study were almost the same as theirs. While, the absolute vapor pressure values of Sr(g) and SrO(g) obtained in this work were about one order of magnitude higher than their values. The main reason for this discrepancy might have resulted from the fact that the phases considered by Minato et al. were composed of many different substance, while the present specimen was two component mixture. So, if $SrUO_3$ is added to the multi-component system of Minato et al., the vapor pressures of Sr(g) and SrO(g) are expected to increase up to the present results. While, $BaUO_3$ seems to have been produced in their multi-component system since the same vapor pressures of BaO(g) and Ba(g) were reported in both the studies.

On the other hand, the oxygen potential in graphite Knudsen cell for both the samples was roughly calculated to be below about −800 kJ/mol. Usually such a low oxygen potential can be found only in the very initial stage of irradiation of the coated particles where the amount of fission products is too small to react with each other or to form reaction products with fuel material. However, in case of failure of the coating layers the fission products such as Sr or Ba may be released from the coated particle into the graphite region, where such a low oxygen potential can be realized as shown in the simulation with graphite cell of this study.

The difference in the effect of graphite cell between $SrUO_3$ and $BaUO_3$ can be attributed to the different ratios of vapor pressures of oxide-form and metallic-form vapor species such as $P_{SrO(g)}/P_{Sr(g)}$ or $P_{BaO(g)}/P_{Ba(g)}$. The result of this study is important in assessing the fission products behavior both in normal and accidental conditions in HTGR.

5. Conclusion

The vaporization properties of $SrUO_3$ and $BaUO_3$ have been investigated by Knudsen effusion mass spectrometry either with platinum Knudsen cell or with graphite Knudsen cell in the temperature range of 1510–1920K. The latter cell was employed to simulate the graphite circumstance in HTGR. The pressure-temperature dependences of the main vapor species over either the mixture of $SrUO_3$+23wt%UO_2 or pure $BaUO_3$ were obtained separately. The detected vapor species over the $SrUO_3$+23wt%UO_2 mixture in Pt cell were Sr(g), UO_2(g) and SrO(g) in the decreasing order of their pressures. In graphite cell, it was found that the vapor pressure of Sr(g) increased by about two times compared to that in platinum cell. On the other hand, the vapor species over $BaUO_3$ in Pt cell were BaO(g), Ba(g) and UO_2(g), while in graphite cell, the partial vapor pressure of Ba(g) increased up to about three orders of magnitude higher than the pressure of the whole Ba-containing vapor species in Pt cell. Compared to the case of $SrUO_3$+23wt%UO_2 mixture, the effect of reducing graphite cell on the vaporization behavior of $BaUO_3$ was much more significant. In both cases, carbon acts to decrease oxygen potential so that the partial vapor pressures of Ba(g) and Sr(g) increase in graphite cell while those of oxides decreased. The difference in the effect of graphite cell between $SrUO_3$ and $BaUO_3$ can be attributed to the different ratios of vapor

pressures of oxide-form and metallic-form vapor species. The result of this study is important in assessing the fission products behavior both in normal and accidental conditions in HTGR.

Acknowledgments

The authors wish to express their thanks to Dr. Yasufumi Suzuki, Department of Chemistry and Fuel Research, Japan Atomic Energy research Institute, for his useful comments on this study.

References

1. P. E. Brown and R. L. Faircloth, J. Nucl. Mat. 59(1976)29-41.
2. T. Ogawa, K. Fukuda, H. Sekino, M. Numata and K. Ikawa, J. Nucl. Mat. 135(1985) 18-31.
3. S. Imoto, J. Nucl. Mat. 140(1986) 19-27.
4. M. Akabori and K. Fukuda, J. Nucl. Mat. 183(1991)70-75.
5. K. Minato, T. Ogawa, K. Fukuda, M. Shimizu, Y. Tayama and I. Takahashi, J. Nucl. Mat. 208(1994)266-281.
6. H. Kleykamp, J. Nucl. Mat. 131(1985)221-246.
7. Y. Hinatsu, J. Solid State Chem. 102(1993)566-569.
8. M. Yamawaki, M. Yasumoto, C. Nakano and M. Kanno, High Temp. High Press. 14(1982)423.
9. K. Hilpert, in Structure and Bonding, ed. M. J. Clarke and C. Hill (Springer-Verlag Berlin Heidelberg 1990) Vol. 73, p.107.
10. J. B. Mann, in Recent Development in Mass Spectrometry, ed. K. O.gata and T. Hayakawa, (the Univ. of Tokyo Press 1970), p.814.
11. K. Hilpert and H. Gerads, High Temp. Sci. 7(1975)11.
12. T. B. Lindemer and H. J. de Nordwall, Oak Ridge National Laboratory, Report ORNL-4926(1974).

6.15 Plant Concept of Heat Utilization of High Temperature Gas-Cooled Reactors

—— Co-generation and Coal-Gasification ——

HTR-HUC (HTR Heat Utilization Core Group in FAPIG*)
M.Tonogouchi, S.Maeda,(Ube Ind.), A.Ide, H.Hayakawa, T.Yasuno(Fuji Electric),
Y.Takenaka, S.Hayashi, T.Kobayashi(Kawasaki Heavy Ind.), M.Takeda(Shimizu Corp.)
M.Horie(Kobe Steel), K.Handa, Y.Nakamura(Furukawa Elec.),
M.Kaneko(Nuclear Fuel Ind.), T.Masuda(Nippon Light Metal),
M.Ikehara(Nissho Iwai), Y.Takase(Asahi Denka), M.Ishiwatari(FAPIG)

*FAPIG(The First Atomic Power Industry Group) is a supplier group of nuclear plant and consists of 22 companies representing variety of industries such as Electric, Chemical, Steel, Heavy industries etc..

ABSTRACT

The world energy demand is increasing along with the increase of population and rise of the standard of living and if this would be supplied only by the fossil fuels, much limitation will be imposed on human activities by the environmental problem.

The use of nuclear energy for generating electricity is now well established all over the world. Because more than 50% of the energy cunsumed in nonelectrical energy, it is important to develop methods to apply nuclear energy to the fields other than generating electricity. Since the modular high Temperature gas-cooled reactor (M-HTR) can supply high temperature energy of 700℃ to 1000℃ and possesses high level inherent safety, the M-HTR seems to be most suitable to apply the industries that need high temperature energy.

In Japan, JAERI is now constructing the High temperature Engineering Test Reactor (HTTR) and the new era is coming for the development and utilization of HTR.

Recognizing that the heat utilization of HTR would mitigate problems of environment and resources and contribute the effective use and steady supply of the energy, FAPIG organized a working group named " HTR-HUC " to study the heat

utilization of HTR in the field other than electric power generation.

We chose three kinds of plants to study, 1)a co-generation plant in which the existing power units supplying steam and electricity can be replaced by a nuclear plant, 2)Coal gasification plant which can accelerate the clean use of coal and contribute stable supply of the energy and preservation of the environment in the world and 3)Hydrogen production plant which can help to break off the use of the new energy carrier HYDROGEN and will release people from the dependence of fossil energy.

In this paper the former two plants, Co-generation chemical plant and Coal-gasification plant are focussed on. The main features of these plants are as follows.

(1) Co-generation chemical plant

A typical chemical plant in Japan was selected as the reference plant. The reactor system consists of 2 modules of HTR with the thermal output of 450MWt each and the reactor outlet temperature of 700℃. 640ton/hr of steam of 200 ℃ to 450℃ and 210MW of electricity are supplied to the chemical plant in which 1800ton/day of ammonia, 1200ton/day of methanol, 1700t/day of ammonium sulphate and so on are produced. The total heat untilization efficiency in this plant comes up to 74%.

(2) Coal-gasification plant

The coal gasification/ammonia production plant was selected as the reference plant of coal gasification. The reactor system consists of 4 modules of HTR with IHX, with the thermal output of 170MWt each and the reactor outlet temperature of 950℃. The coal is gasified by the steam gasification process using fluidized bed gasification furnace with gasification temperature of 750 ℃ and the product gas is supplied to the ammonia plant of the capacity of 1700ton/day. The amount of CO_2 emission from this plant is reduced by 20% than that from current coal-gasification plant.

1. INTRODUCTION

The FAPIG(First Atomic Power Industry Group) joined in the construction of two Japanese gas-cooled reactors. Through these experiences, FAPIG has the confidence with usefulness of the gas-cooled reactors. In this paper, we introduce the two types of heat utilization plant of HTGR.

2. PLANT SELECTION

We have started this work by getting information on energy consumption status of energy utilizing plant from our group companies to image a realistic model plant for the study.

Among the 10 companies who answered, 4 companies consume energy more than 100MW in a plant. They are a steel making, aluminium refining and cement & chemical production companies.

Considering the purpose of the present study, we have selected two types of plant:1)Co-generation plant to substitute the existing power plant in the chemical plant. 2)Coal gasification plant to produce ammonia by using reformed H2 from coal.

As a reference reactor, we chose 450 Mwt MHTGR and 200 Mwt HTR-M.

3. CO-GENERATION PLANT

The theme of this study is the utilization of nuclear energy for industrial plant as steam and electricity.

3.1 Plant Specification

We studied best match of HTGR co-generation system with chemical plant and got the result as follows.

(1) Nuclear reactor system

Type of Reactor	MHTGR
Thermal Output of Reactor	450 MW x 2
Inlet and Outlet Coolant Temperature	288 / 704 ℃
Coolant Pressure	7.09 Mpa
Steam Temperature	540 ℃
Steam Pressure	17.8 Mpa
Power Generated	117 Mwe x 2

(2) Chemical plant

a.Extracted Steam Conditions

Pressure (Mpa)	10.6	3.6	1.1
Temperature (℃)	490	330	220
Flow Rate (t/h)	264	108	269

b.Products

Ammonia	1,800 t/d
Methanol	1,200 t/d
Nitric Acid	430 t/d
Sulfuric Acid	1,200 t/d
Caprolactum	290 t/d
Nylon	220 t/d
Ammonium Sulfate	1,670 t/d

3.2 PROCESS FLOW

Process flow is showed in the attached Fig.1.

4. COAL GASIFICATION PLANT

The theme of this section is the utilization of high temperature helium from HTR-M for coal gasification.

4.1 Plant specification

The most important problem to be discussed is how to utilize the helium enthalpy for coal gasification. For heating indirectry, outlet temperature of helium shold be higher. We adopted two step gasification that has pre-reforming fluidized bed to use as much energy of helium as possible for gasification.

(1) Nuclear Reactor System

Type of Reactor	HTR-M
Thermal Output of Reactor	170 MW x 4
Inlet and Outlet Coolant Temperature	300 / 950 ℃
Coolant Pressure	4.05 Mpa

(2) Intermediate Heat Exchanger

Helium Flow Rate (kg/s)	50.3	47.3
Inlet and Outlet Gas Temperature (℃)	950/292	200/900
Inlet and Outlet Gas Pressure (Mpa)	4.04/4.02	4.44/4.25

(3) Coal Gasification / Ammonia Synthesis System

Ammonia Production Rate	1,500 t/d
Coal Gasification Rate	2,200 t/d
Number of Gasifier	4
Type of Gasifier	Flidized Bed
Helium Temperature at Gasifier (Out/In)	900/650 ℃
Gasifier Operating Temperature	750 ℃
Gasifier Operating Pressure	1.01 Mpa
Steam Carbon Ratio	3

4.2 PROCESS FLOW

Process Flow is showed in the attached Fig.2

5. SAFETY ASSESSMENT

We are studying on the following items for the safety assessment.

a. Safety improvement for adjacent demand plant

b. Discussion on reactor safety system

c. Possibility of adaptations for adjacent demand plant

d. Protective consideration against the gas explosion at demand plant

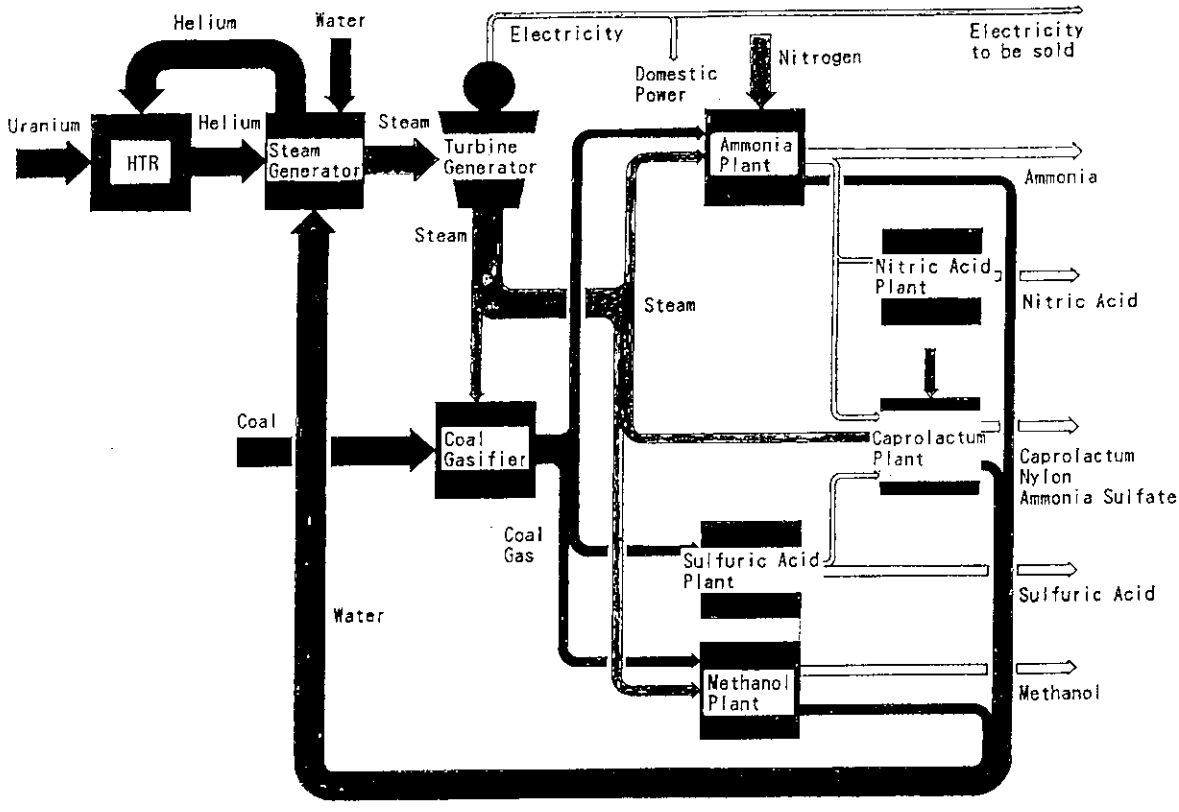


Fig.1 Diagram of HTR Co-Generation Plant

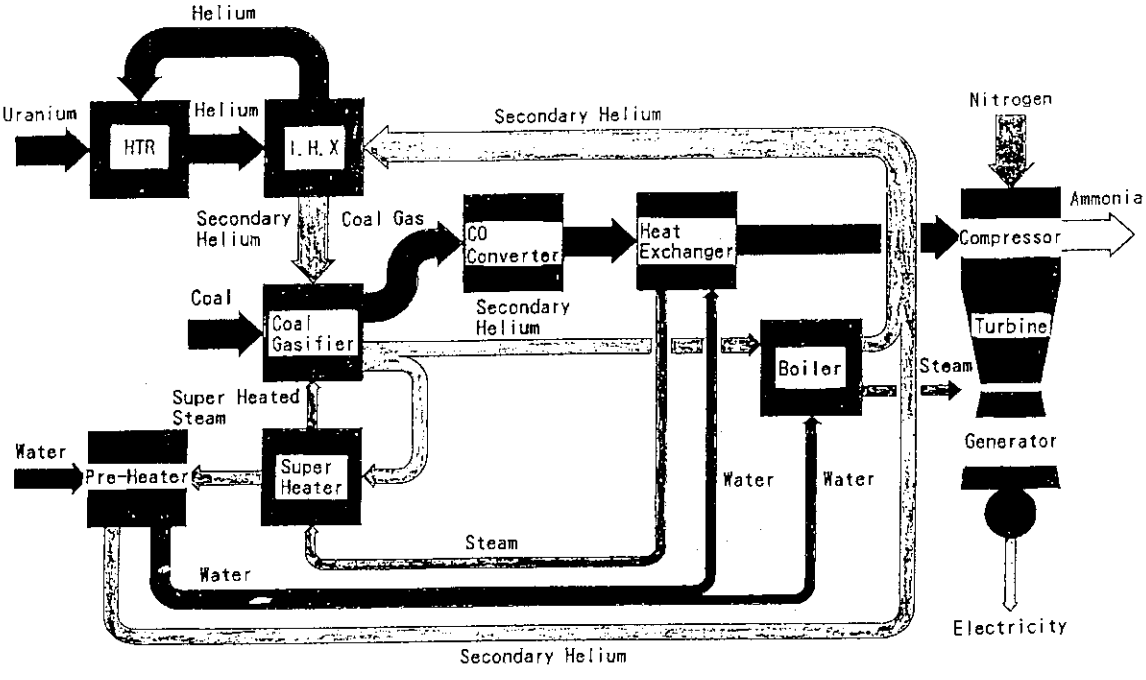


Fig.2 Diagram of HTR Coal-Gasification Ammonia Production Plant

6.16 Performance of High Temperature Chemical Heat Pump with Metal Hydride Reaction

S.Ishiyama, H.Ugachi and M.Eto

Department of High Temperature Engineering,
Japan Atomic Energy Research Institute
Tokai-mira, Ibaraki-ken 319-11 Japan

Abstract

The Japan Atomic Energy Research Institute(JAERI) has been constructing the High Temperature Engineering Test Reactor(HTTR) since 1991. The HTTR(thermal out put;30 MW) has been designed to be operated at very high temperature(Max. temperature;950°C) and hydrogen gas production plant, such as steam reforming methanol-hydrogen system will be jointed to this reactor to testify its productivity and efficiency. To improve the total efficiency of hydrogen mass production systems and extend the end-user of nuclear thermal energy, (1)hydrogen storage system and (2)thermal energy amplifier system are required to be with highly storage efficiency and amplify thermal energy at the temperature of 100C-500C° to above 1000°C. The concept of high temperature heat pump systems is composed of high and low temperature pressure vessels with MH materials, hydrogen gas removal and helium coolant passes between those vessels and around the vessel, and auxiliary equipment(such as heat exchanger, compressor) The function of high temperature pressure vessel is mainly to contribute heat up the wasted energy at 100°C-500°C to above 1000°C and low pressure vessel has mainly the function of mass hydrogen storage and supplier to the high temperature vessel.

To testify the efficiency of thermal conversion of the chemical heat pump system above-mentioned, the heat pump element test facility has been constructed and its performance tests are planted. The heat pump element test facility is composed of high temperature pressure vessels of about 1m length with 355 diameter and, hydrogen supplier and helium coolant suppler with Ar purge lines. A TiCr intermetallic compound powder(mean grain size~20μm) of about 3kg are filled

in the pressure vessel of SUS 316 with insulator(Micro thermo^{R}, outer and inner diameter of 120mm and 60mm with 960mm in length)) and ceramic holder tube(outer and inner diameter of 60mm and 50mm with 960mm in length; alumina of 3.0g/cm^3 density with mean micro pore size of 2μm). Heater of hastelloy X^{R} with 50mm in diameter with 850mm in length and heat exchanger tube(hastelloy X; total length 3400mm, out an inner diameter, 6.35mm and 4.35mm) are set at the center of the pressure vessel(length;1048mm, diameter;155mm, SUS316). From the thermal analysis of the system, it can be concluded that after exoergic reaction of H_2 absorption in the MH material of the order of 3wt/%H_2, calorific power of 5.7MJ is expected and considering total heat capacity of the facility, thermal output or heat gain, ΔT of the outlet He coolant will reaches up to about 870°C, thus the maximum temperature of outlet He coolant temperature reaches up to above 1000°C, if inlet He coolant is heated up to 500°C by the heater. Helium gas coolant of 4MPa supplied from He gas cylinder at R.T. is heated up to the designed temperature(~1000°C) by the exoergic reaction of the MH materials and then cooled down to the low temperature before blow out to the atmosphere. Hydrogen gas is introduced from H_2 cylinder into the pressure vessel through the three side inlets and after MH reaction, H_2 gas absorbed in MH materials which is cooled down to the temperature of the heater(~500°C), is to be dissociated from the MH by evacuation of the vessel by vacuum pump and blow out to the atmosphere. This MH absorption and dissociation procedure will be repeated to measure the coolant and MH temperature at every cycle, and built up the design data base for the high temperature chemical heat pump systems

Performance of High Temperature Chemical Heat Pump with Metal Hydride Reaction

S. Ishiyama, K. Fukaya and M.Eto

Japan Atomic Energy Research Institute(JAERI)
JAPAN

ABSTRACT

JAERI has been developing a hydrogen storage type high temperature chemical heat pump not only to amplify thermal energy of the temperature 373K to 1273K as well as store mass hydrogen energy, but hydrogen transportation to remote side. To testify the concept of this type of heat pump, heat pump element test facility was constructed and has been testing its performance. Heat conversion from 773K to 1173K was achieved with high heat exchanged coefficient by helium cooling technique.

Present paper reports the recent tests results of the facility, including R&D on metal-hydride and structural materials for this system.

1. Introduction

The Japan Atomic Energy Research Institute(JAERI) has been constructing the High Temperature Engineering Test Reactor(HTTR) since 1991. The HTTR(30MW) has been designed to be operated at very high temperatures(maximum temperature, 1223K) and jointed to hydrogen gas production plant or gas turbine generator to testify its productivity or efficiency[1-3]. To improve the total efficiency of hydrogen mass production and electrical generation and extend the end-user of nuclear thermal energy, the concept of hydrogen storage type high temperature chemical heat pump system proposed[4,5] is very attractive, because of (i)re-use of exhaust heat from nuclear plants for mass hydrogen production, (ii)mass hydrogen storage and (iii)transportation of hydrogen energy to remote side.

Present paper reports the recent activities of the R&D on the hydrogen storage type high temperature chemical heat pump system with metal hydride reactions and describes high performance of the system.

2. The concept of hydrogen storage type of high temperature chemical heat pump system.

2.1 *What is hydrogen storage type chemical heat pump?*

The concept of hydrogen storage type chemical heat pump is based on the metal-hydride reaction as following;

$$\underset{\downarrow}{M(Metal)} + H_2 \leftrightarrow \underset{\downarrow}{MH_2(Metal\ hydride)} + \underset{\downarrow}{\Delta Q(heat\ of\ reaction)} \quad (1)$$

(i)**Dissociation pressure** (ii)**Hydrogen storage** (iii)**Hydrogen production**

In this equation, there is three of merits, that is, (i)heat of reaction yielded in metal hydride reaction is to be utilized to amplify lower temperature of exhaust heat up to the temperature high enough to electricity or hydrogen production, and (ii)hydride energy produced is to be stored such as metal hydride materials(MH_2) in the equation, and (iii)high dissociation pressure, by which hydrogen energy is to be transported to remote aria.

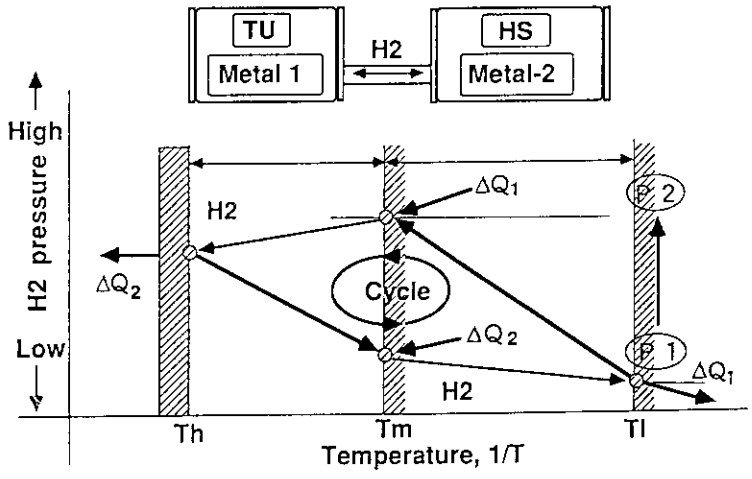


Fig. 1 The driving principle of the hydrogen storage type chemical heat pump system.

Therefor, hydrogen storage type chemical heat pump system with these reactions has a potential not only to amplify thermal energy of low temperatures as well as store mass hydrogen energy, but hydrogen transportation to remote side.

Chemical heat pump system is consisted of hydrogen storage reactor(HS) and temperature up reactor(TU), and hydrogen gas removes between these reactors at its operation. In the system, two of metal alloys, which exhibit different hydrogen absorption behaviors at the different temperature ranges, are filled in these reactors. The metal-1 in the HS, which behaves hydrogen absorption at temperature between lower(T_l) and middle temperature(T_m) levels with higher hydrogen absorption rate and lower enthalpy, and the other, the metal-2 in TU, which absorbs hydrogen between T_m and higher temperature(T_h) levels with higher enthalpy are required, respectively. Fig. 1 shows driving principle of simple model of this system. There is three temperature levels

round the system, that is, low temperature(T_l; room temperature level, at 303K), middle temperature(T_m; exhaust heat level, lower than 373K) and high temperature(T_h;673K~1473K). At first, hydrogen gas is absorbed in metal in HS reactor kept at T_l and TU kept at T_m is evacuated. Then, HS reactor is heated up to T_m and jointed to TU. At this time, the metal-1 absorbs heat energy ΔQ_1(= enthalpy of the metal-1) from exhaust heat source. There is differential pressure between TU and HS due to dissociation pressure yielded in HS($P_1 \rightarrow P_2$), then hydrogen gas absorbed in HS with metal-hydride reaction removes to HS. In TU, metal hydrogen reaction starts and releases reaction heat ΔQ_2(= enthalpy of the metal-2) at T_h. After finishing metal hydride reaction in HS, the temperature of the reactor returns to T_m and dissociates hydrogen from metal hydride in the reactor with heat absorption of ΔQ_2 from the exhaust heat source. Parallely, HS is cooled off to T_l level again to remove hydrogen from TU to HS with differential pressure between TU and HS.

In this process, this system consumes totally heat energy ($\Delta Q_1+\Delta Q_2$) from the exhaust energy source at T_m and amplifies these energy up to T_h and releases with ΔQ_2. Therefor, total energy conversion rate, η as mentioned below in the chapter 4(4.4), can be roughly estimated as the following equation;

$$\eta(T_m \rightarrow T_h) = \Delta Q_2/(\Delta Q_1+\Delta Q_2) \qquad (2)$$

From the eq. (2), it is clear that the choice and best matching of higher enthalpy material in TU and lower enthalpy material in HS, as mentioned above, is very important to maintain high conversion efficiency of the system.

This process can be operated cyclically by the control of hydrogen flow rate and temperature of the reactors.

2.2 *For what the system is required?(Nuclear Heat Utilization Net Work System)*

If the heat pump system with metal hydride materials, which is to amplify exhaust heat from the temperature of lower than 373K to more than 1274K with high thermal conversion rate, is available, the following functions can be expected to this system, such as Nuclear Heat Utilization Net Work System(NHU), as shown in Fig. 2;

(1) Re-use of exhaust heat from nuclear plants to power generation for hydrogen mass production.

(2) Mass hydrogen storage in this system to satisfy demand-supply interaction.

(3) Transportation of mass hydrogen energy to remote side with large scale hydrogen storage ring.

With these functions of the heat pump system,
lower cost mass hydrogen production, storage and transportation can be

achieved.

In the NHU net work system, metropolitan area integrated with industrial, residential and office areas is jointed to large hydrogen storage ring and supplied hydrogen energy from this system to maintain heat and electricity demand.

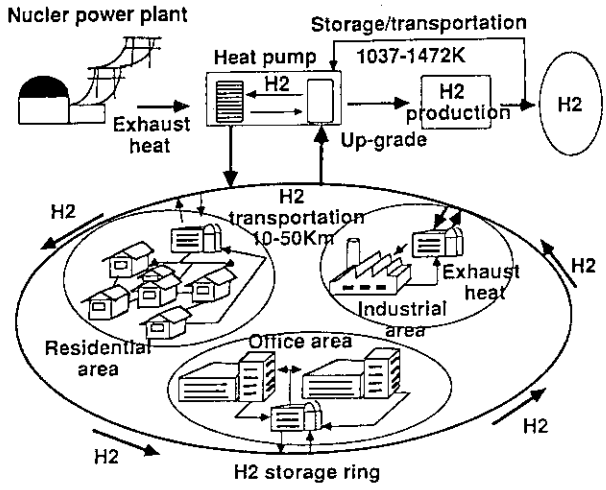


Fig. 2 The concept of Nuclear Heat Utilization Net Work System.

3. Experiments

In practical use, the heat pump system, which can amplify exhaust heat level of less than 373K to more than 1073K, becomes more complicated than such as the model as shown in Fig. 1. The operation temperature of the metals in HS is expected between 373 to 573K, and another metals in original and second TU tanks are between 573K to 773K and 773K to more than 1073K, respectively, as shown in Fig. 3. In the figure, heat exchange between HS reactor and original TU reactors or between original and secondary TU reactors is designed mainly to supply heat energy sustain dissociation reaction of metal-hydride reactions in these reactors.

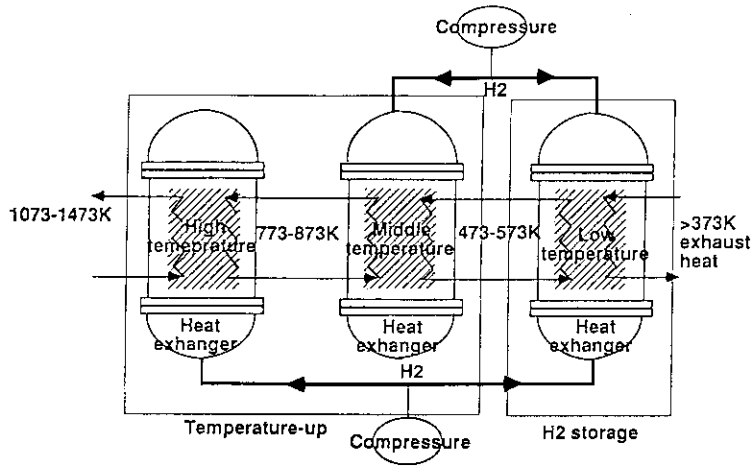


Fig. 3 The concept of the high temperature chemical heat pump system.

This is the reason that R&D of new metal hydride materials are required in higher temperatures to construct the chemical heat pump system. Fig. 4 shows the temperature ranges required for this type of heat pump system, which are classified into three region, that is, the low temperature(333-573K), the middle temperature(573-600K) and the high temperature(773-1473K) regions.

In the lower temperature range, a lot of materials are studied in the world[6], however, the reports is very limited[4,5] in the middle and high temperature ranges, as shown in the figure. Thus, the difficulty of construct of

this type of chemical heat pump is emphasized on the R&D of high temperaturehydrogen absorption materials.

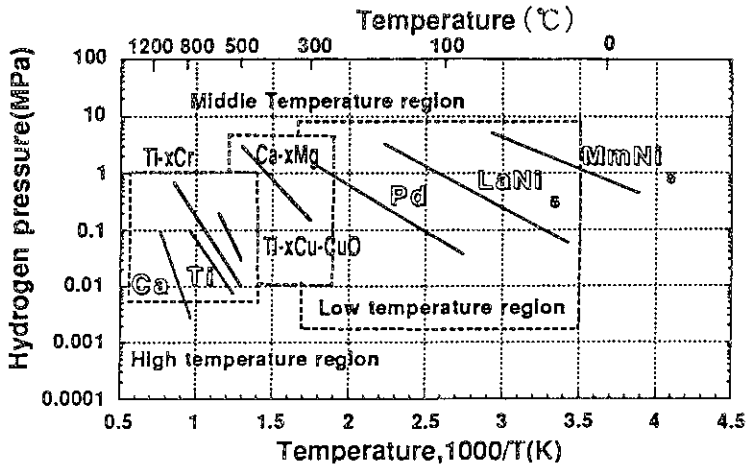
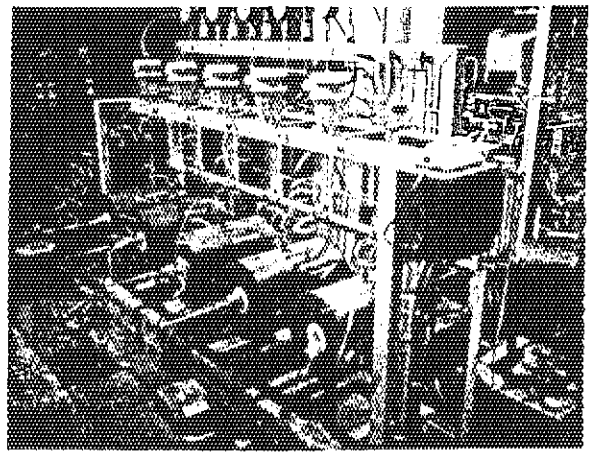


Fig. 4 P-C-T diagram of MH materials developed.

3.1 Materials, preparations and specimens.

For hydrogen absorption materials, Ca intermetallic compounds(Ca-*x*Mg and Ca-*x*Ni) and Ti intermetallic compounds(Ti-xCr and Ti-1.1Cu, Ti-1.1Cu-CuO) are composed by arc melting method. The detailed preparation procedures and materials should be refereed in REF.[4,5].

Prior to heat pump element construction, severance tests of candidate refractory materials are performed with molybdenum alloy, HA188, Hastelloy-X[8-10], SUS316 [11] and F82H[12] exposed under high pressurized hydrogen gas at high temperature for a long duration and compatibility with hydrogen absorption materials at high temperature.
Fig. 5 shows long time hydrogen exposing test equipment.


Fig. 5 Hydrogen exposing test equipment.

Tensile specimen of 2mm thickness with 15mm gage length and charphy specimen of 5mmx5mm and 50mm length with 2mm notch are machined from these materials and exposed under 5MPa hydrogen pressure at 803K for a long duration.

Disk type specimens of 5mm diameter with 4mm thickness are prepared for the compatibility testswith Ti-Cr alloy at 1073-1472k in a vacuum.

3.2 P-C-T measurements.

Absorption and dissociation tests at a constant temperature were performed at temperatures from R.T. to 1273K, employing a P-C-T measuring systems. Detailed operation conditions should be refereed in REF.[4,5].

3.3 High temperature material evaluations for chemical heat pump system.

To evaluate heat conversion performance of the chemical heat pump from 673K to more than 1037K, high temperature chemical heat pump element system was constructed with ca. 3kg Ti-5Cr alloy in the reactor, as shown in Fig. 6. Detailed specifications of the element are listed in the Table 1.

Table 1 Specification of the heat pump

Out/in diameter of helium tube(HA188)	6.35/4.35mm
Total length of helium tube	3400mm
Total weight of Ti-5Cr alloy	3075.6g
Diamter/length of heater element	12.7/850mm
Enthalpy of Ti-5Cr alloy	125kJ/molH2
Hydrogen absorption rate at 1073K	1.5wt.%H2
Out/in diamter of alumina tube	60/50mm
Total length of alumina tube	960mm
Out/in diamter of insulator	120/60mm
Total length of insulator	960mm
Length of pressreu vessle(SUS316)	1500mm

Main test purposes with this system are that;

(1) Demonstrate maximum out put temperature up to 1473K.

(2) Demonstrate off take maximum tempered out-put from the reactor.

For the purposes of (1), pressure and flow rate of hydrogen gas, which is removed from hydrogen cylinder to the reactor and evacuated by rotary pump after metal hydride reaction, were controlled by computer system and measured six points of temperature inside the reactor. Two of thermocouples are located at the in-let and out-let inside positions in heat exchange tube for the measurement of the in-let and out-let gas coolant temperatures. In this system, inert gas, such as helium gas, is removed from helium cylinder under the pressure and flow rate controlled and blow out in air thought the water cooler. Prior to hydrogen removal into the reactor, the element was heated up to 773K by heater element located in the reactor.

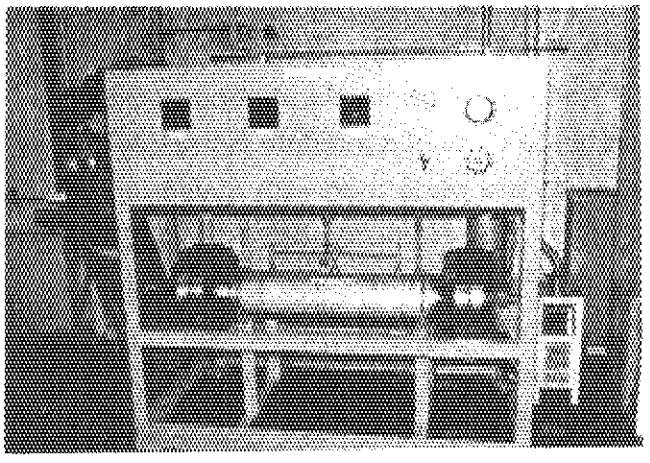


Fig. 6 Chemical heat pump element system with ca.3kg Ti-5Cr alloy.

4. Results and discussions

4.1 High temperature hydrogen absorption materials.

In practical use, Ti and Ca based materials are expected to satisfy the middle and high temperature range use with reasonable production cost and without extra difficulty of its handling, thus Ca/Mg or Ca/Ni alloy system for middle and Ti/Cr or Ti/Cu alloy system for high temperature uses were developed, respectively[4,5]. Fig. 7 shows typical P-C-T

curves of Ca/Mg tested at 593-673K. Ca-1Mg exhibits good absorption(→) /dissociation(←) reversibility and temperature dependency of 1.5-2.5wt.%H_2 absorption/dissociation in these temperatures with plateaus between 0.3-2MPaH_2. Ca-xMg systems also show constitutional dependency on maximum hydrogen absorption rate, as shown in Fig. 8. The results indicated that Mg element have a important role to the metal-hydride characterizations in these alloy systems.

Fig. 9 shows P-C-T curves of TiCu-5CuO. This material exhibits good hydrogen absorption/dissociation characteristics with plateaus between 0.0001 and 0.1MPaH_2 at 673-803K at maximum hydrogen absorption rate up to 1.5wt.%H_2 below 2MPaH_2.

Ti-*x*Cr alloy systems(*X*=5-15wt.%Cr) good exhibit hydrogen absorption/dissociation behaviors up to 1073K[4,5].

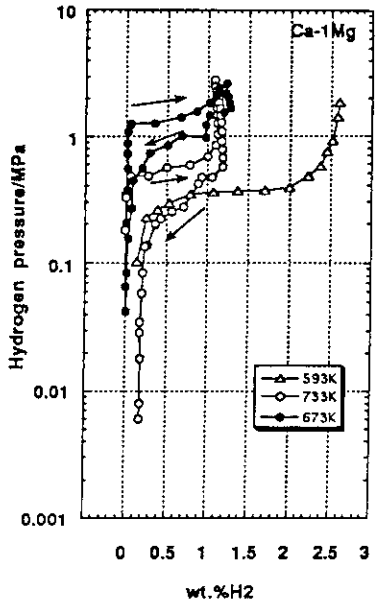


Fig. 7 P-C-T curves of Ca/Mg

With these data, Vanthoff curves of these materials are plotted in Fig. 3. It is clear that P-T characteristics of Ca/Mg alloy systems and Ti/Cr or Ti/Cu alloy are classified into middle and high temperature region in the figure, respectively.

Characteristics of Ti-5Cr alloy after absorption/dissociation cycles are measured at 903K.In this test, P-C-T characteristics and reaction rate in absorption and dissociation processes are obtained. Fig. 10 shows the change in maximum hydrogen absorption as a function of cycle number. Degradation in the value is observed within 200 cycles, but there is no remarkable change after these cycles.

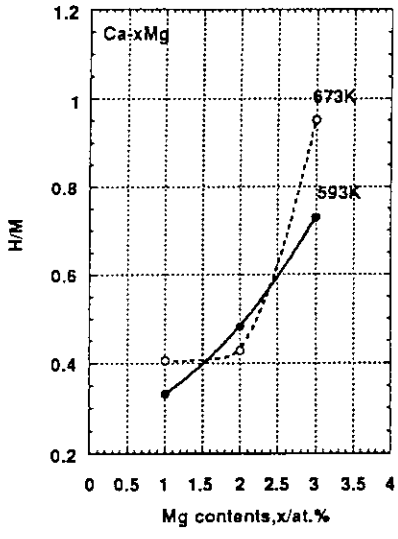


Fig. 8 Maximum absorption rate of Ca-xMg.

4.2 Mechanical properties of the refractory materials under pressurized hydrogen at high temperatures.

Mechanical properties of refractory materials, Molybdenum, Hastelloy-X, F82H(ferrite), SUS 316, HA188 exposed under 5MPaH2 at 803K for over 1200 hours were tested. Fig. 11 shows tensile stress-strain curves of Hastelley-X after 580 hours H_2 exposure. It is clear that Hastelloy-X exhibits good

ductility after long time hydrogen exposure and no tensile strength degradation due to hydrogen embrittelemnt was found in the materials.

Figs. 12 and 13 show the results of charpy impact tests of these materials at R.T..

There is impact energy degradation in these materials except HA188 and F82H, and lateral expansion changes are observed in these materials.

Vicker's hardness of F82H, SUS316, HA188 and Hastelloy-X after long term hydrogen exposure were tested, but there is not so remarkable changes in these materials.

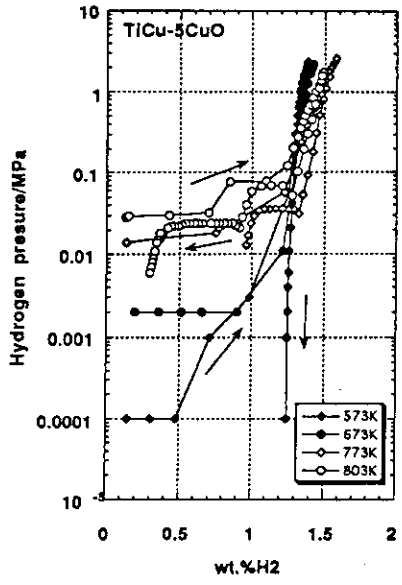


Fig. 9 P-C-T curves of TiCu-5CuO.

Fig. 14 shows bending strength of molybdenum alloy specimens exposed for 827 hours as a function of hydrogen contents in the tested specimen. The results indicated that there is no remarkable change in the material below 0.9ppmH_2 contents.

With these mechanical strength tests results, it can be concluded that degradation mechanical properties due to hydrogen embrittelemnt after a long termed hydrogen exposure at high temperatures are observed in SUS316, Hastelloy-X, but HA188 and F82H shows no remarkable change in these testing conditions.

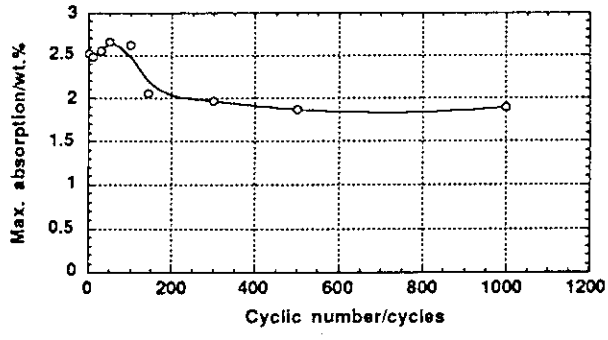


Fig. 10 Cycle effect on maximum H2 absorption of Ti-5Cr

4.3 Compatibility between the refractory materials and Ti/Cr alloy under high temperature.

Fig. 15 shows microstructual interface between Ti-5Cr(right side) and refractory materials(left side) after exposed at 1073-1473K in a vacuum.

Reaction zone are observed in the interface between Hastelloy-X or HA188 and Ti-5Cr alloy at 1273K, as shown in Fig. 15(a) and 15(b), but no remarkable change is found between RuAl and Ti-5Cr alloy, as shown in Fig. 15(c).

With this compatibility tests, It can be concluded that under 1173K Hastelloy-X and HA188 materials is applicable for the structural materials, such as heat exchange tube,

which has the interface with Ti-5Cr alloy under 1173K.

4.4 Performance of the chemical heat pump element system.

(1) H_2 absorption tests of the chemical heat pump system.

To testify the heat conversion from the temperature of 773K to more than 1073K, the reactor evacuated by rotary pump are heated up to 773K by heater element prior to hydrogen removal, then hydrogen gas was introduced into the reactor from gas cylinder with pressure and gas flow controlled.

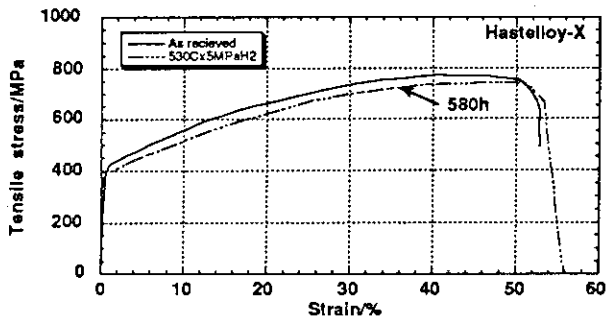


Fig. 11 S-S curves of Hastelloy-X after H_2 long term exposure

In present experiment, hydrogen pressure and flow rate in the present experiment were controlled at 0.5- 2MPa or 50 -100 liter/min, respectively.

Fig. 16 shows the heat up testing results of the reactor from 773K to 1073K with typical meant reactor temperature, hydrogen flow rate and hydrogen absorption rate as a function of testing time. After 200 sec heat up by the heater, the reactor was isolated from the heater warm-up and then introduce with hydrogen gas controlled at 2MPaH_2. Immediately, the mean temperature inside the reactor risen up and then reached up to 1073K within 10 sec after hydrogen introduction. After peak hydrogen flow rate reached up about 400 liter/min ,the hydrogen gas introduction was cut off to keep peak reactor temperature at 1073K. After then, cyclical hydrogen introductions were repeated till the end of metal hydrogen reaction inside the reactor. The take-out of thermal out-put in the reactor was performed by heat transfer with helium gas coolant though heat exchanger pipe. Helium

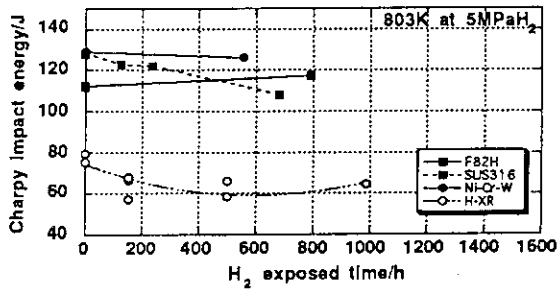


Fig. 12 Charpy impact energy of the materials afte long term H_2 exposure.

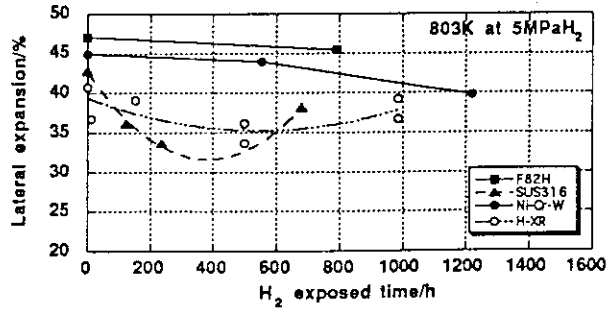


Fig. 13 Lateral expansion of the materials exposed in H_2.

gas at 291K with the pressure of 3MPa and flow rate of 60 liter/min was introduced after peak temperature of the reactor, and out-put temperature of the gas immediately also reached up to the peak temperature of the reactor. With these cyclical hydrogen introduction and helium gas flow control, the peak temperature of the reactor was maintained at 1073K for about 400 sec, after then hydrogen flow rate returned to zero after 600 sec from the beginning of these tests due to the finishing of metal hydride reaction. The introductions of hydrogen and helium gas into the reactor were stopped after 720 sec and hydrogen gas inside the reactor was evacuated with heat up of the reactor by the heater element at 783K. This evacuation procedure was continued about three hours before another cyclic reaction operation.

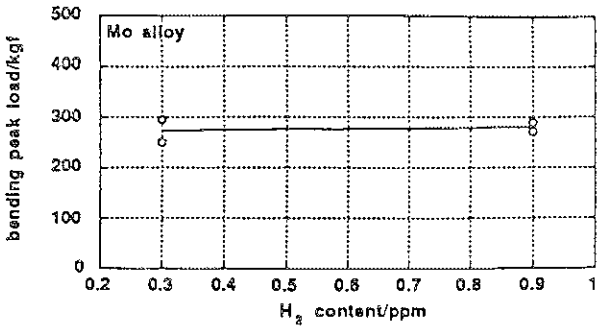


Fig. 14 Bending strength of Mo after H_2 exposure.

(2) Evaluation of heat conversion efficiency of the element

Fig. 17 shows the thermal in-put and out-put inside the reactor during metal hydride reaction with total hydrogen absorption into the metal. Total exothermic energy out-put of metal hydride reaction increases as increase of the hydrogen absorption. A part of this exothermic energy is to be utilized such as heat-up energy of the reactor from 773K to 1073K, thus temperature up heating value of the reactor was evaluated with consideration of total heat capacity of the reactor including that of metal and structural materials, and plotted in the figure. Drastic change in the heating up value are found within 20 sec after hydrogen introduction, then almost saturated till the end of the reaction.

Total heat exchanged value with helium coolant is also plotted in the figure, and exhibits monotomically increases till coolant cut-off.

Thus the heat balance of thermal and heat conversion efficiency inside the reactor can be evaluated with these results. The summation of total heat exchanged value and temperature up heating values are also plotted in the figure, comparing with total exothermic energy. It is of

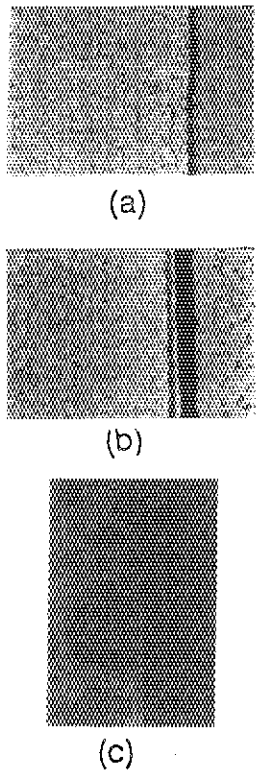


Fig. 15 Compatibility between Ti-5Cr and the materials.

interesting that summation of the heating value is almost balanced with the exothermic energy before 500 sec from the start point, but becomes higher then after. This fact indicated that before 500sec, almost full heat exchange of exothermic energy is achieved by helium coolant except temperature up energy of the reactor and unbalanced heat balance is considered to be due to transformation of the Ti-5Cr alloy from α→β at 1155K[4] observed.

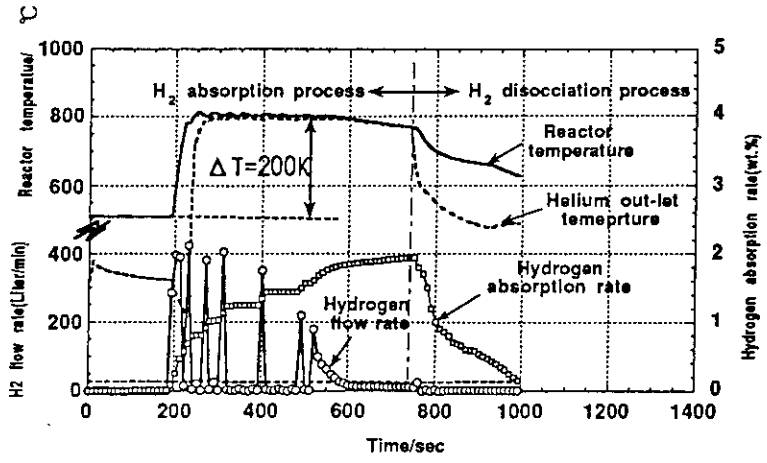


Fig. 16 Heat-up of the heat pump element with H_2 and He flow controlled.

(3) Heat conversion efficiency of the hydrogen storage type chemical heat pump.

Heat conversion efficiency of the hydrogen storage type chemical heat pump models, as shown in Fig. 3 is evaluated with the following equation;

$$\eta = \frac{\{\Delta H_h - (C_{ph} + C_{pH2})(T_h - T_m)\}}{\{\Delta H_h + 2\Delta H_l + \Delta H_m + C_{pl}(T_m - T_l)\}} \quad (3)$$

where ΔH_h, ΔH_l and ΔH_m; enthalpy of alloys used in high, middle and low temperature reactors.

C_{ph}, C_{pl} and C_{pH2}; Heat capacity of alloys used in high and low temperature reactors and hydrogen gas.

T_h, T_m and T_l; Temperature of maximum out-put temperature of the heat pump, exhaust energy and room temperature.

With eq.(3), heat conversion efficiency of the chemical heat pump is calculated with a parameter of the temperature levels of exhaust energy on the assumption that;

$$\Delta H_h = 5\Delta H_l \quad (4)$$

and

$$\Delta H_m = 2\Delta H_l \quad (5)$$

Fig. 18 shows the heat conversion efficiency of the heat pump model calculated by eq.(3). It is noted that a very high efficiency η at T_l = 323K is expected to be more than 50% between out-put temperature of 773K and 1273K. This fact indicates that nuclear

plant under service generates electricity with about 33% efficiency and releases about 70% energy of lower temperature in air, but if this type of heat pump is available to amplify these exhaust energy of the low temperature, the collection of about 50% usable energy for electrical generation can be attained from 70% energy loss of the plant, thus 35%(= 0.7x0.5) thermal energy or 10% electricity(=0.7x0.5x0.33) gain is obtained. This re-usable electricity is applicable for mass hydrogen production with lower production cost.

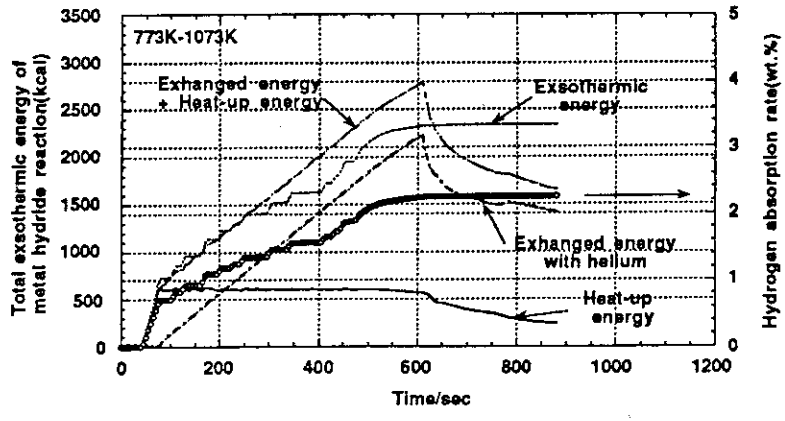


Fig. 17 Total energy balance of the heat pump element.

5. Conclusion

Hydrogen storage type high temperature chemical heat pump has been developing in JAERI. This type of heat pump is one of promising technologies not only to up-grade exhaust energy from nuclear plant to produce lower cost hydrogen and its storage, but to transport the hydrogen produced to remote side. To testify the concept of the system, present study demonstrated the performance of the system including R&D on the high temperature hydrogen absorption and structural materials.

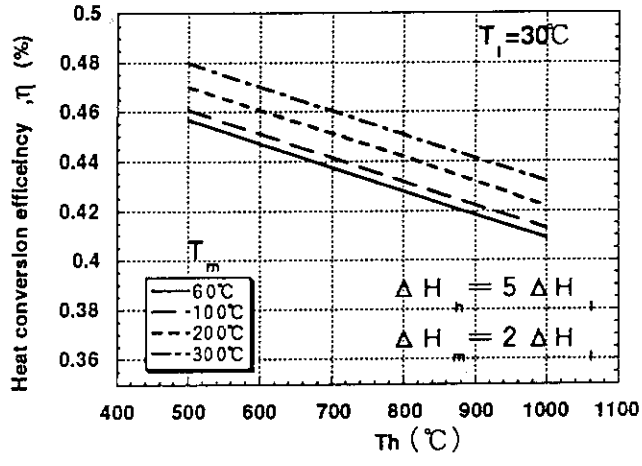


Fig. 18 Heat conversion efficiency calculated by eq.(3).

With these results, it can be concluded that high temperature hydrogen absorption materials with good performance, such as Ti/Cr, T/Cu and Ca/Mg systems are found and high temperature heat pump reactor element was constructed with Ti/Cr alloy and refractory structural materials tested. and its performance was demonstrated.

The results of the element system indicates that heat conversion from 773K up to 1173K was achieved and heat exchange by helium cooling technique is applicable to this system with very high heat exchanged efficiency.

REFERENCES

1. K.Hada,N.Fujimoto and Y.Sudo; IAEA-TECDOC-761,138(1994)pp.124-134.
2. K.Sanogawa; NIPPON GENSHIRYOKU GAKKAI-SHI, Vol.35(1)(1993)pp.70-74.
3. K.Sanogawa; ibid. Vol.35(2)(1993)pp.139-146.
4. S Ishiyama, H.Ugachi and M.Eto; J. of The Hydrogen Energy Systems Society of Japan, Vol.12,No.1(1994)pp.33-40.
5. S Ishiyama,H.Ugachi and M.Eto; J. of alloys and compounds,(1996) to be published.
6. New Energy and Industrial Technology Development Organization(NEDO); Proceeding of International Hydrogen and Clean Energy Symposium '95,(1995) Feb.6-8. D.Stover,H.P.Buchkremer,R.Hecker and H.J.Leyers;J. of Nucle. Mater. V.123(1-3)(1984)pp.1541-1546.
9. H.Nickel and K.Koizlik; Thin Solid Films, V.108(4)(1983)pp.401-414.
10. T.Matsuda,A.Kitsunezaki,H.Saito and S.Seki; J. of Nucle. Mater. V.76-77,pp.608-610(1978).
11. H.Saito,K.Miyazawa,N.Nogawa,M.Mori and Y.Ishida; Proceeding of 4th Inter. Symp. on Radiation Physics, San Paulo, SP(Brazil);3-7 Oct. 1988, p.213.
12. Y.Kohno and A.Kohyama; J. of Nucle. Mater., V.191-194(PT.6)(1992)pp.868-873.

6.17 Disposition of Plutonium with HTGRs using Pu Burner Balls and Th Breeder Balls

K.YAMASHITA, K.TOKUHARA, and N. FUJIMOTO
Department of HTTR Project
Japan Atomic Energy Research Institute
Narita-cho, Oarai-machi, Ibaraki-ken, 311-13 JAPAN
Ph: 029-264-8532 / Fx: 029-264-8486

Abstract

It has been proposed to burn plutonium (Pu) in form of mixed-oxide fuel or in form of pure plutonium fuel with burnable poisons. In former case, the Pu transmuted from ^{238}U remains in spent fuels even if initially loaded plutonium is burned. In latter case, a achievable burnup is limited by parasitic neutron absorption of the burnable poisons.

We have found a reactor system with which Pu can be burned out so that the reprocessing of spent fuels is no more valuable. This system is a pebble bed type HTGR using Pu burner balls (Pu balls) and Th breeder balls (Th balls). The Pu ball contains plutonium, not mixed with fertile material, such as ^{238}U or Th. The Th ball contains only fertile material of Th. The core is loaded with these two types of fuel balls randomly. They are removed continuously from the core. The burnups of Pu balls are evaluated by measuring the strength of γ-rays. The Pu balls are reloaded again from the top of core if the burnup is still under the maximum burnup to be achieved. The Pu balls are discharged from the reactor system as spent fuels if the burnup reaches to the maximum value. The reactivity necessary for the reactor operation is maintained by loading fresh Pu balls. The Th balls are reloaded so far as the fuel integrity is maintained.

The achievable maximum burnup of the Pu ball is about 740 GWd/T_{Pu}. This was evaluated with the following relation:

$$B_n = \frac{2n \cdot B_1}{n+1}$$

where

B_n: burnup of spent fuel of reactors with n-batch fuel loading(GWd/T)

B_1: burnup of spent fuel of reactors with one-batch fuel loading(GWd/T).

The burnup of the pebble bed type HTGR (B_n) is twice than B_1 because the n can be regarded as the infinite due to the continuous loading.

The amount of total Pu is reduced to about 20% for the burnup of 740GWd/T_{Pu}. After the decay of ^{241}Pu to ^{241}Am, only ^{239}Pu remains in the Pu balls finally as fissile material. Thus, total fissile materials will be less than 1% of the initial amount of total Pu. For such small residuum of fissile material, there are no more merits to reprocess and/or to reuse them for nuclear fuels or nuclear weapons. Therefore, they can be disposed directly for waste.

Reactors using ^{239}Pu as fuel have a tendency to possess positive power coefficients due to increase in the fission reaction rate at the giant resonance peak of ^{239}Pu (0.3 eV) by the temperature elevation. It is succeeded to make the power coefficient negative by making the thermal neutron spectrum peak near the giant resonance peak small. The increase in the fission reaction rate at the giant resonance peak by the temperature elevation is reduced by the small thermal neutron spectrum peak. The achievable burnup is high because any additional material like burnable poison is used.

From the results, we think the reactor system concept innovated here is one of the most promising options for deposition of Pu due to the high burnup ability.

Disposition of Plutonium with HTGRs using Pu Burner Balls and Th Breeder Balls

Kiyonobu YAMASHITA, Kazumi TOKUHARA and Nozomu FUJIMOTO
Department of HTTR Project
Japan Atomic Energy Research Institute
Narita-cho, Oarai-machi, Ibaraki-ken, 311-13 JAPAN

Abstract

A concept of reactor system was developed with which weapons-grade Plutonium could be made perfectly worthless in use for weapons. It is a pebble bed type HTGR using Pu burner ball fuels and Th breeder ball fuels. The residual amounts of ^{239}Pu in spent Pu balls become less than 1% of the initial loading. The power coefficient was made negative by reducing the parasitic neutron absorption reaction rate of ^{135}Xe.

1. Introduction

About two hundred tons of weapons-grade plutonium (WG-Pu) will be surplus when nuclear weapons are dismantled in United states and Russia[1]. Unlike highly enriched uranium, simple denaturing cannot make this plutonium worthless for use in future weapons. The use of physical security and institutional barriers to provide secure storage for centuries is questionable when considering government instability and the possibility of national recidivism. This question will be solved by burning of ^{239}Pu. The high burnup is expected from a view point of effective use of the fissile materials.

The WG-Pu burning was studied by using LWR-, FBR- and HTGR- type reactors. The approaches can be classified in two groups from the fuel types. In the first group, Pu is mixed with the fertile materials such as ^{238}U or ^{232}Th[2,3]. The fertile materials are used to mitigate the reactivity change without loss of neutron economy. In the second group, Pu is burned without mixing of fertile materials[1,2,4,5]. Burnable poisons are used to mitigate the reactivity change. In the first case, a problem arises. New fissile materials produced from fertile materials remain in the spent fuels. In the second case, the achievable fuel burnup is reduced by the burnable poisons due to bad neutron economy. Therefore, fissile materials remain in the spent fuel. The problem is also not solved in the second case.

We have found a reactor system in which ^{239}Pu can be burned out almost perfectly. This system is a pebble bed type HTGR(PBR) using Pu burner ball fuels (Pu balls) and Th breeder ball fuels (Th balls). The Pu ball contains only plutonium not mixed with fertile material of Th. The Th ball contains only fertile material of Th. We intend to avoid production of new fissile materials except ^{241}Pu in Pu ball. Therefore, fissile and fertile materials are loaded into Pu balls and Th balls, separately. The core is loaded with these two types of fuel balls randomly.

They are removed continuously from the core and reloaded into the core. The reactivity is controlled through a continuous fuel loading. Pu ball is discharged when the burnup reaches the expected high value. The residual fissile material of ^{239}Pu in Pu ball is extremely small. As a result, Pu in the spent Pu ball becomes perfectly worthless for use in weapons with combination of a large amount of absorption materials of ^{240}Pu, ^{242}Pu and ^{241}Am. Energy is produced effectively by high burnup of ^{239}Pu and burnup of ^{233}U converted from Th.

Power coefficient of any reactor has to be negative to maintain the inherent safety characteristics. However, it is known from operation experiences of Calder Hall type power reactor that the power coefficients may become positive due to shift of the neutron spectrum to the giant fissile resonance peak of ^{239}Pu. The problem was solved by using ^{167}Er as burnable poison in the block-type HTGR design(PC-MHR)[1,4,5]. However the burnup is limited in this way because the neutron economy becomes worse by the parasitic neutron capture reaction of ^{167}Er. We have found a new method to obtain a negative power coefficient without any burnable poisons. The thermal neutron spectrum peak is lowered by heavy loading of Pu in a Pu ball. The positive contribution to the power coefficient, neutron absorption reaction of ^{135}Xe, is reduced by it. In this way, the neutron economy is not made worse and the high burnup can be achieved.

This paper presents the idea of the reactor system, burnup characteristics, power coefficients and resistance to divisions when WG-Pu (94% ^{239}Pu and 6% ^{240}Pu) is burned in the reactor system.

2. Movements of balls in core

Schematic movements of the Pu balls and Th balls are shown in **Fig.1**. The multi-pass fuel loading is applied to achieve an ultimate high burnup of Pu. The burnups of the Pu balls are evaluated by measuring the strength of γ-rays after they are taken out from the bottom of the core. The Pu balls will be reloaded again if the burnup is less than the expected burnup value. The Pu ball and Th ball are distinguished by the difference in γ-ray spectrums. The Pu balls will be discharged from the reactor system as spent Pu balls if the burnup reaches to the expected burnup value. The same number of fresh Pu balls is loaded from top of the core. The reactivity necessary for the reactor operation is provided by the loading of fresh Pu balls. In this way, burnable poisons are not necessary for the reactivity control. Th balls are reloaded repeatedly as far as the fuel integrity is maintained. The technics for the multi-pass fuel loading have been accumulated through the operation of the pebble bed type experimental HTGR of the AVR in Germany for about 20 years. The technics can be applied for the reactor system[6].

3. Pu burning

The maximum burnup of the Pu ball was evaluated with the following relation[7]:

$$B_n = \frac{2n \cdot B_1}{n+1} \qquad (1)$$

where

B_n: burnup of spent fuel for reactors in which the whole fuels are replaced with n-time reloading (GWd/t)

B_1: burnup of spent fuel for reactors in which the whole fuels are replaced for once (GWd/t).

The burnup of the pebble bed type HTGR (B_n) is twice than B_1 because the n can be regarded as the infinite due to the continuous loading. B_1 was calculated with HTGR fuel lattice burnup calculation code DELIGHT[8]. The specifications in **Table 1** were used for the study[9,10]. A simplified model is used for the evaluation of the burnup. Pu, Th and ^{233}U are distributed in the fuel kernel of the coated fuel particles (CFPs) in the ball fuel in the evaluation model. The effective cross section of Th was evaluated by the resonance calculation. The change in the effective multiplication factor k_{eff} is given in **Fig.2**. The burnup B_1 becomes 370 GWd/t_{Pu} if the reactor operation margin is considered. The maximum burnup is 740 GWd/t_{Pu}. This is obtained by substituting 370 Gwd/t_{Pu} into B_1 in the equation (1). The change in Pu isotopes with burnup is shown in **Fig. 3**. The amount of total Pu for 740 GWd/t_{Pu} is 20% of the initial value. The amount of ^{239}Pu becomes less than 1% of the initial values.

The irradiation test of coated fuel particles of Pu (Pu-CFP) had been done by in Belgonucleaire in 1974[11]. It was shown the integrity of the Pu-CFP was maintained for burnup of 600 GWd/t_{Pu}. The density of the fuel kernel was lowered in the Pu-CFP to avoid the pressure rise by fission products. A further reduction in the fuel kernel density may be necessary to realize the burnup of 740 Gwd/t_{Pu}.

Studies on Pu disposition were reported for the advanced LMR (ALMR), advanced BWR (ABWR)[2] and PC-MHR[1,4,5]. **Table 2** shows residual amounts of Pu isotopes when the WG-Pu of 1000 kg is burned in one burnup cycle with the ALMR, ABWR, PC-MHR and PBR. Pu fuel without fertile materials was burned in case of the ALMR. Pu was mixed with natural uranium in the case of the ABWR. Pu was burned without fertile material but with burnable poison of ^{167}Er in case of the PC-MHR. The residual amount of total Pu for the PBR is about one-third of the ALMR and ABWR and about half of the PC-MHR. The residual amount of ^{239}Pu of the PBR is negligible small to the ALMR and ABWR and about 14 times smaller than that of the PC-MHR. The high burnup characteristics of PBR make the residual amount of Pu extremely small. It results from the separation of fissile and fertile materials, continuous fuel loading and no use of burnable poisons. The generated energy by loading of 1000 kg for the PBR is lager than those of the other type reactors. It results from high burnup of ^{239}Pu and burnup of ^{233}U converted from Th. From the results, it can be concluded that the quality of the

WG-Pu can be extremely degraded by the PBR and the WG-Pu can be converted to energy effectively.

The amount of ^{233}U in Th ball will be saturated to about 0.2 g after a certain duration in the core. The burnup of the Th ball is about 7 GWd /t_{Th} for a year. The Th ball can be used for 16 years if it is supposed that the integrity is maintained to the average burnup of Thorium, Hochtemperatur-Reaktor(THTR-300)(109 GWd/t)[12].

4. Negative temperature coefficient

The power coefficient always has to be negative for any reactors to maintain the inherent safety characteristics. ^{135}Xe and ^{239}Pu possess positive contributions to power coefficients in thermal reactors. The shift of the thermal neutron spectrum peak in high energy causes a decrease in the neutron absorption reaction rate of ^{135}Xe and an increase in the fission reaction rate of ^{239}Pu. Isothermal temperature coefficients (ITC) were studied here instead of the power coefficients because the power coefficient is negative if the ITC is negative. The same temperatures are assumed for the fuel and moderator. The temperatures are changed simultaneously in the study. **Figure 4** shows the change in the ITC with the burnup of the Pu ball for 0.5 and 1 g Pu loading. The amounts of ^{233}U and Th were maintained in the equilibrium values. The ITC was evaluated with the lattice cell burnup model of the SRAC code[13]. The ITC increases with burnup even if the amount of the positive contributor of ^{239}Pu decreases. The ITC for 1 g Pu loading in a Pu ball is still negative for the representative burnup of 370 GWd/t_{Pu}. The representative burnup corresponds to the average burnup of fresh and old Pu balls randomly loaded in the equilibrium core of the PBR. **Figure 5** shows the relations of thermal neutron spectrums with σ_a of ^{135}Xe, σ_f of ^{239}Pu and σ_a of ^{240}Pu for the burnup of 370 GWd/t_{Pu}. The spectrum peak for the case of 1 g Pu loading is smaller than that for the case of 0.5 g Pu loading. The small spectrum peak results to small positive contribution to the ITC because the decrease in the neutron absorption reaction rate of ^{135}Xe becomes small due to the neutron spectrum shift. The absorption reaction rate for the case of 1 g Pu loading was a half of that for the case of 0.5 g Pu loading. As a result, the ITC becomes negative with combination of the negative Doppler coefficients of ^{240}Pu and Th. On the other hand, the ITC for the case of 0.5 g is positive for the representative burnup. The fission reaction rate with giant resonance peak(E=0.3 eV) is hardly changed by increase in Pu loading in a Pu ball. Therefore the positive contribution of ^{239}Pu is practically same for different Pu loading between 0.5 and 1 g.

From the results, it can be concluded that the power coefficient of the PBR can be made negative by reducing absorption reaction rate of ^{135}Xe. The reduction of the neutron absorption of ^{135}Xe is obtained by a heavy loading of Pu in Pu ball. Any additional material like ^{167}Er[5,14] which reduces fuel burnup is not used for PBR to make the power coefficient

negative.

5. Pu ball power

Power is large in the fresh Pu ball. The Pu ball power decreases with progress in burnup. The maximum Pu loading in Pu ball is limited by the maximum permissible power in a ball. The power of 4.5 kW was used in the design of HTR module as the maximum permissible value for irradiated fuel balls of 6 cm diameter[15]. It was determined by the limit of thermal stress in the ball. **Figure 6** shows the change in the Pu ball power with burnup days when the Pu ball is loaded with 1 g Pu. Amount of Th in a Th ball is 14 g. Axial power peaking is not considered in the evaluation of power changes in **Fig. 6**. The maximum power appears at the beginning of burnup. The real maximum power in the core is about 4.9 kW. It was evaluated by using the axial power peaking of the HTR module (1.7)[15]. The real maximum power is slightly lager than the maximum permissible power of 4.5 kW. The maximum permissible power will increase if the large thermal conductivity of graphite of fresh fuel balls is considered for the evaluation of the thermal stress limit. The power of the Th ball is almost constant after the saturation of ^{233}U concentration. The power distribution in the core is homogenized by using the Th ball. The Th ball works as a power producer in the zone where the Pu ball power becomes small as shown in **Fig. 6**.

6 Resistance to diversion and proliferation

Although any mixture of plutonium isotopes can be used to make a nuclear device, the plutonium being high in ^{240}Pu and ^{242}Pu contents is much more difficult to use in weapons applications. The increased difficulty in weapons design, construction, and delivery results from the higher critical mass required, the higher spontaneous neutron emission rate, higher radiation hazard and higher decay heat. The plutonium discharged from the PBR is the lowest in the ratio of ^{239}Pu to total plutonium as shown in **Table 2**. The fissile material ^{241}Pu transmuted from ^{240}Pu in the Pu ball becomes worthless for use in weapons because ^{241}Pu decays to the strong neutron absorber of ^{241}Am with a relatively short half-life time(14 years). The difficulty increases during storage of the spent Pu balls. Finally, the fissile material that could be applied for weapons will be only ^{239}Pu in Pu ball. The ratio of the fissile material to the total residual Pu is about 0.3 % in the spent Pu ball. It can be concluded that Pu burned in the PBR becomes perfectly worthless for use in weapons due to the small amount of residual fissile material of ^{239}Pu and a large amount of absorption materials of ^{240}Pu, ^{242}Pu and ^{241}Am.

The amount of Pu destroyed in the PBR is small. It is only 33 kg for a year. The reason is that Pu is burned in the PBR extremely effectively. However, the WG-Pu destruction speed is important to prevent the diversion. This can be solved well by the spiking[2] of Pu balls in

the PBR. The Pu balls are made radioactive by loading in the core so that the diversion of Pu will be made difficult. Large number of Pu balls can be made radioactive in the reactor system because Pu balls are continuously irradiated in operation in the PBR. The irradiated Pu ball will be stored temporary and be burned again in the reactor system later. The diversion of WP-Pu can be prevented by the spiking without loss of Pu as a valuable energy source.

The total amount of ^{233}U in the core is 36 kg. It does not increase because ^{233}U produced from Th burns soon. ^{233}U does not come out from the reactor system because Th balls are reloaded into the core repeatedly. Th balls are used for the whole reactor life without reprocessing. ^{233}U in Th balls can be well controlled with safeguards system as far as they are kept in the core. The Th balls possess a high resistance to diversion due to the high γ ray of ^{232}U even if some broken Th balls are discharged from the reactor system. 36 kg ^{233}U will be produced for destruction of 1000 kg of WG-Pu for a reactor life of 30 years. The fissile materials can be reduced to 0.36% of the initial amount.

7. Conclusion

The total amount of Pu can be reduced to about 20% of the initial value by the PBR. The amount of ^{239}Pu in the spent Pu ball will be less than 1% of the initial value. The substantive amount of fissile material will be the same as the amount of ^{239}Pu after decay of ^{241}Pu. Finally the ratio of the fissile material to the total residual Pu is 0.3 % in the spent Pu ball. It could be concluded from extremely low quality that the residual Pu is perfectly worthless for reuse for the weapons. The spent Pu ball possesses high resistance to diversion and proliferation due to small content of ^{239}Pu in Pu. A direct disposal to rock salt mining may be possible due to the small amount of fissile material in the spent Pu ball[16]. The large amount of WP-Pu can be made resistible to diversion and proliferation by the spiking of Pu balls.

Energy generated by the PBR is more for the same consumption of Pu amount than those by the PC-MHR, ALMR and ABWR. The WG-PU can be burned in the PBR as a valuable energy source effectively.

Furthermore, a method was found that the power coefficient could be made negative without any additional material like ^{167}Er which reduces fuel burnup. The neutron absorption ratio of ^{135}Xe is reduced. It is realized by a heavy loading of Pu in Pu ball.

ACKNOWLEDGMENTS

The authors express their sincere thanks to Messrs. R.Shindo, S.Shiozawa, T.Tanaka and T.Tobioka for valuable comments and support.

References

(1) Brian G. Chow, "Economics and Proliferation Resistance of Weapons Plutonium

Disposal," TANSAO 721-408 (1995), 284PP.
(2) USDOE:"Plutonium Disposition Study"(1993).
(3) Akie, H.,et al.,:Nuclear Technology, Vol.107, 182pp. ,(1994)
(4) Alberstein, D., Baxter, A.M. and Simon, W.A."The Plutonium Consumption Modular Helium Reactor(PC-MHR), IAEA TCM on unconventional Options for Plutonium Disposition", in Obninsk (1994).
(5) Baxter, A.M. and Neylan, A.J.,"The GT-MHR for Destruction of Weapons Plutonium", TANSAO72-408 (1995), 391pp.
(6) IAEA: "Operation Experience with Nuclear Power Stations in Member States", (1974-89)
(7) Graves, H.W., "Nuclear Fuel Management", (1979).
(8) Shindo, R., Yamashita, K.,and Murata,I. ,:JAERI-M90-048, (1990),(in Japanese).
(9) Grebennik, V.N., Mosevitskii, I.S.:JAERI-M92-215, (1993)
(10)Hubel, H.J., Lornert,G.H.,:Kerntechnuk,47,(1985),159pp.
(11)Bairoit,H.,et al.,:Nucl.Technol. ,23,240, (1974).
(12)Assoziation EURATOM/BBC-Krupp /KFA:"Sicherheits bericht des THTR Prototyp 300 MWe",(1992).
(13)Tsuchihasi, K., Ishigro,Y.,Kaneko,K. and Ido,M.,JAERI-1302,(1986).
(14)Obara,T. and Sekimoto,H.:Ann Nucl.Energy Vol.22,No.6,331pp.,(1995).
(15)Teuchert,E.,Ruetten,H.J., and Haas,K.A.:Juel-2618,(1992).
(16)Kirch,K.,et al.:Nucl.Eng.Des.,121, (1990), 241pp.

Table 1 Specifications of core and fuel

Thermal power*	200 MW
Core height*	9.4 m
Core diameter*	3.0 m
Moderator	Graphite
Coolant	Helium
Pu ball	
Pu amount	1 g/ball
Number in core	about 180000
239Pu:240Pu	94:6
Th ball	
Th amount	14 g/ball
Number in core	about 180000

* Specifications referred to Russian HTR-Module in development[9]

Table 2 Residual plutonium and generated energy by loading of 1000kg plutonium in different reactor types

	Before burnup	After burnup			
		ALMR*	ABWR*	PC-MHR[4]	PBR
Total Pu(kg)	1000	618	648	350	199
^{239}Pu(kg)	940	476	279	85	6
^{240}Pu(kg)	60	130	233		72
^{241}Pu(kg)	0	12	97	265	55
^{242}Pu(kg)	0	0	39		66
Generated energy (J)**	------	4×10^{13}	*** 9.2×10^{13}	-------	1.1×10^{14}

* :They were referred to "plutonium disposition study" in USDOE[2].

** :Energy generated by burnup of fissile materials converted from Th and 238U was included.

***:Enrichment was regarded as 3.5w/o. This was evaluated from burnup of 37.1 GWd/t given in reference[2].

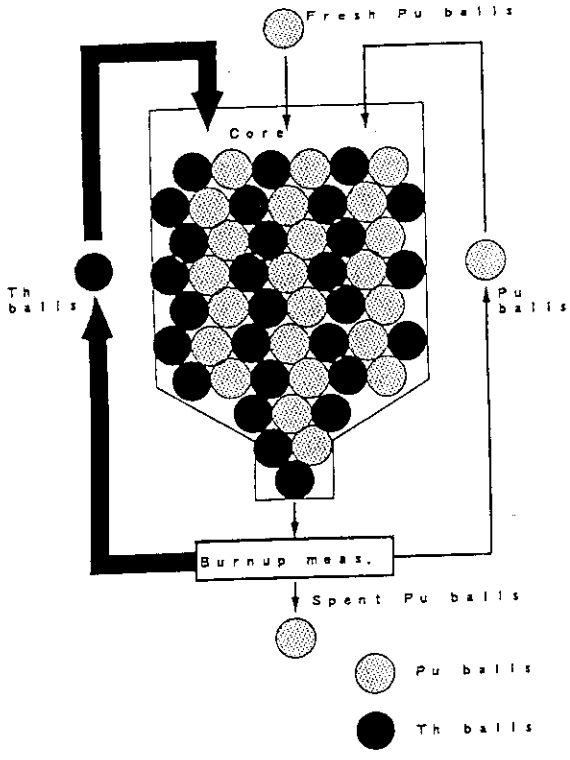


Fig. 1 Schematic movements of The Pu balls and Th balls

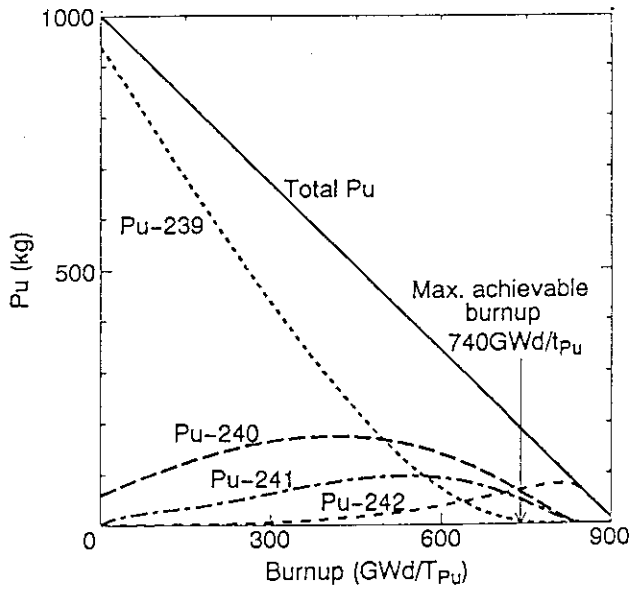


Fig.3 Change in amounts of Pu isotopes with burnup of Pu ball (Initial amount of Pu is normalized to 1000kg)

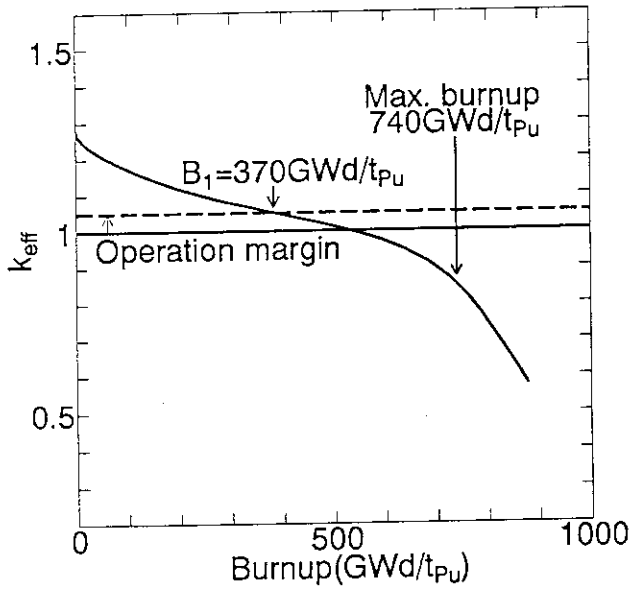


Fig. 2 Change in the effective multiplication factor k_{eff}

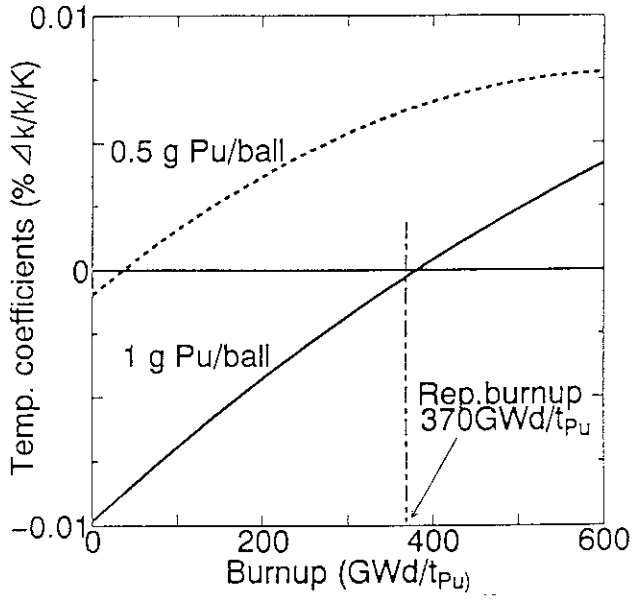


Fig. 4 Change in the isothermal temperature coefficients between 500 K and 900 K with burnup of Pu ball

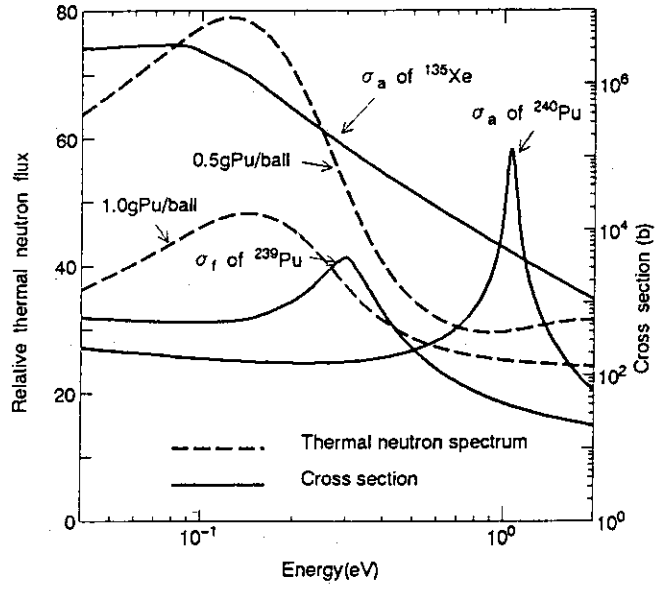


Fig. 5 Relations of thermal neutron spectrums with σ_a of ^{135}Xe, σ_f of ^{239}Pu and σ_a of ^{240}Pu

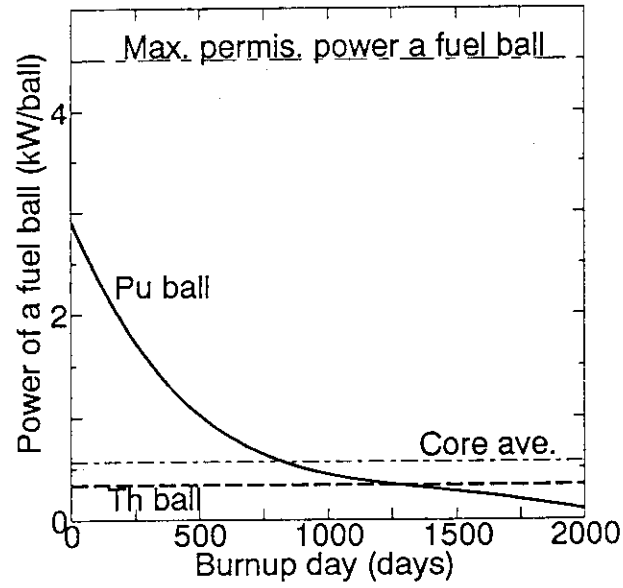


Fig. 6 Change in the Pu ball power with burnup days

6.18 Abstract of paper to be presented at "The 3rd JAERI Symposium on HTGR Technologies"

Title: Studies on Water Splitting Hydrogen Production

Authors: Kaoru ONUKI, Ryutaro HINO, Hayato NAKAJIMA, Masatoshi FUTAKAWA, Ikuo IOKA, and Saburo SHIMIZU (JAERI)

Abstract:

Hydrogen will play an important role in future energy system because of its ideal characteristics as an energy carrier. The high temperature gas-cooled reactor (HTGR) has a potential to spread the utilization of nuclear energy in the non-electricity energy sector. The hydrogen production using HTGR is therefore a quite attractive option in future energy system. In Japan, the importance of such a new technology should be emphasized because of the lack of domestic energy resources and the increasing requirement for cleaner energies.

Studies on two kinds of water splitting process for hydrogen production, i.e. thermochemical Iodine-Sulfur(IS) Process and high temperature steam electrolysis, have been conducted at JAERI which utilize high temperature nuclear heat supplied by HTGR.

IS process, which is composed of three chemical reactions, works as a chemical engine producing hydrogen driven by HTGR. A laboratory scale experimental study has been conducted to demonstrate the continuous hydrogen production by IS process, using a glass-made apparatus designed to include all the elemental unit operations. So far, stable production of hydrogen and oxygen at the rate of 1.5 liter-H_2/hr has been successfully demonstrated for over 8 hours. In parallel with the demonstration study, studies for improving the process thermal efficiency have been conducted focusing on the hydrogen iodide decomposition step. Also, a study on the materials of construction suitable for the corrosive process environments is under way for large scale realization of the process.

High temperature steam electrolysis is an advanced electrolysis process using solid oxide electrolytes working at high temperature ranging from 850℃ to 1000℃. The electrolysis process features its simple process scheme and lower working electricity than the conventional water electrolysis. Through laboratory-scale experiments, electrolysis cells such as tubular cells and planar cells have been developed to improve hydrogen production performance. Using a planar cell, hydrogen could be produced at a rate of 2.4 liter/hr at steam temperature of 850℃.

STUDIES ON WATER SPLITTING HYDROGEN PRODUCTION

Kaoru ONUKI, Ryutaro HINO, Hayato NAKAJIMA, Masatoshi FUTAKAWA,
Ikuo IOKA, and Saburo SHIMIZU

Japan Atomic Energy Research Institute

JAPAN

1. Introduction

Hydrogen has been widely recognized to have ideal characteristics as an energy carrier from the viewpoints of storability, low transportation loss, wide utilization area, and clean burning product etc. Emerging concern on the global environmental pollution accelerates the needs for such cleaner energies. On the other hand, the peaceful utilization of nuclear energy is still limited to the electricity production area, although it has been realized in industrial scale for over 40 years. The high temperature gas-cooled reactor (HTGR) has a potential to change the situation by supplying the nuclear heat for non-electricity energy carrier production. Therefore, the hydrogen production utilizing high temperature nuclear heat supplied by HTGR is a quite attractive concept in a future energy system. Especially, in Japan, the importance should be strongly emphasized because of the lack of domestic energy resources.

From these viewpoints, in JAERI, two kinds of innovative hydrogen production processes are under study. Both processes produce hydrogen by decomposing water utilizing nuclear heat supplied by HTGR, the maximum temperature of which is supposed to be ～950℃. One is a thermochemical Iodine-Sulfur (IS) process, which works as a chemical engine combining three chemical reactions. The other is a high temperature electrolysis of steam (HTES) process using a solid oxide electrolyte which shows large oxide ion conductivity at temperature range higher than ca. 800℃. The present status of the R&D's is presented in this paper.

2. IS Process

2.1 Outline of the Process

IS process is composed of the following three chemical reactions.

$$I_2 + SO_2 + 2H_2O = 2HI + H_2SO_4 \quad (1)$$

$$2HI = H_2 + I_2 \quad (2)$$

$$H_2SO_4 = H_2O + SO_2 + 0.5O_2 \quad (3)$$

Here, the sulfuric acid decomposition reaction (3) is an endothermic reaction, and the so-called Bunsen reaction (1) is an exothermic reaction. The process has a lot of attractive features such that all the chemicals circulate in the process in fluid state, the sulfuric acid decomposition proceeds stoi-

chiometrically with high conversion ratio and large entropy change at the temperature range of 800 ～900℃, etc. The process was first proposed by General Atomic Co. (GA)[1], and has been widely studied by several research institutions[2-4]. Studies on the catalysts for the gas phase decomposition reactions (2) and (3), on the separation method of HI and H_2SO_4, and on the process flowsheet etc. have clarified the basic characteristics of the process. The thermal efficiency of the process based on the Higher Heating Value (HHV) of hydrogen has been estimated using the thermodynamic data to be 46～52% depending on the process scheme and the operating conditions.

However, the process has not yet been demonstrated even in a laboratory scale. The main problems lie in the lack of knowledge on the complicated chemical reaction and separation phenomena relating to the Bunsen reaction step, and in the lack of construction materials suitable for the corrosive process environments. Therefore, we are studying on the following three subjects.

(1) Laboratory scale demonstration

To show the feasibility of the continuous hydrogen production by studying mainly on the chemistry relating to the four component system, HI-H_2SO_4-I_2-H_2O.

(2) Process improvement

To find alternative process schemes which improve the process thermal efficiency and mitigate the corrosive process environments, as well.

(3) Development of the structural materials and the reactor vessels

2.2 Laboratory Scale Demonstration

The simplified flowsheet of the laboratory scale demonstration apparatus is shown in **Fig. 1**. The apparatus was made of glass and can produce hydrogen at the rate of 1.5 liter (STP) per hour. It was designed based on the data acquired in our laboratory for the continuous operation. The detailed data and the mass flow's were reported elsewhere[2]. A brief description of the flowsheet is as follows.

The Bunsen reaction is carried out as gas absorption reaction with I_2

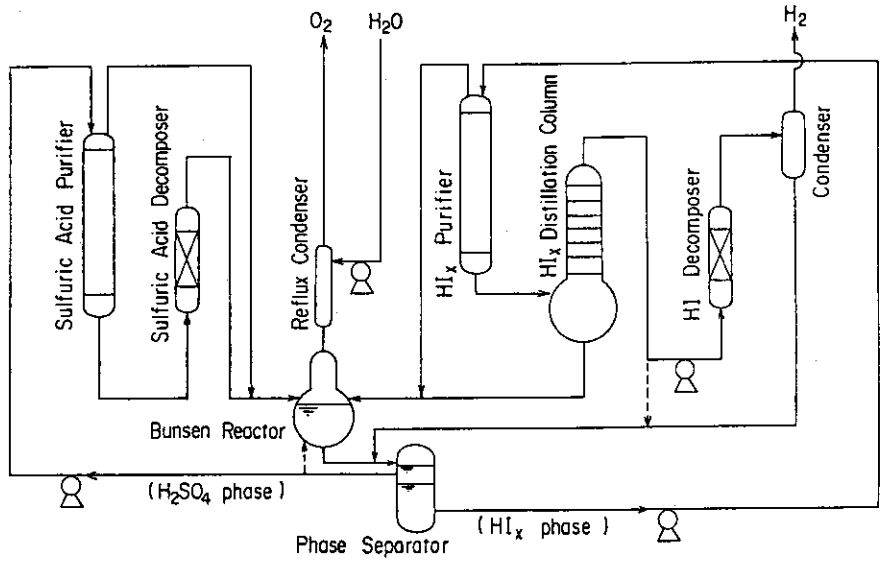


Fig. 1 Scheme of the labo-scale apparatus for IS process.

from the HI decomposition step, SO_2 from the H_2SO_4 decomposition step, and the feed water. The O_2 produced by the H_2SO_4 decomposition is separated in the Bunsen reactor by the selective absorption of SO_2. The HI and H_2SO_4 produced is separated owing to the liquid-liquid phase separation phenomena under presence of excess amount of iodine. The obtained HI rich phase (HI-I_2-H_2O system, so-called HI_x phase) is then purified to separate the minor component, H_2SO_4. Then, hydriodic acid (HI-H_2O) is separated from I_2 by distillation, and then vaporized and decomposed with Pt catalyst. The separation of H_2 from the product mixture is carried out by selective condensation of other components on cooling down. Similarly, the H_2SO_4 rich phase (H_2SO_4-H_2O system) is purified, concentrated, vaporized and decomposed with Pt catalyst.

So far, the stable and stoichiometric production of H_2 and O_2 for over 8 hours could be realized with the apparatus showing the continuous operation of the process is possible[5], although the process flowsheet was not optimized from the viewpoint of thermal efficiency. At present, modification of reactor designs is under study to overcome some technical problems still remaining. One problem is a condensation of I_2 at the Bunsen reactor inlet, which may cause a plugging. The other one is a gradual composition change of the phase separated solutions. **Fig. 2** shows a time profile of iodine concentration in the H_2SO_4 phase observed in the continuous operation experiment. The change is due to a decrease of HI content in the phase separator which causes the increase of I_2/HI ratio and the separation factor. The decrease of HI was estimated to be caused by the unsuitable design of either the Bunsen reactor or the HI decomposer. After achieving steady-state operation with the present flowsheet, it is planned to increase the operation temperature at the Bunsen reaction step to realize the continuous operation under efficient conditions.

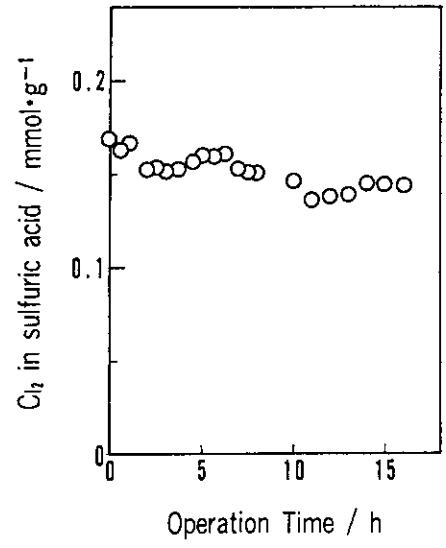


Fig. 2 Time profile of I_2 concentration in the sulfuric acid phase. (labo-scale demonstration exp.)

2.3 Process Improvement by Electrodialysis of HI_x solution

In IS process, the separation of HI and I_2 from the purified HI_x solution is carried out by distillation. With the atmospheric pressure distillation, azeotropic hydriodic acid is distilled, the molar ratio of which is $HI/H_2O \fallingdotseq 5/1$. Since the evaporation of the H_2O causes a decrease of the process thermal efficiency, efficient methods such as an extractive distillation using phosphoric acid[1], and a reactive distillation under high pressure ($\sim$ 20 bar)[3] have been proposed. However, the process environments of these methods are very corrosive and practical structural materials for the columns have not yet been found.

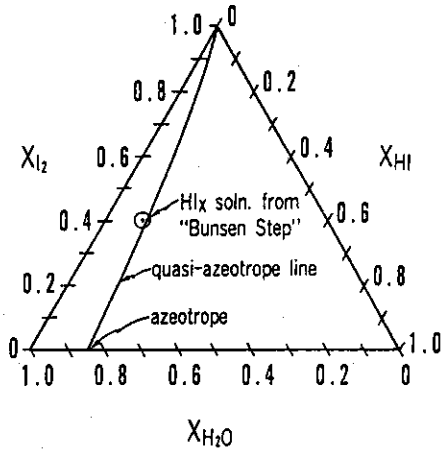


Fig. 3 VLE of HI-I_2-H_2O system.
(1) Quasi-azeotrope composition

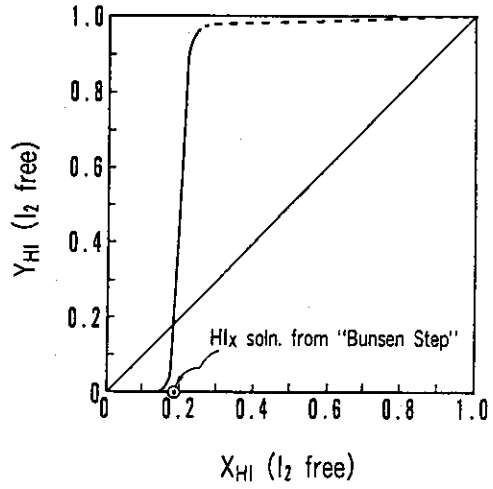


Fig. 4 VLE of HI-I_2-H_2O system.
(2) x-y curve at 40mol% iodine

Fig. 3 shows the quasi-azeotrope line of HI-I_2-H_2O system at 1 bar based on the thermodynamic data obtained at RWTH Aachen[6]. At the quasi-azeotropic composition, the HI/H_2O ratio in the vapor phase is equal to that in the liquid phase. In the figure, the composition of HI_x solution obtained from the Bunsen reaction step is also shown which is considered to be the "best" composition from the viewpoint of the process thermal efficiency. The figure shows that the HI_x solution from the Bunsen reaction step has a composition very close to the quasi-azeotropic one. In **Fig. 4**, the x-y curve of HI-I_2-H_2O system at 40mol% I_2 is shown, which indicates that the volatility of HI sharply increases in the higher HI composition region than the quasi-azeotropic one. From these facts, it is considered that highly concentrated HI could be obtained by distillation, if the HI_x solution from the Bunsen reaction step could be concentrated even slightly. The distillation environment would become far milder than the other proposals because of the low boiling temperature of the concentrated HI_x solution. The key technology to realize the concept is a method to concentrate the HI_x solution. From these viewpoints, the feasibility of the electrodialysis of HI_x solution is under study.

(1) Experimental

Fig. 5 shows a schema of the experimental apparatus. The electrodialysis cell was made of glass with a pair of ion exchange membranes(ϕ 20 mm), the distance between which is 28～40 mm. Glassy Carbon (Tokai Carbon Co.) was used as the electrode. Experiments were carried out by applying a

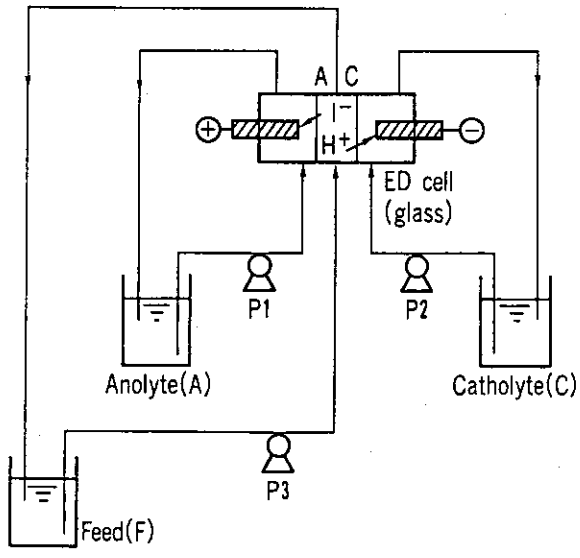


Fig. 5 Experimental Setup for Electrodialysis.

specified voltage while circulating three kinds of HI_x solutions (Anolyte, Catholyte, Feed) in the cell. The electrodialysis rate was calculated by measuring the content changes in each compartment of the cell, after applying the electricity equal to the several percents of the initial amount of HI. Ion exchange membranes tested were Selemion (CMV&AMV, ASAHI GLASS Co.), NEOSEPTA CMH (TOKUYAMA SODA Co.), Nafion 117 (Dupon Co.), and TOSFLEX IE-DF34 (TOSOH Co.).

(2) Results and Discussion

First, the current voltage relationship of the system was measured without the ion exchange membranes to see the electrode reactions. **Fig. 6** shows the results obtained by varying the iodine concentration. Here, the composition of the solution is expressed as HI_x(W %), where x is the ratio of $(I+I^-)/I^-$ in mol and W is the ratio of $HI/(HI+H_2O)$ in mass %. In the case of hydriodic acid (x=1.0), little current was observed up to 1.0V, and at the voltage higher than 1.5V current was observed with H_2 gas evolution at the cathode. On the other hand, with increasing the iodine concentration, current was observed proportional to the applied voltage without gas evolution, and the current was increased with the iodine concentration. The results indicate that the current observed in the HI_x solution is due to the following redox reactions,

$$I_2 + 2e \rightarrow 2I^- \quad \text{(cathode)} \qquad (4)$$

$$2I^- \rightarrow I_2 + 2e \quad \text{(anode)} \qquad (5)$$

while in the hydriodic acid electrolysis of HI occurs.

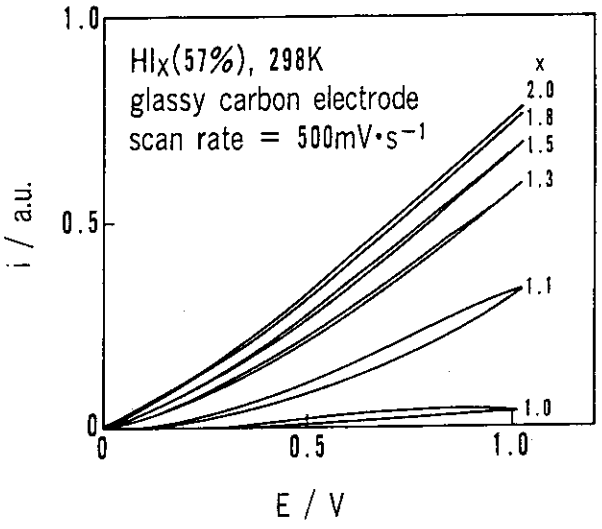


Fig. 6 Current-voltage relationship. HI_x(57%) soln./glassy carbon

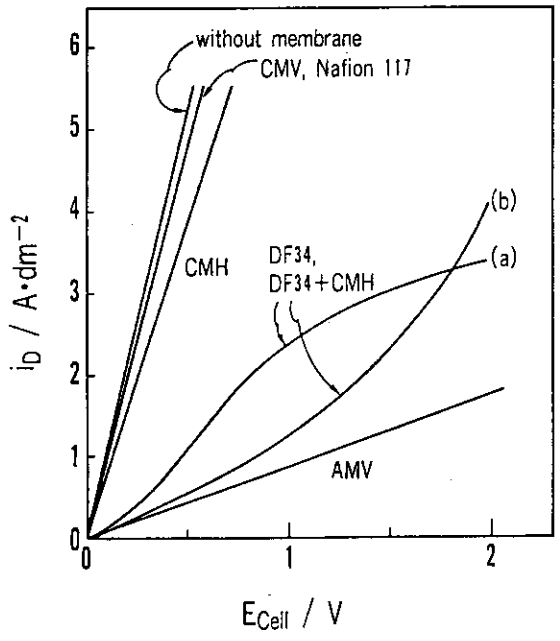


Fig. 7 Currnt density vs cell voltage with ion exchange membranes. $HI_{1.8}$(52%) soln./glassy carbon

Next, the electric resistance of the ion exchange membranes were measured. **Fig. 7** shows the relationships between current density and the cell voltage. Here, the curve (a) was obtained when the smaller ion exchange capacity side of DF34 was faced to the anode, and the curve (b) was obtained with the reverse setting of DF34. As seen in the figure,

Table 1 The Material Balance of the Electrodialysis of HI_x solution

Run No.	membrane	v_e*1)	v_i*2)			
				HI	I_2	H_2O
ED-12	CMV/AMV	0.15	Anolyte*3)	-0.04	+0.018	+0.04
			Feed*4)	-0.12	+0.054	-0.7
			Catholyte*3)	+0.14	-0.072	+0.9
ED-28	CMH/DF34	0.13	Anolyte*3)	-0.03	+0.041	-0.05
			Feed*4)	-0.12	+0.015	-0.4
			Catholyte*3)	+0.13	-0.054	+0.5

*1) current density in mmol-electron $\cdot h^{-1} \cdot dm^{-2}$. *2) changing rate of the component i in mmol $\cdot h^{-1} \cdot dm^{-2}$. *3) $HI_{1.8}$(54%). *4) $HI_{1.8}$(40%).

the electric resistance's of cation exchange membranes (CMV, CMH, Nafion 117) were far smaller than those of anion exchange membranes (AMV, DF34). The current density obtained when a pair of DF34 and CMH was set in the cell was nearly equal to that obtained when only DF34 was used. These results showed the required voltage is determined by the electric resistance of the anion exchange membrane.

Table 1 shows examples of the material balance obtained by the electrodialysis experiments. The following characteristics can be pointed out from the results.

① The sum of the changing rates of the three solutions equals to zero within experimental error in each component, indicating there was no net chemical change. This is due to the electrode reaction is a redox one, and also means the membranes were stable under the experimental conditions.

② In case the ion exchange membranes show ideal selectivity, the following changing rates, v_i, are expected compared with the current density, v_e.

Anolyte: $v_{HI} = 0$, $v_{I_2} = +0.5\ v_e$

Feed: $v_{HI} = -v_e$, $v_{I_2} = 0$

Catholyte: $v_{HI} = +v_e$, $v_{I_2} = -0.5\ v_e$

The experimental results of the catholyte are in accord with the expectation, indicating the cation exchange membranes shows good ion selectivity. On the other hand, the v_i's of the feed and the anolyte are smaller than the ideal ones, indicating the selectivity of the anion exchange membranes are low, and iodine permeates the membrane as well.

③ Water permeates through cation exchange membranes. The permeability was in the following order; CMV ≒ Nafion 117 >> CMH.

The ion selectivity governs the current efficiency, and the water permeation determines the concentration limit. The results shows the importance of the selectivity of anion exchange membrane and the water permeability of cation exchange membrane.

The above results clarified the required characteristics of the ion exchange membrane for the electrodialysis of HI_x solution. Among the membranes tested, the combination of CMH/DF34 was found to be promising. The following experiments will be carried out focusing on the characteristics such as current efficiency, concentration limit and required voltage considering the effects of the solution composition and temperature.

2.4 Structural Materials

The corrosion tests of commercially available materials in the representative process environments[2] clarified the difficulty of finding the structural materials for the concentrator and evaporator of sulfuric acid with the concentration of 50-96 wt% and for the distillation column of HI_x solution. We have adopted the following strategy on the problem. Concerning the latter environment, alternative process schemes such as the above mentioned electrodialysis should be pursued. While for the former environment, new materials and/or reactor vessels should be developed.

Following the strategy, corrosion resistance's of two candidate materials were examined in the boiling condition of 95-96% sulfuric acid. One candidate is ceramics such as SiC and Si_3N_4. Test tubes made of the ceramics were fabricated to examine the corrosion resistance under simulated condition of the evaporator. Sulfuric acid was filled in the test tube which was connected to a quartz condenser, and the test tube was heated in a cylindrical electric furnace. After heating for a specified duration under the reflux condition of the sulfuric acid, weight change of the test tube was measured. In the corrosion test of 1000 hrs, there was no detectable weight change in the both ceramics. At present, the effect of the environment on the mechanical properties of the ceramics is under study. The other candidate is a Fe-Si alloy. Using test pieces with different alloy composition, the effect of the alloy composition on the corrosion resistance was examined and found Si content of ca. 13 wt% is critical. The alloy with Si content below 13 % corroded severely while that with higher Si showed excellent corrosion resistance. At present, corrosion resistance of a new hybrid alloy is under study considering the Fe-Si alloy with Si content higher than 13 wt% is brittle. The bulk composition of the hybrid alloy is ca. 3 wt% Si which shows ductility, while the surface has a Si content of ca. 14 wt%.

3. HTES Process

3.1 Outline of the Process

In the water electrolysis, there is no commercial large scale units except the conventional alkaline electrolysis unit which have rather low current efficiency of 80% or less. Many advanced concepts have been proposed to improve hydrogen production efficiency and to reach high hydrogen production density. A water electrolysis using solid polymer membranes (solid polymer electrolysis, SPE) and a high temperature electrolysis of steam (HTES) using ceramic electrolysis cells are the representatives of new advanced technologies. Current efficiency of the SPE is of the order of 85-

90% in the laboratory-scale and prototype experiments, and that of the HTES is around 100% in the laboratory-scale experiments.

The theoretical electric energy demand decreases with increasing temperature; the electric energy demand in the HTES at 1000℃ is about 30% lower than the water electrolysis at room temperature. Also, high temperature operation helps lowering the electrode overvoltages, and increasing the current density. Thus, the HTES is favored from both thermodynamic and kinetic standpoints, i.e., lower cell voltage and higher current density are simultaneously achievable. Furthermore, there is little corrosion problem owing to the high corrosion resistance of the ceramic electrolyte.

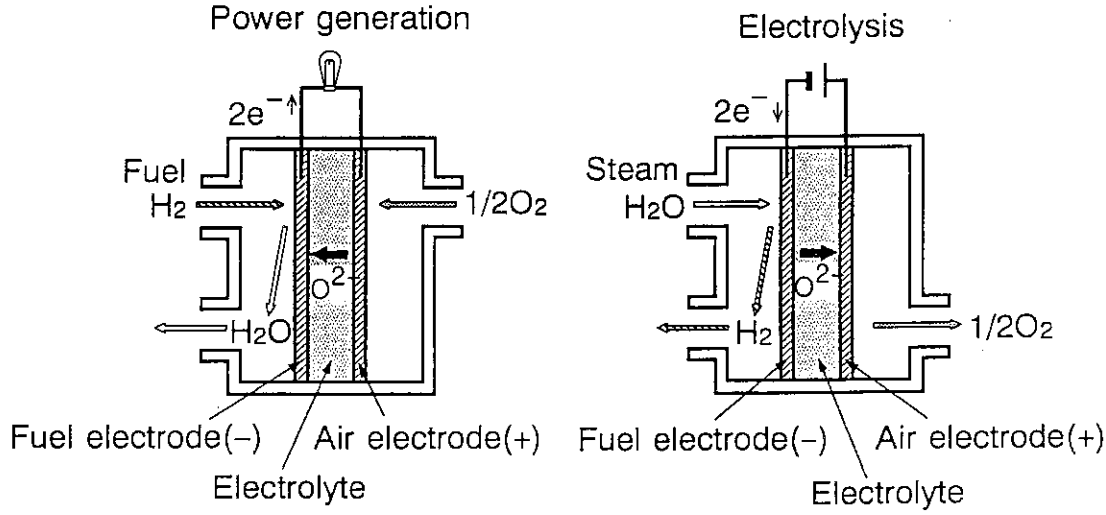
The process of HTES is a reaction reverse to solid oxide fuel cell (SOFC) being under vigorous development worldwide, where an oxide ion conducting solid oxide is mainly used as the electrolyte as shown in **Fig. 8**. The electrolysis cell consists of the gas tight electrolyte, a porous fuel electrode (cathode) and a porous air electrode (anode). The electrode reactions are expressed as follows.

$$H_2O(g) + 2e^- \rightarrow H_2(g) + O^{2-} \quad \text{(cathode)} \quad (6)$$

$$O^{2-} \rightarrow 0.5O_2(g) + 2e^- \quad \text{(anode)} \quad (7)$$

At the fuel electrode, hydrogen and oxide ion are produced from steam. The oxide ion produced migrates through oxygen vacancies in the lattice of the electrolyte, a mixed oxide such as ZrO_2/Y_2O_3. Oxygen is formed on the air electrode surface.

The HTES is at a very early stage of technology, and thus, significant development effort is required to solve severe problems relating to the materials and the fabrication techniques caused by the high temperature operation. We are now conducting laboratory-scale experiments to improve



at fuel electrode	$H_2+O^{2-} \rightarrow H_2O+2e^-$	$H_2O+2e^- \rightarrow H_2+O^{2-}$
at air electrode	$1/2O_2+2e^- \rightarrow O^{2-}$	$O^{2-} \rightarrow 2e^-+1/2O_2$
Total reaction	$H_2+1/2O_2 \rightarrow H_2O$	$H_2O \rightarrow H_2+1/2O_2$

Fig. 8 Principle of high-temperature electrolysis of steam (Reverse reaction of solid oxide fuel cell).

and upgrade the HTES technology. In the followings, recent progress is presented focusing on the test results obtained by a planar electrolysis cell.

3.2 Tubular-type Cell

At the beginning of the HTES tests, we used electrolysis tube of the banded-cell structure shown in **Fig. 9**. The electrolysis tube was composed of 12 electrolysis cells of 19mm in length.

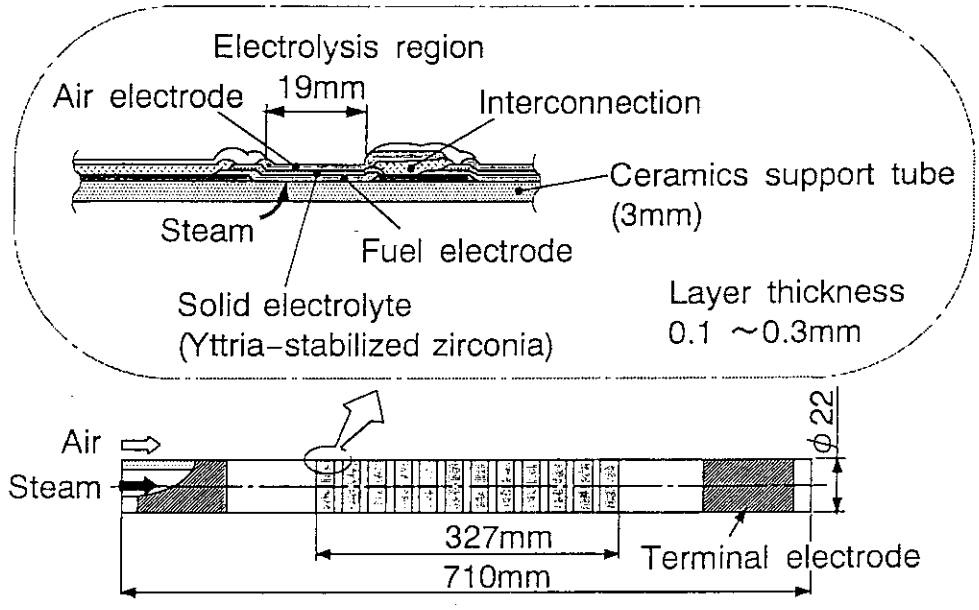


Fig. 9 Structural drawing of electrolysis tube with 12 cells.

These cells were connected in series electrically. The electrolyte was zirconia stabilized with 8 mol% yttria (YSZ) which is popular material in the SOFC as described before. The electrolyte layer was sandwiched between the porous electrode layers: Ni cermet for the fuel electrode and $LaCoO_3$ for the air electrode. At both ends of the electrolysis tube, platinum (Pt) wires were welded on copper coating layers for electric leads. Pt wires were connected with a DC power supply. The copper coating layers were connected with thin layers of the electric conductors. Outside of the electrolysis tube except the cells and the copper coatings was coated by thin gas tight layers. These layers were formed on a porous calcia-stabilized ZrO_2 tube (support

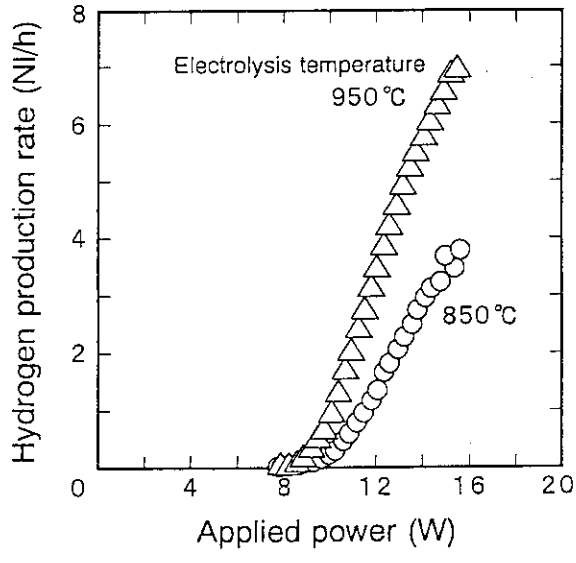


Fig. 10 Hydrogen production rate vs applied power. (Electrolysis tube)

tube or ceramic tube) of 22mm in outer diameter and 3mm in thickness by plasma spraying method. Thickness of each layers was in a range from 0.1mm to 0.3mm.

Fig. 10 shows a relationship between hydrogen production rate and applied power. Hydrogen was produced at the maximum rate of 3.9 Nl/h at 850℃, and at 7.0 Nl/h at 950℃, respectively. The maximum energy efficiency, a quotient of combustion heat of generated hydrogen/ applied power, was about 80% at 950℃. This rather low energy efficiency was considered to be caused by following reasons:

- Ohmic loss was high at the interconnections and the electric lead layers,
- Concentration overvoltage at the fuel electrode increased with the reaction progress, due to the high diffusion resistance of the support tube to steam and hydrogen.

In addition, the steam conversion ratio indicating an efficiency of steam utilization was less than 40%. The reason of the low steam conversion ratio was considered that steam could not permeate easily through the support tube to the cathode since the support tube had rather low porosity of around 38%. If steam could be supplied to the cathode sufficiently, hydrogen production rate would increase more than the present results. The self-supporting cell structure, therefore, is considered to be better in the HTES than the banded-cell structure supported by the ceramic tube.

3.3 Planar-type Cell

Then, we focused on the planar cells, particularly self-supporting planar cell, from the viewpoint of mass production of the cell. Quality control in the course of the cell fabrication is much easier than the banded-cell tube, and the fabrication technologies has been in great progress in the SOFC development. Present production cost of the self-supporting planar cell is 1/7 or less compared with that of the banded-cell tube and will be reduced further by mass production. In developing the HTES technology, especially in the electrolysis cell technology, cooperation with cell-production companies is indispensable. So, we have started to cooperate with Fuji Electric Co. who is obtaining good results in the planar type SOFC research field.

Fig. 11 shows a structural drawing of the self-supporting planar cell made by Fuji Electric Co. The cell consists of the electrolyte plate of YSZ and porous

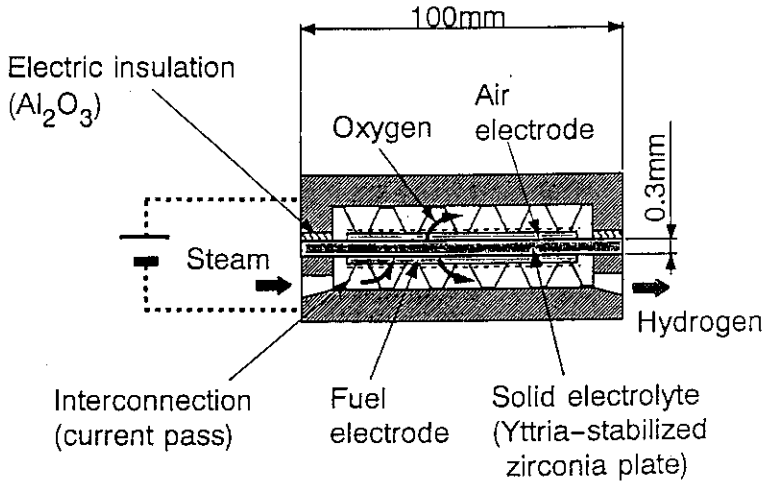


Fig. 11 Structural drawing of self-supporting planar cell.

electrodes. The YSZ plate is a 100mm square plate with thickness of 0.3mm, and electrodes are coated on the area of 80 x 80mm with thickness of less than 0.03mm. Material of the cathode is Ni cermet, and that of anode is strontium-doped $LaMnO_3$. The cell is sandwiched with metal housings made of SUS-310S. Each housings have a metal rod for the electric lead, an inlet and an outlet pipings for gases, and Pt sheet of 0.1mm thick is welded on inner surface of each housings opposite to the electrodes of the cell. Metal rods and pipings are also made of SUS-310S. DC power is supplied through the metal rods, housings, Pt sheets and wavy electrical lead plates of interconnections to the cell. The interconnection made of Pt mesh is installed in each electrode compartment to work as the support of the cell against the pressure difference between electrodes as well as the electric lead. Compression seals are done at the edge of the cell plate with the compression load up to 20kg. Then, an alumina sheet of 0.3mm thick is inserted between the cell plate and the housing in the anode side to prevent from current leak through the cell plate edge.

The cell with housings was installed in a electric furnace and was heated to the test temperature. Steam was supplied to the cathode compartment with argon and hydrogen gases from a steam generator. Argon gas was the carrier gas of steam, and hydrogen a reduced gas to keep Ni of the cathode material from oxidation. Dry air was supplied to the anode compartment. Steam flow rate was controlled by controlling water feed rate to the steam generator, and the flow rates of other gases were controlled by mass flow controllers. Hydrogen concentration was measured at the outlet of the cathode compartment by the gas chromatograph. Electrolysis voltage was applied by a DC power supply. The test was conducted under following conditions:

Electrolysis temperature : 850℃.
Inlet gas flow rate: 0.2 Nl/min (Ar),
0.1 Nl/min (H_2).
Steam flow rate : 0.3 g/min.
Air flow rate : 1 Nl/min
(dew point is less than -20℃).
Inlet pressure : ~0.14 MPa
(~1.4 bar(abs)).

Fig. 12 shows a relationship between hydrogen production and current densities: hydrogen production density is a hydrogen production rate per unit electrode area, and current density is a applied current per unit electrode area. The solid line shows the theoretical hydrogen production densities with the current

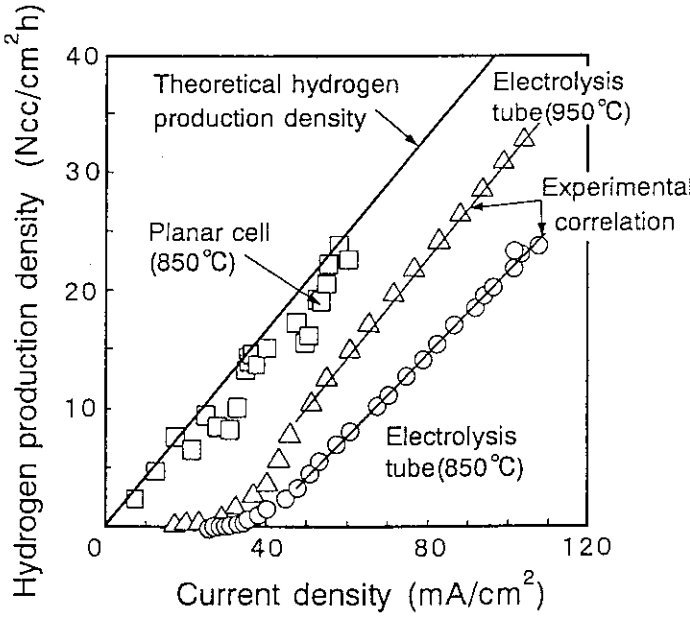


Fig. 12 Hydrogen production density vs current density. (Self-supporting planar cell & Electrolysis tube)

efficiency of 100%. Test results obtained with the electrolysis tube are also shown in the figure. In the case of the electrolysis tube, net hydrogen production starts at about 20mA/cm^2, which shows that there is large leak current. In test results obtained by the planar cell, there is almost no leak current, and the hydrogen production densities agree well with the theoretical values. The energy efficiency, however, was less than 50%, which was almost the same with that of the electrolysis tube at the same temperature, 850℃. This was considered to be caused by ohmic loss by contact resistance between electrodes of the cell and the interconnections. The interconnections is now being improved to reduce the contact resistance.

The planar cell shown in Fig. 11 was found to be fragile, especially it was easily damaged when installing in the metal housings. To improve the mechanical strength of the cell, new type electrolysis cell was fabricated as shown in **Fig. 13.** The cell was supported by the air electrode plate. The electrolyte and the fuel electrode layers were coated on the air electrode plate by plasma spraying to increase adhesion performance of those layers. The electrolysis test with this cell will be conducted from the end of this March.

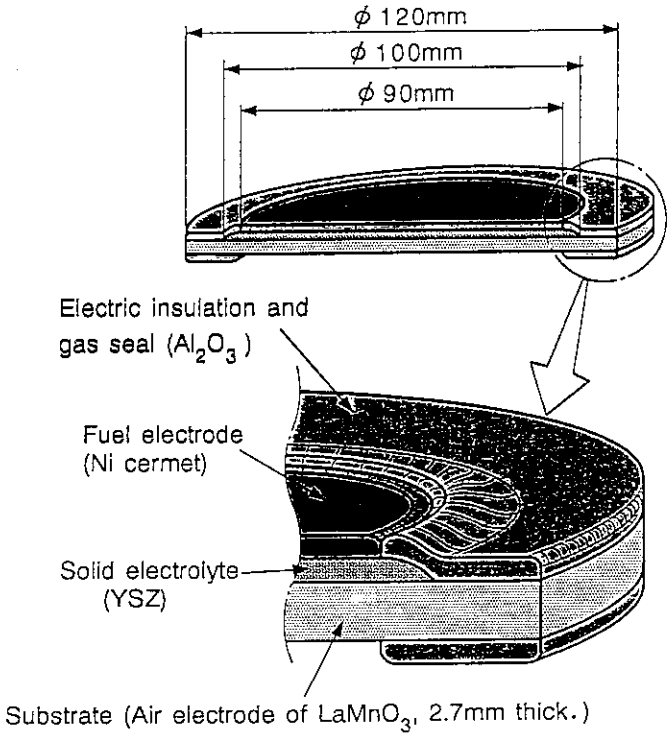


Fig. 13 Structural drawing of planar cell supported by air electrode plate.

References

(1) Norman, J. H. et al., GA-A16713, May 1982.
(2) Onuki, K. et al., JAERI-Review 94-006, Nov. 1994.
(3) Berndhäuser, C. and K. F. Knoche, Int. J. Hydrogen Energy, 19, 239-244(1994).
(4) Öztürk, I. T. et al., Trans IChemE, 72, Part A, 241-250(1994).
(5) Nakajima, H. et al., Proc. Int. Hydrogen and Clean Energy Symp. '95 (IHCE '95), Tokyo, Feb. 1995, pp.251-254.
(6) Neumann, D., Diplom Thesis, LTT RWTH Aachen, May 1987.

6.19 Transmutation of minor actinides (MA) with pebble bed type HTGRs

N. Fujimoto, K. Yamashita and K. Tokuhara

Department of HTTR Project
Japan Atomic Energy Research Institute
Oarai-machi, Higashiibaraki-gun, Ibaraki-ken 311-13, Japan

Abstract

It has been proposed to transmute minor actinides (MA) in LWRs, FBRs or actinide burning reactors. In FBRs and actinide burning reactor, MA is transmuted only about 10%. In LWRs, MA could not transmuted because MA is produce more than that of transmuted. Therefore, the large number of reprocessing process has to be carried out for further transmutation of MA repeatedly.

HTGRs can achieve higher burnup with its coated fuel particles. We have found a reactor system that can transmuted more of MA in fuel for one burnup cycle. This system is a pebble bed type HTGR using MA balls and Pu balls. The Pu is obtained from reprocessing LWR fuel. The criticality maintains with the Pu. MA is converted to fissile nuclides by neutron absorption reaction, then transmuted by fission reaction.

The fuels are loaded and removed from the core continuously. The burnups of the fuel ball are evaluated by measuring the strength of γ-rays when they are exhausted from the core. They are reloaded again if the burnups are still under the expected burnups. They are discharged form the reactor system as spent fuels if the expected burnups are achieved.

So for, the achievable burnup of the fuel is about 600GWd/t. The ratio of the residual MA to initially loaded MA is about 40%. The MA transmutation ratio is five times higher than that of reactors above mentioned. As the same time, about 50% of plutonium is also transmuted.

Moreover, it is expected that the MA will transmuted nearly 100% by many improvements. For example, MA balls are reloaded into the core more times than Pu balls, low outlet coolant temperature, diluted fuel kernel, and so on.

We think that the reactor system is one of the most promising options with which the transmutation of MA can be carried out effectively.

Transmutation of minor actinides(MA) with pebble bed type HTGRs

N. Fujimoto, K. Yamashita and K. Tokuhara

Department of HTTR Project
Japan Atomic Energy Research Institute
Oarai-machi, Higashiibaraki-gun, Ibaraki-ken 311-13, Japan

1. Introduction

Minor actinides (MA) transmutation is one of the superior way to reduce the amount of high level wastes from fuel reprocessing. So far, some MA transmutation nuclear reactor have been proposed such as fast reactor type transmutation reactor[1], transmuting MA in power reactor of FBRs or LWRs[1], etc..

MA has large neutron absorption cross section at thermal energy region. In thermal reactor, MA would be transmuted effectively under long irradiation duration. It is thought that high-temperature gas-cooled reactor (HTGR) can achieve high MA transmutation ration because HTGRs can achieve high fuel burnup with its coated fuel particle. Moreover, it is thought that HTGRs with reprocessed plutonium fuel produce less MA than uranium fueled HTGRs because reprocessed plutonium fuel contains less fertile nuclide than uranium fuel. Therefore, we think that HTGRs would achieve higher MA transmutation reactor. In this work, MA transmutation behavior of an HTGR-type MA transmutation reactor with reprocessed plutonium fuel have been studied. As a result, it is clear that the reactor can achieve about 50 % of MA transmutation ratio, also can achieve about 70 % of MA transmutation ratio by fuel loading improvement.

2. Outline of reactor

In thermal reactor, higher neutron absorption of MA brings higher MA transmutation

ratio. Higher neutron absorption of MA is resulted from higher fuel burnup. It is important to achieve high fuel burnup for high MA transmutation ratio. Therefore, we choose pebble bed type HTGR for MA transmutation reactor because of its high fuel burnup.

MA have large neutron cross section. The fuel of the reactor should contains much fissile materials than that of commercial LWRs, etc.. Moreover, a fuel which contains less fertile nuclide produce less MA during burnup. Therefore, we choose a reprocessed plutonium as the fuel of the reactor. About 70% of the reprocessed plutonium is fissile nuclides. The reprocessed plutonium fuel would contribute to effective utilization of fissile materials instead of high-enriched uranium fuel.

The fuel is a ball-type fuel which consists of coated fuel particles with MA and plutonium fuel kernel. The fuel balls are loaded into the core from the top of the core. The balls move from top to bottom in the core, then they are removed to outside from the bottom of the core. The fuel balls removed from the core are checked its burnup. The fuel balls which do not attain a burnup limit, are reloaded into the core again. The fuel balls which attain the burnup limit are removed from the reactor as spent fuels. The fuel loading procedure have been demonstrated at the AVR[2].

Table 1 shows a major specification of the reactor and fuel. The power density and fuel specification are based on the design of HTR-module of Germany. Isotope composition of MA and plutonium is based on the isotope composition of LWR spent fuel with five years cooling. The ratio of fissile plutonium to the total heavy metals is 50% and an initial loading amount of heavy metals is about 250kg. The fuel specification aims not only higher burnup but also much heavy metals loading in the core.

3. MA transmutation behavior

MA transmutation behavior is evaluated by changes in MA amount during burnup obtained by lattice cell burnup calculation. The calculation was carried out with lattice cell

model of coated fuel particle with MA and plutonium fuel kernel. The calculation was carried out by SRAC[3] code with JENDEL-3 nuclear data library.

Figure 1 shows a change in an effective multiplication factor k_{eff} with burnup. The burnup is based on the amount of MA and plutonium initially loaded in the core. In the reactor of continuous refueling, the reactor can achieve a burnup of which the area that k_{eff} is higher than 1.0 (as shown A) is equal to the area that k_{eff} is less than 1.0 (as shown B)[4]. From the Fig. 1, the reactor can achieve about 500GWd/T of burnup. The burnup is achieved by 630 days of effective full power operation (630EFPD).

Change in MA amount in the core are shown in Fig. 2. At the maximum burnup of about 500 GWd/T, ^{237}Np and ^{241}Am are reduced to about 50 % and 6 % of initial loading amount, respectively. ^{234}Am and ^{244}Cm are slightly increased due to neutron absorption of another nuclide. However, the amount of increase is little compared to the decrease of ^{237}Np and ^{241}Am. In the model, total amount of MA is reduced to about 57% of initial loading amount. In the model, MA and plutonium are loaded into same ball. Therefore, we call this model as MA mixing model.

Higher MA transmutation ratio would be achieved by longer irradiation duration of MA. Therefore, new fuel loading procedure is applied. The fuel are separated into two kinds of fuel balls. One is a fuel ball which contains MA coated fuel particle (MA ball), another is a fuel ball which is a fuel ball that contains plutonium coated fuel particle (Pu ball). These fuel balls are loaded into the core randomly. The Pu ball are removed from the core when a burnup limit attained. However, MA balls stay more time in the core than the Pu balls. This model is called MA separation model.

Figure 3 shows a change in MA with the MA separation model. In the case, Pu balls are removed from the core when its attain a burnup equal to 500GWd/T which is shown in Fig.1. In the case, a transmutation velocity of ^{237}Np is decreased with increasing burnup. The ^{237}NP is reduced to about 15% of initial loading amount at the 1900 EFPD. The 1900 EFPD

is equal to three times of the duration in which the fuel can achieve 500GWd/T at the case shown in Fig. 1. Total amount of MA is also reduced to about 15% of initial loading amount.

Table 2 shows a comparison of MA transmutation performance in various kind of MA transmutation reactors. L-ABR[1] is a Pb-cooled metal fuel actinide burner reactor, P-ABR[1] is a particle bed type of actinide burner reactor. The L-ABR and P-ABR are both proposed by JAERI. U-PWR[1] is a PWR power reactor in which MA is mixed with uranium fuel. MOX-FBR[1] is a mix-oxide fuel FBR power reactor in which MA is added into the fuel. LMR is a liquid metal cooled metal fuel fast reactor in which MA is added into the fuel. The L-ABR and P-ABR achieve about 20 % of MA transmutation ratio because these reactor achieve about 100GWd/T. The U-PWR achieve about 10% of MA transmutation ratio only. It is because that ^{238}U contained in the fuel produce much MA by neutron absorption reaction. The MOX-FBR and LMR achieve about 40% of MA transmutation ratio due to its long cycle length.

In the HTGR type reactor, about 40% of MA transmutation ratio can be achieved. Moreover, about 70% of MA transmutation ratio can be achieved in MA separation model.

In the expression of MA transmutation per 1GW per year, The L-ABR and P-ABR transmute much more than HTGR type of reactor, However, HTGR type of reactor can achieve higher MA transmutation that of U-PWR, MOX-FBR and LMR.

4. Conclusion

The MA transmutation behavior of HTGR type MA transmutation reactor with plutonium fuel have been studied. As a results, it becomes clear that the reactor can achieve about 40% of MA transmutation ratio per burnup cycle with fuel burnup of 500GWd/T. In each element of MA, ^{237}Np is transmuted up to about 50%, ^{243}Am and ^{244}Cm are increased during fuel burnup. However, the amount of increase is small and half-life of these nuclide are shorter than that of ^{237}Np. Therefore, effective half-life of MA is shortened. In MA separation model,

in which MA fuel balls and Pu fuel balls are loaded into the core, MA transmuted up to about 70%. The higher MA transmutation ratio can contribute to decrease the times of fuel reprocessing.

Plutonium coated fuel particles have been irradiated and demonstrated its integrity up to 600GWd/T[5]. The burnup of 500GWd/t of the reactor is based on MA and plutonium in the reactor, then it is equivalent to 700 GWd/T for plutonium coated fuel particle. therefore, the value of 500GWd/T of the reactor has a possibility with further investigation.

From these results, HTGR type of MA transmutation reactor has a possibility to further investigation.

Reference

(1) Atomic Energy Society of Japan, "Present Status of Transmutation Research and Development", 1994

(2) IAEA,"Operating Experience with Nuclear Power Stations in Member States", (1974-1989)

(3) Tsuchihashi, K., et al., "Revised SRAC Code System", JAERI 1302 (1986)

(4) Graves, H.W.,"Nuclear Fuel Management",John Wiley & Sons, New York (1979)

Table 1 Major specification of reactor and fuel

Reactor type	Pebble bed type HTGR	
Thermal output	200MW	
Power density	3W/cc	
Fuel composition	Pu	MA
	^{239}Pu : 60%	^{237}Np : 50%
	^{240}Pu : 25%	^{241}Am : 35%
	^{241}Pu : 10%	^{243}Am : 10%
	^{242}Pu : 5%	^{244}Cm : 5%
Initial Loading amount	Pu : 180kg MA : 72kg	
Loading amount per fuel ball	Pu : 1g/fuel ball MA : 0.4g/fuel ball	

Table 2 Comparison of MA transmutation in various reactors

	HTGR type reactor		L-ABR[1)]	P-ABR[1)]	U-PWR[1)]	MOX-FBR[1)]	LMR[1)]
	MA mixing model	MA separation model					
Thermal power (MW)	200	200	180	1200	3410	2600	2632
Cycle length (EFPD)	630	1900	550	300	850	1368	900
MA loaded (kg)	72	72	573	1865	180	1450	1200
MA transmutation*) (%/cycle)	43	70	16.0	18.8	9.0	33.5	29.8
MA transmutation*) (kg/1GW·year)	75	40	278	292	1.7	40.9	44.5

*) $MA\ transmutation = \frac{MA(BOC)-MA(EOC)}{MA(BOC)}$

MA(BOC) : Amount of MA at the beginning of cycle

MA(EOC) : Amount of MA at the end of cycle

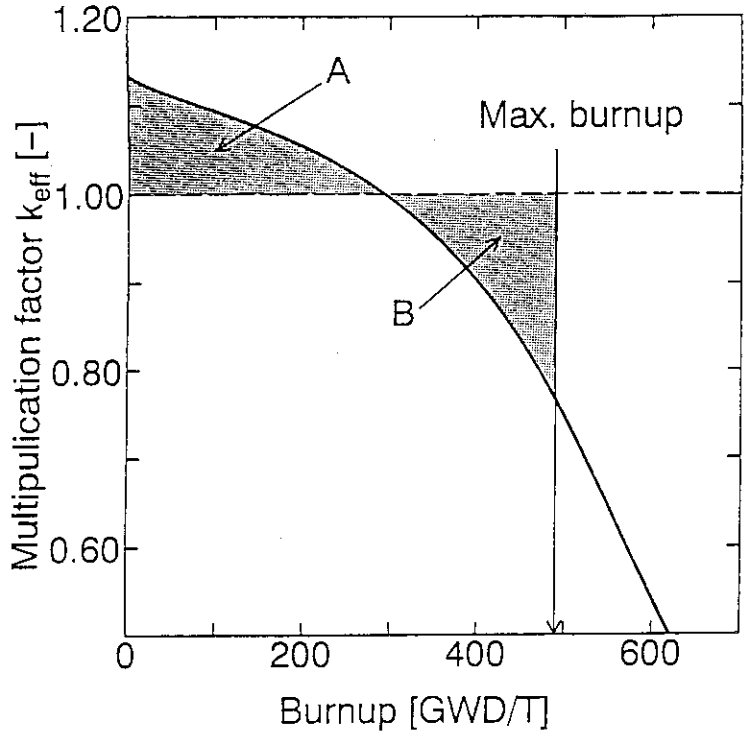


Fig. 1 Change in effective multiplication factor with burnup

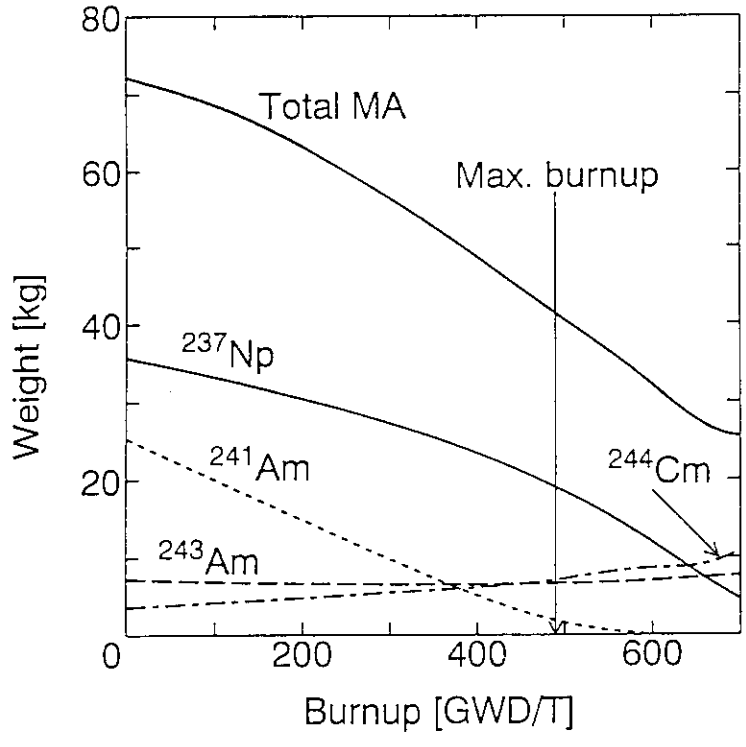


Fig. 2 Change in MA amount and composition with brunup under MA mixing model

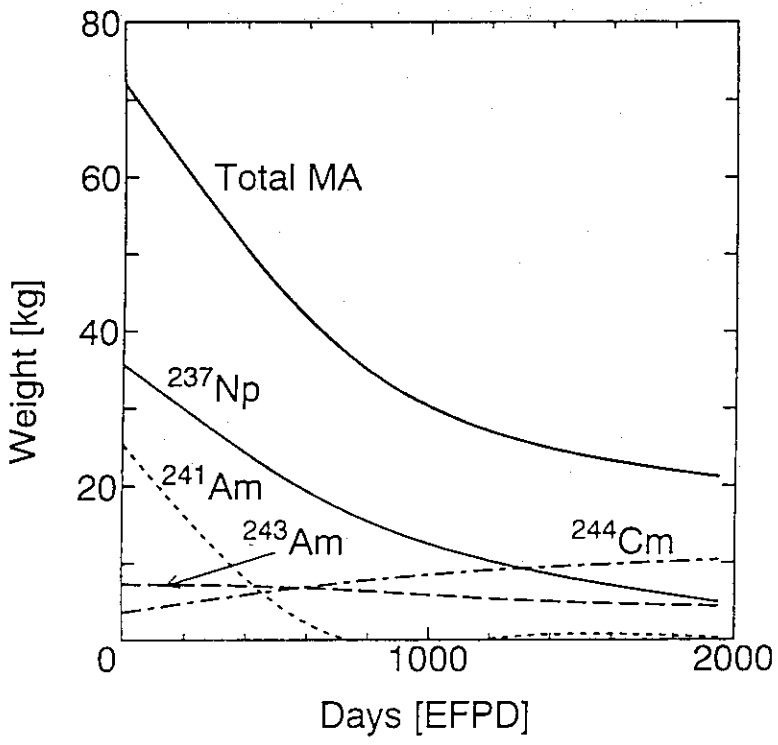


Fig. 3 Change in MA amount and composition with burnup under MA separation model

6.20 Start-up Physics Test Plan of the HTTR

M.TAKEUCHI, N.FUJIMOTO, T.TAKEDA, K.TOKUHARA,
S.NAKAGAWA, N.NOJIRI, H.SAWAHATA and K.YAMASHITA

Department of HTTR Project
Japan Atomic Energy Research Institute
Narita-cho, Oarai-machi, Ibaraki-ken, 311-13 JAPAN
Ph: 029-264-8532 / Fx: 029-264-8486

Abstract

The initial fuel loading of the High Temperature engineering Test Reactor (HTTR) is scheduled to start in the middle of 1997. The first criticality is expected in December 1997. The start-up physics tests are planned in the period from the middle of 1997 to the end of 1998. The full power operation will be achieved in December 1998. The items of the start-up physics tests are selected from the following two viewpoints,

(1) to carry out the function tests necessary for governmental inspection
(2) to grasp the HTTR's characteristics

The first criticality is approached by replacement of mock fuel blocks with fresh fuel blocks. The replacement begins from the outer fuel column bordering the side graphite reflectors. The first criticality will be attained when all outer fuel columns are replaced with fresh fuel blocks. The horizontal profile of fuel region becomes a ring form.

The excess reactivity will be measured with two methods. One is the fuel addition method. The excess reactivity is obtained by addition of reactivity of each fuel column. In the other method, the excess reactivity is evaluated from the control rod reactivity worth curve. The reactivity is measured by the inverse kinetics method for the both methods.

The temperature coefficient is measured in isothermal conditions. The core is heated up to 150°C by energy injected with helium circulator of the main cooling system.

In the reactor scram, the control rods are inserted in two steps to avoid a damage of control rods by high temperature exposure in the core. At first, the control rods in the side reflector are inserted. Secondly, the control rods in the core are inserted after the reactor outlet coolant temperature becomes 750°C or the time of 2400 sec is elapsed after the scram. The subcriticalty is measured continuously by the neutron multiplication method. The applicability of the neutron multiplication method is tested in the Very High Temperature Reactor Criticality Assembly (VHTRC).

The measurements for reactor shutdown margin, kinetics parameters, power coefficient, etc. are carried out also in the start-up physics tests. The power adjustments are carried out in the low and high power. The data obtained through all tests are used for the validation of nuclear design code systems, in combination of the VHTRC tests and as well as for understanding the HTGR's characteristics.

Start-up Physics Test Plan of the HTTR

Mitsuo TAKEUCHI, Takeshi TAKEDA, Nozomu FUJIMOTO, Kazumi TOKUHARA,
Shigeaki NAKAGAWA, Naoki NOJIRI and Kiyonobu YAMASHITA

Department of HTTR Project, Oarai Research Establishment,
Japan Atomic Energy Research Institute

Abstract

Start-up physics tests (SPTs) of the High Temperature engineering Test Reactor (HTTR) are planned to establish High Temperature Gas-cooled Reactor (HTGR) technologies and to be used for the validation of the HTGR core design code system. The SPTs consist of first criticality approach, measurement of reactivity change after scram and so on. At the first criticality approach, mock-up fuel blocks are replaced with flesh fuel blocks. The replacement begins from outer columns bordering the side reflector block to obtain core physics data of the ring type core. Reactivity of the Control Rods (CRs) are measured by the Inverse Kinetics method. Excess reactivity and reactivity shut down margin are measured by using the CR worth curve. This paper describes purposes, conditions and expected results of the SPTs.

1. Introduction

The High Temperature engineering Test Reactor (HTTR)[1] which is under construction by Japan Atomic Energy Research Institute (JAERI) is a graphite-moderated and helium gas-cooled reactor with an outlet temperature of 950°C and thermal output of 30MW. Start-up physics tests (SPTs) of the HTTR are planned to establish the High Temperature Gas-cooled Reactor (HTGR) technologies and to be used for the validation of the HTGR core design code system[2],[3],[4]. Table 1 shows the schedule for the SPTs of the HTTR. The first criticality is expected in December 1997. The SPTs are planned in the period from the middle of 1997 to the end of 1998. The power elevation begins in the middle of 1998.

The SPTs are first criticality approach, measurement of reactivity change after scram and so on. The first criticality is approached by replacing mock-up fuel blocks with flesh fuel blocks. The replacement begins from the outer fuel column bordering the side graphite reflectors, thus the horizontal profile of the fuel region will become a ring form at the first criticality.

Reactivity is controlled by Control Rods (CRs) which are individually supported by CR drive mechanism. The CRs are inserted into control rod guide columns in the

fuel and replaceable reflector regions. In the scram, the two-step CR insertion method[5] is employed mainly to prevent the CR sleeves in the fuel region from overheating. First, 9 pairs of the CRs are inserted immediately into the reflector region at the time of a scram. Second, the other 7 pairs are inserted into the fuel region after the reactor outlet coolant temperature decreases to 750°C or the time of 2400seconds is elapsed after the scram. Both change in reactivity from the CR insertion into the reflector region to that into the fuel region are measured by the Inverse Kinetics (IK) method[6].

The overview of the HTTR core and the instrumentation for monitoring the neutron and temperature are described in chapter 2 and 3, respectively. Chapter 4 shows the purposes, conditions and expected results of the SPTs.

2. Overview of the HTTR core

Table 2 shows the major specifications of the HTTR. The active core, 2.9m in height and 2.3m in equivalent diameter, consists of 30 fuel columns and 7 CR guide columns. Vertical and horizontal cross sections of the HTTR are shown in Figs. 1 and 2, respectively. Each fuel column consists of 5 fuel blocks and 4 graphite blocks of the top and bottom reflectors. Fig. 3 shows the structure of a pin-in-block type fuel (fuel block) used in the HTTR. A fuel rod consists of a graphite sleeve with 14 fuel compacts. Fuel rods are inserted into coolant holes of fuel blocks. Each fuel compact consists of Coated Fuel Particles (CFPs) embedded in the graphite matrix. The coolant gas flows downwards through annular channels formed by a graphite block and fuel rods. Burnable Poison (BP) which consists of boron carbide is inserted into the holes under the dowel pins.

3. Instrumentation

3.1 Temporary neutron instrumentation system

Temporary neutron instrumentation system is used in air atmosphere. The detectors for instrumentations of temporary BF_3 counter, temporary Fission Counter (FC) and temporary Compensated Ionization Chamber (CIC) are located at three irradiation holes (E05, E13 and E21) as shown in Fig. 4. The temporary BF_3 counter instrumentation is designed to monitor the state of reactor core loaded partially with fuel blocks. The temporary FC instrumentation is used to measure the axial neutron flux distribution and the reactivity shutdown margin with the Rod Drop (RD) method for the initial core construction. The temporary CIC instrumentation is used to measure the CR worth by the IK method.

Table 3 shows the major specifications of the detectors for the temporary

neutron instrumentation system. The pre-amplifiers for the instrumentations of the temporary BF_3 counter and the temporary FC are located outside the reactor vessel. The pulse signal from the pre-amplifier is gained by the linear amplifier and then is transferred to the count rate meter and the recorder through the pulse signal shaping circuit. The current signal from the detector for the temporary CIC instrumentation is converted into the voltage signal through the amplifier with the gain from 10^1 to 10^7. This voltage signal is transferred to the recorder and the computer.

3.2 Permanent neutron instrumentation system

Permanent neutron instrumentation system is used in helium gas atmosphere. Table 4 shows the major specifications of the detectors for the permanent neutron instrumentation system. The permanent neutron instrumentation system consists of the wide range monitoring system (WRMS), the power range monitoring system (PRMS) and the BF_3 counter instrumentation system. The WRMS and the PRMS have three channels each and are used actually for the safety protection system. The signal from the PRMS is used to control the reactor power. The BF_3 counter instrumentation system has three BF_3 proportional counters and is not included in the safety protection system.

When the reactor is started up, the WRMS monitors the neutron flux in the power range from 10^{-8}% to 35% by one FC. Since the FC is located at the top of a permanent reflector as shown in Fig. 5, it is designed to endure the high temperature condition of 600°C at this position. On the other hand, the PRMS monitors the neutron flux during the reactor operation in the power range from 0.1% to 120% by one UIC. The UIC covered with the guide tube is located in the inner concrete surrounding the reactor vessel as shown in Fig. 5. Since the neutron flux from 1.45×10^4nv (0.1% reactor power) to 1.45×10^7nv (120% reactor power) is very low around the UIC, each channel of the PRMS is composed of three UICs which are high sensitivity to the neutron. The neutron flux after the scram is measured by the BF_3 counter which is located above the UIC in the guide tube as shown in Fig. 5. The signal from three instrumentation systems above-mentioned is used to evaluate the core characteristics (the CR reactivity worth, reactivity shutdown margin, temperature coefficient of reactivity, etc.). The core characteristics are evaluated by the IK method, the RD method and the period method.

3.3 Temperature measurement system

In order to monitor the core outlet coolant temperature, 4 thermocouples are arranged at each hot plenum block. The N-type thermocouples (Nicrosil-Nisil) are

used because the deviation of thermo-electromotive force is small compared with the other type thermocouples in a high temperature region. Fig. 6 shows the arrangement of thermocouples in the hot plenum block. In order to monitor the temperature of the core internal structure (the permanent reflector block, core restraint mechanism, side shielding block, carbon block, etc.), about 100 thermocouples are arranged inside the reactor pressure vessel.

4. Start-up physics tests

4.1 First criticality test

The purpose of this test is to make up a reactor core so as to achieve first criticality in room temperature and in air atmosphere. The first criticality is approached by replacing the mock-up fuel blocks with the flesh fuel blocks. The mock-up fuel blocks are replaced in the fuel column which consists of 5 fuel blocks and 4 graphite blocks of the top and bottom reflector. In order to obtain core physics data of the ring type core, the replacement begins from outer columns boarding the side reflector blocks in clockwise as shown in Fig. 4. The criticality is estimated by the Inverse Multiplication (IM) method. The measurement of the criticality is conducted at the columns of 12, 15, 18, 19, 20, etc. and the first criticality may be attained at about 20 columns loaded into the core.

During the test, a neutron flux level is measured by the temporary BF_3 counters and the temporary CICs. Three temporary BF_3 counters measure neutron count rate with the IM method. Two temporary CICs are used to confirm the first criticality of the core. These temporary neutron detectors and one temporary neutron source are installed into three irradiation columns at the corner of the reflector region. Criticality mass determined by the test is used to confirm the validity of the HTGR core design code system.

4.2 Initial core construction

The purpose of this test is to construct an initial reactor core loaded fully with the fresh fuel blocks in air atmosphere. The excess reactivity and the reactivity shutdown margin of the representative reactor core are measured by the IK method or the RD method. In the IK method, the increase in reactivity of the core is obtained from the neutron flux change. In the RD method, the reactivity worth of the CRs are obtained from by the integral. We confirm that these measured values satisfy the criteria as follows :

(1) The excess reactivity is below 0.165Δk/k.

(2) The shutdown margin exceeds 1%Δk/k in stuck condition of a pair of the CRs.

4.3 CR reactivity worth test

The purpose of this test is to obtain the reactivity worth curves of the CRs in air and helium gas atmosphere. After constructing the initial core, integrated reactivity worth curves and reactivity worth of each pair of the CRs are obtained by the IK method. We confirm that these measured values satisfy the criteria as follows :

(1) Reactivity addition rate of each CR is below $2.4\times10^{-4}\Delta k/k/s$.

(2) Reactivity by the CRs without a pair of the CRs which has maximum reactivity worth exceeds $1.8\times10^{-1}\Delta k/k$.

4.4 Excess reactivity test

The purpose of this test is to measure excess reactivity of fully loaded reactor core by estimating reactivity worth of the CRs inserted into the fuel region and in air and helium gas atmosphere. The reactivity worth of the CRs inserted into the critical core is defined as the excess reactivity. The reactivity worth of all the CRs inserted into the critical core is obtained by using the reactivity worth curves. The excess reactivity is determined considering the interaction and temperature effects of the CRs. Since the excess reactivity of the initial core is equal to the reactivity worth of the CRs inserted into the critical core, the excess reactivity is obtained by estimating the reactivity worth of the CRs from the reactivity worth curves. The criterion of the excess reactivity is below $0.165\Delta k/k$ and we confirm that this measured value satisfies the criterion.

4.5 Reactivity shutdown margin test

The purpose of this test is to measure reactivity shutdown margin of the core in air and helium gas atmosphere in case that all the CRs are inserted except a pair of the CRs which has maximum reactivity worth. The reactivity shutdown margin of the core is obtained by the RD method, while the CR worth curve is obtained by the IK method. The criterion is that the reactivity shutdown margin exceeds $1\%\Delta k/k$. We confirm that these measured values satisfy the criterion.

4.6 Nuclear power correlation test

The purpose of this test is to adjust the WRMS to the nuclear reactor power in air and helium gas atmosphere by the reactor noise analysis using the two-detector correlation method[7], which can be eliminated the detector noise component. The reactor noise is based on statistical nuclear reaction phenomena. The use of two detectors with independent electronic circuits for direct analysis of the spectral density brings mutual elimination of the detector noises.

At zero power after the initial core construction, it is necessary to adjust the WRMS. The nuclear reactor power is measured by the reactor noise analysis using the two-detector correlation method. The validity of the reactor noise analysis is confirmed by comparing the nuclear reactor power obtained through the reactor noise method with that measured by using the temporary FCs which are calibrated beforehand. The critical points are confirmed in the neighborhood of the reactor power of 8W in both air and helium gas atmosphere, 80W and 800W in helium gas atmosphere. The reactor noise instrumentation (the temporary CICs, pico-ammeter, band pass filter, etc.) is located out of the reactor vessel. It is also connected to the instrumentations through the electric cables. Two pico-ammeters not only multiply output electric current of two CICs but also transform the current into voltage. Two band pass filters measure the reactor noise in the neighborhood of its center frequency. In order to obtain the nuclear reactor power, mean electric current and voltage of two temporary CICs and the transfer function of the instrumentations are measured. The transfer function of the reactor core is evaluated by using the center frequency of the band pass filters, an effective delayed neutron fluctuation of β_{eff} and a mean prompt neutron life time of ℓ. Final, the WRMS is adjusted to the nuclear reactor power by the reactor noise analysis.

4.7 Measurement of maximum reactivity insertion rate

The purpose of this test is to confirm that the maximum reactivity insertion rate is below the limit of $2.4\times10^{-4}\Delta k/k/sec$ in air and helium gas atmosphere. The CRs are categorized into 4 groups (C-, R1-, R2- and R3- CR) by its horizontal position in the core as shown in Fig. 4. The C-CR is located at the center of the core. The R1-CRs have 6 pairs of the CRs and are located in the fuel region. The R2-CRs have 6 pairs of the CRs and are located in the removable reflector region. The R3-CRs have three pairs of the CRs and are located at the corner of the removable reflector region. The maximum reactivity insertion ratio is measured in every CR groups. The reactivity insertion ratio is the amount of differential CR reactivity worth divided by the maximum CR insertion speed of 10mm/s. The differential reactivity worth of the CRs in each group is measured by the CR reactivity tests in advance. The reactivity insertion ratio is evaluated from the reactivity worth curves and insertion speed of the CRs.

4.8 Measurement test for kinetics parameter

The purpose of this test is to determine the value of β_{eff}/ℓ at critical state experimentally in air atmosphere, where β_{eff} is an effective delayed neutron fraction and ℓ is a mean prompt neutron life time. The kinetics parameter β_{eff}/ℓ is measured

by the reactor noise analysis using the two-detector correlation method, which can be eliminated the detector noise component.

Two temporary CICs are used as the detectors. The reactor noise signal from the detectors is measured by using the reactor noise instrumentation (the temporary CICs, pico-ammeters, band pass filters, etc.). The critical points are confirmed in the neighborhood of the reactor power of 0.8W and 8W. The reactor noise instrumentation is located out of the reactor core. First, the power spectrum density of the reactor noise at proper frequency is evaluated by using the electric current of the CIC through the band pass filter. Second, the power spectrum density ratio between one CIC and the other chamber is calculated. Final, the corner angular frequency β_{eff}/ℓ is estimated by using the proper frequency and the power spectrum density ratio. It is difficult to measure the kinetics parameter β_{eff}/ℓ for the graphite-moderated reactor because the parameter is smaller than that of the light water reactor. However, the kinetics parameter β_{eff}/ℓ for the graphite-moderated reactor can be measured by the reactor noise analysis using the two-detector correlation method.

4.9 Neutron flux distribution measurement

The purpose of this test is to measure the neutron flux distribution in the core in a lower thermal power and in air atmosphere. The neutron flux is measured by the temporary FCs containing fission material of ^{235}U. The FCs are installed in three irradiation columns which are located at the corner of the replaceable reflector region as shown in Fig. 4. Vertical neutron flux distributions are measured at 6 different positions in each irradiation column and by traversing the FC inside the irradiation ones. During the test, the reactor is kept at a critical condition in the neighborhood of the reactor power of 8W. The reactor power is estimated as shown in section 4.6. The data is used to confirm the validity of the HTGR core design code system.

4.10 Measurement test for temperature coefficient of reactivity

The purposes of this test are to determine temperature coefficient of reactivity experimentally keeping an uniform core temperature in helium gas atmosphere and to confirm that the temperature coefficient of reactivity is negative. The test is performed at four elevated reactor core temperatures (23°C, 70°C, 110°C and 150°C) in order. The reactor core temperature defined as an average between temperature of the reactor core inlet and outlet measured by the N type thermocouples as shown in Fig. 6. The core is heated by energy injected with the helium gas circulators of the HTTR main cooling system as shown in Fig. 7. Difference between reactivities of present and previous temperature points is measured by the IK method. The validity

of the design value is confirmed by comparing the temperature coefficient of reactivity obtained by the test with the design one. The critical point is confirmed in the neighborhood of the reactor power of 30W. The reactivity difference by the IK method is measured by the WRMS.

4.11 Thermal power correlation test

The purposes of this test are to measure a thermal power and to correlate the permanent power−measuring instrumentation in the neighborhood of the reactor power of 9MW, 21MW and 30MW and in helium gas atmosphere. During the test, the HTTR is operated at the rated operation under a single operation mode. At the single loaded operation mode, the primary pressurized water cooler is operated and both the secondary pressurized water cooler and the intermediate heat exchanger are not operated.

The measurement of the thermal power is conducted by the calorimetric method. In the calorimetric method, the thermal power is obtained as the summation of heat removed by the main cooling system, the auxiliary cooling system and the vessel cooling system as shown in Fig. 7. Each removal heat of the cooling system is measured by temperature and flow rate of pressurized water circuit of each cooling system and heat input from the gas circulators and related pumps. The thermal power is expressed in the following equation :

(HTTR thermal power)=(heat removed by main cooling system)+(heat removed by auxiliary cooling system)+(heat removed by vessel cooling system)−(heat generated by gas circulators and related pumps)

We confirm that the HTTR can attain 30MW thermal output, 850°C outlet coolant temperature and 395°C inlet coolant temperature so as to satisfy the operational parameter limit.

4.12 Power coefficient measurement

The purpose of this test is to confirm that the power coefficient is negative in helium gas atmosphere. The reactor power is varied by the fuel and moderator temperature changes due to the Doppler effect and the thermal neutron shift. The reactor is kept a certain power level in a period so as to saturate the effect of xenon and samarium. The reactor power is varied into different power levels in stepwise by changing the setpoint of the power control system. The reactor power is kept stable at the setpoint and then the CR positions are recorded. The reactivity change is evaluated by the change of the CR positions and the CR worth curves. The power coefficient is obtained from the reactivity change divided by the reactor power change

(from 30% to 20%, from 70% to 60% and from 100% to 90%). These measured data are used to confirm the validity of the HTGR core design code system.

4.13 Measurement test for reactivity change after scram

The purposes of this test are to measure subcriticality by the scram in helium gas atmosphere, to measure reactivity change in the period from the CR insertion into the reflector region to that into the fuel region continuously and to measure the reactivity by the CR insertion into the fuel region under the subcritical condition. The subcriticality by the scram is measured by the IK method and the RD method. It is confirmed that subcriticality by the scram is more than 4%Δk/k. Both change in reactivity change by the CR insertion into the fuel region are measured by the IK method. It is confirmed that subcriticality by the CR insertion into the fuel region is more than 1%Δk/k.

Before the reactor scram is simulated by the manual operation, the critical point is confirmed by using the CRs. In the neighborhood of the reactor power of 30kW, 1MW and 27MW, the CRs are inserted in two steps by making a simulated signal so as to exceed 750°C of the outlet temperature of the reactor core. The reactivity under above−mentioned reactor core conditions is measured by the PRMS (three permanent UICs and three permanent BF_3 detectors). On the other hand, the subcriticality by the scram with the RD method is measured by three permanent BF_3 detectors.

5. Conclusions

The followings are the major characteristics of the SPTs of the HTTR :

(1) The first criticality is approached by replacing the mock−up fuel blocks with the flesh fuel blocks. The replacement begins from outer columns bordering the side reflector block.

(2) The WRMS is adjusted to the nuclear reactor power by the reactor noise analysis using the two−detector correlation method.

(3) Both change in reactivity from the CR insertion into the reflector region to that into the fuel region are measured by the IK method.

Acknowledgements

The authors would like to thank Messrs. T. TANAKA, O. BABA, Drs. S. SHIOZAWA, Y. KANEKO of JAERI for their useful comments.

References

(1) S. SAITO et al., Design of High Temperature Engineering Test Reactor (HTTR),

JAERI 1332, (1994).

(2) R. SINDO et al., DELIGHT-7; One Dimensional Fuel Cell Burnup Analysis Code for High Temperature Gas-cooled Reactors (HTGR), JAERI-M 90-048, (1990).

(3) K. D. LATHEROP and F. W. BRINKLEY, LA-4848-MS, (1973).

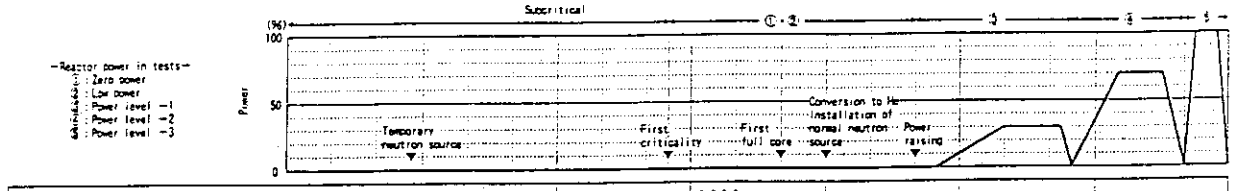
(4) H. HARADA and K. YAMASHITA, The Reactor Core Analysis Code CITATION 1000-VP for High Temperature Engineering Test Reactor, JAERI-M 89-135, (1989).

(5) I. MURATA et al., Evaluation of Shut Down Margin in Scram Condition for High Temperature Engineering Test Reactor (HTTR), JAERI-M 91-165, (1991).

(6) Y. KANEKO et al., Present Art of Reactivity Determination, J. At. Energy Soc. Japan 19(6) 26-36, (1977).

(7) T. NOMURA, Reactivity Measurements by Reactor Noise Analysis using Two-Detector Correlation Method, J. Nucl. Sci. Technol. 3(1) 14-19, (1966).

Table 1 Schedule for start-up physics tests of the HTTR



No.	Test items	1997 4	5	6	7	8	9	10	11	12	1998 1	2	3	4	5	6	7	8	9	10	11	12
NT-1	First criticality test									○												
NT-2	Initial core construction											○										
NT-3	Control rod reactivity worth test									○		○	○	○	○							
NT-4	Excess reactivity test												○	○				○			○	○
NT-5	Reactivity shutdown margin test												○	○							○	○
NT-6	Nuclear power correlation test												○	○								
NT-7	Measurement of maximum reactivity insertion rate												○	○								
NT-8	Reactivity control effect of control rod												○	○	○							
NT-9	Response confirmation of neutron detectors						○			○			○									
NT-10	Shutdown margin (RSS)												○									
NT-11	Measurement test for kinetics parameter												○									
NT-12	Neutron flux distribution measurement												○									
NT-13	Measurement test for temperature coefficient of reactivity														○							
NT-14	Thermal power correlation test																					
NT-15	Power coefficient measurement																					
NT-16	Plant stability																					
NT-17	Measurement of reactivity change after scram																					
NT-18	Xe decay effect																					

Table 2 Major specifications of the HTTR

Thermal power	30MW
Core structure	Graphite
Core equivalent diameter	2.3m
Core height	2.9m
Average power density	2.5W/cm^3
Fuel	UO_2
Fuel type	Pin-in-block Coated Fuel Particle (CFP)
Fuel loading	off-load, 1 batch
Maximum fuel temperature	1492°C
Excess reactivity	15%Δk
Uranium enrichment	3 – 10wt%
(Average)	about 6wt%
Fuel burnup (average)	22GWd/t
Burnup days in a cycle	660days
Reactivity coefficients	
Fuel temperature coefficient	$-(1.5 \text{ to } 4.6)\times10^{-5}$Δk/k/°C
Moderator temperature coefficient	$(-17.1 \text{ to } 0.99)\times10^{-5}$Δk/k/°C
Power coefficient	$-(2.4 \text{ to } 4.0)\times10^{-5}$Δk/k/MW
Prompt neutron lifetime	0.67 – 0.70ms
Effective delayed neutron fraction	0.0047–0.0065
Inlet coolant temperature	395°C
Outlet coolant temperature	850°C/950°C
Power peaking factor	
radial	1.1
axial	1.7
Coolant	Helium gas
Primary coolant pressure	4MPa
Coolant flow in core	Downward
Effective core coolant flow rate	88%

Table 3 Major specifications of detectors for temporary neutron instrumentation system

Instrumentation system	Specifications of detector
Temporary BF_3 instrumentation system	BF_3 proportional counter Type : ND8534 Sensitivity : 0.1 cps/nv Dimension : ϕ25mm × 348mm
Temporary FC instrumentation system	Fission counter Type : WL23092 Sensitivity : 0.0015 cps/nv Dimension : ϕ5.3mm with 12m MI cable
Temporary CIC instrumentation system	Gamma ray compensated ionization chamber Type : WL23196 Sensitivity : 2.3×10^{-14} A/nv Dimension : ϕ50.8mm × 1310mm

Table 4 Major specifications of detectors for permanent neutron instrumentation system

Instrumentation system	Specifications of detector
WRMS	Fission counter Type : ND8668 Sensitivity : Pulse mode : 0.1 cps/nv MSV mode : 4×10^{-27} A^2/Hz/nv Dimension : ϕ38mm × 400mm
PRMS	Gamma ray uncompensated ionization chamber Type : ND8707 Sensitivity : 3.0×10^{-12} A/nv Dimension : ϕ110mm × 2,900mm
BF_3 counter instrumentation system	BF_3 proportional counter Type : ND8557 Sensitivity : 50 cps/nv Dimension : ϕ50mm × 648mm

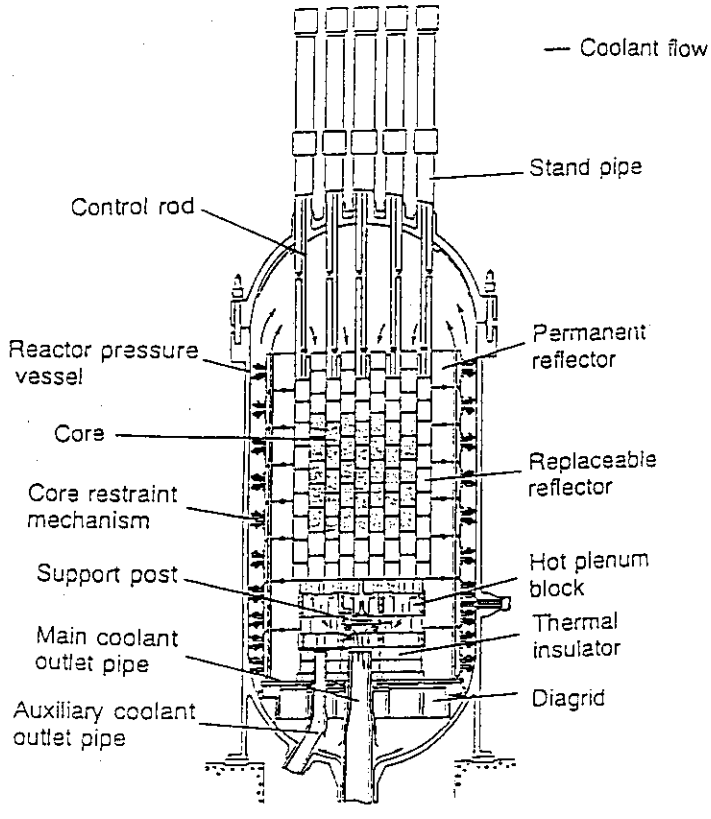


Fig.1 Vertical cross sections of the HTTR

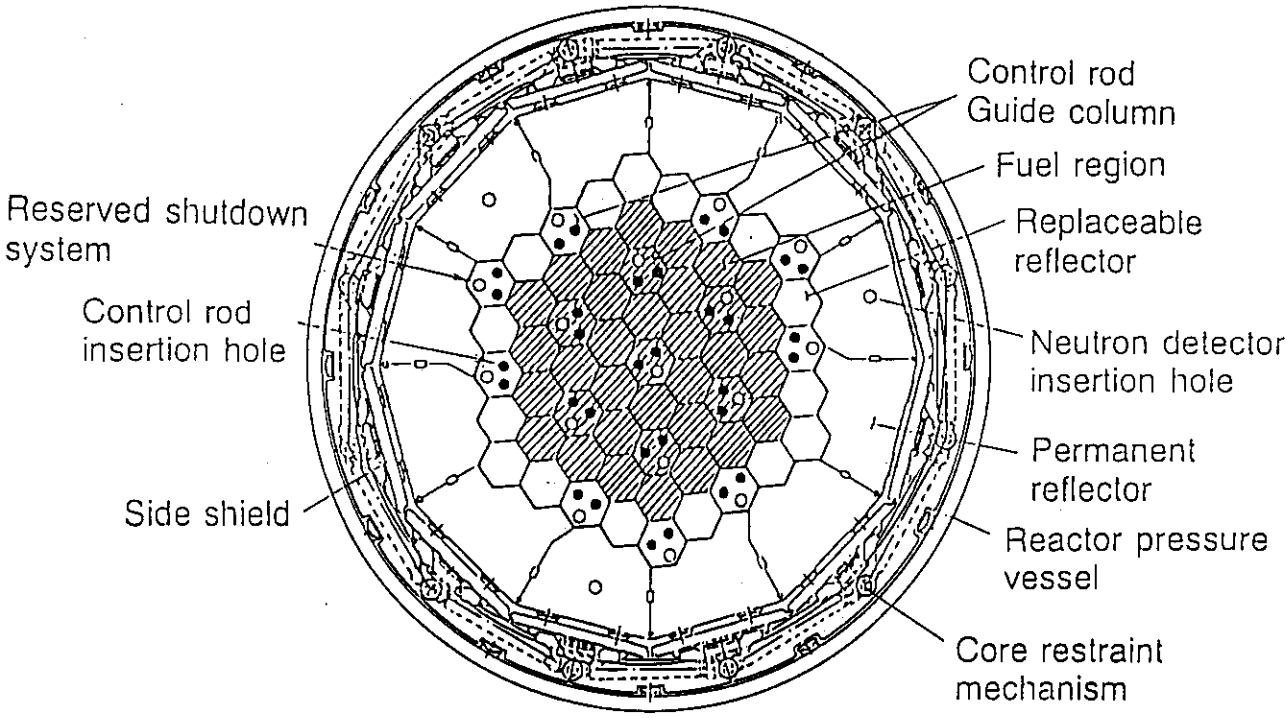


Fig.2 Horizontal cross sections of the HTTR

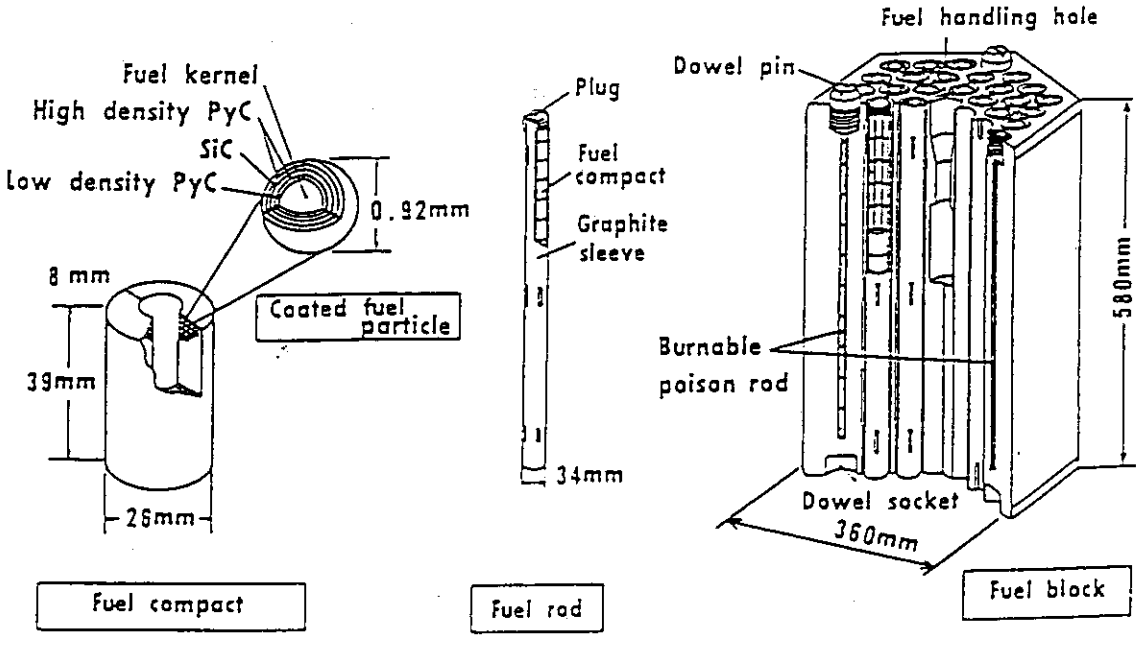


Fig.3 Block-type fuel of the HTTR

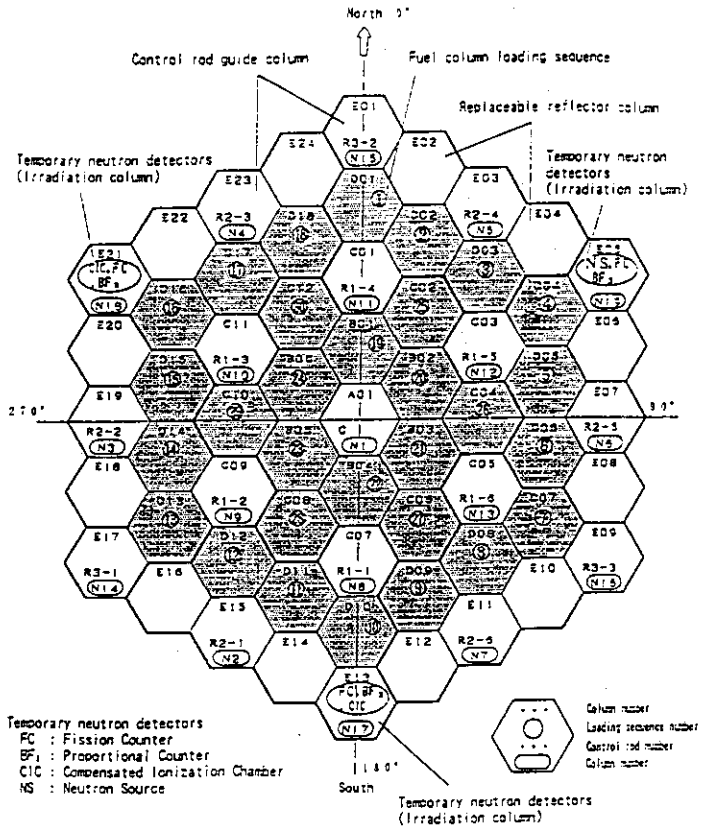


Fig.4 Fuel column loading sequence and positions of extra neutron detectors

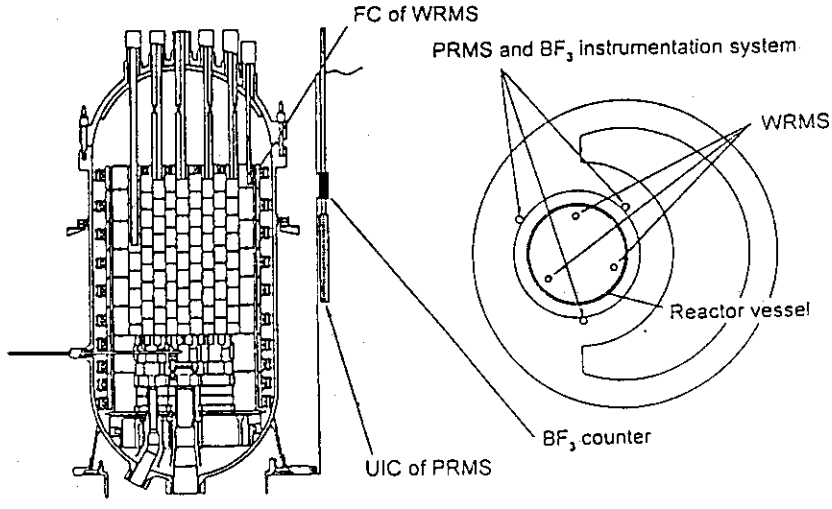


Fig.5 Arrangement of regular neutron instrumentation system

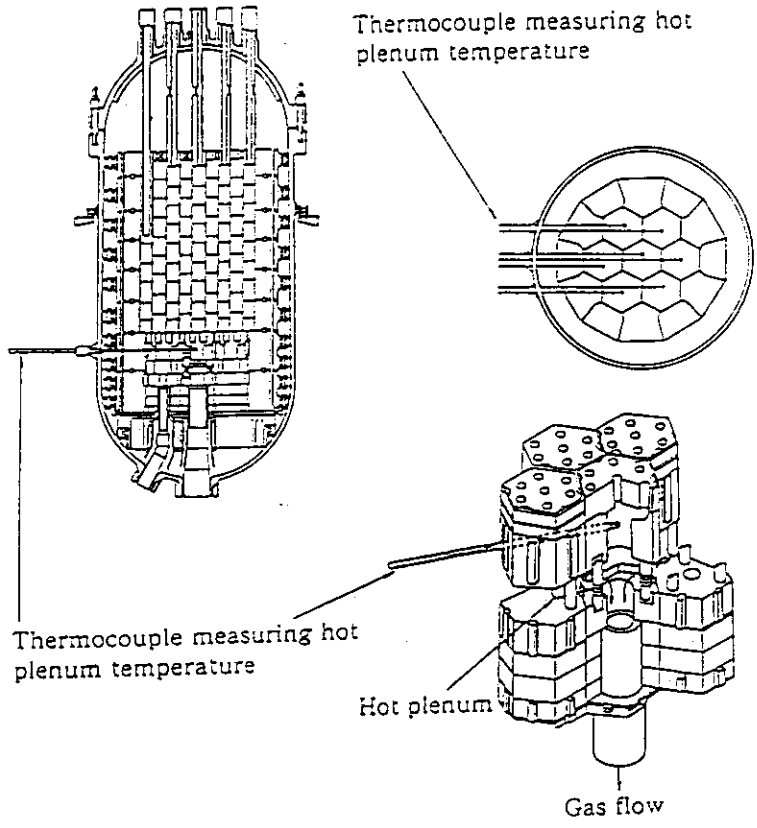


Fig.6 N-typed thermocouple arrangement at hot plenum

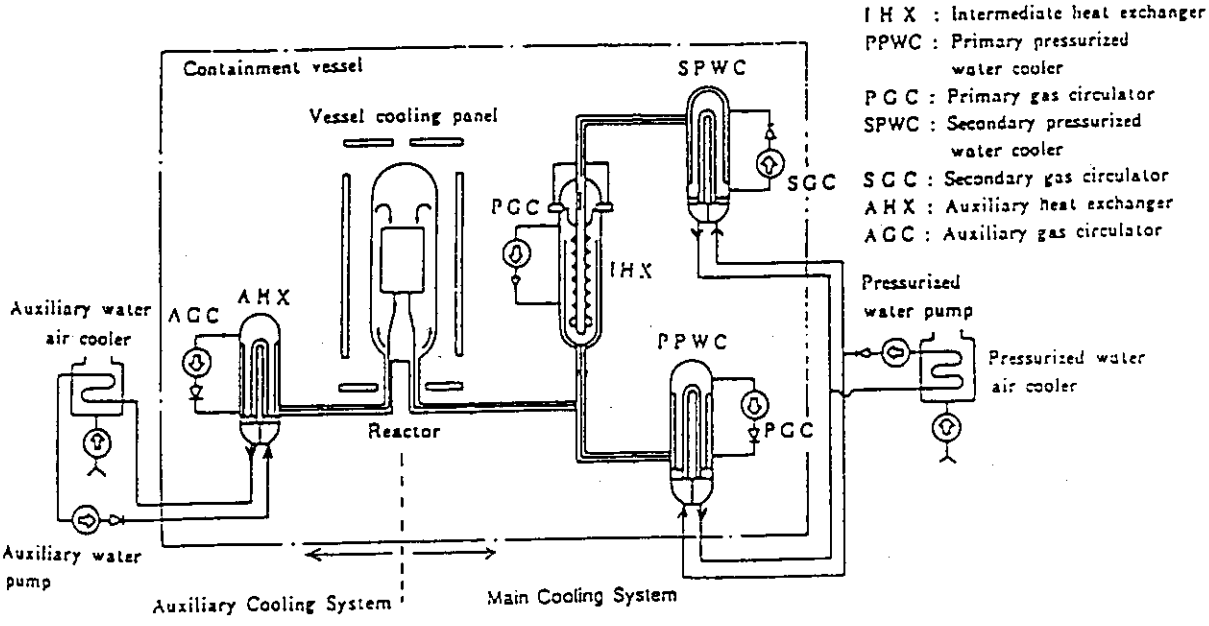


Fig. 7 Reactor cooling system of the HTTR

Third JAERI Symposium on HTGR Technology 15-16 February 1996 Oarai, Japan
Section IV: Safety of HTGR, Development of Fuel and Component, Operation Experience

6.21 Highlights from the IAEA Coordinated Research Programme on Fuel Performance and Fission Product Data

Authors: H. Nabielek, W. Schenk, K. Verfondern (KFA Germany), K. Fukuda (JAERI Japan), A. Khroulev (RRC Kurchatov Russia), Xu Shijiang (INET China), B. Myers (ORNL USA), D. Hanson (GA USA), R. Gillet (CEA France), R. Williamson (Harwell UK) and J.C. Cleveland (IAEA Austria)

Abstract:

Seven countries are cooperating with the objectives (i) to document the status of the experimental data base and of the predictive methods for Gas-Cooled Reactor fuel performance and fission product behaviour; (ii) to verify and validate methods in fuel performance and fission product retention prediction. These countries are China, France, Germany, Japan, Russia, USA and the UK. Duration of the programme is 1993—96.

The technology areas addressed in this IAEA Coordinated Research Programme are:

- Fuel design and manufacture
- Normal operation fuel performance and fission product behaviour
- Accident condition fuel performance and fission product behaviour
  - core heatup
  - fast transients
  - oxidising conditions (water and air ingress)
- Plateout, re-entrainment of plateout, fission product behaviour in the reactor building
- Performance of advanced fuels

Work performed so far has generated a 300-page draft document with important information for normal operations (Germany, Japan, China, Russia) and accident conditions (USA, Japan, Germany, Russia) and, additionally, a special chapter on advanced fuels (Japan).

Highlights from this work will be presented during the Symposium.

SUMMARY

The investigation of fundamental characteristics of **HTGR fuel** has taken place since 30 years. For all countries' reference concepts, the fuel is based on TRISO coated fuel particles with low-enriched uranium. Two directions for the fuel element design have been pursued, the block type in Japan and the US, and the spherical fuel element in Germany, Russia, and China.

Particle and fuel production in **China** is still on a laboratory scale, but will soon go over to prototype scale. Experimental data on her national fuel revealed a low level of free uranium at $4*10^{-6}$. The qualification program concentrates on characterization and inspection of fuel to be used in the HTR-10 experimental reactor with special focus on the observation of coating microstructure and the investigation of SiC strength and Youngs modulus as important parameters.

In **Germany**, high quality fuel was achieved due to large-scale production experience. Measurements of "free uranium" outside an intact SiC layer have shown a reduction of the U_{free} fraction by a factor of 5 compared to fuel production before 1985. An expected value of $1.1*10^{-5}$ is to be used in radiological analyses. Measurement data on uranium contamination of the matrix graphite are usually below the detection limit, i.e., $< 10^{-6}$. In 1989, it was decided to terminate the German activities on HTGR fuel production and development.

The **Japan**ese fuel development has also managed to produce high quality fuel by modification of manufacturing conditions and of both coating and compacting processes. The result is a 95 % confidence level of less than one defective particle per fuel compact. The expected free uranium fraction is $5.5*10^{-4}$ which is way below the regulatory requirement for the U_{free} fraction to be $< 2*10^{-3}$. The fuel production for the HTTR first loading has begun in June 1995 and will last for about three years.

The **US** reference fuel design is based upon a two-particle concept of fissile and fertile UCO coated particles. Operational requirements for burnup and neutron fluence are much stronger compared to other countries' designs. Specification limits are 10^{-5} for the heavy metal contamination and $5*10^{-5}$ for the fraction of defective particles.

Russia has gained a broad experience with its fuel in pre-reactor, reactor, and post-reactor experiments where even sharp pulse irradiation conditions were applied. The fuel design for the 250 MW(th) modular reactor VGM has a fraction of defective particles $< 10^{-4}$ and a U-235 contamination of $4*10^{-6}$. The fuel production, however, is on a laboratory scale so far. Therefore focus was laid upon the development of quality control methods. One that is being widely used is the method of "weak" irradiation of the fuel.

The design of modern HTGRs is based on **high-quality fuel.** In manufacturing, this fuel quality has been achieved in the early 1980s and since has been further improved. This improvement consisted of steps to reduce TRISO particle defects during sphere pressing and in minimizing uranium contamination in the fuel element. Another important aspect was the development of a sensitive quality control method: the burn-leach technique provides

the necessary data to establish a design limit of less than $6*10^{-5}$ free uranium which has been identified as arising from particle defects. With newer data, this design limit can be reduced to $3*10^{-5}$.

Fuel testing under off-normal non-oxidizing conditions has provided fuel performance information as a function of fuel temperature up to 2500 °C. In small, modular HTGRs, temperatures are limited to below 1600 °C. Here the fuel does not suffer from irreversible changes and continues to retain all safety-relevant fission products. When accident temperatures are limited to less than 1600 °C, the heating data confirm that licensing applications can be based on 1 coated particle failure in 4 fuel elements and no additional release of safety-relevant fission products, especially from iodine, beyond normal operation.

During 500 h heating at 1600 °C and 100 h tests at 1800 °C, progressive changes in the silicon carbide lead to fission product release for fuel irradiated to burnup and fast neutron fluence levels beyond design values for present reactor concepts. Cesium release is initiated upon **failure of the silicon carbide**, likely by fission product enhanced local changes of SiC structure. After SiC failure, cesium release is controlled by a SiC grain boundary diffusion mechanism. Finally, Kr-85 and Sr-90 are released, krypton being retained by its slow transport through the remaining intact pyrocarbon, and strontium being strongly bound in the oxide kernel and in the matrix graphite.

The primary mechanism for coating failure and fission product release in the 1900 – 2500 °C temperature range is **thermal decomposition** of silicon carbide. Heating tests have provided the activation energy of this process and the correlation of SiC decomposition with coating failure and subsequent fission product release. The process of fission product release proceeds in several stages. A certain amount of SiC removal at high temperatures leads to SiC deterioration which renders a fraction of particles permeable to cesium and strontium. During 50 °C/h ramped heating tests, the cesium release approaches 100 % at 2500 °C. With the onset of SiC failure, the release process of xenon, krypton, and iodine via diffusion through the pyrocarbon is initiated. Under all heating conditions examined, krypton release is significantly delayed relative to cesium release due to the higher diffusivity of cesium in PyC.

The release behavior of metallic fission products from TRISO coated UO_2 particles was studied by postirradiation isothermal heating tests in the temperature range 1600 to 1900 °C. The fission gas release monitoring and the postheating examinations revealed that no pressure vessel failure occurred in the tests. The ceramographic observations showed no palladium attack and thermal decomposition of SiC. The diffusion coefficient of Cs-137 in the SiC layer was evaluated from the release curves based on a one-layer coated particle model. Fractional release measurements suggested that the diffusion coefficient of Ag-110m in SiC be larger than that of Cs-137.

A model to predict the ultimate failure of TRISO coated fuel particles in hypothetical core heatup events was proposed. The features of the model allow treatment of the statistical variation of the number of particles and a thermodynamic estimation of the stoichiometry of irradiated UO_2 kernels and the equilibrium CO pressures. The model predictions agreed well with the results of the postirradiation temperature ramp tests. However, the model tended to overpredict at lower failure fraction at a low ramp rate. Inspection of the

ceramographs and the X-ray microradiographs of the heated samples revealed the effect of thermal creep of the PyC layer in a range of temperatures around 2100 °C.

Irradiation tests of the fuel compacts at very high temperatures were performed. No crack was observed on the fuel compacts after **high temperature irradiation.** No deterioration of the SiC coating layer of the particles was found even after irradiation at 1998 °C, but a small fraction of the particles failed in the severest case of 1998 °C irradiation.

The RIA tests were carried out in the NSRR. The coating failure fraction increased with the amount of energy deposition. The coating failure may have been caused by the internal high pressure due to UO_2 evaporation. To clarify the mechanisms of the coating failure, analyses of temperature and stresses of the coated particles are needed.

Among the postulated accidents in gas-cooled reactors are those of **water and air ingress.** These accidents involving oxidation of exposed fuel kernels, carbonaceous materials, SiC and ZrC can lead to a significantly enhanced release of fission products and to extensive degradation of the core components. Recent experiments have focused mainly on the effect of water vapor on exposed fuel kernels; the focus is now shifting to the effect of oxygen.

The interaction of water vapor with particles having exposed fuel kernels has been investigated both during and after irradiation. although these types of experiments differ severely, their complementary is yet to be determined.

Three irradiation experiments, HRB-17/-18, HFR-K6, and HFR-B1, have been conducted. The fuel particles contained UO_2 and a known small portion had exposed kernels. A series of discrete tests was conducted with water vapor at partial pressures in the range 0.003 to 2 kPa. The released fission gas was monitored for the isotopes Kr-85m, Kr-87, Kr-88, Xe-133, Xe-135, and Xe-138. The general sequential **response of the exposed fuel kernels to water vapor** consists of three stages:

1. a rapid release of fission gas with a concomitant increase in the steady state release,
2. a period of constant steady state release, and
3. a decline in the release to prehydrolysis values upon cessation of water vapor injection.

During stage 1, collectives (bubbles containing gas atoms) and interstitial gas atoms are sources of released fission gas. These sources were identified and evaluated on the basis of the slope $|\partial ln(R/B) / \partial ln(\lambda)|$; here R/B is the fractional fission gas release of the monitored isotopes and λ the corresponding decay constants. For release of collectives, the slope has values $\approx$ 1 to $\approx$ 0.5.

The transient release of collectives at 800 °C is proportional to P^{α} where P is the partial pressure of water vapor. For P < 1 kPa, α is 1.7 and for P > 1 kPa, α apparently will be significantly smaller. Further analysis indicates that α is temperature dependent A small value of α above 1 kPa could signal the onset of a transport-limiting mechanism. Evidence indicates the fractional release of fission gas from collectives to be the same for

all isotopes of Kr and Xe provided the I-133 precursor contribution is taken into account. The activation energy for the transient release is estimated to be 393 kJ/mol.

During stage 2, which begins after completion of the transient release, interstitials are diffusively released. This stage is characterized by the ratio $h_o = (R/B)_{stage\ 2} / (R/B)_{stage\ 0}$. The ratio is constant in time, depends on the temperature, but is independent of P_{H2O} (at least for $P < 0.2$ kPa) and of isotopic variation. The latter si also theoretically expected. The ratio differs for the elements Kr and Xe to the same extent as do their atomic volumes. The activation energies of R/B in the presence and absence of water vapor are, respectively, 65.8 kJ/mol and 23.6 kJ/mol.

During stage 3, which begins after the injection of water vapor ceases, the fractional release declines to $(R/B)_{stage\ 0}$, i.e., to a fuel structure equivalent in release to the fuel structure existing before water vapor was injected. The characteristic time, Δt, for decline to within 5 % of $(R/B)_{stage\ 0}$, is equal to $3/\delta$. δ is the governing parameter in the corresponding exponential function. It is small at zero neutron flux and passes through a maximum with increasing neutron flux.

In conclusion, in modern HTR fuel the defect level of coated particles during manufacture is practically zero. Only during pressing of fuel bodies, particle failure occurs, but is less than $1*10^{-4}$. In-pile fuel performance is demonstrated by irradiation testing under HTGR-typical conditions with no additional failure of particles. Accident behaviour resulting from unrestricted core heatup is investigated by heating of irradiated fuels: at 1600 °C, all safety-relevant fission products are retained and only at 1800 °C and higher temperatures, particles start to fail and to release fission products. Fission gases and iodine are partially only released from defective or failed particles. The level of release increases during water ingress. For licensing applications, a complete set of codes and data is provided for fission product behaviour in-core and ex-core including plateout. Alternative advanced fuels are studied for better coated particle fission product retention at extreme temperatures and for an inherent corrosive protection of fuel elements.

FORSCHUNGSZENTRUM JÜLICH KFA

Highlights from the IAEA Coordinated Research Programme on Fuel Performance and Fission Product Data

Presented by:
H. Nabielek (KFA) and K. Fukuda (JAERI)
Contributions by:
W. Schenk (KFA)
A. Khroulev (Kurchatov)
S. Xu (INET)
B. Myers (ORNL)
D. Hanson (GA)
R. Gillett (CEA)
R. Williamson (AEA)
J. Cleveland (IAEA)
Supervised and edited by:
K. Verfondern (KFA)

Contents

HTR fuel
- Design
- Manufacture
- Irradiation performance

Accident conditions
- Heatup
- Water ingress
- Air ingress

Ex-core fission product transport
- Plateout
- Liftoff
- Washoff

Advanced fuels
- ZrC particles
- Corrosion resistant fuel elements
- Monolithic fuel rods

Schedule

June 95 First draft (230 pages)
May 96 Second draft
Sep. 96 Third draft
Dec. 96 Final Version (500 pages)

High-Temperature Gas-cooled Reactors have an all-ceramic core with coated fuel particles and graphitic fuel elements. Modern fuel retains fission products up to 1250 °C during irradiation and 1600 °C during heatup accidents.

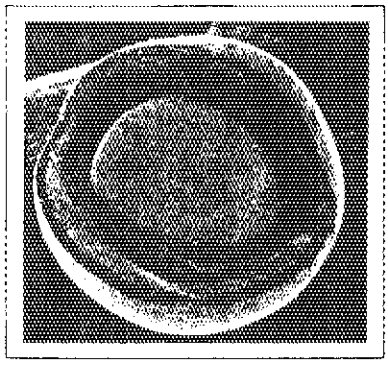
			China	Germany	Japan	Russia	U.S.	
							Fissile	Fertile
Coated particle design								
	Kernel							
		Composition	UO_2	UO_2	UO_2	UO_2	UCO	ThO_2
		Diameter	500 µm	500 µm	600 µm	500 µm	350 µm	500 µm
		Enrichment	17 %	~ 10 %	3 – 9 %	8 %	< 20 %	
	Coating thickness							
		Buffer	90 µm	95 µm	60 µm	100 µm	100 µm	65 µm
		Inner PyC	40 µm	40 µm	30 µm	80 µm	40 µm	40 µm
		SiC	35 µm	35 µm	25 – 35 µm	60 µm	35 µm	35 µm
		Outer PyC	40 µm	40 µm	45 µm	60 µm	40 µm	40 µm
Fuel element design								
	Type		Sphere	Sphere	Block	Sphere	Block	
	Volume packing fraction		7 %	10 %	33 %	15 %	51 %	
Maximum fuel performance requirements								
	Temperature		1000 °C	1250 °C	1495 °C	1400 °C	1250 °C	
	Burnup (FIMA)		10 %	10 %	4 %	9 %	26 %	

Participating countries: China, France, Germany, Japan, Russia, U.S., UK

FORSCHUNGSZENTRUM JÜLICH KFA

HTR coated particle

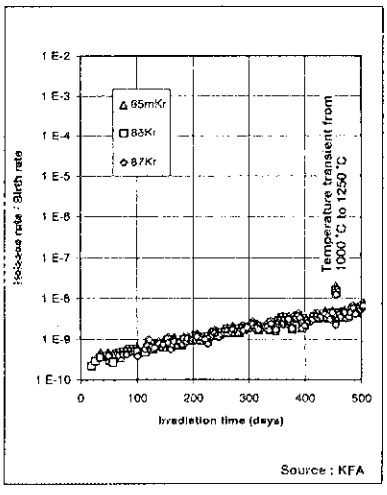
Artificially cracked particle of 1 mm diameter shows structure of UO_2 kernel and coating



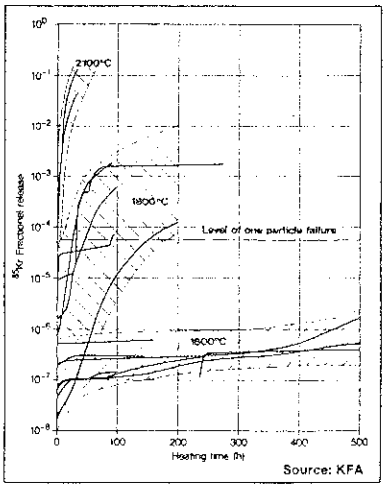
Dense ceramic coating layers retain fission products in normal operation and in accidents

Fission gas release

during normal operation
simulated in irradiation tests
(FRJ2-K15/1, DIDO reactor Jülich)



during core heatup accidents
simulated in heating tests
(KÜFA furnace)

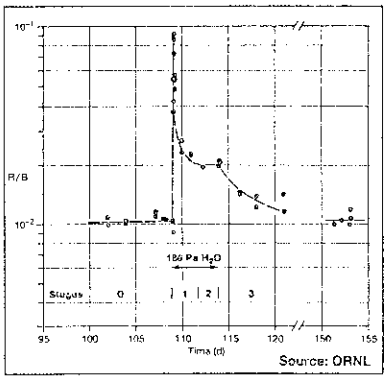


Defective and failed particles

Design limits

	Defects from manufacture	Failures during irradiation
China	3×10^{-4}	5×10^{-4}
Germany	6×10^{-5}	2×10^{-4}
Japan	2×10^{-3}	8×10^{-3}
Russia	1×10^{-4}	1×10^{-4}
U.S.	1.2×10^{-4}	2×10^{-4}

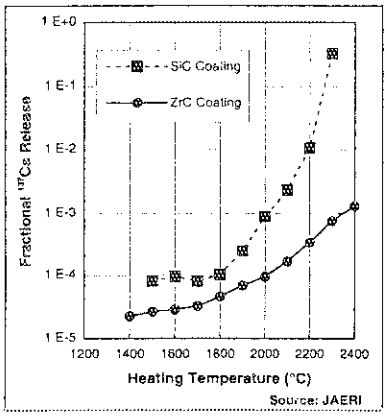
In-pile release from failed particles at 775 °C
with intermittent water vapour injection
(gas release return to "normal" R/B
after termination of water ingress)



Advanced fuels

- ZrC particle coating (instead SiC) for extreme temperature resistance
- Fuel element / graphite coating for inherent protection against water ingress
- Monolithic fuel block for better temperature distribution and more economic manufacture

Results of 2 hour heating tests show better ^{137}Cs retention by ZrC



Conclusions

In modern HTR fuel, the defect level of coated particles during manufacture is practically zero. Only during pressing of fuel bodies, particle failure occurs, but is less than 1×10^{-4}.

In-pile fuel performance is demonstrated by irradiation testing under HTGR-typical conditions with no additional failure of particles.

Accident behaviour resulting from unrestricted core-heatup is investigated by heating of irradiated fuels: at 1600 °C, all safety-relevant fission products are retained and only at 1800 °C and higher temperatures, particles start to fail and to release fission products.

Fission gases and iodine are partially only released from defective or failed particles. The level of release increases during water ingress.

For licensing applications, a complete set of codes and data is provided for fission product behaviour in-core and ex-core including plateout.

Alternative advanced fuels are studied for better coated particle fission product retention at extreme temperatures and for an inherent corrosive protection of fuel elements.

Planned TABLE OF CONTENTS of full 500 pages IAEA Technical Document

Foreword
Table of Contents
0. EXECUTIVE SUMMARY
1. INTRODUCTION & OVERVIEW
2. FUEL DESIGN & FABRICATION
2.1. Coated Particle
2.2. Fuel Element
2.3. Fuel Quality during Manufacture
2.3.1. The Chinese Program
2.3.1.1. Design Specification of the HTR-10 Fuel Element
2.3.1.2. Manufacture Technology
2.3.1.3. Characterization and Inspection
2.3.1.4. Strength and Young's Modulus of Pyrolytic SiC Coatings
2.3.1.4.1. Deposition of SiC Coating
2.3.1.4.2. Effect of Deposition Temperature on Strength and Young's Modulus of Deposited SiC
2.3.1.4.3. Discussion and Conclusions
2.3.2. The German Program
2.3.2.1. Manufacturing Defects
2.3.2.2. Design Basis for Free Uranium
2.3.2.3. Uranium Contamination
2.3.2.4. In-Pile Failure
2.3.3. The Japanese Program
2.3.3.1. Design Criteria for HTTR First Loading Fuel
2.3.3.2. Manufacturing Defects
2.3.4. The Russian Program
2.4. Summary of Chapter 2
2.5. References of Chapter 2
3. NORMAL OPERATION TRISO FUEL PERFORMANCE UNDER IRRADIATION
3.1. Fission Product Inventories in the Active Core
3.2. Fuel Failure Mechanisms and Models
3.2.1. Kernel Migration ("Amoeba Effect")
3.2.2. Fission Product Interaction with Silicon Carbide
3.2.3. Pressure Vessel Failure

3.3. Fission Product Release Models

3.3.1. Gas Release
3.3.2. Metal Release

3.3.2.1. Calculation Models
3.3.2.2. Model Valuation
3.3.2.3. Uptake of Fission Product Metals by Silicon Carbide

3.4. Fuel Irradiation Test Programs

3.4.1. The German Program

3.4.1.1. In-Pile Failure
3.4.1.2. HTR-MODUL Source Terms

3.4.2. The Japanese Program
3.4.3. The Russian Program

3.4.3.1. Weak Irradiation Method (Activation Method)
3.4.3.2. Methods and Results of Reactor and Post-Reactor Investigations
3.4.3.3. Main Conclusions

3.4.4. The US Program

3.5. Reactor Operating Experience

3.5.1. DRAGON
3.5.2. Peach Bottom
3.5.3. Fort St. Vrain
3.5.4. AVR
3.5.5. THTR-300

3.6. Summary of Chapter 3
3.7. References of Chapter 3

4. FUEL PERFORMANCE AND FISSION PRODUCT RELEASE UNDER HEATUP, NON-OXIDIZING CONDITIONS

4.1. Postirradiation Heating Experiments

4.1.1. Postirradiation Heating Tests in Germany

4.1.1.1. Equipment
4.1.1.2. Data of Fuel Samples
4.1.1.3. Experimental Results

4.1.1.3.1. Results Obtained at 1600 - 1800 °C
4.1.1.3.2. Fission Product Release from Heavy Metal Contamination
4.1.1.3.3. Results Obtained at 1900 - 2500 °C

4.1.1.4. Modeling

4.1.1.4.1. Particle Failure
4.1.1.4.2. Metallic Fission Product Release
4.1.1.4.3. Fission Gas and Iodine Release
4.1.1.4.4. Fission Product Transport within the Core Cavern

4.1.2. Postirradiation Heating Tests in Japan

4.1.2.1. Equipment
4.1.2.2. Data of Fuel Samples
4.1.2.3. Results of Isothermal Heating Tests
4.1.2.4. Results of Temperature Ramp Tests
4.1.2.5. Modeling

4.1.2.5.1. Particle Failure
4.1.2.5.2. Fission Product Release

4.1.3. Russia
4.1.4. Heating of Irradiated Particles in the USA

4.1.4.1. Experimental Details
4.1.4.2. Heating Test Results
4.1.4.3. Discussion of Experimental Results
4.1.4.4. Modeling

4.1.4.4.1. Particle Failure
4.1.4.4.2. Fission Product Release

4.2. Irradiation Testing at Very High Temperatures (1500 - 2000 °C)

4.2.1. High Temperature Irradiation in Japan

4.2.1.1 Irradiation Capsules
4.2.1.2. Data of Fuel Samples
4.2.1.3. Results of Irradiation Tests

4.2.2. High Temperature Irradiation in the USA

4.3. Reactivity-Initiated Accident Testing

4.3.1. Pulse Tests in NSRR, Japan

4.3.1.1. Pulse Irradiation Conditions
4.3.1.2. Data of Fuel Samples
4.3.1.3. Results of RIA Tests

4.3.2. Pulse Tests in HYDRA and IGR, Russia

4.3.2.1. Tests Using the HYDRA Reactor

4.3.2.1.1. Pulse Irradiation Conditions
4.3.2.1.2. Data of Fuel Samples
4.3.2.1.3. Results of RIA Tests Using the HYDRA

4.3.2.2. Tests Using the IGR Reactor

4.3.2.2.1. Pulse Irradiation Conditions
4.3.2.2.2. Data of Fuel Samples
4.3.2.2.3. Results of RIA Tests Using the IGR

4.3.2.3. Temperature and Stress Calculations

4.3.2.3.1. Temperature Calculation
4.3.2.3.2. Stress Calculation

4.4. Summary of Chapter 4
4.5. References of Chapter 4

5. FUEL PERFORMANCE UNDER OXIDIZING CONDITIONS

5.1. General Course of the Accidents
5.2. Experimental and Analytical Approach to the Accidents

5.2.1. Experimental Efforts
5.2.2. Encodemental Efforts

5.3. Water Ingress Accidents

5.3.1. Response of Graphite and Carbonaceous Material
5.3.2. Response of Coated Fuel Particles

5.3.2.1. Particles with Exposed Fuel

5.3.2.1.1. Water Vapor Injection During Irradiation
5.3.2.1.2. Postirradiation Water Vapor Injection

5.3.2.2. Particles with Intact Coating(s)

5.3.3. Mobilization of Fission Products

5.3.3.1. Water Vapor
5.3.3.2. Water

5.4. Air Ingress Accidents

5.4.1. Response of Graphite and Carbonaceous Material
5.4.2. Response of Coated Fuel Particles

5.4.2.1. Particles with Exposed Fuel
5.4.2.2. Particles with Intact Coating(s)

5.4.3. Mobilization of Fission Products

5.4.3.1. Air

5.4.4. Long Term, Massive Air Ingress

5.5. Summary of Chapter 5
5.6. References of Chapter 5

6. EX-CORE FISSION PRODUCT TRANSPORT DURING NORMAL AND ACCIDENT CONDITIONS

6.1. Fission Product Transport in Primary Coolant Circuit

6.1.1. Fission Product Transport during Normal Operation ("Plateout")

6.1.1.1. Plateout Models and Computer Codes

6.1.1.1.1. FRG Contribution
6.1.1.1.2. Japanese Contribution
6.1.1.1.3. US Contribution

6.1.1.2. Material Property Data

6.1.1.2.1. FRG Contribution
6.1.1.2.2. Japanese Contribution
6.1.1.2.3. US Contribution

Mass Transfer Coefficients
Sorption Isotherms
Solid-State Diffusion Coefficients

6.1.1.3. Aerosol ("Dust") Effects

6.1.1.3.1. British Contribution
6.1.1.3.2. FRG Contribution
6.1.1.3.3. Japanese Contribution
6.1.1.3.4. US Contribution

6.1.1.4. Integral Plateout Data

6.1.1.4.1. British Contribution
6.1.1.4.2. FRG Contribution

Out-of-Pile Loop Data
In-Pile Loop Data
Gas-Cooled Reactor Data

6.1.1.4.3. Japanese Contribution
6.1.1.4.4. US Contribution

Out-of-Pile Loop Data
In-Pile Loop Data
CPL-2 Test Program
COMEDIE Test Programs
Gas-Cooled Reactor Data

6.1.2. Fission Product Transport during Accidents (Reentrainment)

6.1.2.1. Chemical Desorption

6.1.2.1.1. Physical Models and Computer Codes

FRG Contribution
Japanese Contribution
US Contribution

6.1.2.1.2. Single-Effects Data
6.1.2.1.3. Integral Data

FRG Contribution
Japanese Contribution
US Contribution

6.1.2.2. Mechanical Reentrainment ("Liftoff")

6.1.2.2.1. Physical Models and Computer Codes

British Contribution
FRG Contribution
Japanese Contribution
US Contribution

6.1.2.2.2. Single-Effects Data

FRG Contribution
Japanese Contribution
US Contribution

GAIL IV Results
GA Deposition Loop Results
CPL-2 Test Program Results
Peach Bottom Steam Generator Tube Samples

6.1.2.2.3. Integral Data

Japanese Contribution
US Contribution

CPL-2/4 Loop Blowdown Test
COMEDIE BD-1 Blowdown Tests

6.1.2.3. Removal by Liquid Water ("Washoff")

6.1.2.3.1. Physical Models and Computer Codes

FRG Contribution
Japanese Contribution
US Contribution

6.1.2.3.2. Single-Effects Data

FRG Contribution
Japanese Contribution
US Contribution

6.1.2.3.3. Integral Data

6.1.2.4. Steam-Induced Vaporization ("Steamoff")

6.1.2.4.1. Physical Models and Computer Codes

FRG Contribution
Japanese Contribution
US Contribution

6.1.2.4.2. Single-Effects Data
6.1.2.4.3. Integral Data

6.2. Decontamination of Primary Circuit Components

6.2.1. Mechanical Decontamination Methods
6.2.2. Chemical Decontamination Methods
6.2.3. Electrochemical Decontamination Methods

6.3. Fission Product Transport in Reactor Building

6.3.1. FRG Contribution

6.3.1.1. Deposition Constants and Escape Probabilities
6.3.1.2. Filter Efficiencies

6.3.2. Japanese Contribution
6.3.3. US Contribution

6.4. Summary of Chapter 6
6.5. References of Chapter 6

7. ADVANCED FUELS

7.1. ZrC-Coated Fuel Particles

7.1.1. Fuel Particle Designs
7.1.2. Coating Processes
7.1.3. Characterization Techniques
7.1.4. Fuel Performance during Normal Operation
7.1.5. Fuel Performance during Accidents

7.1.5.1. Non-Oxidizing Conditions
7.1.5.2. Oxidizing Conditions

7.1.6. Fission Product Retentiveness

7.2. Fuel Element

7.2.1. Corrosion Resistant Spherical Fuel Element

7.2.1.1. Process for Production of Corrosion Resistant Spherical Fuel Elements
7.2.1.2. Properties of Corrosion Resistant Spherical Fuel Elements

7.2.1.2.1. Composition of the Protective Layer
7.2.1.2.2. Density and Porosity of the Protective Layer
7.2.1.2.3. Thickness of the Protective Layer
7.2.1.2.4. Mechanical and Thermal Properties

7.2.1.3. Corrosion

7.2.2. Monolithic Fuel Rod

7.2.2.1. Process for Production of Monolithic Fuel Rod
7.2.2.2. Irradiation Experiment

7.3. Summary of Chapter 7
7.4. References of Chapter 7

Appendix A: MATERIAL PROPERTY DATA

A.1. Transport Data for Diffusion Model

A.1.1. Fuel Kernel
A.1.2. Pyrocarbon
A.1.3. Silicon Carbide

A.1.4. Graphite

A.1.4.1. Matrix Graphite
A.1.4.2. Structural Graphite
A.1.4.3. Concentration Dependence of the Diffusion Coefficient

A.2. Sorption of Fission Products over Graphitic Surfaces

A.2.1. Sorption Isotherms
A.2.2. The FRESCO Approach of Sorption Modeling

A.3. Input Data for Particle Failure Models under Accident Conditions

A.3.1. The FRG Particle Failure Model PANAMA
A.3.2. The Japanese Particle Failure Model
A.3.3. The US Particle Failure Model

A.4. References of Appendix A

Appendix B: THE RUSSIAN "ACTIVATION MODEL" OF FISSION PRODUCT RELEASE FROM HTGR FUEL ELEMENTS

B.1. Introduction
B.2. The Basic Principles
B.3. Brief Characterization of Some Models

B.3.1. Stationary Mode, Diffusion Model
B.3.2. Non-Stationary Temperature Mode, One-Group Model, the CORSOR (CORSOR-M) Code

B.4. The Activation Model of Fission Product Release
B.5. Use of the Activation Model for the Analysis of Fission Product Transport

B.5.1. Fission Product Release at Simultaneous Irradiation and Heating
B.5.2. Release during Isothermal Heating of Previously Irradiated Fuel
B.5.3. Fission Product Spatial Distribution

B.6. Main Correlations for the Calculation of Coolant Activity
B.7. Method and Results of Determination of thye Fission Product Release Constants
B.8. Comparison of the Considered Moderl Parameters
B.9. Preliminary Analysis of Kr-85m Release (Experiment FRJ2-P28)
B.10. References of Appendix B

6.22 Some Topics on Improvement in Production Technology and Fission Product Behavior of HTTR Coated Particle Fuel

K. Hayashi, K. Minato, H. Kikuchi, T. Tobita,
T. Shiratori, H. Serizawa and K. Fukuda

Department of Chemistry and Fuel Research
Japan Atomic Energy Research Institute
Toka−mura, Naka−gun, Ibaraki−ken, 319−11, Japan

Abstract

In collaborations of the Japan Atomic Energy Research Institute (JAERI) and the Nuclear Fuel Industries, Ltd. (NFI), various improvements have been made on the production processes of coated fuel particles and fuel compacts, in order to reduce the failure fraction of the fuel for the High Temperature Engineering Test Reactor (HTTR). Irradiation performance of the fuels recently produced by the improved technology was successfully demonstrated by the 13th OGL−1 fuel assembly irradiation, performed in an in−pile gas loop, OGL−1.

In the field of fission product behavior, a peculiar distribution of ^{110m}Ag was noticed in its radial profile in the graphite sleeve; the concentration of this nuclide was markedly reduced with increasing concentration of metallic impurities including ^{60}Co. This behavior may be ascribed to competitive co−sorption of Ag and the impurities for the trapping sites on the surface of open pores in the graphite material. Obtained results so far suggest that this nuclide should be retained effectively in the highly−purified graphite sleeve under the HTTR conditions.

As for the ZrC−coated particle fuel being developed as an advanced HTTR fuel, much better retention of Cs was observed than for SiC−coated particles in isochronal annealing experiments at temperatures between 1500 and 2300°C; while relatively poor retention of Ru was observed for ZrC−coated particles in this temperature range.

1. Introduction

The High Temperature Engineering Test Reactor (HTTR) is under construction at Oarai Research Establishment of Japan Atomic Energy Research Institute (JAERI) [1,2]. HTTR is

a high−temperature gas−cooled reactor (HTGR) of a thermal output of 30 MW [2,3]. Fabrication of the HTTR fuel was started in June 1995, and will be completed in 1997, before its loading into the HTTR core to attain the first criticality in December, 1997 [1,2].

The structure of the HTTR fuel (type A) is given in Fig.1 [3]. The fuel assembly is a pin−in−block type with 30 or 33 fuel rods comprising graphite sleeves and fuel compacts. The fuel compact is a consolidated body of coated fuel particles, dispersed in graphite matrix. The coated particle consists of a UO_2 kernel and four−layer coating of porous, low−density pyrolytic carbon (PyC), inner high−density PyC (IPyC), SiC and outer high−density PyC (OPyC).

In this paper, some topics are reviewed in the following fields of the recent research and development of the HTTR fuel:

- improvement in production technology of coated fuel particles and fuel compacts,
- migration behavior of metallic fission products, particularly ^{110m}Ag, in fuel assembly, and
- release behavior of fission products from ZrC−coated fuel particles during heating at high temperatures up to 2400°C.

2. Improvement in Production Technology

Improvement in production technology of the HTTR fuel was fully described [4−7] and reviewed elsewhere [8]. A brief summary of these references is given in the present paper, together with descriptions of recent advancement in fuel compact production and of irradiation performance tests.

2.1 Kernel Production Process

The UO_2 kernels are produced by an external sol−gel method, in which the microsphere drops are made by vibrating nozzles, shown in Fig. 2 [8]. Comparison between appearances of the products by the conventional nitrogen−injection type nozzles and by the vibrating nozzles in Fig. 3 [8] indicates clearly that sphericity of the kernels has been markedly improved by the new device.

2.2 Coating Process

A recent joint work of JAERI and NFI was focused on improvement in quality of the SiC layer by optimizing the fluidization conditions. As a result, imperfections like circumeferential flaws were almost completely removed [6].

In a separate effort, an improved method, namely, a successive coating, has been developed, in which the unloading and loading of the porous PyC−, IPyC− and SiC−coated particles are not needed [7]. This method has therefore eliminated coating failure during unloading and loading of the particles except during unloading after the OPyC coating.

Figure 4 [7] compares results of the conventional and the improved coating examinations. The fraction of the defective SiC layer was significantly reduced by using the successive four−layer coating without particle unloading (step II), together with the optimization of fluidizing conditions (step I).

2.3 Fuel Compact Production Process

(1) Double−overcoating method

For recent several years, a double−overcoating method was attempted by NFI to mitigate the mechanical damage of coating layers during pressing and curing by using the first overcoating layer for the protection [9]. However, an irradiation test by a gas−swept capsule, 90F−1A, using coated fuel particles with low defective−coating fractions revealed no significant difference between the fission gas releases from fuel compacts produced by the single− and the double−overcoating methods. The double−overcoating method has not been adopted in the HTTR fuel production.

(2) Optimization of pressing conditions

In a collaboration of JAERI and NFI in 1994, a further effort was made to optimize the pressing temperature and speed in the single−overcoating method [10]. The purpose is to preserve an appropriate overcoat thickness of each coated fuel particle, which corresponds to the spacing among the particles.

The phenol binder, which is mixed in the overcoating graphite matrix, begins to become soft at a temperature around 60°C, and to become hard above ca. 150°C. If the pressing temperature is too high within this temperature range, the spacing may be lost due to an excessive fluidity. The function of the overcoat, namely, protection of the coating layer of coated fuel particles, is considered to be deteriorated in this dispersion state. Shrinkage of the overcoat matrix [11] during the subsequent heat treatment and irradiation may lead to intolerable stresses onto the coating layers of adjacent coated fuel particles in mutual contact, and eventually to failure of the coating layers.

In the compaction tests, the overcoat spacings in longitudinal cross−sections of fuel compacts were examined after pressing at different temperatures and speeds; see Fig.5 [10]. Thus, an optimum pressing conditions were sought. The results will be described elsewhere.

2.4 Irradiation Tests of Fuels Produced by the Advanced Technologies

(1) 13th OGL−1 fuel irradiation

The optimum coating conditions described in section 2.2 were applied to the coating process of the coated fuel particles loaded in the 13th OGL−1 fuel assembly in 1989. The OGL−1, Oarai Gas Loop−1, was an in−pile helium gas loop, which had been installed in JMTR until 1995 [12]. Figure 6 [8] shows that the fraction of defective SiC−layer was reduced by two orders of magnitude, compared with those up to the 12th fuel assembly [13].

The improvement in the fuel quality was confirmed in the fission gas release during irradiation. Figure 7 [8] indicates that the release−to−birth ratio, R/B, of ^{88}Kr for the 13th OGL−1 fuel assembly was reduced by more than an order of magnitude, compared with those for the assemblies up to the 12th [13].

(2) Gas−swept capsule irradiation (94F−9A)

Another irradiation program is on going, with a gas−swept capsule, 94F−9A, to be tested in the Japan Materials Testing Reactor (JMTR) of JAERI. The capsule is to be loaded with fuel compacts which were produced by the advanced technologies described above; namely, i) the vibration method for kernels, ii) the successive four−layer coating without particle unloading, and iii) the optimum pressing conditions in fuel compact production.

The coated fuel particles and the compaction method for the capsule test fuel are the same as those for the first charge fuel of HTTR. Fuel compacts for the irradiation test were already produced. Irradiation of the capsule is scheduled to start in January, 1997 and to complete in 1998 after attaining a burnup of about 5% FIMA (fissions per initial metal atom) at 1300°C.

3. Migration Behavior of Fission Products in Fuel Assembly

A series of measurements of metallic fission products were conducted using graphite sleeves and blocks of the OGL−1 fuel assemblies [14−16]. The objective of the studies is to examine the in−pile behavior of metallic fission products under simulated HTTR conditions. Main results of the measurements are briefly reviewed in the present paper, with a special focus on the migration behavior of ^{110m}Ag in the graphite sleeve.

3.1 Experimental Procedures

The graphite sleeves and blocks of the OGL−1 fuel assemblies were irradiated in simulated

conditions of the HTTR core, with respect to the fuel temperatures, burnups and coolant flow. Figure 8 [16] shows a schematic structure of the OGL−1 fuel assembly and the method to measure the fission product distribution in the graphite sleeve.

3.2 Cesium and Other Fission Products

Typical results of radial distribution of fission products in graphite sleeves of OGL−1 fuel assemblies are depicted in Fig. 9 [14,15]. The retention by the sleeve is almost complete for ^{155}Eu, ^{144}Ce and ^{90}Sr, and effective for ^{125}Sb and ^{110m}Ag; while not so effective for ^{137}Cs and ^{134}Cs.

The in−pile diffusion coefficients of Cs in the graphite, IG−110, were determined from the measured profile through comparison with calculated profiles in unsteady state conditions. The obtained equation at temperatures between 750 and 1000°C is as follows [14]:

$$D_{in-pile}(m^2/s) = 9.0\times10^{-6}\exp(-1.57\times10^5(J/mol)/RT), \quad (1)$$

where R is the gas constant (8.314 J/mol·K) and T the temperature (K).

The larger activation energy (157 kJ/mol) obtained for the in−pile diffusion than those (112 and 95 kJ/mol) for diffusion in un−irradiated IG−110 graphite led to an extended model on trapping of the diffusant Cs by the irradiation−induced defects on the surface of open pores [17].

3.3 Ag−110m

Silver−110m is regarded as one of the most important fission products in HTGR, particularly in gas−turbine HTGR systems, from a viewpoint of the plate−out activity in the primary system [18]. A main reason is that intact SiC layer is considered to be permeable to Ag at high temperatures above ca. 1300°C [19].

In normal cases of OGL−1 experiments so far, the radial profile of ^{110m}Ag was as that depicted in Fig. 9. This nuclide was effectively retained in the graphite sleeve. The very low activity of ^{110m}Ag observed at depths adjacent to the outer surface may be ascribed to influx of Ag as impurities from the coolant side. The temperature of the sleeve was calculated to be lower than 1100°C.

On the other hand, a peculiar distribution of ^{110m}Ag was observed in the graphite sleeve of the 12th OGL−1 fuel assembly, as shown in Fig. 10 [16]. The concentration profile of ^{110m}Ag exhibited an inverse tendency to that of ^{60}Co. Namely, the concentration of ^{110m}Ag increased, while that of ^{60}Co decreased, with increasing depth from the inner−surface. The inverse tendency for ^{110m}Ag and ^{60}Co is also observed in their profiles from around the middle

depth to the outer-surface.

The ^{60}Co is considered to have been contained in the sheath material of the thermocouple inserted in the central hole of the irradiated fuel compact stack. That is, the ^{60}Co was an metallic impurity transported through the fuel compacts to the inner-surface of the sleeve.

The mechanism of the inverse tendency of the ^{110m}Ag and ^{60}Co profiles has not been clarified at the moment. A possible cause is that the transport of ^{110m}Ag in the graphite had been affected by the co-sorption process in the diffusion-trap mechanism along open pore surfaces in the graphite. Namely, silver and metallic impurities including Co is considered to have competed for the trapping (or adsorption) sites in the pore surface diffusion.

It is emphasized that the case depicted in Fig. 10 was an accidental case with abnormally large influx of metallic impurities into the graphite. Thus, it can be concluded that Ag-110m will be effectively retained in the graphite sleeve under normal operating conditions using the highly purified graphite without significant influx of impurity metals from outside.

4. Release Behavior of Fission Products form ZrC-coated Fuel Particles

Zirconium carbide (ZrC)-coated fuel particles have been developed at JAERI for more than 20 years as an advanced HTGR fuel to be substituted for SiC-coated fuel particles. A series of research and development works were reviewed [20,21], and integrity of the fuel was assessed in order to use it in a test fuel assembly of the HTTR [22].

As compared with the SiC-coated fuel particles, pronounced features of the ZrC-coated particles are the following:

- better performance against kernel migration failure [20] and chemical attacks by fission products including Pd [23],
- better durability against pressure vessel failure at extremely high temperatures above 2000°C [24], and
- better retention of important fission products, except Ru, particularly at high temperatures of 1600°C [25] and above [26].

A result of a heating experiment [26] to study the fission product release behavior at extremely high temperatures is reviewed below.

4.1 Experimental Procedures

ZrC-coated particles used in the present experiment were sampled by electrochemical deconsolidation of the same fuel compact as was used by Minato [25]. The specifications and

irradiation conditions were given in ref.[25].

A single particle, taken from the samples, was heated in a graphite electrode (Fig.11 [27]), under flowing argon gas for each isochronal heating series at temperatures from 1400 to 2400°C, as shown in Fig. 12 [26]. After each heating step at different temperatures, radioactivity measurement was made by gamma−ray spectrometry for the upper and lower graphite electrodes and the graphite cover, into which fission products were released from the coated particle.

4.2 Results

A typical result of the heating experiment is shown in Fig. 12. The fractional release of ^{137}Cs was much smaller for the ZrC− than for the SiC−coated fuel particles, in particular at temperatures above 2000°C.

On the contrary, the fractional release of ^{106}Ru was much larger for the ZrC−coated particle, at 2000 − 2300°C. This result is consistent with observations by other researchers in isothermal heating at 1400°C [28] and 1600°C [25]. The observed high diffusivity of Ru in the ZrC layer may limit the feasibility of the ZrC−coated particle fuel in utilization for the gas−turbine HTGR system. The higher diffusivity of Ru is presumably concerned with its small atomic radius. Full description of the results and discussion will be given elsewhere.

4.3 Further Research Prospect

The following are further research items for developing the ZrC−coated particle fuel in a reactor scale as an advanced fuel, which can be utilized at higher temperatures up to higher burnups than the SiC−coated particle fuel.

(a) producibility by scaled−up facilities,

(b) property changes and performance in irradiation at higher temperatures up to higher burnups in normal operating conditions,

(c) safety under accident conditions:

- mechanical integrity and fission product release behavior of highly burned−up fuel at extremely high temperatures,
- oxidation behavior under design base and hypothetical accidents with air and water ingress [29], and

(d) reactor safety design with effective measures against air and water ingress [30].

5. Summary

The advanced production technologies above described have been adopted in the production of the first-charge fuel of the HTTR. And fine control on the processes is being made in a reactor core scale.

The studies on ^{110m}Ag distribution in the OGL-1 fuel assemblies have revealed the possibility of retention of this nuclide in the graphite sleeve. Of great interest are the plate-out activity in the primary system and the distribution in the fuel assemblies of HTTR.

Results of research and development (R&D) so far at JAERI have revealed the excellent performance of ZrC-coated fuel particles. However, R&D works thereon are very limited, and further research in an engineering scale is required to develop the fuel as an advanced HTRG fuel with commercial feasibility.

References

[1] T. Tanaka, O. Baba, S. Shiozawa, M. Okubo and Y. Kambayashi, 3rd JAERI Symp. on HTGR Technologies, Oarai, Japan, Feb. 15-16, 1996, 2-5.

[2] Japan Atomic Energy Research Institute, Present Status of HTGR Research and Development, 1996.

[3] S. Saito et al., JAERI-1332 (1994) p.46.

[4] K. Fukuda et al., J. Nucl. Sci. Technol. (Tokyo) 28 (1991) 570.

[5] S. Yoshimuta, N. Suzuki, M. Kaneko and K. Fukuda, Proc. IAEA Specialists Meeting on Behavior of Gas Cooled Reactor Fuel under Accident Conditions, (Oak Ridge, USA, 5-8 Nov. 1990) IWGGCR/25, p.37.

[6] K. Minato, H. Kikuchi, K. Fukuda, N. Suzuki, H. Tomimoto, N. Kitamura and M. Kaneko, Nucl. Technol. 106 (1994) 342.

[7] K. Minato, H. Kikuchi, K. Fukuda, N. Suzuki, H. Tomimoto, N. Kitamura and M. Kaneko, Nucl. Technol. 111 (1995) 260.

[8] K. Hayashi et al., JAERI-Conf 96-006 (1996) p. 128.

[9] S. Yoshimuta, N. Suzuki, F. Takano, N. Kitamura and M. Kaneko, 1989 Annual Meeting of Atomic Energy Society of Japan, (Osaka Univ., April 4-6, 1989) G15 (in Japanese).

[10] H. Kikuchi, K. Minato, T. Tobita, K. Fukuda, T. Oda, H. Tomimoto, S. Yoshimuta, K. Watarumi, 1995 Annual Meeting of Atomic Energy Society of Japan, (Tokyo Inst. Technol., March 28-30, 1995) B55 (in Japanese).

[11] M. R. Everett and B. Blackstone, Nuclear Fuel Performance: Proc. BNES Conf., 15-19

Oct., 1973, London, 29-5.

[12] T. Ishii, T. Saruta, I. Arase, and T. Niiho, 3rd JAERI Symp. on HTGR Technologies, Oarai, Japan, Feb. 15-16, 1996, 6-12.

[13] K. Hayashi, K. Minato, F. Kobayashi, H. Kikuchi, K. Fukuda, T. Kikuchi, T. Saruta and T. Kitajima, JAERI-Research 94-017 (1994) (in Japanese) p.16.

[14] K. Hayashi, T. Kikuchi, K. Kobayashi, K. Minato, K. Fukuda, K. Ikawa and K. Iwamoto, J. Nucl. Mater. 136 (1985) 207.

[15] K. Hayashi, K. Kobayashi, K. Minato, K. Ikawa and K. Fukuda, J. Nucl. Mater. 149 (1987) 57.

[16] K. Hayashi, K. Fukuda, H. Tsuruta and T. Kikuchi, JAERI-M 94-075 (1994) (in Japanese).

[17] K. Hayashi and K. Fukuda, J. Nucl. Mater. 168 (1989) 328.

[18] K. Sawa and T. Tanaka, JAERI-Research 95-071 (1995) (in Japanese).

[19] H. Nabielek, P. E. Brown and P. Offermann, Nucl. Technol. 35 (1977) 483.

[20] T. Ogawa, K. Ikawa, K. Fukuda, S. Kashimura and K. Iwamoto, Nuclear Fuel Performance, BNES, London, 1985, p. 163.

[21] K. Minato, T. Ogawa and K. Fukuda, JAERI-Review 95-004 (1995).

[22] K. Hayashi et al., JAERI-M 90-115 (1990) (in Japanese).

[23] T. Ogawa and K. Ikawa, High Temp. Sci. 22 (1986) 179.

[24] T. Ogawa, K. Fukuda, S. Kashimura, T. Tobita, K. Kobayashi, S. Kado, H. Miyanishi, I. Takahashi and T. Kikuchi, J. Am. Ceram. Soc. 75 (1992) 2985.

[25] K. Minato, T. Ogawa, K. Fukuda, H. Nabielek, H. Sekino, Y. Nozawa and I. Takahashi, J. Nucl. Mater. 224 (1995) 85.

[26] K. Hayashi, T. Ogawa and K. Fukuda, 1992 Annual Meeting of Atomic Energy Society of Japan, (Tokai Univ., March 28-30, 1992) K33 (in Japanese).

[27] K. Hayashi and K. Fukuda, J. Nucl. Sci. Technol. (Tokyo) 27 (1990) 320.

[28] T. Ogawa and K. Ikawa, J. Nucl. Mater. 105 (1982) 331.

[29] K. Minato and K. Fukuda, IAEA-TECDOC-784 (1995) p.86.

[30] K. Sawa, JAERI-Research 95-072 (1995) (in Japanese).

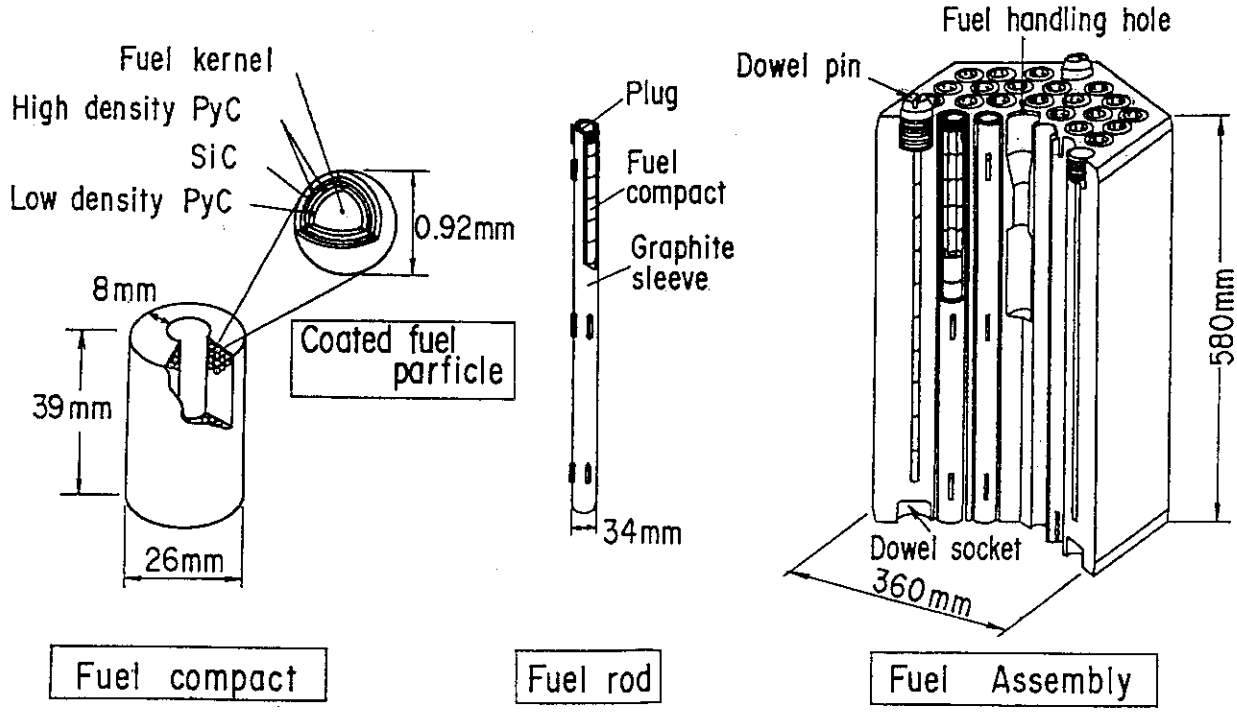


Fig. 1 Structure of a fuel assembly of the High Temperature Engineering Test Reactor (HTTR) [3].

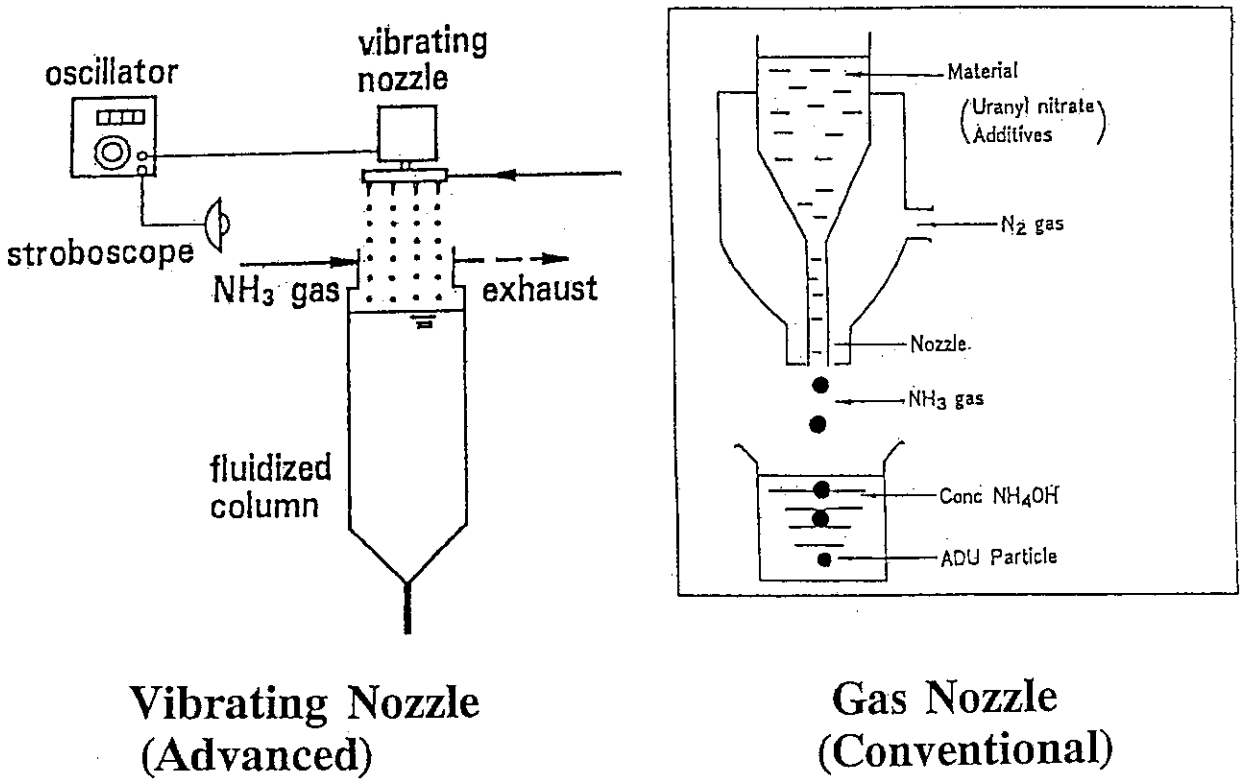


Fig. 2 Comparison of conventional and advanced nozzles for drop formation in the kernel production process [8].

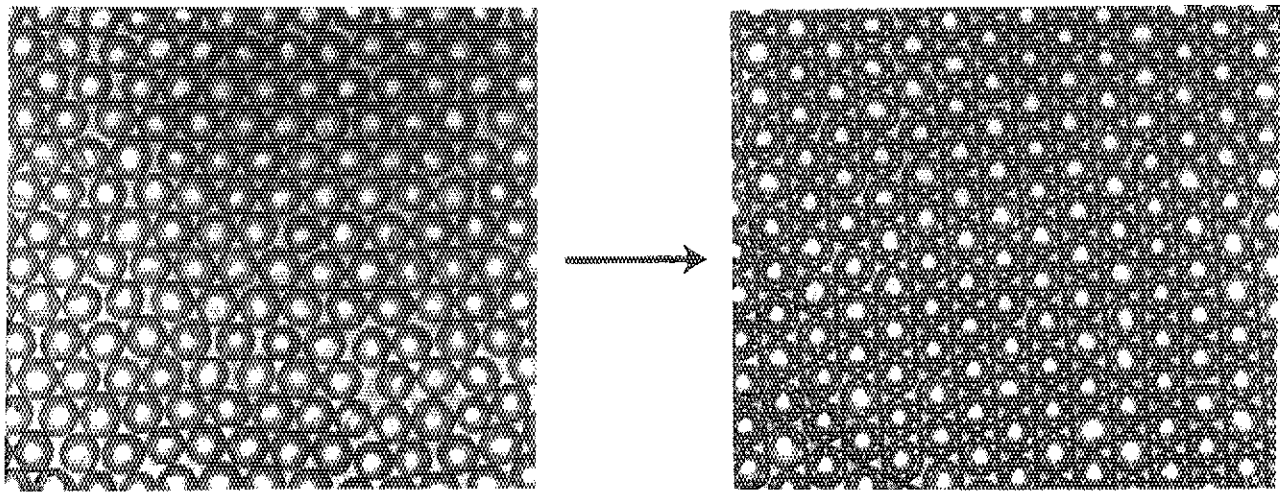


Fig. 3 Improvement in sphericity of fuel kernels produced by the vibrating nozzles, compared with those by the conventional gas nozzles [8].

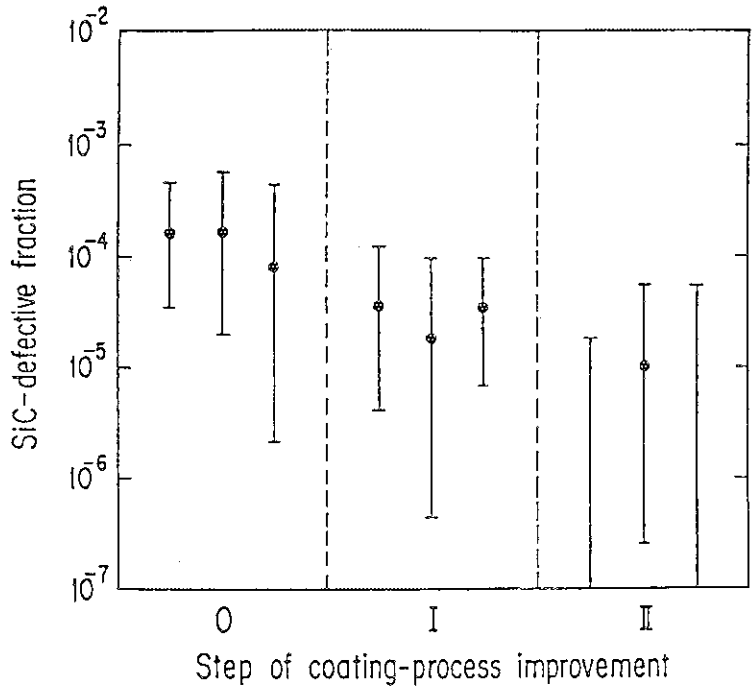


Fig. 4 Typical examples of SiC−defective fraction of the coated fuel particles as a function of the steps in the coating−process improvement. Step 0 is the conventional process. Step I is the improved process in the control of the particle fluidization. Step II is the further improved process without unloading and loading of the SiC−coated particles. Solid circles show measured values, and vertical bars indicate the 95% confidence limits [7].

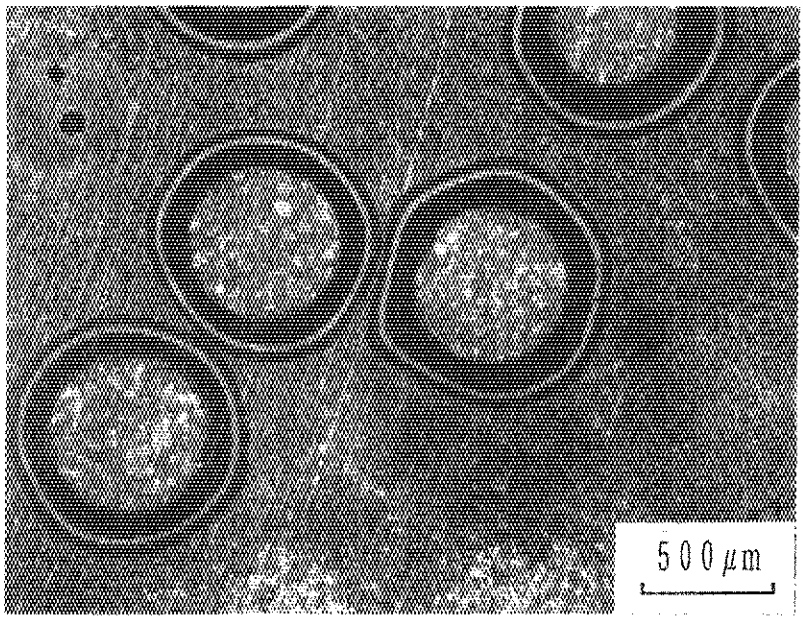


Fig. 5 Longitudinal cross-section of a fuel compact [10].

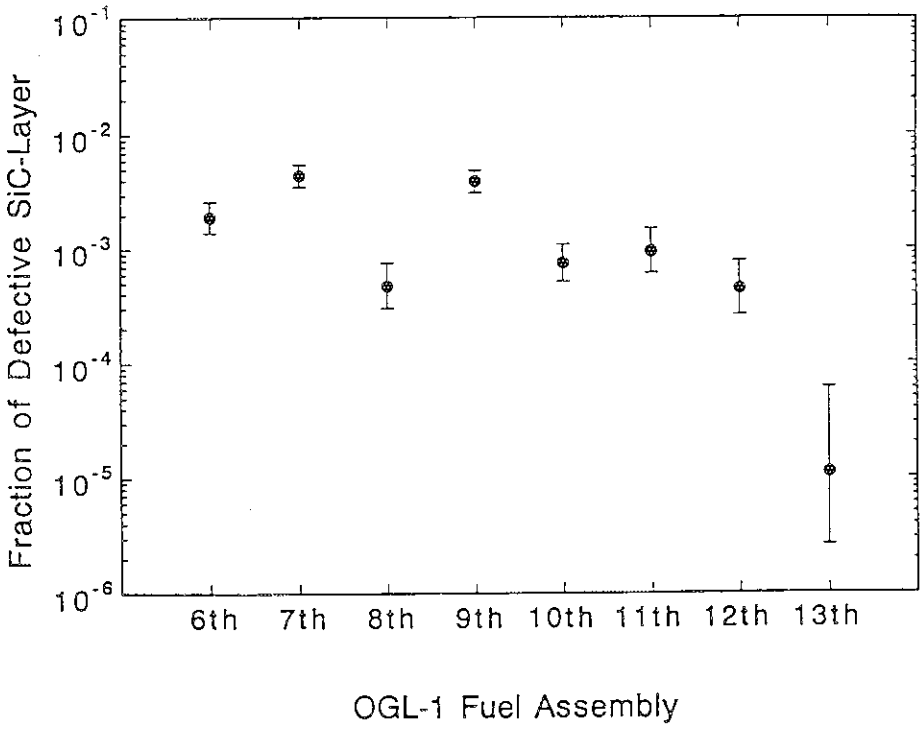


Fig. 6 Change in the fraction of defective SiC layer of coated fuel particles used in recent OGL－1 irradiation experiments [8]. The upper and lower values of the 95% confidence limits of the fractions are indicated in the figure.

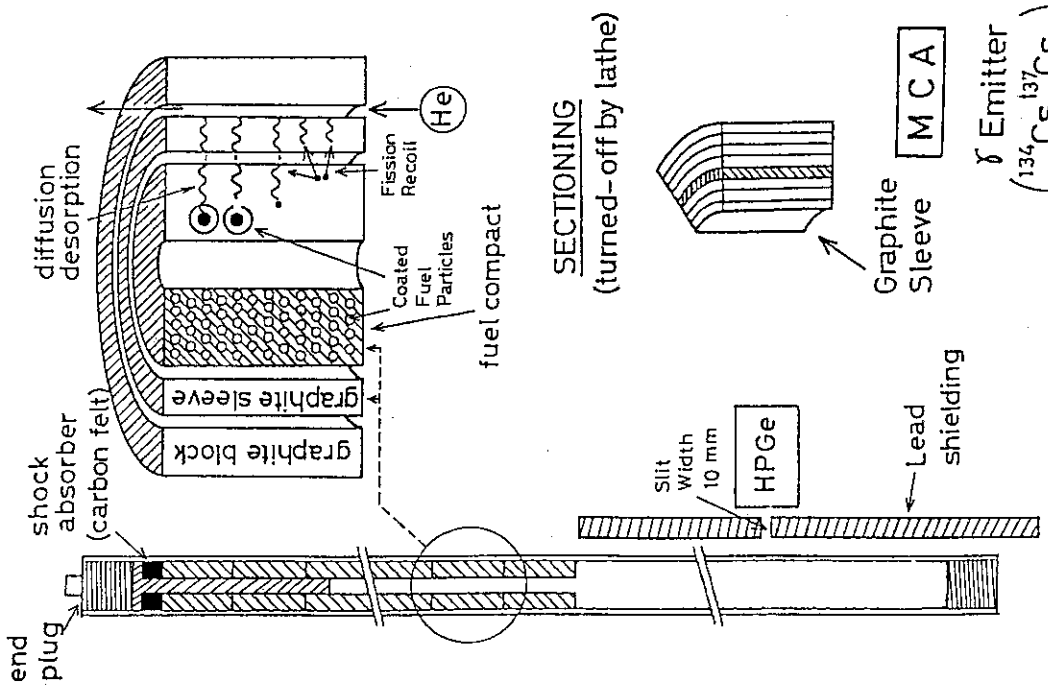


Fig. 8 Schematic diagram of an OGL−1 fuel assembly and the method to measure the distribution of fission products in the graphite sleeve [16].

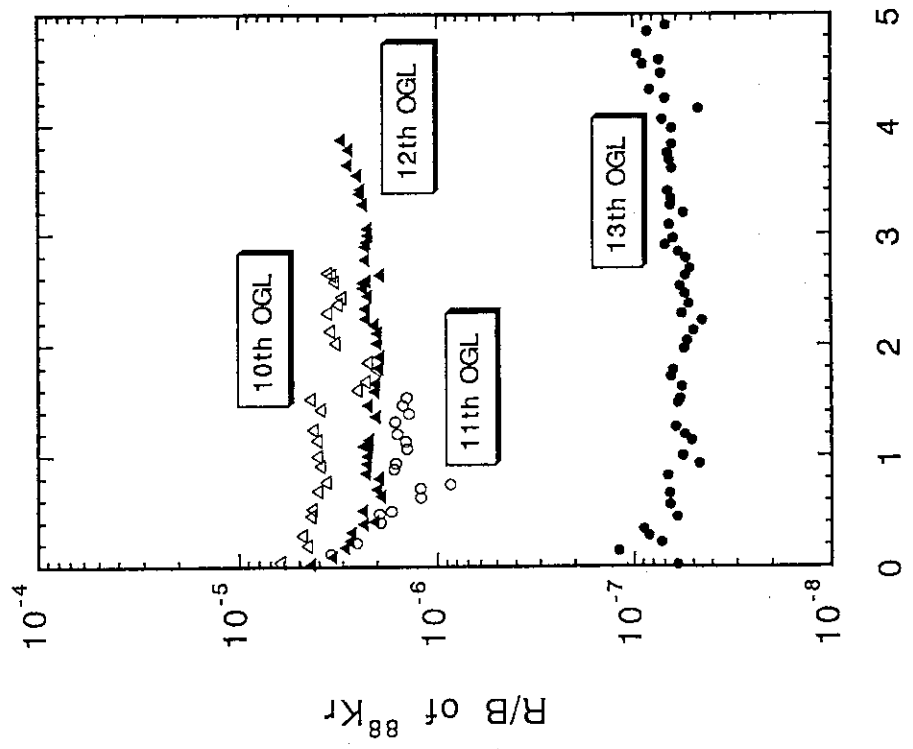


Fig. 7 Comparison of the release−to−birth ratios, R/B, of ^{88}Kr in recent OGL−1 fuel irradiation in steady state operation [8].

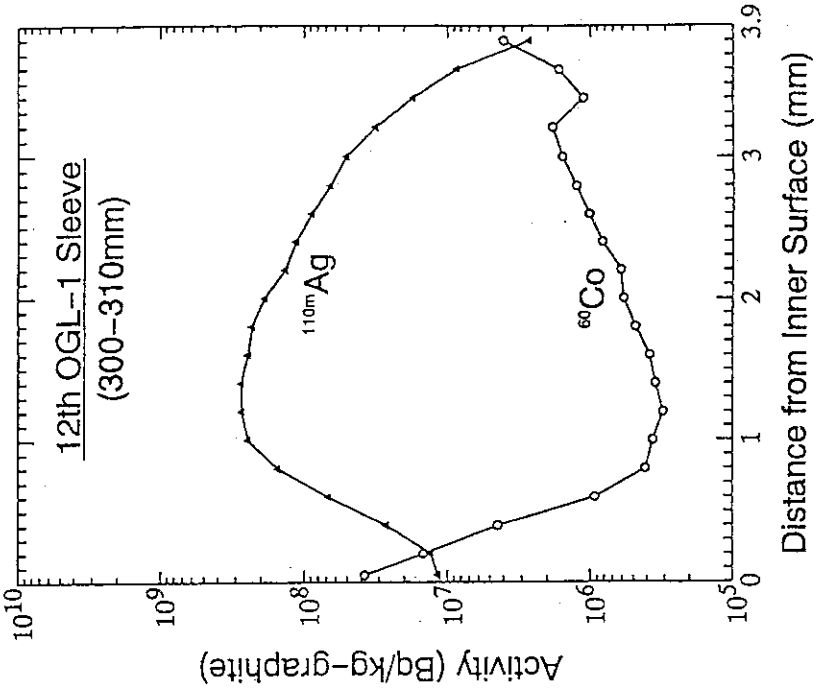


Fig. 10 Radial profiles of fission products in the graphite sleeve of the 12th OGL-1 fuel assembly; 300-310 mm from the axial top [16].

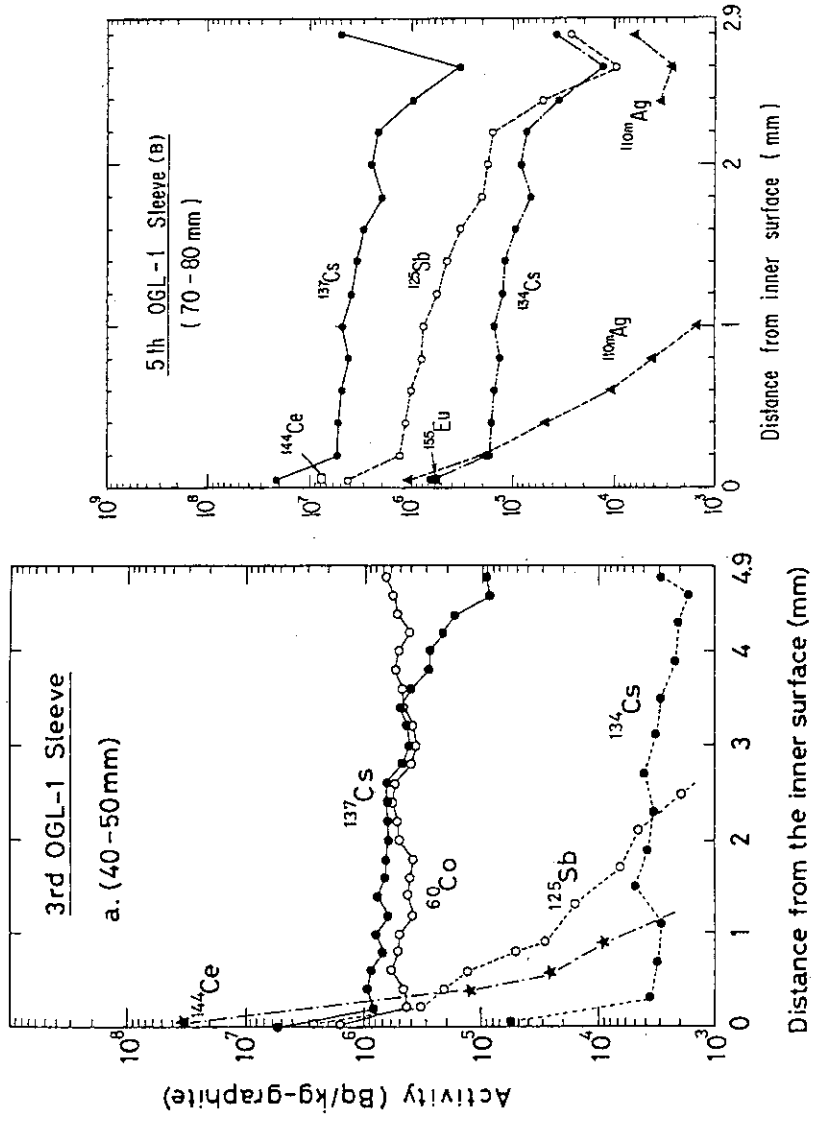


Fig. 9 Typical radial profiles of fission products in graphite sleeves of the 3rd [14] and 5th [15] OGL-1 fuel assemblies.

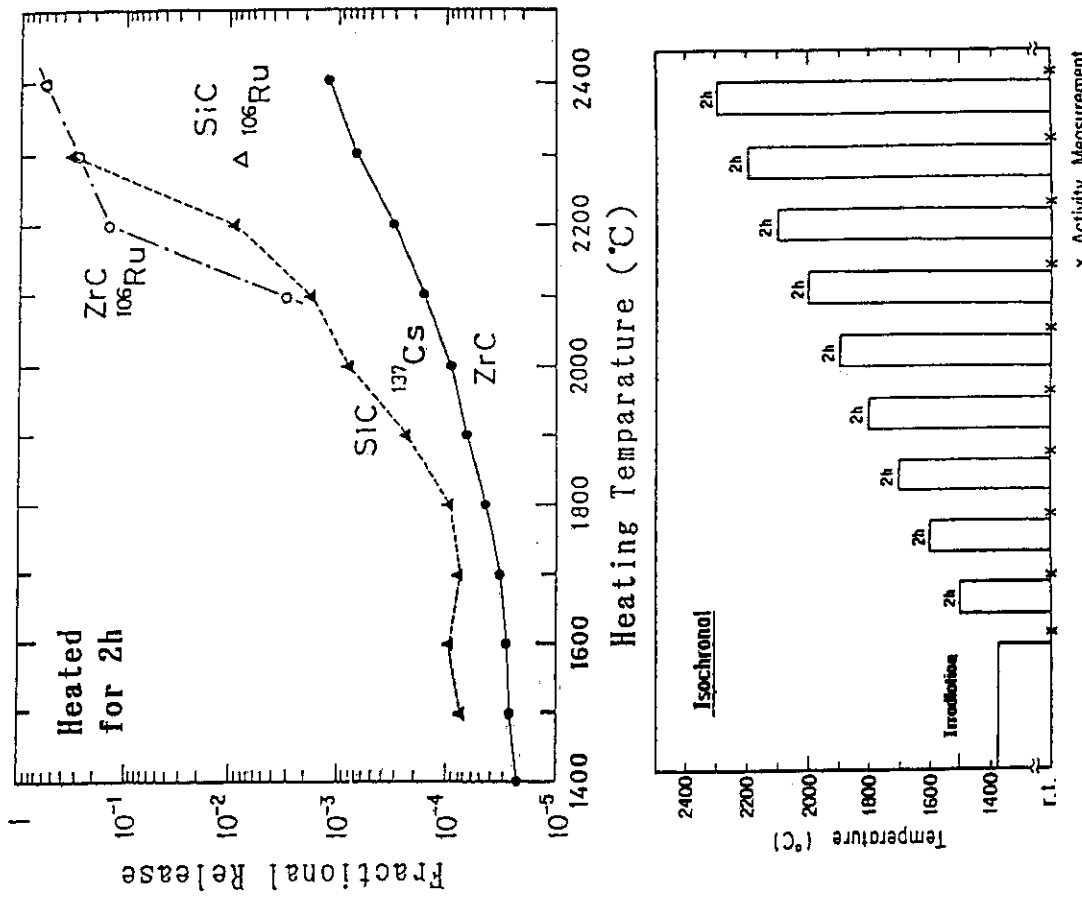


Fig. 12 **Isochronal annealing process (lower) and comparison of fractional release of fission products from ZrC− and SiC−coated fuel particles (upper) [26].**

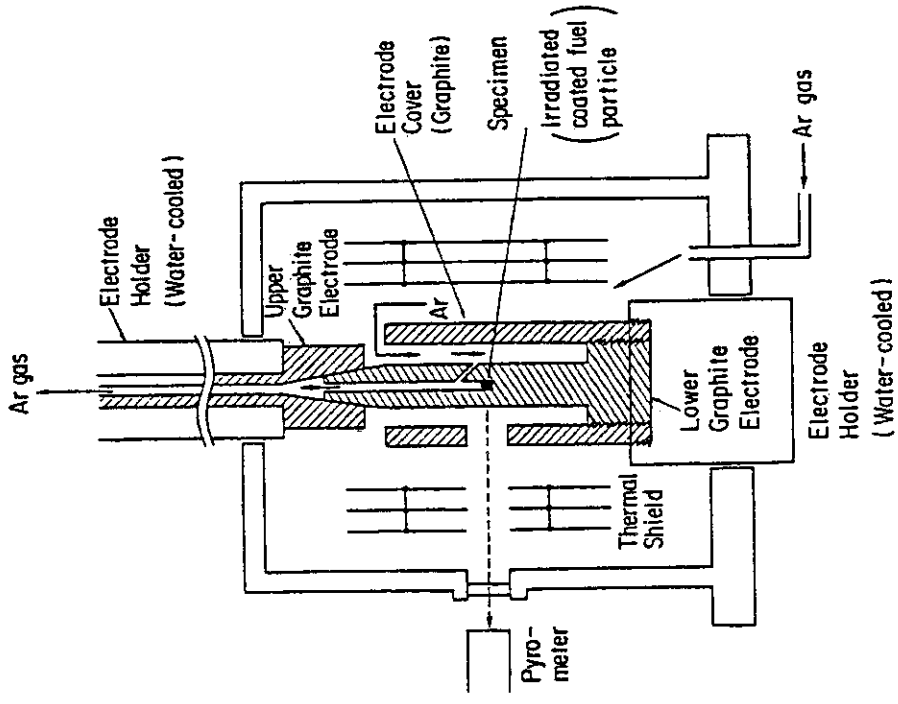


Fig. 11 Schematics of heating furnace for a single particle [27].

Closing Address

Toshiyuki Tanaka

Ladies and gentlemen.

Closing address is originally planned to be given by Dr. Konomo Sanokawa, Technical Advisor of the Japan Atomic Energy Research Institute, JAERI, but he can't attend this meeting because he caught a bad cold. I was asked by him to convey his sincere regards and good success of the meeting.

Instead of him and on behalf of the Organizing Committee, I'd like to briefly summarize the outcome of this Symposium. This Symposium is, as you know, the third one and the last 2nd Symposium was held in October 1992 when the installation of the HTTR containment vessel was almost finished and the reactor building came up to the second floor underground. Since then, the construction of the HTTR has proceeded rather well and comes to be approaching its final stage.

Just I will give you some statistics. We had 24 participants from abroad and 115 Japanese participants including JAERI's researchers. Number of participants has decreased reflecting the change of the circumstances and atmosphere in three years. However we had 17 oral presentations and 22 poster presentations with good success.

Anyway, I'd like to express my sincere gratitude to the authority, people of the town of Oarai, who welcomed us to have this Symposium, and also to all of the participants.

In this Symposium, we had an honor to have two invited lectures by highly distinguished persons, namely, Professor Komiyama from University of Tokyo and Professor Kugeler from KFA Germany.

It is quite obvious that the green house effect by carbon dioxide is one of the key issues in global environmental problems. Prof. Komiyama gave us a clear idea on the mechanism of green house effect and countermeasures for it. He stated that photovoltaic energy and fixation of CO_2 are not enough, and he recommends promotion of utilization of solar energy such as "Kojo no tsuki" project and nuclear energy are the effective and major solution for this problem. And he concluded solar should be more efficient and nuclear should be more open and safe.

Prof. Kugeler impressed us a great change in nuclear safety requirements in Germany,

and showed us a catastrophe-free reactor concept fully applying the HTGR safety characteristics, which can be demonstratable, with some further upgrading technologies which can answer this highly safety requirements in parallel with the EPR with a core catcher.

In the second session, present statuses of HTGR project in China, Russia, the Netherlands, the USA and Japan are explained and discussed.

China and Japan are constructing High-temperature Reactors, HTR-10 and HTTR aiming first criticality early 1999 and late 1997, respectively, and Russia and the USA are making effort on designing of direct cycle gas turbine HTRs while the Netherlands has an activity on the development of a small scale HTR for a combined heat and power generation in a WHITE reactor program.

In the third session, safety research, development of new material and experience in construction and operation of the HTGR were presented and discussed.

In safety research, some useful and comprehensive interesting results on after heat removal and fuel performance in accident conditions were shown and reviewed.

In the research of material development, a new ceramic material using Carbon-Carbon composite for future application in high-temperature in-core component in the HTGR was introduced, and some experiences in design and construction of HTR-10 and HTTR and also in decommissioning of AVR were presented and discussed.

In the forth session, research activities on heat utilization of the HTGR were introduced and discussed.

International Cooperation in IAEA on design and evaluation of heat utilization systems for the HTTR was presented and some research results on the activity were explained.

Examination on design of small pebble bed HTGR for electric generation and some results on comparative study on refueling method were shown.

Test results of CO-2 Reforming of Methane in a closed loop using solar energy were reported and discussed its potential use in nuclear heat application. And significance of the design features of steam reforming system to be connected the HTTR was also introduced.

In the last session, we had a panel discussion chaired by Dr. Tobioka. Due to the participants' beautiful contribution, a very interesting and informative discussion had been carried out on Future Perspectives of Nuclear Energy Utilization and Expected Role of the HTGR. As for the realization or introduction of a commercial HTGR, we need, at first, demonstrate the technical feasibility or viability of the HTGR based on the upgraded concept through the reactor experiments using the HTR-10 and HTTR, and also an international cooperation is highly requested to be introduced in order to make effective use of limited resources available.

Through this Symposium, I, as a secretariat, recognized again a steady and new progress in HTGR technology development despite the several changes since the last Symposium. Nevertheless, we are all aware that there still remain many items to be overcome or upgraded in technical, economical, social and political fields. We plan to hold the next symposium after about three years later. Being very much encouraged with the outcome of this symposium, let us promise ourselves to make further efforts and bring together our progress at the next meeting.

Expressing my hearty thanks to all contributors, participants as well as the staffs of this Symposium, I now declare the Symposium is closed.

Thank you very much indeed.